

**Density Functional Theory Studies on D- $\pi$ -A Systems Used in  
Dye-Sensitized Solar Cells: Donor-Acceptor Effect, Spacer Effect,  
and Molecular Design Strategies**

By

**Divya Velayudhan V. V.**

Registration No: 10CC15A39004

A thesis Submitted to the  
Academy of Scientific & Innovative Research  
for the award of the degree of  
**DOCTOR OF PHILOSOPHY**  
in  
**SCIENCE**

Under the supervision of

**Dr. C. H. Suresh**



**CSIR-National Institute for Interdisciplinary  
Science and Technology (CSIR-NIIST),  
Thiruvananthapuram-695019, Kerala, India**



Academy of Scientific and Innovative Research  
AcSIR Headquarters, CSIR-HRDC campus  
Sector 19, Kamla Nehru Nagar,  
Ghaziabad, U.P. - 201 002, India

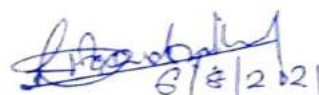
**August 2021**

## DECLARATION

I hereby declare that the Ph.D. thesis entitled "**Density Functional Theory Studies on D- $\pi$ -A Systems Used in Dye-Sensitized Solar Cells: Donor-Acceptor Effect, Spacer Effect, and Molecular Design Strategies**" is an original work carried out by me at Chemical Science and Technology Division(CSTD), CSIR-National Institute for Interdisciplinary Science and Technology (CSIR-NIIST), Thiruvananthapuram, under the supervision of Dr. C. H. Suresh, Senior Principal Scientist, CSTD, CSIR-NIIST, and it has not been submitted elsewhere for any other degree, diploma or title.

CSIR-NIIST

06/08/2021



**Divya Velayudhan V. V.**

**Council of Scientific & Industrial Research  
National Institute for Interdisciplinary Science and Technology  
Thiruvananthapuram-695019, Kerala, India**



**Dr. C. H. Suresh**  
Senior Principal Scientist  
Chemical Sciences and Technology Division

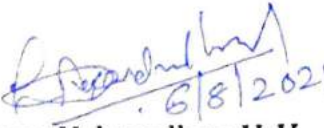


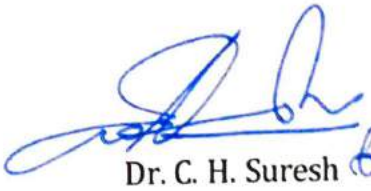
Tel: +91- 471-2515472  
E-mail: sureshch@gmail.com  
sureshch@niist.res.in

06<sup>th</sup> August, 2021

## **CERTIFICATE**

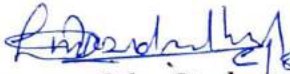
This is to certify that the work incorporated in this Ph.D. thesis entitled "**Density Functional Theory Studies on D- $\pi$ -A Systems Used in Dye-Sensitized Solar Cells: Donor-Acceptor Effect, Spacer Effect, and Molecular Design Strategies**" submitted by Ms. Divya Velayudhan V. V. to the Academy of Scientific and Innovative Research (AcSIR), in partial fulfillment of the requirements for the award of the Degree of Doctor of Philosophy in Science, embodies original research work carried-out by the student. We, further certify that this work has not been submitted to any other University or Institution in part or full for the award of any degree or diploma. Research materials obtained from other sources and used in this research work has been duly acknowledged in the thesis. Images, illustrations, figures, table etc., used in the thesis from other sources, have also been duly cited and acknowledged.

  
Divya Velayudhan V. V.  
(Student)

  
Dr. C. H. Suresh  
(Thesis Supervisor)

## Statements of Academic Integrity

I Divya Velayudhan V. V., a Ph. D. student of the Academy of Scientific and Innovative Research (AcSIR) with Registration No. 10CC15A39004 hereby undertake that, the thesis entitled "**Density Functional Theory Studies on D- $\pi$ -A Systems Used in Dye-Sensitized Solar Cells: Donor-Acceptor Effect, Spacer Effect, and Molecular Design Strategies**" has been prepared by me and that the document reports original work carried out by me and is free of any plagiarism in compliance with the UGC Regulations on "*Promotion of Academic Integrity and Prevention of Plagiarism in Higher Educational Institutions (2018)*" and the CSIR Guidelines for "*Ethics in Research and in Governance (2020)*."

  
Signature of the Student 6/8/2021

Name: Divya Velayudhan V. V.

Date: 6/8/2021

Place: Thiruvananthapuram

---

It is hereby certified that the work done by the student, under my supervision, is plagiarism free in accordance with the UGC Regulations on "*Promotion of Academic Integrity and Prevention of Plagiarism in Higher Educational Institutions (2018)*" and the CSIR Guidelines for "*Ethics in Research and in Governance (2020)*".

  
Signature of the Supervisor

Name: Dr. C. H. Suresh

Date: 6/8/2021

Place: Thiruvananthapuram



## **Acknowledgement**

*First and foremost, I am folding my hands with great gratitude to the GOD ALMIGHTY for without His grace and blessings, this study would not have been possible.*

*I would like to express my deep and sincere gratitude to my research supervisor, Dr. C. H. Suresh, for giving me the opportunity to do research and providing invaluable guidance throughout this research period. His dynamism, vision, sincerity and motivation have deeply inspired me.*

*I express my sincere thanks to Dr. A. Ajayaghosh, Director, CSIR-NIIST, for providing the academic support and excellent infrastructure facilities which made my Ph.D. experience productive and stimulating.*

*I thank to the AcSIR coordinator Dr. V. Karunakaran for his timely advice and support for the conduct of academic procedures. I would like to keep memory lane in Dr. Mangalam S. Nair and Dr. Luxmi Varma, former AcSIR coordinators for their valuable advice, constructive criticisms and warm back up in times of need.*

*My sincere thanks to HoD, Dr. P. Sujatha Devi for all their support and guidelines. I also extend my sincere thanks to former HoDs Dr. K. R. Gopidas and Dr. Luxmi Varma for their valuable advice and support.*

*I also express my gratitude to my Doctoral Advisory Committee Members Dr. C. Vijayakumar, Dr. Kaustabh Kumar Maiti and Dr. S. Savithri for their valuable suggestions, timely help, and support.*

*I am truly excited to reveal a sense of owe to my fellow lab mates in CHS Group for their support and friendship. Dr. Prabha, Dr. Remya K., Dr. Remya P. R, Dr. Della Therese Davis, Dr. Rakhi R., Dr. Renjith S. Pillai, Dr. Anjali B., and Dr. Remya G. S are acknowledged for their help, support and guidelines in understanding the computational tools, research methods and for the created pleasant working atmosphere in the lab. I also extend my gratefulness to the current members of the lab; Bijina, Anila, Anjalikrishna, Krishnapriya, and Haritha for their warm friendship.*

*I gratefully acknowledge CSIR for providing me financial support.*

*I would also like to thank the administrative and technical staff members of CSIR-NIIST for the cooperation and help in their respective roles.*

*I gratefully acknowledge the high-performance computational facilities at CSIRNCL, Pune, and CSIR-CMMACS, Bangalore.*

*I am also grateful to all of my teachers who sacrificed their lives to mould me into the person I am today.*

*I would like to thank my family. I sought inspiration and I owe a great deal to my mother, A.K. Vilasini and my father Velayudhan V.V who have unquestionably given their ears for the primrose path in my life. I also wish to offer my gratefulness to my understanding brother Mr. Vivek Velayudhan. This triumphant trip would not have been possible without them.*

*I am really very much grateful to my better half Dr. Shiju K.J. Thanks for your great support, guidelines, motivation and unwavering concern.*

*Also, thank you to my two cutie pies, Athiradh and Aadikesh, for allowing me to experience love and for helping me relax during the difficult times of my studies. They were incredibly patient and understanding during the entire journey of my research.*

*Last but not the least, I extend my thankfulness to all those persons who supported me directly or indirectly to complete my research without any glitches.*

*Divya Velayudhan V.V.*

# CONTENTS

	Page
Declaration	i
Certificate	ii
Statements of Academic Integrity	iii
Acknowledgements	iv
Contents	vi
List of Figures	x
List of Tables	xiii
List of Abbreviations	xvii
Preface	xix

## Chapter 1

### Introduction

#### Part A: Dye-sensitized Solar Cells

1.1	Introduction	2
1.1.1	Overview of dye-sensitized solar cell (DSSC)	3
1.1.2	Working principle and major components of DSSC	3
1.1.2.1	Photoanode	5
1.1.2.2	Electrolyte	5
1.1.2.3	Counter electrode	7
1.1.2.4	Dye-sensitizers	7
1.1.3	Theoretical background for computing photovoltaic properties of dye-sensitizers	8
1.1.4	Classification of dye-sensitizers	10
1.1.4.1	Metal-based dye-sensitizers	10
1.1.4.2	Porphyrins	11
1.1.4.3	Phthalocyanines	12
1.1.4.4	Metal-free organic dyes	13

1.1.5	Distinctive design strategies in metal-free organic sensitizers	14
1.1.6	Influence of spacer units	17
1.1.7	Significance of acceptors or anchoring units	19
1.1.8	Importance of theoretical study in the design of dye sensitizers	21
1.1.9	Objective of the study	23

## **Part B: Computational Chemistry Methods**

1.2	An overview of computational Chemistry	25
1.2.1	Ab initio quantum chemical methods	26
1.2.1.1	Hartree-Fock theory	28
1.2.1.2	Post-Hartree-Fock methods	31
1.2.1.2.1	Møller-Plesset perturbation theory	32
1.2.1.2.2	Configuration interaction (CI) method	32
1.2.1.2.3	Multi-configurational self-consistent field (MCSCF)	33
1.2.1.2.4	Coupled cluster theory	34
1.2.2	Semiempirical methods	35
1.2.3	Density functional theory	36
1.2.3.1	Thomas-Fermi model	37
1.2.3.2	Hohenberg-Kohn theorem	38
1.2.3.3	Kohn-Sham equations	38
1.2.3.4	Exchange-correlation functionals	40
1.2.3.4.1	Local density approximation (LDA)	41
1.2.3.4.2	Generalized gradient approximation (GGA)	42
1.2.3.4.3	Meta GGA	42
1.2.3.4.4	Hybrid density functional (H-GGA)	42
1.2.3.5	Dispersion corrections	43
1.2.3.6	Time-Dependent density functional theory (TDDFT)	43
1.2.4	Theoretical methods used in the study	46
1.2.5	Basis sets	46
1.2.6	Molecular electrostatic potential (MESP)	49



1.2.7	Solvation models	52
1.3	Conclusions	54
1.4	References	54

## **Chapter 2**

### **Quantification of Donating Strength and Substituent Effect Transmission Power of Various Spacers**

#### **Part A: Substituent Effect Transmission Power of Alkyl, Alkenyl, Alkynyl, Phenyl, Thiophenyl and Polyacene Spacers**

2.1	Abstract	72
2.2	Introduction	72
2.3	Computational methodology	74
2.4	Results and discussion	74
2.4.1	MESP topography and spacer effects	74
2.4.2	$V_{\min}$ based quantification of substituent effect transmission power of spacers	81
2.4.3	Combination of two different spacers and substituent selectivity	83
2.4.4	Conclusions	85

#### **Part B: Density Functional Theory Study on the Donating Strength of Donor Systems in Dye-Sensitized Solar Cells**

2.6	Abstract	86
2.7	Introduction	87
2.8	Computational methodology	90
2.9	Results and discussion	91
2.9.1	MESP analysis of donor molecules	91
2.9.2	MESP analysis of D- $\pi$ -A systems	94
2.9.3	Absorption spectra of donor and D- $\pi$ -A systems	96
2.9.4	Analysis of photovoltaic parameters	102
2.10	Conclusions	103

2.11	References	104
------	------------	-----

## **Chapter 3**

### **Tuning the Donating Strength of Dye-sensitizers Using Molecular Electrostatic Potential Analysis**

3.1	Abstract	114
3.2	Introduction	114
3.3	Computational methodology	117
3.4	Results and discussion	121
3.4.1	MESP analysis	121
3.4.2	Absorption spectra	127
3.4.3	Photovoltaic performance	132
3.4.4	Conclusions	137
3.4.5	References	138

## **Chapter 4**

### **Design and DFT Study of Nitrogen-Rich Donor Systems for Improved Photovoltaic Performance in Dye-sensitized Solar Cells**

4.1	Abstract	144
4.2	Introduction	145
4.3	Computational methodology	149
4.4	Results and discussion	150
4.4.1.	MESP analysis of donors	150
4.4.2	Donating strength of D- $\pi$ -A systems	150
4.4.3	Absorption spectra	154
4.4.4	Photovoltaic performance	162
4.5	Conclusions	163
4.6	References	164
	Abstract	170
	List of publications	171

## List of Figures

			Page
1	Figure 1.1	Major components and working principle of dye-sensitized solar cell.	4
2	Figure 1.2	Molecular structures of Ru-based dye-sensitizers, where TBA = tetra butyl ammonium.	10
3	Figure 1.3	Molecular structure of metalloporphyrin (M: Zn <sup>2+</sup> , Cu <sup>2+</sup> , etc.), b) Representative example of Zn-porphyrin photosensitizer.	12
4	Figure 1.4	Representative example of phthalocyanine photosensitizer.	12
5	Figure 1.5	Schematic representation of D- $\pi$ -A based organic sensitizer.	13
6	Figure 1.6	Representative examples of TPA and coumarin-based D- $\pi$ -A type dye-sensitizers (From left to right).	14
7	Figure 1.7	Examples of D-D- $\pi$ -A type dye-sensitizers.	15
8	Figure 1.8	Representative example of D-A- $\pi$ -A-type dye-sensitizer.	15
9	Figure 1.9	Typically used auxiliary acceptors in DSSCs: a) benzothiadiazole (BTD), b) benzotriazole, c) quinoxaline, d) phthalimide, e) TPD, f) diketo-pyrrolopyrrole (DPP), g) thienopyrazine, h) thiazole, i) cyano-substituted phenyl, j) fluoro-substituted phenyl, and k) cyano vinyl.	16
10	Figure 1.10	Representative examples of a) D- $\pi$ -A- $\pi$ -A b) D- $\pi$ -(A) <sub>2</sub> c) D-A-A and d) double D- $\pi$ -A bridge types metal-free dye sensitizers.	16
11	Figure 1.11	The generally used spacers for DSSC applications.	18
12	Figure 1.12	Widely used anchoring groups in DSSCs viz. carboxylic acid, cyanoacrylic acid, and rhodanine 3-acetic acid (left to right).	20

13	Figure 1.13	The possible adsorption configurations for carboxylic acid onto the metal oxide semiconductor (M = Si, Sn, Ti, etc.).	21
14	Figure 1.14	Representation of “Jacob’s ladder” of exchange-correlation functionals proposed by J. P. Perdew.	40
15	Figure 1.15	Molecular electrostatic potential surface of benzene, benzene, fluorobenzene, chlorobenzene, and bromobenzene (left to right).	50
16	Figure 1.16	Representations of solvent models.	52
17	Figure 2.1	Various spacers considered to quantify the transmission power of spacers. The double bond marked in red is the region where MESP minimum is located for X = NH <sub>2</sub> , OH, CH <sub>3</sub> , H, F, Cl, CF <sub>3</sub> , CHO, CN and NO <sub>2</sub>	75
18	Figure 2.2	MESP isosurface at -13.0 kcal/mol for <b>1a</b> , <b>2a</b> , <b>3a</b> , <b>4a</b> , <b>5a</b> and <b>6a</b> . $V_{\min}$ values in kcal/mol are also depicted	76
19	Figure 2.3	Correlation between the $V_{\min}$ of <b>1a-1c</b> with the inductive parameter ( $\sigma_I$ ).	76
20	Figure 2.4	Correlation of $V_{\min}$ with Hammett parameter ( $\sigma_p$ ) of a) alkenyl b) alkynyl c) phenyl d) thiophenyl and e) polyacene systems.	81
21	Figure 2.5	Spacers considered to quantifying the effect of the combination of two different spacers.	83
22	Figure 2.6	ChemDraw representation of donors (D1 - D13) and D- $\pi$ -A systems. The bond shown in red colour is replaced with $\pi$ -A part to design the D- $\pi$ -A system.	89
23	Figure 2.7	Chemdraw representations of known systems ( <b>1</b> – <b>6</b> ).	91
24	Figure 2.8	MESP minima at the donor site, $V_{mD}$ of the donor systems. Isosurface values in kcal/mol are given in brackets. Here carbon atoms are in green colour, while nitrogen, sulfur, and oxygen atoms are shown in pink, yellow, and red in colours.	92



25	Figure 2.9	MESP isosurface plot of a) representative D- $\pi$ -A system, b) reference system.	94
26	Figure 2.10	Correlation between donating strength ( $\Delta V_{mA}$ ) of D- $\pi$ -A system and change in absorption maxima ( $\Delta\lambda_{max}$ ).	98
27	Figure 2.11	Frontier molecular energy level diagram of D- $\pi$ -A systems at B3LYP/cc-pVDZ level.	99
28	Figure 2.12	Frontier molecular orbitals of representative D- $\pi$ -A systems at B3LYP/cc-pVDZ level.	100
29	Figure 2.13	ChemDraw representation of D1- $\pi$ -A system.	101
30	Figure 2.14	Correlation between $\Delta V_{mA}$ (kcal/mol) and $eV_{OC}$ (eV)	103
31	Figure 3.1	Chemdraw diagram of D- $\pi$ -A system (top) and the donors D1 – D6. The R substituents are CH <sub>3</sub> , C <sub>5</sub> H <sub>11</sub> , isopropyl, t-butyl, OH, OCH <sub>3</sub> , O-C <sub>2</sub> H <sub>5</sub> , NH <sub>2</sub> , N(CH <sub>3</sub> ) <sub>2</sub> , Ph-CH <sub>3</sub> , and Ph-NH <sub>2</sub> . The bond shown in red colour indicates the connecting position of D with $\pi$ -A. rrelation between $\Delta V_{mA}$ (kcal/mol) and $eV_{OC}$ (eV).	116
32	Figure 3.2	Labeled bonds employed to calculate the BLA index	118
33	Figure 3.3	MESP isosurfaces at various sites of a) reference system, b) D1 and D1- $\pi$ -A system, and c) D4 and D4- $\pi$ -A system. $V_m$ values are in kcal/mol.	121
34	Figure 3.4	Correlation between MESP parameters $\Delta V_{mS}$ , $\Delta V_{m(OH)}$ , $\Delta V_{m(CO)}$ , and $\Delta V_{mA}$ .	125
35	Figure 3.5	Correlation between $\Delta V_{mD}$ and $\Delta V_{mA}$ .	126
36	Figure 3.6	Correlation between absorption maximum ( $\lambda_{max}$ ) and donating strength ( $\Delta V_{mA}$ ) of various D- $\pi$ -A systems with different substituents.	131
37	Figure 3.7	Frontier molecular energy levels of phenothiazine based $\pi$ -A with various substituents at B3LYP/cc-pVDZ level.	132
38	Figure 3.8	Frontier molecular orbitals of representative N(CH <sub>3</sub> ) <sub>2</sub> substituted D- $\pi$ -A systems at B3LYP/cc-pVDZ level.	132

39	Figure 3.9	Correlation between donating strength $\Delta V_{mA}$ and open-circuit voltage $eV_{OC}$ of D- $\pi$ -A systems.	133
40	Figure 4.1	Designed donor systems. MESP minimum over the phenyl ring ( $V_{mD}$ ) is given in kcal/mol.	147
41	Figure 4.2	ChemDraw structure of a) Julolidine b) 1,2,4,5-tetrahydropyrrolo[3,2,1-hi] indole	148
42	Figure 4.3	MESP isosurface at various sites of the reference system, and b) representative D- $\pi$ -A system (D1- $\pi$ -A). Where MESP minimum is shown in kcal/mol.	152
43	Figure 4.4	Correlation between $\Delta V_{mA}$ and $\Delta\lambda_{max}$ of D- $\pi$ -A systems. (R value has been calculated by excluding the deviations shown in green colour.	156
44	Figure 4.5	Optimized geometry of representative D- $\pi$ -A system on $(TiO_2)_9$ cluster (D12- $\pi$ -A/ $TiO_2$ ). The electron density shift during excitation can be visualized from b) HOMO and (c) LUMO features	158
45	Figure 4.6	a) Correlation between $\Delta V_{mA}$ and $E_{ads}$ b) $E_{ads}$ and $eV_{oc}$ .	160
46	Figure 4.7	Correlation between donating strength ( $\Delta V_{mA}$ ) of D- $\pi$ -A system and open-circuit voltage ( $eV_{oc}$ ).	163

## List of Tables

		Page
1	Table 2.1	$V_{min}$ (in kcal/mol) obtained over the terminal double bond of various spacer systems. 77
2	Table 2.2	Hammett parameters for the substituents employed in the study. 78
3	Table 2.3	$\Delta V_{min}$ in kcal/mol of various spacer systems. 79

4	Table 2.4	Slope, intercept, reaction constant ( $\rho_s$ ), correlation coefficient (R) and transmission coefficient ( $\gamma$ ) of various spacers.	82
5	Table 2.5	$V_{\min}$ values (kcal/mol) obtained for hetero spacers.	84
6	Table 2.6	Benchmark time-dependent DFT calculations using DFT/SMD/cc-pVDZ method to obtain the absorption spectra. The absorption maxima $\lambda_{\max}$ (nm) and oscillator strength (f) are given along with experimentally known $\lambda_{\max}$ . All the geometries are optimized at B3LYP/cc-pVDZ level.	91
7	Table 2.7	$V_m$ (kcal/mol) of the D- $\pi$ -A systems calculated with B3LYP/cc-pVDZ level.	95
8	Table 2.8	Maximum absorption wavelength (nm), oscillator strength f, absorptional shift $\Delta\lambda_{\max}$ and percentage MO contribution of donor and D- $\pi$ -A systems at TD-CAM-B3LYP/SMD/cc-pVDZ//B3LYP/cc-pVDZ level.	97
9	Table 2.9	Absorption maxima of methyl substituted pyrene based D1- $\pi$ -A systems at TD-CAM-B3LYP/SMD/cc-pVDZ//B3LYP/cc-pVDZ level. Here D1 represents unsubstituted pyrene-based D- $\pi$ -A system, while D1-1, D1-2, D1-3, <i>etc.</i> represents the methyl substitution at 1, 2, 3, 4 and 5 positions of D1- $\pi$ -A	100
10	Table 2.10	Calculated vertical excitation energy, absorption maxima, oscillator strength f, HOMO LUMO energy, HOMO-LUMO energy gap (HLG), ground and excited-state oxidation potentials ( $E^{dye}$ , $E^{dye*}$ ), electron injection free energy change ( $\Delta G_{inject}$ ), dye regeneration driving force ( $\Delta G_{reg}$ ), and open circuit voltage ( $eV_{oc}$ ) of D- $\pi$ -A systems at TD-CAM-B3LYP/SMD/cc-pVDZ//B3LYP/cc-pVDZ level.	102

11	Table 3.1	a) BLA index for the unsubstituted D1 – D3- $\pi$ -A systems in ground state with B3LYP and CAM-B3LYP functional.	118
		b) BLA index for the unsubstituted D4 – D6- $\pi$ -A systems in ground state with B3LYP and CAM-B3LYP functional.	119
12	Table 3.2	BLA index for the TPA (D3) based $\pi$ -A systems in $S_0$ and $S_1$ states at CAM-B3LYP/cc-pVDZ level.	120
13	Table 3.3	$V_m$ (kcal/mol) at various sites of D- $\pi$ -A systems calculated at B3LYP/cc-pVDZ level.	122
14	Table 3.4	HOMO, LUMO and HOMO-LUMO energy gap (HLG) (in eV) observed for the ground state at B3LYP/cc-pVDZ level and absorption maximum $\lambda_{max}$ (nm), and oscillator strength (f) at CAM-B3LYP/SMD/cc-pVDZ// B3LYP/cc-pVDZ level.	128
15	Table 3.5	HOMO, LUMO and HOMO-LUMO energy gap (HLG) (in eV) observed for the ground state at B3LYP/cc-pVDZ level. Excitation energy, ground and excited state oxidation potential ( $E^{dye}$ , $E^{dye^*}$ ), electron injection free energy change $\Delta G_{inject}$ , free energy change for dye regeneration $\Delta G_{reg}$ , and open-circuit voltage $eV_{OC}$ at TD-CAM-B3LYP/SMD/cc-pVDZ//B3LYP/cc-pVDZ level.	134
16	Table 4.1	$V_m$ (kcal/mol) of the D- $\pi$ -A systems calculated at B3LYP/cc-pVDZ level.	153
17	Table 4.2	Maximum absorption wavelength $\lambda_{max}$ (nm), oscillator strength f, MO contribution, percentage of MO contribution (MO %), and shift in absorption maximum $\Delta\lambda_{max}$ (nm) of donor and D- $\pi$ -A systems at	155



		TD-CAM-B3LYP/cc-pVDZ/SMD//B3LYP/cc-pVDZ level.	
18	Table 4.3	HOMO (eV), LUMO (eV), and HOMO-LUMO energy gap, HLG (eV) for the D- $\pi$ -A/TiO <sub>2</sub> systems at B3LYP/GenECP level. Maximum absorption wavelength $\lambda_{\max}$ (nm), and oscillator strength (f) adsorbed on TiO <sub>2</sub> are simulated at TD CAM-B3LYP/GenECP/SMD//B3LYP/GenECP level.	157
19	Table 4.4	The adsorption energies ( $E_{\text{ads}}$ ) of all the D- $\pi$ -A/(TiO <sub>2</sub> ) <sub>9</sub> systems where $E_{\text{ads}}$ values are given in kcal/mol.	159
20	Table 4.5	HOMO (eV), LUMO (eV), and HOMO-LUMO energy gap (eV) at B3LYP/cc-pVDZ level. Ground and excited state oxidation potential ( $E^{\text{dye}}$ , $E^{\text{dye*}}$ ), excitation energy, electron injection free energy change $\Delta G_{\text{inject}}$ , free energy change for dye regeneration $\Delta G_{\text{reg}}$ , and open-circuit voltage $eV_{\text{OC}}$ at TD-CAM-B3LYP/SMD/cc-pVDZ//B3LYP/cc-pVDZ level.	161

## List of Abbreviation

BO	: Born-Oppenheimer
CB	: Conduction band
CC	: Coupled-cluster
CE	: Counter electrode
CGTO	: Contracted gaussian function
CI	: Configuration interaction
CSFs	: Configurational state functions
DFT	: Density functional theory
DSSCs	: Dye-sensitized solar cells
ECP	: Effective core potentials
<i>FF</i>	: Fill factor
GGA	: Generalized gradient approximation
GTO	: Gaussian type orbitals
HF	: Hartree-Fock
HOMO	: Highest occupied molecular orbital
ICT	: Intramolecular charge transfer
LDA	: Local density approximation
LHE	: Light-harvesting efficiency
LUMO	: Lowest unoccupied molecular orbital
MCSCF	: Multi-configurational self-consistent field
MD	: Molecular dynamics
MESP	: Molecular electrostatic potential
MM	: Molecular mechanics
MP	: Møller–Plesset perturbation
MRCI	: Multiconfiguration-reference configuration interaction
PAH	: Polycyclic aromatic hydrocarbon
PCE	: Power conversion efficiency
PCM	: Polarizable continuum model
QM	: Quantum mechanics
SCF	: Self-consistent field
SCRf	: Self-consistent reaction field

SMD      Solvation model density  
STO      Slater type orbitals  
TD DFT   Time-dependent DFT

## PREFACE

Dye-sensitized solar cells (DSSCs) are considered as a safe and sustainable energy source for the world's future energy demand. The less expensive and eco-friendly property of DSSCs over conventional silicon-based solar cells make them promising in the area of photovoltaics. DSSCs are categorized mainly into four: metal-based dye-sensitizers, porphyrins, phthalocyanines, and metal-free dye-sensitizers. Even if metal-free sensitizers have been shown lower power conversion efficiency (PCE) than metal-based ones, the former attained a noteworthy role in DSSCs due to their abundant, cost-effective synthetic procedures. The theoretical studies now play a dominant role in dye design, understanding the mechanism involved in DSSC devices, and thereafter predicting their efficiency. Hence, the thesis entitled "***Density Functional Theory Studies on D- $\pi$ -A Systems Used in Dye-Sensitized Solar Cells: Donor-Acceptor Effect, Spacer Effect, and Molecular Design Strategies***" focused on the quantification of donor strength and electronic effect transmitting power of spacers in dye-sensitizers, which are crucial for the prediction PCE in DSSCs. For the well-organized modelling of a new class of dye molecules, thereafter for the prediction of PCE, a theoretical model is essential. In the thesis work, MESP based topographical analysis has been employed for quantifying the electron donor strength and electronic effect transmission power of spacer moieties in DSSCs. The findings will afford a new pathway for effective dye design in DSSCs. The thesis is organized into four chapters.

The first part of Chapter 1 gives an overview on dye-sensitized solar cells. Working principle, theoretical background, major components, modifications, theoretical advancements, etc. in DSSCs are briefly explained. Computational chemistry is an exciting and fast-emerging field which becomes vital for the progresses made in photovoltaic area. A brief account of computational methodologies employed in the thesis is presented in part B of Chapter 1.

Chapter 2 gives an outline of the quantification of substituent effect transmission power of various spacers and donor strength in dye-sensitizers. It is divided into two parts. Part A discusses the electronic effect transmission power of ( $\gamma$ ) of alkyl, alkenyl, alkynyl, phenyl, thiophenyl, and polyacene spacer units in Y-G-X

molecular model, where Y, G, X represent reaction centre, spacer moiety, and substituent, respectively. Among the studied spacers, alkenyl spacers with shorter chain length ( $n=2$ ) exhibit the highest transmission power while alkyl spacers show the lowest transmission power. The analysis advises shorter spacer chain length for better electronic transmission to a reaction centre. In part B, the electron-donating strength of thirteen typically used donors in D- $\pi$ -A type dye-sensitizers has been quantified as a change in MESP minimum ( $\Delta V_{mA}$ ) at acceptor region (A) using B3LYP/cc-pVDZ level density functional theory (DFT). It is found that  $\Delta V_{mA}$  shows an excellent linear correlation with absorption redshift ( $\Delta\lambda_{max}$ ), which has been observed by the alteration of D to D- $\pi$ -A. The above correlation pinpoints the importance of donor strength towards the fine-tuning of  $\lambda_{max}$  in a preferred region. The close resemblance of frontier molecular orbital energies of D- $\pi$ -A systems with the corresponding energies of donors and  $\pi$ -A system show that donor tunes HOMO, while  $\pi$ -A tunes LUMO. Further, donating strength is found to be proportional to the open-circuit voltage ( $eV_{oc}$ ), which is a fundamental parameter in power conversion efficiency calculation. Among the thirteen D- $\pi$ -A systems, N, N-dialkylaniline, and julolidine are evaluated as the best donors for photovoltaic applications. Overall, this MESP based computation offers a powerful rational design strategy for the development of efficient dyes for DSSC applications.

In Chapter 3, using MESP analysis the influence of substituents for tuning the donating strength of six commonly used donors in D- $\pi$ -A type dye-sensitizers are analysed. The substituent effect enhances electron donation from D to A through the  $\pi$ -spacer, thereby increases the donating strength of donor in D- $\pi$ -A. It is found that electron releasing substituents at donors tune the HOMO and LUMO energies of all the corresponding D- $\pi$ -A systems for better optical properties than the unsubstituted systems. Photovoltaic performance of D- $\pi$ -A system is also enhanced with enhanced donating strength conveys the role of tuning the donor strength for better PCE in DSSCs.

Chapter 4 focused on the impact of nitrogen-rich donor moieties in D- $\pi$ -A type dye-sensitizers for the enhanced donor strength. The N-annulation at donor moiety improves donor strength, maximum absorption wavelength, and photovoltaic

properties of dye-sensitizer. Adsorption stability of D- $\pi$ -A systems on TiO<sub>2</sub> is evaluated and indicates that adsorption stability ( $E_{ads}$ ) increased with enhanced electron-donating strength of D- $\pi$ -A system which has a fundamental role in the enhancement of open-circuit voltage. Consequently, we could conclude that the N-annulated designing strategy will pave the way for attaining high efficiency in dye-sensitized solar cells.

It may be mentioned that each chapter of the thesis is presented as an independent unit and therefore the structural formulae, schemes, and figures are numbered chapter-wise.

---

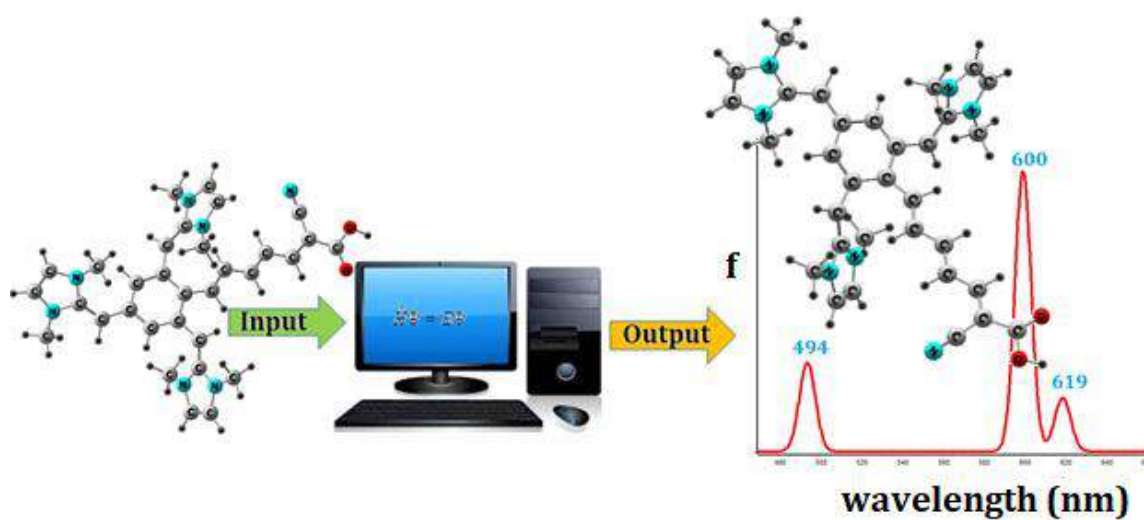
# Introduction

## Part A- Dye-sensitized Solar Cells

### &

## Part B- Computational Chemistry Methods

---







# Part A: Dye-sensitized Solar Cells

---

## 1.1 Introduction

In the 21<sup>st</sup> century, renewable energy, preferably solar energy is becoming the most powerful alternative as well as a sustainable energy source for the fast-growing fossil fuel depletion. The increasing population and severe global climate change make energy depletion more dangerous and impart rapid progress in the development of photovoltaic technologies. Solar energy is considered as the most abundant green energy resource for the upcoming energy demand.<sup>1-3</sup> For the conversion of light energy to electrical energy, the solar cell is the safest promising device. In a photovoltaic cell or a solar cell, the basic operating principle is the photovoltaic effect, which converts light energy into electrical energy.<sup>4-6</sup> It is noted that solar energy that strikes on earth in one hour is sufficient for the world's one year's full energy demand.<sup>7-9</sup> The real challenge of today is gathering and storing solar energy cost-effectively. Consequently, the conversion of solar energy to electrical energy turns into the most important scientific and technological challenge in the world, introducing well-advanced photovoltaic technology, the problems associated with energy scarcity and the environment can be avoided.<sup>6</sup> Also, the invention of the photovoltaic effect by Edmond Becquerel in 1839 promoted research progress in this area, and later he is considered as the father of solar panel.<sup>2, 10, 11</sup>

The scientific and industrial challenges for sustainable energy are linked with its efficiency, cost of production, and stability. To address these concerns, three generations of solar cells are explored *viz.* first, second and third generations, and those classifications depend on the material employed in the solar cell.<sup>11, 12</sup> Crystalline silicon-based solar cell is the first-generation solar cell. It is the most efficient solar cell technology currently available in the world.<sup>13, 14</sup> Till date, a record power conversion efficiency (PCE) of 26.7 % has been attained with a crystalline silicon-based solar cell.<sup>15</sup> While, the high cost of production and environmental issues limited its practical application, which prompted the search for an alternate inexpensive solar cell. Second-generation solar cells namely thin-film solar cells are made by a thin layer of photovoltaic materials (only a few micrometers thickness) such as gallium arsenide (GaAs), cadmium telluride (CdTe), etc. Those provide low production cost and

reduced power conversion efficiency (PCE) to the conventional silicon-based solar cell.<sup>14</sup> Third-generation solar cell technology is modest and comparatively non-toxic than the first-and second-generation solar cells. It also claims minor environmental issues.<sup>16</sup> Dye-sensitized solar cells (DSSCs), perovskite cells, and organic photovoltaic (OPV) solar cells belong to third-generation photovoltaic technology. Even if DSSC attains lower PCE than a first-generation solar cell, the chances for better improvements are still existing in DSSCs than in a conventional silicon-based solar cell.<sup>1</sup>

### **1.1.1 Overview of dye-sensitized solar cell (DSSC)**

DSSCs have specific advantages over traditional silicon-based solar cells due to their reasonable cost of production, easier structure modification, and simple synthetic procedures. It is well known as Grätzel cell, which is originally co-invented by Michael Grätzel and Brian O'Regan in 1988. Whereas, DSSCs achieved prominence in the scientific field just after they invented the first effective DSSC in 1991 using a Ru-based sensitizer (PCE of over 7%).<sup>17</sup> In fact, Ru-based dye-sensitizers afford more PCE than Ru-free photosensitizers, the highly expensive and rare earth nature of Ruthenium metal, its practical application should be restricted for future endeavours. The failure of the expected efficiency is the major challenge faced by the researchers in DSSCs compared to the conventional silicon-based solar cell. To overcome the challenge, a reframing in major components which are involved in DSSC is essential. The four major components involved in a DSSC include photosensitizer, photoanode, counter-electrode, and an electrolyte.<sup>18</sup> The modifications in those major components lead to improvement in power conversion efficiency.<sup>7,19</sup> The highlight feature of DSSC is that it could wonderfully imitate natural photosynthesis, allowing it to function even in mild light conditions.<sup>20</sup> The systematic modifications in the major framework resulted in an approximate power conversion efficiency of 14 %; nevertheless, additional improvements in PCE are still in high demand, and persistent efforts in this area are continuing.<sup>21</sup>

### **1.1.2 Working principle and major components of DSSC**

The basic working principle of a dye-sensitized solar cell is shown in (Figure 1.1). In the figure, the transparent conducting glass sheet treated as an anode (FTO, fluorine-

doped tin oxide) has been coated with a mesoporous oxide layer, preferably TiO<sub>2</sub> (anatase) to activate electronic conduction. The mesoporous oxide layer (photoanode) provides a high surface area to active dye adsorption, thereby increases the light-harvesting efficiency (LHE) of the solar cell.<sup>22</sup> Because of the higher electronic band gap of TiO<sub>2</sub> (3.2 eV), it fails to absorb most of the solar spectrum than silicon (1.1 eV). Whereas due to the less expensive, stable, and abundant features of TiO<sub>2</sub>, it got an extensive range of acceptance in DSSC. For absorbing the incident light, a monolayer of dye is covalently bonded to the mesoporous metal oxide layer. Further, the glass rod coated with a catalyst, typically Pt has been treated as a counter electrode that facilitates efficient regeneration of the redox couple in the electrolyte. Finally, an electrolyte containing redox mediator is sandwiched between the glass rods to enable effective dye regeneration of the oxidized dye.<sup>1, 7, 17</sup>

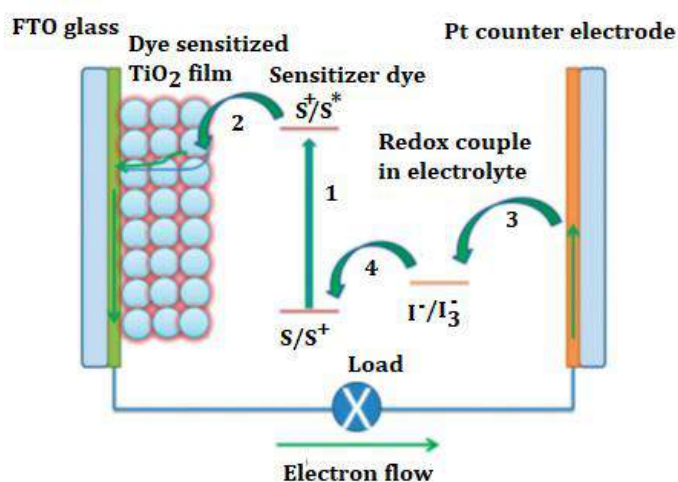


**Figure 1.1** Major components and working principle of the dye-sensitized solar cell.<sup>23</sup>

In DSSC, when the light gets incident on the adsorbed dye molecule, it gets excited from HOMO (highest occupied molecular orbital) to LUMO (lowest unoccupied molecular orbital) of the dye-sensitizer. The excited electron is then injected into the conduction band (CB) of the semiconductor, leaving the dye in its oxidised state. Then, the electrons are moved to an anode and are reached at the counter electrode through an external circuit before it gets collected by the electrolyte. The oxidised dye is regenerated by the electron transfer from the redox electrolyte. Finally, the entire circuit is completed by the reduction at the electrolyte. The entire processes demonstrate the generation of electric power without any chemical transformation. The two main failures occurring in DSSC include

recombination of the injected electron with a) oxidised dye and b) with an electrolyte. Thus, the long life of the injected electron is very essential for the better performance of DSSC. Also, the optimization in all four components should be considered not only as a single component alone for improving the performance of DSSC.<sup>23</sup>

### **1.1.2.1 Photoanode**

Photoanode plays a substantial role in PCE. It effects the critical parameters those are involved in the determination of PCE such as open-circuit voltage ( $eV_{oc}$ ), short-circuit current density ( $J_{sc}$ ), absorption maximum, and fill factor (FF).<sup>24</sup> In DSSC, the photoanode which has been deposited on the transparent glass plate has two major roles *viz.* charge carrier and light harvester, considered as the back bone of DSSC.<sup>25</sup> For the photovoltaic application, the key component of photoanode termed as semiconductors having an electronic band width of 1-2 eV are appropriate.<sup>26</sup> But the small band width metal oxide semiconductors suffer corrosion from the electrolyte, thereby high band width semiconductors such as  $TiO_2$  (3.0 to 3.4 eV) and ZnO (3.1 to 3.3 eV) are chosen extensively.<sup>26</sup> ZnO was the initially used photoanode which is developed in 1972 by Tributsch.<sup>27</sup> The poor PCE, reduced surface area for dye adsorption, lower photostability, and reduced light-harvesting efficiency than  $TiO_2$  are the main challenges handled by ZnO.<sup>28</sup> Practically,  $TiO_2$  is the widely used semiconductor in DSSC due to its stable, abundant, cost-effective, and non-toxic characteristics over ZnO.<sup>24, 29, 30</sup> The three polymorphs of  $TiO_2$  available for DSSC application are anatase (3.2 eV), rutile (3.0 eV), and brookite (3.4 eV),<sup>31</sup> respectively. Among those,  $TiO_2$  anatase is the extensively used polymorph due to its high mobility, high reactivity, and fast electron injection rate to the CB of semiconductor. The various other semiconductors used in DSSCs are  $SnO_2$ ,<sup>32</sup>  $Nb_2O_5$ ,<sup>33-36</sup>  $WO_3$ ,<sup>37</sup>  $In_2O_3$ ,<sup>38</sup>  $SrTiO_3$ ,<sup>36, 39</sup>  $Zn_2SnO_4$ ,<sup>40</sup>  $BaSnO_3$ ,<sup>41</sup>  $CoTiO_3$ ,<sup>42</sup> etc. For improving the efficiency of photoanodes, doping with other metal atoms, and surface treatment with other metals are also explored in the literature.<sup>25</sup>

### **1.1.2.2 Electrolyte**

Apart from metal oxide semiconductors, the electrolytes used in DSSC devices have a strong influence on key parameters such as  $J_{sc}$ ,  $V_{oc}$ , FF, resulting in PCE.<sup>11, 43, 44</sup> During the device operation, the electrolyte manages charge transport between the counter

electrode and semiconductor and acts as a source for the regeneration of oxidized dye.<sup>45</sup> Classically in DSSCs, liquid-electrolytes based on organic solvents are used.<sup>7</sup> In the first efficient DSSC reported by Grätzel and O'Regan, a liquid electrolyte based on carbonate solvent with  $I^-/I_3^-$  redox couple has been utilized.<sup>17</sup> For an efficient DSSC, the electrolyte should be stable, less volatile, and must be a good solvent for the redox-couple components. However, the major problem detected with widely used liquid  $I^-/I_3^-$  electrolyte has been related to its high volatility, which leads to low ion mobility and long-term stability issues in DSSCs.<sup>44, 46</sup> Since iodine is corrosive to metals, it reduces the stability of DSSCs. Also, the higher concentration of iodine induces dye aggregation at the dye/semiconductor interface which may result in smaller  $eV_{oc}$ .<sup>1, 19</sup> To avoid dye aggregation, several additives such as 4-tert-butylpyridine (4TBP),<sup>47</sup> and guanidium thiocyanate<sup>48</sup> have been introduced along with liquid electrolytes for improving the efficiency. Hence, for the best functioning of charge transport kinetics in DSSCs, the liquid electrolyte should consist a solvent, redox couple, and an additive.<sup>11</sup> The other explored redox mediators for DSSC application include  $Br^- / Br_3^-$ ,<sup>49</sup>  $SCN^- / SCN_3^-$ ,<sup>50</sup>  $SeCN^- / SeCN_3^-$ ,<sup>51</sup>  $FeCN_6^{3-/4-}$  Co(II)/Co(III) complex,<sup>52</sup> etc., and found that the advantage of those alterations leads to a record PCE of 12.3 % with  $[Co(bpy)_3]^{2+/3+}$  couple.<sup>53, 54</sup>

Further, to overcome the main difficulties in liquid electrolytes with organic solvents, vivid varieties of electrolytes are explored such as non-volatile ionic electrolytes, solid electrolytes, quasi-solid electrolytes, etc.<sup>11, 54</sup> In ionic electrolyte, in place of volatile solvent, an aromatic or non-aromatic organic cations, and anions as solvent has been used. It is found that the incorporation of non-volatile ionic liquid improves stability issues and showed reasonable efficiency.<sup>55</sup> For better performance, the charge transport issues involved in ionic electrolytes should be rectified by further modifications. In solid-state electrolyte, the liquid electrolyte has been replaced with inorganic p-type semiconductors or organic hole transporting materials and found that it could achieve better stability than the ionic electrolyte. While, due to the poor interface contact (at semiconductor/electrolyte) and lower conductivity, this class of electrolyte shows lower PCE. In quasi-solid electrolytes, the problems associated with liquid and solid electrolytes have been rectified by combining those two electrolytes to form a gel electrolyte.<sup>56, 57</sup> It shows better

stability, durability, and volatility compared to other known electrolytes. However, its low ionic mobility through the viscous medium results in lower PCE than the dye sensitizers with liquid electrolytes. The above findings explain the importance of stability, interface contact property, viscosity, and durability of electrolytes for the better performance of DSSC.<sup>11</sup>

### **1.1.2.3 Counter electrode**

In DSSCs, the counter electrode (CE) acts as a conducting material ensures effective electron transport between the external circuit and the cathode. By reducing the electrolyte, it acts as a catalyst for the regeneration of oxidised dye. For the effective regeneration of the oxidized redox couple, CE collects electrons from the external circuit (anode) and returns those electrons backs to the electrolyte. So, it is found that CE has an important role in the photovoltaic parameters of DSSC.<sup>2, 58, 59</sup> For the effective working of DSSC device, CE should have good conductivity, stability, high catalytic property, and large surface area. Because of the excellent electro-catalytic property, platinum is the widely accepted counter electrode in DSSC applications.<sup>58</sup> While due to the high cost, scarcity, and weak stability of Pt with redox couple, DSSCs demand alternate counter electrodes, which results in the development of other low-cost-abundant materials such as graphene, carbon, and graphite. The synthesis and modification in those platinum-free counter electrodes give a new outlook for the future dye design with an affordable making cost.<sup>60 61 44, 62-64</sup>

### **1.1.2.4 Dye-sensitizers**

The key difference in DSSC that of the conventional silicon-based solar cell appears in electron transport and incident light absorption processes, those are not performed by the same material in DSSC. In DSSCs, light absorption has been taken place in dye molecules, while electron-hole transport has been carried out by metal oxide semiconductors and electrolytes.<sup>65</sup> In this regard, the light-harvesting efficiency of a solar cell depends on a dye sensitizer, which has been considered as an integral part of the DSSC. Since dye sensitizer is as important as photoanode, extensive research efforts have been performed for the structural design of dye molecule alone and show that dye-sensitizer has a noteworthy role towards LHE, electron-injection, charge-recombination, and dark current (dye aggregation on semiconductor), etc.<sup>7, 18, 66, 67</sup>

The specific requirements for an efficient dye-sensitizer include: a) wide absorption spectrum in the visible and near IR region for efficient LHE, b) the anchoring groups in the dye molecule such as -COOH, -SO<sub>3</sub>H, -H<sub>2</sub>PO<sub>3</sub>, etc. should have a capability of permanent chemisorption to OH group of TiO<sub>2</sub> semiconductor surface, which implies good chemical adsorption stability, c) for effective electron-injection to the semiconductor, LUMO should be higher than the CB of the metal oxide semiconductor, d) HOMO of the dye should be lower than the redox potential of the electrolyte used for ensuring the efficient dye regeneration of the oxidized dye, finally, e) for limiting the non-radioactive decay of the excited dye to the ground state, the dye aggregation on the surface should be avoided, which often increases with the reduced oxide film thickness.<sup>67-69</sup>

### 1.1.3 Theoretical background for computing photovoltaic properties of dye-sensitizers

The overall efficiency ( $\eta$ ) of a dye-sensitized solar cell as compared to incident solar power on the cell ( $P_{inc}$ ) can be calculated as<sup>70</sup>:

$$\eta = FF \frac{V_{OC} J_{SC}}{P_{inc}} \quad \text{Eq. (1.1)}$$

where  $V_{OC}$ ,  $J_{SC}$ , FF characterize open-circuit voltage, short-circuit current density, and fill factor, respectively. In the above equation, the short-circuit current density  $J_{SC}$ , which is related to quantum yield for electron injection efficiency ( $\phi_{inject}$ ) and absorption coefficient can be assessed as:

$$J_{SC} = \int LHE(\lambda) \phi_{inject} \eta_{collect} d\lambda \quad \text{Eq. (1.2)}$$

where LHE is the light-harvesting efficiency at a given wavelength, which can be calculated as:

$LHE = 1 - 10^{-f}$ , where  $f$  denotes the oscillator strength of the dye molecule.<sup>71</sup> If higher the oscillator strength, higher will be the LHE, which leads to better  $J_{SC}$ . Electron collection efficiency,  $\eta_{collect}$  is a property associated with structure of semiconductor.<sup>72</sup> For simplification  $\eta_{collect}$  value can be considered to be constant (when we are using the same photoanode and different sensitizers). Further, In DSSCs

the photo-induced electron injection from dye to the semiconductor can be considered as charge transfer (CT) process, which is related with  $\Delta G_{inject}$ .<sup>73, 74</sup> In other words,  $\Delta G_{inject}$  measures electron injection rate, more negative  $\Delta G_{inject}$  gives greater electron injection efficiency. As a result,  $J_{SC}$  could be improved by enhancing LHE and  $\phi_{inject}$ . The electron injection-free energy change can be computed as<sup>72</sup>:

$$\Delta G_{inject} = E^{dye} - |E_{CB}| \quad (\text{Eq. 1.3})$$

In (Eq. 1.3),  $E^{dye*}$  denotes excited state oxidation potential and  $E_{CB}$  represents the energy of the conduction band edge of the  $\text{TiO}_2$  semiconductor (-4.0 eV). The excited state oxidation potential is connected with ground state oxidation because electron injection always begins from an unrelaxed excited state  $E^{dye*}$ . Thus,

$$E^{dye*} = E^{dye} - \lambda_{\max} \quad (\text{Eq. 1.4})$$

In the above equation,  $E^{dye}$  and  $\lambda_{\max}$  represent ground state oxidation potential, and the vertical transition energy (eV), respectively.<sup>75, 76</sup> The ground state oxidation potential could be computed as negative HOMO energy, according to Koopmans theorem.<sup>77</sup>

Also, it is important that the oxidized dye should be regenerated from the electrolyte. The free energy change for dye regeneration computed from ground state oxidation potential can be written as:<sup>78</sup>

$$\Delta G_{reg} = E^{dye} - 4.8 \text{ eV} \quad (\text{Eq. 1.5})$$

Finally, to compute the overall performance of DSSC, the open-circuit voltage ( $eV_{OC}$ ) must be calculated. Open-circuit voltage can be defined as the difference between the Fermi level of the electron in  $\text{TiO}_2$  and the redox potential of the electrolyte  $\text{I}^-/\text{I}_3^-$ . It is also related to LUMO energy which can be theoretically estimated as:

$$eV_{OC} = E_{LUMO} - E_{CB} \quad (\text{Eq. 1.6})$$

Based on the aforesaid critical parameters, we could predict the efficiency of the designed or synthesized system and found that by improving  $J_{sc}$  and  $eV_{OC}$ , we could enhance overall PCE.



### 1.1.4 Classification of dye-sensitizers

The different dye-sensitizers developed for DSSC application can be broadly classified into four 1) metal-based dye-sensitizers 2) porphyrins, 3) phthalocyanines and 4) metal-free organic dyes.<sup>7, 66, 79, 80</sup>

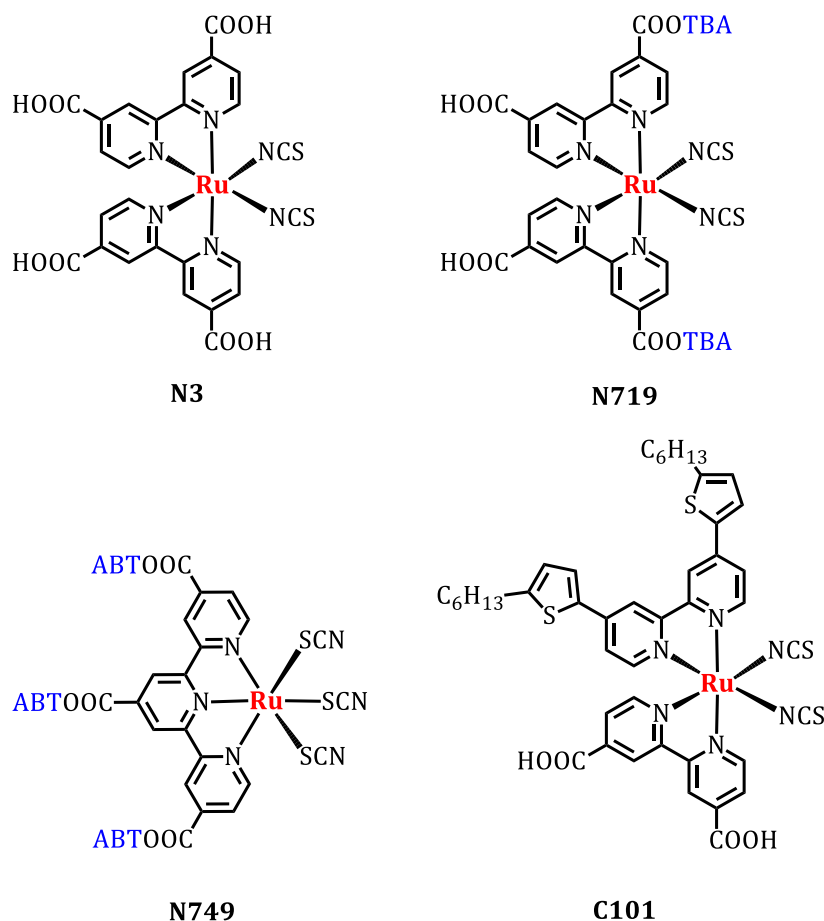


**Figure 1.2** Molecular structures of Ru-based dye-sensitizers, where TBA = tetra butyl ammonium.<sup>81-84</sup>

#### 1.1.4.1 Metal-based dye-sensitizers

The history of metal-based dye sensitizer starts with the discovery of Ru-based dye sensitizer in 1991.<sup>17</sup> The widely accepted Ru based dyes (Figure 1.2) includes N3 (red dye),<sup>81</sup> N179,<sup>82</sup> N749 (black dye),<sup>83</sup> C101,<sup>84</sup> etc., all those dyes showed a PCE more than 10 %. The Ru-based dyes are broadly classified into carboxylate polypyridyl Ru-dyes, phosphonate Ru-dyes, and polynuclear bipyridyl Ru-dyes.<sup>85</sup> The high efficiency observed in Ru-dyes can be attributed to their fast electron injection, good adsorption stability with TiO<sub>2</sub>, stable oxidation state, broad range of visible light absorption, and good photovoltaic properties.<sup>86</sup> The reviews on Ru based sensitizers and their

application in DSSC help us to interpret the charge transfer characteristics in ruthenium complexes and give an outline on the current advancements for DSSC application.<sup>65, 80, 86-89</sup> The other metal ion sensitizers promising for DSSC application include OS, Re, Fe, Pt, and Cu, etc.,<sup>90-94</sup> and found that those are having limited use in DSSC application.

#### **1.1.4.2 Porphyrins**

Porphyrins are naturally occurring macrocyclic compounds which hold a central ring cavity to coordinate metals, yielding metalloporphyrins (Figure 1.3a).<sup>95</sup> The metalloporphyrin (Metals: Zn<sup>2+</sup>, Cu<sup>2+</sup>, etc.) based dyes are less toxic and cheaper than Ru-based photo-sensitizers.<sup>96</sup> A representative example is given in Figure 1.3b. Metalloporphyrins show high absorption and emission spectra in the visible region which can be attributed to the effective charge separation between donor and acceptor region.<sup>95, 97</sup> The high molar extinction coefficient and excellent light-harvesting efficiency make them suitable for solar cell application. Because of the planar structure of porphyrins, that possesses dye aggregation at semiconductor surface and results in poor PCE.<sup>98</sup> A common strategy used for the rectification of dye aggregation includes the incorporation of bulky substituents at the donor site which shows improved efficiency in porphyrins. The method used for the rectification of dye aggregation includes the incorporation of bulky substituents at the donor site which shows improved efficiency in porphyrins. In recent years, substantial work progress has been made in porphyrin-based DSSCs to improve the photovoltaic performance, that reached up to a PCE of 13 %.<sup>13</sup> It is also found that metal-free porphyrins are having lower PCE than Zn-porphyrins. The detailed developments in porphyrin-based DSSCs are reviewed in literature and those provide further insight into the structure-performance relationship in porphyrin-based DSSCs.<sup>13, 98, 99</sup>

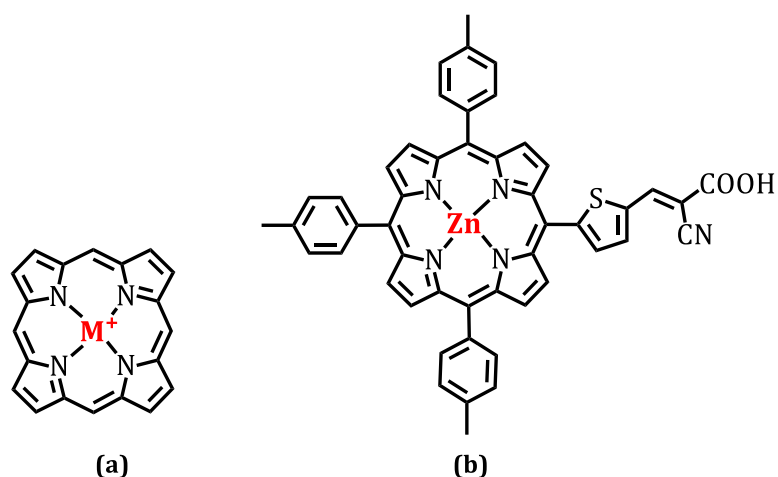


**Figure 1.3** a) Molecular structure of metalloporphyrin (M:  $\text{Zn}^{2+}$ ,  $\text{Cu}^{2+}$ , etc.)  
 b) Representative example of Zn-porphyrin photosensitizer.<sup>96</sup>

### 1.1.4.3 Phthalocyanines

For overcoming the drawbacks of porphyrins, phthalocyanines have been explored. It consists of four isoindole subunits linked together through nitrogen atoms and forming a planar 18  $\pi$ -electron system as shown in (Figure 1.4).<sup>100, 101</sup> The distinguished extraordinary light-harvesting efficiency, robustness, and thermal stability over porphyrin offer significant importance in photovoltaics.<sup>101</sup> The tendency of dye aggregation on the semiconductor surface is the main issue with phthalocyanines, which can be rectified by the incorporation of co-adsorber.<sup>7</sup> The recent advancements in this class of DSSCs reached up to a PCE of 6%,<sup>101</sup>

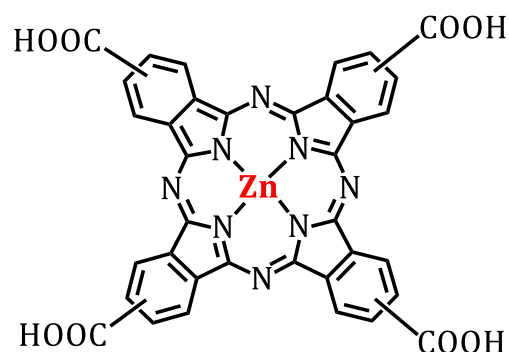


**Figure 1.4** Representative example of phthalocyanine photosensitizer.<sup>99</sup>

Further, the enhancement in the PCE of metal-based dyes has been attained by co-sensitization, where two or more dyes are added to enhance the desired optical and photovoltaic properties.<sup>80, 102</sup> Even if the metal-based class of dye sensitizers are

having comparable PCE to silicon-based solar cells, the high cost of production, low molar absorption coefficient, limited functionalization, short range of absorption in the near infra-red (NIR) region, and environmental toxicity are the major weaknesses possessed, and those concerns directed toward the search for metal-free sensitizers.

#### 1.1.4.4 Metal-free organic dyes

The metal-free class of organic dyes can be prepared relatively less expensively than metal-based dye-sensitizers, and these classes of dyes incorporate different light-absorbing groups into the organic framework for the fine-tuning of the spectral range. The high molar extinction coefficient observed in the metal-free class of organic dyes reports remarkable importance in the field of DSSCs. The general structure of metal-free organic sensitizers includes a D- $\pi$ -A framework (Figure 1.5), where the three major parts comprise donor (D),  $\pi$ -spacer, and an acceptor (A), respectively. The  $\pi$ -spacers, usually  $\pi$ -conjugated systems connect the donor and acceptor groups by forming bridges. The donor groups involved in the structural framework should be electron-rich for the effective intramolecular charge transfer (ICT) of electrons from D to A through  $\pi$ -spacer. The acceptor part involved in the basic structure helps the sensitizers for effective anchoring onto the semiconductor.<sup>103</sup> The rapid progress on the development of metal-free sensitizers increased after 2011 and became the most potential alternative for Ru-based sensitizers. So far, the modifications on the basic structural framework of organic dye sensitizers reached up to a maximum PCE of 13.6 %, <sup>104</sup> while using co-sensitization with an alkoxy silyl-anchor dye and a carboxy-anchor organic dye, a maximum PCE of 14.3 % has been attained.<sup>21</sup> According to the working principle of DSSC, when the light incident on the dye molecule, there is an intramolecular charge transfer (ICT) from D to A through  $\pi$ -spacer, which excites an electron to the LUMO of the dye. This electron transport is considered to be essential for the electron injection from dye molecule to TiO<sub>2</sub> surface.

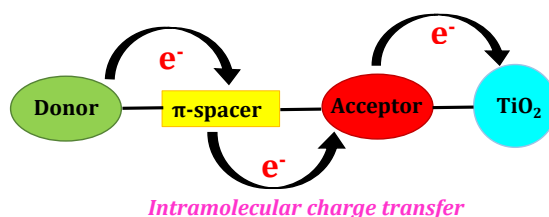


**Figure 1.5** Schematic representation of D- $\pi$ -A based dye-sensitizer.

### 1.1.5 Distinctive design strategies in metal-free organic sensitizers

The frequently used molecular design strategy in metal-free sensitizers comprises a D- $\pi$ -A type architecture, the examples are given in Figure 1.6. In literature, several theoretical, as well as experimental groups, have been considered different combinations of D,  $\pi$ -spacer, and A in the general D- $\pi$ -A framework and analysed their structure-performance relationship in DSSCs. Since the electron-donating ability of donors has a significant role in light-harvesting efficiency, various functional groups *viz.* triphenylamine (TPA),<sup>105</sup> carbazole,<sup>106</sup> phenothiazine,<sup>107, 108</sup> perylene,<sup>109</sup> coumarin,<sup>110</sup> indolines,<sup>111</sup> fluorene,<sup>112</sup> merocyanine,<sup>113</sup> hemicyanine,<sup>114</sup> N,N-dialkylaniline,<sup>115</sup> phenothiazine,<sup>116</sup> tetrahydroquinoline,<sup>117</sup> Squaraine,<sup>118</sup> ullazine,<sup>119</sup> indolizine,<sup>120</sup> julolidine,<sup>121</sup> etc. have been incorporated as donors in D- $\pi$ -A and all those systems gained diverse effects on PCE. The planarity of donor molecules is also studied for estimating the effective ICT and confirms that the planar nature of the donor has a vital role toward open-circuit voltage. Also, the planarity increases the electron delocalization in donors result in a redshift of the absorption peak, thereby improves PCE.<sup>122</sup> Since the modifications with appropriate design strategies extend the absorption of the organic dyes to NIR region, several other design strategies like D-A- $\pi$ -A-type and D-D- $\pi$ -A-type have been developed, and those models facilitate electron migration, inhibit dye aggregation, and improve photostability.<sup>103, 123, 124</sup>

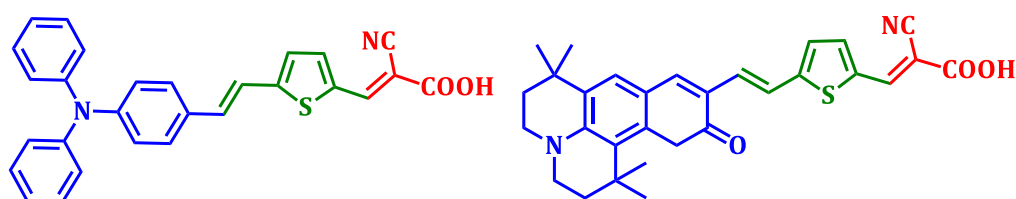


**Figure 1.6** Examples of TPA and coumarin-based D- $\pi$ -A type dye-sensitizers (from left to right).<sup>110, 125</sup>

In D-D- $\pi$ -A approaches, the expansion of the donor part with an additional donor group could be considered as the one easy method for enhancing the electron-donating strength of the donors. Examples of this class are shown in Figure 1.7. By introducing additional donors in the structural unit, we can enhance the molar extinction coefficient and also tunes the HOMO - LUMO energy level of the dye sensitizers to a preferred absorption range. Further, the addition of extra electron-donating groups like OCH<sub>3</sub>, and alkyl chains, onto the D-D- $\pi$ -A framework had a better

enhancement in the overall performance of DSSC compared to the corresponding bare D-D- $\pi$ -A systems.<sup>126-129</sup> In the above said studies, the incorporation of bulky groups could prevent dye aggregation on the semiconductor surface effectively, thereby improves photovoltaic performance.<sup>127</sup>

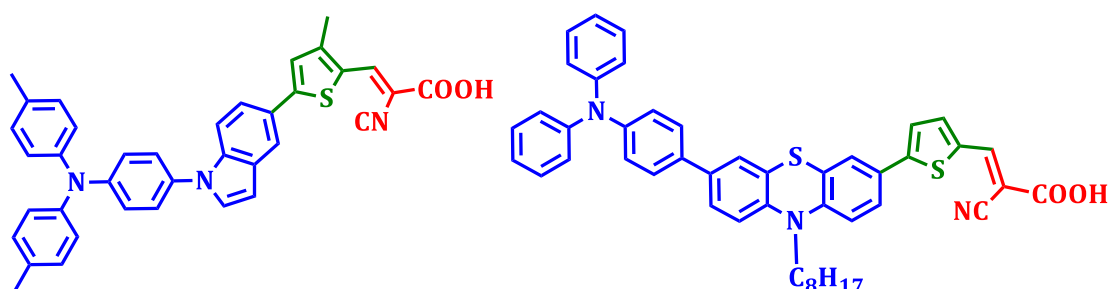


**Figure 1.7** Examples of D-D- $\pi$ -A-type dye-sensitizers.<sup>126, 129</sup>

In D-A- $\pi$ -A-type (Figure 1.8), for improving the performance of DSSC, additional electron-withdrawing units such as diketopyrrolopyrrole (DPP),<sup>130</sup> benzothiadiazole (BTD),<sup>131, 132</sup> and isoindigo<sup>133</sup> have been introduced between the donor and the  $\pi$ -bridge as an auxiliary acceptor.<sup>134, 135</sup> Zhu and Wu, jointly proposed the above novel concept, in which a series of auxiliary acceptors such as benzotriazole, quinoxaline, and phthalimide has been introduced for the design of D-A- $\pi$ -A-type sensitizers. They treated additional anchoring units as “electron trappers,” which can enhance ICT, tune the HOMO - LUMO energy gap, reduce dye-aggregation, and improve photo-thermal stability of dye-sensitizers for improving the overall PCE.<sup>136</sup> The detailed description about the other known auxiliary acceptors (Figure 1.9) and their role for improving the optical and photovoltaic properties of D-A- $\pi$ -A type sensitizers are reviewed by Zhu and Wu, and found that additional electron acceptor units are helpful for improving the dye stability and efficiency.<sup>136</sup>

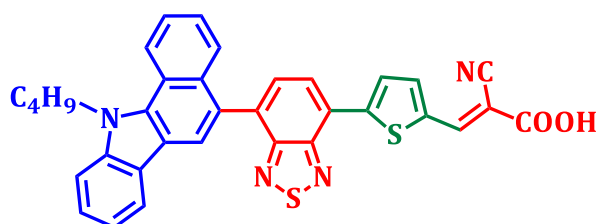


**Figure 1.8** Representative example of D-A- $\pi$ -A-type dye-sensitizer.<sup>137</sup>

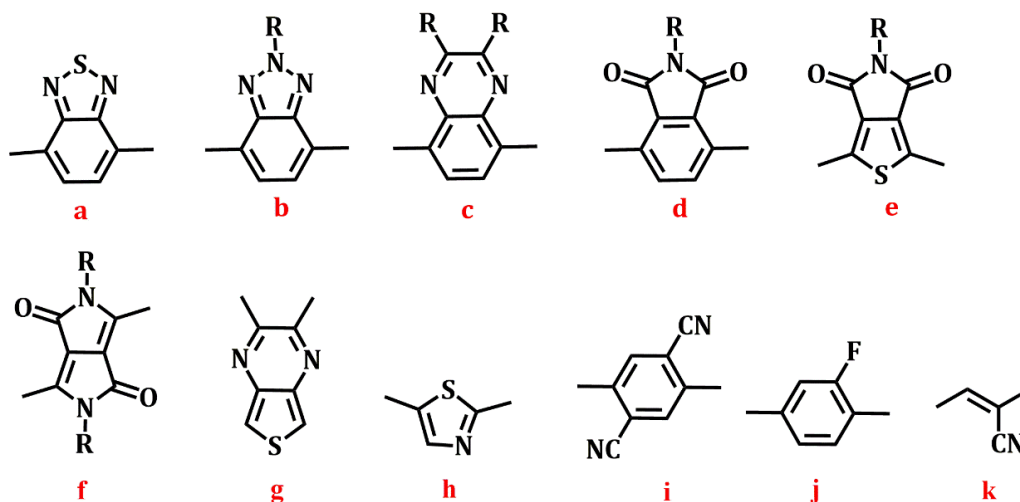


**Figure 1.9** Typically used auxiliary acceptors in DSSCs: a) benzothiadiazole (BTDA), b) benzotriazole, c) quinoxaline, d) phthalimide, e) TPD, f) diketo-pyrrolopyrrole (DPP), g) thienopyrazine, h) thiazole, i) cyano-substituted phenyl, j) fluoro-substituted phenyl, and k) cyano vinyl.

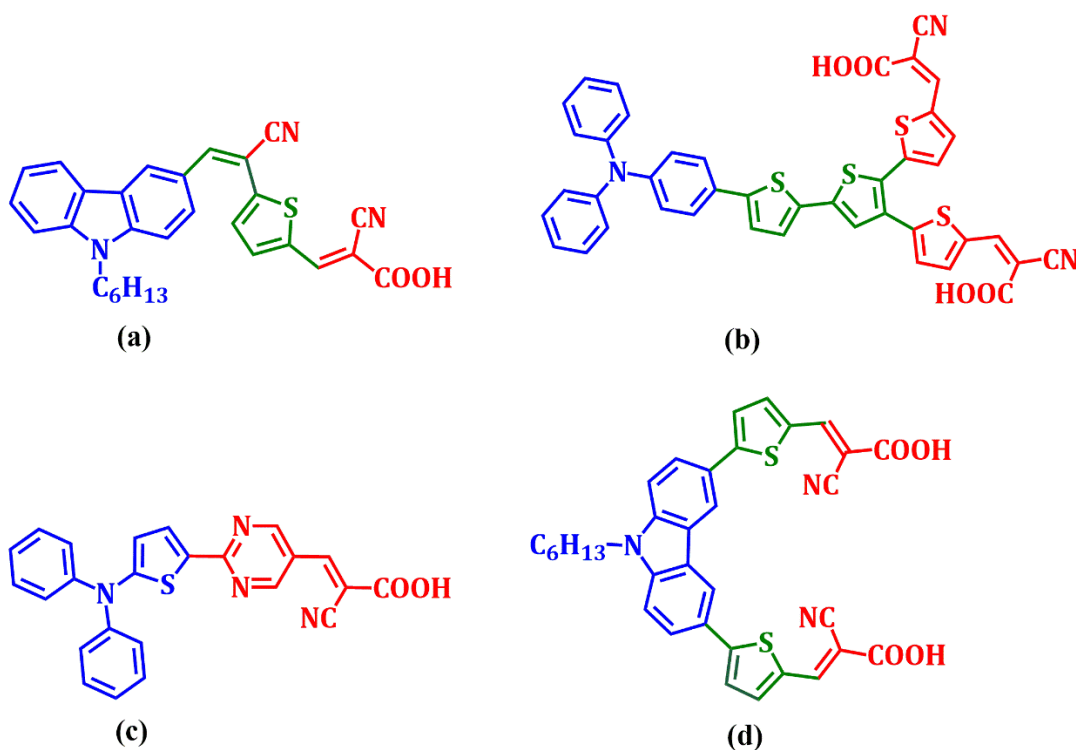


**Figure 1.10** Representative examples of a) D- $\pi$ -A- $\pi$ -A b) D- $\pi$ -(A)<sub>2</sub> c) D-A-A and d) double D- $\pi$ -A bridge types metal-free dye sensitizers.<sup>138, 139, 140-145</sup>

The other known metal-free architectures (Figure 1.10) developed for DSSC application include D- $\pi$ -A- $\pi$ -A,<sup>143-145</sup> D-A-A,<sup>139</sup> D- $\pi$ -(A)<sub>2</sub>,<sup>138</sup> and double D- $\pi$ -A bridges.<sup>140-142</sup> The incorporation of rigid conjugated electron donors and  $\pi$ -spacers

results in excellent DSSC performance. Also, Han *et al.* proved that the introduction of non-planar donor groups with large-steric hindrance resists dye aggregation and electron-charge recombination without any co-adsorbent.<sup>146</sup> The reviews on metal-free dye sensitizers offer a better understanding of the different structure-performance relationship in DSSC and proves that the introduction of additional donors, acceptors, and  $\pi$ -spacers results in wide absorption coverage, higher molar extinction coefficients, lower HOMO - LUMO energy gap, and dark current suppression etc.<sup>18,147</sup>

Apart from conventional donors, several push-pull heterocyclic  $\pi$ -conjugated systems such as thiophene, n-hexyl-2,2'-bithiophene, dithieno [3,2-b:2',3'-d] thiophene, furan and pyrrole, as donors have been developed by various groups<sup>148-150</sup> for scrutinising their excellent charge-transfer characteristics. According to the above studies, the incorporation of push-pull compounds as donors enhances their charge transport properties and offers a bathochromic shift on the absorption maximum when compared to the standard system involved in those studies. There are only limited studies regarding heterocyclic compounds as donors and are found to be beneficial for DSSC application.

In addition to the abovementioned design strategies, the inclusion of co-adsorber like deoxycholic acid (DCA), improves the performance of DSSC by enhancing the electron injection efficiency. The co-adsorber can be considered as a molecule not having any absorption properties but it gets adsorb on the semiconductor surface reduces dye aggregation of the dye on the semiconductor, consequently improves the performance of DSSC.<sup>151</sup>

### **1.1.6 Influence of spacer units**

In DSSC fabrication, the individual design approaches on spacers have a promising role in enhancing the LHE of the dye-sensitizer.<sup>152, 153</sup> The major design strategies in spacers focused on the variation of spacer types, spacer chain length, and planarity of spacers.<sup>154</sup> The spacer length and types involved could significantly influence the HOMO - LUMO energy gap and are expected to tune the region of absorption spectra to a longer wavelength region.<sup>84,155-157</sup> The commonly used spacers in DSSC



application involves 1,3 butadiene,<sup>69</sup> phenyls,<sup>158</sup> ethynyls,<sup>159</sup> phenyl ethynyl,<sup>160</sup> furan,<sup>137,161,162</sup> thiophene,<sup>137,163,164</sup> fused thiophenes,<sup>165,166</sup> pyrrole,<sup>167</sup>

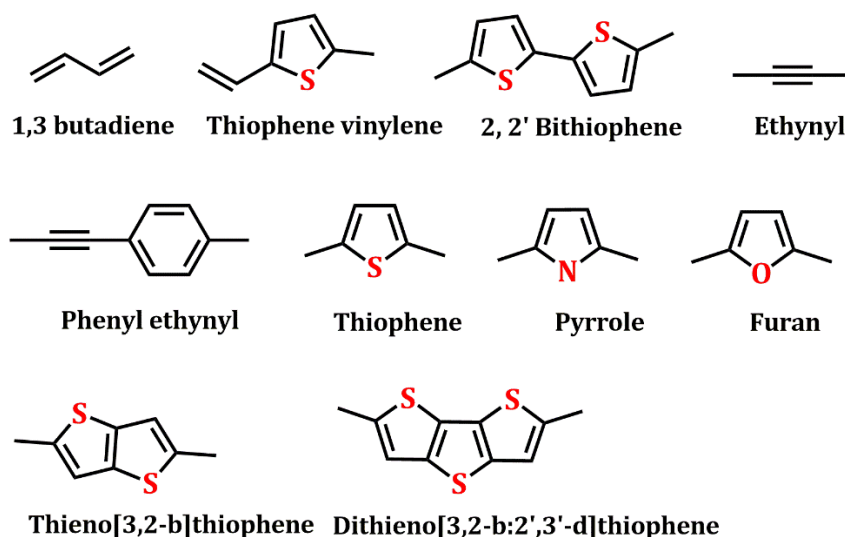


**Figure 1.11** The generally used spacers for DSSC applications.

thieno [3, 2-b] thiophene,<sup>168</sup> etc. (Figure 1.11). Furthermore, it is found that type of spacer moiety has a leading role on the photovoltaic properties of dye molecules. For example, Liu *et al.* reported that D- $\pi$ -A systems with thiophene and furan spacers exhibit better photovoltaic performance than phenyl spacers.<sup>169</sup> Also, the replacement of olefinic spacers by rigid  $\pi$ -spacers for instance phenyl, thiophene, and furan improved the overall performance of the DSSC device.<sup>157</sup> Lin, Ko, and co-workers described that thiophene conjugated spacers have better absorption properties than phenyl spacers, which can be attributed to the more planar structure of thiophene unit with the neighbouring rings. Thus, thiophene is the widely used spacer moiety in DSSC and noted that its photophysical properties improved with spacer length.<sup>156,157,170-172</sup> From the above remarks, we could understand that choice of spacers in DSSC is the one key tactic to improve the efficiency of DSSCs. The effect of spacers on the photophysical properties of D- $\pi$ -A systems is theoretically studied by Tsai and workers and described that spacer type, length and planarity have a substantial role in absorption maximum and charge transfer rate.<sup>173</sup> In that study the increased number of thiophene spacers in D- $\pi$ -A system exhibits better electron injection rate and absorption properties than phenyl moieties. Moreover, spacer length influences the back electron transfer kinetics associated with the performance of dye in DSSCs. A Theoretical study conducted by He *et al.* showed that dye

regeneration efficiency and electron injection efficiency decrease with an increase of  $\pi$ -spacer length.<sup>174</sup> Also, lower the dye regeneration efficiency, greater the charge transfer rate, which is needed for the high-performance DSSCs.<sup>175</sup> Hartland and co-workers showed that shorter spacer length reduces the electronic coupling element and thereby reduces open-circuit voltage ( $eV_{OC}$ ).<sup>176</sup> The effect of spacer length on recombination rate (back electron transfer) and electron-injection have been investigated by various groups and found that optimal spacer chain length controls dynamics of electron injection, and recombination at dye/semiconductor interfaces.<sup>152,177,178</sup>

The studies regarding the planarity and size of rigid spacer systems showed that the incorporation of a rigid system affects the geometrical and electronic properties of the dyes and plays a key role in enhancing the performance of dye sensitizers.<sup>179, 180</sup> The planar conjugated spacers have a higher molar absorption coefficient as well as red-shifted absorption maximum compared to its non-planar analogue. For example, sensitizers with indeno [1,2-b] thiophene spacer displayed better ICT and higher molar absorption coefficient relative to non-planar analogue, thiophene-phenyl unit.<sup>181</sup> Following the above principle, several other planar units have been introduced in DSSC such as fluorene,<sup>182, 183</sup> cyclopentadithiophene,<sup>184</sup> indenofluorene,<sup>185</sup> and dithieno-[3,2-b;2',3'-d]thienyl.<sup>117</sup> The incorporation of rigid fused units like benzotriazole (BTZ), quinoxaline (QX), or benzothiadiazole as electron-deficient spacers had a significant improvement in PCE than coplanar  $\pi$ -spacers, which can be attributed to their enhanced electron delocalization, reduced electron-hole recombination, and improved optical properties, etc.<sup>186-188</sup> Zhang and co-workers also studied the influence of rigid fused electron-rich and electron-deficient units as  $\pi$ -spacers, which provides more insight into the structure-performance relationship of dye-sensitizers for DSSC applications.<sup>72</sup> Finally, we could conclude that the modifications of  $\pi$  spacers are an effective way to achieve highly efficient sensitizers for DSSC applications.<sup>170, 180</sup>

### **1.1.7 Significance of acceptors or anchoring units**

As one of the essential parts of a dye sensitizer, the effect of the acceptor or anchoring group on the optical and photovoltaic properties of a dye-sensitizer has been studied

by various experimental and theoretical groups.<sup>189-191</sup> Anchoring groups help the dye molecule to adsorb onto the TiO<sub>2</sub> surface and allows electron transfer from the dye to TiO<sub>2</sub>, by forming a coordinate bonding or bidentate bridging linkage with the Lewis acid site of TiO<sub>2</sub>. Consequently, the interaction between the acceptor of the dye and the TiO<sub>2</sub> surface has a crucial role in the photovoltaic performance of DSSCs.<sup>192-194</sup> Additionally, the electron-withdrawing ability of the anchoring unit (A) could tune HOMO and LUMO energies of the dye molecule, resulting in a different electron injection capability in dye molecules, which in turn finally affects  $J_{sc}$  and  $eV_{oc}$  of dye sensitizers.<sup>195</sup>

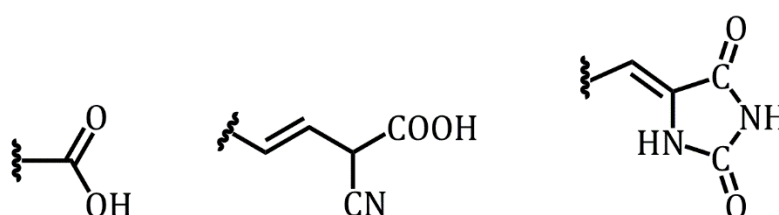


**Figure 1.12** The frequently used anchoring groups in DSSCs viz. carboxylic acid, cyanoacrylic acid, and rhodanine 3-acetic acid (left to right)

The frequently utilized acceptors in DSSCs are cyanoacrylic acid, carboxylic acid, and rhodanine/rhodanine-3-acetic acid, respectively (Figure 1.12).<sup>66, 152</sup> The good adsorption stability and excellent electron-withdrawing ability make cyanoacrylic acid highly appropriate for DSSC applications.<sup>196</sup> Covalent bonding is the major adsorption mechanism involved in dye/semiconductor surfaces.<sup>197</sup> The different adsorption configurations between carboxylic acid and TiO<sub>2</sub> surface have been identified as monodentate ester, bidentate chelating, bidentate bridging, monodentate and bidentate H-bonding, and as a monodentate coordinating mode through CO, respectively, which is shown in Figure 1.13.<sup>152, 192</sup> Among those various adsorption modes bidentate chelate and bidentate bridging configurations showed superior stability over other adsorption modes.<sup>7</sup> Since the adsorption configuration affects LUMO energy, the choice of preferred configuration is central in DSSC for improving efficiency.<sup>198</sup>

The other reported anchors for DSSC application include perylene<sup>199</sup> dicarboxylic acid anhydride,<sup>200-202</sup> 2-hydroxybenzotrile,<sup>203</sup> 8-hydroxyquinoline,<sup>203</sup> 3-hydroxy-N-methylpyridinium,<sup>204</sup> catechol,<sup>205-207</sup> hydroxamate,<sup>208, 209</sup> sulfonic

acid,<sup>210, 211</sup> acetylacetonate (acac),<sup>212, 213</sup> boric acid,<sup>214</sup> nitro groups,<sup>215</sup> tetrazole groups, salicylic acid<sup>216</sup> and aldehyde groups,<sup>199, 217</sup> those studies offered a detailed outlook regarding the electronic structure, stable adsorption configuration, and photo-physical properties of each anchor in detail. Also, those findings highlight the necessity of the choice of anchoring unit for further design rules in dye sensitizers.<sup>192, 195, 218</sup>

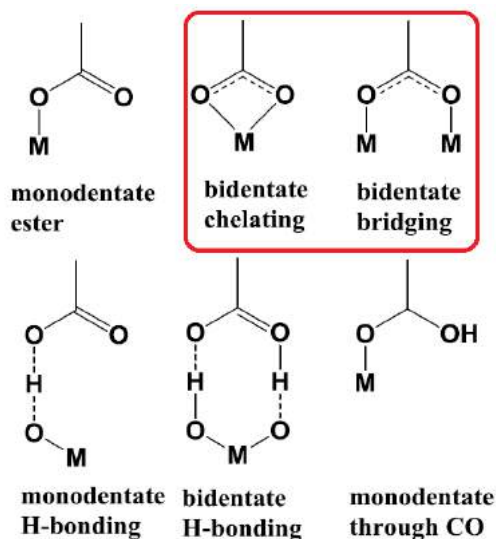


**Figure 1.13** The possible adsorption configurations for carboxylic acid onto the metal oxide semiconductor (M = Si, Sn, Ti, etc.)<sup>192</sup>

### 1.1.8 Importance of theoretical study in the design of dye sensitizers

Computational strategies for developing highly efficient DSSCs are having paramount importance in photovoltaics. It provides a deep insight regarding the fundamental molecular information which are not accessible with experimental studies.<sup>219</sup> Accordingly, over the past 30 years density functional theory (DFT) and time-dependent DFT (TD DFT) have a significant role in optimal dye design, screening molecular properties, and understanding the in-depth mechanism of the photovoltaic process. Another way, the accurate description of electronic structure, dye-semiconductor interaction, and electrolyte interactions could offer an overview of the fundamental process that takes place in DSSCs.<sup>220</sup> The main properties that are studied with electronic structure include rationalization of optical properties of dyes, frontier molecular analysis, and photovoltaic properties, while it is also found that all

the properties associated with the performance of DSSC are not equally predictable with electronic structure method.<sup>220</sup> TD-DFT calculation is reliable for analysing the excited state properties and provides in-depth knowledge about the charge transfer processes in dye sensitizers.

In the literature, the quantum chemical parameters such as electrophilicity index ( $\omega$ ), electron-accepting power ( $\omega^+$ ), and electronic chemical hardness ( $h$ ) have been used for the examination of molecular properties of the dye and found that those are helpful for the prediction of dye stability, electron injection efficiency, and ICT rate.<sup>221-223</sup> Chemical hardness is defined as the resistance of the dye to intramolecular charge transfer, thus by lowering chemical hardness we could improve the short-circuit current density ( $J_{SC}$ ).<sup>224, 225</sup> The higher electrophilicity defines better dye-stability. Apart from those parameters, HOMO - LUMO orbital energy analysis, life time of excited state, absorption spectra, NBO analysis, investigation of charge carriers, electrostatic potential, charge transfer function ( $C^+/C^-$ ), and analysis of dye/TiO<sub>2</sub> adsorption stability, etc. are very helpful for finding the structure-performance relationships in DSSCs.<sup>226</sup> Recently Yang *et al.* described that molecular electrostatic potential (MESP) can be considered as a new tool in theoretical chemistry to predict chemical reactivity. It is found that MESP plot is helpful to locate electron-dense and deficient regions in a molecule, hence it could be suitable for the analysis of the electron transport process in DSSC.<sup>72</sup>

The other primary factors that affect the overall performance of DSSCs such as  $\Delta G_{inject}$ ,  $\Delta G_{reg}$ ,  $J_{SC}$ ,  $eV_{oc}$ , and LHE are possible to compute theoretically, and those studies offer an accurate description of electron injection and regeneration efficiency of dye molecules in DSSCs.<sup>227</sup>

Apart from the above concerns, the selection of reliable exchange-correlation functional-based DFT method is important for the calculation of the electronic structure of isolated dye and dye adsorbed TiO<sub>2</sub> (dye/TiO<sub>2</sub>). Pure DFT functionals often underestimate (or) overestimate the HOMO - LUMO energy gap values. Hence the choice of exact exchange correlational DFT method which is more reliable than pure DFT is necessary for the simulation of absorption spectra and calculation of energy gap values.<sup>228</sup> Since the interaction between dye and semiconductor shift the

position of LUMO of the dye molecule, thereby affecting the electron injection efficiency of dye to the semiconductor, the theoretical studies on the dye/semiconductor interaction have a significant role in determining the overall efficiency.<sup>195, 220</sup> The good adsorption stability results in better photovoltaic performance. Thus, by calculating adsorption energy, we can predict the characteristics of DSSC.<sup>229,230</sup> Theoretically, adsorption energy between dye and TiO<sub>2</sub> can be calculated as  $E_{\text{ads}} = E_{\text{dye+TiO}_2} - (E_{\text{dye}} + E_{\text{TiO}_2})$ , where  $E_{\text{dye+TiO}_2}$ ,  $E_{\text{dye}}$ , and  $E_{\text{TiO}_2}$  represent the energies of adsorbed dye, isolated dye, and bare TiO<sub>2</sub> respectively. It should also be noted that adsorption configurations of anchoring group onto the semiconductor surface display a substantial role in adsorption stability and affects the electron-charge transfer kinetics in DSSC, the selection of the best adsorption configuration is the first step in the theoretical simulation of the adsorption process.<sup>195</sup> Most of the theoretical studies considered TiO<sub>2</sub> surface for adsorption. Among the several polymorphs of TiO<sub>2</sub>, anatase and rutile are the commonly used ones.

The detailed theoretical advancements that happened in this area have been systematically and comprehensively reviewed by Izadyar and Arkan. The review highlights different aspects of molecular properties and charge transfer processes such as selection of appropriate method/basis set, effect of substituents on donor, frontier molecular analysis, importance of chemical descriptors, solvent effect, influence of electrolyte, dye-semiconductor interactions, etc, which are crucial for the dye design are explained in detail.<sup>226</sup> Finally, we could conclude that first principle studies have been contributed numerous advancements in dye design, which is beneficial to reveal the structure-performance relationship in DSSC. <sup>72,226,231-236</sup>

### **1.1.9 Objective of the study**

From the detailed examination of theoretical and experimental studies about DSSCs, we noticed that the electron-rich nature of donor motif, their modifications, spacer modifications such as type, and chain length bring advancements in optical, and photovoltaic properties of dye-sensitizer. However, to the best of our knowledge, a theoretical quantification of donor strength, as well as electronic effect transmitting power of spacers are not explored in the literature. So, in the thesis, we intend to

calculate and analyze the aforesaid fundamental parameters with the help of advanced DFT methodology and analysis of electronic features using MESP. It is anticipated that the theoretical judgement regarding those quantities will help us to choose a particular dye for further structural advancements, which may lead to the development of new electron-rich donors with improved photovoltaic performance. Moreover, to effectively compete with the existing energy shortage, the emerging theoretical simulation is beneficial by maintaining a low-cost than experimental studies.

# Part B: Computational Chemistry Methods

---

## 1.2 An overview of computational chemistry

Computational chemistry is an emerging field of chemistry in which mathematical approximations implemented on computers are utilized to tackle chemical problems. The foundation of computational chemistry is based on two important theories *viz.* classical mechanics based on Newton's equations of motion and quantum mechanics based on Schrödinger equation. The basics of quantum mechanics developed at the earliest of 1920, while the application is limited to small molecular systems. After the development of efficient computer technology, the application for complex systems began to be realised, and thus it could be considered as a product of the digital age. Computational chemistry got its distinct field of study when Walter Kohn and John Pople won the nobel Prize in Chemistry in 1998 for their work on density functional theory (DFT) and computational methods in quantum chemistry.<sup>237</sup> In practice, computational methods have now become an integral component in all the disciplines of chemistry as they increase the microscopic, atomistic, and dynamic understanding of molecular systems.<sup>238</sup> It is extensively used in quantum mechanics for the study of molecular structures, analysis, and interpretation of experimental data, study of reaction mechanism, predicting IR, NMR, and UV-Visible spectra of molecular species, etc. Its application is now extended in computer modelling and simulation techniques to understand the structure and properties of different states of matter.

For determining the molecular structure by geometry optimization, total energy approximation by solving the time-dependent Schrödinger equation is the basic or first step. There are different methods included in computational chemistry for the determination of total energy, which could be classified as *ab initio* quantum chemical methods (Latin term for "from the beginning"), density functional theory (DFT) methods, semiempirical quantum chemical methods, molecular mechanics (MM), molecular dynamics (MD), Monte-Carlo (MC) simulations and hybrid quantum mechanics/molecular mechanics (QM/MM) methods. In the *ab initio* method, empirical or semi-empirical parameters are not involved to solve the Schrödinger equation, while parameters that are derived directly from theoretical principles, for example, constants such as speed of light, mass, and charge of electrons, Plank's



constant, etc. are used. *Ab initio* method is expensive and applies to small systems. In semi-empirical methods, the determination of wave function and energy of quantum many-body systems are determined using experimental data (parametrization). In DFT, the total energy is not expressed in terms of wave function instead it is expressed in terms of electron density. This method shows a balance between accuracy and computational cost and could be applied from smaller systems to complex systems. For modelling the molecular systems ranging from small to large, molecular mechanics simulations can be used. It uses vibrational and conformational motions of the system for the calculation of energy. MM is otherwise known force field method where atoms are considered as balls and bonds as springs.<sup>239-242</sup> To examine the time-dependent behaviour of the system, MD uses quantum mechanics, molecular mechanics, or the mixture of both to calculate the forces which comprise Newton's laws of motion.<sup>243</sup>

### 1.2.1 *Ab initio* quantum chemical methods

*Ab initio* method comes under the electronic structure method, where quantum mechanics is the basis of computation with direct use of theoretical principles. According to quantum mechanics, the energy and other related properties are obtained by solving the Schrödinger equation,<sup>244</sup>

$$H\Psi = E\Psi \quad (\text{Eq. 1.7})$$

where  $H$  is the Hamiltonian operator,  $\Psi$  is the N-body wave function, and  $E$  is the energy eigenvalue of the system. *Ab initio* method considers electronic and nuclear interactions in an atom and hence it is used to describe the inter atomic interactions in a quite different environment. Consequently, in the *ab initio* method, the electronic Schrödinger equation for many-electron systems is solved. The Hamiltonian operator for a system of N electrons and M nuclei can be written in the atomic unit as:

$$H = -\sum_{i=1}^N \frac{1}{2} \nabla_i^2 - \sum_{A=1}^M \frac{1}{2M_A} \nabla_A^2 - \sum_{i=1}^N \sum_{A=1}^M \frac{Z_A}{r_{iA}} + \sum_{i=1}^N \sum_{j>i}^N \frac{1}{r_{ij}} + \sum_{A=1}^M \sum_{B>1}^M \frac{Z_A Z_B}{R_{AB}} \quad (\text{Eq. 1.8})$$

In the above equation, the first two terms represent the electronic and nuclear kinetic energy operators, the third, fourth, and fifth terms in Hamiltonian represent the potential energy operators corresponding to nuclear-electron, electron-electron, and

nuclear-nuclear interactions, respectively. The notations  $\mathbf{R}_A$  and  $\mathbf{r}_i$  stand for the position vectors of nuclei and electrons.  $\mathbf{r}_{iA}$  represents the distance between  $i^{\text{th}}$  electron and  $A^{\text{th}}$  nucleus, and  $\mathbf{r}_{ij}$  is the distance between  $i^{\text{th}}$  and  $j^{\text{th}}$  electrons. Further,  $\mathbf{R}_{AB}$  denotes the distance between  $A^{\text{th}}$  and  $B^{\text{th}}$  nucleus.  $M_A$  is the ratio of the mass of the nucleus to the mass of an electron and  $Z_A$  is the atomic number. Finally,  $\nabla_i^2$  and  $\nabla_A^2$  are Laplacian operators.

According to the basic principle, the Schrödinger wave equation can be exactly solvable for hydrogen and hydrogen-like atoms. Since the solution of the Schrödinger equation is the basis for quantum chemical calculations, approximation methods are needed to solve the wave equation for many-electron systems. The best-known approximation method used in many-electron systems is Born-Oppenheimer (BO) approximation, which considers electronic and nuclear motion are separable.<sup>245, 246</sup> BO approximation neglects nuclear motion while describing the electronic motion in a molecule. Because nuclei are heavier than the electron and moves moderately than the electrons. Thus, BO approximation makes the second term (nuclear kinetic energy term) in Eq. 1.8 as zero and nuclear-nuclear repulsion term as constant (fifth term of Hamiltonian). The remaining terms in the Hamiltonian (Eq. 1.8) constitute the motion of  $N$  electrons in the field of  $M$  point charges, the electronic Hamiltonian  $H_{elec}$  can be written as:

$$H_{elec} = -\sum_{i=1}^N \frac{1}{2} \nabla_i^2 - \sum_{i=1}^N \sum_{A=1}^M \frac{Z_A}{\mathbf{r}_{iA}} + \sum_{i=1}^N \sum_{j>i}^N \frac{1}{\mathbf{r}_{ij}} \quad (\text{Eq. 1.9})$$

In (Eq. 1.9), the third term stands for electron-electron interactions, the determination of the exact solution for this term is highly demanding. To estimate the solution for electron-electron interactions, consider an approximation in which  $N$  electrons are moving completely independent of each other, the corresponding term becomes zero. Hence the total wave function can be written as the product of  $N$  electron wave function as given below:

$$\Psi = \Psi_1(\mathbf{r}_1)\Psi_2(\mathbf{r}_2)\dots\Psi_N(\mathbf{r}_N) \quad (\text{Eq. 1.10})$$

Also, the Schrodinger equation to the electronic Hamiltonian  $H_{elec}$  which is separated out for electronic motion can be represented as:

$$H_{elec} \Phi_{elec}(\{\mathbf{r}_i\}; \{\mathbf{R}_A\}) = E_{elec} \Phi_{elec}(\{\mathbf{r}_i\}; \{\mathbf{R}_A\}) \quad (\text{Eq. 1.11})$$

where  $\{\mathbf{r}_i\}$  and  $\{\mathbf{R}_A\}$  characterise the position of electrons and nuclei, respectively. The electronic wave function which depends on electronic co-ordinates  $\{\mathbf{r}_i\}$  (explicitly) and the position of the nuclei  $\{\mathbf{R}_A\}$  (implicitly) is denoted as  $\Phi_{elec}$ . On solving Eq. 1.11, we will get the energy of the electronic wave function which defines the motion of electrons.<sup>247</sup> The above relation shows that BO approximation effectively separates electronic and nuclear Hamiltonians and their corresponding wave functions. Thus, using the wave function from the Schrödinger equation, any experimentally observable properties can be calculated as the anticipated value of the appropriate operator. Finding an exact solution to the many-body Schrödinger equation is not so easy, for which an appropriate approximation method is required.

### 1.2.1.1 Hartree-Fock theory

The Hartree-Fock (HF) method is a variational, wavefunction-based approach in which motion of each electron can be defined by a single-particle function (orbital) by assuming that electrons are non-interacting. It is the most popular *ab initio* method established to solve the time-independent Schrödinger equation, after applying the Born-Oppenheimer approximation.<sup>248</sup> In HF method, due to the non-interacting nature of electrons, the total Hamiltonian of the many-electron system ( $H$ ) can be expressed as a sum of one electron Hamiltonian given in Eq. (1.12).<sup>245</sup>

$$H = - \sum_{i=1}^N h(i) \quad (\text{Eq. 1.12})$$

Where  $h(i)$  is the one-electron Hamiltonian and the corresponding one-electron wavefunction can be obtained as the product of single-electron spin-orbital wavefunctions; which is known as Hartree product ( $\Psi^{HP}$ ). i.e.,

$$\Psi^{HP}(\mathbf{x}_1, \mathbf{x}_2, \dots, \mathbf{x}_N) = \chi_i(\mathbf{x}_1) \chi_j(\mathbf{x}_2) \dots \chi_k(\mathbf{x}_N) \quad (\text{Eq. 1.13})$$

where,  $\chi_i, \chi_j, \chi_k$  etc. represent spin orbitals and  $\mathbf{x}_1, \mathbf{x}_2, \dots$  etc. represent combined spatial and spin coordinates of each electron, respectively. Also, this N electron wavefunction shows that the probability to find one electron in many electrons

system is independent of the position of other electrons.<sup>249</sup> But in reality, this does not happen, where the electronic motion is interrelated as they experience coulombic repulsion due to the same charge. Further,  $\Psi^{HP}$  is considered as the eigenfunction to the total Hamiltonian ( $H$ ) and one of the problems with the Hartree product is that electrons are indistinguishable, which means the antisymmetric principle is not obeyed. This additional requirement on electronic wavefunction can be rectified by arranging the N-electron wavefunction in the form of Slater determinant (Eq. 1.14) as given below.

$$\Psi(\mathbf{x}_1, \mathbf{x}_2, \dots, \mathbf{x}_N) = \frac{1}{\sqrt{N!}} \begin{vmatrix} \chi_i(\mathbf{x}_1) & \chi_j(\mathbf{x}_1) & \dots & \chi_N(\mathbf{x}_1) \\ \chi_i(\mathbf{x}_2) & \chi_j(\mathbf{x}_2) & \dots & \chi_N(\mathbf{x}_2) \\ \dots & \dots & \dots & \dots \\ \chi_i(\mathbf{x}_N) & \chi_j(\mathbf{x}_N) & \dots & \chi_N(\mathbf{x}_N) \end{vmatrix} \quad (\text{Eq. 1.14})$$

where  $\frac{1}{\sqrt{N!}}$  is a normalization factor. The interesting consequence of the Slater determinant is that the electrons are all indistinguishable and the motion of electrons with parallel spins is correlated when the many-electron wave function is represented in Slater determinant form.<sup>250, 251</sup> The normalized Slater determinant can be represented as given in Eq. 1.15.

$$\Psi(\mathbf{x}_1, \mathbf{x}_2, \dots, \mathbf{x}_N) = \left| \chi_i \chi_j \dots \chi_N \right\rangle \quad (\text{Eq. 1.15})$$

According to variational principle, the wave function giving the lowest energy is the finest and can be calculated as an expectation value of the Hamiltonian over this approximate wave function. It is noted that by increasing the size of the basis set, the energy goes on decreasing, until a limit, named the Hartree-Fock limit. Thus, the finest approximate wave function  $\Psi_0$  that gives the lowest energy ( $E_0$ ), is given by the (Eq. 1.16).

$$E_0 = \langle \Psi_0 | H | \Psi_0 \rangle \quad (\text{Eq. 1.16})$$

By choosing appropriate spin orbitals  $\chi_i$ , minimum energy can be attained and the corresponding eigenvalue equation is named as Hartree-Fock equation; represented as:

$$f(i)\chi(\mathbf{x}_i) = \varepsilon\chi(\mathbf{x}_i) \quad (\text{Eq. 1.17})$$

where  $f(i)$  is a one-electron operator called the Fock operator, which can be written as,

$$f(i) = -\frac{1}{2}\nabla_i^2 - \sum_{A=1}^M \frac{Z_A}{r_{iA}} + V^{\text{HF}}(i) \quad (\text{Eq. 1.18})$$

In Eq. (1.18),  $V^{\text{HF}}(i)$  symbolizes the Hartree-Fock potential which could be defined as the average potential experienced by the  $i^{\text{th}}$  electron due to the remaining electrons. Thus, in the HF method, the elaborated many-electron problem is replaced by a one-electron problem where the electronic interaction is considered in an average way. Generally, the HF potential of a particular electron (1) depends on the spin orbitals of the remaining electrons; hence it can be denoted as,

$$V^{\text{HF}}(1) = \sum_j^N (J_j(1) - K_j(1)) \quad (\text{Eq. 1.19})$$

where the term  $J_j$  is the coulomb operator which comprises the coulombic repulsion between the electrons and  $K_j$  is the exchange operator which characterizes the quantum correlation due to the Pauli's exclusion principle. The coulomb and exchange operators can be written as given below.

$$J_i(1) = \int d\mathbf{x}_2 |\chi_j(2)|^2 \frac{1}{r_{12}} \quad (\text{Eq. 1.20})$$

And

$$K_j(1)\chi_i(1) = \left[ \int d\mathbf{x}_2 \chi_j(2) \frac{1}{r_{12}} \chi_i(2) \right] \chi_j(1) \quad (\text{Eq. 1.21})$$

In closed-shell molecules or atoms, Roothaan and Hall introduced a single matrix form named Roothaan equations for solving the HF equation.<sup>252, 253</sup> It is a representation of HF equation in a non-orthonormal basis set and commonly known as Restricted Hartree-Fock theory. It is independently established in 1951 by Clemens C. J. Roothaan and George G. Hall, henceforth it is also named as Roothaan-Hall equations. According to Roothaan equations, the HF equation (Eq. 1.17) is rewritten by

substituting the unknown molecular orbitals  $\Psi_i$  (Eq. 1.22) as a linear combination of known basis functions  $K$  and leads to (Eq. 1.23).

$$\Psi_i(\mathbf{r}) = \sum_{\mu=1}^K C_{\mu i} \varphi_{\mu}(\mathbf{r}) \quad \text{Where } i=1, 2, 3, \dots, K \quad (\text{Eq. 1.22})$$

$C_{\mu i}$  are the coefficients of  $\varphi_{\mu}$ , and  $K$  is the total number of basis functions. Thus Roothaan-Hall equation for closed-shell systems can be written in a single matrix form as:

$$\mathbf{FC} = \mathbf{SC}\boldsymbol{\varepsilon} \quad (\text{Eq. 1.23})$$

where  $\boldsymbol{\varepsilon}$ ,  $\mathbf{S}$ ,  $\mathbf{F}$  are orbital energies, overlap matrix, and Fock matrix, respectively. In the equation, Fock matrix is the matrix representation of Fock operator (Eq. 1.18) in the basis function  $\Phi_{\mu}$ . Further, to determine the eigen values from the Roothaan-Hall equation, the unknown molecular orbital coefficients which could be obtained from diagonalization of the Fock matrix have been used.

The major limitation observed with the HF method relates to electron correlation, which is ignored in HF theory formulated using Roothaan approach. Even if the electron correlation is exceedingly small, it has large deviations from experimental results. To overcome this weakness several post-Hartree Fock method has been explored.

### 1.2.1.2 Post-Hartree-Fock methods

Post-Hartree-Fock methods are generally developed to improve the limitations of the HF method or self-consistent field (SCF) method. The major problem with HF method is that it does not consider the electronic correlation/repulsion between the electrons while the average repulsions are only considered.<sup>254</sup> Therefore, to correct the limitations of the HF method, Post Hartree-Fock methods add electron correlation which can be considered as the most accurate way of comprising electronic repulsions. The electron correlation energy,  $E_{corr}$  is calculated by subtracting the energy in Hartree-Fock limit ( $E_{HF}$ ) from the exact nonrelativistic energy of the system ( $\varepsilon_0$ ).

$$E_{Corr} = \varepsilon_0 - E_{HF} \quad (\text{Eq. 1.24})$$

Generally, post-Hartree-Fock methods give more precise results than the HF method, the accuracy is good with the price of added computational cost. The major post Hartree-Fock methods are Møller-Plesset perturbation theory MP<sub>n</sub> (where n is the order of correlation),<sup>255, 256</sup> configuration interaction (CI),<sup>257</sup> coupled-cluster theory,<sup>258</sup> and multi-configurational self-consistent field (MCSCF).

#### 1.2.1.2.1 Møller-Plesset perturbation theory

Møller-Plesset perturbation (MP) theory, established in 1934 by Christian Møller and Milton S. Plesset is a quantum chemistry Post-Hartree-Fock *ab initio* method.<sup>256</sup> Being a Post-Hartree-Fock method, MP theory rectified the limitation of HF theory by incorporating electron correlation (called perturbation) to the HF Hamiltonian. Since the calculation involved in Møller-Plesset is not variational, the energy obtained may be lower than the true ground state energy. Thus, the actual Hamiltonian operator in MP theory becomes:

$$H = H_0 + \lambda V \quad (\text{Eq. 1.25})$$

where  $\lambda$  is an arbitrary real parameter that controls the size of the perturbation. The term  $H_0$  denotes the unperturbed Hamiltonian operator and  $V$  is the perturbation. In this theory, the difference between the exact Hamiltonian and the Fock operator is considered as the perturbation.<sup>255, 256</sup> It can be seen that the first MP energy as zero ( $E_{\text{MP1}} = 0$ ), hence total energy looks like that obtained from HF method. Hence a meaningful amount of electronic correlation is added by using MP2 energy. Third-order (MP3) and fourth-order (MP4) calculations are also frequently used in small systems while higher-level MP calculations, especially (MP5) are possible only in few computational chemistry codes. Among the MP<sub>n</sub> methods, MP2 are the most popular, and those MP calculations are restricted to a single point where the geometry optimization is performed at a lower level of theory as the expensive computational cost.<sup>256, 259, 260</sup>

#### 1.2.1.2.2 Configuration interaction (CI) method

*Ab initio* method in which excited and transition state properties are solved to describe the electronic state is called configuration interaction method. In this

method, configuration of the electron can be expressed as a linear combination of Slater determinants and the term interaction implies the mixing of different electronic configurations.<sup>261</sup> Also, interaction among the electronic configurations can be solved using a variational wave function that can be written as a linear combination of configurational state functions (CSFs) resulting from spin orbitals; hence CI wave function can be written as:

$$|\Phi_0\rangle = C_0 |\Psi_0\rangle + \sum_{ar} C_a^r |\Psi_a^r\rangle + \sum_{\substack{a<b \\ r<s}} C_{ab}^{rs} |\Psi_{ab}^{rs}\rangle + \sum_{\substack{a<b<c \\ r<s<t}} C_{abc}^{rst} \Psi_{abc}^{rst} + \dots \quad (\text{Eq. 1.26})$$

The first term in the above equation represents the Slater determinant corresponding to the HF wave function, and the remaining terms create singly, doubly, triply, etc. excited determinants with appropriate expansion coefficients. Occupied orbitals are denoted as  $a, b$ , etc. indices, whereas orbitals involved in the electron excitations are represented as  $r, s$ , etc. Depending on the number of electronic excitations involved, the number of newly constructed determinants may vary. As per the number of excitations, CI methods are classified as configuration interaction single-excitation (CIS), single and double excited CI method (CISD), triple (CISDT) and quadruple (CISDTQ) excitation calculations.<sup>262</sup> Here triple and quadruple excitations are used only when extremely high accuracy is required. If only one spin-orbital differs, we describe this as a single excitation determinant. If two spin orbitals differ, it is a double excitation determinant and so on. It is noted that truncating the CI space as in CID, CISD, etc. will reduce the computational cost by limiting the electronic excitations. For example, in CID, the excitation is limited to double, while in CISD the excitation is limited to single and double. In full CI method, all possible excitations are permitted and hence accuracy and computational cost increases.<sup>245, 263</sup>

### 1.2.1.2.3 Multi-configurational self-consistent field (MCSCF)

We know that in CI method SCF wavefunction is used for constructing the configuration state function. While in MCSCF, we can use multiple determinants for constructing the wavefunctions, gives the most accurate result with a given computational cost. It has been generally used to create qualitatively correct reference states of molecules where HF and DFT are inadequate.<sup>264</sup> However, for



doing calculations, this method requires technical support from the user. We have to find which molecular orbits are to be used and there should be a correlation between bonding and antibonding orbits. Also, we can consider a combination between CI (Where the molecular orbitals are not varied, but the expansion of the wave function) and HF (there is only one determinant, but the molecular orbitals are varied). Consequently, MCSCF wavefunctions are generally used as a reference state for multiconfiguration-reference configuration interaction (MRCI)<sup>262</sup> or multi perturbation theory called complete active space perturbation theory (CASPT2). These methods can be used in an accurate way for the study of ground and excited state properties, where other all methods fail, rarely computed due to the demand of massive amount of computational cost.

#### 1.2.1.2.4 Coupled cluster (CC) theory

Whenever high accuracy is required, the coupled-cluster method (CC method) has been extensively used for the computation of atomic and molecular electronic structure, which includes calculations in excited state properties. As a post-Hartree Fock method, CC comprises electron correlation and enables efficient, accurate, and size-extensive solution of electronic Schrödinger equation. This method was initially used in the 1950s for many-body quantum systems in nuclear physics, latter Cizek (1966) and Paldus (1991) initiated those calculations in quantum chemical calculations.<sup>265</sup> In CC theory method, the Schrödinger equation has been reformulated as a non-linear equation by parametrization *via* an exponential excitation operator.<sup>266</sup> The wavefunction for a multielectron system can be formulated by the operation of an exponential operator (T) on a single determinant. Moreover, it is the perturbation variant of many-electron theory (MET), consequently, the solution derived from this method is exact. Comparing with MET, CC theory is somewhat simpler and gives highly accurate results. Depending on the highest number of allowed electronic excitations in the cluster operator (T), it is classified as CCSD, CCSD(T), and CCSDTQ, where S, D, T, and Q stand for singles, doubles, triples, and quadruples excitations, respectively. Thus, the cluster operator (T) for CCSD (T) can be written as:

$$T = T_1 + T_2 + T_3 \quad (\text{Eq. 1.27})$$

In (Eq. 1.27),  $T_1, T_2, T_3$  denote the operators of all single, double, and triple excitations. Also in the notations, the terms in the round bracket indicate that the contributions from those excitations can be calculated using many-body perturbation theory.<sup>245</sup>

### 1.2.2 Semiempirical methods

Semiempirical methods are based on HF method, which holds the position between *ab initio* method and molecular mechanics.<sup>267</sup> It is noted that *ab initio* method gives highly accurate results as experiments for the heat of formation, whereas moderate accuracy is given for molecular structure determination. The excited properties are also determined by *ab initio* method where the cost in terms of computational resource is the key concern. MM methods are extremely fast and handle big systems, but those methods are not adequate to represent the geometries involved in bond-breaking and bond-making processes. Here comes the importance of semiempirical methods. As in molecular mechanics, the semi-empirical method employs empirical parameters, and it is quantum chemical in nature as *ab initio*. In semiempirical methods, the extensive use of approximations allows us to study bulkier systems where the full HF method without approximation is too costly. In this approximation, the electrons which are not effectively involved in chemical reactions are not considered for Hamiltonian calculation, therefore reduces the complexity of the calculation (inclusion of electron correlation), and found to be effective in larger systems. If there are  $N$  orbitals involved in the calculation, then the two-electron repulsion integral scales as  $N^4$ , whereas by applying approximation the repulsion integrals are reduced to  $N^2$ , thereby simplifies the calculation.

Basically, to reduce the complexity of computation, semiempirical methods use three approximations *viz.* the elimination of the core electrons from the calculation, the use of a minimum number of basis sets, and the reduction of two-electron repulsion integral. One of the first semiempirical method called CNDO/2 (complete neglect of differential overlap) is introduced by John Pople where core approximation and zero-differential overlap (ZDO) have been considered.<sup>268</sup> INDO (Intermediate neglect of differential overlap), and NDDO (Neglect of Diatomic Differential Overlap) - the most successful basis of the modern semiempirical method are the other two methods proposed by John Pople. Later in 1977, Michael Dewar and Walter Thiel

proposed modified Neglect of Diatomic Overlap, MNDO where parameters are assigned for different orbit types and such kinds of approximations could reproduce properties such as dipole moments, heat of formation, geometric variables, etc. Current MNDO methods are Austin Model 1 (AM1) by Dewar and co-workers, and Parametric Method 3 (PM3) by James Stewart. In AM1, a similar approach to MNDO is considered along with a modified expression for nuclear-nuclear core repulsion. In PM3, a similar Hamiltonian that of AM1 has been used while the slightly different nuclear repulsion parameterization strategy improves the accuracy of thermochemical predictions.<sup>269</sup> Another MNDO method is PDDG/PM3 (Pairwise Distance Directed Gaussian) which is suitable for calculating intermolecular interactions. The reparameterization improves the accuracy for determining the heat of formation, however, the common limitations in NDDO remain unchanged like calculation of conformational energies, activation barriers, and description of radicals, etc.<sup>270</sup>

### **1.2.3 Density functional theory (DFT)**

Density Functional Theory (DFT) has been used for the investigation of the electronic structure of many-body systems and has revolutionized the quantum-chemical development of the last 30 years. Since 1970, DFT method was incredibly famous for calculations in solid physics, latter 1990s, this method attains enough accuracy in quantum chemistry calculation where it uses better model exchange and correlation interactions.<sup>271, 272</sup> In DFT, functions of another function (functionals) has been used for calculating the properties of many-electron system without considering the higher-order parameters (fundamental material parameters). In DFT, to compute the ground state energy of a many-electron system, we do not consider the  $3N$  coordinates of the wavefunction, rather we can consider the one variable called the density of electron in terms of 3 coordinates, which reduces the complexity in the calculation for large systems. According to DFT, the energy of the electronic system can be calculated from electron density  $\rho(\mathbf{r})$ , which is the function of space and time rather than wavefunction (which is used in HF theory), and the integration of electron density over all space gives the total number of electrons,  $N$ .<sup>273</sup>

$$N = \int \rho(\mathbf{r}) d\mathbf{r} \quad (\text{Eq. 1.28})$$

In the modern DFT method, the total energy of the molecular system can be calculated using electronic potential acting on the molecular system, which could be constructed as the sum of external potentials  $V_{\text{ext}}$  (depends on the structure and the elemental composition of the system) and effective potential  $V_{\text{eff}}$  (represents the interelectronic interactions). Thus, a system of ' $n$ ' electrons can be written as a set of ' $n$ ' one-electron Schrödinger-like equations called Kohn–Sham equations.

### 1.2.3.1 Thomas Fermi model

DFT, which is originated from Thomas–Fermi (TF) model for the electronic structure of many-body systems was developed shortly after the invention of the Schrödinger equation in 1927.<sup>274-276</sup> According to this model, an electronic state of a uniform electron gas is assumed to be a solution of the Schrödinger equation based on electron density.<sup>277</sup> That is, if the electrons in a solid crystal are distributed uniformly and there is no external magnetic field, then the external potential (corresponds to the nuclear–electron interaction potential) depends only on the distances from the nuclei, and thus it can be calculated from the nuclear charge and electron density. Consequently, the kinetic energy functional of the electron density in TF model,  $T_{\text{TF}}[\rho(\mathbf{r})]$  is formulated as:

$$T_{\text{TF}}[\rho(\mathbf{r})] = \frac{3}{10} (3\pi^2)^{2/3} \int (\rho)^{5/3}(\mathbf{r}) d\mathbf{r} \quad (\text{Eq. 1.29})$$

The total energy in terms of electron density can be expressed by incorporating the interaction between electron-nucleus and electron-electron as follows:

$$E[\rho(\mathbf{r})] = \frac{3}{10} (3\pi^2)^{2/3} \int d\mathbf{r} \rho^{5/3}(\mathbf{r}) - Z \int \frac{\rho(\mathbf{r})}{r} d\mathbf{r} + \frac{1}{2} \iint \frac{\rho(\mathbf{r}_1)\rho(\mathbf{r}_2)}{|\mathbf{r}_1 - \mathbf{r}_2|} d\mathbf{r}_1 d\mathbf{r}_2 \quad (\text{Eq. 1.30})$$

In the above equation, the second and third terms correspond to electron-nucleus interaction and electron-electron interactions, respectively. Although the method provides an interesting theory for representing the Hamiltonian as a function of electron density, the accuracy of the method is not reliable. Since the method does not consider the exchange energy of an atom, the resulting kinetic energy function

becomes approximate. Later in 1928 Paul Dirac added exchange-energy functional, however, the accuracy remained unaltered.

### 1.2.3.2 Hohenberg-Kohn theorems

The limitations of Thomas–Fermi model has been reviewed in 1964 by a theorem called, Hohenberg-Kohn (HK) theorems.<sup>278</sup> The theorems can be applied to any system having electrons moving in presence of an external magnetic field. According to the first HK theorem, external potential can be considered as a unique functional of electron density and states that ground-state density exclusively predicts all the properties of a many-electron system. The second HK theorem states that, if the input electron density is true, the functional delivers ground state energy of the system gives the lowest energy. Since those two theorems were proven mathematically, they can be considered as the basics of DFT method. According to the theorems, the energy functional  $E[\rho(\mathbf{r})]$  can be determined from the ground state density and could be calculated as the sum of two terms as follows:

$$E[\rho(\mathbf{r})] = \int V_{ext}(\mathbf{r})\rho(\mathbf{r})d\mathbf{r} + F[\rho(\mathbf{r})] \quad (\text{Eq. 1.31})$$

In the above equation, the first term represents the interaction of the electrons with an external potential  $V_{ext}(\mathbf{r})$  typically due to the coulomb interaction with the nuclei, and the second term denotes the universal function of electron density  $F[\rho(\mathbf{r})]$ . To obtain minimum energy, a Lagrangian multiplier,  $\mu$  (electronic chemical potential) can be introduced as:

$$\left( \frac{\delta E[\rho(\mathbf{r})]}{\delta \rho(\mathbf{r})} \right)_{V_{ext}} = \mu \quad (\text{Eq. 1.32})$$

The Eq. (1.32) is the DFT equivalent of Schrödinger equation. Also, it has been found that HK theorems lack accurate approximations for ground-state density  $F[\rho(\mathbf{r})]$ . In practice, computation of energy of the interacting electron is not exactly accurate with HK theorem.

### 1.2.3.3 Kohn-Sham equations

In 1965 Kohn and Sham reconstructed the DFT into a practical electronic structure theory. Hohenberg-Kohn theorem fails to provide a way of finding the ground state

density or kinetic energy of the system. To address this problem, Kohn-Sham proposed an alternative approach where a fictitious non-interacting system is constructed and assumes that the density of this fictitious system is same as that of interacting electrons.<sup>279</sup> Thus Kohn-Sham Equations are focused on the outcome of a fictitious system of non-interacting electrons, the energy functional  $E[\rho(\mathbf{r})]$  can be written as a combination of three terms as follows

$$E[\rho(\mathbf{r})] = E_{KE}[\rho(\mathbf{r})] + E_H[\rho(\mathbf{r})] + E_{XC}[\rho(\mathbf{r})] \quad (\text{Eq. 1.33})$$

where the terms  $E_{KE}[\rho(\mathbf{r})]$ ,  $E_H[\rho(\mathbf{r})]$ , and  $E_{XC}[\rho(\mathbf{r})]$  denote kinetic energy of non-interacting electrons, Hartree electrostatic energy of the electrons and the contributions of exchange and correlation to energy, respectively. Here the first two terms in (Eq. 1.33) can be rewrite as

$$E_{KE}[\rho(\mathbf{r})] = \sum_{i=1}^N \int \Psi_i(\mathbf{r}) \left( -\frac{\nabla^2}{2} \right) \Psi_i(\mathbf{r}) d\mathbf{r} \quad (\text{Eq. 1.34})$$

$$E_H[\rho(\mathbf{r})] = \frac{1}{2} \iint \frac{\rho(\mathbf{r}_1) \rho(\mathbf{r}_2)}{|\mathbf{r}_1 - \mathbf{r}_2|} d\mathbf{r}_1 d\mathbf{r}_2 \quad (\text{Eq. 1.35})$$

By substituting Eq. (1.34) and Eq. (1.35) in Eq. (1.33), the full expression for energy functional  $E[\rho(\mathbf{r})]$  becomes:

$$E[\rho(\mathbf{r})] = \sum_{i=1}^N \int \Psi_i(\mathbf{r}) \left( -\frac{\nabla^2}{2} \right) \Psi_i(\mathbf{r}) d\mathbf{r} + \frac{1}{2} \iint \frac{\rho(\mathbf{r}_1) \rho(\mathbf{r}_2)}{|\mathbf{r}_1 - \mathbf{r}_2|} d\mathbf{r}_1 d\mathbf{r}_2 + E_{XC}[\rho(\mathbf{r})] - \sum_{A=1}^M \int \frac{Z_A}{|\mathbf{r} - \mathbf{R}_A|} \rho(\mathbf{r}) d\mathbf{r} \quad (\text{Eq. 1.36})$$

where the contribution of exchange and correlation to energy is defined as the difference between the exact and non-interacting kinetic energy of the system along with the contribution due to exchange and correlation. As per the theorem, the electron density of an N electron system can be defined as the sum of the square moduli of N one-electron orbitals:

$$\rho(\mathbf{r}) = \sum_{i=1}^N |\Psi_i(\mathbf{r})|^2 \quad (\text{Eq. 1.37})$$

By using the expression for entire electron density (Eq. (1.37) and appropriate variational theorem, we can solve the Schrödinger equation for each one-electron Kohn-Sham equation as:

$$\left\{ -\frac{\nabla_1^2}{2} - \left( \sum_{A=1}^M \frac{Z_A}{r_{1A}} \right) + \int \frac{\rho(\mathbf{r}_2)}{r_{12}} d\mathbf{r}_2 + V_{xc}[\mathbf{r}_1] \right\} \Psi_i(\mathbf{r}_1) = \varepsilon_i \Psi_i(\mathbf{r}_1) \quad (\text{Eq. 1.38})$$

where  $\varepsilon_i$  represents the molecular orbital energies, and  $V_{xc}$  is the exchange-correlation functional which is related to exchange-correlation energy as

$$V_{xc}[\mathbf{r}] = \frac{\delta E_{xc}[\rho(\mathbf{r})]}{\delta \rho(\mathbf{r})} \quad (\text{Eq. 1.39})$$

Unfortunately, in the Kohn–Sham approach, the exchange-correlation potential and corresponding exchange-correlation energy are the two unknown terms included in the calculation of total energy. Since  $E_{xc}$  is not known exactly, which has to be solved for the practical applications of DFT. To address the problem, several approximations have been introduced and which are discussed in the next section.

### 1.2.3.4 Exchange-correlation functionals

For the practical application of Kohn–Sham approach, we have to address the solution for exchange-correlation energy  $E_{xc}$ . However, in a closed mathematical form, the solution for the problem is not exactly known yet. Thus, from the beginning stage itself, DFT methods have been used several approximations for  $E_{xc}$ . By this time, several approximated functionals have been introduced with varying levels of complexity and Perdew proposed a useful way of categorizing complexity known as “Jacob’s ladder.”<sup>280</sup> (Figure 1.14)

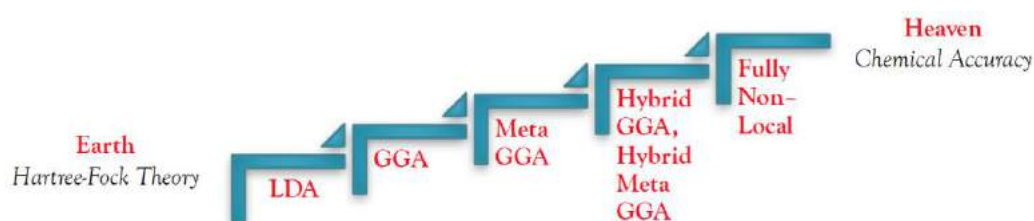


Figure 1.14 Schematic diagram of “Jacob’s ladder” of exchange exchange-correlation functionals proposed by J. P. Perdew.<sup>281</sup>

The exchange-correlation energy,  $E_{XC}$  can be expressed as a sum of two terms, one exchange term  $E_X$  (associated with the interaction of electrons of the same spin) and a correlation term  $E_C$  (associated with the interaction of electrons of opposite spin). The corresponding functionals are exchange functional and correlation functional, respectively. Thus, we can write exchange correlation functional as:

$$E_{XC}[\rho(\mathbf{r})] = E_X[\rho(\mathbf{r})] + E_C[\rho(\mathbf{r})] \quad (\text{Eq. 1.40})$$

The functional dependence of  $E_{XC}$  on electron density can be written as:

$$E_{XC}[\rho(\mathbf{r})] = \int \rho(\mathbf{r}) \varepsilon_{XC}[\rho(\mathbf{r})] d\mathbf{r} \quad (\text{Eq. 1.41})$$

where  $\rho(\mathbf{r})$  and  $\varepsilon_{XC}$  represent electron density and energy density, respectively. Finally, for the practical application of DFT, approximations for  $E_{XC}$  functionals are introduced and the most common types of exchange-correlation functionals are discussed below.

#### 1.2.3.4.1 Local density approximation (LDA)

Local density approximation (LDA) is the simplest known density functional approach where the approximations are derived from homogenous electron gas. In this regard, a heterogeneous system is divided into infinitesimal volumes, and electron density in each volume can be taken as constant. Based on this assumption, the obtained exchange-correlation energy from each volume is assumed to be the exchange-correlation energy of a homogeneous electron gas of the same density. The expression for exchange energy can be written as<sup>282</sup>:

$$E_X^{\text{LDA}}[\rho(\mathbf{r})] = -\frac{3}{4} \left( \frac{3}{\pi} \right)^{1/3} \int \rho^{4/3}(\mathbf{r}) d\mathbf{r} \quad (\text{Eq. 1.42})$$

It is noted that the calculation of correlation energy is more complicated and which leading to numerous different approximations.<sup>283</sup> The analytical expression for correlation energy is available in low- and high-density limits and hence for the full range of densities many-body perturbation theories have been proposed, more accurate results are obtained from quantum Monte Carlo simulations.<sup>284</sup>



### 1.2.3.4.2 Generalized gradient approximation (GGA)

In generalized gradient approximation methods, the exchange-correlation potential depends on the electron density and its gradient  $\vec{\nabla} \rho(\mathbf{r})$ . So, there is a significant improvement in the accuracy by GGA than LDA.<sup>285</sup> The general form of exchange-correlation energy obtained from GGA is:

$$E_{XC}[\rho_{\alpha}(\mathbf{r}), \rho_{\beta}(\mathbf{r})] = \int \varepsilon_{XC}(\rho_{\alpha}(\mathbf{r}), \rho_{\beta}(\mathbf{r}), \vec{\nabla} \rho_{\alpha}(\mathbf{r}), \vec{\nabla} \rho_{\beta}(\mathbf{r})) d^3\mathbf{r} \quad (\text{Eq. 1.43})$$

The GGA functionals are made by adding a correction term to the LDA functionals. These methods have followed two main lines: the first one is the numerical fitting procedures proposed by Becke. And the second group of GGA has been developed by Perdew which is a more rational-based one and gives importance to the development of exchange-correlation functionals.<sup>286</sup> The popular examples of GGA functionals include Becke88 (B88),<sup>287</sup> Perdew 86,<sup>288</sup> Perdew-Wang 91 (PW91),<sup>289</sup> Perdew-Burke-Ernzerhof (PBE),<sup>290</sup> and Lee-Yang-Par (LYP).<sup>287, 291</sup>

### 1.2.3.4.3 Meta GGA

Meta GGA functionals are known as third-generation functionals and they used second-order derivatives of density and kinetic energy densities as additional degrees of freedom to offer enhanced performance over LDA and GGA.<sup>292, 293</sup> The highly parameterized approximate functionals developed by Truhlar and coworkers named Minnesota is based on meta GGA functional. In Minnesota functionals, there are different family of functionals, published in different years starting from 2005 to 2015.<sup>294, 295</sup>

### 1.2.3.4.4 Hybrid density functional (H-GGA)

These are fourth-generation functionals in which “exact exchange” extracted from HF exchange energy has been included as a functional of the Kohn-Sham molecular orbitals. By adding HF exchange energy with DFT exchange-correlation, H-GGA shows a significant improvement over GGA and hence widely used in quantum chemical calculations. The most widely used H-GGA functional is B3LYP, where to control the mixing of HF exchange 3-parameters are employed.<sup>296</sup> The other examples are B3P86, B3PW91, B97-1, MPWB1K, and X3LYP. Another new class of exchange correlational

functionals is Hybrid-meta GGA (HM-GGA), these depend on HF exchange, electron density, the gradient of electron density, and the kinetic energy density. HM-GGA methods are similar to H-GGA, and the only difference that occurs is that they start from meta GGA as a substitute for GGA.<sup>286</sup> The main outcome of these functionals is the improvement in the determination of barrier heights and atomization energies. The examples for HM-GGA methods are B1B95, BB1K, MPW1B95 and TPSS1KCIS. In summary, the performance of H-GGA and HM-GGA is better than GGA and LDA, while the performance of each functional depends on the property under evaluation, and on the type of system under study.

### 1.2.3.5 Dispersion corrections

The long-range van der Waals (vdW) type interactions have significant importance for predicting the electronic structure, stability, and reaction mechanism for a many-electron system. So, in molecules having Van der Waals type interactions, we have to incorporate dispersion corrections to the KS-DFT functionals (exchange-correlation functional).<sup>297-299</sup> According to this principle the total energy of the system can be represented as:

$$E_{DFT-D} = E_{KS-DFT} + E_{disp} \quad (\text{Eq. 1.44})$$

The mathematical expression for dispersion energy can be expressed as:

$$E_{disp} = -S_6 \sum_{i=1}^{N_{at}-1} \sum_{j=i+1}^{N_{at}} \frac{C_6^{ij}}{R_{ij}^6} f_{dmp}(R_{ij}) \quad (\text{Eq. 1.45})$$

In the above equation  $N_{at}$  denotes the number of atoms in the system,  $S_6$  is a global scaling factor that depends on the used dispersion function.  $C_6^{ij}$  represents the dispersion coefficient for an atom pair  $ij$ .  $R_{ij}$  is the interatomic distance, and  $f_{dmp}$  is the damping function that must be used to avoid near-singularities for small interatomic distances.

### 1.2.3.6 Time-Dependent density functional theory (TD DFT)

Time-dependent density functional theory is used for the study of excited-state properties of many-electron systems in the presence of time-dependent potentials,

such as electric or magnetic fields.<sup>300-302</sup> It extends the basic ideas of ground-state properties formulated by DFT to excitations. The approach is same as DFT and the only variable involved in this approach is electron density which is a function of space and time.<sup>303</sup> In TD DFT, density has been obtained from the fictitious non-interacting system named Kohn-Sham system, and the final analytical expression for the time-dependent variant of effective potential called Kohn-Sham potential can be obtained by several sophisticated approximations.<sup>304</sup>

The basics of TD DFT calculation has been published in 1984 by Erich Runge and Eberhard K. U and known as Runge-Gross (RG) theorem.<sup>302</sup> The RG theorem can be considered as the analogue of HK theorem in DFT. It suggests Hamiltonian in presence of time-dependent function as:

$$\hat{H}(\{\mathbf{r}\}, t) = \hat{T}(\{\mathbf{r}\}) + \hat{W}(\{\mathbf{r}\}) + \hat{V}_{ext}(\{\mathbf{r}\}, t) \quad (\text{Eq. 1.46})$$

Here the first two terms *viz.*  $\hat{T}$  and  $\hat{W}$  symbolise kinetic energy of electrons, and electronic interactions, respectively. The last term  $\hat{V}_{ext}$  represents the external potential which defines the electrons' interaction with the nuclei of the system. In the case of non-trivial time-dependence, an additional explicitly time-dependent potential can also exist from a time-dependent electric or magnetic field. In general, the time-dependent many-body Schrödinger equation is,

$$i \frac{\partial \Psi}{\partial t}(\{\mathbf{r}\}, t) = H(\{\mathbf{r}\}, t) \Psi(\{\mathbf{r}\}, t) \quad (\text{Eq. 1.47})$$

where  $H$  is the Hamiltonian operator which has a general form given in Eq. (1.47). As RG theorem,<sup>302</sup> by starting from the Schrödinger equation, we can calculate electron density, from which we can determine the external potential. Also, it is noted that the absolute square of wavefunction  $|\Psi(\{\mathbf{r}\}, t)|^2$ , probability of finding the electron at position  $\mathbf{r}$ , takes the form:

$$\rho(\mathbf{r}, t) = N \int d^3\mathbf{r}_2 \dots d^3\mathbf{r}_N |\Psi(\mathbf{r}_1, \mathbf{r}_2, \dots, \mathbf{r}_N, t)|^2 \quad (\text{Eq. 1.48})$$

Unfortunately, RG theorem failed to suggest how to calculate that valuable quantity named electron density. To address this problem, Kohn-Sham utilized a fictitious system of non-interacting systems, subject to an external potential. In this approach,

the electron density obtained from the fictitious non-interacting system is taken as the density of the original interacting system. In time-dependent case, the fictitious systems obey the time-dependent Schrödinger equation, and density obtained from the time-dependent Kohn-Sham (KS) orbital is represented as:

$$\rho(\mathbf{r}, t) = \sum_{i=1}^N |\varphi_i(\mathbf{r}, t)|^2 \quad (\text{Eq. 1.49})$$

In this approach, kinetic energy of the non-interacting system can be calculated and the only problem raised is the determination of external potential  $V_{ext}(\mathbf{r}, t)$ . So, to calculate  $V_{ext}(\mathbf{r}, t)$ , the time-dependent KS potential can be written as<sup>279</sup>

$$v_{KS}[\rho](\mathbf{r}, t) = v_{ext}(\mathbf{r}, t) + v_{Hartree}[\rho](\mathbf{r}, t) + v_{xc}[\rho](\mathbf{r}, t) \quad (\text{Eq. 1.50})$$

The first term in (Eq. 1.50) denotes the external potential and the second term, the Hartree potential constitutes the classical electrostatic interaction between the electrons. The Hartree potential can be rewrite as:

$$v_{Hartree}[\rho](\mathbf{r}, t) = \int d^3 \mathbf{r}' \frac{\rho(\mathbf{r}', t)}{|\mathbf{r} - \mathbf{r}'|} \quad (\text{Eq. 1.51})$$

The last term in the expression (Eq. 1.51) represents the exchange-correlation potential, which constitutes all properties of a many-electron system. As ground-state DFT, the exact solution for  $V_{xc}$  as a functional of the density is unknown, and to obtain an appropriate solution for  $V_{xc}$  several approximations have been proposed. Comparing with ground-state DFT, the approximation methods are still in the first phase and the simplest approximation is the adiabatic local density approximation (ALDA), which is analogues to LDA in DFT. ALDA assumes that xc at  $(\mathbf{r}, t)$  is equivalent to the xc potential of a homogeneous electron gas and retains all the faintness of the LDA approximation. Even though it suffers drawbacks, ALDA-based exchange correlational functionals is the most widely used approximation approach and it executes well to define features like excitation energies.<sup>305</sup> The interests in developing xc functionals are continuing with the demand for computational resources. Recently, Nonadiabatic electron dynamics in time-dependent density functional theory has been developed by Gulevich and Zhumagulov, named oscillator model for xc kernels (OMXC). The approach is based on the representation of the frequency-dependent

exchange-correlation kernel, which enables one to replace the costly memory integrals and reduces the computational cost to that of ALDA-based TD DFT.<sup>306</sup>

### 1.2.4 Theoretical methods used in the study

In the thesis, the widely used hybrid GGA density functional, B3LYP is used for the ground state optimization of the systems. In 1993, Axel Becke developed hybrid B3LYP method to investigate the vibrational spectra and circular dichroism.<sup>307</sup> It offers wide range of application in various fields of chemistry and emerged as a standard tool for the estimation of electronic structure analysis of dye-sensitizers. As a hybrid (i.e., mixed) functional, B3LYP has been constructed as a linear combination of exchange or correlational functionals of LDA, GGA and HF exchange energy. It employs three empirical parameters, which regulates the mixing of HF exchange energy ( $E_X^{HF}$ ) and density functional exchange and correlation energies. In B3LYP, the mixing of 5-components such as Hartree-Fock, LDA, Becke88 exchange, VWN and LYP correlations are involved. Here, B3 term denotes Becke -3-parameter and LYP refers Lee-Yang-Parr correlation functional.<sup>308</sup> Thus, the exchange-correlation energy of B3LYP can be written as:

$$E_{XC}^{B3LYP} = (1-a)E_X^{LDSA} + aE_X^{HF} + b\Delta E_X^B + (1-c)E_c^{LDSA} + cE_c^{LYP} \quad (\text{Eq. 1.52})$$

In the above equation (Eq.1.52), Beck 88 and LYP have been used as GGA exchange and correlation functionals. For the evaluation of optical and photovoltaic properties, the long-range corrected TD-CAM B3LYP hybrid functional has been used. It is the most efficient and widely used method for the estimation of excited-state properties and found that range-separated functionals provide better results in optical properties than hybrid or pure functionals.

### 1.2.5 Basis sets

A basis set is a mathematical description of functions called basis functions which in turn are combined to makes molecular orbitals. The basic functions are atomic orbitals which are used to approximate the electronic wavefunction of a molecular system. Consequently, to construct the wavefunction of a molecular system we can use molecular orbital as a function of basis set. The mathematical expression for molecular orbital  $\psi_i$ , as a linear combination of basis functions  $\varphi_j$  is given by

$$\psi_i = \sum_j C_{ij} \varphi_j \quad (\text{Eq. 1.53})$$

In equation (1.53), the constant term ( $C_{ij}$ ) and parameters involved in the basis functions are solved using variational theorem to produce a self-consistent field (SCF) for the electrons. The major types of atomic orbitals involved in quantum chemical calculation are Slater type orbitals, and Gaussian type orbitals. Out of these, Gaussian type orbitals (GTO) are widely used, which can be attributed to the efficient implementations of Post-Hartree-Fock methods. Further for the better approximate wavefunction, we can also use a larger basis set where the cost of computation will be high.

Since hydrogenic basis functions are not sufficient for the description of an atom exactly, a better level atomic orbital named Slater type orbitals (STO) are invented by J. C. Slater.<sup>309</sup> A minimal basis set comprises a minimum number of atomic orbitals needed for the construction of molecular orbital. In STO, the minimal basis set is represented as STO-nG, where  $n$  is an integer and G is a Gaussian type orbital. The mathematical expression for STO is given by:

$$\Phi_{abc}^{\text{STO}}(x, y, z) = Nx^a y^b z^c e^{-\zeta r} \quad (\text{Eq. 1.54})$$

where  $x, y, z$  represents the angular part of the orbital, and  $N$  is a constant called the normalization constant. Further,  $a, b, c$  denotes the components of angular momentum ( $L = a + b + c$ ), and  $\zeta$  is the orbital exponent which determines the width or spread of the orbital. The STO basis sets are highly effective for atoms and diatomic molecules and provide a radial component of orbital function. But for the evaluation of a many-center two-electron system, STO provides complicated calculations. It has been found that STO provides an improvement over hydrogenic orbitals to describe accurate electronic contribution in a molecule, that improvement in computational efficiency in terms of the accurate description of atomic orbital are attained by combining STOs with Gaussian functions.<sup>310-312</sup> In GTOs the dependence of radial part with radius is  $r^2$ , while it is  $r$  in STO. Hence, it is understood that, in all the basis sets, the changes always occur in the radial part and the spherical harmonic functions are

used to describe the angular part of the orbital. Thus, the mathematical expression for GTO<sup>310-312</sup> is:

$$\Phi_{abc}^{\text{GTO}}(x, y, z) = Nx^a y^b z^c e^{-\zeta r^2} \quad (\text{Eq. 1.55})$$

Unfortunately, in Gaussian functions, the exact shape of an atomic orbital cannot be obtained and this could be attained by replacing each STO with several Gaussian functions.<sup>313</sup> These Gaussian functions form primitive Gaussian basis set and the corresponding linear combination of primitive Gaussian functions are known as contracted Gaussian function(CGTO). The Gaussian type orbitals are represented as N-MPG\*, where N represents the number of Gaussian primitives used for each inner-shell orbital. The hyphen denotes a split-basis set where the valence orbitals are double zeta. The terms M and P indicate the number of primitives used for constructing inner (large zeta function), and outer valence (small zeta function) regions. The asterisk to the notation G means that a single set of Gaussian 3d polarization functions is included on heavy atoms. A double asterisk (\*\*) means that a single set of Gaussian 2p functions is included for each hydrogen atom.<sup>313</sup> Another important addition is the diffuse functions that allow electron density to occupy a large area of space. This kind of diffuse functions are significant for the systems having lone pairs, anions, the systems in their excited state, etc.<sup>314</sup> The diffuse functions are generally added by + or ++ signs. These are essential for treating anions and electronegative atoms. The single + version adds the diffuse function to heavy atoms while in the double ++ version, the diffuse function is added to the hydrogen atom.<sup>315</sup>

The majority of quantum chemical calculations employ a contracted GTO (CGTO) set where the optimization of GTO functions with coefficients improves the quality of the basis set.<sup>316-318</sup> Typically, there are two kinds of contractions-segmented contraction and general contraction. The Pople-style basis set families (3-21G, 6-31G,...) and the Karlsruhe basis sets come under segmented contraction, while the correlation-consistent (cc) basis set families by Dunning and co-workers are included in general contracted basis sets. i.e., the quality of basis set can be increased using an increased number of contracted Gaussians. Further, a complete basis set (CBS) which is developed by the systematic increase in the number of basis functions could be able to define the system completely. Dunning's basis sets (cc-pVDZ, cc-pVTZ,

ccpVQZ, etc.) are intended to converge smoothly towards the CBS limit by extrapolation. Those are constructed by adding shells of functions to a core atomic HF function. For example, in cc-pVDZ, 1s, 1p, and 1d functions are added to the core atomic HF function and in cc-pVTZ, an extra f-function is added along with 1s, 1p, and 1d to atomic HF function.<sup>319</sup>

In addition, for reducing the computational cost needed for the calculation on heavier systems such as transition metals, lanthanides, polyatomic molecules, and molecules containing heavy atoms, effective core potentials (ECP) have been used.<sup>320, 321</sup> It is found that heavy metals with large inner electrons require a large set of Gaussians to describe them. This issue can be simplified by introducing effective core potential for the inner electrons, thereby we could eliminate the need for the core basis functions. Here, the replacement of inner core electrons with ECPs treats only the valence electrons explicitly, which are generally involved in bonding. Further, ECPs are also used for representing relativistic effects, which are usually confined with core electrons. Thus, in ECPs both the scalar (spin-free) relativistic effects and spin-orbit (spin-dependent) relativistic effects are included. The frequently used ECPs are Los Alamos National Laboratory (LANL) ECPs and Stuttgart/Cologne ECPs.

The thesis work includes three distinct kinds of basis sets. To construct the basis functions for smaller atoms such as C, H, N, O, F, S, and Cl, Pople basis set 6-31G(d, p),<sup>322</sup> and Dunning's correlation consistent basis set cc-pVDZ have been utilized. To describe transition metal atom Ti, the ECP LANL2DZ is used.

### **1.2.6 Molecular electrostatic potential (MESP)**

The molecular electrostatic potential (MESP) surfaces illustrate the charge distributions in a molecule three-dimensionally as shown in Figure 1.15. This charge distribution gives an overall idea regarding the charged regions in the molecule, thereby gives knowledge regarding the molecular reactivity.<sup>323,324</sup> In typical MESP plots, the red colour regions correspond to high electron density while blue colour regions show low electron density. The intermediate levels have been shown by yellow and green colours. Molecular electrostatic potential (MESP) at a given point  $p(x, y, z)$  in the vicinity of a molecule can be defined as "a force that is acting on a positive test charge (a proton) located at  $p$  through an electron charge cloud



generated by its electron and nuclei.” The concept was introduced by Scrocco and Tomasi, and thereafter it has been emerged as an excellent tool for predicting various

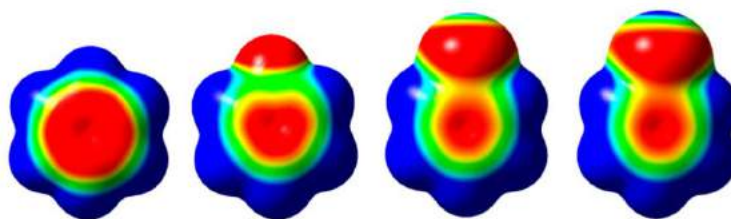


**Figure 1.15** Molecular electrostatic potential surface of benzene, benzene, fluorobenzene, chlorobenzene, and bromobenzene (left to right).<sup>324</sup>

chemical as well as biological properties<sup>325</sup>. The basic principle behind MESP is Coulomb’s law. According to Coulomb’s law, “the force of attraction or repulsion between two point charges is directly proportional to the product of the charge and inversely proportional to the square of the distance between the charges”:

$$F = \frac{q_1 q_2 \hat{r}}{4\pi\epsilon_0 r^2} \quad (\text{Eq. 1.56})$$

where  $q_1$  and  $q_2$  are the two stationary electrically charged particles,  $\hat{r}$  denotes a unit vector joining the position vectors of  $q_1$  and  $q_2$ . ‘ $r$ ’ represents the distance of separation between the point charges  $q_1$  and  $q_2$ , and  $4\pi\epsilon_0$  is the proportionality constant. The electric field,  $E$  produced by a fixed-point charge  $q$  at  $\mathbf{r}$  is given by the equation:

$$E = \frac{q\mathbf{r}}{4\pi\epsilon_0 |\mathbf{r}|^3} \quad (\text{Eq. 1.57})$$

Further, the electrostatic potential,  $V$  at a point  $\mathbf{r}$  in the field generated by a point charge  $q_0$  can be calculated as:

$$V = \frac{q_0}{4\pi\epsilon_0 r} \quad (\text{Eq.1.58})$$

Since the allocation of electric charge generates potential in the surrounding space, the MESP,  $V(r)$  at a point  $r$  around a molecule by its electron and nuclei can be computed as:<sup>326-328</sup>

$$V(r) = \sum_A^N \frac{Z_A}{|\mathbf{r} - \mathbf{R}_A|} - \int \frac{\rho(\mathbf{r}')d^3\mathbf{r}'}{|\mathbf{r} - \mathbf{r}'|} \quad (\text{Eq. 1.59})$$

In the above equation,  $Z_A$  represents the charge on the nucleus  $A$  located at a distance  $\mathbf{R}_A$ ,  $\rho(\mathbf{r}')$  is the electron density, and  $\mathbf{r}'$  is a dummy integration variable. In Eq. 1.61, the first and second terms denote the potential by the bare nucleus and its electron distribution, respectively. Here, the possible net charges finally obtained with  $V(r)$  viz. positive, and negative provide information regarding molecular reactivity. If Both terms in the above equation are positive, that equation follows subtraction, which are generally obtained from three different situations. If the contribution from the two terms is equal, MESP becomes zero. If the first term dominates over the second, MESP will be positive which shows the closeness at the nucleus, while the second term dominates, MESP becomes negative which shows the proximity at lone pair sites,  $\pi$ -bonds, etc. In this regard, the most negative valued MESP minimum denotes electron localization in a molecule, which is known as the electron-rich site.

Further, MESP can be determined experimentally by X-ray diffraction techniques. It is widely used as a tool for determining the active sites in the molecule. For this purpose, the correct position of MESP minimum and corresponding MESP value at that position is essential. For the more precise determination of active site, the topographical analysis of MESP minimum which is based on critical points (CPs) is essential. The CPs define a point at which the partial derivatives of MESP vanishes. In general, a CP can be represented as an ordered pair  $(R, S)$ . Here, rank  $R$  denotes the number of non-zero eigenvalues of the Hessian matrix and signature  $S$  represents the algebraic sum of the signs of these eigenvalues, respectively. The CPs  $(3, +3)$ , and  $(3, -3)$  correspond to MESP minimum ( $V_{\min}$ ), and maximum, respectively. While  $(3, +1)$ , and  $(3, -1)$  denotes saddle points.<sup>326,327,329</sup>

## 1.2.7 Solvation models

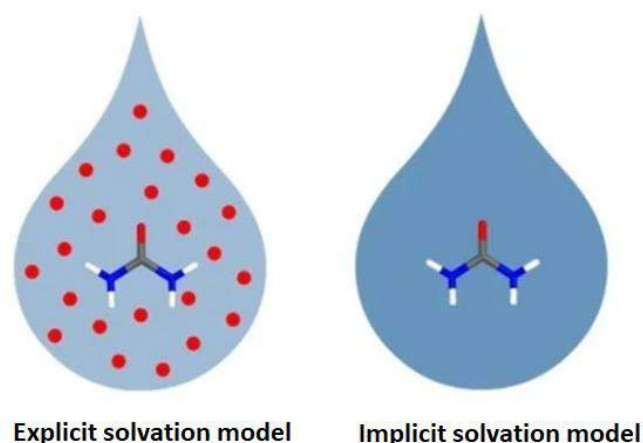


**Figure 1.16** Schematic representations of solvent models.<sup>310</sup>

Surrounding effects are crucial for the successful simulation of the experiment. In computational chemistry, solvation models are used as a computational method which incorporates solvent-effect on the photo-physical properties of molecular systems. The term “solvation” refers the interaction between solvent and solute, which leads to a stable solute-solvent complex formation. The widely used solvation models are: explicit and implicit solvent models (Figure 1.16).<sup>330, 331</sup> In the explicit solvent model, molecular details of each solvent have been considered, shows an accurate simulation of the natural environment. While, if we are considering multiple interaction configurations of each solvent, that model becomes computationally expensive. In the implicit solvent model, solvents are treated as a continuous polarizable medium with a fixed dielectric constant where the solute molecule is kept inside the cavity in the solvent medium. Since it provides a continuous solvent medium instead of individual explicit solvent molecules, it is also named as the continuum solvation model. It is found that the charge distribution and polarizability of a solute have an significant role on static interaction between solute and solvent. In the implicit solvent model, solute polarization in solution has been explained using a concept called reaction field. Further, for the effective description of solute polarization, a method called self-consistent reaction field (SCRF) has been employed for accounting the effect of polarizable medium on a solute system. Depends on the nature of the solvent cavity and reaction field, the SCRF methods are grouped into

two: polarizable continuum model (PCM), and solvation model based on density (SMD).<sup>239,332</sup>

In the polarizable continuum model (PCM), the solvent cavity has been made as a set of interlocking spheres centered on atoms constituting the molecule. It is developed by Tomasi and co-workers.<sup>333-335</sup> In PCM, the free energy of solvation,  $\Delta G_{sol}$  has been calculated as follows:

$$\Delta G_{sol} = \Delta G_{elec} + \Delta G_{disp} + \Delta G_{cav} \quad (\text{Eq. 1.60})$$

where  $\Delta G_{elec}$ , and  $\Delta G_{disp}$ , denote electrostatic solute-solvent interaction, and solute-solvent dispersion interaction and the resulting repulsion, respectively. While  $\Delta G_{cav}$  represents cavitation energy which is vital to create a molecular cavity inside the continuum. There are three variants of PCM are available for analyzing the solvent effect on a chemical system<sup>336</sup> such as dielectric PCM (D-PCM), conductor PCM (C-PCM), and integral equation formalism PCM (IEFPCM). D-PCM is the original method for analysing the solvation effect while in C-PCM, a conductor medium is used for modelling the surrounding instead of the dielectric. In the last one, PCM equations used an integral equation formalism.

Solvation model density (SMD) method is the widely accepted universal model because of its applicability to both charged or neutral solutes in any solvent.<sup>337</sup> In SMD, the electron density of the solute as a whole has been considered for solvent interaction instead of its partial atomic charge. Also, the cavities for the solvent interactions are made by the superpositions of nuclear-centered spheres. In this model, the solvation free energy is calculated as a sum of two main components *viz.* electrostatic term and cavity-dispersion solvent-structure term. The first component arises from the SCRF treatment and contributes the solution for an electrostatic term in terms of IEF-PCM. The second term is the contribution arises from short-range interactions between the solute and solvent molecules in the first solvation shell. This contribution is a sum of terms that are proportional (with geometry-dependent proportionality constants called atomic surface tensions) to the solvent-accessible surface areas of the individual atoms of the solute. In the thesis, SCRF-SMD solvation model is used for computing optical and photovoltaic properties.

## 1.3 Conclusions

The dye-sensitized solar cells are considered as an emerging photovoltaic technique for the ever-growing energy demand. The increased global population in recent years surges the demand for an alternative source of renewable energy like solar energy. In this context, DSSCs have a key role in the production of electrical energy by the effective harvesting of direct sunlight. In the first part of chapter 1, an overview of DSSCs is given. It gives a brief description of the working principle, major components in DSSC, types of dye-sensitizers, the typical structure of dye-sensitizer and its modifications, etc. in detail. The importance of theoretical studies for the design of DSSCs and the theoretical background for the estimation of efficiency of DSSC devices are also comprised in part A of chapter 1.

Nowadays computationally driven dye design strategies for the improved PCE have a vital role in DSSC. It is found that theoretical studies are immensely helpful for the prediction of efficiency and gives an outlook on fundamental photophysical processes involved in DSSC. In part B of chapter 1, an overview on computational chemistry methods is given. It also comprises the basic principles of DFT, and MESP, which has been utilized to compute the electronic effect transmission power of spacers and to quantify the electron-donating strength of donors in dye sensitizers.

## 1.4 References

1. J. Gong, J. Liang and K. Sumathy, *Renew. Sustain. Energy Rev.*, 2012, **16**, 5848-5860.
2. J. Wu, Z. Lan, J. Lin, M. Huang, Y. Huang, L. Fan, G. Luo, Y. Lin, Y. Xie and Y. Wei, *Chem. Soc. Rev.*, 2017, **46**, 5975-6023.
3. V. Smil, *General Energetics*, 1991.
4. Q. Schiermeier, J. Tollefson, T. Scully, A. Witze and O. Morton, *Nature* 2008, **454**, 816-823.
5. A. L. Hammond, *Science*, 1972, **177**, 1088-1090.
6. N. S. Lewis, *science*, 2007, **315**, 798-801.
7. A. Hagfeldt, G. Boschloo, L. Sun, L. Kloo and H. Pettersson, *Chem. Rev.*, 2010, **110**, 6595-6663.
8. G. W. Crabtree and N. S. Lewis, *Phys. Today*, 2007, **60**, 37-42.

9. O. Morton, *Nature*, 2006, **443**, 19-23.
10. M. Becquerel, *Comptes Rendus.*, 1839, **9**, 561-567.
11. J. Wu, Z. Lan, J. Lin, M. Huang, Y. Huang, L. Fan and G. Luo, *Chem. Rev.* , 2015, **115**, 2136-2173.
12. S. Chu and A. Majumdar, *Nature*, 2012, **488**, 294-303.
13. K. Zeng, Z. Tong, L. Ma, W.-H. Zhu, W. Wu and Y. Xie, *Energy Environ. Sci.*, 2020, **13**, 1617-1657.
14. M. A. Green, Y. Hishikawa, E. D. Dunlop, D. H. Levi, J. Hohl-Ebinger and A. W. Ho-Baillie, *Prog. Photovoltaics Res. Appl.*, 2018, **26**, 3-12.
15. L. C. Andreani, A. Bozzola, P. Kowalczewski, M. Liscidini and L. Redorici, *Adv. Phys-X*, 2019, **4**, 1548305.
16. K. Ranabhat, L. Patrikeev, A. Antal'evna-Revina, K. Andrianov, V. Lapshinsky and E. Sofronova, *J. Eng. Appl. Sci.*, 2016, **14**, 481-491.
17. B. O'Regan and M. Grätzel, *Nature*, 1991, **353**, 737-740.
18. S. Chaurasia and J. T. Lin, *Chem. Rec.*, 2016, **16**, 1311-1336.
19. K. E. Jasim, *Dye Sensitized Solar Cells-Working Principles, Challenges and Opportunities*, 2011.
20. N. Anscombe, *Nat. Photonics*, 2011, **5**, 266.
21. K. Kakiage, Y. Aoyama, T. Yano, K. Oya, J.-i. Fujisawa and M. Hanaya, *Chem. Commun*, 2015, **51**, 15894-15897.
22. S. Ardo and G. J. Meyer, *Chem. Soc. Rev.*, 2009, **38**, 115-164.
23. Y. Wu and W. Zhu, *Chem. Soc. Rev.*, 2013, **42**, 2039-2058.
24. M. S. Ahmad, A. K. Pandey and N. Abd Rahim, *Renew. Sustain. Energy Rev.*, 2017, **77**, 89-108.
25. A. Pallikkara and K. Ramakrishnan, *Int. J. Energy Res.*, 2021, **45**, 1425-1448.
26. N. Prabavathy, S. Shalini, R. Balasundaraprabhu, D. Velauthapillai, S. Prasanna and N. Muthukumarasamy, *Int. J. Energy Res.* , 2017, **41**, 1372-1396.
27. H. Tributsch, *Photochem. Photobiol.*, 1972, **16**, 261-269.
28. A. Wibowo, M. A. Marsudi, M. I. Amal, M. B. Ananda, R. Stephanie, H. Ardy and L. J. Diguna, *RSC Adv.*, 2020, **10**, 42838-42859.
29. R. Jose, V. Thavasi and S. Ramakrishna, *J. Am. Ceram. Soc.*, 2009, **92**, 289-301.
30. Q. Wang, S. Ito, M. Grätzel, F. Fabregat-Santiago, I. Mora-Seró, J. Bisquert, T. Bessho and H. Imai, *J. Phys. Chem. B*, 2006, **110**, 25210-25221.

31. W. Hu, L. Li, G. Li, C. Tang and L. Sun, *Cryst. Growth Des.*, 2009, **9**, 3676-3682.
32. B. N. DiMarco, R. N. Sampaio, E. M. James, T. J. Barr, M. T. Bennett and G. J. Meyer, *ACS Appl. Mater. Interfaces*, 2020, **12**, 23923-23930.
33. J. Z. Ou, R. A. Rani, M. H. Ham, M. R. Field, Y. Zhang, H. Zheng, P. Reece, S. Zhuiykov, S. Sriram, M. Bhaskaran, R. B. Kaner and K. Kalantar-zadeh, *ACS nano*, 2012, **6**, 4045-4053.
34. W. Liu, C. Hong, H.-g. Wang, M. Zhang and M. Guo, *Appl. Surf. Sci.*, 2016, **364**, 676-685.
35. P. Guo and M. A. Aegerter, *Thin Solid Films*, 1999, **351**, 290-294.
36. F. Lenzmann, J. Krueger, S. Burnside, K. Brooks, M. Grätzel, D. Gal, S. Rühle and D. Cahen, *J. Phys. Chem. B*, 2001, **105**, 6347-6352.
37. H. Zheng, Y. Tachibana and K. Kalantar-zadeh, *Langmuir*, 2010, **26**, 19148-19152.
38. S. Mahalingam and H. Abdullah, *Renew. Sustain. Energy Rev.*, 2016, **63**, 245-255.
39. S. Gholamrezaei, M. S. Niasari, M. Dadkhah and B. Sarkhosh, *J. Mater. Sci. Mater. Electron.*, 2016, **27**, 118-125.
40. B. Tan, E. Toman, Y. Li and Y. Wu, *J. Am. Chem. Soc.*, 2007, **129**, 4162-4163.
41. D. W. Kim, S. S. Shin, S. Lee, I. S. Cho, D. H. Kim, C. W. Lee, H. S. Jung and K. S. Hong, *ChemSusChem*, 2013, **6**, 449-454.
42. S. Ayneband, E. Nouri, M. Mohammadi and Y. Li, *New J. Chem.*, 2019, **43**, 3760-3768.
43. M. Grätzel, *Acc. Chem. Res.*, 2009, **42**, 1788-1798.
44. P. Semalti and S. N. Sharma, *J. Nanosci. Nanotechnol*, 2020, **20**, 3647-3658.
45. J. Wu, Z. Lan, S. Hao, P. Li, J. Lin, M. Huang, L. Fang and Y. Huang, *Pure Appl. Chem.*, 2008, **80**, 2241-2258.
46. G. Boschloo and A. Hagfeldt, *Acc. Chem. Res.*, 2009, **42**, 1819-1826.
47. G. Boschloo, L. Häggman and A. Hagfeldt, *J. Phys. Chem. B*, 2006, **110**, 13144-13150.
48. N. Kopidakis, N. R. Neale and A. J. Frank, *J. Phys. Chem. B*, 2006, **110**, 12485-12489.
49. C. Teng, X. Yang, C. Yuan, C. Li, R. Chen, H. Tian, S. Li, A. Hagfeldt and L. Sun, *Org. Lett.*, 2009, **11**, 5542-5545.

50. G. Oskam, B. V. Bergeron, G. J. Meyer and P. C. Searson, *J. Phys. Chem. B* 2001, **105**, 6867-6873.
51. P. Wang, S. M. Zakeeruddin, J.-E. Moser, R. Humphry-Baker and M. Grätzel, *J. Am. Chem. Soc.*, 2004, **126**, 7164-7165.
52. M. K. Kashif, J. C. Axelson, N. W. Duffy, C. M. Forsyth, C. J. Chang, J. R. Long, L. Spiccia and U. Bach, *J. Am. Chem. Soc.*, 2012, **134**, 16646-16653.
53. A. Yella, H.-W. Lee, H. N. Tsao, C. Yi, A. K. Chandiran, M. K. Nazeeruddin, E. W.-G. Diau, C.-Y. Yeh, S. M. Zakeeruddin and M. Grätzel, *science*, 2011, **334**, 629-634.
54. F. Bella, C. Gerbaldi, C. Barolo and M. Grätzel, *Chem. Soc. Rev.*, 2015, **44**, 3431-3473.
55. M. Gorlov and L. Kloo, *Dalton Trans.*, 2008, 2655-2666.
56. Y. Ren, Z. Zhang, E. Gao, S. Fang and S. Cai, *J. Appl. Electrochem.*, 2001, **31**, 445-447.
57. W. Kubo, K. Murakoshi, T. Kitamura, S. Yoshida, M. Haruki, K. Hanabusa, H. Shirai, Y. Wada and S. Yanagida, *J. Phys. Chem. B*, 2001, **105**, 12809-12815.
58. Y.-L. Lee, C.-L. Chen, L.-W. Chong, C.-H. Chen, Y.-F. Liu and C.-F. Chi, *Electrochem. commun.*, 2010, **12**, 1662-1665.
59. S. Ito, G. Rothenberger, P. Liska, P. Comte, S. M. Zakeeruddin, P. Péchy, M. K. Nazeeruddin and M. Grätzel, *Electrochem. commun.*, 2006, 4004-4006.
60. H. Wang and Y. H. Hu, *Energy Environ. Sci.*, 2012, **5**, 8182-8188.
61. S. Thomas, T. G. Deepak, G. S. Anjusree, T. A. Arun, S. V. Nair and A. S. Nair, *J. Mater. Chem. A*, 2014, **2**, 4474-4490.
62. G. Yue, J. Wu, Y. Xiao, M. Huang, J. Lin, L. Fan and Z. Lan, *Electrochim. Acta*, 2013, **92**, 64-70.
63. Y. Saito, T. Kitamura, Y. Wada and S. Yanagida, *Chem. Lett.*, 2002, **31**, 1060-1061.
64. L. Bay, K. West, B. Winther-Jensen and T. Jacobsen, *Sol. Energy Mater. Sol. Cells*, 2006, **90**, 341-351.
65. J. N. Clifford, E. Martínez-Ferrero, A. Viterisi and E. Palomares, *Chem. Soc. Rev.*, 2011, **40**, 1635-1646.
66. A. Mishra, M. K. Fischer and P. Bäuerle, *Angew. Chem. Int. Ed.*, 2009, **48**, 2474-2499.



67. Y. Ooyama and Y. Harima, *Eur. J. Org. Chem.*, 2009, **2009**, 2903-2934.
68. J. H. Yum, P. Chen, M. Grätzel and M. K. Nazeeruddin, *ChemSusChem*, 2008, **1**, 699-707.
69. K. Hara, M. Kurashige, Y. Dan-oh, C. Kasada, A. Shinpo, S. Suga, K. Sayama and H. Arakawa, *New J. Chem.*, 2003, **27**, 783-785.
70. J. Preat, D. Jacquemin and E. A. Perpete, *Energy Environ. Sci.*, 2010, **3**, 891-904.
71. W. Sang-aroon, S. Saekow and V. Amornkitbamrung, *J. Photochem. Photobiol. A Chem.*, 2012, **236**, 35-40.
72. P. Li, Z. Wang, C. Song and H. Zhang, *J. Mater. Chem. C*, 2017, **5**, 11454-11465.
73. J. Chen, F.-Q. Bai, J. Wang, L. Hao, Z.-F. Xie, Q.-J. Pan and H.-X. Zhang, *Dyes Pigm.*, 2012, **94**, 459-468.
74. J. Chen, J. Wang, F.-Q. Bai, L. Hao, Q.-J. Pan and H.-X. Zhang, *Dyes Pigm.*, 2013, **99**, 201-208.
75. R. Katoh, A. Furube, T. Yoshihara, K. Hara, G. Fujihashi, S. Takano, S. Murata, H. Arakawa and M. Tachiya, *J. Phys. Chem. B* 2004, **108**, 4818-4822.
76. J. Zhang, H.-B. Li, S.-L. Sun, Y. Geng, Y. Wu and Z.-M. Su, *J. Mater. Chem.*, 2012, **22**, 568-576.
77. T. Koopmans, *Physica*, 1933, **1**, 104-113.
78. G. Boschloo and A. Hagfeldt, *Acc. Chem. Res.*, 2009, **42**, 1819-1826.
79. A. Listorti, B. O'Regan and J. R. Durrant, *Chem. Mater.*, 2011, **23**, 3381-3399.
80. A. Carella, F. Borbone and R. Centore, *Front. Chem.*, 2018, **6**, 481.
81. M. K. Nazeeruddin, A. Kay, I. Rodicio, R. Humphry-Baker, E. Mueller, P. Liska, N. Vlachopoulos and M. Graetzel, *J. Am. Chem. Soc.*, 1993, **115**, 6382-6390.
82. R. Buscaino, C. Baiocchi, C. Barolo, C. Medana, M. Grätzel, M. K. Nazeeruddin and G. Viscardi, *Inorganica Chim. Acta*, 2008, **361**, 798-805.
83. M. K. Nazeeruddin, P. Pechy and M. Grätzel, *Chem. Comm.*, 1997, 1705-1706.
84. F. Sauvage, J.-D. Decoppet, M. Zhang, S. M. Zakeeruddin, P. Comte, M. Nazeeruddin, P. Wang and M. Grätzel, *J. Am. Chem. Soc.*, 2011, **133**, 9304-9310.
85. N. Sekar and V. Y. Gehlot, *Resonance*, 2010, **15**, 819-831.
86. Y. Qin and Q. Peng, *Int. J. Photoenergy*, 2012, **2012**.
87. G. C. Vougioukalakis, A. I. Philippopoulos, T. Stergiopoulos and P. Falaras, *Coord. Chem. Rev.*, 2011, **255**, 2602-2621.

88. S. Shalini, R. Balasundaraprabhu, T. S. Kumar, N. Prabavathy, S. Senthilarasu and S. Prasanna, *Int. J. Energy Res.*, 2016, **40**, 1303-1320.
89. S. Aghazada and M. K. Nazeeruddin, *Inorganics*, 2018, **6**, 52.
90. R. Juwita, J.-Y. Lin, S.-J. Lin, Y.-C. Liu, T.-Y. Wu, Y.-M. Feng, C.-Y. Chen, H.-H. Gavin Tsai and C.-G. Wu, *J. Mater. Chem. A*, 2020, **8**, 12361-12369.
91. G. Sauv e, M. E. Cass, G. Coia, S. J. Doig, I. Lauermann, K. E. Pomykal and N. S. Lewis, *J. Phys. Chem. B*, 2000, **104**, 6821-6836.
92. S. Ferrere, *Chem. Mater.*, 2000, **12**, 1083-1089.
93. E. A. M. Geary, L. J. Yellowlees, L. A. Jack, I. D. H. Oswald, S. Parsons, N. Hirata, J. R. Durrant and N. Robertson, *Inorg. Chem.*, 2005, **44**, 242-250.
94. Y.-J. Yuan, Z.-T. Yu, J.-Y. Zhang and Z.-G. Zou, *Dalton Trans.*, 2012, **41**, 9594-9597.
95. D. Daphnomili, G. Sharma, S. Biswas, K. J. Thomas and A. Coutsolelos, *J Photochem Photobiol A: Chem*, 2013, **253**, 88-96.
96. J. Mikroyannidis, G. Charalambidis, A. Coutsolelos, P. Balraju and G. Sharma, *J Power Sources*, 2011, **196**, 6622-6628.
97. M. P. Balanay, C. V. P. Dipaling, S. H. Lee, D. H. Kim and K. H. Lee, *Sol. Energy Mater. Sol. Cells*, 2007, **91**, 1775-1781.
98.  . Birel, S. Nadeem and H. Duman, *J. Fluoresc.*, 2017, **27**, 1075-1085.
99. Z. Parsa, S. S. Naghavi and N. Safari, *J. Phys. Chem. A*, 2018, **122**, 5870-5877.
100. C. Leznoff and A. Lever, *Properties and Applications*, VCH, New York, 1989.
101. M. Urbani, M.-E. Ragoussi, M. K. Nazeeruddin and T. Torres, *Coord. Chem. Rev.*, 2019, **381**, 1-64.
102. A. Islam, M. Akhtaruzzaman, T. H. Chowdhury, C. Qin, L. Han, I. M. Bedja, R. Stalder, K. S. Schanze and J. R. Reynolds, *ACS Appl. Mater. Interfaces*, 2016, **8**, 4616-4623.
103. M. Ye, X. Wen, M. Wang, J. Iocozzia, N. Zhang, C. Lin and Z. Lin, *Mater. Today*, 2015, **18**, 155-162.
104. L. Zhang, X. Yang, W. Wang, G. G. Gurzadyan, J. Li, X. Li, J. An, Z. Yu, H. Wang and B. Cai, *ACS Energy Lett.*, 2019, **4**, 943-951.
105. Q.-Y. Yu, J.-Y. Liao, S.-M. Zhou, Y. Shen, J.-M. Liu, D.-B. Kuang and C.-Y. Su, *J. Phys. Chem. C*, 2011, **115**, 22002-22008.

106. Z.-S. Wang, N. Koumura, Y. Cui, M. Takahashi, H. Sekiguchi, A. Mori, T. Kubo, A. Furube and K. Hara, *Chem. Mater.*, 2008, **20**, 3993-4003.
107. A. S. Hart, C. B. K. C, N. K. Subbaiyan, P. A. Karr and F. D'Souza, *ACS Appl. Mater. Interfaces*, 2012, **4**, 5813-5820.
108. Y. Hua, S. Chang, D. Huang, X. Zhou, X. Zhu, J. Zhao, T. Chen, W.-Y. Wong and W.-K. Wong, *Chem. Mater.*, 2013, **25**, 2146-2153.
109. S. Ferrere and B. A. Gregg, *New J. Chem.*, 2002, **26**, 1155-1160.
110. Z. S. Wang, Y. Cui, K. Hara, Y. Dan-oh, C. Kasada and A. Shinpo, *Adv. Mater.*, 2007, **19**, 1138-1141.
111. B. Liu, Q. Liu, D. You, X. Li, Y. Naruta and W. Zhu, *J. Mater. Chem.*, 2012, **22**, 13348-13356.
112. K. R. Justin Thomas and A. Baheti, *Mater. Technol.*, 2013, **28**, 71-87.
113. A. C. Khazraji, S. Hotchandani, S. Das and P. V. Kamat, *J. Phys. Chem. B*, 1999, **103**, 4693-4700.
114. Z. Wang, Y. Huang, C. Huang, J. Zheng, H. Cheng and S. Tian, *Synth. Met.*, 2000, **114**, 201-207.
115. K. Hara, M. Kurashige, S. Ito, A. Shinpo, S. Suga, K. Sayama and H. Arakawa, *Chem. Commun.*, 2003, 252-253.
116. Z.-S. Huang, H. Meier and D. Cao, *J. Mater. Chem. C*, 2016, **4**, 2404-2426.
117. R. Chen, X. Yang, H. Tian, X. Wang, A. Hagfeldt and L. Sun, *Chem. Mater.*, 2007, **19**, 4007-4015.
118. S. A. Al-horaibi, A. M. Asiri, R. M. El-Shishtawy, S. T. Gaikwad and A. S. Rajbhoj, *J. Mol. Struct.*, 2019, **1195**, 850-858.
119. J. Feng, Y. Jiao, W. Ma, M. K. Nazeeruddin, M. Grätzel and S. Meng, *J. Phys. Chem. C*, 2013, **117**, 3772-3778.
120. A. J. Huckaba, F. Giordano, L. E. McNamara, K. M. Dreux, N. I. Hammer, G. S. Tschumper, S. M. Zakeeruddin, M. Grätzel, M. K. Nazeeruddin and J. H. Delcamp, *Adv. Energy Mater.*, 2015, **5**, 1401629.
121. G. Wu, F. Kong, J. Li, W. Chen, C. Zhang, Q. Chen, X. Zhang and S. Dai, *Synth. Met.*, 2013, **180**, 9-15.
122. K. Do, D. Kim, N. Cho, S. Paek, K. Song and J. Ko, *Org. Lett.*, 2012, **14**, 222-225.
123. Y. M. Hailu, M. T. Nguyen and J.-C. Jiang, *Phys. Chem. Chem. Phys.*, 2018, **20**, 23564-23577.

124. J. He, Y. Liu, J. Gao and L. Han, *Photochem. Photobiol. Sci.*, 2017, **16**, 1049-1056.
125. D. P. Hagberg, T. Marinado, K. M. Karlsson, K. Nonomura, P. Qin, G. Boschloo, T. Brinck, A. Hagfeldt and L. Sun, *J. Org. Chem.*, 2007, **72**, 9550-9556.
126. W. Wu, J. Yang, J. Hua, J. Tang, L. Zhang, Y. Long and H. Tian, *J. Mater. Chem.*, 2010, **20**, 1772-1779.
127. B. Liu, Q. Liu, D. You, X. Li, Y. Naruta and W. Zhu, *J. Mater. Chem.*, 2012, **22**, 13348-13356.
128. T. Sudyoasuk, S. Pansay, S. Morada, R. Rattanawan, S. Namuangruk, T. Kaewin, S. Jungsuttiwong and V. Promarak, *EEur. J. Org. Chem.*, 2013, **2013**, 5051-5063.
129. X. Liu, Z. Cao, H. Huang, X. Liu, Y. Tan, H. Chen, Y. Pei and S. Tan, *J. Power Sources*, 2014, **248**, 400-406.
130. X.-F. Zang, Z.-S. Huang, H.-L. Wu, Z. Iqbal, L. Wang, H. Meier and D. Cao, *J. Power Sources*, 2014, **271**, 455-464.
131. Y. Wu, M. Marszalek, S. M. Zakeeruddin, Q. Zhang, H. Tian, M. Grätzel and W. Zhu, *Energy Environ. Sci.*, 2012, **5**, 8261-8272.
132. W. Zhu, Y. Wu, S. Wang, W. Li, X. Li, J. Chen, Z. s. Wang and H. Tian, *Adv. Funct. Mater.*, 2011, **21**, 756-763.
133. W. Ying, F. Guo, J. Li, Q. Zhang, W. Wu, H. Tian and J. Hua, *ACS Appl. Mater. Interfaces*, 2012, **4**, 4215-4224.
134. X. Li, Z. Zheng, W. Jiang, W. Wu, Z. Wang and H. Tian, *Chem. comm.*, 2015, **51**, 3590-3592.
135. Y. Wu, W.-H. Zhu, S. M. Zakeeruddin and M. Grätzel, *ACS Appl. Mater. Interfaces* 2015, **7**, 9307-9318.
136. Y. Wu and W. Zhu, *C Chem. Soc. Rev.*, 2013, **42**, 2039-2058.
137. L. Han, J. Liu, Y. Liu and Y. Cui, *J. Mol. Struct.*, 2019, **1180**, 651-658.
138. R. Yeh-Yung Lin, F.-L. Wu, C.-H. Chang, H.-H. Chou, T.-M. Chuang, T.-C. Chu, C.-Y. Hsu, P.-W. Chen, K.-C. Ho, Y.-H. Lo and J. T. Lin, *J. Mater. Chem. A*, 2014, **2**, 3092-3101.
139. L.-Y. Lin, C.-H. Tsai, F. Lin, T.-W. Huang, S.-H. Chou, C.-C. Wu and K.-T. Wong, *Tetrahedron*, 2012, **68**, 7509-7516.
140. N. Manfredi, B. Cecconi and A. Abboto, *Eur. J. Org. Chem.*, 2014, **2014**, 7069-7086.

141. Y. Hong, J.-Y. Liao, J. Fu, D.-B. Kuang, H. Meier, C.-Y. Su and D. Cao, *Dye. Pigm.*, 2012, **94**, 481-489.
142. K. D. Seo, B. S. You, I. T. Choi, M. J. Ju, M. You, H. S. Kang and H. K. Kim, *J. Mater. Chem. A*, 2013, **1**, 9947-9953.
143. P. Naik, M. R. Elmorsy, R. Su, D. D. Babu, A. El-Shafei and A. V. Adhikari, *Sol. Energy*, 2017, **153**, 600-610.
144. G.-G. Luo, H. Lu, Y.-H. Wang, J. Dong, Y. Zhao and R.-B. Wu, *Dyes Pigm.*, 2016, **134**, 498-505.
145. T. Khanasa, N. Prachumrak, P. Kochapradist, S. Namuangruk, T. Keawin, S. Jungsuttiwong, T. Sudyoardsuk and V. Promarak, *Tetrahedron Lett.*, 2014, **55**, 3244-3248.
146. Y. Numata, A. Islam, H. Chen and L. Han, *Energy Environ. Sci.*, 2012, **5**, 8548-8552.
147. X. Zhang, M. Grätzel and J. Hua, *Front. Optoelectron.*, 2016, **9**, 3-37.
148. S. S. Fernandes, M. C. R. Castro, I. Mesquita, L. Andrade, A. Mendes and M. M. M. Raposo, *Dyes Pigm.*, 2017, **136**, 46-53.
149. A. B. Marco, N. M. de Baroja, J. M. Andrés-Castán, S. Franco, R. Andreu, B. Villacampa, J. Orduna and J. Garín, *Dyes Pigm.*, 2019, **161**, 205-213.
150. H.-Y. Yang, Y.-S. Yen, Y.-C. Hsu, H.-H. Chou and J. T. Lin, *Org. Lett.*, 2010, **12**, 16-19.
151. K. Hara, Y. Dan-oh, C. Kasada, Y. Ohga, A. Shinpo, S. Suga, K. Sayama and H. Arakawa, *Langmuir*, 2004, **20**, 4205-4210.
152. E. Galoppini, *Coord. Chem. Rev.*, 2004, **248**, 1283-1297.
153. J. Sivanadanam, P. Ganesan, R. Madhumitha, M. K. Nazeeruddin and R. Rajalingam, *J. Photochem. Photobiol. A: Chem.*, 2015, **299**, 194-202.
154. C.-J. Tan, C.-S. Yang, Y.-C. Sheng, H. W. Amini and H.-H. G. Tsai, *J. Phys. Chem. C*, 2016, **120**, 21272-21284.
155. C. Teng, X. Yang, C. Yang, H. Tian, S. Li, X. Wang, A. Hagfeldt and L. Sun, *J. Phys. Chem. C*, 2010, **114**, 11305-11313.
156. M. Velusamy, K. R. Justin Thomas, J. T. Lin, Y.-C. Hsu and K.-C. Ho, *Org. Lett.*, 2005, **7**, 1899-1902.
157. A. Kathiravan, V. Srinivasan, T. Khamrang, M. Velusamy, M. Jaccob, N. Pavithra, S. Anandan and K. Velappan, *Phys. Chem. Chem. Phys.*, 2017, **19**, 3125-3135.

158. N. Duvva, Y. K. Eom, G. Reddy, K. S. Schanze and L. Giribabu, *ACS Appl. Energy Mater.*, 2020, **3**, 6758-6767.
159. É. Torres, S. Sequeira, P. Parreira, P. Mendes, T. Silva, K. Lobato and M. J. Brites, *J. Photochem. Photobiol. A Chem.*, 2015, **310**, 1-8.
160. S. Martins, J. Avó, J. Lima, J. Nogueira, L. Andrade, A. Mendes, A. Pereira and P. S. Branco, *J. Photochem. Photobiol. A Chem.*, 2018, **353**, 564-569.
161. A. F. Buene, N. Boholm, A. Hagfeldt and B. H. Hoff, *New J. Chem.*, 2019, **43**, 9403-9410.
162. J. Yang, F. Guo, J. Hua, X. Li, W. Wu, Y. Qu and H. Tian, *J. Mater. Chem.*, 2012, **22**, 24356-24365.
163. D. M. Almenningen, H. E. Hansen, M. F. Vold, A. F. Buene, V. Venkatraman, S. Sunde, B. H. Hoff and O. R. Gautun, *Dyes Pigm.*, 2021, **185**, 108951.
164. M. Paramasivam, R. K. Chitumalla, S. P. Singh, A. Islam, L. Han, V. Jayathirtha Rao and K. Bhanuprakash, *J. Phys. Chem. C*, 2015, **119**, 17053-17064.
165. X. Cheng, M. Liang, S. Sun, Y. Shi, Z. Ma, Z. Sun and S. Xue, *Tetrahedron*, 2012, **68**, 5375-5385.
166. X. Liu and X. Liu, *RSC Adv.*, 2019, **9**, 24733-24741.
167. Y.-S. Yen, Y.-C. Hsu, J. T. Lin, C.-W. Chang, C.-P. Hsu and D.-J. Yin, *J. Phys. Chem. C*, 2008, **112**, 12557-12567.
168. S. S. M. Fernandes, I. Mesquita, L. Andrade, A. Mendes, L. L. G. Justino, H. D. Burrows and M. M. M. Raposo, *Org. Electron.*, 2017, **49**, 194-205.
169. J. Jia, Y. Zhang, P. Xue, P. Zhang, X. Zhao, B. Liu and R. Lu, *Dyes Pigm.*, 2013, **96**, 407-413.
170. S. Liu, X. Bao, W. Li, K. Wu, G. Xie, R. Yang and C. Yang, *Macromolecules*, 2015, **48**, 2948-2957.
171. S. Jungstittiwong, T. Yakhanthip, Y. Surakhot, J. Khunchalee, T. Sudyoadsuk, V. Promarak, N. Kungwan and S. Namuangruk, *J. Comput. Chem.*, 2012, **33**, 1517-1523.
172. K. R. Justin Thomas, Y.-C. Hsu, J. T. Lin, K.-M. Lee, K.-C. Ho, C.-H. Lai, Y.-M. Cheng and P.-T. Chou, *Chem. Mater.*, 2008, **20**, 1830-1840.
173. C.-J. Tan, C.-S. Yang, Y.-C. Sheng, H. W. Amini and H.-H. G. Tsai, *J. Phys. Chem. C*, 2016, **120**, 21272-21284.

174. N. A. Anderson, X. Ai, D. Chen, D. L. Mohler and T. Lian, *J. Phys. Chem. B*, 2003, **107**, 14231-14239.
175. W. Senevirathna, C. M. Daddario and G. v. Sauvé, *J. Phys. Chem. Lett.*, 2014, **5**, 935-941.
176. I. Martini, J. H. Hodak and G. V. Hartland, *J. Phys. Chem. B*, 1998, **102**, 9508-9517.
177. I. Ciofini, T. Le Bahers, C. Adamo, F. Odobel and D. Jacquemin, *J. Phys. Chem. C*, 2012, **116**, 11946-11955.
178. L.-J. He, J. Chen, F.-Q. Bai, R. Jia, J. Wang and H.-X. Zhang, *Dyes Pigm.*, 2017, **141**, 251-261.
179. X. Zhang, F. Gou, D. Zhao, J. Shi, H. Gao, Z. Zhu and H. Jing, *J. Power Sources*, 2016, **324**, 484-491.
180. S. Chaurasia, C.-J. Liang, Y.-S. Yen and J. T. Lin, *J. Mater. Chem. C*, 2015, **3**, 9765-9780.
181. H. Choi, M. Shin, K. Song, M.-S. Kang, Y. Kang and J. Ko, *J. Mater. Chem. A*, 2014, **2**, 12931-12939.
182. A. Baheti, P. Tyagi, K. R. J. Thomas, Y.-C. Hsu and J. T. s. Lin, *J. Phys. Chem. C* 2009, **113**, 8541-8547.
183. C.-G. Wu, M.-F. Chung, H.-H. G. Tsai, C.-J. Tan, S.-C. Chen, C.-H. Chang and T.-W. Shih, *ChemPlusChem*, 2012, **77**, 832.
184. C.-G. Wu, W.-T. Shieh, C.-S. Yang, C.-J. Tan, C.-H. Chang, S.-C. Chen, C.-Y. Wu and H.-H. G. Tsai, *Dyes Pigm.*, 2013, **99**, 1091-1100.
185. S. Chaurasia, Y.-C. Chen, H.-H. Chou, Y.-S. Wen and J. T. Lin, *Tetrahedron*, 2012, **68**, 7755-7762.
186. Z.-S. Huang, H.-L. Feng, X.-F. Zang, Z. Iqbal, H. Zeng, D.-B. Kuang, L. Wang, H. Meier and D. Cao, *J. Mater. Chem. A*, 2014, **2**, 15365-15376.
187. J.-S. Ni, Y.-C. Yen and J. T. Lin, *Chem. Commun*, 2015, **51**, 17080-17083.
188. Z.-S. Huang, X.-F. Zang, T. Hua, L. Wang, H. Meier and D. Cao, *ACS Appl. Mater. Interfaces*, 2015, **7**, 20418-20429.
189. M. Cheng, X. Yang, C. Chen, J. Zhao, Q. Tan and L. Sun, *Phys. Chem. Chem. Phys.*, 2013, **15**, 17452-17459.

190. A. Slimi, M. Hachi, A. Fitri, A. T. Benjelloun, S. Elkhatabi, M. Benzakour, M. McHarfi, M. Khenfouch, I. Zorkani and M. Bouachrine, *J. Photochem. Photobiol. A: Chem.*, 2020, **398**, 112572.
191. W.-C. Chen, S. Nachimuthu and J.-C. Jiang, *Sci. Rep.*, 2017, **7**, 1-13.
192. L. Zhang and J. M. Cole, *ACS Appl. Mater. Interfaces*, 2015, **7**, 3427-3455.
193. N. Martsinovich and A. Troisi, *Energy Environ. Sci*, 2011, **4**, 4473-4495.
194. N. Martsinovich, D. R. Jones and A. Troisi, *Energy Environ. Sci*, 2010, **114**, 22659-22670.
195. F. Ambrosio, N. Martsinovich and A. Troisi, *J. Phys. Chem. Lett.*, 2012, **3**, 1531-1535.
196. C. O'Rourke and D. R. Bowler, *J. Phys.: Condens. Matter*, 2014, **26**, 195302.
197. K. Kalyanasundaram and M. Grätzel, *Coord. Chem. Rev.*, 1998, **177**, 347-414.
198. C. S. Kley, C. Dette, G. Rinke, C. E. Patrick, J. Čechal, S. J. Jung, M. Baur, M. Dürr, S. Rauschenbach and F. Giustino, *Nano Lett.*, 2014, **14**, 563-569.
199. Y. Ooyama, Y. Hagiwara, Y. Oda, T. Mizumo, Y. Harima and J. Ohshita, *New J. Chem.*, 2013, **37**, 2336-2340.
200. S. Ferrere, A. Zaban and B. A. Gregg, *J. Phys. Chem. B*, 1997, **101**, 4490-4493.
201. S. Ferrere and B. A. Gregg, *New J. Chem.*, 2002, **26**, 1155-1160.
202. C. Zafer, M. Kus, G. Turkmen, H. Dincalp, S. Demic, B. Kuban, Y. Teoman and S. Icli, *Sol. Energy Mater. Sol. Cells*, 2007, **91**, 427-431.
203. H. He, A. Gurung and L. Si, *Chem. Comm.*, 2012, **48**, 5910-5912.
204. J. Zhao, X. Yang, M. Cheng, S. Li and L. Sun, *ACS Appl. Mater. Interfaces* 2013, **5**, 5227-5231.
205. E. L. Tae, S. H. Lee, J. K. Lee, S. S. Yoo, E. J. Kang and K. B. Yoon, *J. Phys. Chem. B*, 2005, **109**, 22513-22522.
206. B.-K. An, W. Hu, P. L. Burn and P. Meredith, *J. Phys. Chem. C*, 2010, **114**, 17964-17974.
207. Y. Ooyama, T. Yamada, T. Fujita, Y. Harima and J. Ohshita, *J. Mater. Chem. A*, 2014, **2**, 8500-8511.
208. W. R. McNamara, R. C. Snoeberger III, G. Li, C. Richter, L. J. Allen, R. L. Milot, C. A. Schmuttenmaer, R. H. Crabtree, G. W. Brudvig and V. S. Batista, *Energy Environ. Sci.*, 2009, **2**, 1173-1175.



209. W. R. McNamara, R. L. Milot, H.-e. Song, R. C. Snoeberger III, V. S. Batista, C. A. Schmuttenmaer, G. W. Brudvig and R. H. Crabtree, *Energy Environ. Sci.*, 2010, **3**, 917-923.
210. L. Zhang, J. M. Cole and C. Dai, *ACS Appl. Mater. Interfaces*, 2014, **6**, 7535-7546.
211. Z.-S. Wang, F.-Y. Li and C.-H. Huang, *Chem. Comm.*, 2000, 2063-2064.
212. T. A. Heimer, S. T. D'Arcangelis, F. Farzad, J. M. Stipkala and G. J. Meyer, *Inorg. Chem.*, 1996, **35**, 5319-5324.
213. W. R. McNamara, R. C. Snoeberger Iii, G. Li, J. M. Schleicher, C. W. Cady, M. Poyatos, C. A. Schmuttenmaer, R. H. Crabtree, G. W. Brudvig and V. S. Batista, *J. Am. Chem. Soc.*, 2008, **130**, 14329-14338.
214. S. Altobello, C. A. Bignozzi, S. Caramori, G. Larramona, S. Quici, G. Marzanni and R. Lakhmiri, *J. Photochem. Photobiol. A: Chem.*, 2004, **166**, 91-98.
215. J. Cong, X. Yang, J. Liu, J. Zhao, Y. Hao, Y. Wang and L. Sun, *Chem. Comm.*, 2012, **48**, 6663-6665.
216. F. Gou, X. Jiang, B. Li, H. Jing and Z. Zhu, *ACS Appl. Mater. Interfaces*, 2013, **5**, 12631-12637.
217. J. Tang, S. Qu, J. Hu, W. Wu and J. Hua, *Sol. Energy*, 2012, **86**, 2306-2311.
218. H.-Q. Xia, C.-P. Kong, J. Wang, F.-Q. Bai and H.-X. Zhang, *RSC Adv.*, 2014, **4**, 50338-50350.
219. F. Labat, T. Le Bahers, I. Ciofini and C. Adamo, *Acc. Chem. Res.*, 2012, **45**, 1268-1277.
220. N. Martsinovich and A. Troisi, *Energy Environ. Sci.*, 2011, **4**, 4473-4495.
221. A. Dreuw, J. L. Weisman and M. Head-Gordon, *J. chem. phys.*, 2003, **119**, 2943-2946.
222. J.-i. Nishida, T. Masuko, Y. Cui, K. Hara, H. Shibuya, M. Ihara, T. Hosoyama, R. Goto, S. Mori and Y. Yamashita, *J. Phys. Chem. C*, 2010, **114**, 17920-17925.
223. R. G. Parr and R. G. Pearson, *J. Am. Chem. Soc.*, 1983, **105**, 7512-7516.
224. Y. Li, Y. Li, P. Song, F. Ma, J. Liang and M. Sun, *RSC Adv.*, 2017, **7**, 20520-20536.
225. W. Zhang, Y. Wu, H. Zhu, Q. Chai, J. Liu, H. Li, X. Song and W.-H. Zhu, *ACS Appl. Mater. Interfaces*, 2015, **7**, 26802-26810.
226. F. Arkan and M. Izadyar, *Renew. Sustain. Energy Rev.*, 2018, **94**, 609-655.
227. W. Zhang, L. Wang, L. Mao, J. Jiang, H. Ren, P. Heng, H. Ågren and J. Zhang, *J. Phys. Chem. C*, 2020, **124**, 3980-3987.

228. J. Yang, X. Wang, W.-L. Yim and Q. Wang, *J. Phys. Chem. C*, 2015, **119**, 26355-26361.
229. P. McGill and H. Idriss, *Surf. Sci*, 2008, **602**, 3688-3695.
230. U. Terranova and D. Bowler, *J. Phys. Chem. C*, 2010, **114**, 6491-6495.
231. J. K. Roy, S. Kar and J. Leszczynski, *ACS Sustainable Chem. Eng.*, 2020, **8**, 13328-13341.
232. M. Karuppusamy, V. S. K. Choutipalli, D. Vijay and V. Subramanian, *J. Chem. Sci.*, 2020, **132**, 1-22.
233. P. N. Samanta, D. Majumdar, S. Roszak and J. Leszczynski, *J. Phys. Chem. C*, 2020, **124**, 2817-2836.
234. N. Agnihotri, *J. Photochem. Photobiol C: Photochem. Rev.*, 2014, **18**, 18-31.
235. Y. M. Hailu, M. T. Nguyen and J.-C. Jiang, *Phys. Chem. Chem. Phys.*, 2018, **20**, 23564-23577.
236. C. Sun, Y. Li, Y. Shi and Y. Li, *ChemistrySelect*, 2018, **3**, 6622-6637.
237. H. A. Wahab, R. E. Amaro and Z. Cournia, *J. Chem. Inf. Model.*, 2018, **58**, 2175-2177.
238. R. J. Sension, in *Advances in Teaching Physical Chemistry*, American Chemical Society, 2007, vol. 973, ch. 13, pp. 220-234.
239. J. Thyssen, T. Fleig and H. J. A. Jensen, *J. Chem. Phys.*, 2008, **129**, 034109.
240. A. K. Rappé and C. J. Casewit, *Molecular Mechanics Across Chemistry*, University Science Books, 1997.
241. N. Allinger, *Advances in Physical Organic Chemistry*, Elsevier, 1976, vol. 13, pp. 1-82.
242. E. G. Lewars, in *Computational Chemistry*, Springer, 2016, pp. 51-99.
243. B. Leimkuhler and C. Matthews, *Molecular Dynamics*, Springer, 2016.
244. E. Schrödinger, *Ann. Phys.*, 1926, **79**, 734.
245. A. Szabo and N. S. Ostlund, *Modern Quantum Chemistry: Introduction to Advanced Electronic Structure Theory*, Courier Corporation, 2012.
246. M. Born and R. Oppenheimer, *Ann. Phys.*, 1927, **389**, 457-484.
247. A. Szabão and N. S. Ostlund, *Modern Quantum Chemistry: Introduction to Advanced Electronic Structure Theory*, Free Press, 1982.
248. C. D. Sherrill, *An introduction to Hartree-Fock molecular orbital theory*, 2000.
249. W. Pauli, *Zeitschrift für Physik A Hadrons and Nuclei*, 1925, **31**, 765-783.

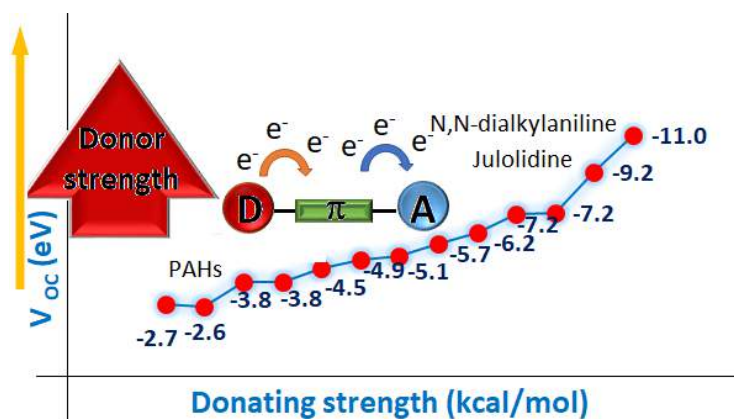
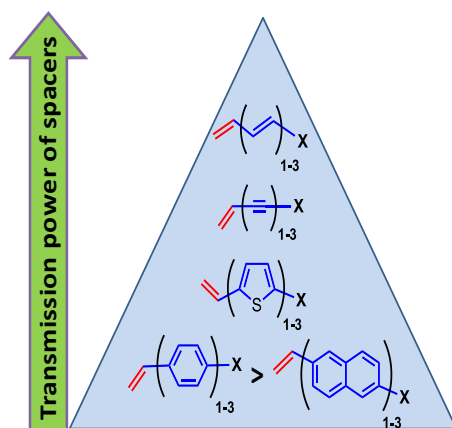
250. V. Fock, *Zeitschrift für Physik A Hadrons and Nuclei*, 1930, **61**, 126-148.
251. J. C. Slater, *Phys. Rev.*, 1930, **35**, 210-211.
252. G. G. Hall, *Proc. Royal Soc. A*, 1951, **205**, 541-552.
253. C. C. J. Roothaan, *Rev. Mod. Phys.*, 1951, **23**, 69-89.
254. D. C. Young, *Computational Chemistry, New York*, 2001, **9**, 390.
255. D. Cremer, *Wiley Interdiscip. Rev. Comput. Mol. Sci.*, 2011, **1**, 509-530.
256. C. Møller and M. S. Plesset, *Phys. Rev.*, 1934, **46**, 618-622.
257. I. Shavitt, *Mol. Phys.*, 1998, **94**, 3-17.
258. R. J. Bartlett and M. Musiał, *Rev. Mod. Phys.*, 2007, **79**, 291.
259. D. Cremer, *Encyclopedia of computational chemistry*, 1998.
260. D. G. Fedorov and K. Kitaura, *J. Chem. Phys.*, 2004, **121**, 2483-2490.
261. J. Pople, R. Seeger and R. Krishnan, *Int. J. Quantum Chem.*, 1977, **12**, 149-163.
262. P. J. Knowles and H.-J. Werner, *Chem. Phys. Lett.*, 1988, **145**, 514-522.
263. D. C. Young, *Computational Chemistry: A Practical Guide for Applying Techniques to Real World Problems*, 2001, 19-31.
264. H. Nakano, *J. Chem. Phys.*, 1993, **99**, 7983-7992.
265. J. Čížek, *J. Chem. Phys.*, 1966, **45**, 4256-4266.
266. P. R. Taylor, in *Lecture Notes in Quantum Chemistry II*, Springer, 1994, pp. 125-202.
267. C. J. Cramer, *Essentials of Computational Chemistry: Theories and Models*, John Wiley & Sons, 2013.
268. J. A. Pople, D. P. Santry and G. A. Segal, *J. Chem. Phys.*, 1965, **43**, S129-S135.
269. M. J. Dewar and W. Thiel, *J. Am. Chem. Soc.*, 1977, **99**, 4899-4907.
270. J. J. Stewart, *J. Mol. Model.*, 2013, **19**, 1-32.
271. E. K. Gross and R. M. Dreizler, *Density Functional Theory*, Springer Science & Business Media, 2013.
272. N. Argaman and G. Makov, *Am. J. Phys.*, 2000, **68**, 69-79.
273. W. Kohn, A. D. Becke and R. G. Parr, *J. Phys. Chem. A*, 1996, **100**, 12974-12980.
274. E. Fermi, *Rend. Acad. Lincei*, 1927, **6**, 602.
275. E. Fermi, *Z. Phys.*, 1928, **48**, 73.
276. L. H. Thomas, *Proc. Cambridge Phil. Soc.*, 1927, **23**, 542.
277. T. Tsuneda, *Density Functional Theory in Quantum Chemistry*, Springer, 2014.
278. A. D. Becke, *J. Chem. Phys.*, 2014, **140**, 18A301.

279. W. Kohn and L. J. Sham, *Phys. rev.*, 1965, **140**, A1133.
280. J. P. Perdew and K. Schmidt, *AIP Conference Proceedings*, 2001, **577**, 1-20.
281. E. Awoonor-Williams, Brief Overview on Density Functional Theory, <https://awoonor.github.io/DFT/>.
282. R. G. Parr, in *Horizons of Quantum Chemistry*, Springer, 1980, pp. 5-15.
283. S. H. Vosko, L. Wilk and M. Nusair, *Can. J. Phys.*, 1980, **58**, 1200.
284. D. M. Ceperley and B. J. Alder, *Phys. Rev. Lett.*, 1980, **45**, 566-569.
285. T. J. Giese and D. M. York, *J. Chem. Phys.*, 2010, **133**, 244107.
286. S. F. Sousa, P. A. Fernandes and M. J. Ramos, *J. Phys. Chem. A*, 2007, **111**, 10439-10452.
287. A. D. Becke, *Phys. Rev. A*, 1988, **38**, 3098-3100.
288. J. P. Perdew, *Phys. Rev. B*, 1986, **33**, 8822-8824.
289. K. Burke, J. P. Perdew and Y. Wang, in *Electronic Density Functional Theory*, Springer, 1998, pp. 81-111.
290. J. P. Perdew, K. Burke and M. Ernzerhof, *Phys. Rev. Lett.*, 1996, **77**, 3865.
291. C. Lee, W. Yang and R. G. Parr, *Phys. Rev. B* 1988, **37**, 785.
292. G. I. Csonka, J. P. Perdew, A. Ruzsinszky, P. H. Philipsen, S. Lebègue, J. Paier, O. A. Vydrov and J. G. Ángyán, *Phys. Rev. B*, 2009, **79**, 155107.
293. S. K. Ghosh and R. G. Parr, *Phys. Rev. A*, 1986, **34**, 785.
294. R. Peverati and D. G. Truhlar, *J. Chem. Theory Comput.*, 2012, **8**, 2310-2319.
295. Y. Zhao and D. G. Truhlar, *J. Chem. Phys.*, 2006, **125**, 194101.
296. A. D. Becke, *J. Chem. Phys.*, 1992, **96**, 2155-2160.
297. K. Berland, V. R. Cooper, K. Lee, E. Schröder, T. Thonhauser, P. Hyldgaard and B. I. Lundqvist, *Reports on Progress in Physics*, 2015, **78**, 066501.
298. S. Grimme, J. Antony, T. Schwabe and C. Mück-Lichtenfeld, *Org. Biomol. Chem.*, 2007, **5**, 741-758.
299. S. Grimme, L. Goerigk and R. Fink, *Rev.: Comput. Mol. Sci*, 2011, **1**, 211-228.
300. S. Botti, A. Schindlmayr, R. Del Sole and L. Reining, *Rep. Prog. Phys.*, 2007, **70**, 357.
301. C. A. Ullrich and Z.-h. Yang, *Braz. J. Phys.*, 2014, **44**, 154-188.
302. E. Runge and E. K. U. Gross, *Phys. Rev. Lett.*, 1984, **52**, 997-1000.
303. Y. Takimoto, F. Vila and J. Rehr, *J. chem. phys.*, 2007, **127**, 154114.
304. E. Gross, J. Dobson and M. Petersilka, *Density functional theory II*, 1996, 81-172.

305. C. Fiolhais, F. Nogueira and M. A. Marques, *A Primer in Density Functional Theory*, Springer Science & Business Media, 2003.
306. D. R. Gulevich, Y. V. Zhumagulov, A. Vagov and V. Perebeinos, *Phys. Rev. B*, 2019, **100**, 241109.
307. A. D. Beck, *J. Chem. Phys.*, 1993, **98**, 5648-5646.
308. B. Komjáti, Á. Urai, S. Hosztafi, J. Kökösi, B. Kováts, J. Nagy and P. Horváth, *Spectrochim. Acta A Mol. Biomol. Spectrosc.*, 2016, **155**, 95-102.
309. L. C. Allen and A. M. Karo, *Rev. Mod. Phys.*, 1960, **32**, 275-285.
310. P. M. W. Gill, in *Advances in Quantum Chemistry*, eds. J. R. Sabin and M. C. Zerner, Academic Press, 1994, vol. 25, pp. 141-205.
311. D. Feller and E. R. Davidson, in *Rev. Computat. Chem.*, John Wiley & Sons, Inc., 2007, pp. 1-43.
312. S. F. Boys, *Proc. Royal Soc. A*, 1950, **200**, 542-554.
313. *Gaussian Basis Sets* <https://chem.libretexts.org/@go/page/210880> (accessed Aug 2, 2021).
314. M. J. Frisch, J. A. Pople and J. S. Binkley, *J. Chem. Phys.*, 1984, **80**, 3265-3269.
315. J. B. Foresman and A. Frisch, *Exploring Chemistry with Electronic Structure Methods.*, Gaussian Inc., Pittsburg, USA, 1996.
316. Y. Sakai, H. Tatewaki and S. Huzinaga, *J. Comput. Chem.*, 1981, **2**, 100-107.
317. R. F. Stewart and W. J. Hehre, *J. Chem. Phys.*, 1970, **52**, 5243-5247.
318. H. Tatewaki and S. Huzinaga, *J. Chem. Phys.*, 1979, **71**, 4339-4348.
319. T. H. Dunning Jr, *J. Chem. Phys.*, 1989, **90**, 1007-1023.
320. S. Kritikou and J. G. Hill, *J. Quantum Chem.*, 2015, **11**, 5269-5276.
321. T. V. Russo, R. L. Martin and P. J. Hay, *J. Phys. Chem.*, 1995, **99**, 17085-17087.
322. W. J. Hehre, *Acc. Chem. Res.*, 1976, **9**, 399-406.
323. A. J. Shusterman and L. M. Hoistad, *Chem. Educ.*, 2001, **6**, 36-40.
324. J. D. Mottishaw, A. R. Erck, J. H. Kramer, H. Sun and M. Koppang, *J. Chem. Educ.*, 2015, **92**, 1846-1852.
325. E. Scrocco and J. Tomasi, in *New concepts II*, Springer, 1973, pp. 95-170.
326. P. Politzer and D. G. Truhlar, *Chemical Applications of Atomic and Molecular Electrostatic Potentials*, Plenum Press, New York, 1981.
327. S. R. Gadre, P. K. Bhadane, S. S. Pundlik and S. S. Pingale, *Molecular Electrostatic Potential: Concepts and Applications*, Elsevier, Amsterdam, 1996.

328. S. R. Gadre and R. N. Shirsat, *Electrostatics of Atoms and Molecules*, Universities Press, Hyderabad, India, 2000.
329. F. J. Luque, M. Orozco, P. K. Bhadane and S. R. Gadre, *J. Chem. Phys.*, 1994, **100**, 6718.
330. C. J. Cramer and D. G. Truhlar, *Chem. Rev.*, 1999, **99**, 2161-2200.
331. M. Steiner, T. Holzknecht, M. Schauerl and M. Podewitz, *Molecules*, 2021, **26**, 1793.
332. J. Tomasi and M. Persico, *Chem. Rev.*, 1994, **94**, 2027-2094.
333. B. Mennucci, *Wiley Interdiscip. Rev. Comput. Mol. Sci.*, 2012, **2**, 386-404.
334. B. Mennucci, J. Tomasi, R. Cammi, J. R. Cheeseman, M. J. Frisch, F. J. Devlin, S. Gabriel and P. J. Stephens, *J. Phys. Chem. A* 2002, **106**, 6102-6113.
335. S. Miertuš, E. Scrocco and J. Tomasi, *Chem. Phys.*, 1981, **55**, 117-129.
336. J. Tomasi, E. Cancès, C. S. Pomelli, M. Caricato, G. Scalmani, M. J. Frisch, R. Cammi, M. V. Basilevsky, G. N. Chuev and B. Mennucci, in *Continuum Solvation Models in Chemical Physics*, John Wiley & Sons, Ltd, 2007, pp. 1-123.
337. A. V. Marenich, C. J. Cramer and D. G. Truhlar, *J. Phys. Chem. B* 2009, **113**, 6378-6396.

# Quantification of Donating Strength and Substituent Effect Transmission Power of Various Spacers



# Part A: Substituent Effect Transmission Power of Alkyl, Alkenyl, Alkynyl, Phenyl, Thiophenyl and Polyacene Spacers

---

## 2.1 Abstract

*The transmission of substituent effect through a variety of spacers viz. alkyl, alkenyl, alkynyl, phenyl, thiophenyl, and polyacene has been studied by modeling Y-G-X type molecular systems (Y- reaction center, G - spacer moiety and X - substituent) using B3LYP/6-31G(d,p) density functional theory. The reaction center is always kept as a CC double bond and the molecular electrostatic potential (MESP) minimum ( $V_m$ ) observed for this bond showed subtle variation with respect to the changes in the spacer unit and the nature of substituent. Strong linear correlations are observed between Hammett substituent constants ( $\sigma_I$  and  $\sigma_p$ ) and  $V_m$ , which recommend the aptness of  $V_m$  as an electronic descriptor to quantify the substituent effect. Since  $V_m$  offers an alternative measure of substituent effect, the correlation between  $V_m$  and  $\sigma_p$  has been used for assessing the transmission of substituent effect through a variety of spacer moieties. The highest transmission coefficient ( $\gamma$ ) is always observed for smaller spacer length. Among all the spacers, alkenyl showed the highest and alkyl showed the lowest transmission power. The study recommends the use of short chains of CC double, CC triple or a combination of both as spacers for the effective transmission of substituent effect to the reaction center.*

## 2.2 Introduction

Substituents in molecules are regarded as functional groups and tuning of various chemical properties can be achieved by controlling the substituent effects.<sup>1, 2</sup> The theory of substituent effect has been considered as fundamental to the prediction of molecular reactivity.<sup>1-6</sup> The electronic effect of a substituent can be transmitted to the reaction center *via* a transmitting moiety. For example in a molecule Y-G-X, (Y- reaction center, G - spacer moiety and X - substituent), the effect of X at Y through G can be interpreted with the famous Hammett relationship  $\log(K_X/K_0) = \rho\sigma$ , where  $\rho$



is the reaction constant and  $\sigma$  is the substituent constant. Hammett equation and several of its modifications<sup>3, 7</sup> have been used in a quantitative way for the effective interpretation of substituent effects.<sup>8</sup> The applicability of  $\sigma$ -constants for a variety of molecules assisted the understanding of structure-activity and structure-property relationships in chemistry.<sup>9-21</sup>

Substituent effects are classified into inductive (through  $\sigma$  bond),  $\pi$  - resonance and through space (field) effects.<sup>1, 3, 22, 23</sup> The separation of the substituent effect into inductive ( $\sigma_I$  or F) and resonance effect ( $\sigma_R$  or R) was done by Swain and Lupton.<sup>24</sup> They interpreted that the negative and positive values of substituent constant indicate the electron-donating and withdrawing nature of substituents, respectively. Using quantum chemical approaches, many efforts have been made to model the substituent effect.<sup>8-21, 25-30</sup> Substituent effects are responsible for small perturbations on the molecular electron density distribution, which can be measured by means of correlating them with the computed quantities of total energy, atomic charges, and electrostatic potentials resulting from *ab initio* quantum chemical or semiempirical methods.<sup>15, 31-35</sup> Further, several experimental studies have utilized Y-G-X type systems to understand the substituent effect transmission ability of various spacer moieties using geometrical variables, ionization techniques, and NMR chemical shifts etc.<sup>30, 36-44</sup>

Among the several theoretical quantities used to interpret Hammett constants, topographical analysis of molecular electrostatic potential (MESP) provided a clean approach to substituent effects.<sup>9-11, 27-29</sup> The prediction and rationalization of reactivity trends using MESP have been pioneered by Scrocco, Tomasi, and co-workers.<sup>45, 46</sup> Politzer and Murry widely used the MESP plots calculated using standard electronic structure theory to interpret while the topographical analysis of MESP has been pioneered by Gadre *et al.*<sup>47-50</sup> From the MESP topographical studies on conjugated organic molecular systems, Suresh *et al.* have shown that critical features of MESP are useful for the quantification of inductive,<sup>51</sup> resonance,<sup>52</sup> steric<sup>53</sup> and proximity effects<sup>26</sup> of substituents. Also, MESP minimum ( $V_m$ ) has been used as a powerful electronic descriptor to quantify substituent effect, trans influence, and two electron donor character of ligands.<sup>9, 11, 54-57</sup> Here we intend to study Y-G-X type systems using  $V_m$  analysis. The substituent effect transmission power of X through the

spacer will be assessed by the  $V_m$  observed over Y, an olefinic moiety. Although the significance of such spacers in donor-acceptor systems is well known, quantification of substituent effect transmission power of a variety of spacer systems is yet to be systematically analyzed. Previous studies showed that modifications in spacer units such as their  $\pi$ -bond character, conjugation length, and planarity had a significant role in electron transmission power, absorption wavelength, and other related photophysical properties.<sup>58-61</sup> Here spacers such as alkyl, alkenyl, alkynyl, phenyl, thiophenyl, and polyacenes have been selected to include the inductive, and resonance effect aspects. We envision that this study will provide useful information regarding the future dye designing and other related studies.

## 2.3 Computational methodology

Geometry optimization has been carried out with B3LYP/6-31G(d, p) density functional theory method.<sup>62,63</sup> MESP computations are also done at the same level of theory and basis set. Previous studies showed that this method is adequate for calculating MESP features.<sup>10,16,64</sup> Gaussian 09 programme package has been used for all the calculations.<sup>65</sup> Vibrational frequency analysis is done with the same level of theory to confirm that the number of imaginary frequencies is zero for all the optimized geometries.

## 2.4 Results and discussion

### 2.4.1 MESP topography and spacer effects

MESP is one of the most appropriate electronic descriptors to understand the electron withdrawing and donating nature of substituents and ligands.<sup>9,10,50,54,66,67</sup> It is recognized that electron rich region in a molecule experiences a significant change in MESP minimum ( $V_m$ ) due to substituent effects. Here we consider an olefinic bond (Figure 2.1) as a sensitive region to understand the precise variation of  $V_m$  with respect to the substituent effect. A general notation  $C_2H_3-G_n-X$  has been used to denote the molecule, where  $G_n$  stands for the repeating 'n' spacer G units between  $C_2H_3$  and X. The effect of substituent on  $C_2H_3$  - has been measured in terms of  $V_m$

on its CC double bond. Electron donating and withdrawing substituents used in this study include NH<sub>2</sub>, OH, CH<sub>3</sub>, H, F, Cl, CF<sub>3</sub>, CHO, CN and NO<sub>2</sub>. The spacers selected for the study are alkyl, alkenyl, alkynyl, phenyl, thiophenyl, and polyacenes (Figure 2.1). For a reasonable understanding about the spacer length, systems up to n = 3 have been considered. In studies related to the substituent effect, a system with X = H is described as the unsubstituted reference system. Hence the change in  $V_m$  due to substitution is designated as  $\Delta V_m$  which gives a direct estimation of the substituent effect.<sup>27</sup>

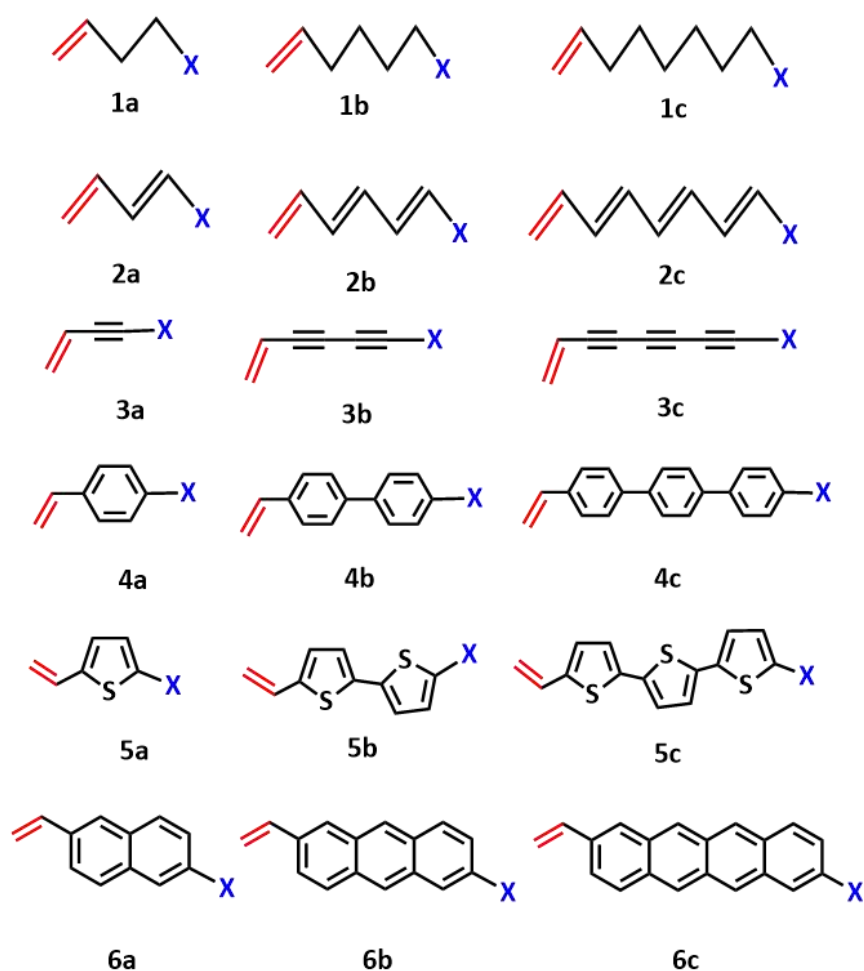


**Figure 2.1** Various spacers considered to quantify the transmission power of spacers. The double bond marked in red is the region where MESP minimum is located for X = NH<sub>2</sub>, OH, CH<sub>3</sub>, H, F, Cl, CF<sub>3</sub>, CHO, CN and NO<sub>2</sub>

MESP isosurface for **1a**, **2a**, **3a**, **4a**, **5a** and **6a** (X = H) is shown in Figure 2.2 along with the respective  $V_m$  values at the terminal double bond, *viz.* -22.2, -18.6, -13.8, -19.5, -18.4, -19.0 kcal/mol. The  $V_m$  at the terminal double bond for all the

substituted systems (total 180 systems) is depicted in Table 2.1. The  $V_m$  ranges from -30.5 to 3.8 kcal/mol which indicates the effect of both spacer moiety and substituent on tuning the electron distribution on the double bond. In  $C_2H_3$ -alkyl-X systems (**1a** - **1c**), the inductive effect is the prime factor for electron transmission.

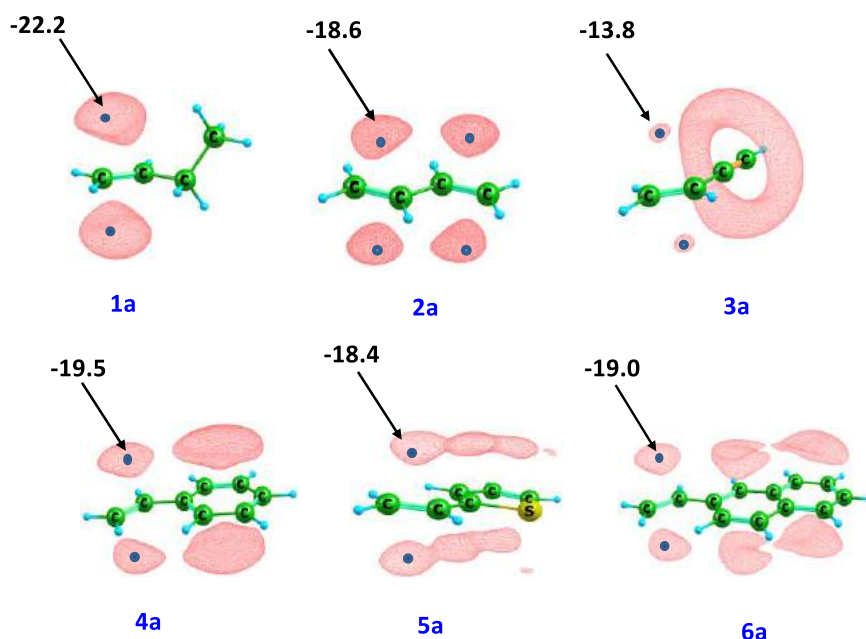


**Figure 2.2** MESP isosurface at -13.0 kcal/mol for **1a**, **2a**, **3a**, **4a**, **5a** and **6a**.  $V_m$  values in kcal/mol are also depicted.

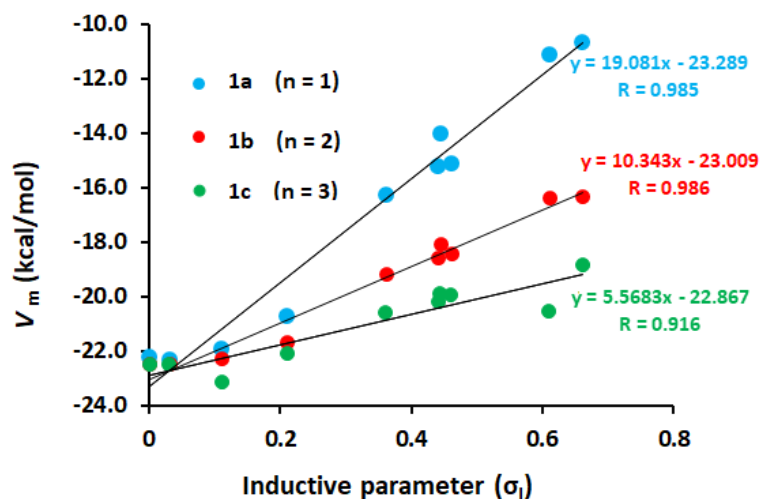


**Figure 2.3** Correlation between the  $V_m$  of **1a**-**1c** with the inductive parameter ( $\sigma_I$ ).

A less negative  $V_m$  is observed for  $X = NH_2$  and  $X = OH$  than  $X = H$  suggesting the electron withdrawing inductive (-I) character of the highly electronegative N and O

atoms. For X = CH<sub>3</sub> and n = 1,  $V_m$  is slightly more negative than X = H indicating the electron donating inductive (+I) effect of the methyl group. An increase in alkyl chain length slightly enhances this electron donation. Further, the -I effect of substituents Cl, CF<sub>3</sub>, CN, NO<sub>2</sub> etc. are clearly reflected on their respective  $V_m$ . The diminishing -I effect with an increase in alkyl chain length is pronounced in the case of CN and NO<sub>2</sub>.

**Table 2.1**  $V_m$  (in kcal/mol) obtained over the terminal double bond of various spacer systems.

	NH <sub>2</sub>	OH	CH <sub>3</sub>	H	F	Cl	CF <sub>3</sub>	CHO	CN	NO <sub>2</sub>
1a	-21.9	-20.7	-22.3	-22.2	-16.3	-14.0	-15.2	-15.1	-11.1	-10.7
1b	-22.3	-21.6	-22.5	-22.5	-19.1	-18.1	-18.6	-18.4	-16.4	-16.3
1c	-23.2	-22.1	-22.5	-22.5	-20.6	-19.9	-20.2	-20.0	-20.5	-18.8
2a	-30.5	-25.4	-21.6	-18.6	-17.0	-13.3	-8.6	-7.3	-3.6	0.1
2b	-28.6	-24.3	-20.8	-18.4	-17.9	-14.8	-10.7	-9.0	-6.8	-3.5
2c	-24.3	-23.3	-20.4	-18.3	-18.1	-15.6	-12.2	-10.5	-8.9	-6.0
3a	-25.9	-20.6	-18.4	-13.8	-14.0	-11.9	-3.7	-3.0	1.4	3.8
3b	-20.1	-16.3	-14.3	-10.2	-11.0	-9.7	-2.7	-2.0	1.3	3.1
3c	-13.2	-13.1	-11.5	-8.0	-8.9	-7.9	-2.1	-1.5	1.1	2.5
4a	-25.8	-21.8	-21.0	-19.5	-17.5	-15.1	-12.5	-11.1	-8.5	-6.7
4b	-22.0	-20.2	-19.8	-19.1	-17.9	-16.7	-15.4	-14.8	-13.2	-12.4
4c	-20.0	-19.4	-19.3	-18.9	-18.1	-15.1	-16.8	-16.4	-15.5	-15.0
5a	-24.5	-20.8	-20.1	-18.4	-16.3	-14.4	-10.5	-8.7	-6.2	-3.5
5b	-20.8	-19.1	-18.2	-17.1	-15.9	-14.8	-12.5	-10.7	-9.6	-7.3
5c	-18.6	-17.4	-17.2	-16.6	-15.8	-15.1	-13.5	-12.3	-11.5	-9.8
6a	-23.5	-20.6	-20.2	-19.0	-17.4	-15.8	-13.9	-12.8	-11.0	-9.5
6b	-22.1	-20.1	-19.6	-18.8	-17.5	-16.1	-14.8	-13.8	-12.4	-11.2
6c	-20.5	-19.5	-19.2	-18.6	-17.4	-16.4	-15.4	-14.6	-13.5	-12.6

For example,  $V_m$  of  $\text{NH}_2$  substituted systems shows a variation of  $\sim 1.3$  kcal/mol from  $n = 1$  to  $n = 3$ , while CN and  $\text{NO}_2$  exhibits a variation of 9.4 and 8.1 kcal/mol, respectively. The inductive control of electronic transmission in alkyl systems is confirmed by the strong linear correlation between  $V_m$  and inductive substituent constant ( $\sigma_I$ ) (Figure 2. 3 and Table 2. 2). The slope of the correlation plot 19.081 observed for spacer length  $n = 1$  is the highest and it decreases to 10.343 for  $n = 2$  and further decreases to 5.568 for  $n = 3$ . This data indicates the rapidly decreasing behavior of I with the increase in the number of CC single bonds.<sup>51</sup>

**Table 2. 2** Hammett parameters for the substituents employed in the study.

X	$\sigma_p^{26}$	$\sigma_I^{51}$
$\text{NH}_2$	-0.66	0.11
OH	-0.37	0.21
Me	-0.17	0.03
H	0.00	0.00
F	0.06	0.36
Cl	0.23	0.44
$\text{CF}_3$	0.54	0.44
CHO	0.51	0.46
CN	0.66	0.61
$\text{NO}_2$	0.78	0.66

For the case of unsubstituted alkenyl systems (**2a - 2c**),  $V_m$  values are observed at -18.6, -18.4, and -18.3 kcal/mol respectively. The small variation in  $V_m$  indicates the negligible impact of spacer length on electronic transmission whereas the individual effect of a substituent on  $V_m$  is very high in **2** series. For instance,  $\Delta V_m$  of  $\text{NH}_2$  and OH in **2** is significantly more negative than those in **1**. In **2**,  $\text{NH}_2$  and OH donate electrons mainly *via* resonance mechanism.  $\text{NH}_2$  is the most electron-donating with  $\Delta V_m$  -11.9, -10.2 and -6.0 kcal/mol for **2a**, **2b**, and **2c**, respectively (Table 2. 3) while the most electron-withdrawing  $\text{NO}_2$  shows  $\Delta V_m$  18.7, 14.9 and 12.4 kcal/mol. Increasing the spacer length diminishes the power of electron transmission. Further, in the case of

CH<sub>3</sub>,  $V_m$  is more negative than the unsubstituted system which can be mainly attributed to the electron-donating hyperconjugation and +I effect of CH<sub>3</sub>. Here the magnitude of electron donation for **2a** - **2c** in terms of  $\Delta V_m$  is -3.1, -2.4, and -2.1

**Table 2. 3**  $\Delta V_m$  in kcal/mol of various spacer systems.

X	$V_m$	$\Delta V_m$								
	H	NH <sub>2</sub>	OH	CH <sub>3</sub>	F	Cl	CF <sub>3</sub>	CHO	CN	NO <sub>2</sub>
1a	-22.2	0.3	1.5	-0.1	6.0	8.2	7.0	7.1	11.1	11.5
1b	-22.5	0.2	0.8	0.0	3.3	4.4	3.9	4.1	6.1	6.1
1c	-22.5	-0.7	0.4	0.0	1.9	2.6	2.3	2.5	1.9	3.6
2a	-18.6	-11.9	-6.8	-3.1	1.6	5.3	10	11.3	15.0	18.7
2b	-18.4	-10.2	-6.0	-2.4	0.5	3.6	7.7	9.3	11.6	14.9
2c	-18.3	-6.0	-5.0	-2.1	0.3	2.7	6.1	7.8	9.4	12.4
3a	-13.8	-12.1	-6.8	-4.6	-0.2	1.9	10.1	10.8	15.2	17.6
3b	-10.2	-9.9	-6.0	-4.1	-0.8	0.5	7.5	8.2	11.5	13.3
3c	-8.0	-5.2	-5.0	-3.5	-0.9	0.1	5.9	6.5	9.2	10.5
4a	-19.5	-6.3	-2.3	-1.4	2.0	4.5	7.1	8.4	11.0	12.8
4b	-19.1	-2.9	-1.1	-0.8	1.2	2.4	3.7	4.3	5.8	6.7
4c	-18.9	-1.1	-0.5	-0.4	0.8	3.8	2.1	2.4	3.4	3.9
5a	-18.4	-6.1	-2.4	-1.7	2.1	4	7.8	9.7	12.2	14.9
5b	-17.1	-3.7	-2.0	-1.1	1.1	2.3	4.6	6.4	7.5	9.7
5c	-16.6	-2.1	-0.8	-0.6	0.8	1.5	3.1	4.2	5.1	6.8
6a	-19.0	-4.5	-1.6	-1.2	1.6	3.3	5.1	6.2	8.0	9.5
6b	-18.8	-3.3	-1.3	-0.9	1.3	2.6	4.0	5.0	6.3	7.5
6c	-18.6	-1.9	-0.9	-0.6	1.1	2.1	3.2	4.0	5.1	6.0

kcal/mol (Table 2. 3). Substituents F, Cl, CF<sub>3</sub>, CHO, CN, and NO<sub>2</sub> show a considerable decrease in the magnitude of  $V_m$  compared to the reference system, which authenticates their electron-withdrawing inductive and resonance effects. The

$\Delta V_m$  18.7, 15.0, 11.3, 10.0, 5.3, 1.6 kcal/mol observed for the substituents  $\text{NO}_2$ , CN, CHO,  $\text{CF}_3$ , Cl and F, respectively suggest that their electron-withdrawing power follows the order  $\text{NO}_2 > \text{CN} > \text{CHO} > \text{CF}_3 > \text{Cl} > \text{F}$  (Table 2. 3). The strong linear correlations observed between  $V_m$  of **2a**, **2b**, and **2c** systems with Hammett constant  $\sigma_p$  (Figure 2.4 and Table 2.2) suggest that the MESP topographical quantity  $V_m$  is highly suited as an electronic descriptor to quantify the electron-donating and withdrawing nature of a substituent. The slope of the correlation plots decreases as  $n$  increase in the spacer length. Since  $\sigma_p = 0$  stands for the unsubstituted systems, the Y-intercept of the correlation plot corresponds to  $V_m$  of the unsubstituted system. Indeed, the Y-intercept and  $V_m$  of the unsubstituted system show very close agreement.

The unsubstituted alkynyl systems, (**3a** - **3c**) show  $V_m$  values at -13.8, -10.2, and -8.0 kcal/mol, respectively. The magnitude of these values is smaller than the unsubstituted alkenyl systems indicating the more electronegative  $\text{C}_{sp}$  hybridized carbons in alkynyl systems than  $\text{C}_{sp^2}$  in alkenyl systems. Similar to **2**, resonance effect dominates in **3** except for  $\text{X} = \text{CH}_3$  and  $\text{X} = \text{CF}_3$ . The magnitude of electron-withdrawing effect ( $\Delta V_m$ ) obtained for substituents such as  $\text{NO}_2$ , CN, CHO,  $\text{CF}_3$ , Cl, and F is very similar to that found for  $\text{C}_2\text{H}_3$ -alkenyl-X systems which indicates that substituent effect transmission power is similar for CC double bonds and CC triple bonds.

The unsubstituted systems with phenyl ring spacers, **4a** - **4c** show  $V_m$  values at -19.5, -19.1, and -18.9 kcal/mol, respectively. The electron-donating  $\text{NH}_2$ , OH, and  $\text{CH}_3$  substituents enhance the negative character of  $V_m$  while the electron-withdrawing F, Cl,  $\text{CF}_3$ , CHO, CN, and  $\text{NO}_2$  substituents diminish it. A similar  $V_m$  feature has been noticed for systems containing thiophenyl spacers, **5a** - **5c**, and polyacene spacers, **6a** - **6c** (Table 2.1). In **4** series with  $n = 2$  and 3, adjacent two phenyl units are twisted away from planarity which gives a diminishing effect on the electron-donating/withdrawing ability of the substituent. The CC single bond connection between two phenyl units in **4** proposes a significant inductive effect along with resonance. In polyacenes, resonance effect dominates over the inductive effect. In **4**, **5**, and **6** series, an increase in spacer length has a decreasing effect on the transmission power of the substituent effect.



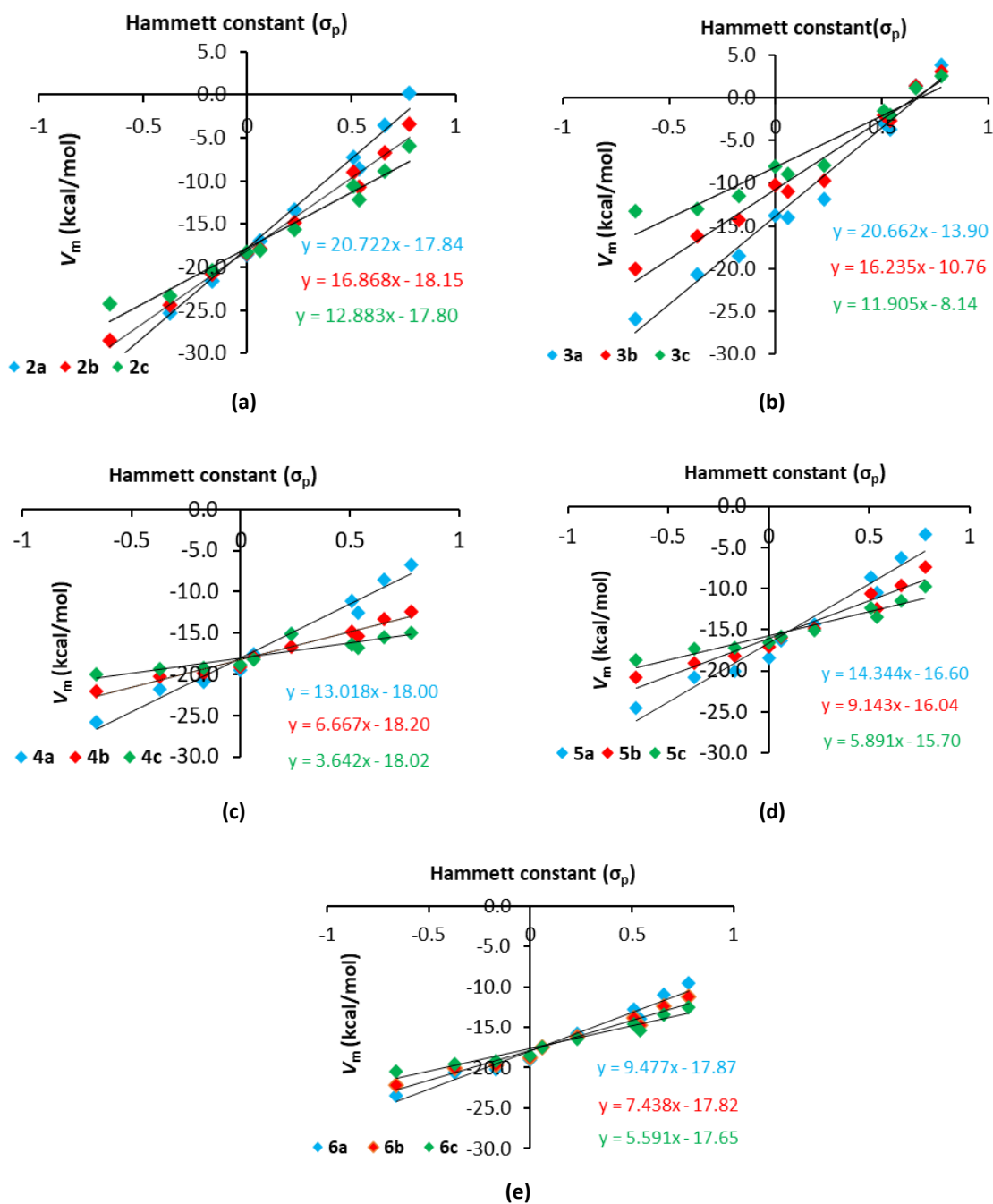


**Figure 2. 4** Correlation of  $V_m$  with Hammett parameter ( $\sigma_p$ ) of a) alkenyl b) alkynyl c) phenyl d) thiophenyl and e) polyacene systems.

## 2.4.2 $V_m$ based quantification of substituent effect transmission power of spacers

When a reacting center and substituent are separated by a variety of spacers, significant variations in the molecular properties can be observed.<sup>68</sup> The transmission of the substituent effect through olefinic systems showed the applicability of  $\rho$  in

calculating the substituent effect transmission power. From the previous studies,<sup>37, 39</sup> it is understood that the transmission power of a spacer can be quantified by the transmission coefficient ( $\gamma$ ) defined as  $\gamma = \rho_s / \rho_0$ , where  $\rho_s$  is the reaction constant of a spacer for which the transmission power has to be quantified and  $\rho_0$  is the reaction constant of the reference group. Since  $V_m$  provides an alternative measure of substituent effects for  $\pi$ -conjugated systems, the correlation of  $V_m$  with  $\sigma_p$  can be used to evaluate the transmission ability of various spacers using the equation,  $V_m = \rho\sigma_p + \text{constant}$ . Therefore, linear regression analysis between  $V_m$  and  $\sigma_p$  values is carried out to find the  $\rho$  values (Table 2.4). In order to calculate the transmission coefficients ( $\gamma$ ), the phenyl group substituted **4a** is taken as the reference system for

**Table 2.4** Slope, intercept, reaction constant ( $\rho_s$ ), correlation coefficient ( $R$ ) and transmission coefficient ( $\gamma$ ) of various spacers.

X	Slope	Intercept	$\rho_s$	$R$	$\gamma$
2a	20.722	-17.84	20.722	0.994	1.592
2b	16.868	-18.15	16.868	0.993	1.296
2c	12.883	-17.80	12.883	0.981	0.989
3a	20.662	-13.90	20.662	0.988	1.587
3b	16.235	-10.76	16.235	0.985	1.247
3c	11.905	-8.14	11.905	0.962	0.914
4a	13.018	-18.00	13.018	0.987	1.000
4b	6.667	-18.20	6.667	0.984	0.512
4c	3.642	-18.02	3.642	0.895	0.280
5a	14.344	-16.60	14.344	0.979	1.102
5b	9.143	-16.03	9.143	0.973	0.702
5c	5.891	-15.70	5.891	0.961	0.452
6a	9.477	-17.87	9.477	0.984	0.728
6b	7.438	-17.81	7.438	0.983	0.571
6c	5.591	-17.65	5.591	0.974	0.429

all the spacers. For **4a** systems,  $V_m = 13.018(\sigma_p) - 18.00$  and the slope of this equation ( $\rho_{4a}$ ) is used as  $\rho_0$  to determine  $\gamma$ . For example, the  $\gamma$  value for **2a** is calculated as  $\gamma = \rho_{2a} / \rho_{4a} = 20.722 / 13.018 = 1.592$  meaning that the transmission power of **2a** is 1.592 times higher than phenyl ring. Among the  $\pi$ -bonded spacers, for  $n = 1$ , the order of substituent effect transmission power of spacers is **2a**  $\approx$  **3a** > **5a** > **4a** > **6a**. On the basis of the average of all the  $\gamma$  values for a particular spacer from  $n = 1 - 3$ , the order of transmission power of substituent effects is as follows: **2a - 2c** > **3a - 3c** > **5a - 5c** > **4a - 4c** > **6a - 6c**. This order is in agreement with the experimental findings<sup>37</sup> and suggesting the appropriateness of  $V_m$  method for the present study.

### 2.4.3 Combination of two different spacers and substituent selectivity

To understand the transmission ability of a combination of two different spacers, we selected six types of spacers as shown in Figure 2. 5. In **7a** and **7b**, the substituent is connected to the double-bonded carbon and an aromatic ring, respectively. In Table 2.5, the  $V_m$  values obtained for all the hetero spacers are reported. For substituent 'H' the  $V_m$  values of **7a** and **7b** are -18.76 and -18.89 kcal/mol showing a variation of 0.13 kcal/mol between the two isomers. However, for other substituents, the difference in  $V_m$  is found to be less than  $\sim 1.0$  kcal/mol suggesting that the electron

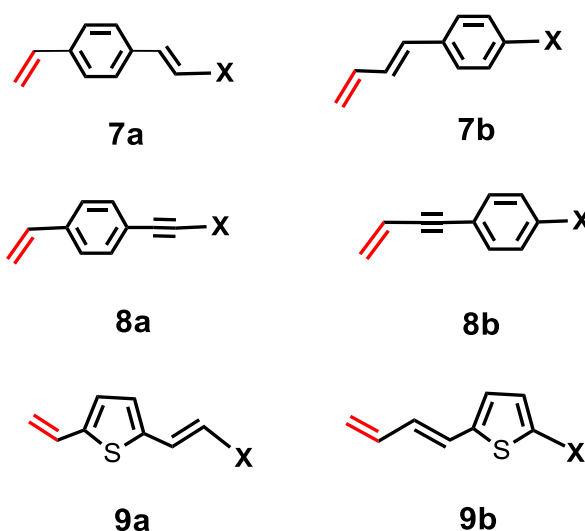


**Figure 2. 5** Spacers considered to quantifying the effect of the combination of two different spacers.

**Table 2. 5**  $V_m$  values (kcal/mol) obtained for hetero spacers.

X	7a	7b	8a	8b	9a	9b
NH <sub>2</sub>	-24.85	-24.22	-22.78	-21.02	-24.16	-23.72
OH	-21.96	-21.08	-20.27	-17.95	-21.52	-20.83
Me	-20.21	-20.21	-18.83	-17.07	-19.39	-19.77
H	-18.76	-18.89	-16.32	-15.88	-17.51	-18.32
F	-17.70	-17.70	-16.50	-14.56	-16.75	-17.13
Cl	-15.81	-15.75	-15.44	-12.80	-14.56	-15.44
CF <sub>3</sub>	-13.24	-13.49	-10.86	-10.67	-11.42	-12.30
CHO	-12.05	-12.17	-9.79	-9.60	-8.85	-10.35
CN	-10.17	-10.48	-10.48	-7.78	-7.97	-8.85
NO <sub>2</sub>	-7.97	-8.79	-8.79	-6.28	-5.21	-6.34

donating or withdrawing nature is not highly affected whether 'X' is attached to the double bond or the phenyl ring. The  $V_m$  values for substituent 'H' of **8a** and **8b** are -16.32 and -15.88 kcal/mol indicating that total electron withdrawing nature of ethynylbenzene is more when ethyne is attached directly to the olefinic moiety. Further, the electron withdrawing and donating substituents show maximum influence when they are attached to the phenyl ring. Additionally, for **9a** and **9b**,  $V_m$  values for the unsubstituted systems are observed at -17.51 and -18.32 kcal/mol, respectively meaning that the variation is only 0.81 kcal/mol. In fact, for all the substituent except CHO and NO<sub>2</sub>, the variation is less than ~1 kcal/mol. This confirms that electronic effect is not highly affected whether 'X' is attached to a double bond or thiophenyl ring. In general, a spacer made up of two different moieties, substituent effect transmission power of 'X' can show a minor variation depending on the connectivity of X with the spacer unit.

## 2.5 Conclusions

The substituent effect transmission power of electron donating and withdrawing substituents on a terminal CC double bond has been assessed using MESP  $V_m$  analysis. The  $V_m$  observed on this bond showed significant change with respect to the electron donating/withdrawing nature of the substituent as well as the nature and length of the spacer unit. The  $V_m$  correlates strongly with an inductive parameter for systems consisting of alkyl spacers. Similarly, for all the  $\pi$ -conjugated systems, strong linear correlations were observed between Hammett substituent constant and  $V_m$ . The decreasing trend of slope values with an increase in the size of spacer length revealed the strongly diminishing nature of the substituent effect transmission. From the slope of the correlation plots, the transmission power of spacers is obtained which can be arranged in the order alkenyl > alkynyl > thiophenyl > phenyl > polyacene. For systems having alkyl spacers, transmission of substituent effect is the least as the inductive effect has a rapidly diminishing character with the increase in the size of the spacer unit. In summary, among all the spacer groups, alkenyl and alkynyl units are the most effective for the substituent effect transmission.

# Part B: Density Functional Theory Study on the Donating Strength of Donor Systems in Dye-Sensitized Solar Cells

---

## 2.6 Abstract

*The electron-donating strength of donor (D) moieties in thirteen donor- $\pi$ -acceptor systems (D1- $\pi$ -A to D13- $\pi$ -A wherein  $\pi$ - and A represent butadiene and cyanoacrylic acid units, respectively) have been studied using B3LYP/cc-pVDZ level density functional theory (DFT) calculations. The selected D moieties are encountered as a part of an organic sensitizer molecule in dye-sensitized solar cell (DSSC) applications. When D moiety is joined with  $\pi$ -A, a certain amount of electron donation from D to A occurs leading to an increase in electron density at the A site of D- $\pi$ -A compared to A site of  $\pi$ -A. This electron reorganization is quantified in terms of the change in molecular electrostatic potential (MESP) minimum ( $\Delta V_{mA}$ ) at the acceptor site, the CN group of the cyanoacrylic acid. The  $\Delta V_{mA}$  is always negative, in the range -11.0 to -2.6 kcal/mol which provides a quick assessment of the rank order of the electron-donating nature of the D moieties in the ground state of D- $\pi$ -A. The optical, and photovoltaic properties of D and D- $\pi$ -A systems are also determined at TD-CAM-B3LYP/cc-pVDZ//B3LYP/cc-pVDZ level. An absorption redshift ( $\Delta\lambda_{max}$ ) in the range 81 – 242 nm is observed when D moieties change to D- $\pi$ -A systems. The ground state property  $\Delta V_{mA}$  showed a strong linear correlation with the excited state property  $\Delta\lambda_{max}$ . Further,  $\Delta V_{mA}$  is found to be proportional to the open-circuit voltage ( $eV_{oc}$ ). The resemblance of highest occupied molecular orbital (HOMO) and lowest unoccupied molecular orbital (LUMO) energies of the D- $\pi$ -A system with the respective energies of donor and  $\pi$ -A system shows that donor tunes HOMO, while  $\pi$ -A tunes LUMO. Among the thirteen D- $\pi$ -A systems, N,N-dialkylaniline, and julolidine are rated as the best donors for photovoltaic applications. This study shows that MESP based assessment of donating strength of donor systems offers a powerful rational design strategy for the development of efficient dyes for DSSC applications.*

## 2.7 Introduction

Dye-sensitized solar cells (DSSCs) have been regarded as a high potential alternative for the conventional silicon-based solar cells due to their high molar extinction coefficient, low production cost, simple synthetic strategy, and easy structural modifications.<sup>69-73</sup> DSSCs also perform relatively better than other traditional solar cells under diffuse light conditions and at a higher temperature.<sup>72-74</sup> In DSSC applications, the sensitizers synthesized can be divided into two broad areas, *viz.* the metal-based systems such as Ru(II) polypyridyl complexes, and Zn(II) porphyrins<sup>75</sup> and the metal-free donor- $\pi$ -acceptor (D- $\pi$ -A) type organic dyes.<sup>76</sup> The Ru-based polypyridyl sensitizers attained the highest power conversion efficiency over 11% than most of the metal-free sensitizers.<sup>77-82</sup> This is due to the ability of metal sensitizers to absorb solar irradiation up to the near-infrared region, while other metal-free dye sensitizers absorb at shorter wavelength region.<sup>76, 83</sup> So, a highly efficient sensitizer should have an absorption maximum near to Vis-NIR region associated with a long-lived charge excited state.<sup>84,85</sup> Due to the highly expensive, and toxic synthetic procedures involved in metal sensitizers, the organic dyes got remarkable importance in DSSC applications.<sup>76</sup> Recent studies proposed important structural modifications on organic dyes<sup>86, 87</sup> to achieve high power conversion efficiency (PCE) and over 12 % has been earned with a metal-free alkoxysilyl carbazole dye as a sensitizer.<sup>88</sup> Yao *et al* reported an improved PCE of 12.5 % with a metal-free indenoperylene based D- $\pi$ -A dye, the best-known metal-free organic dye.<sup>89</sup> In 2017, a simple designing strategy over phenothiazine moiety with ethynyl-pyrene enabled a PCE of 12 %.<sup>90</sup> The other recent milestones in DSSCs include co-sensitization, which enables higher photovoltaic performance over 14 % with a collaborative sensitization by silyl and carboxy anchoring groups.<sup>91</sup> Many studies proposed the structural modification of the donor group of the D- $\pi$ -A dye to achieve higher efficiency as increasing the electron-donating strength generally broadens and intensifies the region of absorption.<sup>92-94</sup> In general, a dye sensitizer with D- $\pi$ -A framework can be modified at donor,<sup>95, 96</sup> spacer,<sup>59, 97-99</sup> and anchoring groups<sup>100-102</sup> to improve the PCE. Typically, the acceptor portion (A) of the dye anchored onto the TiO<sub>2</sub> semiconductor favours charge transfer of the excited electrons to the conduction band of the semiconductor.<sup>103</sup> The oxidized dye is then regenerated by the electron

transfer from the electrolyte ( $I^-/I_3^-$  couple), while the electrolyte couple regains the electron from the platinum counter electrode.<sup>72, 104</sup> Therefore, for an efficient dye sensitizer, an effective electron injection can occur from the dye to  $TiO_2$  semiconductor if its highest occupied molecular orbital (HOMO) is observed at a level slightly below the redox couple of  $I^-/I_3^-$  electrolyte (-4.8 eV) and lowest unoccupied molecular orbital (LUMO) is observed above the conduction band of  $TiO_2$  (-4.0 eV).<sup>76, 105, 106</sup>

Apart from the simple D- $\pi$ -A framework, several other configurations like D-D- $\pi$ -A,<sup>107-109</sup> D-A- $\pi$ -A,<sup>110-113</sup> D- $\pi$ -A-A,<sup>114</sup> (D- $\pi$ -A)<sub>2</sub>,<sup>115</sup> and double D- $\pi$ -A bridges<sup>116</sup> were also introduced and revealed that the introduction of additional donors, acceptors, and extension of  $\pi$  conjugation reduces the HOMO-LUMO energy gap and redshifts the absorption maximum. In other words, for the improved PCE, the donor should be stable, and electron-rich for the effective electron injection to the  $TiO_2$  conduction band,<sup>96, 117, 118</sup> and thereby broaden their absorption to Vis-NIR region.<sup>117, 118</sup> Therefore, for effective dye designing, it is very important to understand the electronic and photophysical properties of the dye systems.<sup>111</sup> Density functional theory (DFT) and Time-dependent density functional theory (TD-DFT) can afford a more efficient approach to understand and predict these structural and electronic features without any time delay than the traditional trial and error methods.<sup>119-130</sup> Previous studies have shown that the donor strength has a significant role in absorption maximum, kinetics of electron injection and light-harvesting efficiency.<sup>131, 132</sup> Recently, the relevance of the theoretical estimation of donor strength in organic electronics has been explained by Köse.<sup>133</sup>

Thirteen typically used donor building blocks (Figure 2.6) in the DSSC applications are selected for this DFT/TDDFT study.<sup>92, 98, 134-139</sup> The estimation of their donating strength is made by molecular electrostatic potential (MESP) topographical features of the donor molecules and the corresponding D- $\pi$ -A systems. The MESP distribution is useful to understand the charge distribution within a molecule,<sup>56, 140-142</sup> and the regions with negative MESP values indicate electron-dense regions while positive-valued areas represent electron-deficient regions.



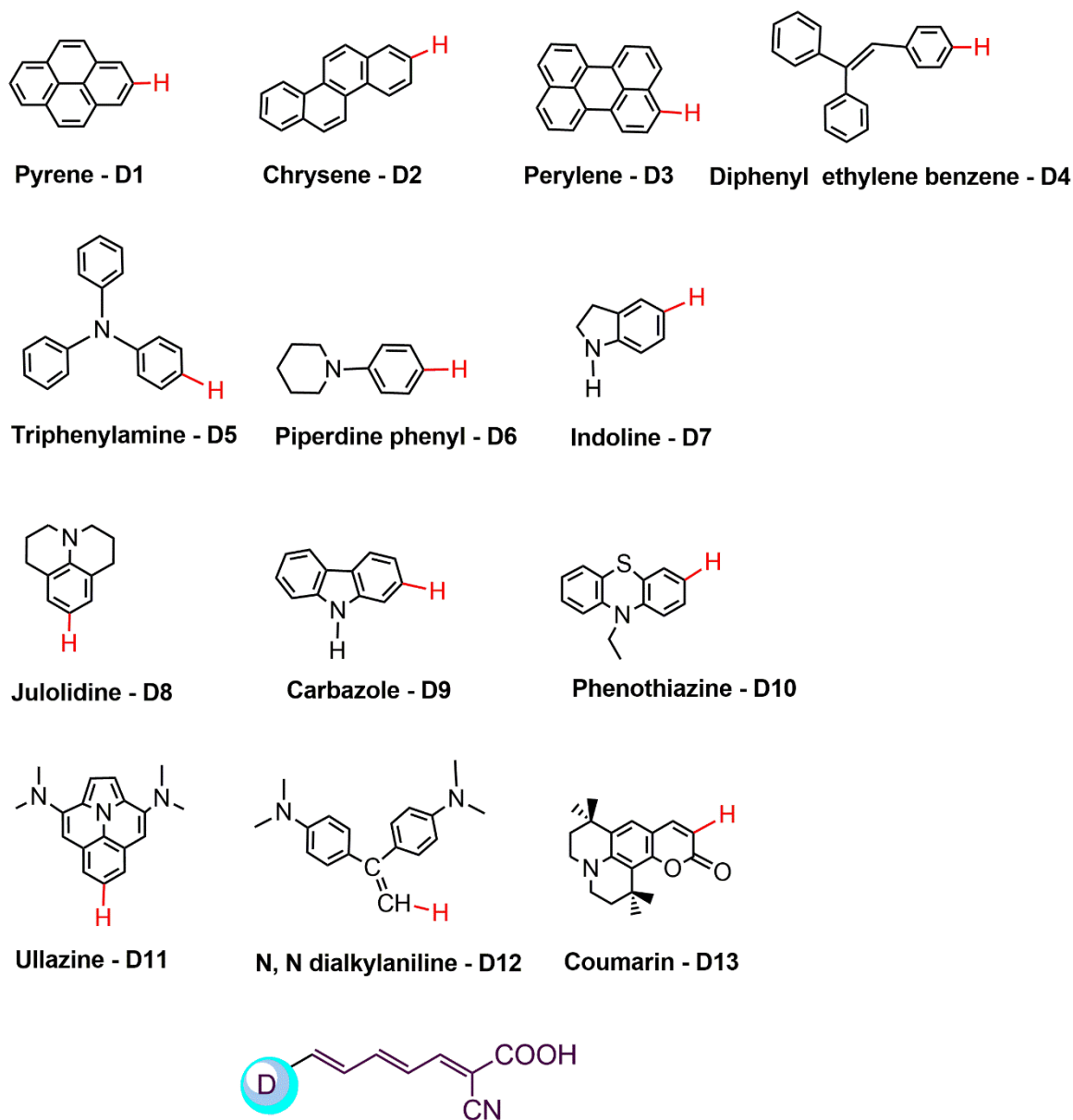


**Figure 2.6** ChemDraw representation of donors (D1 - D13) and D- $\pi$ -A systems (at the bottom). The bond shown in red colour is replaced with  $\pi$ -A part to design the D- $\pi$ -A system.

The MESP based interpretation has been used for the study of substituent effects, intermolecular interactions, non-covalent interactions, hydrogen bonding, cation- $\pi$  interactions, aromaticity, and a variety of chemical phenomena.<sup>143-146</sup> MESP analysis has been used in the field of organometallic chemistry for the quantification of electron-donating strength of phosphine and N-heterocyclic ligands.<sup>140</sup> The global minimum ( $V_m$ ) of MESP near the two-electron donor atom (P or N) indicates the net donating ability of the ligand for making a coordination bond with a metal centre. Further, Suresh and co-workers proved that MESP minimum ( $V_m$ ) analysis is very

effective for the quantification of inductive, resonance, steric, and proximity effects of substituents.<sup>29, 51, 52, 142, 147</sup> Recently the substituent effect transmitting power ( $\gamma$ ) through various spacer units is also calculated *via* MESP analysis and showed that  $V_m$  values are beneficial for the quantification of the transmission power of spacers.<sup>148</sup> The study recommends the usage of short alkenyl systems as spacers for effective electronic transmission. Moreover, the above reliable studies confirmed that MESP is a powerful descriptor, capable to predict electronic properties of the molecular systems effectively. The present study focuses on MESP analysis of D- $\pi$ -A systems towards photovoltaic applications. The butadiene moiety (-HC=CH-CH=CH-) and cyanoacrylic acid unit (-H<sub>2</sub>C=C(CN)-COOH) are used as the  $\pi$ -spacer and anchoring (A) group, respectively.

## 2.8 Computational methodology

The ground state geometry optimization has been carried out using B3LYP density functional theory (DFT) method<sup>149</sup> using cc-pVDZ basis set,<sup>150</sup> this DFT method has been extensively used in the theoretical studies of organic dyes for dye-sensitized solar cell applications.<sup>112, 127</sup> Frequency calculations were also done with the same level of theory and confirmed that there were no imaginary frequencies. Vertical excitation energy calculations have been done for the first 7 states by using long-range and solvation effect-corrected CAM-B3LYP/cc-pVDZ DFT method<sup>123</sup> in dichloromethane. The reliability of this method has been checked by doing the computation on experimentally known systems (Figure 2.7) using three more methods, *viz.* B3LYP,<sup>149</sup> PBE1PBE,<sup>151</sup> and  $\omega$ B97XD<sup>152</sup>. For all these methods, the solvation effects are incorporated through the self-consistent reaction field (SCRf) calculation implemented in SMD (solvation model based on electron density) model.<sup>153</sup> The TD-DFT calculations showed that the result given by CAM-B3LYP is the most reliable to reproduce the experimental absorption maximum (Table 2.6). DFT and TD-DFT calculations are done with the Gaussian 16 program package.<sup>154</sup> For quantifying the electron donating strength of donors in D- $\pi$ -A system, molecular electrostatic potential (MESP) analysis has been performed at B3LYP/cc-pVDZ level.

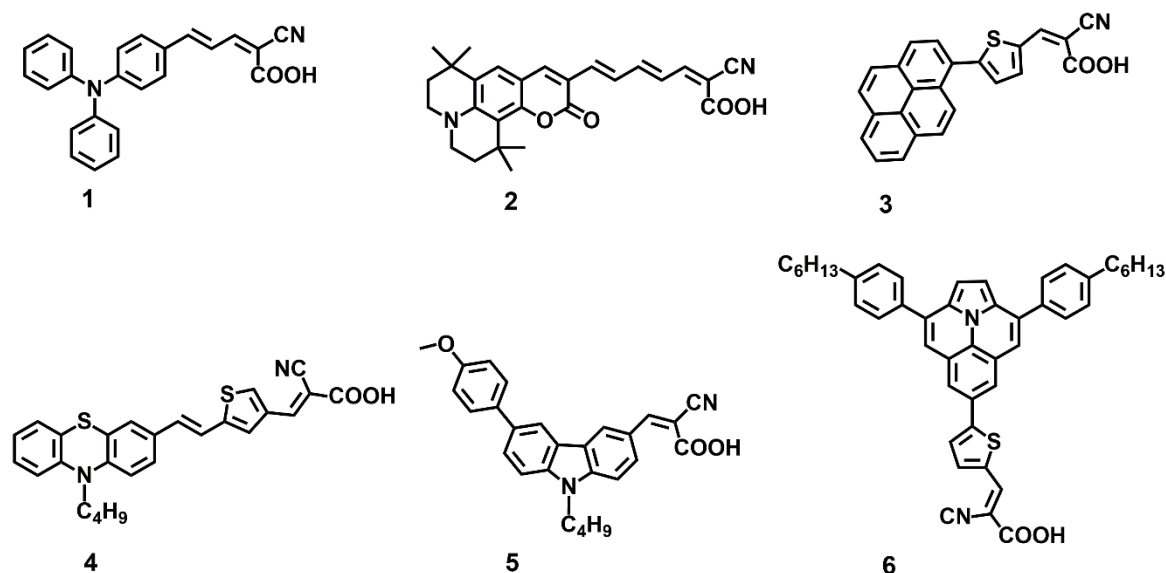


**Figure 2. 7** Chemdraw representations of known systems (1 – 6).

**Table 2. 6** Benchmark time-dependent DFT calculations using DFT/SMD/cc-pVDZ method to obtain the absorption spectra. The absorption maxima  $\lambda_{\max}$  (nm) and oscillator strength (f) are given along with experimentally known  $\lambda_{\max}$ . All the geometries are optimized at B3LYP/cc-pVDZ level.

Systems	CAM-B3LYP		B3LYP		PBE1PBE		$\omega$ B97XD		Exp. $\lambda_{\max}$	Deviation from exp. $\lambda_{\max}$ (CAM-B3LYP)
	$\lambda_{\max}$	f	$\lambda_{\max}$	f	$\lambda_{\max}$	f	$\lambda_{\max}$	f		
1	422	1.52	559	1.44	488	1.24	429	1.48	417 (EtOH) <sup>92</sup>	-5
2	499	1.99	577	1.71	560	1.80	488	2.01	506 (MeOH) <sup>126</sup>	7
3	409	1.25	508	0.65	482	0.75	398	1.35	388 (THF) <sup>98</sup>	-21
4	460	1.41	599	0.78	563	0.90	448	1.44	494 (DCM) <sup>59</sup>	34
5	355	1.09	445	0.39	420	0.49	348	1.15	338 (DCM) <sup>155</sup>	-17
6	388	1.60	462	0.64	436	0.93	382	1.67	388 (DCM) <sup>118</sup>	0

## 2.9 Results and discussion

### 2.9.1 MESP analysis of donor molecules

The MESP minima  $V_m$  are useful to locate the most electron-rich regions in the molecules. The  $V_m$  appears on aromatic rings, on hetero atoms and on CC double bonds of donor molecules (D1 - D13) are shown in Figure 2.8. Since all the systems

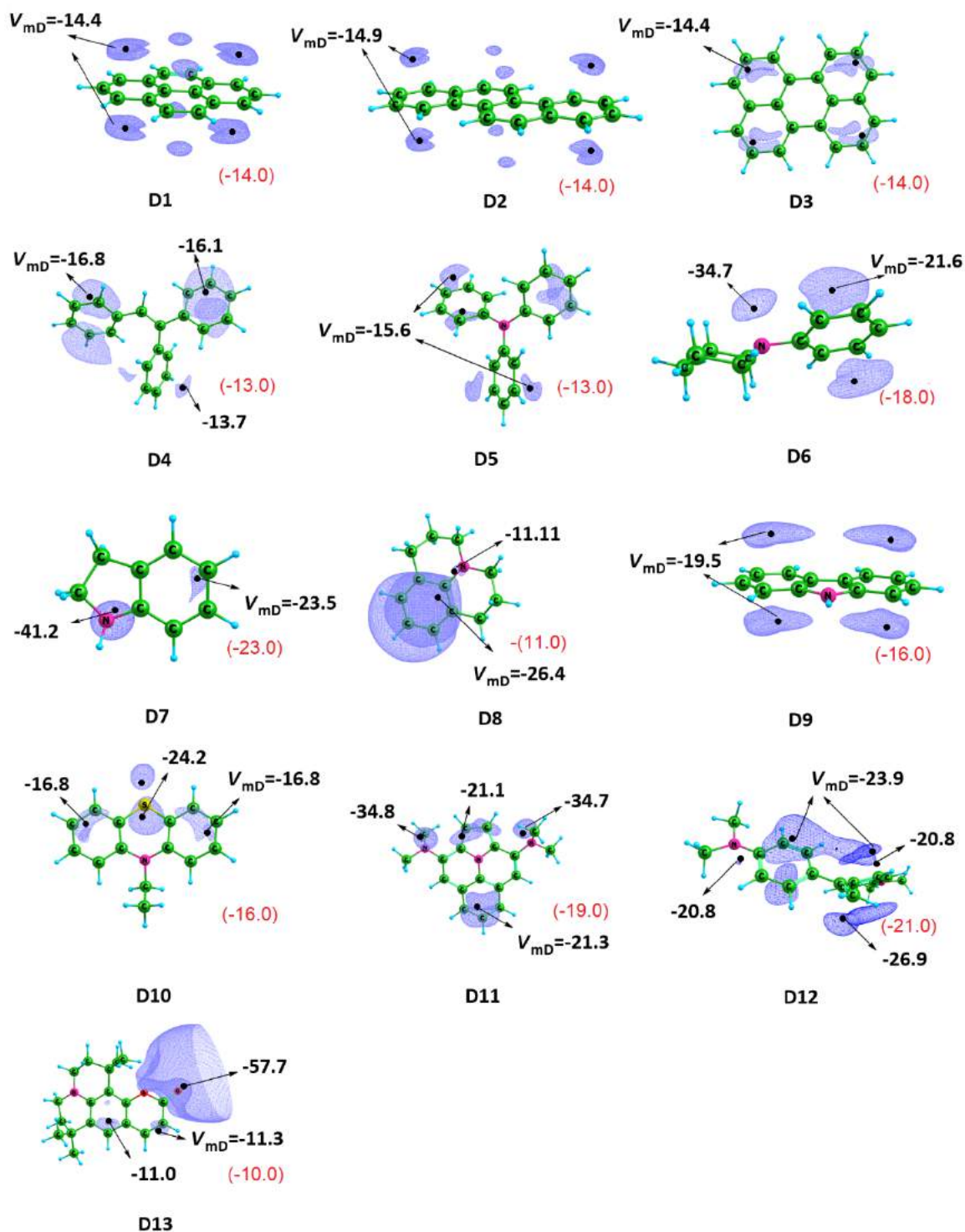


**Figure 2.8** MESP minima at the donor site,  $V_{mD}$  of the donor systems. Isosurface values in kcal/mol are given in brackets. Here carbon, nitrogen, sulfur, and oxygen atoms are shown in green, pink, yellow, and red in colours.

contain at least one aromatic ring, the ring showing the most negative  $V_m$  ( $V_{mD}$ ) is taken for comparing the donor strength of each system. The  $V_{mD}$  of all the systems are

depicted in Figure 2.8 along with other  $V_m$  values. In polycyclic aromatic hydrocarbon (PAH) systems (D1 - D3),  $V_{mD}$  values lie in a small range -14.4 to -14.9 kcal/mol which can be attributed to similar  $\pi$ -conjugation features which are not affected by a hetero atom or a substituent. In the D4 system, two phenyl rings show nearly a coplanar arrangement with the CC double bond and their  $V_{mD}$  (-16.1 and -16.8 kcal/mol) values are more negative than a PAH while the third phenyl ring having a highly twisted arrangement with respect to the CC double bond shows  $V_{mD}$  -13.7 kcal/mol. It appears that the presence of a conjugated CC bond in D4 enhances its electron density over the corresponding aromatic rings. In D5, three phenyl rings share the lone pair electron density from the nitrogen centre leading to a more negative character for  $V_{mD}$  -15.6 kcal/mol than a PAH. In D6, D7, and D8, an amino nitrogen centre is connected with an arene ring. In piperidine-phenyl system D6, the nitrogen centre is more pyramidalized than the other two and shows the least negative  $V_{mD}$  (-21.6 kcal/mol) among the three. In D7 and D8, fusing the N-alkyl unit/s with the aromatic ring improves the planarization of the N-centre, leading to more electron donation *via* +R effect to the arene ring. As result, julolidine D8 shows the most electron-rich arene ring in terms of  $V_{mD}$  (-26.4 kcal/mol) followed by D7 (-23.5 kcal/mol). Compared to a PAH, carbazole arene rings show significantly more negative  $V_{mD}$  (-19.5 kcal/mol); here the sharing of N-centre lone pair is with two aromatic rings which leads to less negative  $V_{mD}$  than D6 - D8. Similarly, in D10, sharing of N-lone pair with two arene rings can be seen in addition to the effect of hetero S atom. In this case,  $V_{mD}$  is less negative than carbazole. In D11, the combined effect of three N-centres can be attributed to the electron-rich nature of the arene ring ( $V_{mD}$  -21.3 kcal/mol) and among the N-centres, the N,N-dimethyl units are not fully effective of +R influence due to slight pyramidalization causing by steric congestions from the alkyl moiety of the adjacent five-membered ring. In D12, along with the +R contribution of N,N-dimethyl substituents, the conjugation effect of CC double bond is leading to relative more electron-rich arene rings. The least negative  $V_{mD}$  -11.0 kcal/mol is observed in D13, the coumarin system. Here, the presence of a highly electron-withdrawing carbonyl group at the heterocyclic ring reduces the electron density on the aromatic ring.

## 2.9.2 MESP analysis of D- $\pi$ -A systems

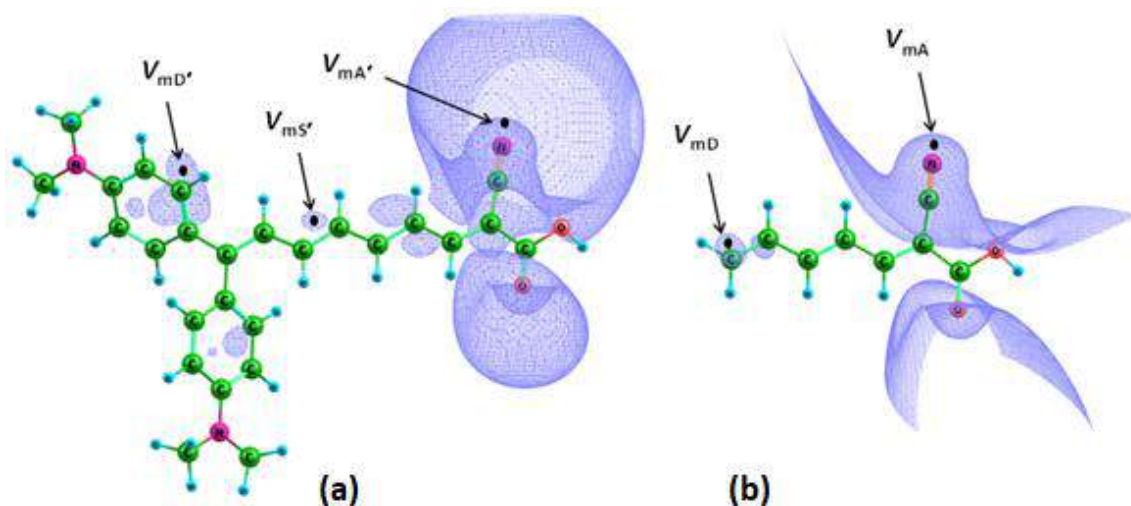


**Figure 2.9** MESP isosurface plot of a) representative D- $\pi$ -A system, b) reference system.

The donating strength of donor fragments in the D- $\pi$ -A system has been studied by MESP analysis. The MESP isosurface plot of a representative D- $\pi$ -A system (D12) is shown in Figure 2.9a along with MESP minimum ( $V_m$ ) values at various positions. The positions selected for  $V_m$  analysis are (i) donor site ( $V_{mD}'$ ), (ii) spacer site nearer to donor ( $V_{mS}'$ ) and (iii) anchor site ( $V_{mA}'$ ). The  $\pi$ -A portion is built by linking a butadiene moiety ( $\pi$ -spacer) with cyanoacrylic acid moiety (A). Since the  $\pi$ -spacer and anchor units are the same for all donors, it has been considered as a reference system and the corresponding MESP minimum at its spacer ( $V_{mS}$ ) and anchoring sites ( $V_{mA}$ ) are evaluated for comparing with those of D- $\pi$ -A system (Figure 2.9b). The various MESP minimum values, *viz.*  $V_{mD}'$ ,  $V_{mS}'$  and  $V_{mA}'$  are shown in Table 2.7 along with the most negative  $V_m$  of the donor molecule ( $V_{mD}$ ). In Table 2.7, the quantities  $\Delta V_{mD}$ ,  $\Delta V_{mS}$ , and  $\Delta V_{mA}$  represent the change occurred on the minimum potential of the donor, spacer and anchoring sites with the introduction of the  $\pi$ -A system. Further, in order to calculate  $\Delta V_{mD}$ , the most negative minima at the phenyl ring of each donor ( $V_{mD}$ ) have been subtracted from the corresponding minima ( $V_{mD}'$ ) of the D- $\pi$ -A system. Similarly,  $\Delta V_{mS}$  and  $\Delta V_{mA}$  have been calculated by subtracting the  $V_m$  values at spacer and anchoring moieties of the reference system ( $V_{mS}$  and  $V_{mA}$ ) from the corresponding minima ( $V_{mS}'$  and  $V_{mA}'$ ) of the D- $\pi$ -A system.

**Table 2.7**  $V_m$  (kcal/mol) of the D- $\pi$ -A systems calculated with B3LYP/cc-pVDZ level.

Systems	$V_{mD}$	$V_{mD'}$	$\Delta V_{mD}$	$V_{mS}$	$V_{mS'}$	$\Delta V_{mS}$	$V_{mA}$	$V_{mA'}$	$\Delta V_{mA}$
D1	-14.4	-8.2	6.2	-2.4	-3.3	-0.9	-50.3	-53.0	-2.7
D2	-14.9	-9.8	5.1	-2.4	-3.3	-0.9	-50.3	-53.0	-2.6
D3	-14.4	-8.0	6.4	-2.4	-4.0	-1.6	-50.3	-54.2	-3.8
D4	-16.8	-7.8	9.0	-2.4	-4.3	-1.9	-50.3	-54.2	-3.8
D5	-15.6	-7.7	7.9	-2.4	-6.3	-3.9	-50.3	-56.0	-5.7
D6	-21.6	-9.3	12.3	-2.4	-8.0	-5.6	-50.3	-57.5	-7.2
D7	-23.5	-8.8	14.7	-2.4	-8.3	-5.9	-50.3	-57.5	-7.2
D8	-26.4	-10.0	16.4	-2.4	-10.8	-8.4	-50.3	-59.5	-9.2
D9	-19.5	-12.0	7.5	-2.4	-4.8	-2.4	-50.3	-54.8	-4.5
D10	-16.8	-9.4	7.4	-2.4	-5.3	-2.9	-50.3	-55.2	-4.9
D11	-21.3	-11.0	10.3	-2.4	-7.5	-5.1	-50.3	-55.4	-5.1
D12	-23.9	-14.1	9.8	-2.4	-12.9	-10.5	-50.3	-61.4	-11.0
D13	-11.0	-1.9	9.1	-2.4	-8.0	-5.6	-50.3	-56.5	-6.2

From Table 2.7, it is clear that when a donor part is being attached with a  $\pi$ -A system, the minimum potential on the donor site ( $V_{mD'}$ ) becomes less negative indicating the electron transferring ability from the donor site to the  $\pi$ -A site. The term  $\Delta V_{mD}$  in Table 2.7 represents the change occurred on the minimum potential at the donor site during the  $\pi$ -A linkage which varies from 5.1 to 16.4 kcal/mol and indicates the intramolecular charge transfer involved in D- $\pi$ -A system. Further, at the spacer site of D- $\pi$ -A, electron density gain is observed represented by negative  $\Delta V_{mS}$  which lies in the range -0.9 to -10.5 kcal/mol. On the basis of  $\Delta V_{mS}$ , the highest donating strength can be attributed to D12, while the least donating strength can be assigned for PAHs.

The  $V_{mA'}$  values indicate that the minimum potential at the anchor moiety, for example at cyano group, shows significant variations with respect to different donor units. The most electron-donating donor is expected to show the most negative  $V_{mA'}$ . In DSSC applications, the cyanoacrylic portion has to be linked to the  $TiO_2$  semiconductor for efficient electron transfer. By making the anchoring group electron-rich, efficient electron transfer from the dye to  $TiO_2$  can occur. In other

words, the efficiency of the DSSC system can be directly related to the electron-donating strength of the donor moieties. Due to this reason, the change in MESP minimum appeared on the anchoring part ( $\Delta V_{\text{mA}}$ ) has been considered as the donating strength of the donor moiety. The PAHs (D1-D3) showed the least negative  $\Delta V_{\text{mA}}$  (-2.7 to -3.8 kcal/mol), indicating their poor electron-donating strength. Also, in D4 system, a similar donating strength -3.8 kcal/mol is observed. In D5, the introduction of N-centre imparts more negative  $\Delta V_{\text{mA}}$  (-5.7 kcal/mol) than PAHs which explains its better electron-donating strength than polyacenes. In D6 and D7, the more planarized nitrogen centres in donor part impart more negative  $\Delta V_{\text{mA}}$  (-7.2 kcal/mol) and suggests its higher electron-donating strength than D5. In D8 system, the fused N-centre with the aromatic ring further improves its planarization and leads to more negative  $\Delta V_{\text{mA}}$  -9.2 kcal/mol than D5, D6, and D7. In carbazole (D9), N-lone pair is shared between two aromatic rings through resonance, and as a result, the electron-donating strength in terms of  $\Delta V_{\text{mA}}$  (-4.5 kcal/mol) appears weaker than those (D6 - D8) having only one aromatic ring for sharing N-lone pair. In D10, the presence of sulfur slightly enhances the negative of  $\Delta V_{\text{mA}}$  to -5.1 kcal/mol. Even though there are three nitrogen centres in ullazine, it shows a donating strength -5.1 kcal/mol which can be attributed to the influence of pyramidalized N,N-dimethyl groups in ullazine. In D12, more negative  $\Delta V_{\text{mA}}$  of -11.0 kcal/mol can be recognized with the +R effect of mostly planarized N,N-dimethyl substituents. Finally, in D13 a more negative  $\Delta V_{\text{mA}}$  (-6.2 kcal/mol) than PAHs has been observed due to the interplay of electron-rich nitrogen centre and the electron-withdrawing carbonyl group. These results strongly suggest that the incorporation of an electron-rich heteroatom in the donor region can have a positive influence on the electronic transmission to the acceptor moiety. On the basis of  $\Delta V_{\text{mA}}$ , the order of donating strength of donor groups can be written as  $D2 < D1 < D3 = D4 < D9 < D10 < D11 < D5 < D13 < D6 = D7 < D8 < D12$ . The julolidine based donor system D8 and the N, N-dialkyl aniline incorporated D12 are the most efficient among the studied systems.

### 2.9.3 Absorption spectra of donor and D- $\pi$ -A systems

The absorption maxima of all the systems (donor and D- $\pi$ -A) along with oscillator strength ( $f$ ) are summarized in Table 2.8. For the assessment of absorptional shift  $\Delta\lambda_{\text{max}}$ , the absorption maximum of the D- $\pi$ -A system was subtracted from the donor



**Table 2.8** Maximum absorption wavelength  $\lambda_{\max}$  (nm), oscillator strength  $f$ , absorptional shift  $\Delta\lambda_{\max}$  and percentage MO contribution of donor and D- $\pi$ -A systems at TD-CAM-B3LYP/SMD/cc-pVDZ//B3LYP/cc-pVDZ level.

Systems	Donor			D- $\pi$ -A			$\Delta\lambda_{\max}$
	$\lambda_{\max}$	$f$	MO contribution	$\lambda_{\max}$	$f$	MO contribution	
D1	320	0.52	H $\rightarrow$ L (93.2%)	401	2.21	H-1 $\rightarrow$ L (94.2 %)	81
				376	0.03	H $\rightarrow$ L (74.6 %)	56
D2	306	0.03	H-1 $\rightarrow$ L (33.6 %)	409	2.47	H $\rightarrow$ L (79.3 %)	103
			H $\rightarrow$ L (19.9 %)				
			H $\rightarrow$ L+1 (39.5 %)				
	300	0.23	H $\rightarrow$ L (68.5 %)				109
D3	408	0.59	H $\rightarrow$ L (98.7 %)	518	1.73	H $\rightarrow$ L (90.4 %)	110
D4	300	0.78	H $\rightarrow$ L (97.0 %)	434	2.21	H $\rightarrow$ L (88.6 %)	134
D5	284	0.03	H $\rightarrow$ L (90.8 %)	453	2.02	H $\rightarrow$ L (86.7 %)	169
	279	0.38	H $\rightarrow$ L+1 (98.8 %)				174
D6	256	0.05	H $\rightarrow$ L (87.8 %)	446	2.00	H $\rightarrow$ L (92.6 %)	190
	236	0.37	H $\rightarrow$ L+1 (91.7 %)				210
D7	261	0.09	H $\rightarrow$ L (90.5 %)	448	1.86	H $\rightarrow$ L (93.7 %)	187
	226	0.18	H $\rightarrow$ L+1 (90.0 %)				222
D8	277	0.08	H $\rightarrow$ L (92.9 %)	480	1.95	H $\rightarrow$ L (93.2 %)	203
	243	0.29	H $\rightarrow$ L+1 (92.9 %)				237
D9	286	0.06	H $\rightarrow$ L (87.6 %)	419	2.21	H $\rightarrow$ L (93.2 %)	133
	262	0.31	H-1 $\rightarrow$ L (84.2 %)				157
D10	319	0.02	H $\rightarrow$ L (95.2 %)	459	1.67	H $\rightarrow$ L (84.8 %)	140
	275	0.18	H $\rightarrow$ L+2 (84.6 %)				184
D11	324	0.38	H $\rightarrow$ L (90.8 %)	448	0.02	H $\rightarrow$ L (89.2 %)	124
				411	2.11	H-1 $\rightarrow$ L (73.6 %)	87
D12	278	0.20	H $\rightarrow$ L (78.0 %)	520	1.95	H $\rightarrow$ L (92.6 %)	242
D13	334	0.64	H $\rightarrow$ L (95.3 %)	503	1.99	H $\rightarrow$ L (89.3 %)	169

system. For calculating  $\Delta\lambda_{\max}$ , HOMO  $\rightarrow$  LUMO orbital transition has been considered, except for D1. In D1,  $\lambda_{\max}$  is observed for HOMO-1  $\rightarrow$  LUMO transition, while its HOMO  $\rightarrow$  LUMO transition is nearly forbidden due to very small  $f$  value. The data in Table 2.8 clearly suggest that the absorption maximum ( $\lambda_{\max}$ ) of D- $\pi$ -A shifts significantly to a higher wavelength region compared to the donor D. Since in all systems, we used same spacer and anchoring moiety (the  $\pi$ -A unit), the influence of them on the absorptional shift ( $\Delta\lambda_{\max}$ ) can be considered as same. This implies that the large variation in  $\Delta\lambda_{\max}$  exhibited by the D- $\pi$ -A system is due to the variation in the donating strength of donor moieties. For instance, among all donor moieties, D1 with  $\Delta\lambda_{\max}$  81 nm is the least donating while D12 with  $\Delta\lambda_{\max}$  242 nm is the most donating (Table 2.8). Further,  $\Delta V_{\text{mA}}$  with  $\Delta\lambda_{\max}$  with correlation coefficient shows a linear correlation 0.966 (Figure 2.10) shows the significance of donating strength  $\Delta V_{\text{mA}}$  on  $\Delta\lambda_{\max}$ . In the linear correlation plot, D1 and D11 based D- $\pi$ -A systems exhibit slight deviation, which can be attributed as their less intense ( $f \rightarrow 0.02 - 0.03$ ) and nearly forbidden HOMO  $\rightarrow$  LUMO charge transfer character of the orbital excitation. From the results the shift in absorption maxima ( $\Delta\lambda_{\max}$ ) follows the order D12 > D8 > D7 > D6 > D10 > D5 > D13 > D9 > D4 > D3 > D2 > D11 > D1, preferably due to the nature of donor groups. Therefore, to improve the wavelength of absorption to a preferred region (Vis to NIR), its donating ability has to be tuned with the introduction of better electron-donating donor groups (preferably more nitrogen centres).

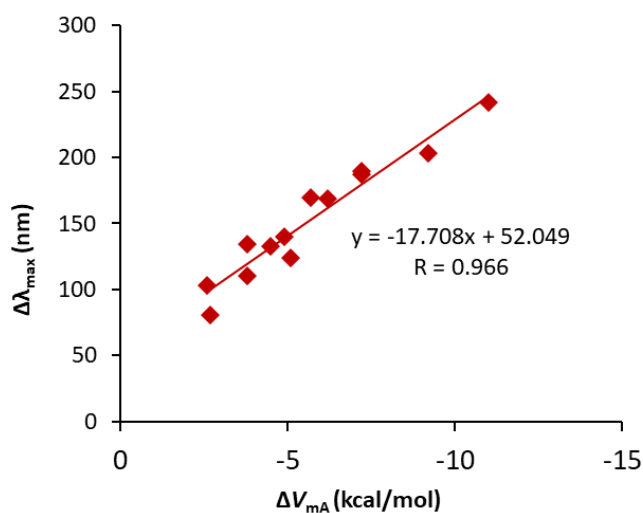


**Figure 2.10** Correlation between donating strength ( $\Delta V_{\text{mA}}$ ) of D- $\pi$ -A system and change in absorption maxima ( $\Delta\lambda_{\max}$ ).

The frontier molecular orbital energy levels given in Figure 2.11 show the HOMO-LUMO band gap features of D, D- $\pi$ -A and  $\pi$ -A (butadiene moiety linked with cyano acrylic acid). The HOMO value ( $\epsilon_h$ ) of the D systems is in the range -4.66 to -5.70 eV, whereas that of D- $\pi$ -A system is in the range -4.96 to -5.89 eV. This data indicates the close resemblance of the HOMO level of D and D- $\pi$ -A. On the other hand, the LUMO energy ( $\epsilon_l$ ) of D shows a large deviation from the  $\epsilon_l$  of D- $\pi$ -A indicating clear dissimilarity. In fact,  $\epsilon_l$  of D- $\pi$ -A in the range -2.52 to -3.10 eV is very close to  $\epsilon_l$  -2.97 eV observed for  $\pi$ -A. Thus, the data in Figure 2.11 indicate that HOMO of D- $\pi$ -A is more like HOMO of donor and its LUMO is more like that of  $\pi$ -A. This feature is well evident in the frontier molecular orbital diagram given in D- $\pi$ -A for representative cases (Figure 2.12). HOMO is more localized towards the donor region with decreasing orbital contributions from the  $\pi$ -A, while the LUMO is mostly localized at the  $\pi$ -A region. D1- $\pi$ -A is an exception wherein HOMO-1 to LUMO is the allowed transition and its HOMO has a different  $\pi$  character, localized exclusively on the pyrene ring. The data in Figure 2.11 clearly suggest that linking the donor system to the  $\pi$ -A unit is very effective for reducing the bandgap. For all cases, the HOMO level is tuned towards the value of  $I^-/I_3^-$  electrolyte couple while the LUMO level appears closer to the conduction band (CB) of TiO<sub>2</sub>. The HOMO and LUMO distribution and their energy levels suggest significant charge separation in the excited state leading to strong electron coupling of the dye with TiO<sub>2</sub> semiconductor which promotes the electron transfer to the conduction band.<sup>156</sup>

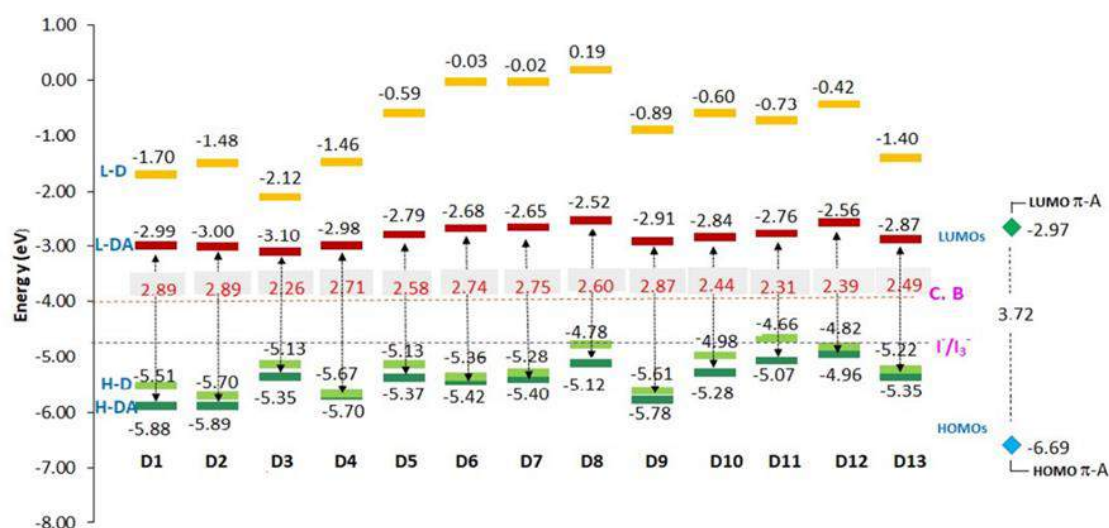


**Figure 2.11** Frontier molecular energy level diagram of D- $\pi$ -A systems at B3LYP/cc-pVDZ level.

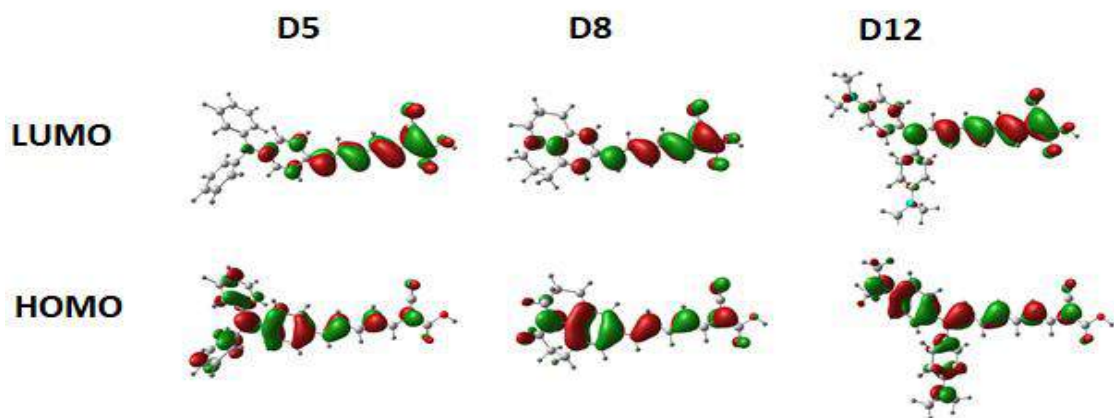


**Figure 2.12** Frontier molecular orbitals of representative D- $\pi$ -A systems at B3LYP/cc-pVDZ level.

**Table 2.9** Absorption maxima of methyl substituted pyrene based D1- $\pi$ -A systems at TD-CAM-B3LYP/SMD/cc-pVDZ//B3LYP/cc-pVDZ level. Here D1 represents unsubstituted pyrene-based D- $\pi$ -A system, while D1-1, D1-2, D1-3, *etc.* represents the methyl substitution at 1, 2, 3, 4 and 5 positions of D1- $\pi$ -A (see Figure 2.13 for numbering).

D- $\pi$ -A systems	HOMO-1 (eV)	HOMO (eV)	LUMO (eV)	HLG (eV)	$\lambda_{\max}$ (nm)	f	MO contribution
D1	-6.02	-5.88	-2.99	2.89	S1 $\rightarrow$ 401	2.22	H-1 $\rightarrow$ L (94.17 %)
					S2 $\rightarrow$ 376	0.03	H $\rightarrow$ L (74.56 %)
D1-1	-5.73	-5.39	-2.81	2.58	430	2.21	H $\rightarrow$ L (72.12%)
D1-2	-5.95	-5.46	-2.92	2.54	404	1.05	H $\rightarrow$ L (45.84%)
D1-3	-5.94	-5.62	-2.92	2.70	405	1.95	H-1 $\rightarrow$ L (69.83%)
							H $\rightarrow$ L (21.06%)
D1-4	-5.93	-5.62	-2.94	2.69	407	2.07	H-1 $\rightarrow$ L (74.28%)
							H $\rightarrow$ L (17.43%)
D1-5	-5.93	-5.83	-2.91	2.92	S1 $\rightarrow$ 405	2.19	H-1 $\rightarrow$ L (94.84%)
					S2 $\rightarrow$ 381		0.03

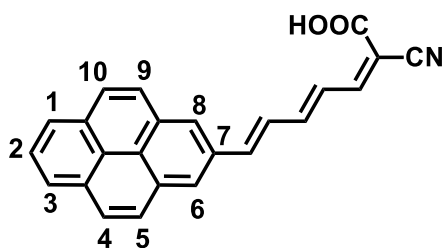


**Figure 2.13** ChemDraw representation of D1- $\pi$ -A system.

In general, compared to D systems, the absorption maxima of D- $\pi$ -A systems show a significant red shift (Table 2.8) in the range 81 – 242 nm. In D1- $\pi$ -A and D2- $\pi$ -A,  $\lambda_{\max}$  is observed at 401 and 409 nm, respectively. The major electronic excitation of pyrene incorporated D1- $\pi$ -A is assigned as HOMO-1 to LUMO. The forbidden HOMO to LUMO transition of D1- $\pi$ -A can be changed to allowed one by appropriate substitution such as a substitution by the methyl group at the first or second position (Table 2.9 and Figure 2.13). The D3- $\pi$ -A showed a broad absorption coverage in the visible region with  $\lambda_{\max}$  518 nm corresponding to the HOMO-LUMO transition. Among all, D3- $\pi$ -A has the lowest HOMO-LUMO band gap, 2.26 eV (Figure 2.11). The D4 in D4- $\pi$ -A is more electron-donating than a PAH moiety and it shows a smaller bandgap 2.71 eV than D1 to D2 incorporated systems. Further, in nitrogen-containing D- $\pi$ -A systems (D5 - D13), the band gap energy decreases to a greater extent 2.31 – 2.75 eV for all except D9- $\pi$ -A (2.87 eV) than hydrocarbon systems. Among the nitrogen-containing systems, D12- $\pi$ -A showed the highest  $\lambda_{\max}$  520 nm with band gap 2.39 eV while D11- $\pi$ -A showed the lowest bandgap 2.31 eV. The  $\lambda_{\max}$  of D11- $\pi$ -A observed at 411 nm is due to HOMO-1 to LUMO transition. Among all, the HOMO energy level of D12- $\pi$ -A appeared nearest to the energy level of redox electrolyte while its LUMO level is 1.44 eV higher than the CB of TiO<sub>2</sub>. The LUMO energy level of all systems offer a favourable electron injection from the excited state to the conduction band of TiO<sub>2</sub> while HOMO energies lower than the oxidation potential of I<sup>-</sup>/I<sub>3</sub><sup>-</sup> electrolyte (-4.8 eV) indicate effective dye regeneration. These results support their effective utilization in the DSSC application. The D3- $\pi$ -A, D11- $\pi$ -A and D12- $\pi$ -A systems are among the lowest band gap systems, desirable for harvesting more light in the UV-visible region.

## 2.9.4 Analysis of photovoltaic parameters

In Table 2.10, the  $\Delta G_{inject}$  values fall in the range -1.04 to -1.94 eV, the D11- $\pi$ -A with the most negative value has the highest electron injection efficiency while D2 to D4 based D- $\pi$ -A systems show the lowest efficiency. The smallest  $\Delta G_{reg}$  0.16 eV is observed for D12- $\pi$ -A and suggests its fastest dye regeneration efficiency. A good

**Table 2.10** Calculated vertical excitation energy, absorption maximum, oscillator strength f, HOMO LUMO energy, HOMO-LUMO energy gap (HLG), ground and excited-state oxidation potentials ( $E^{dye}$  and  $E^{dye*}$ ), electron injection free energy change ( $\Delta G_{inject}$ ), free energy change for dye regeneration ( $\Delta G_{reg}$ ), and open circuit voltage ( $eV_{oc}$ ) of D- $\pi$ -A systems at TD-CAM-B3LYP/SMD/cc-pVDZ//B3LYP/cc-pVDZ level.

Systems	Excitation energy (eV)	$\lambda_{absmax}$ (nm)	f	HOMO (eV)	LUMO (eV)	HLG (eV)	$E^{dye}$ (eV)	$E^{dye*}$ (eV)	$\Delta G_{inject}$ (eV)	$\Delta G_{reg}$ (eV)	( $eV_{oc}$ ) (eV)
D1	3.09	401	2.22	-5.88	-2.99	2.89	5.88	2.79	-1.21	1.08	1.01
D2	3.03	409	2.47	-5.89	-3.00	2.89	5.89	2.86	-1.14	1.09	1.00
D3	2.39	518	1.73	-5.35	-3.10	2.26	5.35	2.96	-1.04	0.55	0.90
D4	2.86	434	2.21	-5.70	-2.98	2.71	5.70	2.84	-1.16	0.90	1.02
D5	2.73	453	2.02	-5.37	-2.79	2.58	5.37	2.64	-1.36	0.57	1.21
D6	2.78	446	2.00	-5.42	-2.68	2.74	5.42	2.64	-1.36	0.62	1.32
D7	2.59	448	1.95	-5.40	-2.65	2.75	5.40	2.81	-1.19	0.60	1.35
D8	2.77	480	1.86	-5.12	-2.52	2.60	5.12	2.35	-1.65	0.32	1.48
D9	2.96	419	2.21	-5.78	-2.91	2.87	5.78	2.82	-1.18	0.98	1.09
D10	2.70	459	1.67	-5.28	-2.84	2.44	5.28	2.58	-1.42	0.48	1.16
D11	3.01	411	2.11	-5.07	-2.76	2.31	5.07	2.06	-1.94	0.27	1.24
D12	2.39	520	1.95	-4.96	-2.56	2.39	4.96	2.57	-1.43	0.16	1.44
D13	2.46	503	1.99	-5.35	-2.87	2.49	5.35	2.89	-1.11	0.55	1.13

linear correlation between  $\Delta V_{mA}$  and  $eV_{oc}$  is observed for all the cases (Figure 2.14) suggesting that the electron-accepting tendency of the acceptor part is well reflected on the LUMO levels. Among all the systems, julolidine based D8- $\pi$ -A possesses the

highest  $\epsilon_1$  value resulting to the highest  $eV_{oc}$  1.48 eV. The second-highest  $eV_{oc}$  1.44 eV is observed for D12- $\pi$ -A. The  $\Delta V_{mA}$  values suggest that the electron-donating ability of PAHs moieties is the lowest among all the donors and the corresponding D1 to D3 based D- $\pi$ -A systems show the lowest range of  $eV_{oc}$ , 0.90 – 1.01 eV.

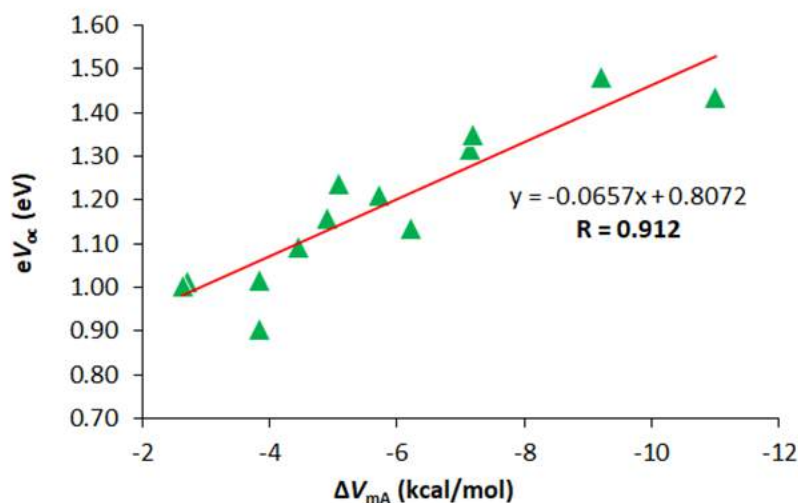


**Figure 2.14** Correlation between  $\Delta V_{mA}$  (kcal/mol) and  $eV_{oc}$  (eV).

## 2.10 Conclusions

Using MESP topographical analysis, the donating strength of thirteen known (D1 – D13) typically used donor systems in the DSSC applications has been quantified. The redshift in absorption maximum ( $\Delta\lambda_{max}$ ) observed for the D- $\pi$ -A systems is rationalized in terms of the amount of electron donation from the donor D moieties to the  $\pi$ -A using the MESP parameter  $\Delta V_{mA}$ . The highest electron-donating strength  $\Delta V_{mA}$  observed in D12- $\pi$ -A shows the highest  $\Delta\lambda_{max}$  and maximum absorption wavelength  $\lambda_{max}$  with a small band gap energy of 2.39 eV. In poor electron-donating D1 and D2 based D- $\pi$ -A systems, the smallest  $\Delta\lambda_{max}$ , and  $\lambda_{max}$  are observed. A linear correlation obtained between  $\Delta V_{mA}$  and  $\Delta\lambda_{max}$  confirms that  $\Delta\lambda_{max}$  increases with increase in  $\Delta V_{mA}$ . The frontier molecular energy levels showed that HOMO of the D- $\pi$ -A resembles more like HOMO of the donor, whereas LUMO resembles more like LUMO of  $\pi$ -A. Thus, the donor tunes the HOMO, while  $\pi$ -A tunes the LUMO energy of the D- $\pi$ -A system for efficient dye regeneration and electron injection. Among all the systems, D12- $\pi$ -A showed the highest electron injection efficiency. Since  $eV_{oc}$  is

directly proportional to the power conversion efficiency of the solar cell, D8- $\pi$ -A and D12- $\pi$ -A having the highest  $eV_{oc}$  can be regarded as the most efficient sensitizers for DSSC while the least  $eV_{oc}$  displayed by PAH based (D1 - D3) D- $\pi$ -A systems offer poor efficiency. The linear correlation between  $\Delta V_{mA}$  and  $eV_{oc}$  shows that  $eV_{oc}$  increases with increase in the negative character of  $\Delta V_{mA}$  and also proves that better sensitizers can be developed by connecting powerful electron donor to a  $\pi$ -A system. One way to do this is by incorporating multiple lone pair bearing nitrogen centres in donors. Thus, the MESP approach offers an easy analysis tool for the quantification of donating strength of D- $\pi$ -A systems in DSSC applications.

## 2.11 References

1. T. M. Krygowski and B. T. Stępień, *Chem. Rev.*, 2005, **105**, 3482-3512.
2. O. Exner and T. M. Krygowski, *Chem. Soc. Rev.*, 1996, **25**, 71-75.
3. C. Hansch, A. Leo and R. W. Taft, *Chem. Rev.*, 1991, **91**, 165-195.
4. W. Adcock and N. A. Trout, *Chem. Rev.*, 1999, **99**, 1415-1435.
5. O. Exner and S. Bohm, *Curr. Org. Chem.*, 2006, **10**, 763-778.
6. L. P. Hammett, *J. Am. Chem. Soc.*, 1937, **59**, 96-103.
7. H. H. Jaffé, *Chem. Rev.*, 1953, **53**, 191-261.
8. T. M. Krygowski, M. A. Dobrowolski, K. Zborowski and M. K. Cyrański, *J. Phys. Chem.*, 2006, **19**, 889-895.
9. C. H. Suresh and S. R. Gadre, *J. Amer. Chem. Soc.*, 1998, **120**, 7049-7055.
10. C. H. Suresh and S. R. Gadre, *J. Phys. Chem. A*, 2007, **111**, 710-714.
11. G. S. Remya and C. H. Suresh, *Phys. Chem. Chem. Phys.*, 2016, **18**, 20615-20626.
12. T. M. Krygowski, K. Ejsmont, B. T. Stępień, M. K. Cyrański, J. Poater and M. Sola, *J. Org. Chem.*, 2004, **69**, 6634-6640.
13. T. M. Krygowski, M. Palusiak, A. Płonka and J. E. Zachara - Horeglad, *J. Phys. Org. Chem.*, 2007, **20**, 297-306.
14. T. M. Krygowski, J. E. Zachara-Horeglad and M. Palusiak, *J. Org. Chem.*, 2010, **75**, 4944-4949.
15. T. M. Krygowski and W. P. Oziminski, *J. Mol. Model.*, 2014, **20**, 2352.
16. S. E. Wheeler and K. N. Houk, *J. Chem. Theory Comput.*, 2009, **5**, 2301-2312.
17. S. E. Wheeler and K. N. Houk, *J. Am. Chem. Soc.*, 2009, **131**, 3126-3127.



18. S. E. Wheeler, *J. Am. Chem. Soc.*, 2011, **133**, 10262-10274.
19. S. E. Wheeler, *Acc. Chem. Res.*, 2013, **46**, 1029-1038.
20. B. Galabov, S. Ilieva and H. F. Schaefer, *J. Org. Chem.*, 2006, **71**, 6382-6387.
21. B. Galabov, V. Nikolova and S. Ilieva, *Chem. Eur. J.*, 2013, **19**, 5149-5155.
22. R. W. Taft, *J. Am. Chem. Soc.*, 1953, **75**, 4231-4238.
23. M. Charton, *Prog. Phys. Org. Chem.*, 1981, **13** 119-251.
24. C. G. Swain and E. C. Lupton, *J. Am. Chem. Soc.*, 1968, **90**, 4328-4337.
25. B. Galabov, S. Ilieva, G. Koleva, W. D. Allen, H. F. Schaefer III and P. von R. Schleyer, *Wiley Interdiscip. Rev. Comput. Mol. Sci*, 2013, **3**, 37-55.
26. F. B. Sayyed and C. H. Suresh, *New. J. Chem.*, 2009, **33**, 2465-2471.
27. F. B. Sayyed, C. H. Suresh and S. R. Gadre, *J. Phys. Chem. A*, 2010, **114**, 12330-12333.
28. F. B. Sayyed and C. H. Suresh, *J. Phys. Chem. A*, 2011, **115**, 9300-9307.
29. F. B. Sayyed and C. H. Suresh, *J. Phys. Chem. A*, 2011, **115**, 5660-5664.
30. F. B. Sayyed and C. H. Suresh, *Chem. Phys. Lett.*, 2012, **523**, 11-14.
31. S. Böhm and J. Kuthan, *Int. J. Quantum Chem*, 1984, **26**, 21-33.
32. K. H. Kim and Y. C. Martin, *J. Org. Chem.*, 1991, **56**, 2723-2729.
33. J. S. Murray, T. Brinck and P. Politzer, *J. Mol. Struct. (THEOCHEM)*, 1992, **255**, 271-281.
34. H. Szatyłowicz, T. Siodła, O. A. Stasyuk and T. M. Krygowski, *Phys. Chem. Chem. Phys.*, 2016, **18**, 11711-11721.
35. T. Krygowski and N. Sadlej-Sosnowska, *Struct. Chem.*, 2011, **22**, 17-22.
36. C. A. van Walree and L. W. Jenneskens, *Tetrahedron*, 1997, **53**, 5825-5830.
37. M. Charton, *J. Org. Chem.*, 1961, **26**, 735-738.
38. S. A. Myers, R. A. Assink, D. A. Loyb and K. J. Sheac, *J. Chem. Soc., Perkin Trans. 2*, 2000, 545-549.
39. K. Bowden, *Can. J. Chem.*, 1963, **41**, 2781-2793.
40. K. Waisser, J. Kunes, L. Kubicova, M. Budesinsky and O. Exner, *Magn. Reson. Chem.*, 1997, **35**, 543-548
41. W. Adcock, *J. Phys. Org. Chem.*, 2009, **22**, 1065-1069.
42. W. Adcock and A. Krstic, R, *Magn. Reson. Chem.*, 2000, **38**, 115-122.
43. W. Adcock and N. Trout, A, *Magn. Reson. Chem.*, 1998, **36**, 181-195.

44. A. R. Campanelli, A. Domenicano, G. Piacente and F. Ramondo, *J. Phys. Chem. A*, 2010, **114**, 5162-5170.
45. E. Scrocco and J. Tomasi, in *New concepts II*, Springer1973, 95-170.
46. E. Scrocco and J. Tomasi, in *Advances in Quantum Chemistry*, Elsevier1978, **11**, pp. 115-193.
47. S. R. Gadre and I. H. Shrivastava, *J. Chem. Phys.*, 1991, **94**, 4384-4390.
48. F. Luque, M. Orozco, P. Bhadane and S. Gadre, *J. Chem. Phys.*, 1994, **100**, 6718-6726.
49. S. R. Gadre and P. K. Bhadane, *J. Chem. Phys.*, 1997, **107**, 5625-5626.
50. S. R. Gadre and C. H. Suresh, *J. Org. Chem.*, 1997, **62**, 2625-2627.
51. C. H. Suresh, P. Alexander, K. P. Vijayalakshmi, P. K. Sajith, and S. R. Gadre, *Phys. Chem. Chem. Phys.*, 2008, **10**, 6492-6499.
52. F. B. Sayyed and C. H. Suresh, *Tetrahedron Lett.*, 2009, **50**, 7351-7354.
53. C. H. Suresh, *Inorg. Chem.*, 2006, **45** 4982-4986.
54. P. K. Sajith and C. H. Suresh, *Inorg. Chem.*, 2012, **51**, 967-977.
55. P. Sajith and C. H. Suresh, *Dalton Trans.*, 2010, **39**, 815-822.
56. J. Mathew, T. Thomas and C. H. Suresh, *Inorg. Chem.*, 2007, **46**, 10800-10809.
57. J. Mathew and C. H. Suresh, *Inorg. Chem.*, 2010, **49**, 4665-4669.
58. C.-J. Tan, C.-S. Yang, Y.-C. Sheng, H. W. Amini and H.-H. G. Tsai, *J. Phys. Chem. C*, 2016, **120**, 21272-21284.
59. C. Teng, X. Yang, C. Yang, H. Tian, S. Li, X. Wang, A. Hagfeldt and L. Sun, *J. Phys. Chem. C*, 2010, **114**, 11305-11313.
60. Y. Hua, J. He, C. Zhang, C. Qin, L. Han, J. Zhao, T. Chen, W.-Y. Wong, W.-K. Wong and X. Zhu, *J. Mater. Chem. A*, 2015, **3**, 3103-3112.
61. Y. Ding, Y. Jiang, W. Zhang, L. Zhang, X. Lu, Q. Wang, G. Zhou, J.-m. Liu, K. Kempa and J. Gao, *J. Phys. Chem. C*, 2017, **121**, 16731-16738.
62. A. D. Becke, *J. Chem. Phys.*, 1993, **98**, 5648-5652.
63. C. Lee, W. Yang and R. G. Parr, *Phys. Rev. B*, 1988, **37**, 785.
64. F. B. Sayyed and C. H. Suresh, *New. J. Chem.*, 2009, **33**, 2465-2471.
65. M. J. Frisch, G. W. Trucks, H. B. Schlegel, G. E. Scuseria, M. A. Robb, J. R. Cheeseman, G. Scalmani, V. Barone, B. Mennucci, G. A. Petersson, H. Nakatsuji, M. Caricato, X. Li, H. P. Hratchian, A. F. Izmaylov, J. Bloino, G. Zheng, J. L. Sonnenberg, M. Hada, M. Ehara, K. Toyota, R. Fukuda, J. Hasegawa, M. Ishida, T.

- Nakajima, Y. Honda, O. Kitao, H. Nakai, T. Vreven, J. J. A. Montgomery, J. E. Peralta, F. Ogliaro, M. Bearpark, J. J. Heyd, E. Brothers, K. N. Kudin, V. N. Staroverov, T. Keith, R. Kobayashi, J. Normand, K. Raghavachari, A. Rendell, J. C. Burant, S. S. Iyengar, J. Tomasi, M. Cossi, N. Rega, J. M. Millam, M. Klene, J. E. Knox, J. B. Cross, V. Bakken, C. Adamo, J. Jaramillo, R. Gomperts, R. E. Stratmann, O. Yazyev, A. J. Austin, R. Cammi, C. Pomelli, J. W. Ochterski, R. L. Martin, K. Morokuma, V. G. Zakrzewski, G. A. Voth, P. Salvador, J. J. Dannenberg, S. Dapprich, A. D. Daniels, O. Farkas, J. B. Foresman, J. V. Ortiz, J. Cioslowski, D. J. Fox, Gaussian 09, Revision D.01; Gaussian, Inc. Wallingford, CT, 2013.
66. F. Massoth, P. Politzer, M. Concha, J. Murray, J. Jakowski and J. Simons, *J. Phys. Chem. B*, 2006, **110**, 14283-14291.
  67. P. Politzer, L. Abrahmsen and P. Sjoberg, *J. Am. Chem. Soc.*, 1984, **106**, 855-860.
  68. J. Frederick and J. Dippy, *Chem. Rev.*, 1939, **25**, 151-211.
  69. B. O'regan and M. Grätzel, *Nature*, 1991, **353**, 737.
  70. N. Anscombe, *Nat. Photonics*, 2011, **5**, 266-267.
  71. F. Odobel, L. Le Pleux, Y. Pellegrin and E. Blart, *Acc. Chem. Res.*, 2010, **43**, 1063-1071.
  72. A. Hagfeldt, G. Boschloo, L. Sun, L. Kloo and H. Pettersson, *Chem. Rev.*, 2010, **110**, 6595-6663.
  73. N. Sharifi, F. Tajabadi and N. Taghavinia, *ChemPhysChem*, 2014, **15**, 3902-3927.
  74. J. Gong, K. Sumathy, Q. Qiao and Z. Zhou, *Renew. Sustain. Energy Rev.*, 2017, **68**, 234-246.
  75. A. Yella, H.-W. Lee, H. N. Tsao, C. Yi, A. K. Chandiran, M. K. Nazeeruddin, E. W.-G. Diau, C.-Y. Yeh, S. M. Zakeeruddin and M. Grätzel, *Science*, 2011, **334**, 629-634.
  76. A. Mishra, M. K. Fischer and P. Bäuerle, *Angew. Chem. Int. Ed.*, 2009, **48**, 2474-2499.
  77. M. K. Nazeeruddin, A. Kay, I. Rodicio, R. Humphry-Baker, E. Mueller, P. Liska, N. Vlachopoulos and M. Graetzel, *J. Am. Chem. Soc.*, 1993, **115**, 6382-6390.
  78. M. K. Nazeeruddin, P. Péchy, T. Renouard, S. M. Zakeeruddin, R. Humphry-Baker, P. Comte, P. Liska, L. Cevey, E. Costa, V. Shklover, L. Spiccia, G. B. Deacon, C. A. Bignozzi and M. Grätzel, *J. Am. Chem. Soc.*, 2001, **123**, 1613-1624.

79. M. K. Nazeeruddin, R. Splivallo, P. Liska, P. Comte and M. Grätzel, *Chem. Commun.*, 2003, **12**, 1456-1457.
80. M. K. Nazeeruddin, F. De Angelis, S. Fantacci, A. Selloni, G. Viscardi, P. Liska, S. Ito, B. Takeru and M. Grätzel, *J. Am. Chem. Soc.*, 2005, **127**, 16835-16847.
81. F. Gao, Y. Wang, J. Zhang, D. Shi, M. Wang, R. Humphry-Baker, P. Wang, S. M. Zakeeruddin and M. Grätzel, *Chem. Commun.*, 2008, 2635-2637.
82. C.-Y. Chen, M. Wang, J.-Y. Li, N. Pootrakulchote, L. Alibabaei, C.-h. Ngoc-le, J.-D. Decoppet, J.-H. Tsai, C. Grätzel, C.-G. Wu, S. M. Zakeeruddin and M. Grätzel, *ACS Nano*, 2009, **3**, 3103-3109.
83. Y. Cao, Y. Bai, Q. Yu, Y. Cheng, S. Liu, D. Shi, F. Gao and P. Wang, *J. Phys. Chem. C* 2009, **113**, 6290-6297.
84. M. Pastore, E. Mosconi and F. De Angelis, *J. Phys. Chem. C*, 2012, **116**, 5965-5973.
85. M. Cheng, X. Yang, J. Li, F. Zhang and L. Sun, *ChemSusChem*, 2013, **6**, 70-77.
86. S. Ito, H. Miura, S. Uchida, M. Takata, K. Sumioka, P. Liska, P. Comte, P. Péchy and M. Grätzel, *Chem. Commun.*, 2008, 5194-5196.
87. W. Zeng, Y. Cao, Y. Bai, Y. Wang, Y. Shi, M. Zhang, F. Wang, C. Pan and P. Wang, *Chem. Mater.*, 2010, **22**, 1915-1925.
88. K. Kakiage, Y. Aoyama, T. Yano, T. Otsuka, T. Kyomen, M. Unno and M. Hanaya, *Chem. Commun.*, 2014, **50**, 6379-6381.
89. Z. Yao, M. Zhang, H. Wu, L. Yang, R. Li and P. Wang, *J. Am. Chem. Soc.*, 2015, **137**, 3799-3802.
90. B. Nagarajan, S. Kushwaha, R. Elumalai, S. Mandal, K. Ramanujam and D. Raghavachari, *J. Mater. Chem. A*, 2017, **5**, 10289-10300.
91. K. Kakiage, Y. Aoyama, T. Yano, K. Oya, J.-i. Fujisawa and M. Hanaya, *Chem. Commun.*, 2015, **51**, 15894-15897.
92. T. Kitamura, M. Ikeda, K. Shigaki, T. Inoue, N. A. Anderson, X. Ai, T. Lian and S. Yanagida, *Chem. Mater.*, 2004, **16**, 1806-1812.
93. Z.-S. Wang, Y. Cui, Y. Dan-oh, C. Kasada, A. Shinpo and K. Hara, *J. Phys. Chem. C*, 2007, **111**, 7224-7230.
94. Z.-S. Wang, N. Koumura, Y. Cui, M. Takahashi, H. Sekiguchi, A. Mori, T. Kubo, A. Furube and K. Hara, *Chem. Mater.*, 2008, **20**, 3993-4003.

95. A. Venkateswararao, K. R. J. Thomas, C.-P. Lee, C.-T. Li and K.-C. Ho, *ACS Appl. Mater. Interfaces*, 2014, **6**, 2528-2539.
96. A. J. Huckaba, F. Giordano, L. E. McNamara, K. M. Dreux, N. I. Hammer, G. S. Tschumper, S. M. Zakeeruddin, M. Grätzel, M. K. Nazeeruddin and J. H. Delcamp, *Adv. Energy Mater.*, 2015, **5**, 1401629.
97. K. Hara, M. Kurashige, Y. Dan-oh, C. Kasada, A. Shinpo, S. Suga, K. Sayama and H. Arakawa, *New J. Chem.*, 2003, **27**, 783-785.
98. A. Baheti, C.-P. Lee, K. J. Thomas and K.-C. Ho, *Phys. Chem. Chem. Phys.*, 2011, **13**, 17210-17221.
99. K. Srinivas, C. R. Kumar, M. A. Reddy, K. Bhanuprakash, V. J. Rao and L. Giribabu, *Synth. Met.*, 2011, **161**, 96-105.
100. Y. Ooyama, S. Inoue, T. Nagano, K. Kushimoto, J. Ohshita, I. Imae, K. Komaguchi and Y. Harima, *Angew. Chem. Int. Ed.*, 2011, **50**, 7429-7433.
101. B. Hosseinzadeh, A. S. Beni, M. Azari, M. Zarandi and M. Karami, *New J. Chem.*, 2016, **40**, 8371-8381.
102. D. Patil, M. Jadhav, K. Avhad, T. H. Chowdhury, A. Islam, I. Bedja and N. Sekar, *New J. Chem.*, 2018, **42**, 11555-11564.
103. J. Feng, Y. Jiao, W. Ma, M. K. Nazeeruddin, M. Grätzel and S. Meng, *J. Phys. Chem. C*, 2013, **117**, 3772-3778.
104. S. Ardo and G. J. Meyer, *Chem. Soc. Rev.*, 2009, **38**, 115-164.
105. R. Argazzi, C. A. Bignozzi, T. A. Heimer, F. N. Castellano and G. J. Meyer, *J. Am. Chem. Soc.*, 1995, **117**, 11815-11816.
106. N. Hirata, J. J. Lagref, E. J. Palomares, J. R. Durrant, M. K. Nazeeruddin, M. Grätzel and D. Di Censo, *Chem. Eur. J.*, 2004, **10**, 595-602.
107. Z. Ning, Q. Zhang, W. Wu, H. Pei, B. Liu and H. Tian, *J. Org. Chem.*, 2008, **73**, 3791-3797.
108. L. Li, Y. Hao, X. Yang, J. Zhao, H. Tian, C. Teng, A. Hagfeldt and L. Sun, *ChemSusChem*, 2011, **4**, 609-612.
109. J. Tang, J. Hua, W. Wu, J. Li, Z. Jin, Y. Long and H. Tian, *Energy Environ. Sci.*, 2010, **3**, 1736-1745.
110. W. Li, Y. Wu, Q. Zhang, H. Tian and W. Zhu, *ACS Appl. Mater. Interfaces*, 2012, **4**, 1822-1830.

111. R. Tarsang, V. Promarak, T. Sudyoasuk, S. Namuangruk, N. Kungwan and S. Jungsuttiwong, *ChemPhysChem*, 2014, **15**, 3809-3818.
112. H.-Q. Xia, C.-P. Kong, J. Wang, F.-Q. Bai and H.-X. Zhang, *RSC Adv.*, 2014, **4**, 50338-50350.
113. A. Dessì, A. Sinicropi, S. Mohammadpourasl, R. Basosi, M. Taddei, F. Fabrizi de Biani, M. Calamante, L. Zani, A. Mordini, P. Bracq, D. Franchi and G. Reginato, *ACS Omega* 2019, **4**, 7614-7627.
114. L.-Y. Lin, C.-H. Tsai, F. Lin, T.-W. Huang, S.-H. Chou, C.-C. Wu and K.-T. Wong, *Tetrahedron*, 2012, **68**, 7509-7516.
115. K. D. Seo, B. S. You, I. T. Choi, M. J. Ju, M. You, H. S. Kang and H. K. Kim, *J. Mater. Chem. A*, 2013, **1**, 9947-9953.
116. Y. Hong, J.-Y. Liao, J. Fu, D.-B. Kuang, H. Meier, C.-Y. Su and D. Cao, *Dyes Pigm.*, 2012, **94**, 481-489.
117. A. Dualeh, R. Humphry - Baker, J. H. Delcamp, M. K. Nazeeruddin and M. Grätzel, *Adv. Energy Mater.*, 2013, **3**, 496-504.
118. J. H. Delcamp, A. Yella, T. W. Holcombe, M. K. Nazeeruddin and M. Grätzel, *Angew. Chem. Int. Ed.*, 2013, **125**, 394-398.
119. K. Srinivas, K. Yesudas, K. Bhanuprakash, V. J. Rao and L. Giribabu, *J. Phys. Chem. C*, 2009, **113**, 20117-20126.
120. J. Preat, C. Michaux, D. Jacquemin and E. A. Perpète, *J. Phys. Chem. C*, 2009, **113**, 16821-16833.
121. J. Preat, *J. Phys. Chem. C*, 2010, **114**, 16716-16725.
122. J. Preat, D. Jacquemin and E. A. Perpète, *Environ. Sci. Technol.*, 2010, **44**, 5666-5671.
123. M. Pastore, E. Mosconi, F. De Angelis and M. Grätzel, *J. Phys. Chem. C*, 2010, **114**, 7205-7212.
124. D. Casanova, F. P. Rotzinger and M. Grätzel, *J. Chem. Theory Comput.*, 2010, **6**, 1219-1227.
125. S. Meng, E. Kaxiras, M. K. Nazeeruddin and M. Grätzel, *J. Phys. Chem. C*, 2011, **115**, 9276-9282.
126. R. Sánchez-de-Armas, M. Á. San Miguel, J. Oviedo and J. F. Sanz, *Phys. Chem. Chem. Phys.*, 2012, **14**, 225-233.

127. J. Zhang, H.-B. Li, S.-L. Sun, Y. Geng, Y. Wu and Z.-M. Su, *J. Mater. Chem.*, 2012, **22**, 568-576.
128. W. Fan, D. Tan and W. Q. Deng, *ChemPhysChem*, 2012, **13**, 2051-2060.
129. J. Zhang, Y.-H. Kan, H.-B. Li, Y. Geng, Y. Wu and Z.-M. Su, *Dyes Pigm.*, 2012, **95**, 313-321.
130. J. Zhang, H.-B. Li, J.-Z. Zhang, Y. Wu, Y. Geng, Q. Fu and Z.-M. Su, *Journal of Materials Chemistry A*, 2013, **1**, 14000-14007.
131. W.-L. Ding, D.-M. Wang, Z.-Y. Geng, X.-L. Zhao and Y.-F. Yan, *J. Phys. Chem. C*, 2013, **117**, 17382-17398.
132. R. Tarsang, V. Promarak, T. Sudyoasuk, S. Namuangruk and S. Jungstittiwong, *J. Photochem. Photobiol.*, 2014, **273**, 8-16.
133. M. E. Köse, *J. Phys. Chem. A*, 2019, **123**, 5566-5573.
134. K. Hara, T. Sato, R. Katoh, A. Furube, Y. Ohga, A. Shinpo, S. Suga, K. Sayama, H. Sugihara and H. Arakawa, *J. Phys. Chem. B*, 2003, **107**, 597-606.
135. J. Li and A. C. Grimsdale, *Chem. Soc. Rev.*, 2010, **39**, 2399-2410.
136. G. Wu, F. Kong, J. Li, W. Chen, X. Fang, C. Zhang, Q. Chen, X. Zhang and S. Dai, *Dyes Pigm.*, 2013, **99**, 653-660.
137. Z.-S. Huang, H. Meier and D. Cao, *J. Mater. Chem.*, 2016, **4**, 2404-2426.
138. Y. Zhang, H. Cheema, L. McNamara, L. A. Hunt, N. I. Hammer and J. H. Delcamp, *Chem. Eur. J.*, 2018, **24**, 5939-5949.
139. Z. Yang, C. Shao and D. Cao, *RSC Adv.*, 2015, **5**, 22892-22898.
140. C. H. Suresh and N. Koga, *Inorg. Chem.*, 2002, **41**, 1573-1578.
141. O. Köhl, *Coord. Chem. Rev.*, 2005, **249**, 693-704.
142. C. H. Suresh, *Inorg. Chem.*, 2006, **45**, 4982-4986.
143. S. Mecozzi, A. P. West and D. A. Dougherty, *J. Am. Chem. Soc.*, 1996, **118**, 2307-2308.
144. S. E. Wheeler and K. N. Houk, *J. Chem. Theory Comput.*, 2009, **5**, 2301-2312.
145. S. E. Wheeler and K. Houk, *J. Am. Chem. Soc.*, 2009, **131**, 3126-3127.
146. F. B. Sayyed and C. H. Suresh, *J. Phys. Chem. A*, 2011, **115**, 9300-9307.
147. F. B. Sayyed and C. H. Suresh, *New J. Chem.*, 2009, **33**, 2465-2471.
148. V. V. Divya, F. B. Sayyed and C. H. Suresh, *ChemPhysChem*, 2019, **20**, 1752-1758.
149. A. D. Becke, *J. Chem. Phys.*, 1993, **98**, 1372-1377.
150. T. H. Dunning Jr, *J. Chem. Phys.*, 1989, **90**, 1007-1023.

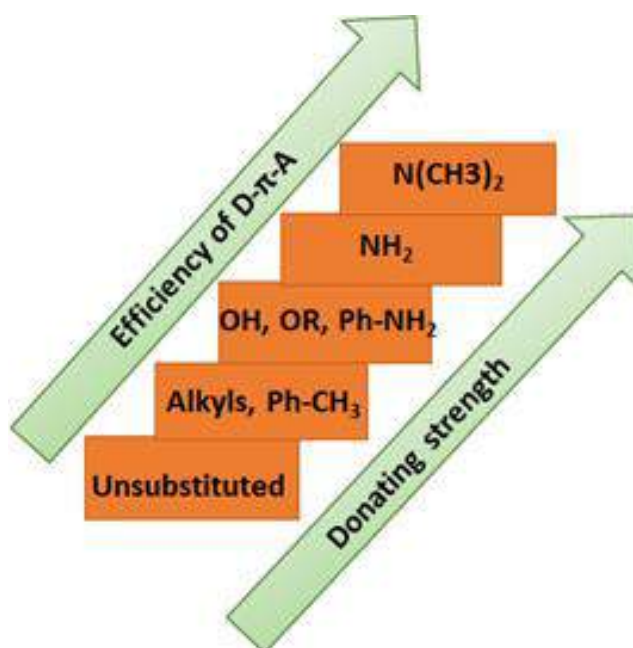
151. C. Adamo and V. Barone, *J. Chem. Phys.*, 1999, **110**, 6158-6170.
152. J.-D. Chai and M. Head-Gordon, *Phys. Chem. Chem. Phys.*, 2008, **10**, 6615-6620.
153. A. V. Marenich, C. J. Cramer and D. G. Truhlar, *J. Phys. Chem. B*, 2009, **113**, 6378-6396.
154. M. J. Frisch, G. W. Trucks, H. B. Schlegel, G. E. Scuseria, M. A. Robb, J. R. Cheeseman, G. Scalmani, V. Barone, G. A. Petersson, H. Nakatsuji, X. Li, M. Caricato, A. V. Marenich, J. Bloino, B. G. Janesko, R. Gomperts, B. Mennucci, H. P. Hratchian, J. V. Ortiz, A. F. Izmaylov, J. L. Sonnenberg, D. Williams-Young, F. Ding, F. Lipparini, F. Egidi, J. Goings, B. Peng, A. Petrone, T. Henderson, D. Ranasinghe, V. G. Zakrzewski, J. Gao, N. Rega, G. Zheng, W. Liang, M. Hada, M. Ehara, K. Toyota, R. Fukuda, J. Hasegawa, M. Ishida, T. Nakajima, Y. Honda, O. Kitao, H. Nakai, T. Vreven, K. Throssell, J. A. Montgomery Jr., J. E. Peralta, F. Ogliaro, M. J. Bearpark, J. J. Heyd, E. N. Brothers, K. N. Kudin, V. N. Staroverov, T. A. Keith, R. Kobayashi, J. Normand, K. Raghavachari, A. P. Rendell, J. C. Burant, S. S. Iyengar, J. Tomasi, M. Cossi, J. M. Millam, M. Klene, C. Adamo, R. Cammi, J. W. Ochterski, R. L. Martin, K. Morokuma, O. Farkas, J. B. Foresman and D. J. Fox, Wallingford, CT, 2016.
155. R. Samae, P. Surawatanawong, U. Eiamprasert, S. Pramjit, L. Saengdee, P. Tangboriboonrat and S. Kiatisevi, *Eur. J. Org. Chem.*, 2016, **2016**, 3536-3549.
156. J. Yang, X. Wang, W.-L. Yim and Q. Wang, *J. Phys. Chem. C*, 2015, **119**, 26355-26361.



---

## Tuning the Donating Strength of Dye- sensitizers Using Molecular Electrostatic Potential Analysis

---



### 3.1 Abstract

*Donor- $\pi$ -acceptor (D- $\pi$ -A) systems typically used in dye-sensitized solar cells (DSSC) have been studied for assessing the donating strength of six donors (D1 – D6) under the influence of substituents such as CH<sub>3</sub>, C<sub>5</sub>H<sub>11</sub>, isopropyl, t-butyl, OH, OCH<sub>3</sub>, OC<sub>2</sub>H<sub>5</sub>, NH<sub>2</sub>, N(CH<sub>3</sub>)<sub>2</sub>, PhCH<sub>3</sub>, and PhNH<sub>2</sub> along with  $\pi$ -spacer butadiene and acceptor moiety cyanoacrylic acid. The substituent effect enhances electron donation from D to A through the  $\pi$ -spacer. The enhancement in electron density at A has been quantified in terms of the difference in the molecular electrostatic potential (MESP) minimum at the cyano nitrogen ( $\Delta V_{mA}$ ) between  $\pi$ -A and D- $\pi$ -A. For unsubstituted D- $\pi$ -A systems,  $\Delta V_{mA}$  is in the range -0.2 to -5.7 kcal/mol, whereas the substitution enhances the negative character of  $\Delta V_{mA}$  in the range -0.8 to -8.0 kcal/mol. In alkyls and Ph-CH<sub>3</sub> substituted D- $\pi$ -A systems,  $\Delta V_{mA}$  lies in the range -0.8 to -6.7 kcal/mol, whereas the N(CH<sub>3</sub>)<sub>2</sub> substituted systems exhibit more negative  $\Delta V_{mA}$  (more enhanced donating strength) in the range -5.1 - -8.0 kcal/mol. The more negative value of  $\Delta V_{mA}$  implies the greater electron-donating ability of the D- $\pi$ -A system. Optical and photovoltaic parameters ( $\Delta G_{reg}$ ,  $\Delta G_{inject}$ ,  $eV_{OC}$ ) are analyzed at TD-CAM-B3LYP/SMD/cc-pVDZ//B3LYP/cc-pVDZ level DFT. An excellent linear correlation observed in all the six sets between  $\Delta V_{mA}$  and absorption maximum ( $\lambda_{max}$ ) showing that  $\lambda_{max}$  increases with enhanced donating strength. The higher absorption maximum obtained by N(CH<sub>3</sub>)<sub>2</sub> substituted D- $\pi$ -A systems lies in the range 430 nm to 490 nm, explains the outstanding donating ability of N(CH<sub>3</sub>)<sub>2</sub> than other substituents. The reduced highest occupied molecular orbital (HOMO) – lowest unoccupied molecular orbital (LUMO) gap (from 3.14 to 2.17 eV) with enhanced donating strength confirms the influence of substituent effects in broadening the absorption maximum. Further, in photovoltaic parameters, a strong influence of the substituent effect is observed. The N(CH<sub>3</sub>)<sub>2</sub> substituted D1- $\pi$ -A (D1-N(CH<sub>3</sub>)<sub>2</sub>) exhibits the highest  $eV_{OC}$  (1.38 eV). The strong linear correlation observed for the ground state property  $\Delta V_{mA}$  and open-circuit voltage  $eV_{OC}$  provides guidelines for developing an effective strategy for designing dye sensitizer for desirable photovoltaic applications.*

### 3.2 Introduction

Over the past 30 years, dye-sensitized solar cells (DSSCs) and its structural modification became an emerging research area in the field of photovoltaics.<sup>1-3</sup> DSSCs

are considered as the most inventive candidate for the next generation clean renewable source due to easier structure modification, simple synthetic strategy, large absorption coefficient, and low production cost.<sup>1, 4-7</sup> Nonetheless, the performance of DSSC is still in the bottleneck due to its lower power conversion efficiency (PCE) than the conventional silicon-based solar cells due to the inherent voltage loss during the dye regeneration and poor long term stability.<sup>8</sup> In order to improve the PCE over conventional silicon-based solar cells, extensive research efforts like modification on electrolytes, semiconductors, and sensitizers have been executed and result in the development of new and efficient dye sensitizers.<sup>3, 5, 9-21</sup> Among the DSSCs, the Ru based sensitizers achieved the best PCE of 11%, which attain the comparable PCE of a silicon-based solar cell.<sup>5, 22, 23</sup> But due to the scarce resource and highly expensive nature of Ru metal, its practical application is limited, and more research efforts have been resulted in the development of Ru-free organic sensitizers.<sup>6, 11, 24</sup> However, the major challenge of organic solar cells is the enhancement of PCE, durability, and stability to compete with silicon-based solar cells. One of the key strategies for the synthesis of Ru free sensitizers is the designing of the D- $\pi$ -A architecture, which enables the efficient electron transfer from a donor (D) to the acceptor (A) through a spacer ( $\pi$ ).<sup>25, 26</sup>

From the literature, it is understood that for the designing of highly efficient photosensitizers, different kinds of building blocks such as donors,<sup>27-35</sup> spacers,<sup>36-41</sup> and anchoring units<sup>42-46</sup> are required in the D- $\pi$ -A architecture to tune the electronic structure of the synthesized product. The fine-tuning of the HOMO - LUMO (highest occupied molecular orbital - lowest unoccupied molecular orbital) energy levels of a photosensitizer is often achieved by adjusting the substituent effect on the donor by the incorporation of electron-donating/withdrawing groups. In most of the cases, the electron-donating groups on donor moiety act as substituents and they have a profound impact on the electronic structure and efficiency of the desired dye sensitizer.<sup>6, 47-49</sup> A priori knowledge on the donating strength of the donor can become helpful for the prediction of the PCE of the designed/synthesized system. A quantitative/mathematical comparison of donating strength of the typically used donors is lacking in the literature.

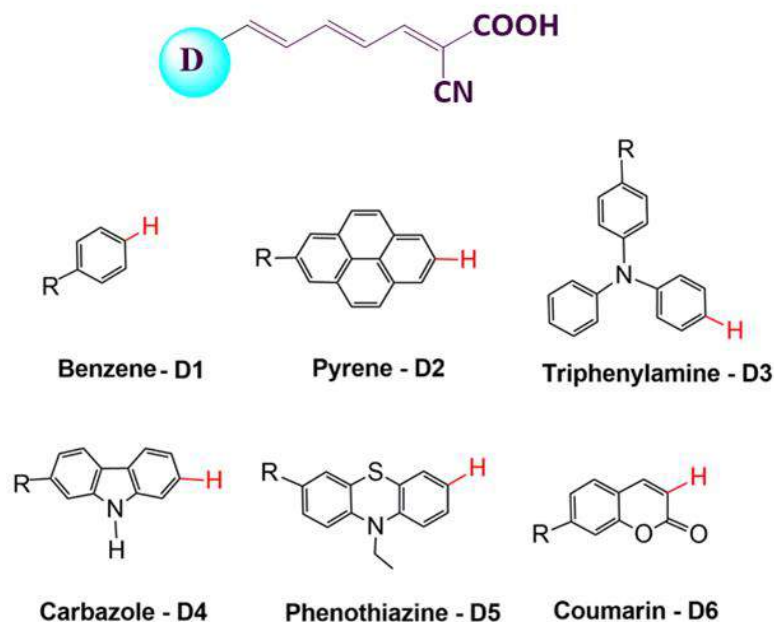


**Figure 3.1** Chemdraw diagram of D- $\pi$ -A system (top) and the donors D1 – D6. The R substituents are CH<sub>3</sub>, C<sub>5</sub>H<sub>11</sub>, isopropyl, t-butyl, OH, OCH<sub>3</sub>, O-C<sub>2</sub>H<sub>5</sub>, NH<sub>2</sub>, N(CH<sub>3</sub>)<sub>2</sub>, Ph-CH<sub>3</sub>, and Ph-NH<sub>2</sub>. The bond shown in red colour indicates the connecting position of D with  $\pi$ -A.

Here we have selected six different donor systems (D1 – D6), substituted with electron-donating groups such as CH<sub>3</sub>, C<sub>5</sub>H<sub>11</sub>, isopropyl, t-butyl, OH, OCH<sub>3</sub>, O-C<sub>2</sub>H<sub>5</sub>, NH<sub>2</sub>, N(CH<sub>3</sub>)<sub>2</sub>, N(C<sub>2</sub>H<sub>5</sub>)<sub>2</sub>, Ph-CH<sub>3</sub>, and Ph-NH<sub>2</sub> to evaluate the donating strength on a  $\pi$ -A system made up of butadiene  $\pi$ -spacer and cyanoacrylic acid (Figure 3.1). According to our previous study, butadiene spacer is rated as having the highest substituent effect transmitting power compared to triple bonded, aromatic, and heteroaromatic conjugated systems.<sup>50</sup> Hence this moiety is employed in the study as  $\pi$ -spacer for effective intramolecular charge transfer (ICT) and cyanoacrylic acid is used as acceptor (A). The molecular electrostatic potential (MESP) topographical analysis is used as a tool to measure the electronic effect of the substituted D on the acceptor A. MESP is a well-established tool for deriving many structure-property relationships for chemical and biological systems.<sup>51-53,54-57</sup> According to Scrocco, Tomasi, and co-workers, the MESP describes the charge distribution around a molecule and the regions with more negative MESP indicate the more electron-dense region of that system.<sup>58, 59</sup> Suresh and co-workers widely used MESP for the quantification of substituent effect,<sup>60</sup> inductive effect,<sup>61</sup> resonance effect,<sup>62</sup> trans influence,<sup>63</sup> cation  $\pi$ -interaction,<sup>64</sup> etc. In a recent study, we have shown that MESP

analysis is very useful for assessing the donating strength of D in D- $\pi$ -A system.<sup>65</sup> MESP becomes a new theoretical tool for predicting the feasibility of organic electrode material for lithium-ion batteries<sup>66</sup>, explained by Shang, Chen, and co-workers. The wide range of applications in various fields supports the validity of MESP based studies for analyzing the photovoltaic properties of dye-sensitized solar cells. The present study focuses on the substituent effect in tuning various ground state electronic and photovoltaic properties of D- $\pi$ -A systems for solar cell application.

### 3.3 Computational methodology

For the ground state geometry optimization of the D- $\pi$ -A systems, widely utilized B3LYP density functional theory (DFT) method<sup>67</sup> with cc-pVDZ basis set<sup>65, 68, 69</sup> has been considered. Vibrational frequency calculation was also done at the same level of theory and basis set, and confirms that there are no imaginary frequencies. Absorption maxima and vertical excitation energies for the first seven states are calculated using time-dependent DFT at the CAM-B3LYP/SMD/cc-pVDZ//B3LYP/cc-pVDZ level.<sup>70, 71</sup> Here SMD stands for the incorporation of the solvation effect of dichloromethane the self-consistent reaction field (SCRF) approach<sup>72</sup> as implemented in Gaussian16 suite of programmes.<sup>73</sup> The dependency of bond localization of single and double bonds in ground state on the excited state properties has been analyzed using bond length alteration index (BLA).<sup>74, 75</sup> The BLA index for the unsubstituted D1 to D6- $\pi$ -A systems are calculated with B3LYP and CAM-B3LYP geometries (Table 3.1a – Table 3.1b). The bonds employed to calculate BLA index are shown in Figure 3.2. For all a positive BLA index has been observed and larger BLA index has been observed with CAM-B3LYP. This indicates that carbon-carbon single and double bond are more localized with CAM-B3LYP than B3LYP. Also, the BLA index for the S<sub>1</sub> state of a representative set of TPA systems has been calculated with CAM-B3LYP (Table 3.2). The reduced BLA index for S<sub>1</sub> than the S<sub>0</sub> state indicates the delocalized nature of the system and also supports the ICT transfer involved in D- $\pi$ -A systems. Previously, González *et al.* noted that B3LYP fails to predict the excitation energies due to its intrinsic problems in describing charge transfer (CT) states whereas the long-range correction on them using CAM delivers good agreement with the experimental UV/vis absorption.<sup>75</sup> They also observed that excited state properties are highly dependent on the localization of single and double bonds in the ground state structure which can

be quantified in terms of the BLA index. Our previous study also showed that the calculated absorption maximum of known D- $\pi$ -A systems at CAM-B3LYP/SMD/cc-pVDZ//B3LYP/cc-pVDZ level of theory agree well with the experimental absorption maximum.<sup>65</sup> The MESP,  $V(r)$  has been evaluated using the electron density  $\rho(\mathbf{r}')$  computed at B3LYP/ cc-pVDZ level. All calculations have been carried out using a Gaussian 16 program package.<sup>73</sup>

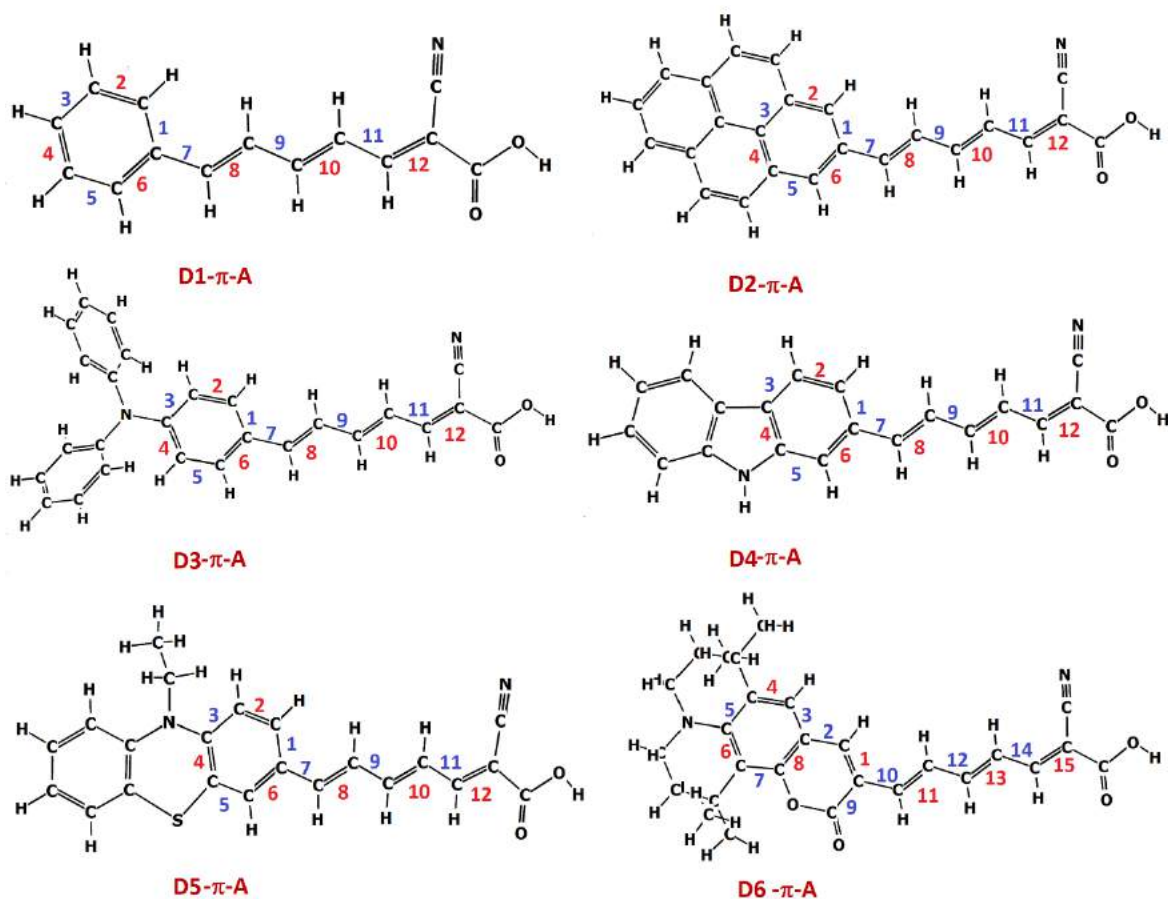


**Figure 3.2** Labeled bonds employed to calculate the BLA index.

**Table 3.1 a)** BLA index for the unsubstituted D1 – D3- $\pi$ -A systems in ground state with B3LYP and CAM-B3LYP functional.

Bond	D1- $\pi$ -A		D2- $\pi$ -A		D3- $\pi$ -A	
	S <sub>0</sub> B3LYP	S <sub>0</sub> CAM-B3LYP	S <sub>0</sub> B3LYP	S <sub>0</sub> CAM-B3LYP	S <sub>0</sub> B3LYP	S <sub>0</sub> CAM-B3LYP
BLA	0.039	0.046	0.039	0.043	0.035	0.046
1	1.413	1.404	1.41	1.4	1.415	1.405

Bond	D1- $\pi$ -A		D2- $\pi$ -A		D3- $\pi$ -A	
	S <sub>0</sub>	S <sub>0</sub>	S <sub>0</sub>	S <sub>0</sub>	S <sub>0</sub>	S <sub>0</sub>
	B3LYP	CAM-B3LYP	B3LYP	CAM-B3LYP	B3LYP	CAM-B3LYP
BLA	0.039	0.046	0.039	0.043	0.035	0.046
2	1.392	1.388	1.4	1.397	1.386	1.383
3	1.401	1.395	1.432	1.420	1.415	1.406
4	1.398	1.391	1.429	1.423	1.411	1.402
5	1.395	1.390	1.402	1.394	1.389	1.386
6	1.411	1.402	1.409	1.402	1.412	1.402
7	1.460	1.464	1.460	1.464	1.451	1.457
8	1.360	1.347	1.360	1.348	1.364	1.35
9	1.435	1.422	1.435	1.422	1.431	1.439
10	1.366	1.353	1.367	1.353	1.369	1.355
11	1.429	1.435	1.428	1.435	1.425	1.432
12	1.370	1.356	1.370	1.356	1.372	1.358

**Table 3.1 b)** BLA index for the unsubstituted D4 – D6- $\pi$ -A systems in ground state with B3LYP and CAM-B3LYP functional.

Bond	D4- $\pi$ -A		D5- $\pi$ -A		D6- $\pi$ -A	
	S <sub>0</sub>	S <sub>0</sub>	S <sub>0</sub>	S <sub>0</sub>	S <sub>0</sub>	S <sub>0</sub>
	B3LYP	CAM-B3LYP	B3LYP	CAM-B3LYP	B3LYP	CAM-B3LYP
BLA	0.036	0.048	0.034	0.045	0.035	0.039
1	1.423	1.415	1.409	1.399	1.37	1.357
2	1.387	1.383	1.389	1.386	1.432	1.436
3	1.406	1.399	1.414	1.406	1.413	1.405
4	1.424	1.413	1.417	1.408	1.388	1.383
5	1.394	1.392	1.391	1.387	1.406	1.401
6	1.409	1.399	1.412	1.402	1.393	1.387
7	1.456	1.461	1.452	1.458	1.397	1.392
8	1.362	1.349	1.363	1.349	1.411	1.400
9	1.433	1.441	1.432	1.440	1.482	1.479

Bond	D4- $\pi$ -A		D5- $\pi$ -A		D6- $\pi$ -A	
	S <sub>0</sub>	S <sub>0</sub>	S <sub>0</sub>	S <sub>0</sub>	S <sub>0</sub>	S <sub>0</sub>
	B3LYP	CAM-B3LYP	B3LYP	CAM-B3LYP	B3LYP	CAM-B3LYP
BLA	0.036	0.048	0.034	0.045	0.035	0.039
10	1.368	1.354	1.369	1.354	1.454	1.459
11	1.427	1.434	1.426	1.433	1.361	1.347
12	1.371	1.357	1.372	1.357	1.435	1.422
13					1.367	1.352
14					1.429	1.436
15					1.369	1.356

**Table 3.2** BLA index for the TPA (D3) based  $\pi$ -A systems in S<sub>0</sub> and S<sub>1</sub> states at CAM-B3LYP/cc-pVDZ level.

Bond	S <sub>0</sub> equilibrium at CAM-B3LYP/cc-pVDZ			S <sub>1</sub> equilibrium at CAM-B3LYP/cc-pVDZ		
	D3			D3	D3-CH <sub>3</sub>	D3-OH
	BLA	0.046		0.010	0.011	0.011
1	1.405			1.428	1.426	1.428
2	1.383			1.373	1.372	1.373
3	1.406			1.415	1.418	1.414
4	1.402			1.418	1.415	1.417
5	1.386			1.372	1.373	1.373
6	1.402			1.426	1.428	1.425
7	1.457			1.421	1.421	1.423
8	1.350			1.39	1.389	1.388
9	1.439			1.404	1.404	1.405
10	1.355			1.390	1.390	1.389
11	1.432			1.403	1.404	1.404
12	1.358			1.388	1.388	1.388



## 3.4 Results and discussion

### 3.4.1 MESP analysis

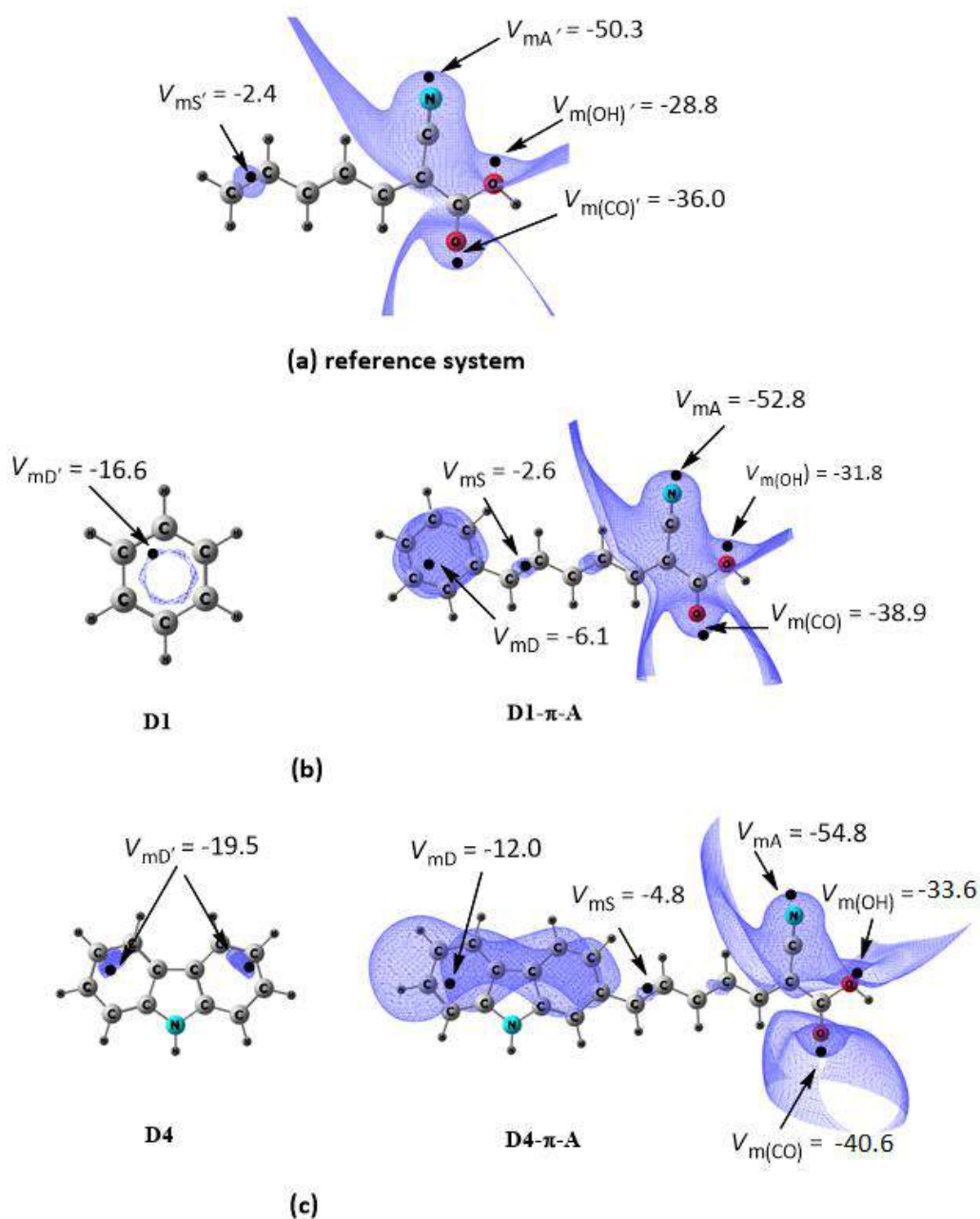


**Figure 3.3** MESP isosurfaces at various sites of a) referencesystem, b) D1 and D1- $\pi$ -A system, and c) D4 and D4- $\pi$ -A system.  $V_m$  values are in kcal/mol.

The MESP plot of two representative donors (D1 and D4) and their corresponding D- $\pi$ -A systems (unsubstituted) are shown in Figure 3.3 along with respective MESP minimum ( $V_m$ ) at various sites. In donor systems,  $V_{mD'}$  represents  $V_m$  of the donor. For example,  $V_{mD'}$  of benzene (D1) and carbazole (D4) are -16.6 and -19.5 kcal/mol

(Figure 3.3). In D- $\pi$ -A systems,  $V_{mD}$  and  $V_{mS}$ , represent the MESP minimum at donor and spacer (nearer to D), respectively, while  $V_{m(OH)}$ ,  $V_{m(CO)}$ , and  $V_{mA}$  represent the MESP minimum at the lone pair regions of OH, CO and CN of the acceptor moiety, respectively. Previous studies by Suresh and Gadre *et al.* have shown that lone pair regions in molecules can be characterized using MESP topographical analysis.<sup>76</sup> The MESP minimum observed at the CN unit of  $\pi$ -A is considered as a reference value,  $V_{mA'}$  (Figure 3.3a) (-50.3 kcal/mol) to monitor the changes observed at this minimum due to the incorporation of D to  $\pi$ -A. One could also consider the MESP minimum  $V_{m(OH)'}$  or  $V_{m(CO)'}$  of  $\pi$ -A as a reference point similar to  $V_{mA'}$  because in general the trends observed for these quantities show a parallel behavior. Here  $V_{mA'}$  is selected as the reference point on the basis of its most negative character compared to all other minima.

In Table 3.3,  $V_m$  of D- $\pi$ -A systems at various sites *viz.* donor ( $V_{mD}$ ), spacer ( $V_{mS}$ ) and acceptor ( $V_{m(OH)}$ ,  $V_{m(CO)}$  and  $V_{mA}$ ) are reported along with  $V_{mD'}$ . The unsubstituted D- $\pi$ -A systems are denoted as D1, D2, D3, D4, D5, and D6, and the substituents attached at D1 – D6 are represented as D1-CH<sub>3</sub>, D1- C<sub>5</sub>H<sub>11</sub>, D2- CH<sub>3</sub>, D2-C<sub>5</sub>H<sub>11</sub>, etc. The quantities  $\Delta V_{mD}$ ,  $\Delta V_{mS}$ ,  $\Delta V_{m(OH)}$ ,  $\Delta V_{m(CO)}$  and  $\Delta V_{mA}$  represent the change in  $V_m$  at respective sites with the attachment of  $\pi$ -A to D.  $\Delta V_{mD}$  has been calculated by subtracting the  $V_m$  observed at donor ( $V_{mD'}$ ) from the respective  $V_m$  observed at D site of D- $\pi$ -A ( $V_{mD}$ ). Likewise  $\Delta V_{mS}$ ,  $\Delta V_{m(OH)}$ ,  $\Delta V_{m(CO)}$ , and  $\Delta V_{mA}$  are estimated by subtracting the respective  $V_m$  at  $\pi$ -A *viz.*  $V_{mS'}$ ,  $V_{m(OH)'}$ ,  $V_{m(CO)'}$  and  $V_{mA'}$  (Figure 3.3) from the corresponding values at D- $\pi$ -A ( $V_{mS}$ ,  $V_{m(OH)}$ ,  $V_{m(CO)}$  and  $V_{mA}$ ) (Table 3.3).

**Table 3.3**  $V_m$  (kcal/mol) at various sites of D- $\pi$ -A systems calculated at B3LYP/cc-pVDZ level.

Donor moiety	D- $\pi$ -A system	$V_{mD'}$	$V_{mD}$	$V_{mS}$	$V_{m(OH)}$	$V_{m(CO)}$	$V_{mA}$	$\Delta V_{mD}$	$\Delta V_{mS}$	$\Delta V_{m(OH)}$	$\Delta V_{m(CO)}$	$\Delta V_{mA}$
<b>Benzene</b>	D1	-16.6	-6.1	-2.6	-31.8	-38.9	-52.8	10.5	-0.2	-2.9	-2.9	-2.5
	D1-CH <sub>3</sub>	-18.1	-6.5	-3.8	-32.7	-39.9	-53.8	11.5	-1.4	-3.9	-3.9	-3.5
	D1-C <sub>5</sub> H <sub>11</sub>	-18.7	-7.2	-4.3	-33.1	-40.1	-54.2	11.5	-1.9	-4.3	-4.1	-3.8
	D1-isopropyl	-17.9	-6.7	-3.8	-32.9	-39.9	-53.8	11.2	-1.4	-4.1	-3.9	-3.5

Donor moiety	D- $\pi$ -A system	$V_{mD'}$	$V_{mD}$	$V_{mS}$	$V_{m(OH)}$	$V_{m(CO)}$	$V_{mA}$	$\Delta V_{mD}$	$\Delta V_{mS}$	$\Delta V_{m(OH)}$	$\Delta V_{m(CO)}$	$\Delta V_{mA}$
	D1-t-but	-18.1	-6.9	-4.0	-32.9	-40.0	-53.9	11.2	-1.6	-4.1	-4.0	-3.6
	D1-OH	-17.9	-5.0	-4.3	-33.8	-40.9	-54.5	12.9	-1.9	-5.0	-4.8	-4.2
	D1-OCH <sub>3</sub>	-18.8	-6.0	-5.0	-34.3	-41.4	-54.8	12.8	-2.6	-5.5	-5.4	-4.5
	D1-OC <sub>2</sub> H <sub>5</sub>	-19.3	-6.5	-5.3	-34.5	-41.6	-55.3	12.7	-2.9	-5.6	-5.6	-5.0
	D1-NH <sub>2</sub>	-23.1	-8.6	-7.6	-36.4	-43.7	-57.1	14.5	-5.2	-7.6	-7.7	-6.8
	D1-N(CH <sub>3</sub> ) <sub>2</sub>	-24.0	-9.1	-9.0	-37.7	-45.1	-58.4	14.9	-6.7	-8.8	-9.0	-8.0
	D1-PhCH <sub>3</sub>	-16.7	-7.0	-3.7	-32.8	-39.8	-53.5	9.7	-1.3	-4.0	-3.8	-3.2
	D1-PhNH <sub>2</sub>	-19.7	-9.5	-5.9	-34.5	-41.7	-55.0	10.2	-3.5	-5.6	-5.6	-4.7
<b>Pyrene</b>	D2	-14.4	-8.2	-3.3	-32.0	-39.3	-53.0	6.2	-0.9	-3.2	-3.3	-2.7
	D2-CH <sub>3</sub>	-15.4	-8.7	-4.0	-32.6	-39.8	-53.7	6.7	-1.6	-3.8	-3.8	-3.3
	D2-C <sub>5</sub> H <sub>11</sub>	-15.8	-9.2	-4.2	-32.8	-40.0	-53.9	6.7	-1.8	-4.0	-4.0	-3.6
	D2-isopropyl	-15.3	-8.8	-4.0	-32.4	-39.7	-53.7	6.5	-1.6	-3.6	-3.7	-3.4
	D2-t-but	-15.5	-8.9	-4.1	-32.4	-39.8	-53.8	6.6	-1.7	-3.6	-3.8	-3.5
	D2-OH	-15.2	-8.2	-4.0	-32.8	-39.9	-53.7	7.0	-1.6	-4.0	-3.9	-3.4
	D2-OCH <sub>3</sub>	-15.9	-8.8	-4.5	-32.9	-40.2	-54.2	7.1	-2.1	-4.1	-4.1	-3.8
	D2-OC <sub>2</sub> H <sub>5</sub>	-16.3	-9.2	-4.6	-33.3	-40.5	-54.3	7.1	-2.3	-4.5	-4.5	-4.0
	D2-NH <sub>2</sub>	-18.1	-11.0	-5.8	-34.1	-41.2	-54.7	7.2	-3.4	-5.3	-5.2	-4.4
	D2-N(CH <sub>3</sub> ) <sub>2</sub>	-18.9	-11.5	-6.7	-34.7	-42.1	-55.8	7.3	-4.3	-5.9	-6.1	-5.5
	D2-PhCH <sub>3</sub>	-14.7	-8.6	-3.8	-32.6	-39.7	-53.7	6.1	-1.4	-3.8	-3.7	-3.3
	D2-PhNH <sub>2</sub>	-16.7	-10.7	-5.0	-33.4	-40.6	-54.5	6.0	-2.6	-4.6	-4.6	-4.1
<b>TPA</b>	D3	-15.6	-7.7	-6.3	-35.6	-42.5	-56.0	7.9	-3.9	-6.8	-6.5	-5.7
	D3-CH <sub>3</sub>	-16.5	-8.3	-6.9	-36.0	-43.2	-56.7	8.2	-4.5	-7.2	-7.2	-6.3
	D3-C <sub>5</sub> H <sub>11</sub>	-16.8	-8.7	-7.2	-36.0	-43.3	-57.0	8.2	-4.8	-7.2	-7.3	-6.7
	D3-isopropyl	-16.4	-8.3	-6.8	-35.8	-43.1	-56.6	8.1	-4.5	-7.0	-7.1	-6.3
	D3-t-but	-16.4	-8.3	-6.9	-36.1	-43.1	-56.4	8.2	-4.5	-7.3	-7.1	-6.0
	D3-OH	-17.5	-8.2	-7.5	-36.3	-43.5	-57.2	9.3	-5.1	-7.5	-7.5	-6.8
	D3-OCH <sub>3</sub>	-17.9	-8.7	-7.7	-36.6	-43.7	-57.2	9.2	-5.3	-7.8	-7.7	-6.9
	D3-OC <sub>2</sub> H <sub>5</sub>	-18.1	-8.9	-7.8	-36.7	-43.9	-57.4	9.2	-5.5	-7.9	-7.9	-7.1

Donor moiety	D- $\pi$ -A system	$V_{mD'}$	$V_{mD}$	$V_{mS}$	$V_{m(OH)}$	$V_{m(CO)}$	$V_{mA}$	$\Delta V_{mD}$	$\Delta V_{mS}$	$\Delta V_{m(OH)}$	$\Delta V_{m(CO)}$	$\Delta V_{mA}$
	D3-NH <sub>2</sub>	-19.4	-10.2	-8.7	-37.3	-44.5	-58.1	9.2	-6.3	-8.5	-8.5	-7.8
	D3-N(CH <sub>3</sub> ) <sub>2</sub>	-20.0	-11.0	-9.2	-37.7	-44.8	-58.3	9.0	-6.8	-8.9	-8.8	-8.0
	D3-PhCH <sub>3</sub>	-15.3	-7.8	-6.4	-35.6	-42.7	-56.3	7.5	-4.0	-6.8	-6.7	-6.0
	D3-PhNH <sub>2</sub>	-17.4	-9.7	-7.5	-36.3	-43.5	-57.2	7.7	-5.1	-7.5	-7.5	-6.8
<b>Carbazole</b>	D4	-19.5	-12.0	-4.8	-33.6	-40.6	-54.8	7.5	-2.4	-4.8	-4.6	-4.5
	D4-CH <sub>3</sub>	-20.6	-12.3	-5.6	-34.2	-41.3	-55.3	8.3	-3.2	-5.4	-5.3	-5.0
	D4-C <sub>5</sub> H <sub>11</sub>	-21.0	-12.7	-5.9	-34.3	-41.4	-55.5	8.3	-3.5	-5.5	-5.3	-5.1
	D4-isopropyl	-20.3	-12.2	-5.5	-34.0	-41.0	-55.1	8.1	-3.1	-5.2	-5.0	-4.8
	D4-t-but	-20.4	-12.4	-5.5	-34.1	-41.1	-54.9	8.0	-3.1	-5.3	-5.1	-4.6
	D4-OH	-21.0	-11.4	-6.0	-34.8	-41.5	-55.7	9.6	-3.6	-6.0	-5.5	-5.4
	D4-OCH <sub>3</sub>	-21.6	-12.0	-6.5	-35.1	-42.0	-56.0	9.5	-4.1	-6.3	-6.0	-5.7
	D4-OC <sub>2</sub> H <sub>5</sub>	-21.8	-12.4	-6.7	-35.1	-42.1	-55.8	9.4	-4.3	-6.3	-6.1	-5.5
	D4-NH <sub>2</sub>	-23.6	-14.5	-7.9	-36.0	-43.2	-57.0	9.1	-5.5	-7.2	-7.2	-6.7
	D4-N(CH <sub>3</sub> ) <sub>2</sub>	-24.6	-14.7	-8.8	-36.8	-43.7	-57.5	9.9	-6.5	-8.0	-7.7	-7.2
	D4-PhCH <sub>3</sub>	-19.5	-12.2	-5.2	-33.9	-41.0	-55.0	7.2	-2.8	-5.1	-5.0	-4.6
	D4-PhNH <sub>2</sub>	-21.8	-14.6	-6.5	-34.9	-42.0	-55.7	7.2	-4.1	-6.1	-6.0	-5.4
<b>Phenothiazine</b>	D5	-16.8	-9.4	-5.3	-34.6	-41.7	-55.2	7.4	-2.9	-5.8	-5.6	-4.9
	D5-CH <sub>3</sub>	-17.6	-9.0	-5.8	-34.7	-42.2	-55.7	8.6	-3.5	-5.9	-6.1	-5.4
	D5-C <sub>5</sub> H <sub>11</sub>	-17.9	-9.5	-6.1	-35.2	-42.5	-55.8	8.4	-3.8	-6.4	-6.5	-5.5
	D5-isopropyl	-17.5	-9.0	-5.9	-35.0	-42.3	-55.3	8.5	-3.5	-6.2	-6.3	-5.0
	D5-t-but	-17.6	-9.0	-6.0	-35.1	-42.4	-55.7	8.6	-3.6	-6.3	-6.3	-5.4
	D5-OH	-18.1	-7.2	-6.3	-35.4	-42.9	-56.1	10.9	-4.0	-6.6	-6.8	-5.8
	D5-OCH <sub>3</sub>	-18.4	-9.4	-6.7	-35.5	-42.7	-56.2	9.0	-4.3	-6.7	-6.7	-5.9
	D5-OC <sub>2</sub> H <sub>5</sub>	-18.6	-9.8	-6.7	-35.7	-43.1	-56.5	8.8	-4.3	-6.9	-7.1	-6.1
	D5-NH <sub>2</sub>	-19.5	-11.4	-7.3	-36.1	-43.4	-56.9	8.2	-5.0	-7.3	-7.4	-6.5
	D5-N(CH <sub>3</sub> ) <sub>2</sub>	-20.6	-12.4	-8.2	-36.6	-44.1	-57.5	8.3	-5.8	-7.8	-8.1	-7.2
	D5-PhCH <sub>3</sub>	-16.7	-9.0	-5.5	-34.8	-42.0	-55.5	7.7	-3.1	-6.0	-6.0	-5.1
	D5-PhNH <sub>2</sub>	-18.2	-11.2	-6.6	-35.4	-42.9	-56.2	7.0	-4.2	-6.6	-6.8	-5.9

Donor moiety	D- $\pi$ -A system	$V_{mD'}$	$V_{mD}$	$V_{mS}$	$V_{m(OH)}$	$V_{m(CO)}$	$V_{mA}$	$\Delta V_{mD}$	$\Delta V_{mS}$	$\Delta V_{m(OH)}$	$\Delta V_{m(CO)}$	$\Delta V_{mA}$
<b>Coumarin</b>	<b>D6</b>	-5.7	-0.1	0.0	-30.1	-37.8	-50.5	5.6	2.4	-1.3	-1.8	-0.2
	D6-CH <sub>3</sub>	-6.5	-0.4	-1.2	-31.0	-38.7	-51.3	6.1	1.2	-2.2	-2.7	-0.9
	D6-C <sub>5</sub> H <sub>11</sub>	-7.2	-1.1	-1.6	-31.2	-39.0	-51.8	6.1	0.8	-2.4	-3.0	-1.5
	D6-isopropyl	-6.7	-0.6	-1.2	-30.7	-38.7	-51.1	6.0	1.2	-1.9	-2.7	-0.8
	D6-t-but	-6.9	-0.9	-1.4	-31.2	-38.9	-51.3	6.0	0.9	-2.4	-2.9	-1.0
	D6-OH	-6.1	-	-1.9	-31.8	-39.5	-52.3	6.1	0.5	-3.0	-3.5	-1.9
	D6-OCH <sub>3</sub>	-7.0	-0.1	-2.6	-32.1	-40.0	-52.6	7.0	-0.2	-3.3	-4.0	-2.3
	D6-OC <sub>2</sub> H <sub>5</sub>	-7.5	-0.4	-2.9	-32.3	-40.2	-52.5	7.0	-0.6	-3.5	-4.2	-2.2
	D6-NH <sub>2</sub>	-10.4	-2.1	-5.0	-33.9	-41.8	-54.3	8.3	-2.6	-5.1	-5.8	-4.0
	D6-N(CH <sub>3</sub> ) <sub>2</sub>	-11.3	-2.6	-6.3	-35.0	-43.0	-55.5	8.7	-4.0	-6.2	-7.0	-5.1
	D6-PhCH <sub>3</sub>	-7.2	-1.6	-1.6	-31.2	-38.8	-51.5	5.6	0.8	-2.4	-2.8	-1.2
	D6-PhNH <sub>2</sub>	-10.2	-4.2	-3.6	-32.8	-40.6	-53.2	6.0	-1.2	-4.0	-4.6	-2.8

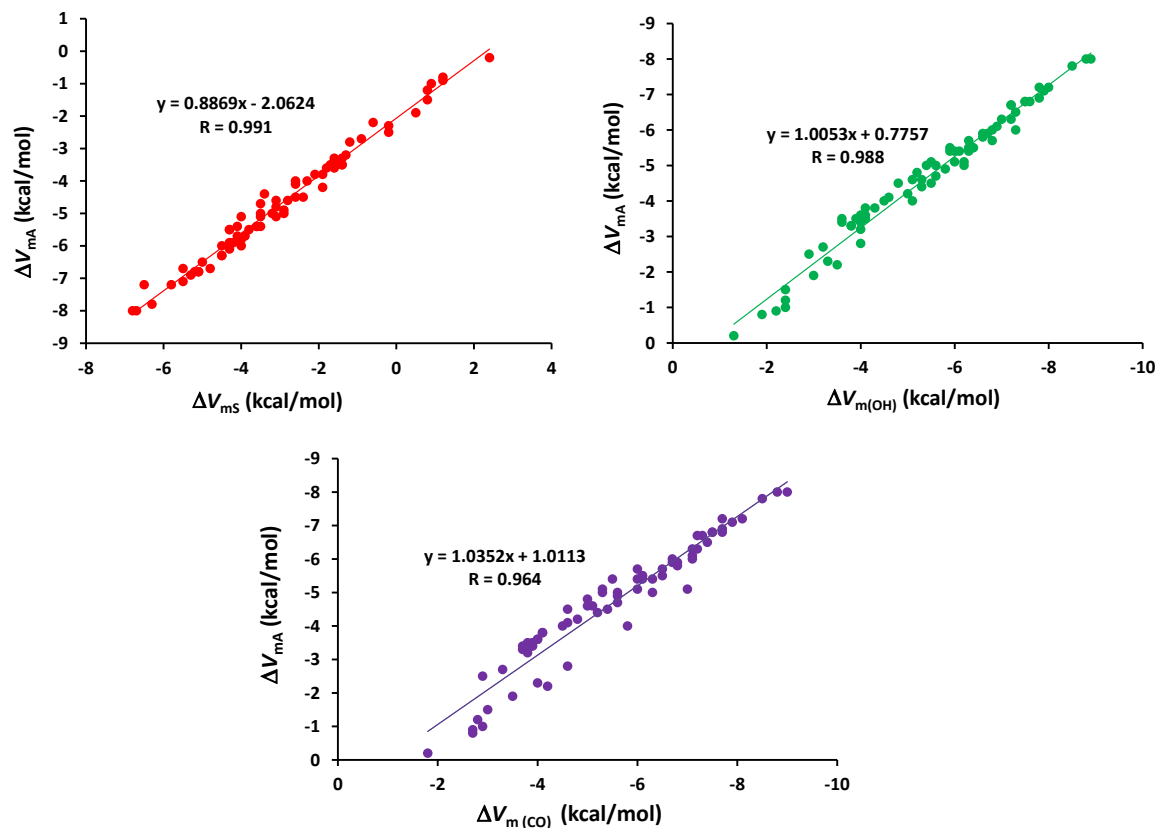


**Figure 3. 4** Correlation between MESP parameters  $\Delta V_{mS}$ ,  $\Delta V_{m(OH)}$ ,  $\Delta V_{m(CO)}$ , and  $\Delta V_{mA}$ .

The data in Table 3.3 show that the  $V_{mD}$  of D- $\pi$ -A system is always less negative than the  $V_{mD}$  of the donor D. For various donor systems,  $\Delta V_{mD}$  lies in the range 5.6 to 14.9 kcal/mol which suggests that the D site of D- $\pi$ -A system becomes electron deficient compared to a normal D. The electron deficiency at D can be attributed to ICT of electrons from D to the  $\pi$ -A region which implies that  $V_m$  at the acceptor sites of D- $\pi$ -A becomes more negative compared to  $\pi$ -A and as a result always negative values are observed for  $\Delta V_{m(OH)}$ ,  $\Delta V_{m(CO)}$ , and  $\Delta V_{mA}$ . For example, when  $\pi$ -A changes to D1- $\pi$ -A,  $V_m$  at cyano region turns out to be more negative ( $V_{mA} = -52.8$  kcal/mol) than the respective  $V_m$  on the reference system ( $\pi$ -A),  $V_{mA}$  (-50.3 kcal/mol). A similar trend in  $V_{mA}$  is observed for all the remaining systems. Also compared to  $\pi$ -A, the  $\pi$ -spacer region of D- $\pi$ -A shows more negative character for  $V_{mS}$  in all cases except some of the coumarin-based systems. Among the donors,  $V_{mD}$  value is the least negative for coumarin systems which can be attributed to the presence of electron-withdrawing carbonyl group in it. The quantities  $\Delta V_{mS}$ ,  $\Delta V_{m(OH)}$ ,  $\Delta V_{m(CO)}$ , and  $\Delta V_{mA}$  show a parallel trend as shown in the correlation plots given in Figure 3.4. This suggests that any of these quantities can be used as a parameter to measure the donating strength of donor moieties to a common acceptor. Here  $\Delta V_{mA}$  (for the CN group) is selected for this purpose. It may be noted that variation in  $\Delta V_{mD}$  is not similar to  $\Delta V_{mA}$  (Figure 3.5) because it accounts for the property of various donors whereas  $\Delta V_{mA}$  accounts for the accepting ability of CN unit from various donors.

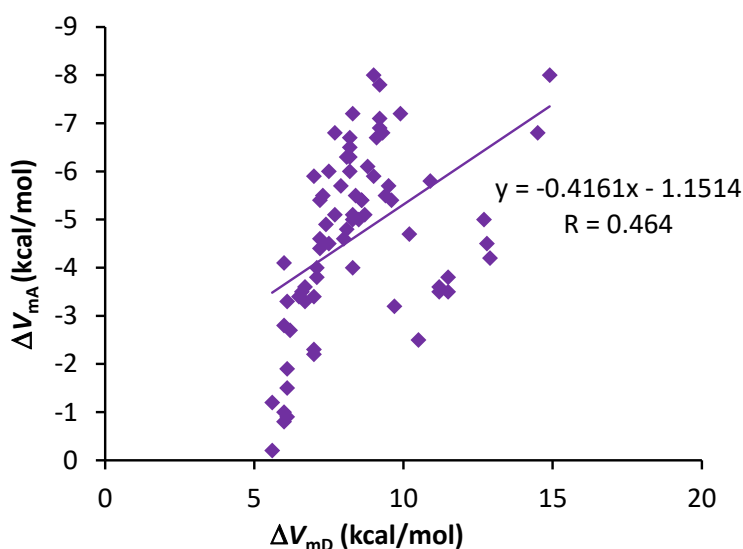


**Figure 3.5** Correlation between  $\Delta V_{mD}$  and  $\Delta V_{mA}$ .

In Table 3.3, the lower  $\Delta V_{mA}$  in the range -0.2 to -5.1 kcal/mol have been attained by coumarin-based D- $\pi$ -A systems which can be attributed to the presence of electron-withdrawing CO group in donor site. In benzene and pyrene-based systems, the strong conjugation feature in donors increases the negative character of  $\Delta V_{mA}$  values (-2.5 to -8.0 kcal/mol) leading to better-donating strength than coumarin systems. In carbazole and phenothiazine systems, the charge transfer to the acceptor is enhanced ( $\Delta V_{mA}$  -4.5 to -7.2 kcal/mol) due to electron-donation from hetero atoms *viz.* nitrogen and sulphur. Among all, the TPA-based systems have the highest electron-donating strength (-5.7 to -8.0 kcal/mol).

Substituents at the donor region can be utilized for tuning the electron-donating strength of the donor. For instance, alkyl substituents *viz.* CH<sub>3</sub>, C<sub>5</sub>H<sub>11</sub>, isopropyl, and t-butyl at the donor unit enhance the electron-donating strength of all the corresponding substituted D- $\pi$ -A systems by an +I inductive effect. The substituents bearing lone pairs such as OH, OCH<sub>3</sub>, NH<sub>2</sub>, and N(CH<sub>3</sub>)<sub>2</sub> improve the electron density of the donor unit, result in better electron-donating power than alkyl substituents ( $\Delta V_{mA}$  in the range -3.4 to -8.0 kcal/mol) +R resonance effect. Among all, N(CH<sub>3</sub>)<sub>2</sub> substituted benzene and TPA-based D- $\pi$ -A systems show the highest donation from donor to acceptor. The donating strength of various substituents attached on D- $\pi$ -A system follows the order PhCH<sub>3</sub> ~ alkyls < -OH, -OR, PhNH<sub>2</sub> < NH<sub>2</sub> < N(CH<sub>3</sub>)<sub>2</sub>.

### 3.4.2 Absorption spectra

In Table 3.4, HOMO, LUMO energies, HOMO-LUMO energy gap (HLG), absorption maximum ( $\lambda_{max}$ ), and oscillator strength (f) of six different D- $\pi$ -A systems with various substituents are reported. In all kinds of D- $\pi$ -A systems, a systematic increase in  $\lambda_{max}$  with respect to various substituents have been observed (388 to 490 nm), which can be correlated to the electron-donating strength of donor in the D- $\pi$ -A system. This is evident in the excellent linear correlations between  $\Delta V_{mA}$  and  $\lambda_{max}$  obtained for all the six kinds of D- $\pi$ -A systems (Figure 3.6). Also, with improved electron-donating strength of a D- $\pi$ -A system, lowering of HLG is noted in every system, which lies in the range 3.14 to 2.17 eV. Among all, the highest  $\lambda_{max}$  490 nm has been shown by (NH<sub>3</sub>)<sub>2</sub> substituted phenothiazine system D5-N(CH<sub>3</sub>)<sub>2</sub>. For the six D- $\pi$ -A systems and the

selected eleven substituents, 102 nm width is available for tuning  $\lambda_{\max}$  to a preferred region. For individual donors, the substituent effect alone can account for a tuning width 69 nm for benzene, 29 nm for pyrene, 19 nm for TPA, 42 nm for carbazole, 31 nm for phenothiazine, and 57 nm for coumarin, respectively.

**Table 3. 4** HOMO, LUMO, and HOMO-LUMO energy gap (HLG) (in eV) observed for the ground state at B3LYP/cc-pVDZ level and absorption maximum  $\lambda_{\max}$  (nm), and oscillator strength (f) at CAM-B3LYP/SMD/cc-pVDZ// B3LYP/cc-pVDZ level.

D- $\pi$ -A system	HOMO	LUMO	HLG	$\lambda_{\max}$	f
<b>Benzene</b>					
D1	-6.13	-2.99	3.14	388	1.74
D1-CH <sub>3</sub>	-6.01	-2.92	3.08	396	1.82
D1-C <sub>5</sub> H <sub>11</sub>	-5.97	-2.90	3.07	398	1.86
D1-isopropyl	-6.01	-2.92	3.08	396	1.86
D1-t-but	-6.00	-2.92	3.08	397	1.89
D1-OH	-5.84	-2.85	2.99	408	1.78
D1-OCH <sub>3</sub>	-5.79	-2.83	2.97	412	1.81
D1-OC <sub>2</sub> H <sub>5</sub>	-5.77	-2.81	2.96	413	1.84
D1-NH <sub>2</sub>	-5.53	-2.69	2.84	434	1.85
D1-N(CH <sub>3</sub> ) <sub>2</sub>	-5.34	-2.62	2.72	457	1.94
D1-PhCH <sub>3</sub>	-5.89	-2.96	2.93	410	2.15
D1-PhNH <sub>2</sub>	-5.52	-2.86	2.66	428	2.17
<b>Pyrene</b>					
D2	-5.88	-2.99	2.89	401	2.22
D2-CH <sub>3</sub>	-5.84	-2.95	2.89	404	2.27
D2-C <sub>5</sub> H <sub>11</sub>	-5.81	-2.94	2.87	404	2.32
D2-isopropyl	-5.83	-2.95	2.88	404	2.30
D2-t-but	-5.82	-2.95	2.87	404	2.33
D2-OH	-5.85	-2.94	2.91	409	2.19
D2-OCH <sub>3</sub>	-5.79	-2.92	2.87	410	2.20
D2-OC <sub>2</sub> H <sub>5</sub>	-5.77	-2.91	2.86	410	2.23
D2-NH <sub>2</sub>	-5.62	-2.86	2.76	419	2.20



D- $\pi$ -A system	HOMO	LUMO	HLG	$\lambda_{\max}$	f
D2-N(CH <sub>3</sub> ) <sub>2</sub>	-5.39	-2.81	2.58	3.17	2.21
D2-PhCH <sub>3</sub>	-5.86	-2.97	2.89	406	2.49
D2-PhNH <sub>2</sub>	-5.53	-2.91	2.62	411	2.53
<b>TPA</b>					
D3	-5.37	-2.79	2.58	453	2.02
D3-CH <sub>3</sub>	-5.31	-2.76	2.55	457	2.03
D3-C <sub>5</sub> H <sub>11</sub>	-5.29	-2.75	2.55	458	2.06
D3-isopropyl	-5.31	-2.76	2.55	457	2.03
D3-t-but	-5.31	-2.76	2.55	457	2.02
D3-OH	-5.26	-2.73	2.53	460	2.02
D3-OCH <sub>3</sub>	-5.24	-2.72	2.52	461	2.03
D3-OC <sub>2</sub> H <sub>5</sub>	-5.23	-2.71	2.51	461	2.03
D3-NH <sub>2</sub>	-5.13	-2.67	2.46	468	2.00
D3-N(CH <sub>3</sub> ) <sub>2</sub>	-5.03	-2.65	2.38	472	2.00
D3-PhCH <sub>3</sub>	-5.31	-2.78	2.52	457	2.12
D3-PhNH <sub>2</sub>	-5.17	-2.73	2.44	460	2.12
<b>Carbazole</b>					
D4	-5.78	-2.91	2.87	419	2.21
D4-CH <sub>3</sub>	-5.69	-2.87	2.83	424	2.27
D4-C <sub>5</sub> H <sub>11</sub>	-5.67	-2.85	2.82	425	2.31
D4-isopropyl	-5.71	-2.88	2.83	424	2.30
D4-t-but	-5.70	-2.87	2.83	424	2.31
D4-OH	-5.58	-2.84	2.74	432	2.22
D4-OCH <sub>3</sub>	-5.54	-2.82	2.72	433	2.27
D4-OC <sub>2</sub> H <sub>5</sub>	-5.52	-2.81	2.71	434	2.29
D4-NH <sub>2</sub>	-5.33	-2.75	2.58	447	2.23
D4-N(CH <sub>3</sub> ) <sub>2</sub>	-5.14	-2.71	2.44	461	2.26
D4-PhCH <sub>3</sub>	-5.66	-2.90	2.76	427	2.53
D4-PhNH <sub>2</sub>	-5.37	-2.83	2.53	433	2.57
<b>Phenothiazine</b>					
D5	-5.28	-2.84	2.44	459	1.67

D- $\pi$ -A system	HOMO	LUMO	HLG	$\lambda_{\max}$	f
D5-CH <sub>3</sub>	-5.22	-2.81	2.41	464	1.69
D5-C <sub>5</sub> H <sub>11</sub>	-5.20	-2.80	2.40	464	1.72
D5-isopropyl	-5.21	-2.81	2.40	465	1.68
D5-t-but	-5.22	-2.81	2.40	464	1.71
D5-OH	-5.15	-2.79	2.36	469	1.66
D5-OCH <sub>3</sub>	-5.14	-2.78	2.36	469	1.70
D5-OC <sub>2</sub> H <sub>5</sub>	-5.12	-2.77	2.35	470	1.71
D5-NH <sub>2</sub>	-4.99	-2.74	2.25	482	1.62
D5-N(CH <sub>3</sub> ) <sub>2</sub>	-4.88	-2.70	2.17	490	1.62
D5-PhCH <sub>3</sub>	-5.22	-2.81	2.41	464	1.69
D5-PhNH <sub>2</sub>	-5.07	-2.78	2.29	469	1.78
<b>Coumarin</b>					
D6	-6.19	-3.34	2.85	424	1.71
D6-CH <sub>3</sub>	-6.09	-3.26	2.82	431	1.78
D6-C <sub>5</sub> H <sub>11</sub>	-6.07	-3.25	2.82	431	1.84
D6-isopropyl	-6.09	-3.27	2.82	431	1.83
D6-t-but	-6.07	-3.25	2.82	432	1.84
D6-OH	-5.98	-3.20	2.78	439	1.77
D6-OCH <sub>3</sub>	-5.94	-3.18	2.76	442	1.82
D6-OC <sub>2</sub> H <sub>5</sub>	-5.92	-3.16	2.76	443	1.85
D6-NH <sub>2</sub>	-5.71	-3.04	2.67	463	1.86
D6-N(CH <sub>3</sub> ) <sub>2</sub>	-5.56	-2.97	2.59	481	1.96
D6-PhCH <sub>3</sub>	-6.00	-3.28	2.72	444	2.10
D6-PhNH <sub>2</sub>	-5.68	-3.17	2.51	461	2.18

The  $\Delta V_{\text{mA}}$  versus  $\lambda_{\max}$  correlations given in Figure 3.6 suggest that the substituent effect tunes the HOMO-LUMO energy gap (HLG). The HLG plot of a representative system D5- $\pi$ -A (phenothiazine-based) is given in Figure 3.7 which shows that the introduction of substituents on the core D unit lowers the HLG from 2.41 to 2.17 eV. The poor electron-donating ability observed in alkyls and PhCH<sub>3</sub> substituted systems display higher HLG (2.40 to 2.41 eV), while the lowest HLG has been attained with N(CH<sub>3</sub>)<sub>2</sub> substituted D5- $\pi$ -A. Similar trend in HLG is observed for

the remaining systems which confirms the significance of the substituent effect in tuning  $\lambda_{\max}$  (Table 3.4). The HOMO and LUMO plots of representative systems are shown in Figure 3.8. HOMO has a more delocalized distribution than LUMO with more orbital contributions from the donor site while the LUMO is largely delocalized along the  $\pi$ -spacer and acceptor moiety.

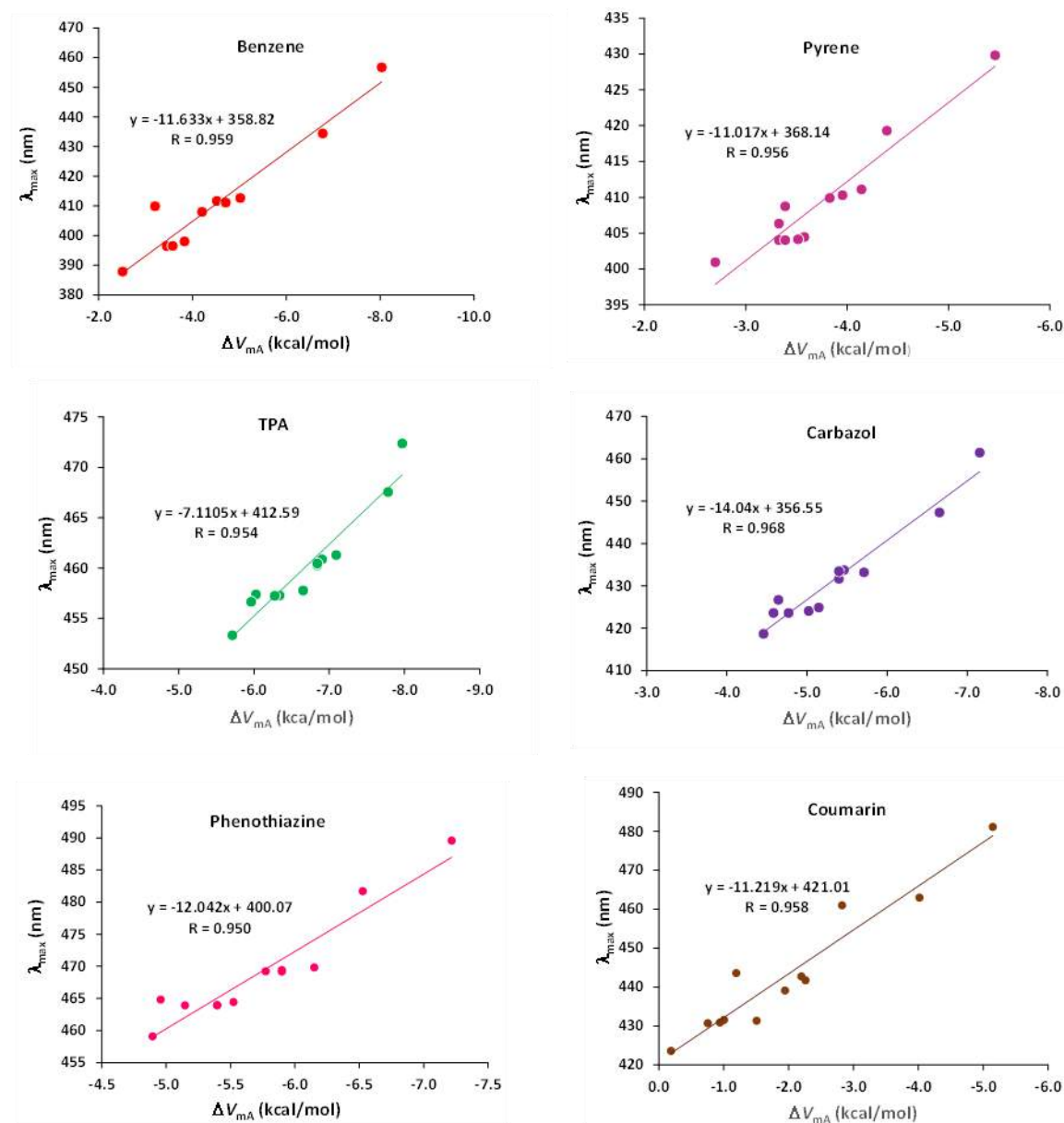


**Figure 3.6** Correlation between absorption maximum ( $\lambda_{\max}$ ) and donating strength ( $\Delta V_{mA}$ ) of various D- $\pi$ -A systems with different substituents.

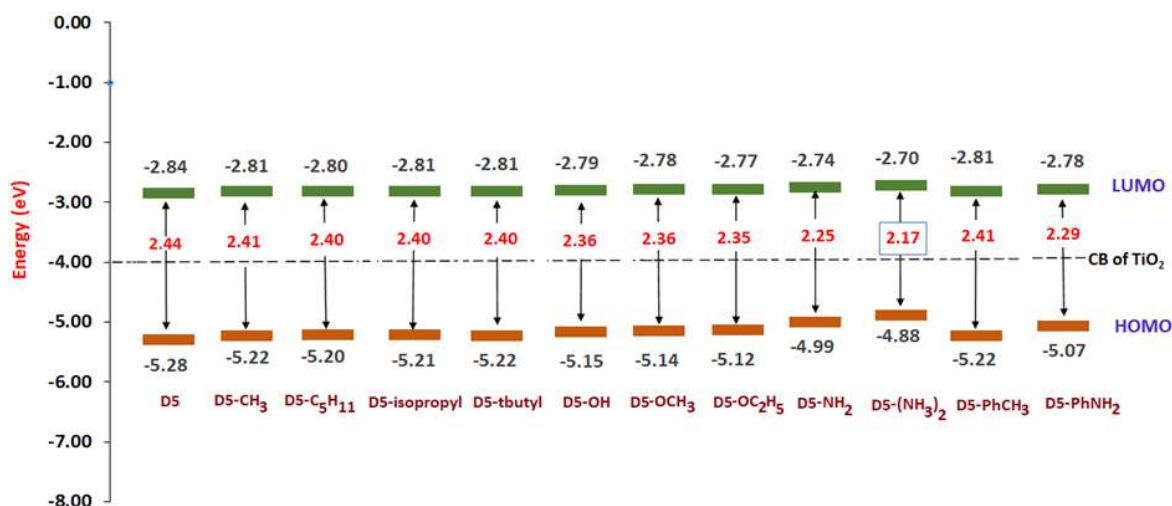


**Figure 3.7** Frontier molecular energy levels of phenothiazine based  $\pi$ -A with various substituents at B3LYP/cc-pVDZ level.

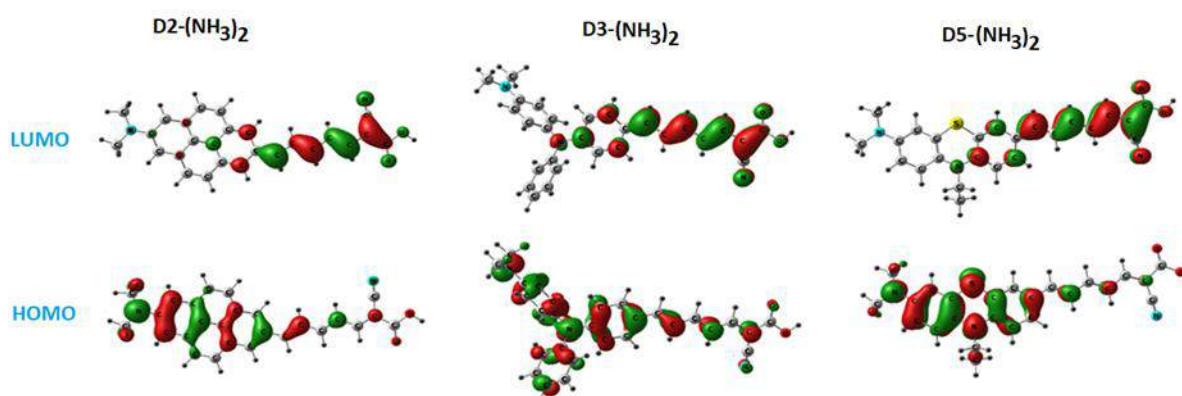


**Figure 3.8** Frontier molecular orbitals of representative  $N(CH_3)_2$  substituted D- $\pi$ -A systems at B3LYP/cc-pVDZ level.

### 3.4.3 Photovoltaic performance

In Table 3. 5, electronic excitation energy, ground state oxidation potential  $E^{dye}$ , excited state oxidation potential  $E^{dye*}$ , free energy change of electron injection  $\Delta G_{inject}$ , free energy change of dye regeneration  $\Delta G_{reg}$ , and open-circuit voltage  $eV_{OC}$  of D- $\pi$ -A systems are described. The negative  $\Delta G_{inject}$  observed in the range -0.73 to -1.65 eV lies above the CB of  $TiO_2$  (-4.0 eV) and indicates the possibility of a spontaneous electron injection process from CB to  $TiO_2$ . Also, a more electron-donating substituent enhances the electron injection process as  $\Delta G_{inject}$  becomes more negative with such substituents. Alkyls and  $PhCH_3$  substituted D- $\pi$ -A systems are less efficient for electron injection than the OH,  $OCH_3$ ,  $OC_2H_5$ ,  $NH_2$ , and  $N(CH_3)_2$

substituted systems. Among all, the most negative  $\Delta G_{inject}$  -1.65 eV is observed for phenothiazine system D5-N(CH<sub>3</sub>)<sub>2</sub>. The smaller electron injection efficiency (-0.79 to -0.81 eV) observed for alkyls and PhCH<sub>3</sub> substituted coumarin systems can be attributed to their lower electron-donating strength than others.

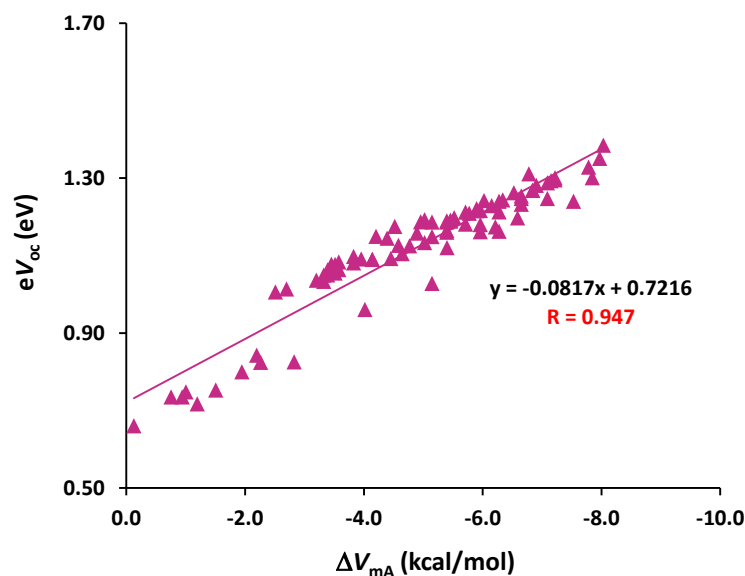


**Figure 3.9** Correlation between donating strength  $\Delta V_{mA}$  and open-circuit voltage  $eV_{OC}$  of D- $\pi$ -A systems.

From the previous studies, it is understood that the PCE of DSSCs depends on the free energy change for dye regeneration.<sup>77, 78</sup> The lower the  $\Delta G_{reg}$ , faster will be the dye regeneration, leading to higher efficiency for the electron injection from dye to TiO<sub>2</sub> semiconductor. In the studied systems, the fastest dye regeneration force 0.08 eV has been attained by N(CH<sub>3</sub>)<sub>2</sub> substituted phenothiazine system (D5- N(CH<sub>3</sub>)<sub>2</sub>), whereas the least dye regeneration (1.27 - 1.29 eV) has been possessed by alkyls, and PhCH<sub>3</sub> substituted coumarin systems. The unsubstituted systems always possessed higher  $\Delta G_{reg}$  values (0.48 - 1.39 eV) than substituted ones (0.08 - 1.29 eV) and suggests that the introduction of electron-donating substituents on the donor moiety gives better  $\Delta G_{reg}$  values and improves electron regeneration efficiency. Similarly, a positive effect of substituents on  $eV_{OC}$  is always observed confirming that by tuning the donating strength of the substituents, significant improvement in the performance of DSSC can be achieved. In all the six sets, N(CH<sub>3</sub>)<sub>2</sub> substituted systems possess the best  $eV_{OC}$  and among them, the highest is observed for D1- N(CH<sub>3</sub>)<sub>2</sub> (1.38 eV) whereas the lowest  $eV_{OC}$  (0.72 eV) is observed for D6-PhCH<sub>3</sub>.

**Table 3. 5** HOMO, LUMO, and HOMO-LUMO energy gap (HLG) (in eV) observed for the ground state at B3LYP/cc-pVDZ level. Excitation energy, ground, and excited state oxidation potential ( $E^{dye}$ ,  $E^{dye*}$ ), electron injection-free energy change  $\Delta G_{inject}$ , free energy change for dye regeneration  $\Delta G_{reg}$ , and open-circuit voltage  $eV_{OC}$  at TD-CAM-B3LYP/SMD/cc-pVDZ//B3LYP/cc-pVDZ level.

D- $\pi$ -A	Excitation energy (eV)	HOMO (eV)	LUMO (eV)	HLG (eV)	$E^{dye}$ (eV)	$E^{dye*}$ (eV)	$\Delta G_{inject}$ (eV)	$\Delta G_{reg}$ (eV)	$eV_{OC}$ (eV)
<b>Benzene</b>									
D1	3.20	-6.13	-2.99	3.14	6.13	2.93	-1.07	1.33	1.01
D1-CH <sub>3</sub>	3.13	-6.01	-2.92	3.08	6.01	2.88	-1.12	1.21	1.08
D1-C <sub>5</sub> H <sub>11</sub>	3.11	-5.97	-2.90	3.07	5.97	2.86	-1.14	1.17	1.10
D1-isopropyl	3.13	-6.01	-2.92	3.08	6.01	2.88	-1.12	1.21	1.08
D1-t-but	3.13	-6.00	-2.92	3.08	6.00	2.87	-1.13	1.20	1.08
D1-OH	3.04	-5.84	-2.85	2.99	5.84	2.80	-1.20	1.04	1.15
D1-OCH <sub>3</sub>	3.01	-5.79	-2.83	2.97	5.79	2.78	-1.22	0.99	1.17
D1-OC <sub>2</sub> H <sub>5</sub>	3.00	-5.77	-2.81	2.96	5.77	2.77	-1.23	0.97	1.19
D1-NH <sub>2</sub>	2.85	-5.53	-2.69	2.84	5.53	2.68	-1.32	0.73	1.31
D1-N(CH <sub>3</sub> ) <sub>2</sub>	2.71	-5.34	-2.62	2.72	5.34	2.63	-1.37	0.54	1.38
D1-PhCH <sub>3</sub>	3.02	-5.89	-2.96	2.93	5.89	2.87	-1.13	1.09	1.04
D1-PhNH <sub>2</sub>	2.90	-5.52	-2.86	2.66	5.52	2.62	-1.38	0.73	1.14
<b>Pyrene</b>									
D2	3.09	-5.88	-2.99	2.89	5.88	2.79	-1.21	1.08	1.01
D2-CH <sub>3</sub>	3.07	-5.84	-2.95	2.89	5.84	2.77	-1.23	1.04	1.05
D2-C <sub>5</sub> H <sub>11</sub>	3.07	-5.81	-2.94	2.87	5.81	2.74	-1.26	1.01	1.06
D2-isopropyl	3.07	-5.83	-2.95	2.88	5.83	2.76	-1.24	1.03	1.05
D2-t-but	3.07	-5.82	-2.95	2.87	5.82	2.75	-1.25	1.02	1.05
D2-OH	3.03	-5.85	-2.94	2.91	5.85	2.82	-1.18	1.05	1.06
D2-OCH <sub>3</sub>	3.02	-5.79	-2.92	2.87	5.79	2.77	-1.23	0.99	1.08
D2-OC <sub>2</sub> H <sub>5</sub>	3.02	-5.77	-2.91	2.86	5.77	2.75	-1.25	0.97	1.09
D2-NH <sub>2</sub>	2.96	-5.62	-2.86	2.76	5.62	2.66	-1.34	0.82	1.14

D- $\pi$ -A	Excitation energy (eV)	HOMO (eV)	LUMO (eV)	HLG (eV)	$E^{dye}$ (eV)	$E^{dye^*}$ (eV)	$\Delta G_{inject}$ (eV)	$\Delta G_{reg}$ (eV)	$eV_{OC}$ (eV)
D2-N(CH <sub>3</sub> ) <sub>2</sub>	2.88	-5.39	-2.81	2.58	5.39	2.51	-1.49	0.59	1.19
D2-PhCH <sub>3</sub>	3.05	-5.86	-2.97	2.89	5.86	2.81	-1.19	1.06	1.03
D2-PhNH <sub>2</sub>	3.02	-5.53	-2.91	2.62	5.53	2.51	-1.49	0.73	1.09
<b>TPA</b>									
D3	2.73	-5.37	-2.79	2.58	5.37	2.64	-1.36	0.57	1.21
D3-CH <sub>3</sub>	2.71	-5.31	-2.76	2.55	5.31	2.60	-1.40	0.51	1.24
D3-C <sub>5</sub> H <sub>11</sub>	2.71	-5.29	-2.75	2.55	5.29	2.58	-1.42	0.49	1.25
D3-isopropyl	2.71	-5.31	-2.76	2.55	5.31	2.60	-1.40	0.51	1.24
D3-t-but	2.71	-5.31	-2.76	2.55	5.31	2.60	-1.40	0.51	1.24
D3-OH	2.69	-5.26	-2.73	2.53	5.26	2.57	-1.43	0.46	1.27
D3-OCH <sub>3</sub>	2.69	-5.24	-2.72	2.52	5.24	2.55	-1.45	0.44	1.28
D3-OC <sub>2</sub> H <sub>5</sub>	2.69	-5.23	-2.71	2.51	5.23	2.54	-1.46	0.43	1.29
D3-NH <sub>2</sub>	2.65	-5.13	-2.67	2.46	5.13	2.48	-1.52	0.33	1.33
D3-N(CH <sub>3</sub> ) <sub>2</sub>	2.62	-5.03	-2.65	2.38	5.03	2.41	-1.59	0.23	1.35
D3-PhCH <sub>3</sub>	2.72	-5.31	-2.78	2.52	5.31	2.60	-1.41	0.51	1.22
D3-PhNH <sub>2</sub>	2.69	-5.17	-2.73	2.44	5.17	2.48	-1.52	0.37	1.27
<b>Carbazole</b>									
D4	2.96	-5.78	-2.91	2.87	5.78	2.82	-1.18	0.98	1.09
D4-CH <sub>3</sub>	2.92	-5.69	-2.87	2.83	5.69	2.77	-1.23	0.89	1.13
D4-C <sub>5</sub> H <sub>11</sub>	2.92	-5.67	-2.85	2.82	5.67	2.75	-1.25	0.87	1.15
D4-isopropyl	2.93	-5.71	-2.88	2.83	5.71	2.78	-1.22	0.91	1.12
D4-t-but	2.93	-5.70	-2.87	2.83	5.70	2.77	-1.23	0.90	1.13
D4-OH	2.87	-5.58	-2.84	2.74	5.58	2.71	-1.29	0.78	1.16
D4-OCH <sub>3</sub>	2.86	-5.54	-2.82	2.72	5.54	2.68	-1.32	0.74	1.18
D4-OC <sub>2</sub> H <sub>5</sub>	2.86	-5.52	-2.81	2.71	5.52	2.66	-1.34	0.72	1.19
D4-NH <sub>2</sub>	2.77	-5.33	-2.75	2.58	5.33	2.56	-1.44	0.53	1.25
D4-N(CH <sub>3</sub> ) <sub>2</sub>	2.69	-5.14	-2.71	2.44	5.14	2.45	-1.55	0.34	1.29
D4-PhCH <sub>3</sub>	2.91	-5.66	-2.90	2.76	5.66	2.75	-1.25	0.86	1.10

D- $\pi$ -A	Excitation energy (eV)	HOMO (eV)	LUMO (eV)	HLG (eV)	$E^{dye}$ (eV)	$E^{dye^*}$ (eV)	$\Delta G_{inject}$ (eV)	$\Delta G_{reg}$ (eV)	$eV_{OC}$ (eV)
D4-PhNH <sub>2</sub>	2.86	-5.37	-2.83	2.53	5.37	2.51	-1.49	0.57	1.17
<b>Phenothiazine</b>									
D5	2.70	-5.28	-2.84	2.44	5.28	2.58	-1.42	0.48	1.16
D5-CH <sub>3</sub>	2.67	-5.22	-2.81	2.41	5.22	2.55	-1.45	0.42	1.19
D5-C <sub>5</sub> H <sub>11</sub>	2.67	-5.20	-2.80	2.40	5.20	2.53	-1.47	0.40	1.20
D5-isopropyl	2.67	-5.21	-2.81	2.40	5.21	2.54	-1.46	0.41	1.19
D5-t-but	2.67	-5.22	-2.81	2.40	5.22	2.55	-1.45	0.42	1.19
D5-OH	2.64	-5.15	-2.79	2.36	5.15	2.51	-1.49	0.35	1.21
D5-OCH <sub>3</sub>	2.64	-5.14	-2.78	2.36	5.14	2.50	-1.50	0.34	1.22
D5-OC <sub>2</sub> H <sub>5</sub>	2.64	-5.12	-2.77	2.35	5.12	2.48	-1.52	0.32	1.23
D5-NH <sub>2</sub>	2.57	-4.99	-2.74	2.25	4.99	2.42	-1.58	0.19	1.26
D5-N(CH <sub>3</sub> ) <sub>2</sub>	2.53	-4.88	-2.70	2.17	4.88	2.35	-1.65	0.08	1.30
D5-PhCH <sub>3</sub>	2.67	-5.22	-2.81	2.41	5.22	2.55	-1.45	0.42	1.19
D5-PhNH <sub>2</sub>	2.64	-5.07	-2.78	2.29	5.07	2.43	-1.57	0.27	1.22
<b>Coumarin</b>									
D6	2.93	-6.19	-3.34	2.85	6.19	3.27	-0.73	1.39	0.66
D6-CH <sub>3</sub>	2.88	-6.09	-3.26	2.82	6.09	3.21	-0.79	1.29	0.74
D6-C <sub>5</sub> H <sub>11</sub>	2.87	-6.07	-3.25	2.82	6.07	3.19	-0.81	1.27	0.75
D6-isopropyl	2.88	-6.09	-3.27	2.82	6.09	3.21	-0.79	1.29	0.73
D6-t-but	2.87	-6.07	-3.25	2.82	6.07	3.20	-0.80	1.27	0.75
D6-OH	2.82	-5.98	-3.20	2.78	5.98	3.15	-0.85	1.18	0.80
D6-OCH <sub>3</sub>	2.81	-5.94	-3.18	2.76	5.94	3.13	-0.87	1.14	0.82
D6-OC <sub>2</sub> H <sub>5</sub>	2.80	-5.92	-3.16	2.76	5.92	3.11	-0.89	1.12	0.84
D6-NH <sub>2</sub>	2.68	-5.71	-3.04	2.67	5.71	3.04	-0.96	0.91	0.96
D6-N(CH <sub>3</sub> ) <sub>2</sub>	2.58	-5.56	-2.97	2.59	5.56	2.98	-1.02	0.76	1.03
D6-PhCH <sub>3</sub>	2.80	-6.00	-3.28	2.72	6.00	3.21	-0.79	1.20	0.72
D6-PhNH <sub>2</sub>	2.69	-5.68	-3.17	2.51	5.68	2.99	-1.01	0.88	0.83



By considering the above-mentioned results, we analyzed the relation between electron-donating strength  $\Delta V_{mA}$  and open-circuit voltage  $eV_{OC}$  (Figure 3.9). The excellent linear correlation observed in all the six series of different D- $\pi$ -A systems show that  $eV_{OC}$  increases with enhancement in the donating strength of substituents. Overall, the study suggests that by selecting the appropriate donor and substituent, precise tuning of the optical and photovoltaic properties of the D- $\pi$ -A systems can be achieved. Also, these results point out that the theoretical examination of donating strength of substituents using MESP analysis is promising for dye designing and efficiency prediction of D- $\pi$ -A systems.

### 3.5 Conclusions

The electron-donating strength of donor in D- $\pi$ -A system affects the optical and photovoltaic performance of DSSC, leading to better PCE in a solar cell. In the study using MESP analysis, we have characterized the donating strength ( $\Delta V_{mA}$ ) of six different sets of D- $\pi$ -A systems, wherein  $\pi$  and A systems are butadiene and cyanoacrylic acid, respectively. The significance of eleven electron releasing groups at donor is also examined for a total of seventy-two D- $\pi$ -A systems and achieved the fine-tuning of the electron donation from the donor to the acceptor. In all the six different sets of D- $\pi$ -A systems, the  $N(CH_3)_2$  substituted D- $\pi$ -A systems show the highest donating strength which can be attributed to the highest electron releasing nature of  $N(CH_3)_2$  group. Also, the electron releasing groups at donors tune the HOMO and LUMO energies of all the corresponding D- $\pi$ -A systems for better optical properties than unsubstituted systems. The optical and photovoltaic performance of D- $\pi$ -A system are described at CAM-B3LYP/cc-pVDZ/SMD//B3LYP/cc-pVDZ level. The enhanced performance of these properties achieved with enhanced donating strength conveys the role of tuning the donating strength for better PCE. Among all,  $N(CH_3)_2$  substituted D1 system (benzene) possess the highest  $eV_{OC}$  which can be attributed to its highest donating strength. These findings suggest that we can improve the photovoltaic performance of DSSC by tuning the ground state property,  $\Delta V_{mA}$  at the acceptor site. All the findings imply that incorporation of more electron-releasing substituents on an electron-rich donor moiety improves/tunes the photovoltaic performance by facilitating efficient intramolecular charge transfer in D- $\pi$ -A system.

The correlation plot of  $\Delta V_{\text{mA}}$  with  $eV_{\text{OC}}$  will provide an efficient guideline for developing an effective dye designing strategy for desirable photovoltaic properties.

### 3.6 References

1. J. Gong, K. Sumathy, Q. Qiao and Z. Zhou, *Renew. Sustain. Energy Rev.*, 2017, **68**, 234-246.
2. Y.-H. Chen, V. S. Nguyen, H.-H. Chou, Y. S. Tingare, T.-C. Wei and C.-Y. Yeh, *ACS Appl. Energy Mater.*, 2020, **3**, 5479-5486.
3. N. Mariotti, M. Bonomo, L. Fagiolari, N. Barbero, C. Gerbaldi, F. Bella and C. Barolo, *Green Chem.*, 2020, **22**, 7168-7218.
4. B. O'regan and M. Grätzel, *Nature*, 1991, **353**, 737.
5. M. K. Nazeeruddin, F. De Angelis, S. Fantacci, A. Selloni, G. Viscardi, P. Liska, S. Ito, B. Takeru and M. Grätzel, *J. Am. Chem. Soc.*, 2005, **127**, 16835-16847.
6. G. Marotta, M. A. Reddy, S. P. Singh, A. Islam, L. Han, F. De Angelis, M. Pastore and M. Chandrasekharam, *ACS Appl. Mater. Interfaces*, 2013, **5**, 9635-9647.
7. S. Yun, Y. Qin, A. R. Uhl, N. Vlachopoulos, M. Yin, D. Li, X. Han and A. Hagfeldt, *Energy Environ. Sci.*, 2018, **11**, 476-526.
8. L. L. Estrella, M. P. Balanay and D. H. Kim, *J. Phys. Chem. A*, 2018, **122**, 6328-6342.
9. M. Grätzel, *Nature*, 2001, **414**, 338-344.
10. S. Ito, S. M. Zakeeruddin, R. Humphry-Baker, P. Liska, R. Charvet, P. Comte, M. K. Nazeeruddin, P. Péchy, M. Takata and H. Miura, *Adv. Mater.*, 2006, **18**, 1202-1205.
11. S. Ito, H. Miura, S. Uchida, M. Takata, K. Sumioka, P. Liska, P. Comte, P. Péchy and M. Grätzel, *ChemComm*, 2008, 5194-5196.
12. Q. Yu, Y. Wang, Z. Yi, N. Zu, J. Zhang, M. Zhang and P. Wang, *ACS Nano*, 2010, **4**, 6032-6038.
13. L. Han, A. Islam, H. Chen, C. Malapaka, B. Chiranjeevi, S. Zhang, X. Yang and M. Yanagida, *Energy Environ. Sci.*, 2012, **5**, 6057-6060.
14. L. E. Polander, A. Yella, J. Teuscher, R. Humphry-Baker, B. F. E. Curchod, N. Ashari Astani, P. Gao, J.-E. Moser, I. Tavernelli, U. Rothlisberger, M. Grätzel, M. K. Nazeeruddin and J. Frey, *Chem. Mater.*, 2013, **25**, 2642-2648.

15. S. Mathew, A. Yella, P. Gao, R. Humphry-Baker, B. F. Curchod, N. Ashari-Astani, I. Tavernelli, U. Rothlisberger, M. K. Nazeeruddin and M. Grätzel, *Nat. Chem.*, 2014, **6**, 242-247.
16. K. Kakiage, Y. Aoyama, T. Yano, T. Otsuka, T. Kyomen, M. Unno and M. Hanaya, *Chem. Commun.*, 2014, **50**, 6379-6381.
17. Y. S. Tingare, N. S. n. Vinh, H. H. Chou, Y. C. Liu, Y. S. Long, T. C. Wu, T. C. Wei and C. Y. Yeh, *Adv. Energy Mater.*, 2017, **7**, 1700032.
18. K. Sharma, V. Sharma and S. S. Sharma, *Nanoscale Res. Lett.*, 2018, **13**, 381.
19. X. Song, X. Yang, H. Wang, J. An, Z. Yu, X. Wang, A. Hagfeldt and L. Sun, *Sol. Energy*, 2019, **187**, 274-280.
20. P. Ferdowsi, Y. Saygili, F. Jazaeri, T. Edvinsson, J. Mokhtari, S. M. Zakeeruddin, Y. Liu, M. Grätzel and A. Hagfeldt, *ChemSusChem*, 2020, **13**, 212-220.
21. Y.-Q. Yan, Y.-Z. Zhu, P.-P. Dai, J. Han, M. Yan and J.-Y. Zheng, *New J. Chem.*, 2020, **44**, 12909-12915.
22. Y. Chiba, A. Islam, Y. Watanabe, R. Komiya, N. Koide and L. Han, *Jpn. J. Appl. Phys*, 2006, **45**, L638.
23. F. Gao, Y. Wang, D. Shi, J. Zhang, M. Wang, X. Jing, R. Humphry-Baker, P. Wang, S. M. Zakeeruddin and M. Grätzel, *J. Am. Chem. Soc.*, 2008, **130**, 10720-10728.
24. S. Tan, J. Zhai, H. Fang, T. Jiu, J. Ge, Y. Li, L. Jiang and D. Zhu, *Chem.: Eur. J.*, 2005, **11**, 6272-6276.
25. A. Mishra, M. K. Fischer and P. Bäuerle, *Angew. Chem. Int. Ed.*, 2009, **48**, 2474-2499.
26. T. Mori, H. Saomoto, K. Machitani, K. Inoue, Y. Aoki, T. Koshitani, N. Koumura and T. N. Murakami, *RSC Adv.*, 2016, **6**, 13964-13970.
27. K. Hara, Y. Dan-oh, C. Kasada, Y. Ohga, A. Shinpo, S. Suga, K. Sayama and H. Arakawa, *Langmuir*, 2004, **20**, 4205-4210.
28. K. Hara, T. Sato, R. Katoh, A. Furube, T. Yoshihara, M. Murai, M. Kurashige, S. Ito, A. Shinpo and S. Suga, *Adv. Funct. Mater.*, 2005, **15**, 246-252.
29. R. Chen, X. Yang, H. Tian, X. Wang, A. Hagfeldt and L. Sun, *Chem. Mater.*, 2007, **19**, 4007-4015.
30. Z.-S. Wang, Y. Cui, Y. Dan-oh, C. Kasada, A. Shinpo and K. Hara, *J. Phys. Chem. C*, 2007, **111**, 7224-7230.

31. S. Hwang, J. H. Lee, C. Park, H. Lee, C. Kim, C. Park, M.-H. Lee, W. Lee, J. Park and K. Kim, *ChemComm*, 2007, 4887-4889.
32. J. Preat, D. Jacquemin, C. Michaux and E. A. Perpète, *Chem. Phys.*, 2010, **376**, 56-68.
33. H. Tian, I. Bora, X. Jiang, E. Gabrielsson, K. M. Karlsson, A. Hagfeldt and L. Sun, *J. Mater. Chem.*, 2011, **21**, 12462-12472.
34. A. Dhar, N. Siva Kumar, M. Asif and R. L. Vekariya, *New J. Chem.*, 2018, **42**, 12024-12031.
35. Y. Ren, D. Sun, Y. Cao, H. N. Tsao, Y. Yuan, S. M. Zakeeruddin, P. Wang and M. Grätzel, *J. Am. Chem. Soc.*, 2018, **140**, 2405-2408.
36. T. Kitamura, M. Ikeda, K. Shigaki, T. Inoue, N. A. Anderson, X. Ai, T. Lian and S. Yanagida, *Chem. Mater.*, 2004, **16**, 1806-1812.
37. D. P. Hagberg, T. Marinado, K. M. Karlsson, K. Nonomura, P. Qin, G. Boschloo, T. Brinck, A. Hagfeldt and L. Sun, *J. Org. Chem.*, 2007, **72**, 9550-9556.
38. H. Tian, X. Yang, R. Chen, R. Zhang, A. Hagfeldt and L. Sun, *J. Phys. Chem. C*, 2008, **112**, 11023-11033.
39. J. Zhang, H.-B. Li, S.-L. Sun, Y. Geng, Y. Wu and Z.-M. Su, *J. Mater. Chem.*, 2012, **22**, 568-576.
40. J. Zhang, Y.-H. Kan, H.-B. Li, Y. Geng, Y. Wu and Z.-M. Su, *Dyes Pigm.*, 2012, **95**, 313-321.
41. Z. Yao, L. Yang, Y. Cai, C. Yan, M. Zhang, N. Cai, X. Dong and P. Wang, *J. Phys. Chem. C*, 2014, **118**, 2977-2986.
42. T. Horiuchi, H. Miura, K. Sumioka and S. Uchida, *J. Am. Chem. Soc.*, 2004, **126**, 12218-12219.
43. W. Xu, B. Peng, J. Chen, M. Liang and F. Cai, *J. Phys. Chem. C*, 2008, **112**, 874-880.
44. J. Preat, *J. Phys. Chem. C*, 2010, **114**, 16716-16725.
45. D. Patil, M. Jadhav, K. Avhad, T. H. Chowdhury, A. Islam, I. Bedja and N. Sekar, *New J. Chem.*, 2018, **42**, 11555-11564.
46. H.-L. Jia, Z.-J. Peng, Y.-C. Chen, C.-Y. Huang and M.-Y. Guan, *New J. Chem.*, 2018, **42**, 18702-18707.
47. L. Zhang, W. Shen, R. He, X. Liu, Z. Fu and M. Li, *J. Mol.*, 2014, **20**, 2489.
48. N. Inostroza, F. Mendizabal, R. Arratia-Pérez, C. Orellana and C. Linares-Flores, *J. Mol. Model*, 2016, **22**, 25.

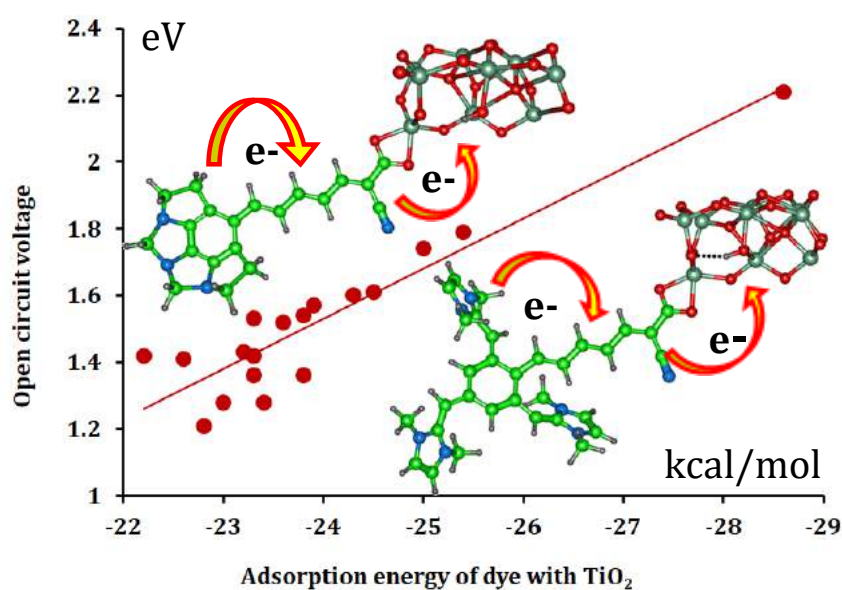
49. S. Gauthier, F. Robin-Le Guen, L. Wojcik, N. Le Poul, A. Planchat, Y. Pellegrin, P. G. Level, N. Szuwarski, M. Boujtita and D. Jacquemin, *Dyes Pigm.*, 2019, **171**, 107747.
50. V. V. Divya, F. B. Sayyed and C. H. Suresh, *ChemPhysChem*, 2019, **20**, 1752-1758.
51. S. R. Gadre, S. A. Kulkarni and I. H. Shrivastava, *J. Chem. Phys.*, 1992, **96**, 5253-5260.
52. S. R. Gadre and R. N. Shirsat, *Electrostatics of Atoms and Molecules*, Universities Press 2000.
53. P. Politzer and D. G. Truhlar, *Chemical Applications of Atomic and Molecular Electrostatic Potentials: Reactivity, Structure, Scattering, and Energetics of Organic, Inorganic, and Biological Systems*, Springer Science & Business Media 2013.
54. C. H. Suresh and N. Koga, *Inorg. Chem.*, 2002, **41**, 1573-1578.
55. C. H. Suresh, *Inorg. Chem.*, 2006, **45**, 4982-4986.
56. J. Mathew, T. Thomas, and C. H. Suresh, *Inorg. Chem. 2007*, 2007, **46**, 10800-10809.
57. G. S. Remya and C. H. Suresh, *Phys. Chem. Chem. Phys.*, 2016, **18**, 20615-20626.
58. E. Scrocco and J. Tomasi, in *New concepts II*, Springer 1973, 95-170.
59. J. S. Murray and P. Politzer, *Wiley Interdiscip. Rev. Comput. Mol. Sci.*, 2011, **1**, 153-163.
60. F. B. Sayyed and C. H. Suresh, *New J. Chem.*, 2009, **33**, 2465-2471.
61. C. H. Suresh, P. Alexander, K. P. Vijayalakshmi, P. K. Sajith and S. R. Gadre, *Phys. Chem. Chem. Phys.*, 2008, **10**, 6492-6499.
62. F. B. Sayyed and C. H. Suresh, *Tetrahedron Lett.*, 2009, **50**, 7351-7354.
63. P. K. Sajith and C. H. Suresh, *Inorg. Chem.*, 2012, **51**, 967-977.
64. F. B. Sayyed and C. H. Suresh, *J. Phys. Chem. A*, 2011, **115**, 9300-9307.
65. V. V. Divya and C. H. Suresh, *New J. Chem.*, 2020, **44**, 7200-7209.
66. L. Liu, L. Miao, L. Li, F. Li, Y. Lu, Z. Shang and J. Chen, *J. Phys. Chem. Lett.*, 2018, **9**, 3573-3579.
67. A. D. Becke, *J. Chem. Phys.*, 1993, **98**, 1372-1377.
68. T. H. Dunning Jr, *Chem. Phys.*, 1989, **90**, 1007-1023.

69. H. Gotfredsen, T. Neumann, F. E. Storm, A. V. Muñoz, M. Jevric, O. Hammerich, K. V. Mikkelsen, M. Freitag, G. Boschloo and M. B. Nielsen, *ChemPhotoChem*, 2018, **2**, 976-985.
70. M. Pastore, E. Mosconi, F. De Angelis and M. Grätzel, *J. Phys. Chem. C*, 2010, **114**, 7205-7212.
71. T. Yanai, D. P. Tew and N. C. Handy, *Chem. Phys. Lett.*, 2004, **393**, 51-57.
72. A. V. Marenich, C. J. Cramer and D. G. Truhlar, *J. Phys. Chem. B*, 2009, **113**, 6378-6396.
73. M. J. Frisch, G. W. Trucks, H. B. Schlegel, G. E. Scuseria, M. A. Robb, J. R. Cheeseman, G. Scalmani, V. Barone, G. A. Petersson, H. Nakatsuji, X. Li, M. Caricato, A. V. Marenich, J. Bloino, B. G. Janesko, R. Gomperts, B. Mennucci, H. P. Hratchian, J. V. Ortiz, A. F. Izmaylov, J. L. Sonnenberg, D. Williams-Young, F. Ding, F. Lipparini, F. Egidi, J. Goings, B. Peng, A. Petrone, T. Henderson, D. Ranasinghe, V. G. Zakrzewski, J. Gao, N. Rega, G. Zheng, W. Liang, M. Hada, M. Ehara, K. Toyota, R. Fukuda, J. Hasegawa, M. Ishida, T. Nakajima, Y. Honda, O. Kitao, H. Nakai, T. Vreven, K. Throssell, J. A. Montgomery Jr., J. E. Peralta, F. Ogliaro, M. J. Bearpark, J. J. Heyd, E. N. Brothers, K. N. Kudin, V. N. Staroverov, T. A. Keith, R. Kobayashi, J. Normand, K. Raghavachari, A. P. Rendell, J. C. Burant, S. S. Iyengar, J. Tomasi, M. Cossi, J. M. Millam, M. Klene, C. Adamo, R. Cammi, J. W. Ochterski, R. L. Martin, K. Morokuma, O. Farkas, J. B. Foresman and D. J. Fox, Wallingford, CT 2016.
74. R. Menzel, D. Ogermann, S. Kupfer, D. Wei, G. Helmar, K. Kleinermanns, L. González\* and R. Beckert, *Dyes Pigm.*, 2012, **94**, 512-524.
75. S. Kupfer, J. Guthmuller and L. González\*, *J. Chem. Theory Comput.*, 2013, **9**, 543-554.
76. A. Kumar, S. R. Gadre, N. Mohan and C. H. Suresh, *J. Phys. Chem. A*, 2014, **118**, 526-532.
77. S. M. Feldt, G. Wang, G. Boschloo and A. Hagfeldt, *J. Phys. Chem. C*, 2011, **115**, 21500-21507.
78. W. Yang, N. Vlachopoulos, Y. Hao, A. Hagfeldt and G. Boschloo, *Phys. Chem. Chem. Phys.*, 2015, **17**, 15868-15875.

---

# Design and DFT Study of Nitrogen-Rich Donor Systems for Improved Photovoltaic Performance in Dye-sensitized Solar Cells

---



## 4.1 Abstract

*Eighteen electron-rich nitrogen incorporated donors with butadiene  $\pi$ -spacer and cyanoacrylic acid acceptor (A) as photosensitizers (D1- $\pi$ -A to D18- $\pi$ -A) for dye-sensitized solar cell (DSSC) applications have been designed for improving the photovoltaic performance. The significance of nitrogen centres for revamping the donating strength ( $\Delta V_{mA}$ ) of D- $\pi$ -A is scrutinized using molecular electrostatic potential (MESP) analysis at B3LYP/cc-pVDZ density functional theory (DFT). During the transformation of a donor (D) to D- $\pi$ -A, a certain delocalization of electron density from D to  $\pi$ -A has occurred, and the change in MESP minimum ( $\Delta V_{mA}$ ) observed at cyano region of D- $\pi$ -A is related to the donating strength of D. Optical and photovoltaic properties are analyzed at TD/CAM-B3LYP/cc-pVDZ/SMD//B3LYP/cc-pVDZ level. In D1- $\pi$ -A to D18- $\pi$ -A,  $\Delta V_{mA}$  are in the range -7.0 to -19.0 kcal/mol and the increase in donating strength is found to be proportional to the number of planar nitrogens in donors. The D12- $\pi$ -A exhibited the most negative  $\Delta V_{mA}$  (-19.0 kcal/mol) indicating the highest electron-donating strength of D12 whereas the least negative  $\Delta V_{mA}$  (-7.0 kcal/mol) displayed by D7- $\pi$ -A is correlated to the weak donating character of D7. By increasing the electron-donating strength of D in D- $\pi$ -A, a red-shift in the absorption maximum ( $\Delta\lambda_{max}$ ) by 162 to 294 nm is observed. Further, the open-circuit voltage ( $eV_{oc}$ ) calculated for the D- $\pi$ -A systems showed a strong linear relationship with  $\Delta V_{mA}$ . The LUMO (lowest unoccupied molecular orbital) energy of all the D- $\pi$ -A systems (-1.79 to -2.79 eV) is observed above the conduction band (CB) energy of the TiO<sub>2</sub> (-4.0 eV) which ensured the desirable electron injection efficiency ( $\Delta G_{inject}$ ) for them. The analysis of the adsorption energy ( $E_{ads}$ ) of D- $\pi$ -A systems on TiO<sub>2</sub> semiconductor (D- $\pi$ -A / TiO<sub>2</sub>) showed that D12- $\pi$ -A has the highest adsorption stability. Improving adsorption stability is better for improving  $eV_{oc}$  and power conversion efficiency (PCE). The maximum absorption wavelength ( $\lambda_{max}$ ) of (D- $\pi$ -A / TiO<sub>2</sub>) systems ranges from 513 to 703 nm and all of them display a red-shift related to bare D- $\pi$ -A systems. The study suggests D12 as the most efficient photosensitizer for DSSC applications. Further, it deepens the understanding of the structure-performance relationship of D- $\pi$ -A systems as photosensitizers.*



## 4.2 Introduction

The utilization of a renewable source of energy, preferably solar energy for the ever-growing energy demand could diminish global climate change which leads to sustainable livelihood on earth.<sup>1-4</sup> Since solar energy is the most abundant green energy alternative for the future energy crisis, more research efforts have to invest in the development of photovoltaic strategies based on solar power.<sup>1, 3-5</sup> Over the past three decades, the third generation photovoltaic technology employed in dye-sensitized solar cell (DSSC) acquired a notable position over conventional silicon-based solar cell due to simple synthetic strategy, easier structure modification, large absorption coefficient, and low production cost.<sup>3, 5-11</sup> The major components employed in a DSSC device include photosensitizers, electrolytes, and electrode materials, the modifications in those components leads to the enhancement of power conversion efficiency (PCE) of the solar cell.<sup>12</sup> Generally in DSSCs, Ru-based sensitizers have more PCE than organic dye sensitizers, which show a comparable PCE as silicon-based solar cells.<sup>3</sup> Whereas, the highly expensive and rare chance of occurrence of Ru-metal its practical application in DSSC is to be limited.<sup>3, 13</sup>

After the invention of the DSSC device by O'Regan and Grätzel in 1991,<sup>6</sup> extensive research efforts have been invested on the synthesis and device modelling of metal-free organic sensitizers which leads to the improvement of PCE.<sup>13-21</sup> Usually, organic sensitizers constitute a D- $\pi$ -A framework where D,  $\pi$ , and A denote donor,  $\pi$ -spacer and acceptor, respectively. So far large varieties of structural modifications in the D- $\pi$ -A structural framework have been performed, reveal that tuning the donating strength of donor could significantly influence the absorption range and photovoltaic parameters.<sup>12, 22-29</sup> In our previous study, we quantified the electron-donating strength of eight typically used donor systems *viz* pyrene, perylene, chrysene, triphenylamine, carbazole, phenothiazine, julolidine, N,N, dialkylaniline, ullazine and coumarin in D- $\pi$ -A system and revealed that julolidine and N,N, dialkylaniline based  $\pi$ -A systems are the most efficient sensitizers for DSSC.<sup>22</sup> For the improved optical and photovoltaic properties of D- $\pi$ -A systems the particular analysis recommends the incorporation of electron-rich hetero atoms (preferably nitrogen) in donors. Literature shows that the non-planar nature of donors, especially triphenylamine, carbazole and indoline reduce the electron transferability and overall conjugation in

the donor group with  $\pi$ -A system leading to lower light-harvesting efficiency of the dye sensitizer.<sup>30, 31</sup> The mentioned reducing factors are rectified through the introduction of planarized nitrogen incorporated donors *viz.* ullazine, and indolizine as photosensitizers.<sup>30-33</sup> Further, the rational designing of photosensitizers with nitrogen annulation at the bay region of polycyclic aromatic hydrocarbon (PAH) system provide remarkable PCE in DSSC.<sup>34</sup> For example, perylene based PAH system as donors in DSSC have disappointing PCE,<sup>35-37</sup> whereas N-annulated perylene (NP) core as a donor with phenyl functional results in improved PCE about 10.5 %.<sup>38</sup> Latter Wang et al. modified the NP core with bulky substituents to obtain PCE up to 10.4 %.<sup>39</sup> This re-engineered chromophore was again modified with an N-annulated indenoperylene unit as the donor and reached up to a PCE of 12.5 %.<sup>40</sup> The aforementioned studies reveal that the structural modifications with N-annulation in PAH systems enhance the intramolecular charge transfer (ICT) due to the planar structure. Also, the multiple substitution sites involved in PAHs increase the possibility of molecular engineering. Recently Subramanian *et al.* described that more N-doped polyaromatic hydrocarbon analogue of ullazine contributes large dipole moment and more planarization to the dye-sensitizers thus resulting in high light-harvesting efficiency (LHE) than the donors with a single N-doping site.<sup>25</sup>

In this context, the most significant approach for an efficient photosensitizer is the engineering of electron-rich planar donors. Correspondingly it is worthwhile to evaluate the role of nitrogen centres in donors for enhancing the donating strength. To tackle the failings of electron transferability and overall conjugation in the donor group with the  $\pi$ -A system, we designed eighteen electron-rich nitrogen incorporated donors (D1 – D18) as dye sensitizers for DSSC application (Figure 4.1). For the  $\pi$ -A framework, butadiene and cyanoacrylic acid have been considered. In our previous study,<sup>41</sup> we proved that butadiene exhibits better electronic effect transmitting power than thiophene, furan and benzylic spacers. Hence for better electronic charge transfer from D to A, butadiene  $\pi$ -spacer and cyanoacrylic acid as acceptor have been considered.

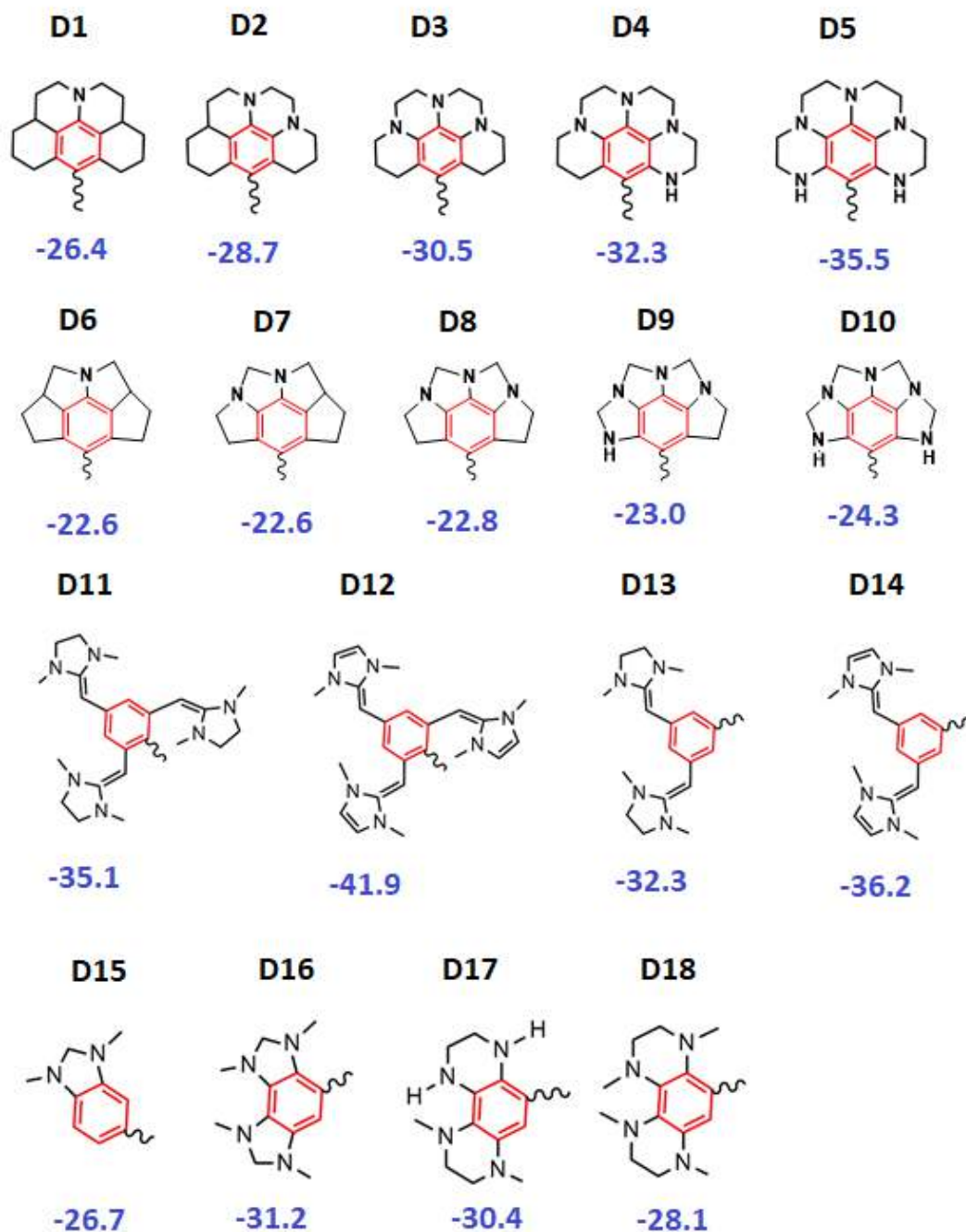


**Figure 4. 1** Designed donor systems. MESP minimum over the phenyl ring ( $V_{mD}$ ) is given in kcal/mol.

In the analysis, D1 – D5 donors are designed from known donor julolidine (Figure 4.2a), where the possibility for the N-annulation in julolidine core has been attempted (D1 to D5) to enhance the electron-donating strength of designed systems compared to julolidine (calculated electron-donating strength,  $\Delta V_{mA}$  of julolidine by MESP analysis is  $-9.2$  kcal/mol<sup>22</sup>). Julolidine is an N-heterocyclic aromatic compound

which comprises alkyl bridges between amino nitrogen and ring ortho carbon atoms.<sup>42, 43</sup> Because of the high efficiency in energy conversion and fluorescent properties, julolidine derivatives have been used in the construction of dye-sensitized solar cells, photoconductive materials and as fluorescent sensors for bio-imaging, etc.<sup>44</sup> The conjugation of the aromatic part of the molecule with its amino substituent is an indicator for the ability of the nitrogen atom to possess the  $sp^2$ -hybridization, which enhances the donating strength of these classes of compounds.<sup>45</sup> In D6 – D10, five-membered rings at aromatic ring system have been considered for N-annulation, those systems are derived from 1,2,4,5-tetrahydropyrrolo[3,2,1-hi] indole (Figure 4.2b).<sup>43</sup> Among the designed N-heterocyclic systems (D1 – D10), some of the derivatives are known and they are the best candidates for intramolecular cyclization and for generating diboronyne nanowires.<sup>46, 47</sup> The donors D11 – D14 are designed from the electron-rich nature of phenyl/ $\pi$ -system. According to various experimental and theoretical studies, the electron-rich nature of phenyl/ $\pi$ -system could be fine-tuned by electron-donating substituents and hence the aromatic ring of 1,3,5-N,N-dimethyltriaminobenzene could be considered as the most electron-rich neutral six-membered ring.<sup>48</sup> Previously, Suresh and Sayyed described that electron density at the phenyl ring could significantly improve by the treatment of N-heterocyclic ring substitution and they proposed two highly electron rich systems *viz.* D11 and D12 as shown in Figure 4.1.<sup>48</sup> Since those systems are considered as electron rich (involves six nitrogen lone pairs), we could test the suitability of those systems as photosensitizers for DSSC application. Finally, two, and four nitrogens have been integrated in D15 – D18, where the likelihood of N-annulation has been attained through N-heterocyclic five and six membered rings.<sup>49, 50</sup>

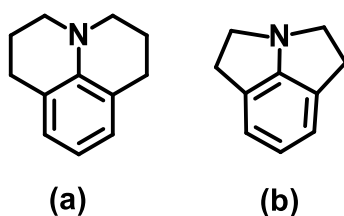


**Figure 4. 2** ChemDraw of a) Julolidine b) 1,2,4,5-tetrahydropyrrolo[3,2,1-hi] indole

For evaluating the donating strength of donors in D- $\pi$ -A, the intramolecular charge transfer (ICT) from D to A has to be assessed. Here it has been quantified in terms of change in molecular electrostatic potential (MESP) minimum,  $\Delta V_m$  at cyano

group of A. Very recently we proved that MESP is an excellent tool to quantify the electron-donating strength ( $\Delta V_m$ ) of D- $\pi$ -A system.<sup>22,26</sup> It is a real physical property which can be experimentally observable from X-ray diffraction studies. To understand the reactivity of molecular system, theoretically derived MESP has been extensively used in the works of Tomasi,<sup>51</sup> Pullman,<sup>52,53</sup> Politzer<sup>54-57</sup> and Gadre,<sup>58-60</sup> and the wide range of applications in chemical and biological phenomena shows the acceptability of this area of research. Further, our group has contributed to several applications of MESP parameter in organic and inorganic chemistry and described that MESP is an excellent tool for the prediction of structure-property relationships.<sup>61-70</sup> In the present study the significance of N-annulation for improved optical and photovoltaic properties has been evaluated using density functional theory (DFT) and time-dependent DFT (TDDFT) calculations. Currently, quantum chemical calculations have been emerged as an elementary tactic to identify the potential sensitizers before long-running expensive synthesis.<sup>71-77</sup> Thus our computationally engineered dye sensitizers could open up new synthetic strategies for the development of photosensitizers for DSSC application.

### 4.3 Computational methodology

Density functional theory (DFT) calculation at B3LYP/cc-pVDZ level has been conducted for the optimization of ground state geometries of D- $\pi$ -A systems.<sup>78,79</sup> It is substantiated that B3LYP level is adequate for the explanation of electronic structure of dye molecules in DSSC applications.<sup>26, 80, 81</sup> The ground state geometries of all D- $\pi$ -A systems after binding to (TiO<sub>2</sub>)<sub>9</sub> cluster are optimized at the same level DFT with LANL2DZ basis set for Ti atom and cc-pVDZ for non-metal atoms.<sup>82</sup> Vibrational frequencies are calculated at the same level and confirmed that there are no imaginary frequencies. The studies show that (TiO<sub>2</sub>)<sub>9</sub> cluster size is sufficient to model the dye-TiO<sub>2</sub> interfaces for simulating the electronic structure, optical properties, and binding modes of TiO<sub>2</sub>.<sup>83</sup> Frontier molecular orbital energies of all D- $\pi$ -A and D- $\pi$ -A adsorbed on (TiO<sub>2</sub>)<sub>9</sub> cluster systems (D- $\pi$ -A/ TiO<sub>2</sub>) are reported for ground-state geometries. The optical properties of D- $\pi$ -A systems before and after binding to (TiO<sub>2</sub>)<sub>9</sub> cluster are simulated at Time-dependent DFT (TD DFT) at CAM-B3LYP level<sup>84</sup> on the ground state geometry with mixed basis sets. To account for the solvent effect (dichloromethane as solvent) SCRFF-SMD (self-consistent reaction field-density

simulation model) incorporated in Gaussian 16 suite of programme has been considered. CAM-B3LYP exchange-correlation functional is widely used in theoretical calculations for the excited state properties and provide results that close to experimental results.<sup>85-87</sup> In our previous study, absorptional properties of experimentally known dye sensitizers have been benchmarked and found that TD-CAM B3LYP/cc-pVDZ/SMD//B3LYP/cc-pVDZ level is adequate to describe electronic, optical and photovoltaic properties.<sup>22</sup> The highest excitation energy associated with CAM-B3LYP exchange functional than B3LYP functional can be attributed to the higher bond length alteration index (BLA) of D- $\pi$ -A systems.<sup>26</sup> Moreover, for the examination of intramolecular charge transfer characteristics of D- $\pi$ -A systems, molecular electrostatic potential based topographical analysis has been performed on ground state geometry at B3LYP/cc-pVDZ level. All the calculations are performed with Gaussian 16 programme package.<sup>88</sup>

## 4.4 Results and discussion

### 4.4.1 MESP analysis of donors

MESP minima  $V_m$  gives a clear idea regarding the most electron-rich region in a molecular system. In all the donor systems (D1 – D18), an aromatic phenyl ring (shown in red colour, Figure 4.1) has been observed and the  $V_m$  observed at those phenyl rings,  $V_{mD}$  has been considered as the donor strength of each system. The most negative  $V_m$  depicts the most electron-rich nature of the molecular system. From D1 to D5, a systematic increase in N-centers (up to 5 nitrogens) is introduced and  $V_{mD}$  reached up to -35.5 kcal/mol from -26.4 kcal/mol. The more negative  $V_{mD}$  in D5 (-35.5 kcal/mol) than those of D1 - D4 characterizes the higher electron-rich nature which can be attributed to the occurrence of five nitrogen centers. In D6 - D10 donors, an increase in the negative character of  $V_{mD}$  (from -22.6 to -24.3 kcal/mol) has been attained by a systematic increase of nitrogen atoms (up to 5 nitrogens). While due to the presence of more pyramidalized nitrogens, D6 - D10 donors provide less negative  $V_{mD}$  than those of D1 - D5.

In D11 - D12 donors, imidazolidine and imidazole ring systems have been introduced at 1,3, and 5 positions of the benzene ring. In D11, the electron-rich amination functional groups increase the electron density over the phenyl ring resulted in a

comparable  $V_{mD}$  of -35.1 kcal/mol as D5 (-35.5 kcal/mol). In D12, the conjugation in CC bond enhances the electron density over phenyl ring leading to more negative  $V_{mD}$  (-41.9 kcal/mol) than D11. Due to the reduced number of aminal functional groups at phenyl ring, D13 shows less negative  $V_{mD}$  (-32.3 kcal/mol) than those of D11 and D12. In D14, conjugation increases the electron density of the donor system resulted in more negative  $V_{mD}$  (-36.2 kcal/mol) than D13. It is noted that imidazolidine and imidazole substituted donor systems *viz.* D12 and D14 exhibit more negative  $V_{mD}$  than the D5 which can be considered as their better donor strength. Finally, for verifying the effectiveness of the introduced strategy, D15 - D18 donors are examined. In D16 the increased number of N-alkyl substitution at phenyl ring resulted in more negative  $V_{mD}$  (-31.2 kcal/mol) than D15 ( $V_{mD} = -26.7$  kcal/mol). Compared to D15, a more negative  $V_{mD}$  is observed for D17 can be attributed to the presence of additional two nitrogen centres. Finally, in D18 the additional two methyl groups at nitrogen atoms promote pyramidalization of N-centres resulted in less negative  $V_{mD}$  (-28.1 kcal/mol) than D17.

#### 4.4.2 Donating strength of D- $\pi$ -A systems

The influence of electron-rich nitrogen lone pairs in donors (D) for enhancing the electron-donating strength of D- $\pi$ -A system ( $\Delta V_{mA}$ ) has been elucidated with MESP analysis. In D- $\pi$ -A systems, the  $\pi$ -A linkage with donor involve an intramolecular charge transfer (ICT) from D to A, the transferred electron density accumulated at A depends on the donor strength of each system.<sup>22, 26</sup> The electron density distribution *via* ICT at various regions of a representative D- $\pi$ -A system (D1- $\pi$ -A) *viz.* D,  $\pi$ -spacer and A have been shown in Figure 4.3a as MESP minima at donor  $V_{mD}$ , spacer  $V_{mS}$  and acceptor  $V_{mA}$  respectively. Since  $\pi$ -A part (butadiene) involved in the study is the same for all D- $\pi$ -A systems, the MESP minimum observed at CN group of A has been considered as the reference  $V_{mA}$  to evaluate the changes observed at that minimum with the attachment of D (Figure 4.3b). Also, it is proved that one could take other  $V_m$  regions at A as reference  $V_m$  *viz.*  $V_{m(OH)}$  and  $V_{m(CO)}$  for monitoring the changes at respective sites due to the parallel behaviour exhibited by those parameters.<sup>26</sup> In the study,  $V_{mA}$  (observed at CN region) has been selected as the reference point due to the most negative  $V_m$  character.

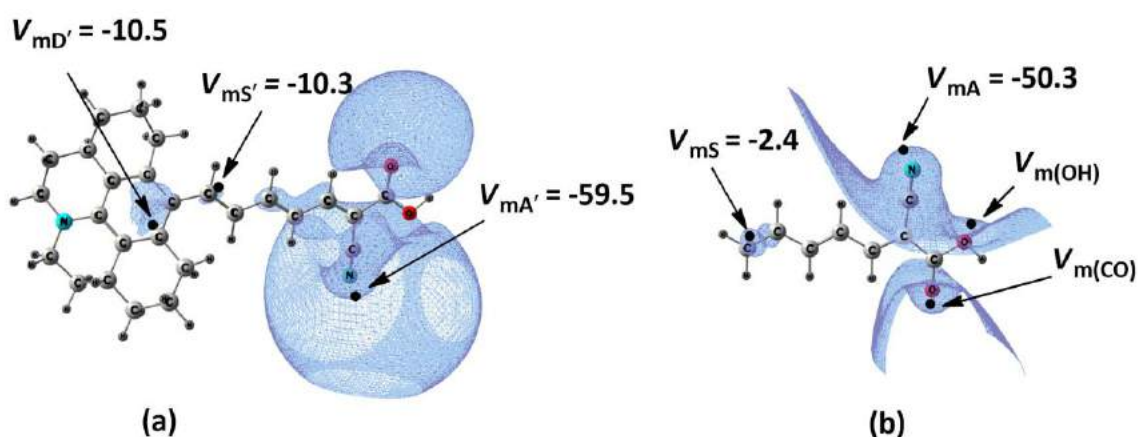


**Figure 4.3** a) MESP isosurface at various sites of the reference system, and b) representative D- $\pi$ -A system (D1- $\pi$ -A). Where MESP minimum is shown in kcal/mol.

In Table 4.1,  $V_m$  at D,  $\pi$ -spacer and A of D- $\pi$ -A systems are reported along with the change in  $V_m$  at those regions with the attachment of  $\pi$ -A to D. The change in  $V_m$  occurs at D site ( $\Delta V_{mD}$ ) has been calculated by subtracting  $V_m$  observed at donor ( $V_{mD}$ ) from the corresponding  $V_m$  observed at D of D- $\pi$ -A ( $V_{mD'}$ ). Likewise,  $\Delta V_{mS}$  and  $\Delta V_{mA}$  have been calculated by subtracting the  $V_m$  observed at respective sites of the reference system ( $V_{mS}$  and  $V_{mA}$ ) from the corresponding values of D- $\pi$ -A systems ( $V_{mS'}$  and  $V_{mA'}$ ). In the table  $\Delta V_{mD}$  ranges from 12.1 to 17.9 kcal/mol, the positive  $\Delta V_{mD}$  value shows the electron deficiency at D. In all, the less negative  $V_m$  observed at the D site of D- $\pi$ -A ( $V_{mD'}$ ) than the  $V_m$  of the donor ( $V_{mD}$ ) confirms the ICT from D to A. Further, the ICT from D to A enhances the electron density at spacer, the gained electron density at spacer has been denoted as negative  $\Delta V_{mS}$  which ranges from -6.0 to -16.3 kcal/mol. As per  $\Delta V_{mS}$ , the highest electron-donating strength has been attained by D5- $\pi$ -A system while the least has been possessed by D8- $\pi$ -A system. The  $V_{mA'}$  ranges from -56.2 to -69.3 kcal/mol. The donors having more electron-donating strength exhibit more negative  $V_{mA'}$ . As a result, the change in MESP appears on acceptor ( $\Delta V_{mA}$ ) with the attachment of D to  $\pi$ -A has been regarded as the donating strength of D- $\pi$ -A system.<sup>22</sup>

In D1 - D5 based  $\pi$ -A systems, the least negative  $\Delta V_{mA}$  (-9.2 kcal/mol) has been attained by one nitrogen involved system D1- $\pi$ -A which shows its poor electron-donating strength. Also, from D1- $\pi$ -A to D5- $\pi$ -A, a systematic enhancement in donating strength has been observed for an increased number of nitrogen centres ( $n = 1 - 5$ ) and the most negative  $\Delta V_{mA}$  (-13.5 kcal/mol) has been shown by D5- $\pi$ -A (incorporate 5 nitrogen lone pairs). In D6 to D10- $\pi$ -A the more pyramidalized



nitrogen centres in donors impart less negative  $\Delta V_{mA}$  in the range -5.9 to -8.4 kcal/mol than D1- $\pi$ -A - D5- $\pi$ -A systems. In D11- $\pi$ -A, the incorporation of six nitrogen lone pairs

**Table 4. 1**  $V_m$  (kcal/mol) of the D- $\pi$ -A systems calculated at B3LYP/cc-pVDZ level.

Systems	$V_{mD}$	$V_{mD'}$	$\Delta V_{mD}$	$V_{mS'}$	$V_{mS}$	$\Delta V_{mS}$	$V_{mA'}$	$V_{mA}$	$\Delta V_{mA}$
D1	-26.4	-10.5	15.9	-10.3	-2.4	-7.9	-59.5	-50.3	-9.2
D2	-28.7	-13.0	15.7	-11.7	-2.4	-9.3	-60.3	-50.3	-10.0
D3	-30.5	-14.1	16.4	-12.3	-2.4	-9.9	-60.8	-50.3	-10.5
D4	-32.3	-14.9	17.4	-13.2	-2.4	-10.9	-61.3	-50.3	-11.0
D5	-35.5	-17.6	17.9	-18.6	-2.4	-16.3	-63.8	-50.3	-13.5
D6	-22.6	-9.0	13.6	-9.3	-2.4	-7.0	-58.2	-50.3	-7.8
D7	-22.6	-9.7	12.9	-8.8	-2.4	-6.4	-57.4	-50.3	-7.0
D8	-22.8	-10.6	12.2	-8.3	-2.4	-6.0	-56.2	-50.3	-5.9
D9	-23.0	-10.5	12.5	-9.5	-2.4	-7.1	-57.9	-50.3	-7.5
D10	-24.3	-12.0	12.4	-10.4	-2.4	-8.0	-58.7	-50.3	-8.4
D11	-35.1	-22.8	12.3	-18.4	-2.4	-16.1	-64.0	-50.3	-13.7
D12	-41.9	-28.7	13.2	-18.4	-2.4	-16.1	-69.3	-50.3	-19.0
D13	-32.3	-20.7	11.6	-11.1	-2.4	-8.7	-58.2	-50.3	-7.9
D14	-36.2	-24.1	12.1	-14.6	-2.4	-12.2	-60.0	-50.3	-9.7
D15	-26.7	-11.6	15.1	-10.4	-2.4	-8.0	-58.5	-50.3	-8.2
D16	-31.2	-13.9	17.3	-13.1	-2.4	-10.7	-62.0	-50.3	-11.7
D17	-30.4	-16.2	14.2	-11.6	-2.4	-9.2	-58.9	-50.3	-8.5
D18	-28.1	-13.5	14.6	-9.9	-2.4	-7.5	-58.4	-50.3	-8.1

through imidazolidine rings at phenyl ring enhances the electron density at donor site resulting in  $\Delta V_{mA}$  of -13.7 kcal/mol. Whereas in D12- $\pi$ -A, the conjugation in CC bond (imidazole ring) enhances the electron density at donor than in D11- $\pi$ -A, which leads to more negative  $\Delta V_{mA}$  of -19.0 kcal/mol. In D13- $\pi$ -A and D14- $\pi$ -A systems, relatively lower donating strength is observed in terms of  $\Delta V_{mA}$  (-7.9 kcal/mol and -9.7 kcal/mol) than those of D11 and D12- $\pi$ -A systems. This can be attributed to their reduced number of nitrogen centres (4 nitrogens). Since nitrogens involved in D1 to D4- $\pi$ -A systems are more planarized than those of D13 and D14- $\pi$ -A, the former

systems show more electron-donating strength. The integration of four nitrogens at donor enhances the donating strength of D16- $\pi$ -A system (-11.7 kcal/mol) than D15- $\pi$ -A (-8.2 kcal/mol). Further, the nearly planar nitrogens involved in D16- $\pi$ -A provide a similar donating strength -11.7 kcal/mol as D4- $\pi$ -A (-11.0 kcal/mol). D17- $\pi$ -A with four nitrogen atoms incorporated through two fused six-membered rings at the phenyl ring attains less negative  $\Delta V_{mA}$  (-8.5 kcal/mol) than D16- $\pi$ -A. The additional two methyl groups in D18- $\pi$ -A at nitrogen atoms are pyramidalized and lead to less negative  $\Delta V_{mA}$  (8.1 kcal/mol) than D17. Finally, from the elucidated examples it is clear that donors having more planarized nitrogen centres enhance the donating strength of D- $\pi$ -A systems. Among all, D12, D11 and D5 based  $\pi$ -A systems are the best candidates for DSSC application.

#### 4.4.3 Absorption spectra

In Table 4.2, the optical properties of donor and D- $\pi$ -A systems are given. Since we have used same  $\pi$ - and A units in all the designed D- $\pi$ -A systems, the influence of  $\pi$ -A on absorption maximum ( $\lambda_{max}$ ) can be considered as same for all donors, and the shift in absorption maximum ( $\Delta\lambda_{max}$ ) occurred during the transformation of D to D- $\pi$ -A can be recognized as the influence of donating strength of donor units. The  $\Delta\lambda_{max}$  is calculated by subtracting  $\lambda_{max}$  of D from the analogous D- $\pi$ -A system. For analysis HOMO  $\rightarrow$  LUMO transition has been considered. The influence of donor strength ( $V_{mD}$ ) has occurred in the  $\lambda_{max}$  of donors from 272 to 329 nm. In Table 4.2, when a donor changes to D- $\pi$ -A, absorption shifts to higher wavelength in the range 454 to 619 nm. According to our previous study,  $\Delta\lambda_{max}$  in the range of 162 to 294 nm can be recognized as the influence of donating strength ( $\Delta V_{mA}$ ) of D- $\pi$ -A systems.<sup>22</sup> A significant correlation observed between  $\Delta V_{mA}$  and  $\Delta\lambda_{max}$  with a correlation coefficient of 0.940 confirms the significance of  $\Delta V_{mA}$  on  $\Delta\lambda_{max}$  (Figure 4.4, deviations are neglected for R calculation). It shows that  $\Delta\lambda_{max}$  increases with enhanced donating strength of D- $\pi$ -A systems. In the table, D1 - D5 based  $\pi$ -A systems display a systematic increase in  $\Delta\lambda_{max}$  (from 203 to 257 nm) which can be recognized as the enhanced donating strength of those systems with an increased number of nitrogen centres ( $n = 1-5$ ). Among those systems, D4 based  $\pi$ -A system shows greater  $\Delta\lambda_{max}$  than D5- $\pi$ -A, which displays a slight deviation in correlation (marked in green colour, Figure 4.4).

**Table 4. 2** Maximum absorption wavelength  $\lambda_{\max}$  (nm), oscillator strength  $f$ , MO contribution, percentage of MO contribution (MO %), and shift in absorption maximum  $\Delta\lambda_{\max}$  (nm) of donor and D- $\pi$ -A systems at TD-CAM-B3LYP/cc-pVDZ/SMD//B3LYP/cc-pVDZ level.

Systems	Donor			D- $\pi$ -A system				
	$\lambda_{\max}$ (nm)	$f$	MO contribution	$\lambda_{\max}$ (nm)	$f$	MO contribution	MO %	$\Delta\lambda_{\max}$ (nm)
D1	272	0.08	H $\rightarrow$ L	476	1.77	H $\rightarrow$ L	92 %	203
D2	286	0.11	H $\rightarrow$ L	513	1.53	H $\rightarrow$ L	92 %	227
D3	280	0.02	H $\rightarrow$ L	520	1.54	H $\rightarrow$ L	92 %	240
D4	285	0.03	H $\rightarrow$ L	542	1.31	H $\rightarrow$ L	89 %	257
D5	285	0.04	H $\rightarrow$ L	527	1.58	H $\rightarrow$ L	91 %	241
D6	285	0.04	H $\rightarrow$ L	471	1.74	H $\rightarrow$ L	94 %	187
D7	301	0.05	H $\rightarrow$ L	481	1.42	H $\rightarrow$ L	92 %	180
D8	304	0.03	H $\rightarrow$ L	475	1.46	H $\rightarrow$ L	91 %	171
D9	329	0.06	H $\rightarrow$ L	531	0.97	H $\rightarrow$ L	92 %	202
D10	341	0.07	H $\rightarrow$ L	522	0.04	H $\rightarrow$ L	87 %	181
D11	304	0.11	H $\rightarrow$ L	549	1.30	H $\rightarrow$ L	88 %	245
D12	325	0.60	H $\rightarrow$ L	619	0.27	H $\rightarrow$ L	79 %	294
				600	1.41	H-1 $\rightarrow$ L	49%	275
D13	292	1.17	H $\rightarrow$ L	454	0.03	H $\rightarrow$ L	91 %	162
				423	1.19	H-1 $\rightarrow$ L	68 %	131
D14	324	1.14	H $\rightarrow$ L	583	0.03	H $\rightarrow$ L	93 %	259
				512	0.14	H-1 $\rightarrow$ L	93 %	188
D15	272	0.18	H $\rightarrow$ L	481	1.62	H $\rightarrow$ L	92 %	209
D16	282	0.06	H $\rightarrow$ L	509	0.99	H $\rightarrow$ L	93 %	227
D17	282	0.09	H $\rightarrow$ L	500	0.83	H $\rightarrow$ L	92 %	218
D18	288	0.07	H $\rightarrow$ L	487	0.97	H $\rightarrow$ L	90 %	199

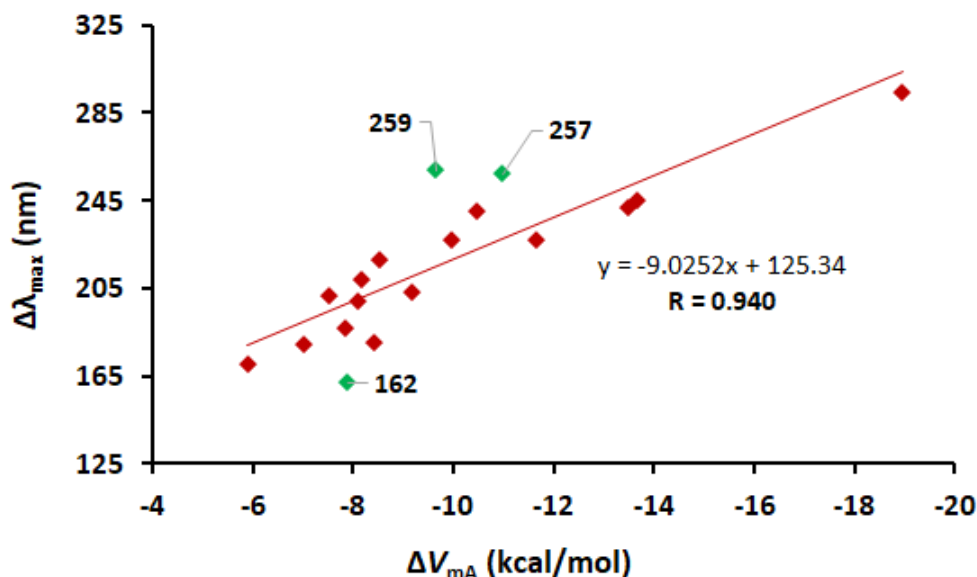


**Figure 4.4** Correlation between  $\Delta V_{mA}$  and  $\Delta\lambda_{max}$  of D- $\pi$ -A systems (R is calculated by excluding the points in green colour).

The lower  $\Delta\lambda_{max}$  exhibited by D6- $\pi$ -A to D10- $\pi$ -A systems in the range of 171-202 nm are recognized as due to the lesser donating strength of those systems. Compared to D6- $\pi$ -A to D10- $\pi$ -A systems, the greater  $\Delta\lambda_{max}$  in D11- $\pi$ -A (245 nm) can be recognized as its larger donating strength. The presence of conjugation in CC bonds enhances the donating strength of D12- $\pi$ -A resulting to the highest  $\Delta\lambda_{max}$  of 294 nm. The highest  $\Delta\lambda_{max}$  (294 nm) can be attributed to the utmost  $\Delta V_{mA}$  and  $\lambda_{max}$  of D12- $\pi$ -A (619 nm). In D13- $\pi$ -A and D14- $\pi$ -A systems,  $\Delta\lambda_{max}$  of 162 and 259 nm are observed with a  $\lambda_{max}$  of 454 and 583 nm, respectively. In those systems slight deviation in correlation has been observed, may be due to the poor oscillator strength ( $f \rightarrow 0.03$ ). The higher  $\Delta\lambda_{max}$  of 227 nm in D16- $\pi$ -A than D15- $\pi$ -A (209 nm) can be spotted as due to the better electron-donating strength (because of increased number of nitrogens (four)) of D16- $\pi$ -A. In D17- $\pi$ -A,  $\lambda_{max}$  and  $\Delta\lambda_{max}$  are 500 nm and 218 nm, respectively. Even though there is an equal number of nitrogens (four) in the donor site, the higher  $\Delta\lambda_{max}$  in D17- $\pi$ -A than D18- $\pi$ -A (199 nm) can be recognized as the influence of more planar NH centres.

Finally, for the dye sensitizers, HOMO (highest occupied molecular orbital) and LUMO (lowest unoccupied molecular orbital) energies are crucial for determining the efficiency of the sensitizers. For the effective regeneration of the oxidized dye, it is

**Table 4.3** HOMO (eV), LUMO (eV), and HOMO-LUMO energy gap, HLG (eV) for the D- $\pi$ -A/TiO<sub>2</sub> systems at B3LYP/GenECP level. Maximum absorption wavelength  $\lambda_{\max}$  (nm), and oscillator strength (f) adsorbed on TiO<sub>2</sub> are simulated at TD CAM-B3LYP/GenECP/SMD//B3LYP/GenECP level.

D- $\pi$ -A/TiO <sub>2</sub> systems	HOMO (eV)	LUMO (eV)	HLG (eV)	$\lambda_{\max}$ (nm)	f
D1	-5.43	-3.68	1.75	538	2.36
D2	-5.17	-3.66	1.52	583	2.03
D3	-5.10	-3.64	1.46	593	2.07
D4	-5.07	-3.62	1.45	611	1.73
D5	-5.09	-3.55	1.54	592	0.60
D6	-5.63	-3.74	1.89	526	2.24
D7	-5.53	-3.76	1.77	538	1.85
D8	-5.57	-3.79	1.77	531	1.87
D9	-5.37	-3.74	1.64	611	1.73
D10	-5.39	-3.71	1.69	574	0.05
D11	-4.85	-3.50	1.34	630	1.79
D12	-4.38	-3.25	1.13	703	0.29
D13	-4.99	-3.78	1.21	513	0.03
D14	-4.32	-3.71	0.61	697	0.02
D15	-5.44	-3.74	1.71	545	2.01
D16	-5.08	-3.60	1.48	610	1.91
D17	-5.25	-3.72	1.53	573	1.02
D18	-5.31	-3.72	1.59	558	1.22

important to have HOMO energy ( $e_h$ ) lower than the redox potential of the I<sup>-</sup>/I<sub>3</sub><sup>-</sup> electrolyte (-4.8 eV). The  $e_h$  of D3 - D5, D11 - D14, and D16 based  $\pi$ -A systems are in the range of -4.68 to -4.74 eV, lying above the redox potential of the I<sup>-</sup>/I<sub>3</sub><sup>-</sup> electrolyte. It is therefore suggesting that the oxidized dye might not efficiently regenerate in those systems from I<sup>-</sup>/I<sub>3</sub><sup>-</sup> electrolyte. Whereas for the rest of the D- $\pi$ -A systems,  $e_h$  (-4.82 to -5.29 eV) lying below the redox potential of the electrolyte facilitates effective dye regeneration. For D1- $\pi$ -A to D18- $\pi$ -A systems, LUMO energies ( $e_l$ ) are in the range of -1.79 to -2.79 eV, lying above the conduction band (CB) energy of the TiO<sub>2</sub>

semiconductor (-4.0 eV), which ensures effective electron injection into the TiO<sub>2</sub> conduction band. HOMO-LUMO gap (HLG) energy of designed D- $\pi$ -A systems ranges from 1.64 to 2.65 eV and it shows a decreasing trend with increasing electron donating strength. In DSSCs, HLG values give a clear idea regarding the PCE of the dye-sensitizer. As per various theoretical studies, Lower HLG ensures better optical and photovoltaic properties, thereby improves the PCE of DSSC devices.<sup>89-91</sup> Herein, we could recognize that lower HLG energy obtained with D12- $\pi$ -A (2.17 eV) shows finest absorption maximum (619 nm), good adsorption stability (-28.6 kcal/mol), and highest  $eV_{oc}$  (2.21 eV). Consequently, among all D12- $\pi$ -A system having lowest LUMO energy (-1.79 eV) may provide better PCE in DSSC device.

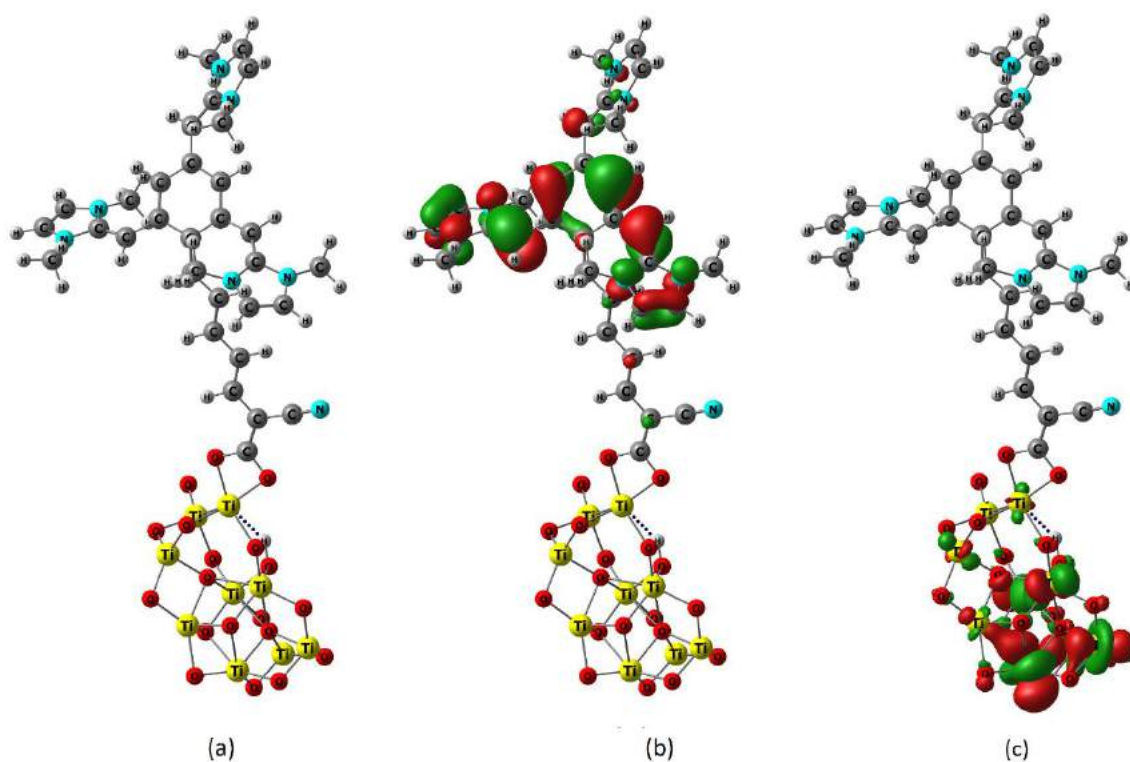


**Figure 4.5** a) Optimized geometry of representative D- $\pi$ -A system on (TiO<sub>2</sub>)<sub>9</sub> cluster (D12- $\pi$ -A/TiO<sub>2</sub>). The electron density shift during excitation can be visualized from b) HOMO and c) LUMO features.

According to the basic principle of DSSC, when the dye molecule gets adsorbed on the TiO<sub>2</sub> semiconductor, the interaction between those dye and semiconductor can shift their energy level and prompt electron injection to semiconductor which is desirable for the better PCE.<sup>72</sup> To determine the energy levels of the adsorbed D- $\pi$ -A

systems on TiO<sub>2</sub>, we have designed a bidentate bridging mode for binding the D- $\pi$ -A systems on TiO<sub>2</sub> (Figure 4.5a). It has been reported that bidentate bridging mode is

**Table 4. 4** The adsorption energies ( $E_{\text{ads}}$ ) of all the D- $\pi$ -A/(TiO<sub>2</sub>)<sub>9</sub> systems where  $E_{\text{ads}}$  values are given in kcal/mol.

D- $\pi$ -A/(TiO <sub>2</sub> ) <sub>9</sub> systems	$E_{\text{ads}}$ (kcal/mol)
D1- $\pi$ -A/(TiO <sub>2</sub> ) <sub>9</sub>	-23.6
D2- $\pi$ -A/(TiO <sub>2</sub> ) <sub>9</sub>	-23.8
D3 - $\pi$ -A/(TiO <sub>2</sub> ) <sub>9</sub>	-23.9
D4 - $\pi$ -A/(TiO <sub>2</sub> ) <sub>9</sub>	-24.3
D5 - $\pi$ -A/(TiO <sub>2</sub> ) <sub>9</sub>	-25.0
D6- $\pi$ -A/(TiO <sub>2</sub> ) <sub>9</sub>	-23.3
D7 - $\pi$ -A/(TiO <sub>2</sub> ) <sub>9</sub>	-23.0
D8 - $\pi$ -A/(TiO <sub>2</sub> ) <sub>9</sub>	-22.8
D9 - $\pi$ -A/(TiO <sub>2</sub> ) <sub>9</sub>	-23.4
D10 - $\pi$ -A/(TiO <sub>2</sub> ) <sub>9</sub>	-23.8
D11- $\pi$ -A/(TiO <sub>2</sub> ) <sub>9</sub>	-25.4
D12- $\pi$ -A/(TiO <sub>2</sub> ) <sub>9</sub>	-28.6
D13 - $\pi$ -A/(TiO <sub>2</sub> ) <sub>9</sub>	-22.2
D14 - $\pi$ -A/(TiO <sub>2</sub> ) <sub>9</sub>	-23.3
D15- $\pi$ -A/(TiO <sub>2</sub> ) <sub>9</sub>	-22.6
D16- $\pi$ -A/(TiO <sub>2</sub> ) <sub>9</sub>	-24.5
D17 - $\pi$ -A/(TiO <sub>2</sub> ) <sub>9</sub>	-23.2
D18- $\pi$ -A/(TiO <sub>2</sub> ) <sub>9</sub>	-23.3

the most stable adsorption mode for anchoring group.<sup>92 93</sup> Further, LUMO energy levels of the adsorbed D- $\pi$ -A systems (-3.25 to -3.79 eV) are deeper than the bare D- $\pi$ -A systems (-1.79 to -2.79 eV), and ensure that LUMO is above the CB energy of TiO<sub>2</sub> which could promote efficient electron injection from the excited dye molecule into CB of TiO<sub>2</sub>. Absorption properties of D1- $\pi$ -A to D18- $\pi$ -A systems adsorbed on TiO<sub>2</sub> are reported in Table 4.3. We denote D- $\pi$ -A adsorbed TiO<sub>2</sub> as D- $\pi$ -A/TiO<sub>2</sub>. The observed  $\lambda_{\text{max}}$  in the range 513 to 703 nm is favourable for improved PCE, shows a red shift with respect to pure D- $\pi$ -A system. Among all, D12- $\pi$ -A/TiO<sub>2</sub> shows the highest  $\lambda_{\text{max}}$  (703 nm), whereas D13- $\pi$ -A/TiO<sub>2</sub> displays the lowest  $\lambda_{\text{max}}$  (513 nm). HLG of

D- $\pi$ -A/TiO<sub>2</sub> systems ranges from 0.61 to 1.89 eV indicating that the adsorption of the dye with the semiconductor significantly reduces the HLG related to bare D- $\pi$ -A systems. The electron density shifts in D- $\pi$ -A/TiO<sub>2</sub> systems between HOMO and LUMO are given in the representative example (D12- $\pi$ -A/TiO<sub>2</sub>) shown in Figure 4.5b and 4.5c. In all the D- $\pi$ -A/TiO<sub>2</sub> systems, HOMO is localized on donor region whereas LUMO is distributed on TiO<sub>2</sub>. This kind of charge delocalization is anticipated for the better PCE of dye sensitizers.

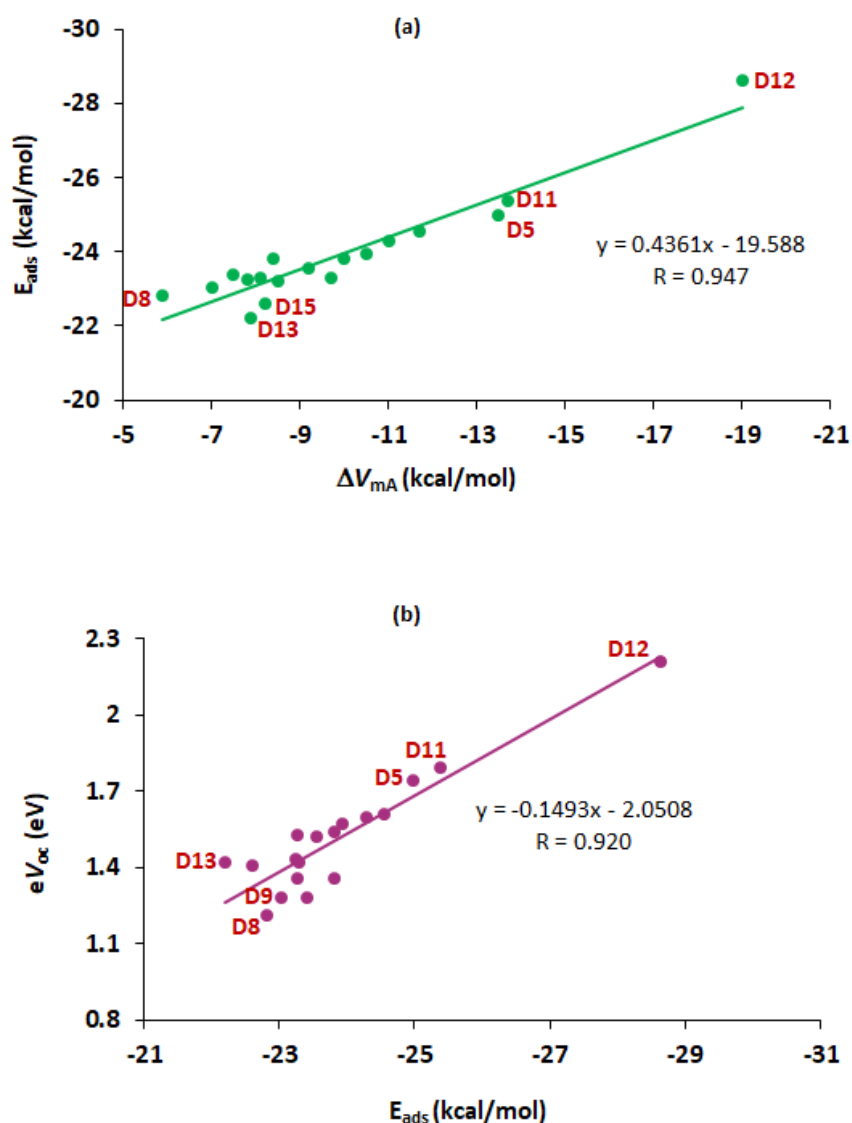


**Figure 4.6** a) Correlation between  $\Delta V_{mA}$  and  $E_{ads}$  b)  $E_{ads}$  and  $eV_{oc}$ .

Quantitatively, adsorption stability of the D- $\pi$ -A systems on (TiO<sub>2</sub>)<sub>9</sub> cluster has been evaluated using adsorption energy ( $E_{ads}$ ) which is listed in Table 4.4. It is defined as  $E_{ads} = E_{dye/TiO_2} - (E_{dye} + E_{TiO_2})$ , where  $E_{dye/TiO_2}$ ,  $E_{dye}$ , and  $E_{TiO_2}$  denote energies of



dye/TiO<sub>2</sub>, isolated dye and TiO<sub>2</sub> cluster respectively.<sup>94</sup> It is clear that, more negative adsorption energy could reveal higher adsorption stability between dye molecule and

**Table 4. 5** HOMO (eV), LUMO (eV), and HOMO-LUMO energy gap (eV) at B3LYP/cc-pVDZ level. Ground and excited state oxidation potential ( $E^{dye}$ ,  $E^{dye*}$ ), excitation energy, electron injection-free energy change  $\Delta G_{inject}$ , free energy change for dye regeneration  $\Delta G_{reg}$ , and open-circuit voltage  $eV_{OC}$  at TD-CAM-B3LYP/SMD/cc-pVDZ//B3LYP/cc-pVDZ level.

Systems	Excitation	HOMO (eV)	LUMO (eV)	HLG (eV)	$E^{dye}$ (eV)	$E^{dye*}$ (eV)	$\Delta G_{inject}$ (eV)	$\Delta G_{reg}$ (eV)	$eV_{OC}$ (eV)
	Energy (eV)								
D1	2.61	-5.09	-2.48	2.61	5.09	2.48	-1.52	0.29	1.52
D2	2.42	-4.82	-2.46	2.36	4.82	2.40	-1.60	0.02	1.54
D3	2.38	-4.74	-2.43	2.31	4.74	2.36	-1.64	-0.06	1.57
D4	2.29	-4.69	-2.40	2.29	4.69	2.40	-1.60	-0.11	1.60
D5	2.35	-4.68	-2.26	2.42	4.68	2.33	-1.67	-0.12	1.74
D6	2.63	-5.29	-2.64	2.65	5.29	2.66	-1.34	0.49	1.36
D7	2.58	-5.22	-2.72	2.50	5.22	2.64	-1.36	0.42	1.28
D8	2.61	-5.27	-2.79	2.48	5.27	2.66	-1.34	0.47	1.21
D9	2.33	-5.05	-2.72	2.33	5.05	2.72	-1.28	0.25	1.28
D10	2.38	-5.04	-2.64	2.40	5.04	2.66	-1.34	0.24	1.36
D11	2.26	-4.50	-2.21	2.29	4.50	2.24	-1.76	-0.30	1.79
D12	2.00	-3.96	-1.79	2.17	3.96	1.96	-2.04	-0.84	2.21
D13	2.73	-4.77	-2.58	2.19	4.77	2.04	-1.96	-0.03	1.42
D14	2.21	-4.11	-2.47	1.64	4.11	1.90	-2.10	-0.69	1.53
D15	2.58	-5.11	-2.59	2.52	5.11	2.53	-1.47	0.31	1.41
D16	2.29	-4.72	-2.39	2.33	4.72	2.43	-1.57	-0.08	1.61
D17	2.48	-4.96	-2.57	2.39	4.96	2.48	-1.52	0.16	1.43
D18	2.55	-5.04	-2.58	2.46	5.04	2.49	-1.51	0.24	1.42

TiO<sub>2</sub>. In Table 4.4, we observed that all the adsorbed systems that have more negative adsorption energy contain a greater number of N-annulation. Among all, the most negative adsorption energy (-28.6 kcal/mol) is attained with D12- $\pi$ -A/TiO<sub>2</sub>, which indicates the most stable adsorption. Apart from N-annulation, adsorption stability

increases with enhanced electron-donating strength of D- $\pi$ -A. The excellent linear correlation between  $\Delta V_{mA}$  and  $E_{ads}$  with a correlation coefficient of 0.947 confirms that the donating strength of the donor systems of D- $\pi$ -A assessed in terms of  $\Delta V_{mA}$  is useful to assess the  $E_{ads}$  values of the dye on the semiconductor (Figure 4.6a). Since stronger adsorption leads to deeper LUMO energy level, a more donating dye is expected to give higher adsorption stability and higher  $eV_{oc}$  (Table 4.4 and Figure 4.6b). In D12- $\pi$ -A/TiO<sub>2</sub> system, the highest adsorption stability and  $eV_{oc}$  (2.21 eV) have been observed, which predicts superior photovoltaic performance of the adsorbed dye.

#### 4.4.4 Photovoltaic performance

The photovoltaic parameters of the D- $\pi$ -A systems are listed in Table 4.5. The electron injection-free energy change ( $\Delta G_{inject}$ ) are in the range -1.28 to -2.10 eV. It is defined as  $\Delta G_{inject} = E^{dye*} - |E_{CB}|$ ,<sup>95-97</sup> where  $E^{dye*}$  is the excited state oxidation potential and  $E_{CB}$  is the energy of the conduction band edge of the TiO<sub>2</sub> semiconductor (-4.0 eV).  $E^{dye*}$  can be calculated as  $(-e_h - \text{vertical excitation energy})$ .<sup>95, 98</sup> The more negative  $\Delta G_{inject}$  will have more ability to inject electrons from the excited state of the D- $\pi$ -A to the CB of TiO<sub>2</sub>. Since  $\Delta G_{inject}$  is related to short-circuit current density  $J_{sc}$ , by improving the electron injection ability, enhancement in PCE can occur.<sup>6, 22, 26, 97</sup> Among all,  $\Delta G_{inject}$  is more negative in D14- $\pi$ -A (-2.10 eV) while it is the least negative in D9- $\pi$ -A (-1.28 eV). Further, it is noted that donating strength improves the electron injection efficiency. The  $\Delta G_{reg}$  (free energy change for dye regeneration) value measures dye regeneration efficiency of the systems which can be written as  $(E^{dye} - 4.8)\text{eV}$  or  $(-e_h) - 4.8 \text{ eV}$ .<sup>99, 100</sup> The smallest  $\Delta G_{reg}$  (-0.84 eV) observed in D12- $\pi$ -A shows the highest dye regeneration efficiency, while the highest value 0.49 observed in D6- $\pi$ -A indicates the lowest dye regeneration efficiency. Finally, open-circuit voltage ( $eV_{oc} = e_l - (-4.0)$ )<sup>101</sup> lies in the range 1.21 eV to 2.21 eV, which shows an excellent correlation with  $\Delta V_{mA}$  (Figure 4.7), and suggests that  $eV_{oc}$  increases with enhanced strength of D- $\pi$ -A systems. The correlation in Figure 4.7 also suggests that MESP approach offers an easy analysis tool for the quantification of the donating strength of D- $\pi$ -A systems in DSSC applications, and the correlation plot provides a guideline for designing dye sensitizers for desirable photovoltaic applications.

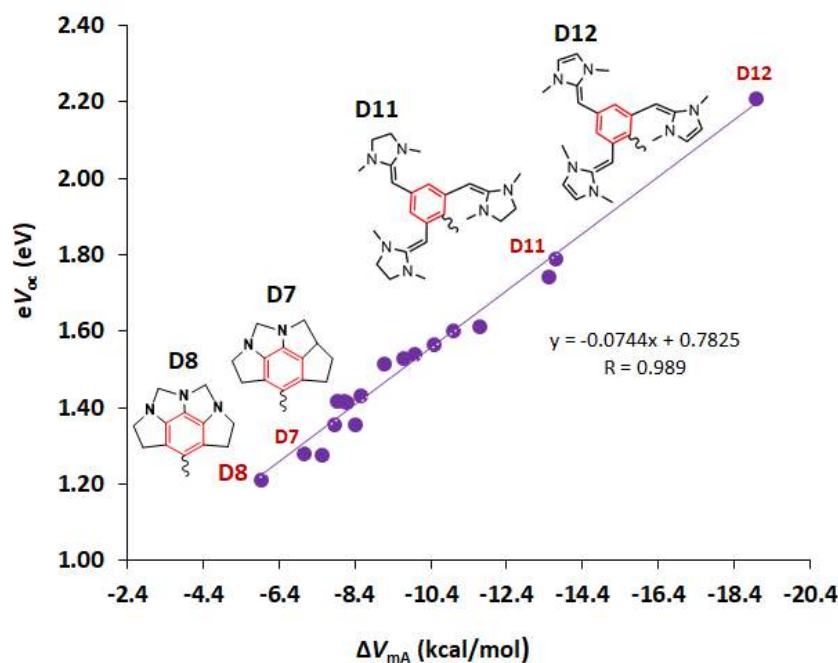


**Figure 4. 7** Correlation between donating strength ( $\Delta V_{mA}$ ) of D- $\pi$ -A system and open-circuit voltage ( $eV_{oc}$ ).

## 4.5 Conclusions

Donor modifications, especially through the integration of electron-rich nitrogen atoms (N-annulation) significantly affect the structure-performance relationship of D- $\pi$ -A systems for dye-sensitized solar cell applications. For tuning the electron-donating ability of D- $\pi$ -A systems, eighteen electron-rich nitrogen incorporated donors are designed with butadiene and cyanoacrylic acid as  $\pi$ -spacer and acceptor, respectively. The implication of planarized nitrogens for improving the electron-donating strength ( $\Delta V_{mA}$ ) of D- $\pi$ -A systems is investigated using MESP topographical analysis, which states that the magnitude of  $\Delta V_{mA}$  increases with an increased number of planar nitrogens. The  $\lambda_{max}$  of D- $\pi$ -A systems are fine-tuned by the extent of  $\pi$ -conjugation and N-annulation in donors. The significance of  $\Delta V_{mA}$  in shifting absorption maximum ( $\Delta\lambda_{max}$ ) is confirmed by the linear correlation observed between  $\Delta V_{mA}$  and  $\Delta\lambda_{max}$ . Regarding the frontier molecular orbitals of D- $\pi$ -A systems, HOMO and LUMO energies are affected by electron-rich nature of donors in D- $\pi$ -A. The sufficiently more negative LUMO energy of D- $\pi$ -A systems to the CB energy of TiO<sub>2</sub> provides efficient electron injection efficiency. Open-circuit voltage ( $eV_{oc}$ ), and

electron injection free energy change ( $\Delta G_{inject}$ ) have been analysed for D- $\pi$ -A systems and reveal that  $eV_{oc}$  is increased with enhanced  $\Delta V_{mA}$ . Also, adsorption stability of D- $\pi$ -A systems on  $TiO_2$  has been evaluated and indicates that adsorption stability ( $E_{ads}$ ) increased with enhanced electron-donating strength of D- $\pi$ -A system. Since adsorption of D- $\pi$ -A system on  $TiO_2$  shifts LUMO energy, the stability of D- $\pi$ -A/ $TiO_2$  system affects  $eV_{oc}$  and thus the efficiency of the solar cell. The strong linear correlation observed between  $E_{ads}$  and  $eV_{oc}$  proves this conclusion. Among all the cases studied, D12- $\pi$ -A/ $TiO_2$  shows the highest adsorption stability, furthermore D12- $\pi$ -A displays the highest  $\Delta\lambda_{max}$ , the best  $eV_{oc}$  and the highest magnitude for  $\Delta V_{mA}$ . Consequently, from the aforementioned fundamental parameters, it can be concluded that D12 based photosensitizer is very effective for improving the PCE. Also, the N-annulated designing strategy will pave the way for attaining high efficiency in the field of dye-sensitized solar cells.

## 4.6 References

1. A. Baheti, C.-P. Lee, K. J. Thomas and K.-C. Ho, *Phys. Chem. Chem. Phys.*, 2011, **13**, 17210-17221.
2. Y.-H. Chen, V. S. Nguyen, H.-H. Chou, Y. S. Tingare, T.-C. Wei and C.-Y. Yeh, *ACS Appl. Energy Mater.*, 2020, **3**, 5479-5486.
3. J. Gong, K. Sumathy, Q. Qiao and Z. Zhou, *Renew. Sustain. Energy Rev.*, 2017, **68**, 234-246.
4. G. Boschloo, *Front. Chem.*, 2019, **7**, 77.
5. M. Grätzel, *Acc. Chem. Res.*, 2009, **42**, 1788-1798.
6. B. O'Regan and M. Grätzel, *Nature*, 1991, **353**, 737-740.
7. M. K. Nazeeruddin, F. De Angelis, S. Fantacci, A. Selloni, G. Viscardi, P. Liska, S. Ito, B. Takeru and M. Grätzel, *J. Am. Chem. Soc.*, 2005, **127**, 16835-16847.
8. G. Marotta, M. A. Reddy, S. P. Singh, A. Islam, L. Han, F. De Angelis, M. Pastore and M. Chandrasekharam, *ACS Appl. Mater. Interfaces*, 2013, **5**, 9635-9647.
9. S. Yun, Y. Qin, A. R. Uhl, N. Vlachopoulos, M. Yin, D. Li, X. Han and A. Hagfeldt, *Energy Environ. Sci.*, 2018, **11**, 476-526.
10. A. Fakharuddin, R. Jose, T. M. Brown, F. Fabregat-Santiago and J. Bisquert, *Energy Environ. Sci.*, 2014, **7**, 3952-3981.

11. A. Hinsch, W. Veurman, H. Brandt, K. F. Jensen and S. Mastroianni, *ChemPhysChem*, 2014, **15**, 1076-1087.
12. A. Hagfeldt, G. Boschloo, L. Sun, L. Kloo and H. Pettersson, *Chem. Rev.*, 2010, **110**, 6595-6663.
13. Y. Kurumisawa, T. Higashino, S. Nimura, Y. Tsuji, H. Iiyama and H. Imahori, *J. Am. Chem. Soc.*, 2019, **141**, 9910-9919.
14. H. Zhou, J.-M. Ji, S. H. Kang, M. S. Kim, H. S. Lee, C. H. Kim and H. K. Kim, *J. Mater. Chem. C*, 2019, **7**, 2843-2852.
15. K. Kakiage, Y. Aoyama, T. Yano, K. Oya, T. Kyomen and M. Hanaya, *Chem. Commun.*, 2015, **51**, 6315-6317.
16. K. Kakiage, Y. Aoyama, T. Yano, K. Oya, J.-i. Fujisawa and M. Hanaya, *Chem. Commun.*, 2015, **51**, 15894-15897.
17. S. Mathew, A. Yella, P. Gao, R. Humphry-Baker, B. F. Curchod, N. Ashari-Astani, I. Tavernelli, U. Rothlisberger, M. K. Nazeeruddin and M. Grätzel, *Nat. Chem.*, 2014, **6**, 242-247.
18. F.-S. Lin, P. Priyanka, M.-S. Fan, S. Vegiraju, J.-S. Ni, Y.-C. Wu, Y.-H. Li, G.-H. Lee, Y. Ezhumalai and R.-J. Jeng, *J. Mater. Chem. C*, 2020, **8**, 15322-15330.
19. Y. Ren, Y. Li, S. Chen, J. Liu, J. Zhang and P. Wang, *Energy Environ. Sci.*, 2016, **9**, 1390-1399.
20. K. Sharma, V. Sharma and S. Sharma, *Nanoscale Res. Lett.*, 2018, **13**, 381.
21. X. Song, X. Yang, H. Wang, J. An, Z. Yu, X. Wang, A. Hagfeldt and L. Sun, *Sol. Energy*, 2019, **187**, 274-280.
22. V. V. Divya and C. H. Suresh, *New J. Chem.*, 2020, **44**, 7200-7209.
23. M. Jadhav, J. V. Vaghasiya, D. Patil, S. S. Soni and N. Sekar, *New J. Chem.*, 2019, **43**, 8970-8981.
24. R. Tarsang, V. Promarak, T. Sudyoasuk, S. Namuangruk and S. Jungstittiwong, *J. Photochem. Photobiol. A: Chemistry*, 2014, **273**, 8-16.
25. M. Karuppusamy, V. S. K. Choutipalli, D. Vijay and V. Subramanian, *J. Chem. Sci.*, 2020, **132**, 20.
26. V. V. Divya and C. H. Suresh, *New J. Chem.*, 2021, **45**, 2496-2507.
27. Y. K. Eom, S. H. Kang, I. T. Choi, Y. Yoo, J. Kim and H. K. Kim, *J. Mater. Chem. A*, 2017, **5**, 2297-2308.

28. Y.-Q. Yan, Y.-Z. Zhu, P.-P. Dai, J. Han, M. Yan and J.-Y. Zheng, *Sol. Energy*, 2020, **207**, 428-435.
29. H. Zhang, Z.-E. Chen and H.-R. Tian, *Sol. Energy*, 2020, **198**, 239-246.
30. A. J. Huckaba, F. Giordano, L. E. McNamara, K. M. Dreux, N. I. Hammer, G. S. Tschumper, S. M. Zakeeruddin, M. Grätzel, M. K. Nazeeruddin and J. H. Delcamp, *Adv. Energy Mater.*, 2015, **5**, 1401629.
31. Y. Zhang, H. Cheema, L. McNamara, L. A. Hunt, N. I. Hammer and J. H. Delcamp, *Chem. Eur. J.*, 2018, **24**, 5939-5949.
32. J. Feng, Y. Jiao, W. Ma, M. K. Nazeeruddin, M. Grätzel and S. Meng, *J. Phys. Chem. C*, 2013, **117**, 3772-3778.
33. J. H. Delcamp, A. Yella, T. W. Holcombe, M. K. Nazeeruddin and M. Grätzel, *Angew. Chem. Int. Ed.*, 2013, **125**, 394-398.
34. C. Yan, W. Ma, Y. Ren, M. Zhang and P. Wang, *ACS Appl. Mater. Interfaces* 2015, **7**, 801-809.
35. U. B. Cappel, M. H. Karlsson, N. G. Pschirer, F. Eickemeyer, J. Schöneboom, P. Erk, G. Boschloo and A. Hagfeldt, *J. Phys. Chem. C*, 2009, **113**, 14595-14597.
36. C. Li, Z. Liu, J. Schöneboom, F. Eickemeyer, N. G. Pschirer, P. Erk, A. Herrmann and K. Müllen, *J. Mater. Chem. C*, 2009, **19**, 5405-5415.
37. Y. Jin, J. Hua, W. Wu, X. Ma and F. Meng, *Synth. Met.*, 2008, **158**, 64-71.
38. J. Luo, M. Xu, R. Li, K.-W. Huang, C. Jiang, Q. Qi, W. Zeng, J. Zhang, C. Chi, P. Wang and J. Wu, *J. Am. Chem. Soc.*, 2014, **136**, 265-272.
39. Z. Yao, H. Wu, Y. Ren, Y. Guo and P. Wang, *Energy Environ. Sci.*, 2015, **8**, 1438-1442.
40. Z. Yao, M. Zhang, H. Wu, L. Yang, R. Li and P. Wang, *J. Am. Chem. Soc.*, 2015, **137**, 3799-3802.
41. V. V. Divya, F. B. Sayyed and C. H. Suresh, *ChemPhysChem*, 2019, **20**, 1752-1758.
42. F. Effenberger, P. Fischer, W. W. Schöllner and W.-D. Stohrer, *Tetrahedron*, 1978, **34**, 2409-2417.
43. A. Zakrzewska, R. Gawinecki, E. Kolehmainen and B. Ośmiński, *Int. J. Mol. Sci.*, 2005, **6**, 52-62.
44. J. O. S. Varejão, E. V. V. Varejão and S. A. Fernandes, *Eur. J. Org. Chem.*, 2019, **2019**, 4273-4310.

45. J. E. Kuder, W. W. Limburg, J. M. Pochan and D. Wychick, *J. Chem. Soc. Perkin II*, 1977, 1643-1651.
46. G. Shishkin, *Chem. Heterocycl. Compd.*, 1983, **19**, 549-553.
47. F. Fantuzzi, C. B. Coutinho, R. R. Oliveira and M. A. C. Nascimento, *Inorg. Chem.*, 2018, **57**, 3931-3940.
48. C. H. Suresh and F. B. Sayyed, *J. Phys. Chem. A*, 2013, **117**, 10455-10461.
49. S. Rohrbach, R. S. Shah, T. Tuttle and J. A. Murphy, *Angew. Chem.*, 2019, **131**, 11576-11580.
50. J. S. Miller, D. A. Dixon, J. C. Calabrese, C. Vazquez, P. J. Krusic, M. D. Ward, E. Wasserman and R. L. Harlow, *J. Am. Chem. Soc.*, 1990, **112**, 381-398.
51. E. Scrocco and J. Tomasi, in *Adv. Quantum Chem.*, ed. P.-O. Löwdin, Academic Press 1978, vol. **11**, pp. 115-193.
52. B. Pullman, *Int. J. Quantum Chem.*, 1990, **38**, 81-92.
53. A. Pullman and B. Pullman, *Q. Rev. Biophys.*, 1981, **14**, 289-380.
54. P. Politzer and J. S. Murray, *J. Mol. Struct.*, 1996, **376**, 419-424.
55. P. Politzer, J. S. Murray and T. Clark, *Phys. Chem. Chem. Phys.*, 2013, **15**, 11178-11189.
56. P. Politzer and J. S. Murray, *Cryst. Growth Des.*, 2015, **15**, 3767-3774.
57. P. Politzer and J. S. Murray, *ChemPhysChem*, 2020, **21**, 579-588.
58. C. H. Suresh and S. R. Gadre, *J. Org. Chem.*, 1999, **64**, 2505-2512.
59. S. R. Gadre and R. N. Shirsat, *Electrostatics of Atoms and Molecules*, Universities Press 2000.
60. S. R. Gadre, S. A. Kulkarni and I. H. Shrivastava, *J. Chem. Phys.*, 1992, **96**, 5253-5260.
61. F. B. Sayyed and C. H. Suresh, *New J. Chem.*, 2009, **33**, 2465-2471.
62. P. Sajith and C. H. Suresh, *Inorg. Chem.*, 2012, **51**, 967-977.
63. J. Mathew and C. H. Suresh, *Organometallics*, 2011, **30**, 1438-1444.
64. K. Sandhya and C. H. Suresh, *Dalton Trans.*, 2014, **43**, 12279-12287.
65. B. A. Anjali, F. B. Sayyed and C. H. Suresh, *J. Phys. Chem. C*, 2016, **120**, 1112-1119.
66. B. A. Anjali and C. H. Suresh, *ACS omega*, 2017, **2**, 4196-4206.
67. P. V. Bijina and C. H. Suresh, *J. Chem. Sci.*, 2016, **128**, 1677-1686.
68. R. Rakhi and C. H. Suresh, *Phys. Chem. Chem. Phys.*, 2016, **18**, 24631-24641.

69. K. Remya and C. H. Suresh, *Phys. Chem. Chem. Phys.*, 2015, **17**, 27035-27044.
70. T. D. Della and C. H. Suresh, *Phys. Chem. Chem. Phys.*, 2016, **18**, 14588-14602.
71. F. Arkan and M. Izadyar, *Renew. Sust. Energ. Rev.*, 2018, **94**, 609-655.
72. W. Zhang, L. Wang, L. Mao, J. Jiang, H. Ren, P. Heng, H. Ågren and J. Zhang, *J. Phys. Chem. C*, 2020, **124**, 3980-3987.
73. A. D. Laurent, C. Adamo and D. Jacquemin, *Phys. Chem. Chem. Phys.*, 2014, **16**, 14334-14356.
74. M. Y. Mehboob, M. U. Khan, R. Hussain, K. Ayub, A. Sattar, M. K. Ahmad, Z. Irshad and M. Adnan, *Spectrochim. Acta A Mol. Biomol. Spectrosc.*, 2021, **244**, 118873.
75. M. Y. Mehboob, M. U. Khan, R. Hussain, R. Fatima, Z. Irshad and M. Adnan, *J. Theor. Comput. Chem.*, 2020, **19**, 2050034.
76. M. Y. Mehboob, R. Hussain, M. U. Khan, M. Adnan, A. Umar, M. U. Alvi, M. Ahmed, M. Khalid, J. Iqbal and M. N. Akhtar, *Comput. Theor. Chem.*, 2020, **1186**, 112908.
77. M. Y. Mehboob, R. Hussain, M. U. Khan, M. Adnan, M. A. Ehsan, A. Rehman and M. R. S. A. Janjua, *J. Phys. Org. Chem.*, 2021, e4204.
78. A. D. Becke, *J. Chem. Phys.*, 1993, **98**, 1372-1377.
79. T. H. Dunning Jr, *Chem. Phys.*, 1989, **90**, 1007-1023.
80. J. K. Roy, S. Kar and J. Leszczynski, *J. Phys. Chem. C*, 2019, **123**, 3309-3320.
81. S. Kupfer, J. Guthmuller and L. Gonzalez, *J. Chem. Theory Comput.*, 2013, **9**, 543-554.
82. P. J. Hay and W. R. Wadt, *J. Chem. Phys.*, 1985, **82**, 270-283.
83. R. Sánchez-de-Armas, M. Á. San Miguel, J. Oviedo and J. F. Sanz, *Phys. Chem. Chem. Phys.*, 2012, **14**, 225-233.
84. T. Yanai, D. P. Tew and N. C. Handy, *Chem. Phys. Lett.*, 2004, **393**, 51-57.
85. G. Deogratias, N. Seriani, T. Pogrebnyaya and A. Pogrebnoi, *J. Mol. Graph. Model.*, 2020, **94**, 107480.
86. J. Zhang, H.-C. Zhu, R.-L. Zhong, L. Wang and Z.-M. Su, *Org. Electron.*, 2018, **54**, 104-113.
87. H.-C. Zhu, C.-F. Li, Z.-H. Fu, S.-S. Wei, X.-F. Zhu and J. Zhang, *Appl. Surf. Sci.*, 2018, **455**, 1095-1105.
88. M. J. Frisch, G. W. Trucks, H. B. Schlegel, G. E. Scuseria, M. A. Robb, J. R. Cheeseman, G. Scalmani, V. Barone, G. A. Petersson, H. Nakatsuji, X. Li, M. Caricato, A. V. Marenich, J. Bloino, B. G. Janesko, R. Gomperts, B. Mennucci, H. P.



- Hratchian, J. V. Ortiz, A. F. Izmaylov, J. L. Sonnenberg, D. Williams-Young, F. Ding, F. Lipparini, F. Egidi, J. Goings, B. Peng, A. Petrone, T. Henderson, D. Ranasinghe, V. G. Zakrzewski, J. Gao, N. Rega, G. Zheng, W. Liang, M. Hada, M. Ehara, K. Toyota, R. Fukuda, J. Hasegawa, M. Ishida, T. Nakajima, Y. Honda, O. Kitao, H. Nakai, T. Vreven, K. Throssell, J. A. Montgomery Jr., J. E. Peralta, F. Ogliaro, M. J. Bearpark, J. J. Heyd, E. N. Brothers, K. N. Kudin, V. N. Staroverov, T. A. Keith, R. Kobayashi, J. Normand, K. Raghavachari, A. P. Rendell, J. C. Burant, S. S. Iyengar, J. Tomasi, M. Cossi, J. M. Millam, M. Klene, C. Adamo, R. Cammi, J. W. Ochterski, R. L. Martin, K. Morokuma, O. Farkas, J. B. Foresman and D. J. Fox, Wallingford, CT, 2016.
89. M. Y. Mehboob, R. Hussain, Z. Irshad and M. Adnan, *J. Phys. Org. Chem.*, 2021, DOI: org/10.1002/poc.4210
90. R. Hussain, M. Y. Mehboob, M. U. Khan, M. Khalid, Z. Irshad, R. Fatima, A. Anwar, S. Nawab and M. Adnan, *J. Mater. Sci.*, 2021, **56**, 5113-5131.
91. M. Y. Mehboob, R. Hussain, Z. Irshad and M. Adnan, *Bull Korean Chem Soc*, 2021.
92. L. Zhang and J. M. Cole, *ACS Appl. Mater. Interfaces*, 2015, **7**, 3427-3455.
93. M. Pastore and F. De Angelis, *Phys. Chem. Chem. Phys.*, 2012, **14**, 920-928.
94. P. Li, Z. Wang, C. Song and H. Zhang, *J. Mater. Chem. A*, 2017, **5**, 11454-11465.
95. R. Katoh, A. Furube, T. Yoshihara, K. Hara, G. Fujihashi, S. Takano, S. Murata, H. Arakawa and M. Tachiya, *J. Phys. Chem. B*, 2004, **108**, 4818-4822.
96. J. Preat, C. Michaux, D. Jacquemin and E. A. Perpète, *J. Phys. Chem. C*, 2009, **113**, 16821-16833.
97. N. N. Ghosh, M. Habib, A. Pramanik, P. Sarkar and S. Pal, *New J. Chem.*, 2019, **43**, 6480-6491.
98. J. Zhang, H.-B. Li, S.-L. Sun, Y. Geng, Y. Wu and Z.-M. Su, *J. Mater. Chem.*, 2012, **22**, 568-576.
99. G. Boschloo and A. Hagfeldt, *Acc. Chem. Res.*, 2009, **42**, 1819-1826.
100. T. Koopmans, *Physica*, 1933, **1**, 104-113.
101. C.-R. Zhang, Z.-J. Liu, Y.-H. Chen, H.-S. Chen, Y.-Z. Wu, W. Feng and D.-B. Wang, *Curr. Appl. Phys.*, 2010, **10**, 77-83.



## ABSTRACT

---

Name of the Student: Divya Velayudhan V. V.

Registration No.: 10CC15A39004

Faculty of Study: Chemical Sciences

Year of Submission: 2021

AcSIR academic centre/CSIRLab: CSIR-NIIST

Name of the Supervisor: Dr. C. H. Suresh

**Title of the thesis:** Density Functional Theory Studies on D- $\pi$ -A Systems Used in Dye-Sensitized Solar Cells: Donor-Acceptor Effect, Spacer Effect, and Molecular Design Strategies

---

Dye-sensitized solar cells (DSSCs) have a fundamental role in photovoltaic technology as an alternative to highly expensive conventional silicon based solar cell. Theoretical studies are greatly acknowledged for the reliable prediction of efficiency of dye-sensitizers and understanding the fundamental processes involved in DSSC device. The thesis is organized into four chapters. Chapter 1 gives an overview of both DSSCs and computational chemistry methods. In chapter 2, using molecular electrostatic potential (MESP) analysis, the electronic effect transmission power ( $\gamma$ ) of various spacer (G in the notation) units in a Y-G-X type molecular model and electron donating strength ( $\Delta V_{mA}$ ) of typically used donors in D- $\pi$ -A type dye-sensitizers have been computed. Among the studied spacers units, alkenyl spacers with shorter spacer chain length showed the highest  $\gamma$ , which will be effective for the better power conversion efficiency (PCE) in DSSCs. Further,  $\Delta V_{mA}$  is found to be proportional to absorptional redshift and open-circuit voltage ( $eV_{OC}$ ) which shows the relevance of  $\Delta V_{mA}$  for the enhancement of optical and photovoltaic properties of dye-sensitizers. In chapter 3, the role of electron donating substituents on the donor region of D- $\pi$ -A systems has been analysed and found that  $\Delta V_{mA}$ , optical, and photovoltaic properties have been improved in substituted D- $\pi$ -A systems than bare D- $\pi$ -A. Finally in chapter 4, the significance of nitrogen centres for revamping the donating strength of D- $\pi$ -A is scrutinized. The results show that absorption maxima, adsorption stability of dye/TiO<sub>2</sub> interface, and photovoltaic properties enhanced with number of N-centres at donor region. In all chapters, the strong linear correlation observed for the ground state property  $\Delta V_{mA}$  and  $eV_{OC}$  provides guidelines for effective dye design with a desirable photovoltaic applications. For the prediction of PCE, the study developed a new theoretical strategy (MESP based).

## List of Publications

### I. Publications related to thesis

1. Substituent Effect Transmission Power of Alkyl, Alkenyl, Alkynyl, Phenyl, Thiophenyl, and Polyacene Spacers, **Velayudhan V. Divya**, Fareed Bhasha Sayyed, and Cherumuttathu H. Suresh,\* *ChemPhysChem* **2019**, 20, 1752– 1758
2. Density functional theory study on the donating strength of donor systems in dye-sensitized solar cells, **Velayudhan V. Divya** and Cherumuttathu H. Suresh,\* *New J. Chem.*, **2020**, 44, 7200
3. Tuning the donating strength of dye sensitizers using molecular electrostatic potential analysis, **Velayudhan V. Divya** and Cherumuttathu H. Suresh,\* *New J. Chem.*, **2021**, 45, 2496
4. Design and DFT study of nitrogen-rich donor systems for improved photovoltaic performance in dye-sensitized solar cells, **Velayudhan V. Divya** and Cherumuttathu H. Suresh,\* *New J. Chem.*, **2021**, 45, 11585-11595

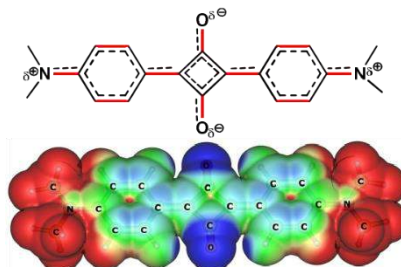
### II. Publications out of thesis

1. Electronic Structure of Bis (4-dimethylaminophenyl) squaraine, **Velayudhan V. Divya** and Cherumuttathu H. Suresh, \* *ChemistrySelect*, **2019**, 4, 3387 –3394
2. Solution Processable Deep-Red Phosphorescent Pt (II) Complex: Direct Conversion from Its Pt(IV) Species via a Base-Promoted Reduction, Ilene Allison, Hyunsoo Lim, Atul Shukla, Viqar Ahmad, Monirul Hasan, Kedar Deshmukh, Robert Wawrzinek, Sarah K. M. McGregor, Jack K. Clegg, **Velayudhan V. Divya**, Chinju Govind, Cherumuttathu H. Suresh, Venugopal Karunakaran, Narayanan Unni K. N., Ayyappanpillai Ajayaghosh, Ebinazar B. Namdas\* and Shih-Chun Lo,\* *ACS Appl. Electron. Mater.*, **2019**, 1, 1304–1313
3. Regulating Back Electron Transfer through Donor and  $\pi$ -Spacer Alterations in Benzothieno[3,2-b]indole-based Dye-sensitized Solar Cells, P. R Nitha, V. Jayadev, Sourava C. Pradhan, **Velayudhan V. Divya**, Cherumuttathu H. Suresh, Jubi John,\* Suraj Soman,\* Ayyappanpillai Ajayaghosh\* *Chem Asian J.*, **2020**, 15, 3 503–3512

### III. Published contributions to academic conferences

1. Presented a poster entitled “Electronic Structure of Bis(4-dimethylaminophenyl) Squaraine” at the Theoretical Chemistry Symposium (TCS), BITS Pilani, Pilani, Rajasthan, 13-16 February, 2019.

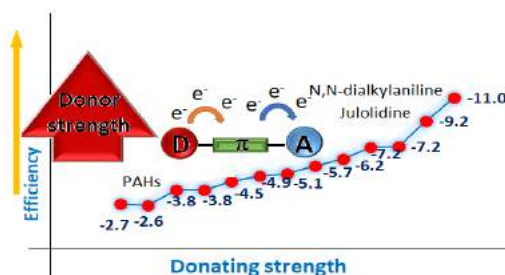
**Abstract:** Squaraine is a well-known organic functional material in the field of photovoltaics due to its energy harvesting characteristics. The aim of the present study is to understand in detail the electronic structure of squaraine dye as well as its



noncovalent interaction with solvent molecules. The structural and electronic features of bis (4dimethylaminophenyl) squaraine (1) has been studied using density functional BLYP/631G(d,p) level of theory. The quinoid character of 1 is correlated to partial double bond character of C-NMe<sub>2</sub> (1.386 Å) and C-O (1.243 Å) bonds which leads to accumulation of positive charge on NMe<sub>2</sub> groups and negative charge on carbonyl oxygen. Further, the diagonal C1C3 (2.089 Å) and C2C4 (2.126 Å) distances of the squaric ring indicated a 1,3 type C-C orbital interaction. Molecular electrostatic potential (MESP) topographical analysis confirmed the charge separated quadrupolar nature of 1. The MESP minimum,  $V_{\min}$  located at the carbonyl oxygen, -63.9 kcal/mol, confirmed its highly electron rich character arising from the quinoid structure. The electronic structure of 1 revealed from MESP confirmed its quadrupolar nature and suggested the location of positive charge on NMe<sub>2</sub> groups. The typically used chemical structure drawing of 1 showing +2 charge on the squaraine ring is inaccurate and misleading. The solvatochromic behaviour of 1 can be attributed to its quadrupolar electronic structure wherein the electron rich carbonyl groups provide room for noncovalent interactions with multiple solvent molecules.

2. Presented a Poster entitled “Density functional theory study on the donating strength of donor systems in dye-sensitized solar cells” - 14th International Conference on Ecomaterials (ICEM-14), CSIR-National Institute for Interdisciplinary Science and Technology (NIIST), Industrial Estate (P.O.), Thiruvananthapuram, Kerala, 5 – 7 February, 2020.

**Abstract:** Developing a highly efficient D- $\pi$ -A system for dye-sensitized solar cell (DSSC) application *via* improved donor strength became an emerging area of interest for the last two decades.<sup>1</sup> Since the electron-donating strength of the donor fragment determines the electronic and optical properties of the system, it is highly essential to know the donating strength of such units beforehand. Herein, a TD-CAM B3LYP/cc-pVDZ//B3LYP/cc-pVDZ density functional theory study has been carried out on 13 typically used donor systems for the analysis of optical, and photovoltaic properties. The electron-donating strength of the donor system has been quantified in terms of the molecular electrostatic potential at anchoring moiety. Further, a remarkable linear correlation obtained between donating strength ( $\Delta V_{mA}$ ) and absorption shift ( $\Delta\lambda_{max}$ ), open-circuit voltage ( $V_{oc}$ ) shows the significance of  $\Delta V_{mA}$  on  $\Delta\lambda_{max}$  and  $V_{oc}$ . Among the investigated D- $\pi$ -A systems, N,N-dialkyl aniline, and julolidine were found to be the best donors for the photovoltaic application. In general, by tuning the donating strength we can able to enhance  $V_{oc}$ , thereby enhances the efficiency of the D- $\pi$ -A system.



# **SCI Publications**

# Substituent Effect Transmission Power of Alkyl, Alkenyl, Alkynyl, Phenyl, Thiophenyl, and Polyacene Spacers

Velayudhan V. Divya,<sup>[a, b]</sup> Fared Bhasha Sayyed,<sup>[a]</sup> and Cherumuttathu H. Suresh<sup>\*[a, b]</sup>

The transmission of substituent effect through a variety of spacers, that is to say, alkyl, alkenyl, alkynyl, phenyl, thiophenyl, and polyacene has been studied by modeling Y-G-X type molecular systems (Y: reaction center; G: spacer moiety; X: substituent) using B3LYP/6-31G(d,p) density functional theory calculations. The reaction center is always kept as a C=C double bond and the molecular electrostatic potential (MESP) minimum ( $V_{\min}$ ) observed for this bond showed subtle variation with respect to the changes in the spacer unit and the nature of substituent. Strong linear correlations are observed between Hammett substituent constants ( $\sigma_I$  and  $\sigma_P$ ) and  $V_{\min}$ , which

recommend the aptness of  $V_{\min}$  as an electronic descriptor to quantify the substituent effect. Since  $V_{\min}$  offers an alternative measure of substituent effect, the correlation between  $V_{\min}$  and  $\sigma_P$  has been used for assessing the transmission of substituent effect through a variety of spacer moieties. The highest transmission coefficient ( $\gamma$ ) is always observed for smaller spacer length. Among all the spacers, alkenyl showed the highest and alkyl showed the lowest transmission power. The study recommends the use of short chains of C=C double, C≡C triple or a combination of both as spacers for the effective transmission of substituent effect to the reaction center.

## 1. Introduction

Substituents in molecules are regarded as functional groups and tuning of various chemical properties can be achieved by controlling the substituent effects.<sup>[1]</sup> The theory of substituent effect has been considered as fundamental to the prediction of molecular reactivity.<sup>[1–2]</sup> The electronic effect of a substituent can be transmitted to the reaction center via a transmitting moiety. For example in a molecule Y-G-X, (Y: reaction center; G: spacer moiety; X: substituent), the effect of X at Y through G can be interpreted with the famous Hammett relationship  $\log(K_X/K_0) = \rho\sigma$ , where  $\rho$  is the reaction constant and  $\sigma$  is the substituent constant. Hammett equation and several of its modifications<sup>[2a,3]</sup> have been used in a quantitative way for the effective interpretation of substituent effects.<sup>[4]</sup> The applicability of  $\sigma$ -constants for a variety of molecules assisted the understanding of structure-activity and structure-property relationships in chemistry.<sup>[5]</sup>

Substituent effects are classified into inductive (through  $\sigma$  bond),  $\pi$  – resonance and through space (field) effects.<sup>[1a,2a,6]</sup> The separation of the substituent effect into inductive ( $\sigma_I$  or F) and resonance effect ( $\sigma_R$  or R) was done by Swain and Lupton.<sup>[7]</sup> They interpreted that the negative and positive values of substituent constant indicate electron donating and withdrawing nature of substituents, respectively. Using quantum chemical approaches, many efforts have been made to model the

substituent effect.<sup>[4–5,8]</sup> Substituent effects are responsible for small perturbations on the molecular electron density distribution, which can be measured by means of correlating them with the computed quantities of total energy, atomic charges, and electrostatic potentials resulting from ab initio quantum chemical or semiempirical methods.<sup>[5a,9]</sup> Further, several experimental studies have utilized Y-G-X type systems to understand the substituent effect transmission ability of various spacer moieties using geometrical variables, ionization techniques, and NMR chemical shifts etc.<sup>[8f,10]</sup>

Among the several theoretical quantities used to interpret Hammett constants, topographical analysis of molecular electrostatic potential (MESP) provided a clean approach to substituent effects.<sup>[5a–c,8c–e]</sup> The prediction and rationalization of reactivity trends using MESP have been pioneered by Scrocco, Tomasi, and co-workers.<sup>[11]</sup> Politzer and Murry widely used the MESP plots calculated using standard electronic structure theory to interpret while the topographical analysis of MESP has been pioneered by Gadre et al.<sup>[12]</sup> From MESP topographical studies on conjugated organic molecular systems, Suresh et al. have shown that critical features of MESP are useful for the quantification of inductive,<sup>[13]</sup> resonance,<sup>[14]</sup> steric<sup>[15]</sup> and proximity effects<sup>[8b]</sup> of substituents. Also, MESP minimum ( $V_{\min}$ ) has been used as a powerful electronic descriptor to quantify substituent effect, trans influence and two electron donor character of ligands.<sup>[5a,c,16]</sup> Here we intend to study Y-G-X type systems using  $V_{\min}$  analysis. The substituent effect transmission power of X through the spacer will be assessed by the  $V_{\min}$  observed over Y, an olefinic moiety. Although the significance of such spacers in donor-acceptor systems is well known, quantification of substituent effect transmission power of a variety of spacer systems is yet to be systematically analyzed. Previous studies showed that modifications in spacer units such as their  $\pi$ -bond character, conjugation length, and planarity had a significant role in electron transmission power, absorption

[a] V. V. Divya, Dr. F. B. Sayyed, Dr. C. H. Suresh  
Chemical Sciences and Technology Division  
CSIR – National Institute for Interdisciplinary Science and Technology  
Thiruvananthapuram, Kerala, 695 019, India  
E-mail: sureshch@niist.res.in

[b] V. V. Divya, Dr. C. H. Suresh  
Academy of Scientific and Innovative Research (AcSIR)  
Ghaziabad-201002, India

Supporting information for this article is available on the WWW under  
<https://doi.org/10.1002/cphc.201900206>



wavelength, and other related photophysical properties.<sup>[17]</sup> Here spacers such as alkyl, alkenyl, alkynyl, phenyl, thiophenyl, and polyacenes have been selected to include the inductive, and resonance effect aspects. We envision that this study will provide useful information regarding the future dye designing and other related studies.

## 2. Results and Discussion

### 2.1. MESP Topography and Spacer Effects

MESP is one of the most appropriate electronic descriptors to understand the electron withdrawing and donating nature of substituents and ligands.<sup>[5a,b,12d, 16a, 18]</sup> It is recognized that electron rich region in a molecule experiences a significant change in MESP minimum ( $V_{min}$ ) due to substituent effects. Here we consider an olefinic bond (Figure 1) as a sensitive region to

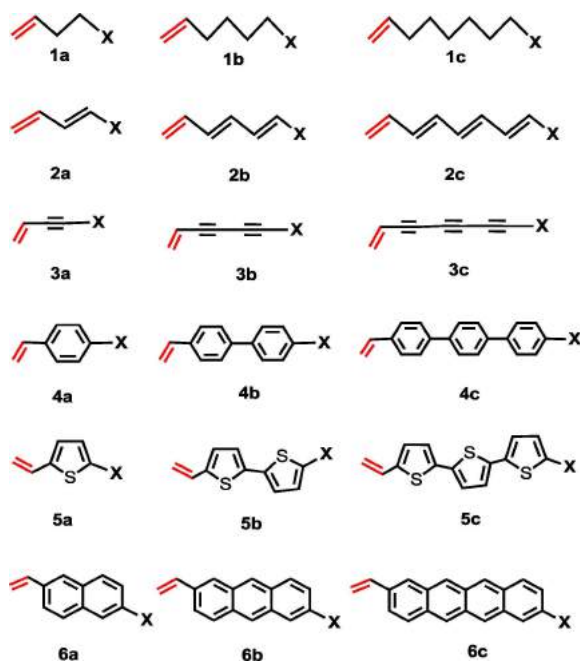


**Figure 1.** Various spacers considered to quantify the transmission power of spacers. The double bond marked in red is the region where MESP minimum is located for  $X=\text{NH}_2$ ,  $\text{OH}$ ,  $\text{CH}_3$ ,  $\text{H}$ ,  $\text{F}$ ,  $\text{Cl}$ ,  $\text{CF}_3$ ,  $\text{CHO}$ ,  $\text{CN}$  and  $\text{NO}_2$ .

understand the precise variation of  $V_{min}$  with respect to the substituent effect. A general notation  $\text{C}_2\text{H}_3\text{-G}_n\text{-X}$  has been used to denote the molecule, where  $\text{G}_n$  stands for the repeating 'n' spacer G units between  $\text{C}_2\text{H}_3$  and X. The effect of substituent on  $\text{C}_2\text{H}_3\text{-}$  has been measured in terms of  $V_{min}$  on its CC double bond. Electron donating and withdrawing substituents used in this study include  $\text{NH}_2$ ,  $\text{OH}$ ,  $\text{CH}_3$ ,  $\text{H}$ ,  $\text{F}$ ,  $\text{Cl}$ ,  $\text{CF}_3$ ,  $\text{CHO}$ ,  $\text{CN}$  and  $\text{NO}_2$ . The spacers selected for the study are alkyl, alkenyl, alkynyl, phenyl, thiophenyl, and polyacenes (Figure 1). For a reasonable understanding about the spacer length, systems up to  $n=3$  have been considered. In studies related to the substituent

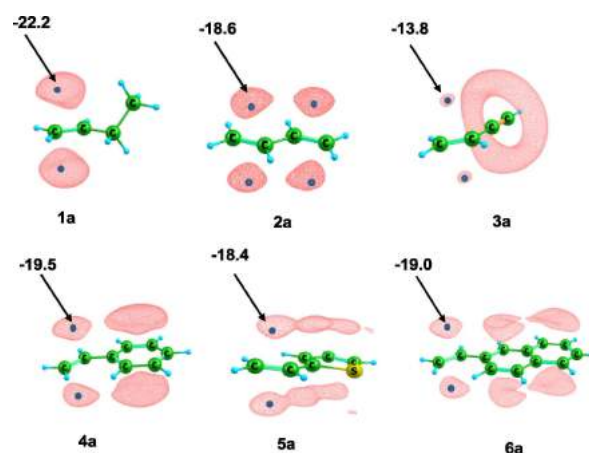


**Figure 2.** MESP isosurface at  $-13.0 \text{ kcal mol}^{-1}$  for 1a, 2a, 3a, 4a, 5a and 6a.  $V_{min}$  values in  $\text{kcal mol}^{-1}$  are also depicted.

effect, a system with  $X=\text{H}$  is described as the unsubstituted reference system. Hence the change in  $V_{min}$  due to substitution is designated as  $\Delta V_{min}$  which gives a direct estimation of the substituent effect.<sup>[8c]</sup>

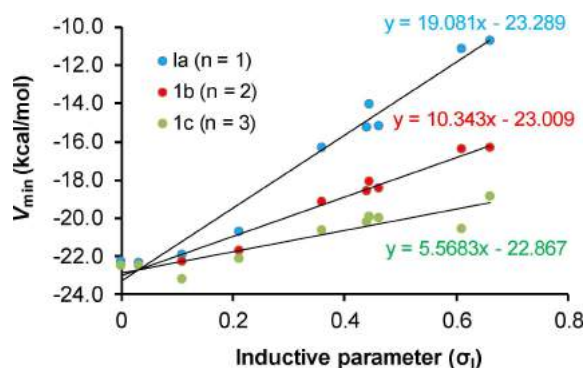
MESP isosurface for 1a, 2a, 3a, 4a, 5a and 6a ( $X=\text{H}$ ) is shown in Figure 2 along with the respective  $V_{min}$  values at the terminal double bond, viz.  $-22.2$ ,  $-18.6$ ,  $-13.8$ ,  $-19.5$ ,  $-18.4$ ,  $-19.0 \text{ kcal/mol}$ . The  $V_{min}$  at the terminal double bond for all the substituted systems (total 180 systems) is depicted in Table 1. The  $V_{min}$  ranges from  $-30.5$  to  $3.8 \text{ kcal/mol}$  which indicates the effect of both spacer moiety and the substituent on tuning the electron distribution on the double bond. In  $\text{C}_2\text{H}_3\text{-alkyl-X}$  systems (1a–1c), the inductive effect is the prime factor for electron transmission. A less negative  $V_{min}$  is observed for  $X=\text{NH}_2$  and  $X=\text{OH}$  than  $X=\text{H}$  suggesting the electron withdrawing inductive ( $-I$ ) character of the highly electronegative N and O atoms. For  $X=\text{CH}_3$  and  $n=1$ ,  $V_{min}$  is slightly more negative than  $X=\text{H}$  indicating the electron donating inductive ( $+I$ ) effect of the methyl group. An increase in alkyl chain length slightly enhances this electron donation. Further, the  $-I$  effect of substituents Cl,  $\text{CF}_3$ , CN,  $\text{NO}_2$  etc. are clearly reflected on their respective  $V_{min}$ . The diminishing  $-I$  effect with an increase in alkyl chain length is pronounced in the case of CN and  $\text{NO}_2$ . For example,  $V_{min}$  of  $\text{NH}_2$  substituted systems shows a variation of  $\sim 1.3 \text{ kcal mol}^{-1}$  from  $n=1$  to  $n=3$ , while CN and  $\text{NO}_2$  exhibits a variation of 9.4 and  $8.1 \text{ kcal mol}^{-1}$ , respectively. The inductive control of electronic transmission in alkyl systems is confirmed by the strong linear correlation between  $V_{min}$  and inductive substituent constant ( $\sigma_I$ ) (Figure 3 and Table S1). The slope of the correlation plot 19.081 observed for spacer length  $n=1$  is the highest and it decreases to 10.343 for  $n=2$  and further decreases to 5.5683 for  $n=3$ . This data indicates the rapidly decreasing behavior of  $I$  with the increase in the number of CC single bonds.<sup>[13]</sup>

For the case of unsubstituted alkenyl systems (2a–2c),  $V_{min}$  values are observed at  $-18.6$ ,  $-18.4$ , and  $-18.3 \text{ kcal/mol}$  respectively. The small variation in  $V_{min}$  indicates the negligible impact of spacer length on electronic transmission whereas the

**Table 1.**  $V_{\min}$  (in kcal mol<sup>-1</sup>) obtained over the terminal double bond of various spacer systems.

X	NH <sub>2</sub>	OH	CH <sub>3</sub>	H	F	Cl	CF <sub>3</sub>	CHO	CN	NO <sub>2</sub>
1a	-21.9	-20.7	-22.3	-22.2	-16.3	-14.0	-15.2	-15.1	-11.1	-10.7
1b	-22.3	-21.6	-22.5	-22.5	-19.1	-18.1	-18.6	-18.4	-16.4	-16.3
1c	-23.2	-22.1	-22.5	-22.5	-20.6	-19.9	-20.2	-20.0	-20.5	-18.8
2a	-30.5	-25.4	-21.6	-18.6	-17.0	-13.3	-8.6	-7.3	-3.6	0.1
2b	-28.6	-24.3	-20.8	-18.4	-17.9	-14.8	-10.7	-9.0	-6.8	-3.5
2c	-24.3	-23.3	-20.4	-18.3	-18.1	-15.6	-12.2	-10.5	-8.9	-6.0
3a	-25.9	-20.6	-18.4	-13.8	-14.0	-11.9	-3.7	-3.0	1.4	3.8
3b	-20.1	-16.3	-14.3	-10.2	-11.0	-9.7	-2.7	-2.0	1.3	3.1
3c	-13.2	-13.1	-11.5	-8.0	-8.9	-7.9	-2.1	-1.5	1.1	2.5
4a	-25.8	-21.8	-21.0	-19.5	-17.5	-15.1	-12.5	-11.1	-8.5	-6.7
4b	-22.0	-20.2	-19.8	-19.1	-17.9	-16.7	-15.4	-14.8	-13.2	-12.4
4c	-20.0	-19.4	-19.3	-18.9	-18.1	-15.1	-16.8	-16.4	-15.5	-15.0
5a	-24.5	-20.8	-20.1	-18.4	-16.3	-14.4	-10.5	-8.7	-6.2	-3.5
5b	-20.8	-19.1	-18.2	-17.1	-15.9	-14.8	-12.5	-10.7	-9.6	-7.3
5c	-18.6	-17.4	-17.2	-16.6	-15.8	-15.1	-13.5	-12.3	-11.5	-9.8
6a	-23.5	-20.6	-20.2	-19.0	-17.4	-15.8	-13.9	-12.8	-11.0	-9.5
6b	-22.1	-20.1	-19.6	-18.8	-17.5	-16.1	-14.8	-13.8	-12.4	-11.2
6c	-20.5	-19.5	-19.2	-18.6	-17.4	-16.4	-15.4	-14.6	-13.5	-12.6

individual effect of a substituent on  $V_{\min}$  is very high in **2** series. For instance,  $\Delta V_{\min}$  of NH<sub>2</sub> and OH in **2** is significantly more negative than those in **1**. In **2**, NH<sub>2</sub> and OH donate electrons


**Figure 3.** Correlation between the  $V_{\min}$  of **1a–1c** with the inductive parameter ( $\sigma_I$ ).

mainly through resonance mechanism. NH<sub>2</sub> is the most electron donating with  $\Delta V_{\min}$  -11.9, -10.2 and -6.0 kcal mol<sup>-1</sup> for **2a**, **2b**, and **2c**, respectively (Table 2 while the most electron withdrawing NO<sub>2</sub> shows  $\Delta V_{\min}$  18.7, 14.9 and 12.4 kcal mol<sup>-1</sup>. Increasing the spacer length diminishes the power of electron transmission. Further, in the case of CH<sub>3</sub>,  $V_{\min}$  is more negative than the unsubstituted system which can be mainly attributed to the electron donating hyperconjugation and +I effect of CH<sub>3</sub>. Here the magnitude of electron donation for **2a–2c** in terms of  $\Delta V_{\min}$  is -3.0, -2.4, and -2.1 kcal/mol (Table 2). Substituents F, Cl, CF<sub>3</sub>, CHO, CN, and NO<sub>2</sub> show a considerable decrease in the magnitude of  $V_{\min}$  compared to the reference system, which authenticates their electron withdrawing inductive and resonance effects. The  $\Delta V_{\min}$  18.7, 15.0, 11.3, 10.0, 5.3, 1.6 kcal mol<sup>-1</sup> observed for the substituents NO<sub>2</sub>, CN, CHO, CF<sub>3</sub>, Cl and F, respectively suggest that their electron withdrawing power follows the order NO<sub>2</sub> > CN > CHO > CF<sub>3</sub> > Cl > F (Table 2). The strong linear correlations observed between  $V_{\min}$  of **2a**, **2b**, and **2c** systems with Hammett constant  $\sigma_p$  (Figure 4 and

**Table 2.**  $\Delta V_{\min}$  in kcal mol<sup>-1</sup> of various spacer systems.

X	$V_{\min}$ H	NH <sub>2</sub>	$\Delta V_{\min}$ OH	CH <sub>3</sub>	F	Cl	CF <sub>3</sub>	CHO	CN	NO <sub>2</sub>
1a	-22.2	0.3	1.5	-0.1	6.0	8.2	7.0	7.1	11.1	11.5
1b	-22.5	0.2	0.8	0.0	3.3	4.4	3.9	4.1	6.1	6.1
1c	-22.5	-0.7	0.4	0.0	1.9	2.6	2.3	2.5	1.9	3.6
2a	-18.6	-11.9	-6.8	-3.1	1.6	5.3	10	11.3	15.0	18.7
2b	-18.4	-10.2	-6.0	-2.4	0.5	3.6	7.7	9.3	11.6	14.9
2c	-18.3	-6.0	-5.0	-2.1	0.3	2.7	6.1	7.8	9.4	12.4
3a	-13.8	-12.1	-6.8	-4.6	-0.2	1.9	10.1	10.8	15.2	17.6
3b	-10.2	-9.9	-6.0	-4.1	-0.8	0.5	7.5	8.2	11.5	13.3
3c	-8.0	-5.2	-5.0	-3.5	-0.9	0.1	5.9	6.5	9.2	10.5
4a	-19.5	-6.3	-2.3	-1.4	2.0	4.5	7.1	8.4	11.0	12.8
4b	-19.1	-2.9	-1.1	-0.8	1.2	2.4	3.7	4.3	5.8	6.7
4c	-18.9	-1.1	-0.5	-0.4	0.8	3.8	2.1	2.4	3.4	3.9
5a	-18.4	-6.1	-2.4	-1.7	2.1	4	7.8	9.7	12.2	14.9
5b	-17.1	-3.7	-2.0	-1.1	1.1	2.3	4.6	6.4	7.5	9.7
5c	-16.6	-2.1	-0.8	-0.6	0.8	1.5	3.1	4.2	5.1	6.8
6a	-19.0	-4.5	-1.6	-1.2	1.6	3.3	5.1	6.2	8.0	9.5
6b	-18.8	-3.3	-1.3	-0.9	1.3	2.6	4.0	5.0	6.3	7.5
6c	-18.6	-1.9	-0.9	-0.6	1.1	2.1	3.2	4.0	5.1	6.0

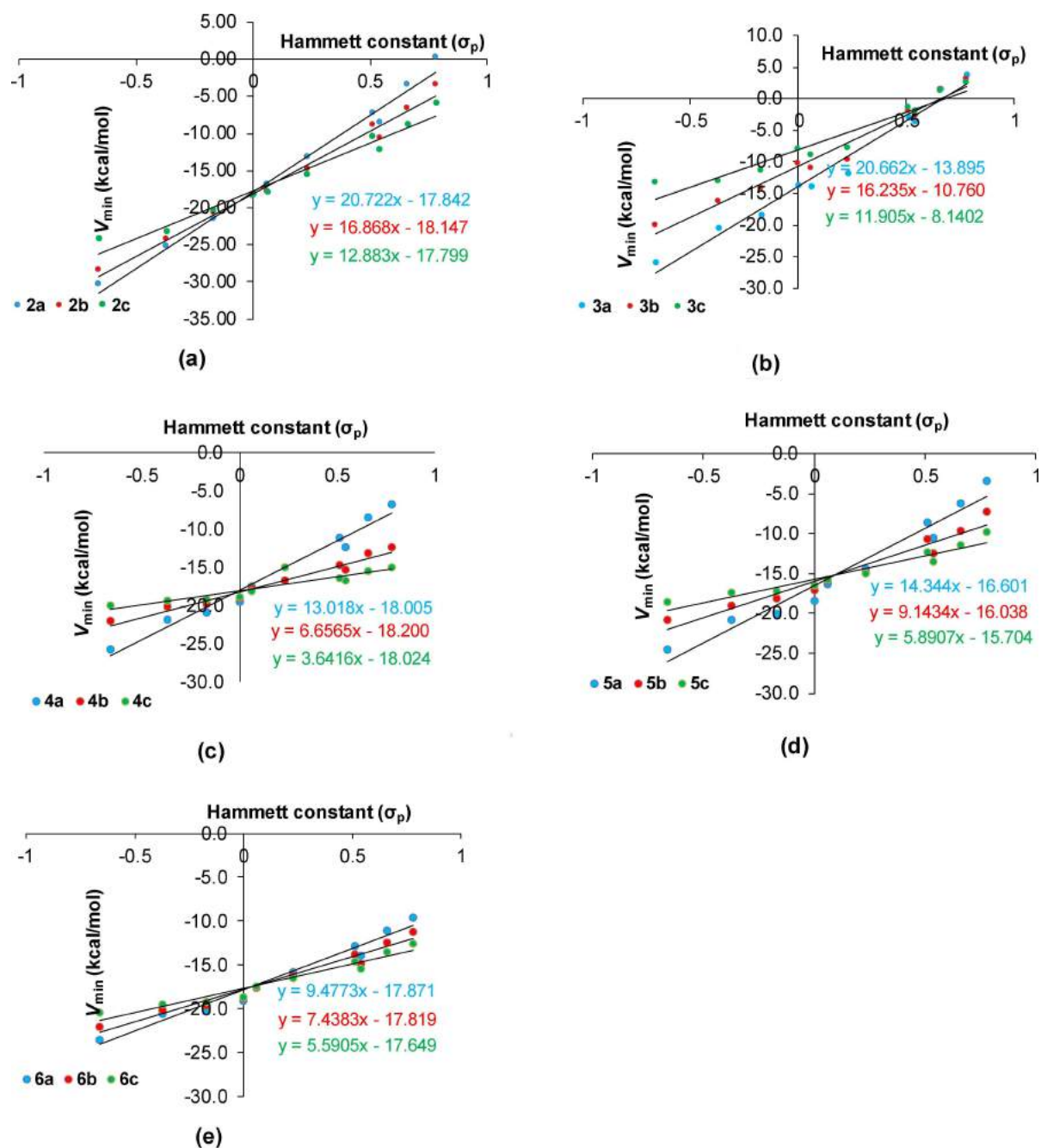


Figure 4. Correlation of  $V_{\min}$  with Hammett parameter ( $\sigma_p$ ) of a) alkenyl, b) alkylnyl, c) phenyl, d) thiophenyl, and e) polyacene systems.

Table S1) suggests that the MESP topographical quantity  $V_{\min}$  is highly suited as an electronic descriptor to quantify the electron donating and withdrawing nature of a substituent. The slope of the correlation plots decreases as  $n$  increase in the spacer length. Since  $\sigma_p = 0$  stands for the unsubstituted systems, the Y-intercept of the correlation plot corresponds to  $V_{\min}$  of the unsubstituted system. Indeed, the Y-intercept and  $V_{\min}$  of the unsubstituted system show very close agreement.

The unsubstituted alkylnyl systems, (**3a–3c**) shows  $V_{\min}$  values at  $-13.8$ ,  $-10.2$ , and  $-8.0$  kcal mol $^{-1}$ , respectively. The magnitude of these values are smaller than the unsubstituted

alkenyl systems indicating the more electronegative  $C_{sp}$  hybridized carbons in alkylnyl systems than  $C_{sp2}$  in alkenyl systems. Similar to **2**, resonance effect dominates in **3** except for  $X=CH_3$  and  $X=CF_3$ . The magnitude of electron withdrawing effect ( $\Delta V_{\min}$ ) obtained for substituents such as  $NO_2$ ,  $CN$ ,  $CHO$ ,  $CF_3$ ,  $Cl$ , and  $F$  is very similar to that found for  $C_2H_3$ -alkenyl- $X$  systems which indicates that substituent effect transmission power is similar for  $C=C$  double bonds and  $C\equiv C$  triple bonds.

The unsubstituted systems with phenyl ring spacers, **4a–4c** show  $V_{\min}$  values at  $-19.5$ ,  $-19.1$ , and  $-18.9$  kcal mol $^{-1}$ , respectively. The electron donating  $NH_2$ ,  $OH$ , and  $CH_3$  substitu-

ents enhance the negative character of  $V_{min}$  while the electron withdrawing F, Cl,  $CF_3$ , CHO, CN, and  $NO_2$  substituents diminish it. The similar  $V_{min}$  feature has been noticed for systems containing thiophenyl spacers, **5a–5c** and polyacene spacers, **6a–6c** (Table 1). In **4** series with  $n=2$  and 3, adjacent two phenyl units are twisted away from planarity which gives a diminishing effect on the electron donating/withdrawing ability of the substituent. The C–C single bond connection between two phenyl units in **4** proposes a significant inductive effect along with resonance. In polyacenes, resonance effect dominates over the inductive effect. In **4**, **5** and **6** series, increase in spacer length has a decreasing effect on the transmission power of the substituent effect.

## 2.2. $V_{min}$ -Based Quantification of Substituent Effect Transmission Power of Spacers

When a reacting center and substituent are separated by a variety of spacers, significant variations in the molecular properties can be observed.<sup>[19]</sup> The transmission of the substituent effect through olefinic systems showed the applicability of  $\rho$  in calculating the substituent effect transmission power. From the previous studies,<sup>[10b,d]</sup> it is understood that the transmission power of a spacer can be quantified by the transmission coefficient ( $\gamma$ ) defined as  $\gamma = \rho_s / \rho_o$ , where  $\rho_s$  is the reaction constant of a spacer for which the transmission power has to be quantified and  $\rho_o$  is the reaction constant of the reference group. Since  $V_{min}$  provides an alternative measure of substituent effects for  $\pi$ -conjugated systems, the correlation of  $V_{min}$  with  $\sigma_p$  can be used to evaluate the transmission ability of various spacers using the equation,  $V_{min} = \rho\sigma_p + \text{constant}$ . Therefore, linear regression analysis between  $V_{min}$  and  $\sigma_p$  values is carried out to find the  $\rho$  values (Table 3). In order to calculate the transmission coefficients ( $\gamma$ ), the phenyl group substituted **4a** is taken as the reference system for all the spacers. For **4a** systems,  $V_{min} = 13.018(\sigma_p) - 18.00$  and the slope of this equation ( $\rho_{4a}$ ) is used as  $\rho_o$  to determine  $\gamma$ . For example, the  $\gamma$  value for **2a** is calculated as  $\gamma = \rho_{2a} / \rho_{4a} = 20.722 / 13.018 = 1.592$  meaning that the transmission power of **2a** is 1.592 times higher than

**Table 3.** Slope, intercept, reaction constant ( $\rho_s$ ), correlation coefficient (R) and transmission coefficient ( $\gamma$ ) of various spacers.

X	Slope	Intercept	$\rho_s$	R	$\gamma$
<b>2a</b>	20.722	−17.84	20.722	0.994	1.592
<b>2b</b>	16.868	−18.15	16.868	0.993	1.296
<b>2c</b>	12.883	−17.80	12.883	0.981	0.989
<b>3a</b>	20.662	−13.90	20.662	0.988	1.587
<b>3b</b>	16.235	−10.76	16.235	0.985	1.247
<b>3c</b>	11.905	−8.14	11.905	0.962	0.914
<b>4a</b>	13.018	−18.00	13.018	0.987	1.000
<b>4b</b>	6.667	−18.20	6.667	0.984	0.512
<b>4c</b>	3.642	−18.02	3.642	0.895	0.280
<b>5a</b>	14.344	−16.60	14.344	0.979	1.102
<b>5b</b>	9.143	−16.03	9.143	0.973	0.702
<b>5c</b>	5.891	−15.70	5.891	0.961	0.452
<b>6a</b>	9.477	−17.87	9.477	0.984	0.728
<b>6b</b>	7.438	−17.81	7.438	0.983	0.571
<b>6c</b>	5.591	−17.65	5.591	0.974	0.429

phenyl ring. Among the  $\pi$ -bonded spacers, for  $n=1$ , the order of substituent effect transmission power of spacers is **2a**  $\approx$  **3a** > **5a** > **4a** > **6a**. On the basis of the average of all the  $\gamma$  values for a particular spacer from  $n=1–3$ , the order of transmission power of substituent effects is as follows: **2a–2c** > **3a–3c** > **5a–5c** > **4a–4c** > **6a–6c**. This order is in agreement with the experimental findings<sup>[10b]</sup> and suggesting the appropriateness of  $V_{min}$  method for the present study.

## 2.3. Combination of Two Different Spacers and Substituent Selectivity

To understand the transmission ability of a combination of two different spacers, we selected six types of spacers as shown in Figure 5. In **7a** and **7b** the substituent is connected to the double bonded carbon and an aromatic ring, respectively. In Table 4, the  $V_{min}$  values obtained for all the hetero spacers are reported. For substituent 'H' the  $V_{min}$  values of **7a** and **7b** are  $-18.76$  and  $-18.89$  kcal/mol showing a variation of  $0.13$  kcal mol<sup>−1</sup> between the two isomers. However, for other substituents, the difference in  $V_{min}$  is found to be less than  $\sim 1.0$  kcal mol<sup>−1</sup> suggesting that the electron donating or withdrawing nature is not highly affected whether 'X' is attached to the double bond or the phenyl ring. The  $V_{min}$  values for substituent 'H' of **8a** and **8b** are  $-16.32$  and  $-15.88$  kcal mol<sup>−1</sup> indicating that total electron withdrawing nature of ethynylbenzene is more when ethyne is attached directly to the olefinic

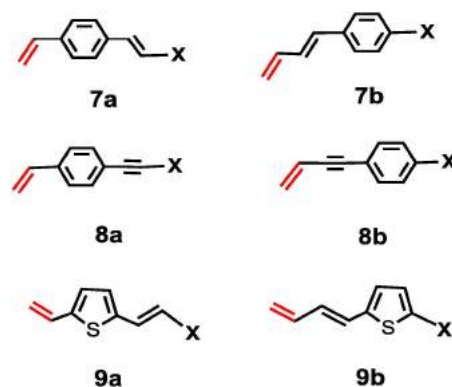


**Figure 5.** Spacers considered to quantifying the effect of the combination of two different spacers.

**Table 4.**  $V_{min}$  values (kcal/mol) obtained for hetero spacers.

X	7a	7b	8a	8b	9a	9b
<b>NH<sub>2</sub></b>	−24.85	−24.22	−22.78	−21.02	−24.16	−23.72
<b>OH</b>	−21.96	−21.08	−20.27	−17.95	−21.52	−20.83
<b>Me</b>	−20.21	−20.21	−18.83	−17.07	−19.39	−19.77
<b>H</b>	−18.76	−18.89	−16.32	−15.88	−17.51	−18.32
<b>F</b>	−17.70	−17.70	−16.50	−14.56	−16.75	−17.13
<b>Cl</b>	−15.81	−15.75	−15.44	−12.80	−14.56	−15.44
<b>CF<sub>3</sub></b>	−13.24	−13.49	−10.86	−10.67	−11.42	−12.30
<b>CHO</b>	−12.05	−12.17	−9.79	−9.60	−8.85	−10.35
<b>CN</b>	−10.17	−10.48	−10.48	−7.78	−7.97	−8.85
<b>NO<sub>2</sub></b>	−7.97	−8.79	−8.79	−6.28	−5.21	−6.34



moiety. Further, the electron withdrawing and donating substituents show maximum influence when they are attached to the phenyl ring. Additionally, for **9a** and **9b**,  $V_{\min}$  values for the unsubstituted systems are observed at  $-17.51$  and  $-18.32$  kcal/mol, respectively meaning that the variation is only  $0.81$  kcal/mol. In fact, for all the substituent except CHO and  $\text{NO}_2$ , the variation is less than  $\sim 1$  kcal/mol. This confirms that electronic effect is not highly affected whether 'X' is attached to a double bond or thiophenyl ring. In general, a spacer made up of two different moieties, substituent effect transmission power of 'X' can show a minor variation depending on the connectivity of X with the spacer unit.

### 3. Conclusions

The substituent effect transmission power of electron donating and withdrawing substituents on a terminal CC double bond has been assessed using MESP  $V_{\min}$  analysis. The  $V_{\min}$  observed on this bond showed significant change with respect to the electron donating/withdrawing nature of the substituent as well as the nature and length of the spacer unit. The  $V_{\min}$  correlates strongly with an inductive parameter for systems consisting of alkyl spacers. Similarly, for all the  $\pi$ -conjugated systems, strong linear correlations were observed between Hammett substituent constant and  $V_{\min}$ . The decreasing trend of slope values with an increase in the size of spacer length revealed the strongly diminishing nature of the substituent effect transmission. From the slope of the correlation plots, the transmission power of spacers are obtained which can be arranged in the order alkenyl > alkynyl > thiophenyl > phenyl > polyacene. For systems having alkyl spacers, transmission of substituent effect is the least as the inductive effect has a rapidly diminishing character with the increase in the size of the spacer unit. In summary, among all the spacer groups, alkenyl and alkynyl units are the most effective for the substituent effect transmission.

### 4. Computational Details

Geometry optimization has been carried out with B3LYP/6-31G(d, p) density functional theory method.<sup>[20]</sup> MESP computations are also done at the same level of theory. Previous studies showed that this method is adequate for calculating MESP features.<sup>[5b,h,21]</sup> MESP,  $V(\mathbf{r})$  at a point  $\mathbf{r}$  due to a molecular system with nuclear charges located at  $\mathbf{R}_A$  and electron density  $\rho(\mathbf{r})$  is expressed in Equation (1) where  $N$  is the total number of nuclei in the molecule and  $Z_A$  is the charge on nucleus  $A$ , located at the distance  $|\mathbf{R}_A|$ .

$$V(\mathbf{r}) = \sum_A^N \frac{Z_A}{|\mathbf{r} - \mathbf{R}_A|} - \int \frac{\rho(\mathbf{r}') d^3r'}{|\mathbf{r} - \mathbf{r}'|} \quad (1)$$

In MESP topography, a negative-valued minimum ( $V_{\min}$ ) is often observed in electron-rich regions such as lone pair,  $\pi$ -bonds, and anionic sites of a molecular system. Gaussian 09

programme package has been used for all the calculations.<sup>[22]</sup> Vibrational frequency analysis is done with the same level of theory to confirm that the number of imaginary frequencies is zero for all the optimized geometries.

### Acknowledgements

Authors thank DST-SERB for funding through GAP137239 and also gratefully acknowledge the CSIR 4th PI for HPC facility and NIIST IT lab for computational support.

### Conflict of Interest

The authors declare no conflict of interest.

**Keywords:** density functional calculations · molecular electrostatic potential · spacers · substituent effect · transmission power.

- [1] a) T. M. Krygowski, B. T. Stepień, *Chem. Rev.* **2005**, *105*, 3482–3512; b) O. Exner, T. M. Krygowski, *Chem. Soc. Rev.* **1996**, *25*, 71–75.
- [2] a) C. Hansch, A. Leo, R. W. Taft, *Chem. Rev.* **1991**, *91*, 165–195; b) W. Adcock, N. A. Trout, *Chem. Rev.* **1999**, *99*, 1415–1435; c) O. Exner, S. Bohm, *Curr. Org. Chem.* **2006**, *10*, 763–778; d) L. P. Hammett, *J. Am. Chem. Soc.* **1937**, *59*, 96–103.
- [3] H. H. Jaffé, *Chem. Rev.* **1953**, *53*, 191–261.
- [4] T. M. Krygowski, M. A. Dobrowolski, K. Zborowski, M. K. Cyranski, *J. Phys. Chem.* **2006**, *19*, 889–895.
- [5] a) C. H. Suresh, S. R. Gadre, *J. Am. Chem. Soc.* **1998**, *120*, 7049–7055; b) C. H. Suresh, S. R. Gadre, *J. Phys. Chem. A* **2007**, *111*, 710–714; c) G. S. Remya, C. H. Suresh, *Phys. Chem. Chem. Phys.* **2016**, *18*, 20615–20626; d) T. M. Krygowski, K. Ejsmont, B. T. Stepień, M. K. Cyranski, J. Poater, M. Sola, *J. Org. Chem.* **2004**, *69*, 6634–6640; e) T. M. Krygowski, M. Palusiak, A. Płonka, J. E. Zachara-Horeglad, *J. Phys. Org. Chem.* **2007**, *20*, 297–306; f) T. M. Krygowski, J. E. Zachara-Horeglad, M. Palusiak, *J. Org. Chem.* **2010**, *75*, 4944–4949; g) T. M. Krygowski, W. P. Oziminski, *J. Mol. Model.* **2014**, *20*, 2352; h) S. E. Wheeler, K. N. Houk, *J. Am. Chem. Soc.* **2009**, *131*, 3126–3127; i) S. E. Wheeler, K. N. Houk, *J. Am. Chem. Soc.* **2009**, *131*, 3126–3127; j) S. E. Wheeler, *J. Am. Chem. Soc.* **2011**, *133*, 10262–10274; k) S. E. Wheeler, *Acc. Chem. Res.* **2013**, *46*, 1029–1038; l) B. Galabov, S. Ilieva, H. F. Schaefer, *J. Org. Chem.* **2006**, *71*, 6382–6387; m) B. Galabov, V. Nikolova, S. Ilieva, *Chem. Eur. J.* **2013**, *19*, 5149–5155.
- [6] a) R. W. Taft, *J. Am. Chem. Soc.* **1953**, *75*, 4231–4238; b) M. Charton, *Prog. Phys. Org. Chem.* **1981**, *119*–251.
- [7] C. G. Swain, E. C. Lupton, *J. Am. Chem. Soc.* **1968**, *90*, 4328–4337.
- [8] a) B. Galabov, S. Ilieva, G. Koleva, W. D. Allen, H. F. Schaefer III, P. von R. Schleyer, *Wiley Interdiscip. Rev.: Comput. Mol. Sci.* **2013**, *3*, 37–55; b) F. B. Sayyed, C. H. Suresh, *New J. Chem.* **2009**, *33*, 2465–2471; c) F. B. Sayyed, C. H. Suresh, S. R. Gadre, *J. Phys. Chem. A* **2010**, *114*, 12330–12333; d) F. B. Sayyed, C. H. Suresh, *J. Phys. Chem. A* **2011**, *115*, 9300–9307; e) F. B. Sayyed, C. H. Suresh, *J. Phys. Chem. A* **2011**, *115*, 5660–5664; f) F. B. Sayyed, C. H. Suresh, *Chem. Phys. Lett.* **2012**, *523*, 11–14.
- [9] a) S. Böhm, J. Kuthan, *Int. J. Quantum Chem.* **1984**, *26*, 21–33; b) K. H. Kim, Y. C. Martin, *J. Org. Chem.* **1991**, *56*, 2723–2729; c) J. S. Murray, T. Brinck, P. Politzer, *J. Mol. Struct.* **1992**, *255*, 271–281; d) H. Szatylowicz, T. Siodla, O. A. Stasyuk, T. M. Krygowski, *Phys. Chem. Chem. Phys.* **2016**, *18*, 11711–11721; e) T. Krygowski, N. Sadlej-Sosnowska, *Struct. Chem.* **2011**, *22*, 17–22.
- [10] a) C. A. van Walree, L. W. Jenneskens, *Tetrahedron* **1997**, *53*, 5825–5830; b) M. Charton, *J. Org. Chem.* **1961**, *26*, 735–738; c) S. A. Myers, R. A. Assink, D. A. Loyb, K. J. Sheac, *J. Chem. Soc. Perkin Trans. 2* **2000**, 545–549; d) K. Bowden, *Can. J. Chem.* **1963**, *41*, 2781–2793; e) K. Waisser, J. Kunes, L. Kubicova, M. Budesinsky, O. Exner, *Magn. Reson. Chem.* **1997**, *35*, 543–548; f) W. Adcock, *J. Phys. Org. Chem.* **2009**, *22*, 1065–1069; g) W. Adcock, A. Krstic, *Magn. Reson. Chem.* **2000**, *38*, 115–122; h) W.

- Adcock, N. Trout, *Magn. Reson. Chem.* **1998**, *36*, 181–195; i) A. R. Campanelli, A. Domenicano, G. Piacente, F. Ramondo, *J. Phys. Chem. A* **2010**, *114*, 5162–5170.
- [11] a) E. Scrocco, J. Tomasi, in *New concepts II*, Springer, **1973**, pp. 95–170; b) E. Scrocco, J. Tomasi, in *Advances in quantum chemistry*, Vol. 11, Elsevier, **1978**, pp. 115–193.
- [12] a) S. R. Gadre, I. H. Shrivastava, *J. Chem. Phys.* **1991**, *94*, 4384–4390; b) F. Luque, M. Orozco, P. Bhadane, S. Gadre, *J. Chem. Phys.* **1994**, *100*, 6718–6726; c) S. R. Gadre, P. K. Bhadane, *J. Chem. Phys.* **1997**, *107*, 5625–5626; d) S. R. Gadre, C. H. Suresh, *J. Org. Chem.* **1997**, *62*, 2625–2627.
- [13] C. H. Suresh, P. Alexander, K. P. Vijayalakshmi, P. K. Sajith, S. R. Gadre, *Phys. Chem. Chem. Phys.* **2008**, *10*, 6492–6499.
- [14] F. B. Sayyed, C. H. Suresh, *Tetrahedron Lett.* **2009**, *50*, 7351–7354.
- [15] C. H. Suresh, *Inorg. Chem.* **2006**, *45*, 4982–4986.
- [16] a) P. K. Sajith, C. H. Suresh, *Inorg. Chem.* **2012**, *51*, 967–977; b) P. K. Sajith, C. H. Suresh, *Dalton Trans.* **2010**, *39*, 815–822; c) J. Mathew, T. Thomas, C. H. Suresh, *Inorg. Chem.* **2007**, *46*, 10800–10809; d) J. Mathew, C. H. Suresh, *Inorg. Chem.* **2010**, *49*, 4665–4669.
- [17] a) C.-J. Tan, C.-S. Yang, Y.-C. Sheng, H. W. Amini, H.-H. G. Tsai, *J. Phys. Chem. C* **2016**, *120*, 21272–21284; b) C. Teng, X. Yang, C. Yang, H. Tian, S. Li, X. Wang, A. Hagfeldt, L. Sun, *J. Phys. Chem. C* **2010**, *114*, 11305–11313; c) Y. Hua, J. He, C. Zhang, C. Qin, L. Han, J. Zhao, T. Chen, W.-Y. Wong, W.-K. Wong, X. Zhu, *J. Mater. Chem. A* **2015**, *3*, 3103–3112; d) Y. Ding, Y. Jiang, W. Zhang, L. Zhang, X. Lu, Q. Wang, G. Zhou, J.-m. Liu, K. Kempa, J. Gao, *J. Phys. Chem. C* **2017**, *121*, 16731–16738.
- [18] a) F. Massoth, P. Politzer, M. Concha, J. Murray, J. Jakowski, J. Simons, *J. Phys. Chem. B* **2006**, *110*, 14283–14291; b) P. Politzer, L. Abrahmsen, P. Sjöberg, *J. Am. Chem. Soc.* **1984**, *106*, 855–860.
- [19] J. Frederick, J. Dippy, *Chem. Rev.* **1939**, *25*, 151–211.
- [20] a) A. D. Becke, *J. Chem. Phys.* **1993**, *98*, 5648–5652; b) C. Lee, W. Yang, R. G. Parr, *Phys. Rev. B* **1988**, *37*, 785.
- [21] F. B. Sayyed, C. H. Suresh, *New J. Chem.* **2009**, *33*, 2465–2471.
- [22] M. J. Frisch, G. W. Trucks, H. B. Schlegel, G. E. Scuseria, M. A. Robb, J. R. Cheeseman, G. Scalmani, V. Barone, B. Mennucci, G. A. Petersson, H. Nakatsuji, M. Caricato, X. Li, H. P. Hratchian, A. F. Izmaylov, J. Bloino, G. Zheng, J. L. Sonnenberg, M. Hada, M. Ehara, K. Toyota, R. Fukuda, J. Hasegawa, M. Ishida, T. Nakajima, Y. Honda, O. Kitao, H. Nakai, T. Vreven, J. J. A. Montgomery, J. E. Peralta, F. Ogliaro, M. Bearpark, J. J. Heyd, E. Brothers, K. N. Kudin, V. N. Staroverov, T. Keith, R. Kobayashi, J. Normand, K. Raghavachari, A. Rendell, J. C. Burant, S. S. Iyengar, J. Tomasi, M. Cossi, N. Rega, J. M. Millam, M. Klene, J. E. Knox, J. B. Cross, V. Bakken, C. Adamo, J. Jaramillo, R. Gomperts, R. E. Stratmann, O. Yazyev, A. J. Austin, R. Cammi, C. Pomelli, J. W. Ochterski, R. L. Martin, K. Morokuma, V. G. Zakrzewski, G. A. Voth, P. Salvador, J. J. Dannenberg, S. Dapprich, A. D. Daniels, O. Farkas, J. B. Foresman, J. V. Ortiz, J. Cioslowski, D. J. Fox, Gaussian 09, Revision D.01; Gaussian, Inc. Wallingford, CT, 2013.

---

Manuscript received: February 28, 2019  
Accepted manuscript online: April 11, 2019  
Version of record online: June 13, 2019



Cite this: *New J. Chem.*, 2020, **44**, 7200

# Density functional theory study on the donating strength of donor systems in dye-sensitized solar cells†

Velayudhan V. Divya<sup>ab</sup> and Cherumuttathu H. Suresh<sup>id</sup> \*<sup>ab</sup>

The electron-donating strengths of donor (D) moieties in thirteen donor- $\pi$ -acceptor systems (D1- $\pi$ -A to D13- $\pi$ -A wherein  $\pi$ - and A represent butadiene and cyanoacrylic acid units, respectively) have been studied using B3LYP/cc-pVDZ level density functional theory (DFT) calculations. The selected D moieties are encountered as a part of an organic sensitizer molecule in dye-sensitized solar cell (DSSC) applications. When the D moiety is joined with  $\pi$ -A, a certain amount of electron donation from D to A occurs leading to an increase in electron density at the A site of D- $\pi$ -A compared to the A site of  $\pi$ -A. This electron reorganization is quantified in terms of a change in molecular electrostatic potential (MESP) minimum ( $\Delta V_{\text{mA}}$ ) at the acceptor site, the CN group of the cyanoacrylic acid. The  $\Delta V_{\text{mA}}$  is always negative, in the range of  $-11.0$  to  $-2.6$  kcal mol<sup>-1</sup> which provides a quick assessment of the rank order of the electron-donating nature of the D moieties in the ground state of D- $\pi$ -A. The optical and photovoltaic properties of D and D- $\pi$ -A systems are also determined at the TD-CAM-B3LYP/cc-pVDZ//B3LYP/cc-pVDZ level. An absorption red shift ( $\Delta\lambda_{\text{max}}$ ) in the range of 81–242 nm is observed when D moieties change to D- $\pi$ -A systems. The ground state property  $\Delta V_{\text{mA}}$  showed a strong linear correlation with the excited state property  $\Delta\lambda_{\text{max}}$ . Furthermore,  $\Delta V_{\text{mA}}$  is found to be proportional to the open-circuit voltage ( $V_{\text{OC}}$ ). The resemblance of highest occupied molecular orbital (HOMO) and lowest unoccupied molecular orbital (LUMO) energies of the D- $\pi$ -A system with the respective energies of donor and  $\pi$ -A systems shows that the donor tunes the HOMO, while  $\pi$ -A tunes the LUMO. Among the thirteen D- $\pi$ -A systems, *N,N*-dialkylaniline, and julolidine are rated as the best donors for the photovoltaic applications. This study shows that the MESP based assessment of the donating strength of donor systems offers a powerful rational design strategy for the development of efficient dyes for DSSC applications.

Received 11th February 2020,  
Accepted 1st April 2020

DOI: 10.1039/d0nj00723d

rsc.li/njc

## Introduction

Dye-sensitized solar cells (DSSCs) have been regarded as a highly potential alternative to conventional silicon-based solar cells due to their high molar extinction coefficient, low production cost, simple synthetic strategy and easy structural modifications.<sup>1–5</sup> DSSCs also perform relatively better than other traditional solar cells under diffuse light conditions and at higher temperatures.<sup>4–6</sup> In DSSC applications, the sensitizers synthesized can be divided into two broad areas, *viz.* metal-based systems such as Ru(II) polypyridyl complexes, and Zn(II) porphyrins<sup>7</sup> and the metal-free donor- $\pi$ -acceptor (D- $\pi$ -A) type organic dyes.<sup>8</sup> The Ru-based

polypyridyl sensitizers attained the highest power conversion efficiency over 11% more than most of the metal-free sensitizers.<sup>9–14</sup>

This is due to the ability of metal sensitizers to absorb solar irradiation up to the near-infrared region, while other metal-free dye sensitizers are absorbed in the shorter wavelength region.<sup>8,13,15</sup> So, a highly efficient sensitizer should have an absorption maximum near to the Vis-NIR region associated with a long-lived charge excited state.<sup>16,17</sup> Due to the highly expensive and toxic synthetic procedures involved in metal sensitizers, the organic dyes exhibit remarkable importance in DSSC applications.<sup>8</sup> Recent studies proposed important structural modifications in organic dyes<sup>18,19</sup> to achieve a high power conversion efficiency (PCE) and over 12% has been achieved with a metal-free alkoxy-silyl carbazole dye as a sensitizer.<sup>20</sup> Yao *et al.* reported an improved PCE of 12.5% with a metal-free indenoperylene based D- $\pi$ -A dye,<sup>21</sup> the best-known metal-free organic dye. In 2017, a simple designing strategy over the phenothiazine moiety with ethynyl-pyrene enabled a PCE of 12%.<sup>22</sup> The other recent milestones in DSSCs include co-sensitization, which enables higher photovoltaic performance

<sup>a</sup> Chemical Sciences and Technology Division, CSIR-National Institute for Interdisciplinary Science and Technology (CSIR-NIIST), Thiruvananthapuram, Kerala 695 019, India. E-mail: sureshch@niist.res.in, sureshch@gmail.com

<sup>b</sup> Academy of Scientific and Innovative Research (AcSIR), CSIR-NIIST Campus, Trivandrum, India

† Electronic supplementary information (ESI) available: See DOI: 10.1039/d0nj00723d

over 14% with a collaborative sensitization by silyl and carboxy anchoring groups.<sup>23</sup> Many studies proposed the structural modification of the donor group of the D- $\pi$ -A dye to achieve higher efficiency as increasing the electron donating strength generally broadens and intensifies the region of absorption.<sup>24-26</sup>

In general, a dye sensitizer with a D- $\pi$ -A framework can be modified at donor,<sup>27,28</sup> spacer,<sup>29-32</sup> and anchoring groups<sup>33-35</sup> to improve the PCE. Typically, the acceptor portion (A) of the dye anchored onto the TiO<sub>2</sub> semiconductor favours the charge transfer of the excited electrons to the conduction band of the semiconductor.<sup>36</sup> The oxidized dye is then regenerated by the electron transfer from the electrolyte (I<sup>-</sup>/I<sub>3</sub><sup>-</sup> couple), while the electrolyte couple regains the electron from the platinum counter electrode.<sup>4,37</sup> Therefore, for an efficient dye sensitizer, an effective electron injection can occur from the dye to the TiO<sub>2</sub> semiconductor if its highest occupied molecular orbital (HOMO) is observed at a level slightly below the redox couple of the I<sup>-</sup>/I<sub>3</sub><sup>-</sup> electrolyte (-4.8 eV) and the lowest unoccupied molecular orbital (LUMO) is observed above the conduction band of TiO<sub>2</sub> (-4.0 eV).<sup>8,38,39</sup>

Apart from the simple D- $\pi$ -A framework, several other configurations like D-D- $\pi$ -A,<sup>40-42</sup> D-A- $\pi$ -A,<sup>43-46</sup> D- $\pi$ -A-A,<sup>47</sup> (D- $\pi$ -A)<sub>2</sub>,<sup>48</sup> and double D- $\pi$ -A bridges<sup>49</sup> were also introduced and revealed that the introduction of additional donors, acceptors, and the extension of  $\pi$  conjugation reduces the HOMO-LUMO energy gap and redshifts the absorption maximum. In other words, for the improved PCE, the donor should be stable, and electron-rich for the effective electron injection to the TiO<sub>2</sub> conduction band,<sup>28,50,51</sup> thereby broadening their absorption to the Vis-NIR region.<sup>50,51</sup> Therefore, for effective dye designing, it is very important to understand the electronic and photophysical properties of the dye systems.<sup>44</sup> Density functional theory (DFT) and Time-dependent density functional theory (TD-DFT) can afford a more efficient approach to understand and predict these structural and electronic features without any time delay compared to the traditional trial and error methods.<sup>52-63</sup> Previous studies have shown that the donor strength has a significant role in absorption maximum, the kinetics of electron injection and light-harvesting efficiency.<sup>64,65</sup> Recently, the relevance of the theoretical estimation of donor strength in organic electronics has been explained by Köse.<sup>66</sup>

Thirteen typically used donor building blocks (Fig. 1) in the DSSC applications are selected for this DFT/TDDFT study (D1-D13).<sup>24,31,67-72</sup> Among them, D1-D4 are aromatic hydrocarbon systems whereas the remaining donor moieties contain at least one lone pair bearing a nitrogen centre (D5-D13). The estimation of the donating strength is assessed by molecular electrostatic potential (MESP) topographical features of these donor molecules and their corresponding D- $\pi$ -A systems. The MESP distribution is useful to understand the charge distribution within a molecule,<sup>73-76</sup> and the regions with negative MESP values indicate electron-dense regions while positive-valued areas represent electron-deficient regions. The MESP based interpretation has been used for the study of substituent effects, intermolecular interactions, non-covalent interactions, hydrogen bonding, cation- $\pi$  interactions, aromaticity and a variety of chemical phenomena.<sup>77-80</sup> MESP analysis has been used in the

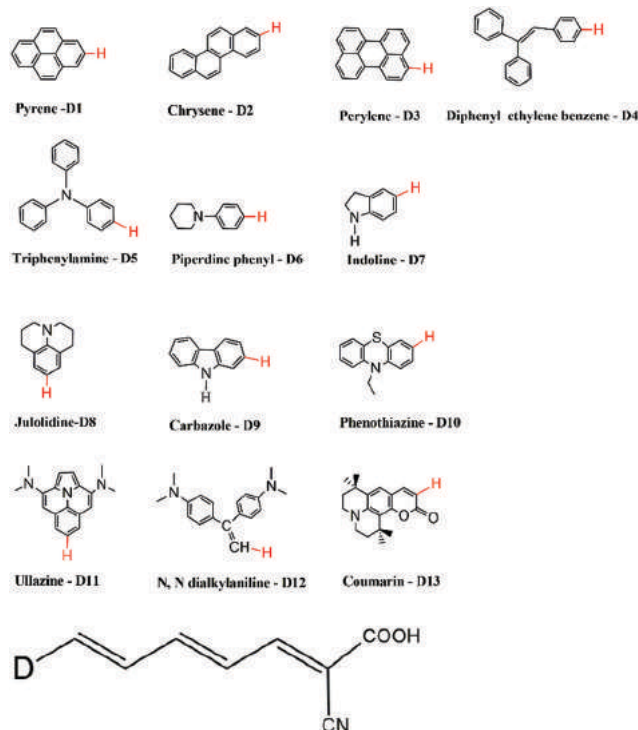


Fig. 1 ChemDraw representation of donors (D1-D13) and D- $\pi$ -A systems. The bond shown in red colour is replaced with the  $\pi$ -A part to design the D- $\pi$ -A system.

field of organometallic chemistry for the quantification of the electron-donating strength of phosphine and N-heterocyclic ligands.<sup>73</sup> The global minimum ( $V_{\min}$ ) of MESP near the two electron donor atom (P or N) indicates the net donating ability of the ligand for making a coordination bond with a metal centre. Furthermore, Suresh and co-workers proved that MESP minimum ( $V_{\min}$ ) analysis is very effective for the quantification of the inductive, resonance, steric and proximity effects of substituents.<sup>75,81-84</sup> Recently the substituent effect transmitting power ( $\gamma$ ) through various spacer units is also calculated *via* MESP analysis and showed that  $V_{\min}$  values are beneficial for the quantification of the transmission power of spacers.<sup>85</sup> The study recommends the usage of short alkenyl systems as spacers for effective electronic transmission. Moreover, the above reliable studies confirmed that MESP is a powerful descriptor, capable of predicting the electronic properties of the molecular systems effectively. The present study focuses on the MESP analysis of D- $\pi$ -A systems towards photovoltaic applications. The butadiene moiety (-HC=CH-CH=CH-) and the cyanoacrylic acid unit (-H<sub>2</sub>C=C(CN)-COOH) are used as the  $\pi$ -spacer and anchoring (A) group, respectively.

## Computational method

The ground state geometry optimization has been carried out using the B3LYP density functional theory (DFT) method<sup>86</sup> with the cc-pVDZ basis set.<sup>87</sup> This DFT method has been extensively used in the theoretical studies of organic dyes for dye-sensitized



solar cell applications.<sup>45,60</sup> Frequency calculations were also done at the same level of theory and confirmed that there were no imaginary frequencies. Vertical excitation energy calculations have been done for the first 7 states by using a long-range and solvation effect-corrected CAM-B3LYP/cc-pVDZ DFT method<sup>56</sup> in dichloromethane. The reliability of this method has been checked by doing the computation on experimentally known systems (Fig. S1, ESI†) using three more methods, *viz.* B3LYP,<sup>86</sup> PBE1PBE,<sup>88</sup> and  $\omega$ B97XD.<sup>89</sup> For all these methods, the solvation effects are incorporated through the self-consistent reaction field (SCRF) calculation implemented in the SMD (solvation model based on electron density) model.<sup>90</sup> The TD-DFT calculations showed that the result given by CAM-B3LYP is the most reliable to reproduce the experimental absorption maximum (Table S1, ESI†). DFT and TD-DFT calculations are done using the Gaussian 16 program package.<sup>91</sup> For quantifying the electron donating strength of donors in the D- $\pi$ -A system, molecular electrostatic potential (MESP) analysis has been performed at the B3LYP/cc-pVDZ level. MESP,  $V(r)$  at point  $r$  in the vicinity of a molecular system in the atomic unit can be calculated from the electron density  $\rho(r')$ , using eqn (1)

$$V(r) = \sum_A^N \frac{Z_A}{|r - R_A|} - \int \frac{\rho(r') dr'}{|r - r'|} \quad (1)$$

where  $N$  is the total number of nuclei present in the molecular system,  $Z_A$  is the charge on the nucleus  $A$  at a distance  $R_A$  and  $r'$  is a dummy integration variable.<sup>92,93</sup>

## Results and discussion

### MESP analysis of donor molecules

The MESP minima  $V_m$  are useful for locating the most electron-rich regions in the molecules. The  $V_m$  appears on the aromatic rings, hetero atoms and CC double bonds of donor molecules (D1–D13) which are shown in Fig. 2. Since all the systems contain at least one aromatic ring, the ring showing the most negative  $V_m$  ( $V_{mD}$ ) is taken for comparing the donor strength of each system. The  $V_{mD}$  values of all the systems are depicted in Fig. 2 along with other  $V_m$  values. In polycyclic aromatic hydrocarbon (PAH) systems (D1–D3),  $V_{mD}$  values lie in a small range of  $-14.4$  to  $-14.9$  kcal mol<sup>-1</sup> which can be attributed to the similar  $\pi$ -conjugation features which are not affected by a hetero atom or a substituent. In the D4 system, two phenyl rings show a nearly coplanar arrangement with the CC double bond and their  $V_{mD}$  ( $-16.1$  and  $-16.8$  kcal mol<sup>-1</sup>) values are more negative than a PAH while the third phenyl ring has a highly twisted arrangement with respect to the CC double bond and shows  $V_{mD} -13.7$  kcal mol<sup>-1</sup>. It appears that the presence of a conjugated CC bond in D4 enhances its electron density over the corresponding aromatic rings. In D5, three phenyl rings share the lone pair electron density from the nitrogen centre leading to a more negative character for  $V_{mD} -15.6$  kcal mol<sup>-1</sup> than a PAH. In D6, D7 and D8, an amino nitrogen centre is connected with an arene ring. In the piperidine-phenyl system D6, the nitrogen centre is more pyramidalized than the other

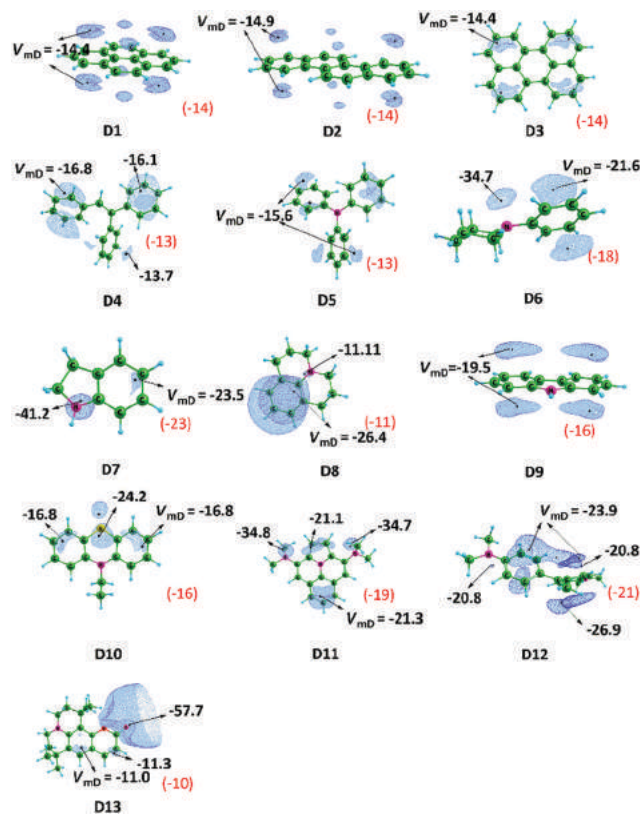


Fig. 2 MESP minima at the donor site, the  $V_{mD}$  of the donor systems. Isosurface values in kcal mol<sup>-1</sup> are given in brackets. Here carbon atoms are shown in green colour, while nitrogen, sulfur and oxygen atoms are shown in pink, yellow and red colours, respectively.

two and shows the least negative  $V_{mD}$  ( $-21.6$  kcal mol<sup>-1</sup>) among the three. In D7 and D8, fusing the  $N$ -alkyl unit/s with the aromatic ring improves the planarization of the  $N$ -centre, leading to more electron donation *via* +R effect to the arene ring. As a result, julolidine D8 shows the most electron-rich arene ring in terms of  $V_{mD} -26.4$  kcal mol<sup>-1</sup> followed by D7 ( $-23.5$  kcal mol<sup>-1</sup>). Compared to a PAH, carbazole arene rings show significantly more negative  $V_{mD}$  ( $-19.5$  kcal mol<sup>-1</sup>); here the sharing of the  $N$ -centre lone pair is with two aromatic rings which leads to less negative  $V_{mD}$  than D6–D8. Similarly, in D10, the sharing of the  $N$ -lone pair with two arene rings can be seen in addition to the effect of the hetero S atom. In this case,  $V_{mD}$  is less negative than carbazole. In D11, the combined effect of three  $N$ -centres can be attributed to the electron-rich nature of the arene ring ( $V_{mD} -21.3$  kcal mol<sup>-1</sup>) and among the  $N$ -centres, the  $N,N$ -dimethyl units are not fully effective for the influence of the +R contribution due to slight pyramidalization caused by steric congestions from the alkyl moiety of the adjacent five-membered ring. In D12, along with the +R contribution of  $N,N$ -dimethyl substituents, the conjugation effect of CC double bonds leads to relatively more electron-rich arene rings. The least negative  $V_{mD} -11.0$  kcal mol<sup>-1</sup> is observed in D13, the coumarin system. Here, the presence of a highly electron-withdrawing carbonyl group at the heterocyclic ring reduces the electron density on the aromatic ring.

### MESP analysis of D- $\pi$ -A systems

The donating strength of donor fragments in the D- $\pi$ -A system has been studied by MESP analysis. The MESP isosurface plot of a representative D- $\pi$ -A system (D12) is shown in Fig. 3a along with MESP minimum ( $V_m$ ) values at various positions. The positions selected for  $V_m$  analysis are (i) the donor site ( $V_{mD}$ ), (ii) the spacer site nearer to the donor ( $V_{mS}$ ) and (iii) the anchor site ( $V_{mA}$ ). The  $\pi$ -A portion is built by linking a butadiene moiety ( $\pi$ -spacer) with the cyanoacrylic acid moiety (A). Since the  $\pi$ -spacer and anchor units are the same for all donors, they have been considered as a reference system and the corresponding MESP minimum at their spacer ( $V_{mS}$ ) and anchoring sites ( $V_{mA}$ ) are evaluated for comparison with those of the D- $\pi$ -A system (Fig. 3b). The various MESP minimum values, *viz.*  $V_{mD}$ ,  $V_{mS}$ , and  $V_{mA}$  (Fig. S3, ESI<sup>†</sup>), are shown in Table 1 along with the most negative  $V_m$  of the donor molecule ( $V_{mD}$ ). In Table 1, the quantities  $\Delta V_{mD}$ ,  $\Delta V_{mS}$ , and  $\Delta V_{mA}$  represent the change that occurs in the minimum potential of the donor, spacer and anchoring sites with the introduction of the  $\pi$ -A system. Furthermore, in order to calculate  $\Delta V_{mD}$ , the most negative minima at the phenyl ring of each donor ( $V_{mD}$ ) have been subtracted from the corresponding minima ( $V_{mD}$ ) of the D- $\pi$ -A system. Similarly,  $\Delta V_{mS}$  and  $\Delta V_{mA}$  have been calculated by subtracting the  $V_m$  values at spacer and anchoring moieties of the reference system ( $V_{mS}$  and  $V_{mA}$ ) from the corresponding minima ( $V_{mS}$  and  $V_{mA}$ ) of the D- $\pi$ -A system.

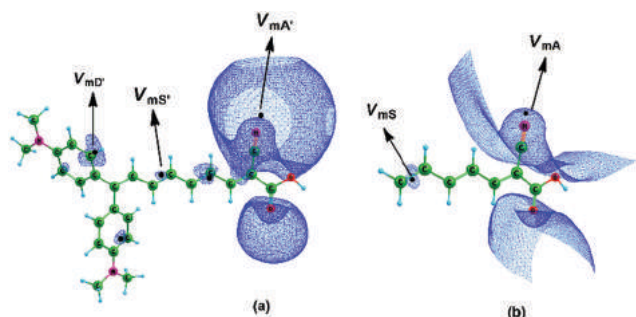


Fig. 3 MESP isosurface plot of (a) representative D- $\pi$ -A system and (b) reference system.

Table 1  $V_m$  (kcal mol<sup>-1</sup>) of the D- $\pi$ -A systems calculated at the B3LYP/cc-pVDZ level

Systems	$V_{mD}$	$V_{mD}'$	$\Delta V_{mD}$	$V_{mS}$	$V_{mS}'$	$\Delta V_{mS}$	$V_{mA}$	$V_{mA}'$	$\Delta V_{mA}$
D1	-14.4	-8.2	6.2	-2.4	-3.3	-0.9	-50.3	-53.0	-2.7
D2	-14.9	-9.8	5.1	-2.4	-3.3	-0.9	-50.3	-53.0	-2.6
D3	-14.4	-8.0	6.4	-2.4	-4.0	-1.6	-50.3	-54.2	-3.8
D4	-16.8	-7.8	9.0	-2.4	-4.3	-1.9	-50.3	-54.2	-3.8
D5	-15.6	-7.7	7.9	-2.4	-6.3	-3.9	-50.3	-56.0	-5.7
D6	-21.6	-9.3	12.3	-2.4	-8.0	-5.6	-50.3	-57.5	-7.2
D7	-23.5	-8.8	14.7	-2.4	-8.3	-5.9	-50.3	-57.5	-7.2
D8	-26.4	-10.0	16.4	-2.4	-10.8	-8.4	-50.3	-59.5	-9.2
D9	-19.5	-12.0	7.5	-2.4	-4.8	-2.4	-50.3	-54.8	-4.5
D10	-16.8	-9.4	7.4	-2.4	-5.3	-2.9	-50.3	-55.2	-4.9
D11	-21.3	-11.0	10.3	-2.4	-7.5	-5.1	-50.3	-55.4	-5.1
D12	-23.9	-14.1	9.8	-2.4	-12.9	-10.5	-50.3	-61.4	-11.0
D13	-11.0	-1.9	9.1	-2.4	-8.0	-5.6	-50.3	-56.5	-6.2

From Table 1, it is clear that when a donor part is being attached with a  $\pi$ -A system, the minimum potential of the donor site ( $V_{mD}$ ) becomes less negative indicating the electron transferring ability from the donor site to the  $\pi$ -A site. The term  $\Delta V_{mD}$  in Table 1 represents the change that occurred on the minimum potential at the donor site during the  $\pi$ -A linkage which varies from 5.1 to 16.4 kcal mol<sup>-1</sup> and indicates the intramolecular charge transfer involved in the D- $\pi$ -A system. Furthermore, at the spacer site of the D- $\pi$ -A system, electron density gain is observed represented by negative  $\Delta V_{mS}$  which lies in the range of -0.9 to -10.5 kcal mol<sup>-1</sup>. On the basis of  $\Delta V_{mS}$ , the highest donating strength can be attributed to the D12, while the least donating strength can be assigned for PAHs.

The  $V_{mA}$  values indicate that the minimum potential at the anchor moiety, for example at the cyano group, shows significant variations with respect to different donor units. The most electron-donating donor is expected to show the most negative  $V_{mA}$ . For the application of DSSCs, the cyanoacrylic portion has to be linked to the TiO<sub>2</sub> semiconductor for efficient electron transfer. By making the anchoring group electron-rich, efficient electron transfer from the dye to TiO<sub>2</sub> can occur. In other words, the efficiency of the DSSC system can be directly related to the electron-donating strength of the donor moieties. Due to this reason, the change in MESP minimum that appeared on the anchoring part ( $\Delta V_{mA}$ ) has been considered as the donating strength of the donor moiety. The PAHs (D1-D3) showed the least negative value of  $\Delta V_{mA}$  (-2.7 to -3.8 kcal mol<sup>-1</sup>), indicating their poor electron-donating strength. Furthermore, in the D4 system, a similar donating strength of -3.8 kcal mol<sup>-1</sup> is observed. In D5, the introduction of the N-centre imparts more negative  $\Delta V_{mA}$  values (-5.7 kcal mol<sup>-1</sup>) than PAHs which explains its better electron-donating strength compared to polyacenes. In D6 and D7, the more planarized nitrogen centres in the donor part impart a more negative  $\Delta V_{mA}$  value of -7.2 kcal mol<sup>-1</sup> and suggests its higher electron-donating strength than D5. In the D8 system, the fused N-centre with the aromatic ring further improves its planarization and leads to more negative  $\Delta V_{mA}$  -9.2 kcal mol<sup>-1</sup> than D5, D6, and D7. In carbazole (D9), the N-lone pair is shared between two aromatic rings through resonance, and as a result, the electron-donating strength in terms of  $\Delta V_{mA}$  (-4.5 kcal mol<sup>-1</sup>) appears weaker than those (D6-D8) having only one aromatic ring for sharing an N-lone pair. In D10, the presence of sulfur slightly enhances the negative value of  $\Delta V_{mA}$  to -5.0 kcal mol<sup>-1</sup>. Even though there are three nitrogen centres in ullazine, it shows a donating strength of -5.1 kcal mol<sup>-1</sup> which can be attributed to the influence of pyramidalized *N,N*-dimethyl groups in ullazine. In D12, a more negative  $\Delta V_{mA}$  value of -11.0 kcal mol<sup>-1</sup> can be recognized with the +R effect of mostly planarized *N,N*-dimethyl substituents. Finally, in D13 a more negative  $\Delta V_{mA}$  value (-6.2 kcal mol<sup>-1</sup>) than that of PAHs has been observed due to the interplay of the electron-rich nitrogen centre and the electron-withdrawing carbonyl group. These results strongly suggest that the incorporation of an electron-rich heteroatom in the donor region can have a positive influence on the electronic transmission to the acceptor moiety. On the basis of  $\Delta V_{mA}$ ,

**Table 2** Maximum absorption wavelength (nm), oscillator strength  $f$ , absorptional shift  $\Delta\lambda_{\max}$  and the percentage MO contribution of donor and D- $\pi$ -A systems at the TD-CAM-B3LYP/SMD/cc-pVDZ//B3LYP/cc-pVDZ level

Donor				D- $\pi$ -A			
Systems	$\lambda_{\max}$	$f$	MO contribution	$\lambda_{\max}$	$f$	MO contribution	$\Delta\lambda_{\max}$
D1	320	0.52	H $\rightarrow$ L (93.2%)	401	2.21	H-1 $\rightarrow$ L (94.2%)	81
D2	306	0.03	H-1 $\rightarrow$ L (33.6%)	376	0.03	H $\rightarrow$ L (74.6%)	56
			H $\rightarrow$ L (19.9%)	409	2.47	H $\rightarrow$ L (79.3%)	103
			H $\rightarrow$ L+1 (39.5%)				
D3	300	0.23	H $\rightarrow$ L (68.5%)				109
	408	0.59	H $\rightarrow$ L (98.7%)	518	1.73	H $\rightarrow$ L (90.4%)	110
D4	300	0.78	H $\rightarrow$ L (97.0%)	434	2.21	H $\rightarrow$ L (88.6%)	134
D5	284	0.03	H $\rightarrow$ L (90.8%)	453	2.02	H $\rightarrow$ L (86.7%)	169
D6	279	0.38	H $\rightarrow$ L+1 (98.8%)				174
	256	0.05	H $\rightarrow$ L (87.8%)	446	2.00	H $\rightarrow$ L (92.6%)	190
	236	0.37	H $\rightarrow$ L+1 (91.7%)				210
D7	261	0.09	H $\rightarrow$ L (90.5%)	448	1.86	H $\rightarrow$ L (93.7%)	187
	226	0.18	H $\rightarrow$ L+1 (90.0%)				222
D8	277	0.08	H $\rightarrow$ L (92.9%)	480	1.95	H $\rightarrow$ L (93.2%)	203
	243	0.29	H $\rightarrow$ L+1 (92.9%)				237
	286	0.06	H $\rightarrow$ L (87.6%)	419	2.21	H $\rightarrow$ L (93.2%)	133
D9	262	0.31	H-1 $\rightarrow$ L (84.2%)				157
	319	0.02	H $\rightarrow$ L (95.2%)	459	1.67	H $\rightarrow$ L (84.8%)	140
D10	275	0.18	H $\rightarrow$ L+2 (84.6%)				184
	324	0.38	H $\rightarrow$ L (90.8%)	448	0.02	H $\rightarrow$ L (89.2%)	124
D11				411	2.11	H-1 $\rightarrow$ L (73.6%)	87
	278	0.20	H $\rightarrow$ L (78.0%)	520	1.95	H $\rightarrow$ L (92.6%)	242
D12	334	0.64	H $\rightarrow$ L (95.3%)	503	1.99	H $\rightarrow$ L (89.3%)	169

the order of the donating strength of donor groups can be written as D2 < D1 < D3 = D4 < D9 < D10 < D11 < D5 < D13 < D6 = D7 < D8 < D12. The julolidine based donor system D8 and the *N,N*-dialkyl aniline incorporated D12 are the most efficient among the studied systems.

### Absorption spectra of donor and D- $\pi$ -A systems

The absorption maxima of all the systems (donor and D- $\pi$ -A) along with oscillator strength ( $f$ ) are summarized in Table 2. For the assessment of the absorptional shift,  $\Delta\lambda_{\max}$ , the absorption maximum of the D- $\pi$ -A system was subtracted from the donor system. For calculating  $\Delta\lambda_{\max}$ , HOMO  $\rightarrow$  LUMO orbital transition has been considered, except for D1. In D1,  $\lambda_{\max}$  is observed for the HOMO-1  $\rightarrow$  LUMO transition, while its HOMO  $\rightarrow$  LUMO transition is nearly forbidden due to very small  $f$  values. The data in Table 2 clearly suggest that the absorption maximum ( $\lambda_{\max}$ ) of D- $\pi$ -A shifts significantly to a higher wavelength region compared to donor D. Since in all systems we used the same spacer and anchoring moiety (the  $\pi$ -A unit), their influence on the absorptional shift ( $\Delta\lambda_{\max}$ ) can be considered to be the same. This implies that the large variation in  $\Delta\lambda_{\max}$  exhibited by the D- $\pi$ -A system is due to the variation in the donating strength of donor moieties. For instance, among all donor moieties, D1 with  $\Delta\lambda_{\max}$  81 nm is the least donating while D12 with  $\Delta\lambda_{\max}$  242 nm is the most donating (Table 2). Furthermore,  $\Delta V_{\text{MA}}$  with  $\Delta\lambda_{\max}$  with a correlation coefficient shows a linear correlation of 0.966 (Fig. 4) which shows the significance of the donating strength of  $\Delta V_{\text{MA}}$  on  $\Delta\lambda_{\max}$ . In the linear correlation plot, D1 and D11 based D- $\pi$ -A systems exhibit a slight deviation, which can be attributed as their less intense ( $f \rightarrow 0.02$ - $0.03$ ) and nearly forbidden HOMO  $\rightarrow$  LUMO charge transfer character of the

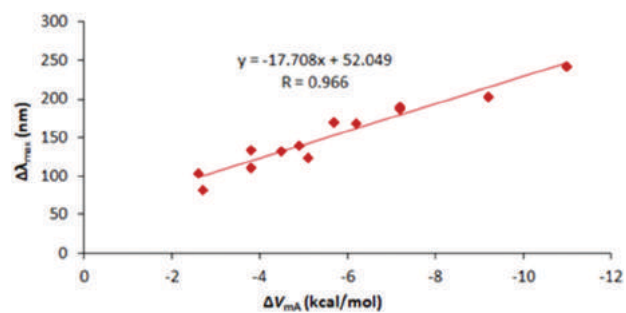


**Fig. 4** Correlation between the donating strength ( $\Delta V_{\text{MA}}$ ) of the D- $\pi$ -A system and the change in absorption maxima ( $\Delta\lambda_{\max}$ ).

orbital excitation. From these results the shift in absorption maxima ( $\Delta\lambda_{\max}$ ) follows the order D12 > D8 > D7 > D6 > D10 > D5 > D13 > D9 > D4 > D3 > D2 > D11 > D1, preferably due to the nature of donor groups. Therefore, to improve the wavelength of absorption to a preferred region (Vis to NIR), its donating ability has to be tuned with the introduction of better electron-donating donor groups (preferably more nitrogen centres).

The frontier molecular orbital energy levels given in Fig. 5 show the HOMO-LUMO band gap features of D, D- $\pi$ -A and  $\pi$ -A systems (butadiene moieties linked with cyano acrylic acid). The HOMO value ( $\epsilon_h$ ) of the D systems is in the range of -4.66 to -5.70 eV, whereas that of the D- $\pi$ -A system is in the range of -4.96 to -5.89 eV. These data indicate the close resemblance of the HOMO level of the D and D- $\pi$ -A systems. On the other hand, the LUMO energy level ( $\epsilon_l$ ) of D shows a large deviation from the  $\epsilon_l$  of the D- $\pi$ -A system indicating clear



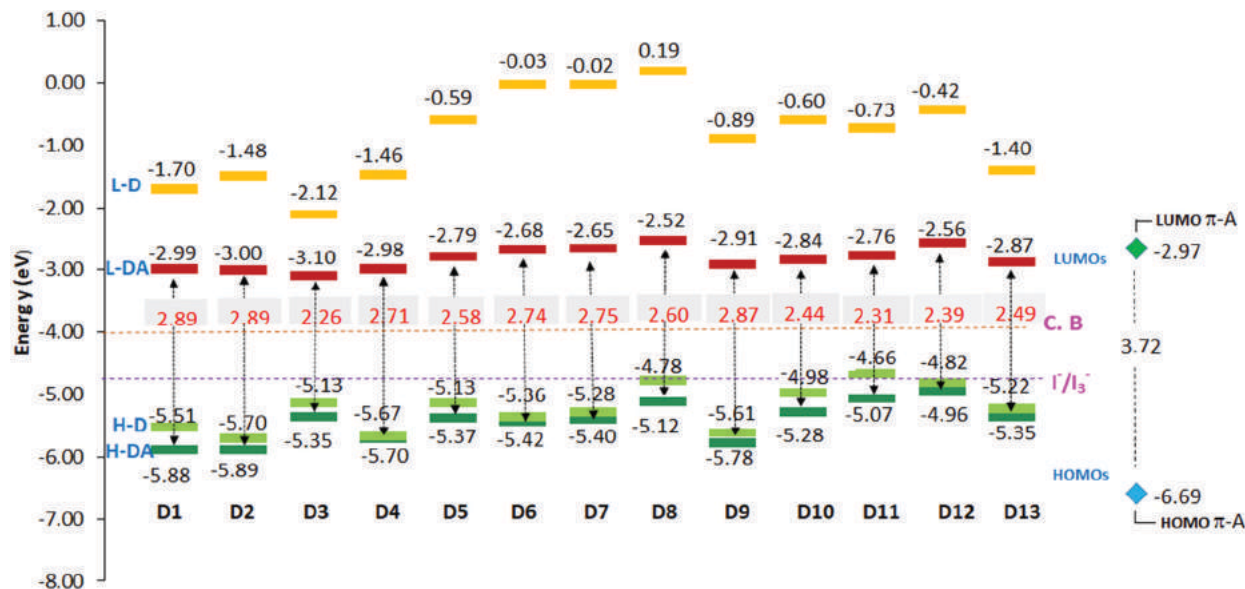


Fig. 5 Frontier molecular energy level diagram of D- $\pi$ -A systems at the B3LYP/cc-pVDZ level.

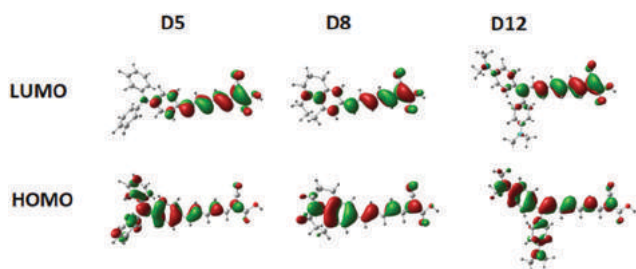


Fig. 6 Frontier molecular orbitals of representative D- $\pi$ -A systems at the B3LYP/cc-pVDZ level.

dissimilarity. In fact,  $\epsilon_1$  of D- $\pi$ -A in the range of  $-2.52$  to  $-3.10$  eV is very close to  $\epsilon_1$   $-2.97$  eV observed for  $\pi$ -A. Thus, the data shown in Fig. 5 indicate that the HOMO of D- $\pi$ -A is more like the HOMO of the donor and its LUMO is more like that of  $\pi$ -A. This feature is clearly evident in the frontier molecular orbital diagram given in the D- $\pi$ -A system for representative cases (Fig. 6). HOMOs are more localized towards the donor region with decreasing orbital contributions from the  $\pi$ -A system, while the LUMO is mostly localized in the  $\pi$ -A region. D1- $\pi$ -A is an exception wherein HOMO-1 to the LUMO is the allowed transition and its HOMO has a different  $\pi$  character, localized exclusively on the pyrene ring. The data shown in Fig. 5 clearly suggest that linking the donor system to the  $\pi$ -A unit is very effective for reducing the band gap. For all cases, the HOMO level is tuned towards the value of the  $\Gamma/I_3^-$  electrolyte couple while the LUMO level appears closer to the conduction band (CB) of  $\text{TiO}_2$ . The HOMO and LUMO distribution and their energy levels suggest a significant charge separation in the excited state leading to the strong electron coupling of the dye with the  $\text{TiO}_2$  semiconductor which promotes the electron transfer to the conduction band.<sup>94</sup>

In general, compared to D systems, the absorption maxima of D- $\pi$ -A systems show a significant red shift (Table 2) in the range of 81–242 nm. In D1- $\pi$ -A and D2- $\pi$ -A,  $\lambda_{\text{max}}$  is observed at

401 and 409 nm, respectively. The major electronic excitation of pyrene incorporated D1- $\pi$ -A is assigned to the transition of HOMO-1 to the LUMO. The forbidden HOMO to LUMO transition of D1- $\pi$ -A can be changed to allow one by appropriate substitution such as a substitution by the methyl group at the first or second position (Table S2 and Fig. S2, ESI<sup>†</sup>). The D3- $\pi$ -A system showed a broad absorption coverage in the visible region with  $\lambda_{\text{max}}$  518 nm corresponding to the HOMO-LUMO transition. Among all, D3- $\pi$ -A has the lowest HOMO-LUMO band gap of 2.26 eV (Fig. 5). The D4 in D4- $\pi$ -A is more electron-donating than a PAH moiety and it shows a smaller band gap of 2.71 eV compared to D1 to D2 incorporated systems. Furthermore, in nitrogen-containing D- $\pi$ -A systems (D5-D13), the band gap energy decreases to a greater extent by 2.31–2.75 eV for all except D9- $\pi$ -A (2.87 eV) than hydrocarbon systems. Among the nitrogen-containing systems, D12- $\pi$ -A showed the highest  $\lambda_{\text{max}}$  520 nm with a band gap of 2.39 eV while D11- $\pi$ -A showed the lowest band gap of 2.31 eV. The  $\lambda_{\text{max}}$  value of D11- $\pi$ -A observed at 411 nm is due to the transition of HOMO-1 to LUMO. Among them all, the HOMO energy level of D12- $\pi$ -A appeared nearest to the energy level of the redox electrolyte while its LUMO level is 1.44 eV higher than the CB of  $\text{TiO}_2$ . The LUMO energy levels of all systems offer a favourable electron injection from the excited state to the conduction band of  $\text{TiO}_2$  while HOMO energies lower than the oxidation potential of the  $\Gamma/I_3^-$  electrolyte ( $-4.8$  eV) indicate effective dye regeneration. These results support their effective utilization in the DSSC application. The D3- $\pi$ -A, D11- $\pi$ -A and D12- $\pi$ -A systems are among the lowest band gap systems, desirable for harvesting more light in the UV-visible region.

#### Analysis of photovoltaic parameters

According to Koopman's theorem,<sup>95</sup> the ground state oxidation potential ( $E_{\text{ox}}^{\text{dye}}$ ) of a dye can be approximated as the negative HOMO energy ( $-\epsilon_{\text{h}}$ ). Furthermore, the excited state dye regeneration

**Table 3** Calculated vertical excitation energy, absorption maxima, oscillator strength  $f$ , HOMO LUMO energy, HOMO–LUMO energy gap (HLG), ground and excited-state oxidation potentials ( $E_{\text{ox}}^{\text{dye}}$  and  $E_{\text{ox}}^{\text{dye*}}$ ), free energy change for electron injection ( $\Delta G_{\text{inject}}$ ), dye regeneration driving force ( $\Delta G_{\text{reg}}$ ), and the open circuit voltage ( $eV_{\text{OC}}$ ) of D– $\pi$ –A systems at the TD-CAM-B3LYP/SMD/cc-pVDZ//B3LYP/cc-pVDZ level

Systems	Excitation energy (eV)	$\lambda_{\text{absmax}}$ (nm)	$f$	HOMO (eV)	LUMO (eV)	HLG (eV)	$E_{\text{ox}}^{\text{dye}}$ (eV)	$E_{\text{ox}}^{\text{dye*}}$ (eV)	$\Delta G_{\text{inject}}$ (eV)	$\Delta G_{\text{reg}}$ (eV)	( $eV_{\text{OC}}$ ) (eV)
D1	3.09	401	2.22	−5.88	−2.99	2.89	5.88	2.79	−1.21	1.08	1.01
D2	3.03	409	2.47	−5.89	−3.00	2.89	5.89	2.86	−1.14	1.09	1.00
D3	2.39	518	1.73	−5.35	−3.10	2.26	5.35	2.96	−1.04	0.55	0.90
D4	2.86	434	2.21	−5.70	−2.98	2.71	5.70	2.84	−1.16	0.90	1.02
D5	2.73	453	2.02	−5.37	−2.79	2.58	5.37	2.64	−1.36	0.57	1.21
D6	2.78	446	2.00	−5.42	−2.68	2.74	5.42	2.64	−1.36	0.62	1.32
D7	2.59	448	1.95	−5.40	−2.65	2.75	5.40	2.81	−1.19	0.60	1.35
D8	2.77	480	1.86	−5.12	−2.52	2.60	5.12	2.35	−1.65	0.32	1.48
D9	2.96	419	2.21	−5.78	−2.91	2.87	5.78	2.82	−1.18	0.98	1.09
D10	2.70	459	1.67	−5.28	−2.84	2.44	5.28	2.58	−1.42	0.48	1.16
D11	3.01	411	2.11	−5.07	−2.76	2.31	5.07	2.06	−1.94	0.27	1.24
D12	2.39	520	1.95	−4.96	−2.56	2.39	4.96	2.57	−1.43	0.16	1.44
D13	2.46	503	1.99	−5.35	−2.87	2.49	5.35	2.89	−1.11	0.55	1.13

driving force ( $\Delta G_{\text{reg}}$ ) can be approximated as ( $E_{\text{ox}}^{\text{dye}} - 4.8$ ) eV or ( $-\epsilon_{\text{h}} - 4.8$ ) eV where  $-4.8$  eV stands for the redox potential of the  $\text{I}^-/\text{I}_3^-$  electrolyte couple.<sup>22,96</sup> The free energy change for electron injection ( $\Delta G_{\text{inject}}$ ) from the excited state of the dye to the semiconductor<sup>53,97,98</sup> is generally defined as,

$$\Delta G_{\text{inject}} = E_{\text{ox}}^{\text{dye*}} - 4.0 \quad (2)$$

where  $E_{\text{ox}}^{\text{dye*}}$  is the excited state oxidation potential and  $-4.0$  eV stands for the conduction band (CB) edge of the  $\text{TiO}_2$  semiconductor.<sup>22,99</sup> Assuming that the electron injection occurs from the unrelaxed excited state,  $E_{\text{ox}}^{\text{dye*}}$  can be explained as the difference between the ground state oxidation potential of the dye and the vertical transition energy  $\lambda_{\text{max}}$ ,<sup>96,97,100</sup>

$$E_{\text{ox}}^{\text{dye*}} = (-\epsilon_{\text{h}}) - \lambda_{\text{max}} \quad (3)$$

Furthermore, the difference between the energy of the LUMO ( $\epsilon_{\text{l}}$ ) of the dye and the energy of the conduction band edge of  $\text{TiO}_2$  is regarded as the open circuit voltage (eqn (4)).<sup>100</sup>

$$eV_{\text{OC}} = \epsilon_{\text{l}} - (-4.0) \quad (4)$$

In Table 3, the  $\Delta G_{\text{inject}}$  values fall in the range of  $-1.04$  to  $-1.94$  eV, and the D11– $\pi$ –A system with the most negative value has the highest electron injection efficiency while D2 to D4 based D– $\pi$ –A systems show the lowest efficiency. The smallest  $\Delta G_{\text{reg}}$  value of 0.16 eV is observed for D12– $\pi$ –A and suggests its fastest dye regeneration efficiency. A good linear correlation between  $\Delta V_{\text{mA}}$  and  $eV_{\text{OC}}$  is observed for all the cases (Fig. 7)

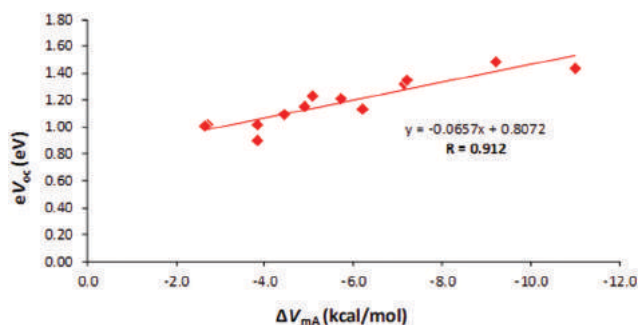


**Fig. 7** Correlation between  $\Delta V_{\text{mA}}$  ( $\text{kcal mol}^{-1}$ ) and  $eV_{\text{OC}}$  (eV).

suggesting that the electron accepting tendency of the acceptor part is well reflected at the LUMO levels. Among all the systems, julolidine based D8– $\pi$ –A possesses the highest  $\epsilon_{\text{l}}$  value resulting in the highest  $eV_{\text{OC}}$  value of 1.48 eV. The second highest  $eV_{\text{OC}}$  value of 1.44 eV is observed for D12– $\pi$ –A. The  $\Delta V_{\text{mA}}$  values suggest that the electron donating ability of PAH moieties is the lowest among all the donors and the corresponding D1 to D3 based D– $\pi$ –A systems show the lowest range of  $eV_{\text{OC}}$  0.90–1.01 eV.

## Conclusions

Using MESP topographical analysis, the donating strength of thirteen known (D1–D13) typically used donor systems in the DSSC applications has been quantified. The red shift in the absorption maximum ( $\Delta\lambda_{\text{max}}$ ) observed for the D– $\pi$ –A systems is rationalized in terms of the amount of electron donation from the donor D moieties to the  $\pi$ –A system using the MESP parameter  $\Delta V_{\text{mA}}$ . The highest electron donating strength  $\Delta V_{\text{mA}}$  observed in D12– $\pi$ –A shows the highest  $\Delta\lambda_{\text{max}}$  and maximum absorption wavelength  $\lambda_{\text{max}}$  with a small band gap energy of 2.39 eV. In poor electron donating D1 and D2 based D– $\pi$ –A systems, the smallest  $\Delta\lambda_{\text{max}}$  and  $\lambda_{\text{max}}$  values are observed. A linear correlation obtained between  $\Delta V_{\text{mA}}$  and  $\Delta\lambda_{\text{max}}$  confirms that  $\Delta\lambda_{\text{max}}$  increases with an increase in  $\Delta V_{\text{mA}}$ . The frontier molecular energy levels showed that the HOMO of the D– $\pi$ –A system has a greater resemblance to the HOMO of the donor, whereas the LUMO has a greater resemblance to the LUMO of  $\pi$ –A. Thus, the donor tunes the HOMO, while  $\pi$ –A tunes the LUMO energy of the D– $\pi$ –A system for efficient dye regeneration and electron injection. Among all the systems, D12– $\pi$ –A showed the highest electron injection efficiency. Since  $eV_{\text{OC}}$  is directly proportional to the power conversion efficiency of the solar cell, D8– $\pi$ –A and D12– $\pi$ –A having the highest  $eV_{\text{OC}}$  can be regarded as the most efficient sensitizers for DSSCs while the lowest  $eV_{\text{OC}}$  values displayed by the PAH based (D1–D3) D– $\pi$ –A systems offer poor efficiency. The linear correlation between  $\Delta V_{\text{mA}}$  and  $eV_{\text{OC}}$  shows that  $eV_{\text{OC}}$  increases with an increase in the negative character of  $\Delta V_{\text{mA}}$  and also proves that better sensitizers can be developed by connecting a powerful electron donor to a  $\pi$ –A system. One way to do this is by incorporating multiple lone pair

bearing nitrogen centres in donors. Thus, the MESP approach offers an easy analysis tool for the quantification of the donating strength of D- $\pi$ -A systems in DSSC applications.

## Conflicts of interest

There are no conflicts to declare.

## Acknowledgements

Authors acknowledge the DST-SERB for funding through GAP1397 and also gratefully acknowledge the CSIR 4th PI for the HPC facility and the NIIST IT lab for computational support. V. V. Divya thanks the CSIR, India, for the senior research fellowship.

## Notes and references

- B. O'regan and M. Grätzel, *Nature*, 1991, **353**, 737.
- N. Anscombe, *Nat. Photonics*, 2011, **5**, 266–267.
- F. Odobel, L. Le Pleux, Y. Pellegrin and E. Blart, *Acc. Chem. Res.*, 2010, **43**, 1063–1071.
- A. Hagfeldt, G. Boschloo, L. Sun, L. Kloo and H. Pettersson, *Chem. Rev.*, 2010, **110**, 6595–6663.
- N. Sharifi, F. Tajabadi and N. Taghavinia, *ChemPhysChem*, 2014, **15**, 3902–3927.
- J. Gong, K. Sumathy, Q. Qiao and Z. Zhou, *Renewable Sustainable Energy Rev.*, 2017, **68**, 234–246.
- A. Yella, H.-W. Lee, H. N. Tsao, C. Yi, A. K. Chandiran, M. K. Nazeeruddin, E. W.-G. Diau, C.-Y. Yeh, S. M. Zakeeruddin and M. Grätzel, *Science*, 2011, **334**, 629–634.
- A. Mishra, M. K. Fischer and P. Bäuerle, *Angew. Chem., Int. Ed.*, 2009, **48**, 2474–2499.
- M. K. Nazeeruddin, A. Kay, I. Rodicio, R. Humphry-Baker, E. Mueller, P. Liska, N. Vlachopoulos and M. Graetzel, *J. Am. Chem. Soc.*, 1993, **115**, 6382–6390.
- M. K. Nazeeruddin, P. Péchy, T. Renouard, S. M. Zakeeruddin, R. Humphry-Baker, P. Comte, P. Liska, L. Cevey, E. Costa, V. Shklover, L. Spiccia, G. B. Deacon, C. A. Bignozzi and M. Grätzel, *J. Am. Chem. Soc.*, 2001, **123**, 1613–1624.
- M. K. Nazeeruddin, R. Splivallo, P. Liska, P. Comte and M. Grätzel, *Chem. Commun.*, 2003, 1456–1457.
- M. K. Nazeeruddin, F. De Angelis, S. Fantacci, A. Selloni, G. Viscardi, P. Liska, S. Ito, B. Takeru and M. Grätzel, *J. Am. Chem. Soc.*, 2005, **127**, 16835–16847.
- F. Gao, Y. Wang, J. Zhang, D. Shi, M. Wang, R. Humphry-Baker, P. Wang, S. M. Zakeeruddin and M. Grätzel, *Chem. Commun.*, 2008, 2635–2637.
- C.-Y. Chen, M. Wang, J.-Y. Li, N. Pootrakulchote, L. Alibabaei, C.-H. Ngoc-le, J.-D. Decoppet, J.-H. Tsai, C. Grätzel, C.-G. Wu, S. M. Zakeeruddin and M. Grätzel, *ACS Nano*, 2009, **3**, 3103–3109.
- Y. Cao, Y. Bai, Q. Yu, Y. Cheng, S. Liu, D. Shi, F. Gao and P. Wang, *J. Phys. Chem. C*, 2009, **113**, 6290–6297.
- M. Pastore, E. Mosconi and F. De Angelis, *J. Phys. Chem. C*, 2012, **116**, 5965–5973.
- M. Cheng, X. Yang, J. Li, F. Zhang and L. Sun, *ChemSusChem*, 2013, **6**, 70–77.
- S. Ito, H. Miura, S. Uchida, M. Takata, K. Sumioka, P. Liska, P. Comte, P. Péchy and M. Grätzel, *Chem. Commun.*, 2008, 5194–5196.
- W. Zeng, Y. Cao, Y. Bai, Y. Wang, Y. Shi, M. Zhang, F. Wang, C. Pan and P. Wang, *Chem. Mater.*, 2010, **22**, 1915–1925.
- K. Kakiage, Y. Aoyama, T. Yano, T. Otsuka, T. Kyomen, M. Unno and M. Hanaya, *Chem. Commun.*, 2014, **50**, 6379–6381.
- Z. Yao, M. Zhang, H. Wu, L. Yang, R. Li and P. Wang, *J. Am. Chem. Soc.*, 2015, **137**, 3799–3802.
- B. Nagarajan, S. Kushwaha, R. Elumalai, S. Mandal, K. Ramanujam and D. Raghavachari, *J. Mater. Chem. A*, 2017, **5**, 10289–10300.
- K. Kakiage, Y. Aoyama, T. Yano, K. Oya, J.-I. Fujisawa and M. Hanaya, *Chem. Commun.*, 2015, **51**, 15894–15897.
- T. Kitamura, M. Ikeda, K. Shigaki, T. Inoue, N. A. Anderson, X. Ai, T. Lian and S. Yanagida, *Chem. Mater.*, 2004, **16**, 1806–1812.
- Z.-S. Wang, Y. Cui, Y. Dan-oh, C. Kasada, A. Shinpo and K. Hara, *J. Phys. Chem. C*, 2007, **111**, 7224–7230.
- Z.-S. Wang, N. Koumura, Y. Cui, M. Takahashi, H. Sekiguchi, A. Mori, T. Kubo, A. Furube and K. Hara, *Chem. Mater.*, 2008, **20**, 3993–4003.
- A. Venkateswararao, K. R. J. Thomas, C.-P. Lee, C.-T. Li and K.-C. Ho, *ACS Appl. Mater. Interfaces*, 2014, **6**, 2528–2539.
- A. J. Huckaba, F. Giordano, L. E. McNamara, K. M. Dreux, N. I. Hammer, G. S. Tschumper, S. M. Zakeeruddin, M. Grätzel, M. K. Nazeeruddin and J. H. Delcamp, *Adv. Energy Mater.*, 2015, **5**, 1401629.
- K. Hara, M. Kurashige, Y. Dan-oh, C. Kasada, A. Shinpo, S. Suga, K. Sayama and H. Arakawa, *New J. Chem.*, 2003, **27**, 783–785.
- C. Teng, X. Yang, C. Yang, H. Tian, S. Li, X. Wang, A. Hagfeldt and L. Sun, *J. Phys. Chem. C*, 2010, **114**, 11305–11313.
- A. Baheti, C.-P. Lee, K. J. Thomas and K.-C. Ho, *Phys. Chem. Chem. Phys.*, 2011, **13**, 17210–17221.
- K. Srinivas, C. R. Kumar, M. A. Reddy, K. Bhanuprakash, V. J. Rao and L. Giribabu, *Synth. Met.*, 2011, **161**, 96–105.
- Y. Ooyama, S. Inoue, T. Nagano, K. Kushimoto, J. Ohshita, I. Imae, K. Komaguchi and Y. Harima, *Angew. Chem., Int. Ed.*, 2011, **50**, 7429–7433.
- B. Hosseinzadeh, A. S. Beni, M. Azari, M. Zarandi and M. Karami, *New J. Chem.*, 2016, **40**, 8371–8381.
- D. Patil, M. Jadhav, K. Avhad, T. H. Chowdhury, A. Islam, I. Bedja and N. Sekar, *New J. Chem.*, 2018, **42**, 11555–11564.
- J. Feng, Y. Jiao, W. Ma, M. K. Nazeeruddin, M. Grätzel and S. Meng, *J. Phys. Chem. C*, 2013, **117**, 3772–3778.
- S. Ardo and G. J. Meyer, *Chem. Soc. Rev.*, 2009, **38**, 115–164.
- R. Argazzi, C. A. Bignozzi, T. A. Heimer, F. N. Castellano and G. J. Meyer, *J. Am. Chem. Soc.*, 1995, **117**, 11815–11816.
- N. Hirata, J. J. Lagref, E. J. Palomares, J. R. Durrant, M. K. Nazeeruddin, M. Grätzel and D. Di Censo, *Chem. – Eur. J.*, 2004, **10**, 595–602.
- Z. Ning, Q. Zhang, W. Wu, H. Pei, B. Liu and H. Tian, *J. Org. Chem.*, 2008, **73**, 3791–3797.

- 41 L. Li, Y. Hao, X. Yang, J. Zhao, H. Tian, C. Teng, A. Hagfeldt and L. Sun, *ChemSusChem*, 2011, **4**, 609–612.
- 42 J. Tang, J. Hua, W. Wu, J. Li, Z. Jin, Y. Long and H. Tian, *Energy Environ. Sci.*, 2010, **3**, 1736–1745.
- 43 W. Li, Y. Wu, Q. Zhang, H. Tian and W. Zhu, *ACS Appl. Mater. Interfaces*, 2012, **4**, 1822–1830.
- 44 R. Tarsang, V. Promarak, T. Sudyoasuk, S. Namuangruk, N. Kungwan and S. Jungstittiwong, *ChemPhysChem*, 2014, **15**, 3809–3818.
- 45 H.-Q. Xia, C.-P. Kong, J. Wang, F.-Q. Bai and H.-X. Zhang, *RSC Adv.*, 2014, **4**, 50338–50350.
- 46 A. Dessi, A. Sinicropi, S. Mohammadpourasl, R. Basosi, M. Taddei, F. Fabrizi de Biani, M. Calamante, L. Zani, A. Mordini, P. Bracq, D. Franchi and G. Reginato, *ACS Omega*, 2019, **4**, 7614–7627.
- 47 L.-Y. Lin, C.-H. Tsai, F. Lin, T.-W. Huang, S.-H. Chou, C.-C. Wu and K.-T. Wong, *Tetrahedron*, 2012, **68**, 7509–7516.
- 48 K. D. Seo, B. S. You, I. T. Choi, M. J. Ju, M. You, H. S. Kang and H. K. Kim, *J. Mater. Chem. A*, 2013, **1**, 9947–9953.
- 49 Y. Hong, J.-Y. Liao, J. Fu, D.-B. Kuang, H. Meier, C.-Y. Su and D. Cao, *Dyes Pigm.*, 2012, **94**, 481–489.
- 50 A. Dualeh, R. Humphry-Baker, J. H. Delcamp, M. K. Nazeeruddin and M. Grätzel, *Adv. Energy Mater.*, 2013, **3**, 496–504.
- 51 J. H. Delcamp, A. Yella, T. W. Holcombe, M. K. Nazeeruddin and M. Grätzel, *Angew. Chem., Int. Ed.*, 2013, **125**, 394–398.
- 52 K. Srinivas, K. Yesudas, K. Bhanuprakash, V. J. Rao and L. Giribabu, *J. Phys. Chem. C*, 2009, **113**, 20117–20126.
- 53 J. Preat, C. Michaux, D. Jacquemin and E. A. Perpète, *J. Phys. Chem. C*, 2009, **113**, 16821–16833.
- 54 J. Preat, *J. Phys. Chem. C*, 2010, **114**, 16716–16725.
- 55 J. Preat, D. Jacquemin and E. A. Perpète, *Environ. Sci. Technol.*, 2010, **44**, 5666–5671.
- 56 M. Pastore, E. Mosconi, F. De Angelis and M. Grätzel, *J. Phys. Chem. C*, 2010, **114**, 7205–7212.
- 57 D. Casanova, F. P. Rotzinger and M. Grätzel, *J. Chem. Theory Comput.*, 2010, **6**, 1219–1227.
- 58 S. Meng, E. Kaxiras, M. K. Nazeeruddin and M. Grätzel, *J. Phys. Chem. C*, 2011, **115**, 9276–9282.
- 59 R. Sánchez-de-Armas, M. Á. San Miguel, J. Oviedo and J. F. Sanz, *Phys. Chem. Chem. Phys.*, 2012, **14**, 225–233.
- 60 J. Zhang, H.-B. Li, S.-L. Sun, Y. Geng, Y. Wu and Z.-M. Su, *J. Mater. Chem.*, 2012, **22**, 568–576.
- 61 W. Fan, D. Tan and W. Q. Deng, *ChemPhysChem*, 2012, **13**, 2051–2060.
- 62 J. Zhang, Y.-H. Kan, H.-B. Li, Y. Geng, Y. Wu and Z.-M. Su, *Dyes Pigm.*, 2012, **95**, 313–321.
- 63 J. Zhang, H.-B. Li, J.-Z. Zhang, Y. Wu, Y. Geng, Q. Fu and Z.-M. Su, *J. Mater. Chem. A*, 2013, **1**, 14000–14007.
- 64 W.-L. Ding, D.-M. Wang, Z.-Y. Geng, X.-L. Zhao and Y.-F. Yan, *J. Phys. Chem. C*, 2013, **117**, 17382–17398.
- 65 R. Tarsang, V. Promarak, T. Sudyoasuk, S. Namuangruk and S. Jungstittiwong, *J. Photochem. Photobiol., A*, 2014, **273**, 8–16.
- 66 M. E. Köse, *J. Phys. Chem. A*, 2019, **123**, 5566–5573.
- 67 K. Hara, T. Sato, R. Katoh, A. Furube, Y. Ohga, A. Shinpo, S. Suga, K. Sayama, H. Sugihara and H. Arakawa, *J. Phys. Chem. B*, 2003, **107**, 597–606.
- 68 J. Li and A. C. Grimsdale, *Chem. Soc. Rev.*, 2010, **39**, 2399–2410.
- 69 G. Wu, F. Kong, J. Li, W. Chen, X. Fang, C. Zhang, Q. Chen, X. Zhang and S. Dai, *Dyes Pigm.*, 2013, **99**, 653–660.
- 70 Z.-S. Huang, H. Meier and D. Cao, *J. Mater. Chem.*, 2016, **4**, 2404–2426.
- 71 Y. Zhang, H. Cheema, L. McNamara, L. A. Hunt, N. I. Hammer and J. H. Delcamp, *Chem. – Eur. J.*, 2018, **24**, 5939–5949.
- 72 Z. Yang, C. Shao and D. Cao, *RSC Adv.*, 2015, **5**, 22892–22898.
- 73 C. H. Suresh and N. Koga, *Inorg. Chem.*, 2002, **41**, 1573–1578.
- 74 O. Kühl, *Coord. Chem. Rev.*, 2005, **249**, 693–704.
- 75 C. H. Suresh, *Inorg. Chem.*, 2006, **45**, 4982–4986.
- 76 J. Mathew, T. Thomas and C. H. Suresh, *Inorg. Chem.*, 2007, **46**, 10800–10809.
- 77 S. Mecozzi, A. P. West and D. A. Dougherty, *J. Am. Chem. Soc.*, 1996, **118**, 2307–2308.
- 78 S. E. Wheeler and K. N. Houk, *J. Chem. Theory Comput.*, 2009, **5**, 2301–2312.
- 79 S. E. Wheeler and K. Houk, *J. Am. Chem. Soc.*, 2009, **131**, 3126–3127.
- 80 F. B. Sayyed and C. H. Suresh, *J. Phys. Chem. A*, 2011, **115**, 9300–9307.
- 81 C. H. Suresh, P. Alexander, K. P. Vijayalakshmi, P. K. Sajith and S. R. Gadre, *Phys. Chem. Chem. Phys.*, 2008, **10**, 6492–6499.
- 82 F. B. Sayyed and C. H. Suresh, *Tetrahedron Lett.*, 2009, **50**, 7351–7354.
- 83 F. B. Sayyed and C. H. Suresh, *New J. Chem.*, 2009, **33**, 2465–2471.
- 84 F. B. Sayyed and C. H. Suresh, *J. Phys. Chem. A*, 2011, **115**, 5660–5664.
- 85 V. V. Divya, F. B. Sayyed and C. H. Suresh, *ChemPhysChem*, 2019, **20**, 1752–1758.
- 86 A. D. Becke, *J. Chem. Phys.*, 1993, **98**, 1372–1377.
- 87 T. H. Dunning Jr, *J. Chem. Phys.*, 1989, **90**, 1007–1023.
- 88 C. Adamo and V. Barone, *J. Chem. Phys.*, 1999, **110**, 6158–6170.
- 89 J.-D. Chai and M. Head-Gordon, *Phys. Chem. Chem. Phys.*, 2008, **10**, 6615–6620.
- 90 A. V. Marenich, C. J. Cramer and D. G. Truhlar, *J. Phys. Chem. B*, 2009, **113**, 6378–6396.
- 91 M. J. Frisch, G. W. Trucks, H. B. Schlegel, G. E. Scuseria, M. A. Robb, J. R. Cheeseman, G. Scalmani, V. Barone, G. A. Petersson, H. Nakatsuji, X. Li, M. Caricato, A. V. Marenich, J. Bloino, B. G. Janesko, R. Gomperts, B. Mennucci, H. P. Hratchian, J. V. Ortiz, A. F. Izmaylov, J. L. Sonnenberg, D. Williams-Young, F. Ding, F. Lipparini, F. Egidi, J. Goings, B. Peng, A. Petrone, T. Henderson, D. Ranasinghe, V. G. Zakrzewski, J. Gao, N. Rega, G. Zheng, W. Liang, M. Hada, M. Ehara, K. Toyota, R. Fukuda, J. Hasegawa, M. Ishida, T. Nakajima, Y. Honda, O. Kitao, H. Nakai, T. Vreven, K. Throssell, J. A. Montgomery, J. E. Peralta, F. Ogliaro, M. J. Bearpark, J. J. Heyd, E. N. Brothers, K. N. Kudin, V. N. Staroverov, T. A. Keith, R. Kobayashi, J. Normand, K. Raghavachari, A. P. Rendell, J. C. Burant, S. S. Iyengar, J. Tomasi, M. Cossi, J. M. Millam, M. Klene, C. Adamo, R. Cammi, J. W. Ochterski, R. L. Martin, K. Morokuma,



- O. Farkas, J. B. Foresman and D. J. Fox, *Gaussian 16, Revision A.03*, Gaussian, Inc., Wallingford CT, 2016.
- 92 S. R. Gadre and R. N. Shirsat, *Electrostatics of atoms and molecules*, Universities Press, 2000.
- 93 P. Politzer and D. G. Truhlar, *Chemical applications of atomic and molecular electrostatic potentials: reactivity, structure, scattering, and energetics of organic, inorganic, and biological systems*, Springer Science & Business Media, 2013.
- 94 J. Yang, X. Wang, W.-L. Yim and Q. Wang, *J. Phys. Chem. C*, 2015, **119**, 26355–26361.
- 95 T. Koopmans, *Physica*, 1933, **1**, 104–113.
- 96 J.-H. Luo, Q.-S. Li, L.-N. Yang, Z.-Z. Sun and Z.-S. Li, *RSC Adv.*, 2014, **4**, 20200–20207.
- 97 R. Katoh, A. Furube, T. Yoshihara, K. Hara, G. Fujihashi, S. Takano, S. Murata, H. Arakawa and M. Tachiya, *J. Phys. Chem. B*, 2004, **108**, 4818–4822.
- 98 N. N. Ghosh, M. Habib, A. Pramanik, P. Sarkar and S. Pal, *New J. Chem.*, 2019, **43**, 6480–6491.
- 99 J. B. Asbury, Y.-Q. Wang, E. Hao, H. N. Ghosh and T. Lian, *Res. Chem. Intermed.*, 2001, **27**, 393–406.
- 100 W. Sang-aroon, S. Saekow and V. Amornkitbamrung, *J. Photochem. Photobiol., A*, 2012, **236**, 35–40.





Cite this: *New J. Chem.*, 2021, 45, 2496

# Tuning the donating strength of dye sensitizers using molecular electrostatic potential analysis†

Velayudhan V. Divya<sup>ab</sup> and Cherumuttathu H. Suresh<sup>id</sup>\*<sup>ab</sup>

Donor- $\pi$ -acceptor (D- $\pi$ -A) systems typically used in dye-sensitized solar cells (DSSC) have been studied for assessing the donating strength of six donors (D1-D6) under the influence of substituents such as CH<sub>3</sub>, C<sub>5</sub>H<sub>11</sub>, isopropyl, *t*-butyl, OH, OCH<sub>3</sub>, OC<sub>2</sub>H<sub>5</sub>, NH<sub>2</sub>, N(CH<sub>3</sub>)<sub>2</sub>, PhCH<sub>3</sub>, and PhNH<sub>2</sub> along with  $\pi$ -spacer butadiene and acceptor moiety cyanoacrylic acid. The substituent effect enhances electron donation from D to A through the  $\pi$ -spacer. The enhancement in electron density at A has been quantified in terms of the difference in the molecular electrostatic potential (MESP) minimum at the cyano nitrogen ( $\Delta V_{\text{mA}}$ ) between  $\pi$ -A and D- $\pi$ -A. For unsubstituted D- $\pi$ -A systems,  $\Delta V_{\text{mA}}$  is in the range -0.1 to -5.7 kcal mol<sup>-1</sup>, whereas the substitution enhances the negative character of  $\Delta V_{\text{mA}}$  in the range -0.8 to -8.0 kcal mol<sup>-1</sup>. In alkyls and Ph-CH<sub>3</sub> substituted D- $\pi$ -A systems,  $\Delta V_{\text{mA}}$  lies in the range -0.8 to -6.7 kcal mol<sup>-1</sup>, whereas the N(CH<sub>3</sub>)<sub>2</sub> substituted systems exhibit more negative  $\Delta V_{\text{mA}}$  (more enhanced donating strength) in the range -5.1 to -8.0 kcal mol<sup>-1</sup>. The more negative value of  $\Delta V_{\text{mA}}$  implies the greater electron-donating ability of the D- $\pi$ -A system. Optical and photovoltaic parameters ( $\Delta G_{\text{reg}}$ ,  $\Delta G_{\text{inject}}$ ,  $eV_{\text{OC}}$ ) are analyzed at the TD-CAM-B3LYP/SMD/cc-pVDZ//B3LYP/cc-pVDZ level of DFT. An excellent linear correlation is observed in all six sets between  $\Delta V_{\text{mA}}$  and the absorption maximum ( $\lambda_{\text{max}}$ ) showing that  $\lambda_{\text{max}}$  increases with enhanced donating strength. The higher absorption maximum obtained by N(CH<sub>3</sub>)<sub>2</sub> substituted D- $\pi$ -A systems lies in the range 430 nm to 490 nm, explaining the outstanding donating ability of N(CH<sub>3</sub>)<sub>2</sub> compared to other substituents. The reduced highest occupied molecular orbital (HOMO) – lowest unoccupied molecular orbital (LUMO) gap (from 3.14 to 2.17 eV) with enhanced donating strength confirms the influence of substituent effects in broadening the absorption maximum. Furthermore, in photovoltaic parameters, a strong influence of the substituent effect is observed. The N(CH<sub>3</sub>)<sub>2</sub> substituted D1- $\pi$ -A (D1-N(CH<sub>3</sub>)<sub>2</sub>) exhibits the highest  $eV_{\text{OC}}$  (1.38 eV). The strong linear correlation observed for the ground state property  $\Delta V_{\text{mA}}$  and open-circuit voltage  $eV_{\text{OC}}$  provides guidelines for developing an effective strategy for designing dye sensitizers for desirable photovoltaic applications.

Received 29th September 2020,  
Accepted 21st November 2020

DOI: 10.1039/d0nj04797j

rsc.li/njc

## Introduction

Over the past 30 years, dye-sensitized solar cells (DSSCs) and their structural modification have become an emerging research area in the field of photovoltaics.<sup>1-3</sup> DSSCs are considered as the most inventive candidate for the next generation of clean renewable sources due to their easier structure modification, simple synthetic strategy, large absorption coefficient, and low production cost.<sup>1,4-7</sup> Nonetheless, the performance of DSSC is still in a bottleneck due to their lower power conversion efficiency (PCE) than the conventional silicon-based solar cells due to the inherent voltage loss during the dye regeneration

and poor long term stability.<sup>8</sup> In order to improve the PCE over conventional silicon-based solar cells, extensive research efforts like modification on electrolytes, semiconductors, and sensitizers have been executed and result in the development of new and efficient dye sensitizers.<sup>3,5,9-21</sup> Among the DSSCs, the Ru based sensitizers achieved the best PCE of 11%, which attains a comparable PCE to a silicon-based solar cell.<sup>5,22,23</sup> But due to the scarce resources and highly expensive nature of Ru metal, its practical application is limited, and more research efforts have resulted in the development of Ru-free organic sensitizers.<sup>6,11,24</sup> However, the major challenge of organic solar cells is the enhancement of PCE, durability, and stability to compete with silicon-based solar cells. One of the key strategies for the synthesis of Ru free sensitizers is the designing of the D- $\pi$ -A architecture, which enables efficient electron transfer from a donor (D) to the acceptor (A) through a spacer ( $\pi$ ).<sup>25,26</sup>

From the literature, it is understood that for the design of highly efficient photosensitizers, different kinds of building

<sup>a</sup> Chemical Sciences and Technology Division, CSIR-National Institute for Interdisciplinary Science and Technology, Thiruvananthapuram, Kerala 695019, India. E-mail: sureshch@niist.res.in, sureshch@gmail.com

<sup>b</sup> Academy of Scientific and Innovative Research (AcSIR), Ghaziabad 201002, India

† Electronic supplementary information (ESI) available. See DOI: 10.1039/d0nj04797j

blocks such as donors,<sup>27–35</sup> spacers,<sup>36–41</sup> and anchoring units<sup>42–46</sup> are required in the D– $\pi$ –A architecture to tune the electronic structure of the synthesized product. The fine-tuning of the HOMO–LUMO (highest occupied molecular orbital – lowest unoccupied molecular orbital) energy levels of a photosensitizer is often achieved by adjusting the substituent effect on the donor by the incorporation of electron-donating/withdrawing groups. In most of the cases, the electron-donating groups on the donor moiety act as substituents and they have a profound impact on the electronic structure and efficiency of the desired dye sensitizer.<sup>6,47–49</sup> *A priori* knowledge on the donating strength of the donor can become helpful for the prediction of the PCE of the designed/synthesized system. A quantitative/mathematical comparison of donating strength of the typically used donors is lacking in the literature.

Here we have selected six different donor systems (D1–D6), substituted with electron-donating groups such as CH<sub>3</sub>, C<sub>5</sub>H<sub>11</sub>, isopropyl, *t*-butyl, OH, OCH<sub>3</sub>, O–C<sub>2</sub>H<sub>5</sub>, NH<sub>2</sub>, N(CH<sub>3</sub>)<sub>2</sub>, N(C<sub>2</sub>H<sub>5</sub>)<sub>2</sub>, Ph–CH<sub>3</sub>, and Ph–NH<sub>2</sub> to evaluate the donating strength on a  $\pi$ –A system made up of a butadiene  $\pi$ -spacer and cyanoacrylic acid (Fig. 1). According to our previous study, the butadiene spacer is rated as having the highest substituent effect transmitting power compared to triple bonded, aromatic, and hetero-aromatic conjugated systems.<sup>50</sup> Hence this moiety is employed in the study as a  $\pi$ -spacer for effective intramolecular charge transfer (ICT) and cyanoacrylic acid is used as an acceptor (A). The molecular electrostatic potential (MESP) topographical analysis is used as a tool to measure the electronic effect of the substituted D on the acceptor A. MESP is a well-established tool for deriving many structure–property relationships for chemical and biological systems.<sup>51–57</sup> According to Scrocco, Tomasi, and coworkers, the MESP describes the charge distribution around a molecule and the regions with more negative MESP indicate the more electron-dense region of that system.<sup>58,59</sup> Suresh and coworkers widely used MESP for the quantification

of the substituent effect,<sup>60</sup> inductive effect,<sup>61</sup> resonance effect,<sup>62</sup> trans influence,<sup>63</sup> cation  $\pi$ -interaction,<sup>64</sup> *etc.* In a recent study, we have shown that MESP analysis is very useful for assessing the donating strength of D in the D– $\pi$ –A system.<sup>65</sup> MESP becomes a new theoretical tool for predicting the feasibility of organic electrode materials for lithium-ion batteries,<sup>66</sup> explained by Shang, Chen, and co-workers. The wide range of applications in various fields supports the validity of MESP based studies for analyzing the photovoltaic properties of dye-sensitized solar cells. The present study focuses on the substituent effect in tuning various ground state electronic and photovoltaic properties of D– $\pi$ –A systems for solar cell applications.

## Theoretical background and computational methodology

The three key parameters involved in the calculations of power conversion efficiency ( $\eta$ ) of a solar cell include open-circuit voltage ( $V_{OC}$ ), short-circuit current density ( $J_{SC}$ ), and the fill factor (FF). Thus, as compared to incident solar power on the cell ( $P_{inc}$ ), the  $\eta$  can be calculated as<sup>67</sup>

$$\eta = FF \frac{V_{OC} J_{SC}}{P_{inc}} \quad (1)$$

In the above equation,  $J_{SC}$  is related to the interaction between a sensitizer and semiconductor. In DSSCs,  $J_{SC}$  is calculated as<sup>39,40,68–70</sup>

$$J_{SC} = \int_{\lambda} \text{LHE}(\lambda) \phi_{\text{inject}} \eta_{\text{collect}} d\lambda \quad (2)$$

From the above equation, it is clear that  $J_{SC}$  is related to the light-harvesting efficiency (LHE) and electron injection efficiency  $\phi_{\text{inject}}$ .

*i.e.*, LHE =  $1 - 10^{-f}$ , where  $f$  represents the oscillator strength of the adsorbed dye molecule.<sup>71</sup>

Furthermore, the electron injection efficiency  $\phi_{\text{inject}}$  is related to electron injection-free energy change ( $\Delta G_{\text{inject}}$ ), and the enhancement in the  $J_{SC}$  can be carried out by the improvement of  $\Delta G_{\text{inject}}$ . Since electron injection takes place from the excited state of the dye to the conduction band of TiO<sub>2</sub>,  $\Delta G_{\text{inject}}$  can be calculated as follows.<sup>71–73</sup>

$$\Delta G_{\text{inject}} = E^{\text{dye}*} - |E_{CB}| \quad (3)$$

where  $E^{\text{dye}*}$  is the excited state oxidation potential and  $E_{CB}$  is the energy of the conduction band edge of the TiO<sub>2</sub> semiconductor. The negative  $\Delta G_{\text{inject}}$  values indicate that free energy change is spontaneous. It is well known that the conduction band (CB) of semiconductors is sensitive to conditions (*e.g.* pH of the solution) and it is very difficult to determine experimentally. Hence in this study, we used a widely accepted value of  $-4.00$  eV (an experimental value where the semiconductor is in contact with aqueous redox electrolytes of fixed pH 7.0) for doing the calculations.<sup>74</sup> For calculating  $E^{\text{dye}*}$ , it is assumed that electron injection occurs from the unrelaxed excited state and  $E^{\text{dye}*}$  can be written as<sup>39,72</sup>

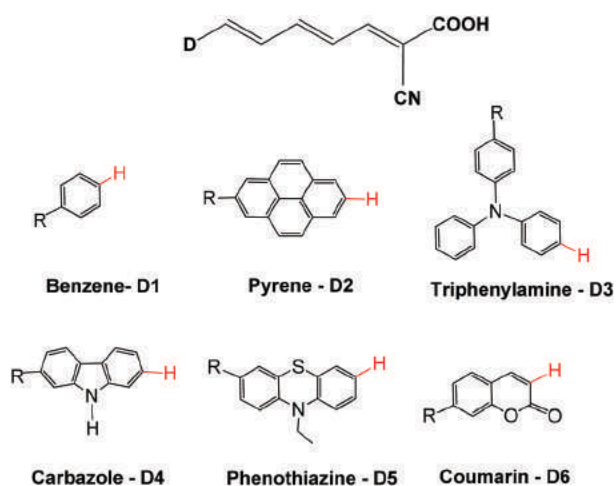


Fig. 1 Chemdraw diagram of the D– $\pi$ –A system (top) and the donors D1–D6. The R substituents are CH<sub>3</sub>, C<sub>5</sub>H<sub>11</sub>, isopropyl, *t*-butyl, OH, OCH<sub>3</sub>, O–C<sub>2</sub>H<sub>5</sub>, NH<sub>2</sub>, N(CH<sub>3</sub>)<sub>2</sub>, Ph–CH<sub>3</sub>, and Ph–NH<sub>2</sub>. The bond shown in red colour indicates the connecting position of D with  $\pi$ –A.

$$E^{\text{dye}*} = E^{\text{dye}} - \lambda_{\text{max}} \quad (4)$$

where  $E^{\text{dye}}$  is the ground state oxidation potential of the dye and  $\lambda_{\text{max}}$  is the vertical transition energy. According to Koopman's theorem, the ground state oxidation potential can be calculated as negative HOMO energy,<sup>75</sup> and this approximation has been giving good agreement with experimental results.<sup>76</sup>

The excited state dye regeneration can be predicted from the ground state oxidation potential as follows.<sup>77</sup>

$$\Delta G_{\text{reg}} = E^{\text{dye}} - 4.8 \text{ eV} \quad (5)$$

Thus from eqn (2)–(4), it is clear that  $J_{\text{SC}}$  will increase with the enhancement of light-harvesting efficiency and  $\Delta G_{\text{inject}}$ .

Theoretically, the open-circuit voltage can be approximated as the difference between the energy of the LUMO of the dye and the energy of the conduction band edge of  $\text{TiO}_2$ .<sup>78</sup>

$$eV_{\text{OC}} = E_{\text{LUMO}} - E_{\text{CB}} \quad (6)$$

Thus, the overall efficiency  $\eta$  of a solar cell can be enhanced by the improvement in  $J_{\text{SC}}$ ,  $eV_{\text{OC}}$  and FF values. (Since FF can be calculated from current–voltage characteristics, it is beyond the scope of this study).

For the ground state geometry optimization of the D- $\pi$ -A systems, the widely utilized B3LYP density functional theory (DFT) method<sup>79</sup> with the cc-pVDZ basis set<sup>65,80,81</sup> has been considered. Vibrational frequency calculation was also carried out at the same level of theory and basis set, and confirms that there are no imaginary frequencies. Absorption maxima and vertical excitation energies for the first seven states are calculated using time-dependent DFT at the CAM-B3LYP/SMD/cc-pVDZ//B3LYP/cc-pVDZ level.<sup>82,83</sup> Here SMD stands for the incorporation of the solvation effect of dichloromethane in the self-consistent reaction field (SCRF) approach<sup>84</sup> as implemented in the Gaussian16 suite of programmes.<sup>85</sup> The dependency of bond localization of single and double bonds in the ground state on the excited state properties has been analyzed using bond length alteration index (BLA).<sup>86,87</sup> The BLA index for the unsubstituted D1 to D6- $\pi$ -A systems are calculated with B3LYP and CAM-B3LYP geometries (Table S1 and Fig. S2, ESI†). For all a positive BLA index has been observed and larger BLA index has been observed with CAM-B3LYP. This indicates that carbon-carbon single and double bonds are more localized with CAM-B3LYP than B3LYP. Also, the BLA index for the S1 state of a representative set of TPA systems has been calculated with CAM-B3LYP (Table S2, ESI†). The reduced BLA index for S1 than the S0 state indicates the delocalized nature of the system and also supports the ICT transfer involved in D- $\pi$ -A systems. Previously, González *et al.* noted that B3LYP fails to predict the excitation energies due to its intrinsic problems in describing charge transfer (CT) states whereas the long-range correction on them using CAM delivers good agreement with the experimental UV/vis absorption.<sup>87</sup> They also observed that excited state properties are highly dependent on the localization of single and double bonds in the ground state structure which can be quantified in terms of the BLA index. Our previous study also showed that the calculated absorption maximum of known D- $\pi$ -A systems at the

CAM-B3LYP/SMD/cc-pVDZ//B3LYP/cc-pVDZ level of theory agrees well with the experimental absorption maximum.<sup>65</sup> The MESP,  $V(\mathbf{r})$  as defined in eqn (1) has been evaluated using the electron density  $\rho(\mathbf{r}')$  computed at the B3LYP/cc-pVDZ level.

$$V(\mathbf{r}) = \sum_A^N \frac{Z_A}{|\mathbf{r} - \mathbf{R}_A|} - \int \frac{\rho(\mathbf{r}') d\mathbf{r}'}{|\mathbf{r} - \mathbf{r}'|}$$

The  $N$  in eqn (1) is the total number of nuclei present in the molecular system,  $Z_A$  is the charge on the nucleus  $A$  at a distance  $R_A$  and  $\mathbf{r}'$  is a dummy integration variable.<sup>52,53</sup> All calculations have been carried out using the Gaussian 16 program package.<sup>85</sup>

### MESP analysis

The MESP plot of two representative donors (D1 and D4) and their corresponding D- $\pi$ -A systems (unsubstituted) are shown in Fig. 2 along with the respective MESP minimum ( $V_m$ ) at various sites.

In donor systems,  $V_{\text{mD}'}$  represents  $V_m$  of the donor. For example,  $V_{\text{mD}'}$  of benzene (D1) and carbazole (D4) are  $-16.6$  and  $-19.5$  kcal mol<sup>-1</sup> (Fig. 2). In D- $\pi$ -A systems,  $V_{\text{mD}}$  and  $V_{\text{mS}}$  represent the MESP minimum at the donor and spacer (nearer to D), respectively while  $V_{\text{m(OH)}}$ ,  $V_{\text{m(CO)}}$ , and  $V_{\text{mA}}$  represent the MESP minimum at the lone pair regions of OH, CO and CN of the acceptor moiety, respectively. Previous studies by Suresh and Gadre *et al.* have shown that lone pair regions in molecules can be characterized using MESP topographical analysis.<sup>88</sup> The

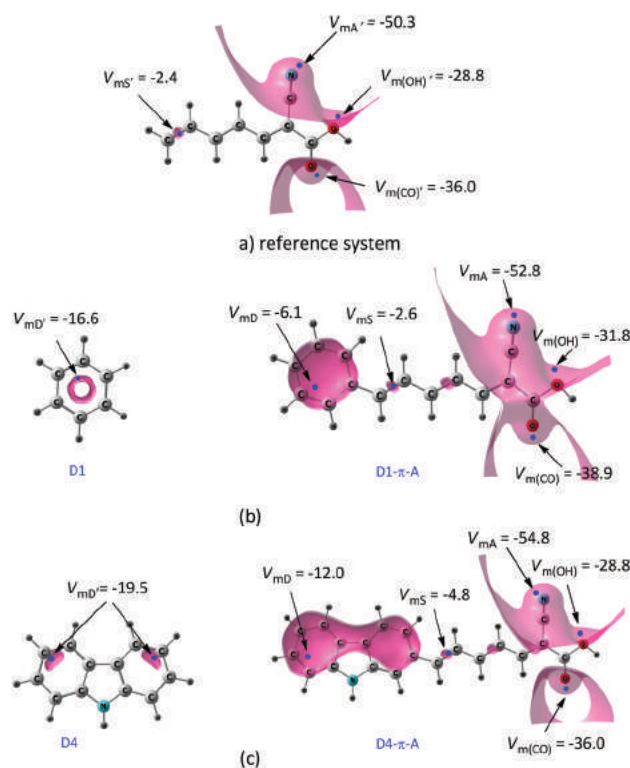


Fig. 2 MESP isosurfaces at various sites of the (a) reference system, (b) D1 and D1- $\pi$ -A system, and (c) D4 and D4- $\pi$ -A system.  $V_m$  values are in kcal mol<sup>-1</sup>.

Table 1  $V_m$  (kcal mol<sup>-1</sup>) at various sites of D- $\pi$ -A systems calculated at B3LYP/cc-pVDZ levels

D moiety	D- $\pi$ -A system	$V_{mD'}$	$V_{mD}$	$V_{mS}$	$V_{m(OH)}$	$V_{m(CO)}$	$V_{mA}$	$\Delta V_{mD}$	$\Delta V_{mS}$	$\Delta V_{m(OH)}$	$\Delta V_{m(CO)}$	$\Delta V_{mA}$	
(a) Benzene	D1	-16.6	-6.1	-2.6	-31.8	-38.9	-52.8	10.5	-0.2	-2.9	-2.9	-2.5	
	D1-CH <sub>3</sub>	-18.1	-6.5	-3.8	-32.7	-39.9	-53.8	11.5	-1.4	-3.9	-3.9	-3.5	
	D1-C <sub>5</sub> H <sub>11</sub>	-18.7	-7.2	-4.3	-33.1	-40.1	-54.2	11.5	-1.9	-4.3	-4.1	-3.8	
	D1-isopropyl	-17.9	-6.7	-3.8	-32.9	-39.9	-53.8	11.2	-1.4	-4.1	-3.9	-3.5	
	D1- <i>t</i> -but	-18.1	-6.9	-4.0	-32.9	-40.0	-53.9	11.2	-1.6	-4.1	-4.0	-3.6	
	D1-OH	-17.9	-5.0	-4.3	-33.8	-40.9	-54.5	12.9	-1.9	-5.0	-4.8	-4.2	
	D1-OCH <sub>3</sub>	-18.8	-6.0	-5.0	-34.3	-41.4	-54.8	12.8	-2.6	-5.5	-5.4	-4.5	
	D1-OC <sub>2</sub> H <sub>5</sub>	-19.3	-6.5	-5.3	-34.5	-41.6	-55.3	12.7	-2.9	-5.6	-5.6	-5.0	
	D1-NH <sub>2</sub>	-23.1	-8.6	-7.6	-36.4	-43.7	-57.1	14.5	-5.2	-7.6	-7.7	-6.8	
	D1-N(CH <sub>3</sub> ) <sub>2</sub>	-24.0	-9.1	-9.0	-37.7	-45.1	-58.4	14.9	-6.7	-8.8	-9.0	-8.0	
	D1-PhCH <sub>3</sub>	-16.7	-7.0	-3.7	-32.8	-39.8	-53.5	9.7	-1.3	-4.0	-3.8	-3.2	
	D1-PhNH <sub>2</sub>	-19.7	-9.5	-5.9	-34.5	-41.7	-55.0	10.2	-3.5	-5.6	-5.6	-4.7	
	Pyrene	D2	-14.4	-8.2	-3.3	-32.0	-39.3	-53.0	6.2	-0.9	-3.2	-3.3	-2.7
		D2-CH <sub>3</sub>	-15.4	-8.7	-4.0	-32.6	-39.8	-53.7	6.7	-1.6	-3.8	-3.8	-3.3
		D2-C <sub>5</sub> H <sub>11</sub>	-15.8	-9.2	-4.2	-32.8	-40.0	-53.9	6.7	-1.8	-4.0	-4.0	-3.6
		D2-isopropyl	-15.3	-8.8	-4.0	-32.4	-39.7	-53.7	6.5	-1.6	-3.6	-3.7	-3.4
		D2- <i>t</i> -but	-15.5	-8.9	-4.1	-32.4	-39.8	-53.8	6.6	-1.7	-3.6	-3.8	-3.5
		D2-OH	-15.2	-8.2	-4.0	-32.8	-39.9	-53.7	7.0	-1.6	-4.0	-3.9	-3.4
		D2-OCH <sub>3</sub>	-15.9	-8.8	-4.5	-32.9	-40.2	-54.2	7.1	-2.1	-4.1	-4.1	-3.8
		D2-OC <sub>2</sub> H <sub>5</sub>	-16.3	-9.2	-4.6	-33.3	-40.5	-54.3	7.1	-2.3	-4.5	-4.5	-4.0
D2-NH <sub>2</sub>		-18.1	-11.0	-5.8	-34.1	-41.2	-54.7	7.2	-3.4	-5.3	-5.2	-4.4	
D2-N(CH <sub>3</sub> ) <sub>2</sub>		-18.9	-11.5	-6.7	-34.7	-42.1	-55.8	7.3	-4.3	-5.9	-6.1	-5.5	
D2-PhCH <sub>3</sub>		-14.7	-8.6	-3.8	-32.6	-39.7	-53.7	6.1	-1.4	-3.8	-3.7	-3.3	
D2-PhNH <sub>2</sub>		-16.7	-10.7	-5.0	-33.4	-40.6	-54.5	6.0	-2.6	-4.6	-4.6	-4.1	
TPA	D3	-15.6	-7.7	-6.3	-35.6	-42.5	-56.0	7.9	-3.9	-6.8	-6.5	-5.7	
	D3-CH <sub>3</sub>	-16.5	-8.3	-6.9	-36.0	-43.2	-56.7	8.2	-4.5	-7.2	-7.2	-6.3	
	D3-C <sub>5</sub> H <sub>11</sub>	-16.8	-8.7	-7.2	-36.0	-43.3	-57.0	8.2	-4.8	-7.2	-7.3	-6.7	
	D3-isopropyl	-16.4	-8.3	-6.8	-35.8	-43.1	-56.6	8.1	-4.5	-7.0	-7.1	-6.3	
	D3- <i>t</i> -but	-16.4	-8.3	-6.9	-36.1	-43.1	-56.4	8.2	-4.5	-7.3	-7.1	-6.0	
	D3-OH	-17.5	-8.2	-7.5	-36.3	-43.5	-57.2	9.3	-5.1	-7.5	-7.5	-6.8	
	D3-OCH <sub>3</sub>	-17.9	-8.7	-7.7	-36.6	-43.7	-57.2	9.2	-5.3	-7.8	-7.7	-6.9	
	D3-OC <sub>2</sub> H <sub>5</sub>	-18.1	-8.9	-7.8	-36.7	-43.9	-57.4	9.2	-5.5	-7.9	-7.9	-7.1	
	D3-NH <sub>2</sub>	-19.4	-10.2	-8.7	-37.3	-44.5	-58.1	9.2	-6.3	-8.5	-8.5	-7.8	
	D3-N(CH <sub>3</sub> ) <sub>2</sub>	-20.0	-11.0	-9.2	-37.7	-44.8	-58.3	9.0	-6.8	-8.9	-8.8	-8.0	
	D3-PhCH <sub>3</sub>	-15.3	-7.8	-6.4	-35.6	-42.7	-56.3	7.5	-4.0	-6.8	-6.7	-6.0	
	D3-PhNH <sub>2</sub>	-17.4	-9.7	-7.5	-36.3	-43.5	-57.2	7.7	-5.1	-7.5	-7.5	-6.8	
(b) Carbazole	D4	-19.5	-12.0	-4.8	-33.6	-40.6	-54.8	7.5	-2.4	-4.8	-4.6	-4.5	
	D4-CH <sub>3</sub>	-20.6	-12.3	-5.6	-34.2	-41.3	-55.3	8.3	-3.2	-5.4	-5.3	-5.0	
	D4-C <sub>5</sub> H <sub>11</sub>	-21.0	-12.7	-5.9	-34.3	-41.4	-55.5	8.3	-3.5	-5.5	-5.3	-5.1	
	D4-isopropyl	-20.3	-12.2	-5.5	-34.0	-41.0	-55.1	8.1	-3.1	-5.2	-5.0	-4.8	
	D4- <i>t</i> -but	-20.4	-12.4	-5.5	-34.1	-41.1	-54.9	8.0	-3.1	-5.3	-5.1	-4.6	
	D4-OH	-21.0	-11.4	-6.0	-34.8	-41.5	-55.7	9.6	-3.6	-6.0	-5.5	-5.4	
	D4-OCH <sub>3</sub>	-21.6	-12.0	-6.5	-35.1	-42.0	-56.0	9.5	-4.1	-6.3	-6.0	-5.7	
	D4-OC <sub>2</sub> H <sub>5</sub>	-21.8	-12.4	-6.7	-35.1	-42.1	-55.8	9.4	-4.3	-6.3	-6.1	-5.5	
	D4-NH <sub>2</sub>	-23.6	-14.5	-7.9	-36.0	-43.2	-57.0	9.1	-5.5	-7.2	-7.2	-6.7	
	D4-N(CH <sub>3</sub> ) <sub>2</sub>	-24.6	-14.7	-8.8	-36.8	-43.7	-57.5	9.9	-6.5	-8.0	-7.7	-7.2	
	D4-PhCH <sub>3</sub>	-19.5	-12.2	-5.2	-33.9	-41.0	-55.0	7.2	-2.8	-5.1	-5.0	-4.6	
	D4-PhNH <sub>2</sub>	-21.8	-14.6	-6.5	-34.9	-42.0	-55.7	7.2	-4.1	-6.1	-6.0	-5.4	
	Phenothiazine	D5	-16.8	-9.4	-5.3	-34.6	-41.7	-55.2	7.4	-2.9	-5.8	-5.6	-4.9
		D5-CH <sub>3</sub>	-17.6	-9.0	-5.8	-34.7	-42.2	-55.7	8.6	-3.5	-5.9	-6.1	-5.4
		D5-C <sub>5</sub> H <sub>11</sub>	-17.9	-9.5	-6.1	-35.2	-42.5	-55.8	8.4	-3.8	-6.4	-6.5	-5.5
		D5-isopropyl	-17.5	-9.0	-5.9	-35.0	-42.3	-55.3	8.5	-3.5	-6.2	-6.3	-5.0
		D5- <i>t</i> -but	-17.6	-9.0	-6.0	-35.1	-42.4	-55.7	8.6	-3.6	-6.3	-6.3	-5.4
		D5-OH	-18.1	-7.2	-6.3	-35.4	-42.9	-56.1	10.9	-4.0	-6.6	-6.8	-5.8
		D5-OCH <sub>3</sub>	-18.4	-9.4	-6.7	-35.5	-42.7	-56.2	9.0	-4.3	-6.7	-6.7	-5.9
		D5-OC <sub>2</sub> H <sub>5</sub>	-18.6	-9.8	-6.7	-35.7	-43.1	-56.5	8.8	-4.3	-6.9	-7.1	-6.1
D5-NH <sub>2</sub>		-19.5	-11.4	-7.3	-36.1	-43.4	-56.9	8.2	-5.0	-7.3	-7.4	-6.5	
D5-N(CH <sub>3</sub> ) <sub>2</sub>		-20.6	-12.4	-8.2	-36.6	-44.1	-57.5	8.3	-5.8	-7.8	-8.1	-7.2	
D5-PhCH <sub>3</sub>		-16.7	-9.0	-5.5	-34.8	-42.0	-55.5	7.7	-3.1	-6.0	-6.0	-5.1	
D5-PhNH <sub>2</sub>		-18.2	-11.2	-6.6	-35.4	-42.9	-56.2	7.0	-4.2	-6.6	-6.8	-5.9	
Coumarin	D6	-5.7	-0.1	0.0	-30.1	-37.8	-50.5	5.6	2.4	-1.3	-1.8	-0.2	
	D6-CH <sub>3</sub>	-6.5	-0.4	-1.2	-31.0	-38.7	-51.3	6.1	1.2	-2.2	-2.7	-0.9	
	D6-C <sub>5</sub> H <sub>11</sub>	-7.2	-1.1	-1.6	-31.2	-39.0	-51.8	6.1	0.8	-2.4	-3.0	-1.5	
	D6-isopropyl	-6.7	-0.6	-1.2	-30.7	-38.7	-51.1	6.0	1.2	-1.9	-2.7	-0.8	
	D6- <i>t</i> -but	-6.9	-0.9	-1.4	-31.2	-38.9	-51.3	6.0	0.9	-2.4	-2.9	-1.0	
	D6-OH	-6.1	-	-1.9	-31.8	-39.5	-52.3	6.1	0.5	-3.0	-3.5	-1.9	
D6-OCH <sub>3</sub>	-7.0	-0.1	-2.6	-32.1	-40.0	-52.6	7.0	-0.2	-3.3	-4.0	-2.3		



Table 1 (continued)

D moiety	D- $\pi$ -A system	$V_{mD'}$	$V_{mD}$	$V_{mS}$	$V_{m(OH)}$	$V_{m(CO)}$	$V_{mA}$	$\Delta V_{mD}$	$\Delta V_{mS}$	$\Delta V_{m(OH)}$	$\Delta V_{m(CO)}$	$\Delta V_{mA}$
	D6-OC <sub>2</sub> H <sub>5</sub>	-7.5	-0.4	-2.9	-32.3	-40.2	-52.5	7.0	-0.6	-3.5	-4.2	-2.2
	D6-NH <sub>2</sub>	-10.4	-2.1	-5.0	-33.9	-41.8	-54.3	8.3	-2.6	-5.1	-5.8	-4.0
	D6-N(CH <sub>3</sub> ) <sub>2</sub>	-11.3	-2.6	-6.3	-35.0	-43.0	-55.5	8.7	-4.0	-6.2	-7.0	-5.1
	D6-PhCH <sub>3</sub>	-7.2	-1.6	-1.6	-31.2	-38.8	-51.5	5.6	0.8	-2.4	-2.8	-1.2
	D6-PhNH <sub>2</sub>	-10.2	-4.2	-3.6	-32.8	-40.6	-53.2	6.0	-1.2	-4.0	-4.6	-2.8

MESP minimum observed at the CN unit of  $\pi$ -A is considered as a reference value,  $V_{mA'}$  (Fig. 2a) ( $-50.3 \text{ kcal mol}^{-1}$ ) to monitor the changes observed at this minimum due to the incorporation of D to  $\pi$ -A. One could also consider the MESP minimum  $V_{m(OH)}$  or  $V_{m(CO)}$  of  $\pi$ -A as a reference point similar to  $V_{mA'}$  because in general the trends observed for these quantities show a parallel behavior. Here  $V_{mA'}$  is selected as the reference point on the basis of its most negative character compared to all other minima.

In Table 1a and b,  $V_m$  of D- $\pi$ -A systems at various sites *viz.* donor ( $V_{mD}$ ), spacer ( $V_{mS}$ ) and acceptor ( $V_{m(OH)}$ ,  $V_{m(CO)}$  and  $V_{mA}$ ) are reported along with  $V_{mD'}$ . The unsubstituted D- $\pi$ -A systems are denoted as D1, D2, D3, D4, D5, and D6, and the substituents attached at D1-D6 are represented as D1-CH<sub>3</sub>, D1-C<sub>5</sub>H<sub>11</sub>, D2-CH<sub>3</sub>, D2-C<sub>5</sub>H<sub>11</sub>, *etc.* The quantities  $\Delta V_{mD}$ ,  $\Delta V_{mS}$ ,  $\Delta V_{m(OH)}$ ,  $\Delta V_{m(CO)}$ , and  $\Delta V_{mA}$  represent the change in  $V_m$  at the respective

sites with the attachment of  $\pi$ -A to D.  $\Delta V_{mD}$  has been calculated by subtracting the  $V_m$  observed at the donor ( $V_{mD'}$ ) from the respective  $V_m$  observed at the D site of D- $\pi$ -A ( $V_{mD}$ ). Likewise  $\Delta V_{mS}$ ,  $\Delta V_{m(OH)}$ ,  $\Delta V_{m(CO)}$ , and  $\Delta V_{mA}$  are estimated by subtracting the respective  $V_m$  at  $\pi$ -A *viz.*  $V_{mS}$ ,  $V_{m(OH)}$ ,  $V_{m(CO)}$  and  $V_{mA'}$  (Fig. 2) from the corresponding values at D- $\pi$ -A ( $V_{mS}$ ,  $V_{m(OH)}$ ,  $V_{m(CO)}$  and  $V_{mA}$ ) (Table 1a and b).

The data in Table 1a and b show that the  $V_{mD}$  of the D- $\pi$ -A system is always less negative than the  $V_{mD'}$  of the donor D. For various donor systems,  $\Delta V_{mD}$  lies in the range 5.6 to 14.9  $\text{kcal mol}^{-1}$  which clearly suggests that the D site of the D- $\pi$ -A system becomes electron deficient compared to a normal D. The electron deficiency at D can be attributed to ICT of electrons from D to the  $\pi$ -A region which implies that  $V_m$  at the acceptor sites of D- $\pi$ -A becomes more negative compared to  $\pi$ -A and as a result always negative values are observed for

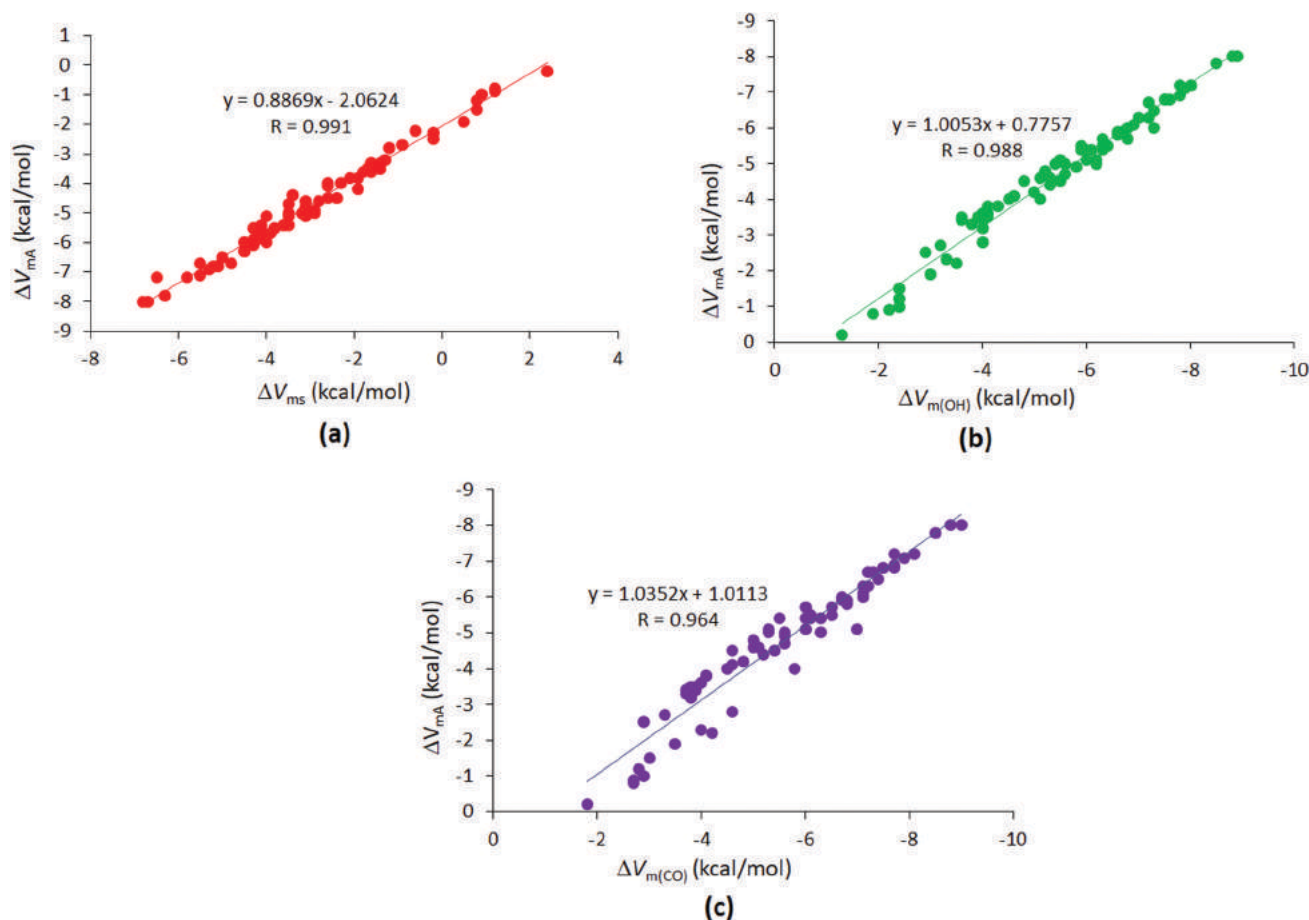


Fig. 3 Correlation between MESP parameters  $\Delta V_{mS}$ ,  $\Delta V_{m(OH)}$ ,  $\Delta V_{m(CO)}$ , and  $\Delta V_{mA}$ .

**Table 2** HOMO, LUMO and HOMO–LUMO energy gap (HLG) (in eV) observed for the ground state at the B3LYP/cc-pVDZ level and absorption maximum  $\lambda_{\max}$  (nm), and oscillator strength ( $f$ ) at the CAM-B3LYP/SMD/cc-pVDZ//B3LYP/cc-pVDZ level

D- $\pi$ -A system	HOMO	LUMO	HLG	$\lambda_{\max}$	$f$	D- $\pi$ -A system	HOMO	LUMO	HLG	$\lambda_{\max}$	$f$
Benzene						Pyrene					
D1	-6.13	-2.99	3.14	388	1.74	D2	-5.88	-2.99	2.89	401	2.22
D1-CH <sub>3</sub>	-6.01	-2.92	3.08	396	1.82	D2-CH <sub>3</sub>	-5.84	-2.95	2.89	404	2.27
D1-C <sub>5</sub> H <sub>11</sub>	-5.97	-2.90	3.07	398	1.86	D2-C <sub>5</sub> H <sub>11</sub>	-5.81	-2.94	2.87	404	2.32
D1-isopropyl	-6.01	-2.92	3.08	396	1.86	D2-isopropyl	-5.83	-2.95	2.88	404	2.30
D1- <i>t</i> -but	-6.00	-2.92	3.08	397	1.89	D2- <i>t</i> -but	-5.82	-2.95	2.87	404	2.33
D1-OH	-5.84	-2.85	2.99	408	1.78	D2-OH	-5.85	-2.94	2.91	409	2.19
D1-OCH <sub>3</sub>	-5.79	-2.83	2.97	412	1.81	D2-OCH <sub>3</sub>	-5.79	-2.92	2.87	410	2.20
D1-OC <sub>2</sub> H <sub>5</sub>	-5.77	-2.81	2.96	413	1.84	D2-OC <sub>2</sub> H <sub>5</sub>	-5.77	-2.91	2.86	410	2.23
D1-NH <sub>2</sub>	-5.53	-2.69	2.84	434	1.85	D2-NH <sub>2</sub>	-5.62	-2.86	2.76	419	2.20
D1-N(CH <sub>3</sub> ) <sub>2</sub>	-5.34	-2.62	2.72	457	1.94	D2-N(CH <sub>3</sub> ) <sub>2</sub>	-5.39	-2.81	2.58	430	2.21
D1-PhCH <sub>3</sub>	-5.89	-2.96	2.93	410	2.15	D2-PhCH <sub>3</sub>	-5.86	-2.97	2.89	406	2.49
D1-PhNH <sub>2</sub>	-5.52	-2.86	2.66	428	2.17	D2-PhNH <sub>2</sub>	-5.53	-2.91	2.62	411	2.53
TPA						Carbazole					
D3	-5.37	-2.79	2.58	453	2.02	D4	-5.78	-2.91	2.87	419	2.21
D3-CH <sub>3</sub>	-5.31	-2.76	2.55	457	2.03	D4-CH <sub>3</sub>	-5.69	-2.87	2.83	424	2.27
D3-C <sub>5</sub> H <sub>11</sub>	-5.29	-2.75	2.55	458	2.06	D4-C <sub>5</sub> H <sub>11</sub>	-5.67	-2.85	2.82	425	2.31
D3-isopropyl	-5.31	-2.76	2.55	457	2.03	D4-isopropyl	-5.71	-2.88	2.83	424	2.30
D3- <i>t</i> -but	-5.31	-2.76	2.55	457	2.02	D4- <i>t</i> -but	-5.70	-2.87	2.83	424	2.31
D3-OH	-5.26	-2.73	2.53	460	2.02	D4-OH	-5.58	-2.84	2.74	432	2.22
D3-OCH <sub>3</sub>	-5.24	-2.72	2.52	461	2.03	D4-OCH <sub>3</sub>	-5.54	-2.82	2.72	433	2.27
D3-OC <sub>2</sub> H <sub>5</sub>	-5.23	-2.71	2.51	461	2.03	D4-OC <sub>2</sub> H <sub>5</sub>	-5.52	-2.81	2.71	434	2.29
D3-NH <sub>2</sub>	-5.13	-2.67	2.46	468	2.00	D4-NH <sub>2</sub>	-5.33	-2.75	2.58	447	2.23
D3-N(CH <sub>3</sub> ) <sub>2</sub>	-5.03	-2.65	2.38	472	2.00	D4-N(CH <sub>3</sub> ) <sub>2</sub>	-5.14	-2.71	2.44	461	2.26
D3-PhCH <sub>3</sub>	-5.31	-2.78	2.52	457	2.12	D4-PhCH <sub>3</sub>	-5.66	-2.90	2.76	427	2.53
D3-PhNH <sub>2</sub>	-5.17	-2.73	2.44	460	2.12	D4-PhNH <sub>2</sub>	-5.37	-2.83	2.53	433	2.57
Phenothiazine						Coumarin					
D5	-5.28	-2.84	2.44	459	1.67	D6	-6.19	-3.34	2.85	424	1.71
D5-CH <sub>3</sub>	-5.22	-2.81	2.41	464	1.69	D6-CH <sub>3</sub>	-6.09	-3.26	2.82	431	1.78
D5-C <sub>5</sub> H <sub>11</sub>	-5.20	-2.80	2.40	464	1.72	D6-C <sub>5</sub> H <sub>11</sub>	-6.07	-3.25	2.82	431	1.84
D5-isopropyl	-5.21	-2.81	2.40	465	1.68	D6-isopropyl	-6.09	-3.27	2.82	431	1.83
D5- <i>t</i> -but	-5.22	-2.81	2.40	464	1.71	D6- <i>t</i> -but	-6.07	-3.25	2.82	432	1.84
D5-OH	-5.15	-2.79	2.36	469	1.66	D6-OH	-5.98	-3.20	2.78	439	1.77
D5-OCH <sub>3</sub>	-5.14	-2.78	2.36	469	1.70	D6-OCH <sub>3</sub>	-5.94	-3.18	2.76	442	1.82
D5-OC <sub>2</sub> H <sub>5</sub>	-5.12	-2.77	2.35	470	1.71	D6-OC <sub>2</sub> H <sub>5</sub>	-5.92	-3.16	2.76	443	1.85
D5-NH <sub>2</sub>	-4.99	-2.74	2.25	482	1.62	D6-NH <sub>2</sub>	-5.71	-3.04	2.67	463	1.86
D5-N(CH <sub>3</sub> ) <sub>2</sub>	-4.88	-2.70	2.17	490	1.62	D6-N(CH <sub>3</sub> ) <sub>2</sub>	-5.56	-2.97	2.59	481	1.96
D5-PhCH <sub>3</sub>	-5.22	-2.81	2.41	464	1.69	D6-PhCH <sub>3</sub>	-6.00	-3.28	2.72	444	2.10
D5-PhNH <sub>2</sub>	-5.07	-2.78	2.29	469	1.78	D6-PhNH <sub>2</sub>	-5.68	-3.17	2.51	461	2.18

$\Delta V_{m(OH)}$ ,  $\Delta V_{m(CO)}$ , and  $\Delta V_{mA}$ . For example, when  $\pi$ -A changes to D1- $\pi$ -A,  $V_m$  at the cyano region turns out to be more negative ( $V_{mA} = -52.8$  kcal mol<sup>-1</sup>) than the respective  $V_m$  on the reference system ( $\pi$ -A),  $V_{mA}$  ( $-50.3$  kcal mol<sup>-1</sup>). A similar trend in  $V_{mA}$  is observed for all the remaining systems. Also compared to  $\pi$ -A, the  $\pi$ -spacer region of D- $\pi$ -A shows more negative character for  $V_{mS}$  in all cases except some of the coumarin-based systems. Among the donors, the  $V_{mD}$  value is the least negative for coumarin systems, which can be attributed to the presence of an electron withdrawing carbonyl group in it. The quantities  $\Delta V_{mS}$ ,  $\Delta V_{m(OH)}$ ,  $\Delta V_{m(CO)}$  and  $\Delta V_{mA}$  show a parallel trend as shown in the correlation plots given in Fig. 3a–c. This suggests that any of these quantities can be used as a parameter to measure the donating strength of donor moieties to a common acceptor. Here  $\Delta V_{mA}$  (for the CN group) is selected for this purpose. It may be noted that variation in  $\Delta V_{mD}$  is not similar to  $\Delta V_{mA}$  (Fig. S3, ESI<sup>†</sup>) because it accounts for the property of various donors whereas  $\Delta V_{mA}$  accounts for the accepting ability of a CN unit from various donors.

In Table 1a and b, the lower  $\Delta V_{mA}$  in the range  $-0.2$  to  $-5.1$  kcal mol<sup>-1</sup> have been attained by coumarin-based D- $\pi$ -A

systems which can be attributed to the presence of an electron-withdrawing CO group in the donor site. In benzene and pyrene based systems, the strong conjugation feature in donors increases the negative character of the  $\Delta V_{mA}$  values ( $-2.5$  to  $-8.0$  kcal mol<sup>-1</sup>) leading to better-donating strength than coumarin systems.

In carbazole and phenothiazine systems, the charge transfer to the acceptor is enhanced ( $\Delta V_{mA} -4.5$  to  $-7.2$  kcal mol<sup>-1</sup>) due to donation from hetero atoms *viz.* nitrogen and sulphur. Among all, the TPA based systems have the highest electron-donating strength ( $-5.7$  to  $-8.0$  kcal mol<sup>-1</sup>).

Substituents at the donor region can be utilized for tuning the electron-donating strength of the donor. For instance, alkyl substituents *viz.* CH<sub>3</sub>, C<sub>5</sub>H<sub>11</sub>, isopropyl, and *t*-butyl at the donor unit enhance the electron-donating strength of all the corresponding substituted D- $\pi$ -A systems by a +I inductive effect. The substituents bearing lone pairs such as OH, OCH<sub>3</sub>, NH<sub>2</sub>, and N(CH<sub>3</sub>)<sub>2</sub> improve the electron density of the donor unit, resulting in better electron-donating power than alkyl substituents ( $\Delta V_{mA}$  in the range  $-3.4$  to  $-8.0$  kcal mol<sup>-1</sup>) +R resonance effect. Among all, N(CH<sub>3</sub>)<sub>2</sub> substituted benzene and TPA based D- $\pi$ -A systems show

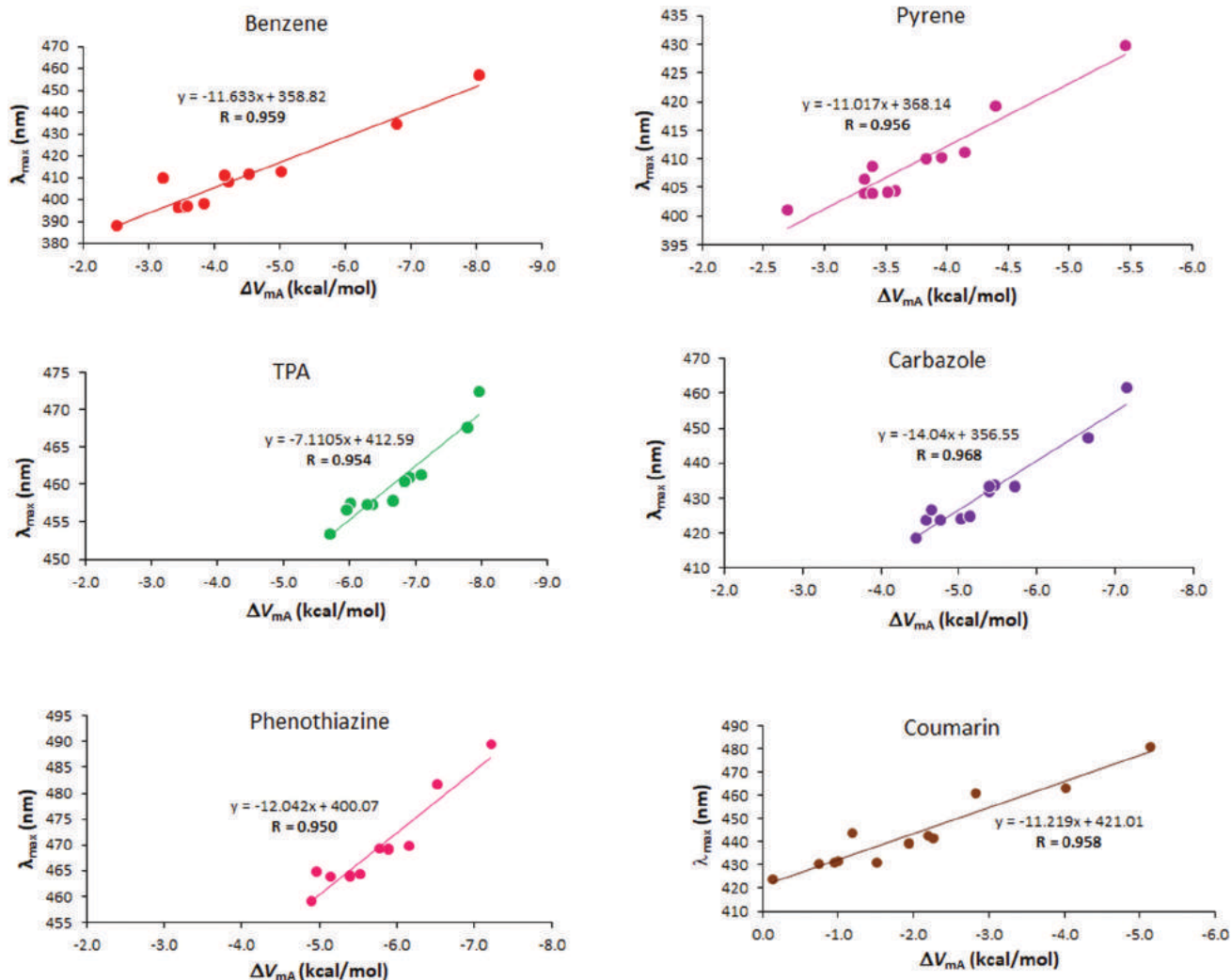


Fig. 4 Correlation between absorption maximum ( $\lambda_{\max}$ ) and donating strength ( $\Delta V_{mA}$ ) of various D- $\pi$ -A systems with different substituents.

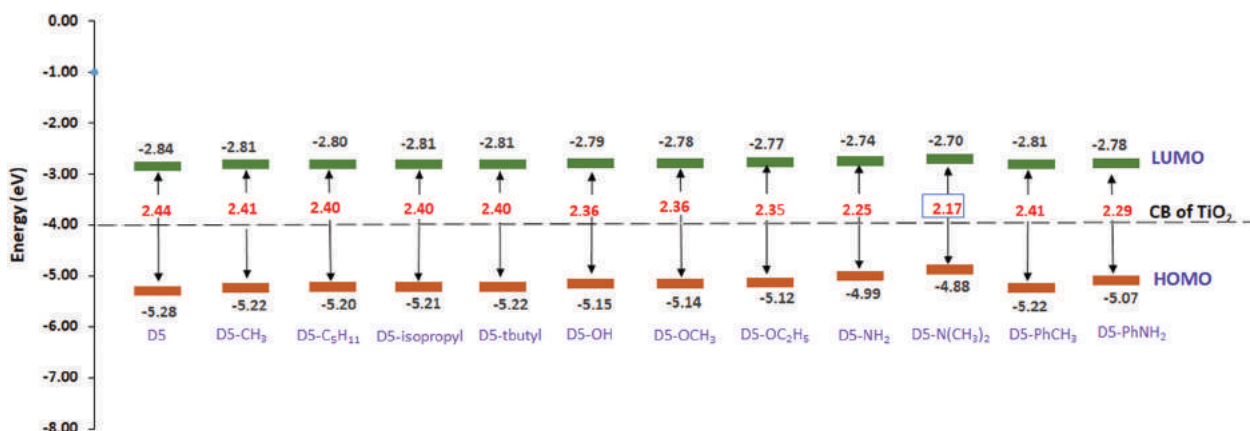


Fig. 5 Frontier molecular energy levels of phenothiazine based  $\pi$ -A with various substituents at the B3LYP/cc-pVDZ level.

the highest donation from donor to acceptor. The donating strength of various substituents attached on the D- $\pi$ -A system follows the order PhCH<sub>3</sub>  $\sim$  alkyls  $<$  -OH, -OR, PhNH<sub>2</sub>  $<$  NH<sub>2</sub>  $<$  N(CH<sub>3</sub>)<sub>2</sub>.

**Table 3** HOMO, LUMO and HOMO–LUMO energy gap (HLG) (in eV) observed for the ground state at the B3LYP/cc-pVDZ level. Excitation energy, ground and excited state oxidation potential ( $E^{\text{dye}}$ ,  $E^{\text{dye*}}$ ), free energy of electron injection  $\Delta G_{\text{inject}}$ , dye regeneration efficiency  $\Delta G_{\text{reg}}$ , and open-circuit voltage  $eV_{\text{OC}}$  at the TD-CAM-B3LYP/SMD/cc-pVDZ//B3LYP/cc-pVDZ level

D- $\pi$ -A	Excitation energy (eV)	HOMO (eV)	LUMO (eV)	HLG (eV)	$E^{\text{dye}}$ (eV)	$E^{\text{dye*}}$ (eV)	$\Delta G_{\text{inject}}$ (eV)	$\Delta G_{\text{reg}}$ (eV)	$eV_{\text{OC}}$ (eV)
(a)									
Benzene									
D1	3.20	-6.13	-2.99	3.14	6.13	2.93	-1.07	1.33	1.01
D1-CH <sub>3</sub>	3.13	-6.01	-2.92	3.08	6.01	2.88	-1.12	1.21	1.08
D1-C <sub>5</sub> H <sub>11</sub>	3.11	-5.97	-2.90	3.07	5.97	2.86	-1.14	1.17	1.10
D1-isopropyl	3.13	-6.01	-2.92	3.08	6.01	2.88	-1.12	1.21	1.08
D1- <i>t</i> -but	3.13	-6.00	-2.92	3.08	6.00	2.87	-1.13	1.20	1.08
D1-OH	3.04	-5.84	-2.85	2.99	5.84	2.80	-1.20	1.04	1.15
D1-OCH <sub>3</sub>	3.01	-5.79	-2.83	2.97	5.79	2.78	-1.22	0.99	1.17
D1-OC <sub>2</sub> H <sub>5</sub>	3.00	-5.77	-2.81	2.96	5.77	2.77	-1.23	0.97	1.19
D1-NH <sub>2</sub>	2.85	-5.53	-2.69	2.84	5.53	2.68	-1.32	0.73	1.31
D1-N(CH <sub>3</sub> ) <sub>2</sub>	2.71	-5.34	-2.62	2.72	5.34	2.63	-1.37	0.54	1.38
D1-PhCH <sub>3</sub>	3.02	-5.89	-2.96	2.93	5.89	2.87	-1.13	1.09	1.04
D1-PhNH <sub>2</sub>	2.90	-5.52	-2.86	2.66	5.52	2.62	-1.38	0.73	1.14
Pyrene									
D2	3.09	-5.88	-2.99	2.89	5.88	2.79	-1.21	1.08	1.01
D2-CH <sub>3</sub>	3.07	-5.84	-2.95	2.89	5.84	2.77	-1.23	1.04	1.05
D2-C <sub>5</sub> H <sub>11</sub>	3.07	-5.81	-2.94	2.87	5.81	2.74	-1.26	1.01	1.06
D2-isopropyl	3.07	-5.83	-2.95	2.88	5.83	2.76	-1.24	1.03	1.05
D2- <i>t</i> -but	3.07	-5.82	-2.95	2.87	5.82	2.75	-1.25	1.02	1.05
D2-OH	3.03	-5.85	-2.94	2.91	5.85	2.82	-1.18	1.05	1.06
D2-OCH <sub>3</sub>	3.02	-5.79	-2.92	2.87	5.79	2.77	-1.23	0.99	1.08
D2-OC <sub>2</sub> H <sub>5</sub>	3.02	-5.77	-2.91	2.86	5.77	2.75	-1.25	0.97	1.09
D2-NH <sub>2</sub>	2.96	-5.62	-2.86	2.76	5.62	2.66	-1.34	0.82	1.14
D2-N(CH <sub>3</sub> ) <sub>2</sub>	2.88	-5.39	-2.81	2.58	5.39	2.51	-1.49	0.59	1.19
D2-PhCH <sub>3</sub>	3.05	-5.86	-2.97	2.89	5.86	2.81	-1.19	1.06	1.03
D2-PhNH <sub>2</sub>	3.02	-5.53	-2.91	2.62	5.53	2.51	-1.49	0.73	1.09
TPA									
D3	2.73	-5.37	-2.79	2.58	5.37	2.64	-1.36	0.57	1.21
D3-CH <sub>3</sub>	2.71	-5.31	-2.76	2.55	5.31	2.60	-1.40	0.51	1.24
D3-C <sub>5</sub> H <sub>11</sub>	2.71	-5.29	-2.75	2.55	5.29	2.58	-1.42	0.49	1.25
D3-isopropyl	2.71	-5.31	-2.76	2.55	5.31	2.60	-1.40	0.51	1.24
D3- <i>t</i> -but	2.71	-5.31	-2.76	2.55	5.31	2.60	-1.40	0.51	1.24
D3-OH	2.69	-5.26	-2.73	2.53	5.26	2.57	-1.43	0.46	1.27
D3-OCH <sub>3</sub>	2.69	-5.24	-2.72	2.52	5.24	2.55	-1.45	0.44	1.28
D3-OC <sub>2</sub> H <sub>5</sub>	2.69	-5.23	-2.71	2.51	5.23	2.54	-1.46	0.43	1.29
D3-NH <sub>2</sub>	2.65	-5.13	-2.67	2.46	5.13	2.48	-1.52	0.33	1.33
D3-N(CH <sub>3</sub> ) <sub>2</sub>	2.62	-5.03	-2.65	2.38	5.03	2.41	-1.59	0.23	1.35
D3-PhCH <sub>3</sub>	2.72	-5.31	-2.78	2.52	5.31	2.60	-1.41	0.51	1.22
D3-PhNH <sub>2</sub>	2.69	-5.17	-2.73	2.44	5.17	2.48	-1.52	0.37	1.27
(b)									
Carbazole									
D4	2.96	-5.78	-2.91	2.87	5.78	2.82	-1.18	0.98	1.09
D4-CH <sub>3</sub>	2.92	-5.69	-2.87	2.83	5.69	2.77	-1.23	0.89	1.13
D4-C <sub>5</sub> H <sub>11</sub>	2.92	-5.67	-2.85	2.82	5.67	2.75	-1.25	0.87	1.15
D4-isopropyl	2.93	-5.71	-2.88	2.83	5.71	2.78	-1.22	0.91	1.12
D4- <i>t</i> -but	2.93	-5.70	-2.87	2.83	5.70	2.77	-1.23	0.90	1.13
D4-OH	2.87	-5.58	-2.84	2.74	5.58	2.71	-1.29	0.78	1.16
D4-OCH <sub>3</sub>	2.86	-5.54	-2.82	2.72	5.54	2.68	-1.32	0.74	1.18
D4-OC <sub>2</sub> H <sub>5</sub>	2.86	-5.52	-2.81	2.71	5.52	2.66	-1.34	0.72	1.19
D4-NH <sub>2</sub>	2.77	-5.33	-2.75	2.58	5.33	2.56	-1.44	0.53	1.25
D4-N(CH <sub>3</sub> ) <sub>2</sub>	2.69	-5.14	-2.71	2.44	5.14	2.45	-1.55	0.34	1.29
D4-PhCH <sub>3</sub>	2.91	-5.66	-2.90	2.76	5.66	2.75	-1.25	0.86	1.10
D4-PhNH <sub>2</sub>	2.86	-5.37	-2.83	2.53	5.37	2.51	-1.49	0.57	1.17
Phenothiazine									
D5	2.70	-5.28	-2.84	2.44	5.28	2.58	-1.42	0.48	1.16
D5-CH <sub>3</sub>	2.67	-5.22	-2.81	2.41	5.22	2.55	-1.45	0.42	1.19
D5-C <sub>5</sub> H <sub>11</sub>	2.67	-5.20	-2.80	2.40	5.20	2.53	-1.47	0.40	1.20
D5-isopropyl	2.67	-5.21	-2.81	2.40	5.21	2.54	-1.46	0.41	1.19
D5- <i>t</i> -but	2.67	-5.22	-2.81	2.40	5.22	2.55	-1.45	0.42	1.19
D5-OH	2.64	-5.15	-2.79	2.36	5.15	2.51	-1.49	0.35	1.21
D5-OCH <sub>3</sub>	2.64	-5.14	-2.78	2.36	5.14	2.50	-1.50	0.34	1.22
D5-OC <sub>2</sub> H <sub>5</sub>	2.64	-5.12	-2.77	2.35	5.12	2.48	-1.52	0.32	1.23
D5-NH <sub>2</sub>	2.57	-4.99	-2.74	2.25	4.99	2.42	-1.58	0.19	1.26
D5-N(CH <sub>3</sub> ) <sub>2</sub>	2.53	-4.88	-2.70	2.17	4.88	2.35	-1.65	0.08	1.30
D5-PhCH <sub>3</sub>	2.67	-5.22	-2.81	2.41	5.22	2.55	-1.45	0.42	1.19
D5-PhNH <sub>2</sub>	2.64	-5.07	-2.78	2.29	5.07	2.43	-1.57	0.27	1.22



Table 3 (continued)

D- $\pi$ -A	Excitation energy (eV)	HOMO (eV)	LUMO (eV)	HLG (eV)	$E^{\text{dye}}$ (eV)	$E^{\text{dye}*}$ (eV)	$\Delta G_{\text{inject}}$ (eV)	$\Delta G_{\text{reg}}$ (eV)	$eV_{\text{OC}}$ (eV)
Coumarin									
D6	2.93	-6.19	-3.34	2.85	6.19	3.27	-0.73	1.39	0.66
D6-CH <sub>3</sub>	2.88	-6.09	-3.26	2.82	6.09	3.21	-0.79	1.29	0.74
D6-C <sub>5</sub> H <sub>11</sub>	2.87	-6.07	-3.25	2.82	6.07	3.19	-0.81	1.27	0.75
D6-isopropyl	2.88	-6.09	-3.27	2.82	6.09	3.21	-0.79	1.29	0.73
D6- <i>t</i> -but	2.87	-6.07	-3.25	2.82	6.07	3.20	-0.80	1.27	0.75
D6-OH	2.82	-5.98	-3.20	2.78	5.98	3.15	-0.85	1.18	0.80
D6-OCH <sub>3</sub>	2.81	-5.94	-3.18	2.76	5.94	3.13	-0.87	1.14	0.82
D6-OC <sub>2</sub> H <sub>5</sub>	2.80	-5.92	-3.16	2.76	5.92	3.11	-0.89	1.12	0.84
D6-NH <sub>2</sub>	2.68	-5.71	-3.04	2.67	5.71	3.04	-0.96	0.91	0.96
D6-N(CH <sub>3</sub> ) <sub>2</sub>	2.58	-5.56	-2.97	2.59	5.56	2.98	-1.02	0.76	1.03
D6-PhCH <sub>3</sub>	2.80	-6.00	-3.28	2.72	6.00	3.21	-0.79	1.20	0.72
D6-PhNH <sub>2</sub>	2.69	-5.68	-3.17	2.51	5.68	2.99	-1.01	0.88	0.83

### Absorption spectra

In Table 2, the HOMO and LUMO energies, HOMO-LUMO energy gap (HLG), absorption maximum ( $\lambda_{\text{max}}$ ), and oscillator strength ( $f$ ) of six different D- $\pi$ -A systems with various substituents are reported. In all kinds of D- $\pi$ -A systems, a systematic increase in  $\lambda_{\text{max}}$  with respect to various substituents has been observed (388 to 490 nm), which can be correlated with the electron donating strength of the donors in the D- $\pi$ -A system. This is evident in the excellent linear correlations between  $\Delta V_{\text{MA}}$  and  $\lambda_{\text{max}}$  obtained for all six kinds of D- $\pi$ -A systems (Fig. 4). Also with an improved electron-donating strength of a D- $\pi$ -A system, lowering of HLG is noted in every system, which lies in the range 3.14 to 2.17 eV. Among all, the highest  $\lambda_{\text{max}}$  490 nm has been shown by (NH<sub>3</sub>)<sub>2</sub> substituted phenothiazine system D5-N(CH<sub>3</sub>)<sub>2</sub>. For the six D- $\pi$ -A systems and the selected eleven substituents, 102 nm width is available for tuning  $\lambda_{\text{max}}$  to a preferred region. For individual donors, the substituent effect alone can account for a tuning width of 69 nm for benzene, 29 nm for pyrene, 19 nm for TPA, 42 nm for carbazole, 31 nm for phenothiazine and 57 nm for coumarin, respectively.

The  $\Delta V_{\text{MA}}$  versus  $\lambda_{\text{max}}$  correlations given in Fig. 4 suggest that the substituent effects tune the HOMO-LUMO energy gap (HLG). The HLG plot of a representative system D5- $\pi$ -A

(phenothiazine-based) is given in Fig. 5 which shows that the introduction of substituents on the core D unit lowers the HLG from 2.41 to 2.17 eV. Poor electron-donating ability is observed in alkyls and PhCH<sub>3</sub> substituted systems display higher HLG (2.40 to 2.41 eV), while the lowest HLG has been attained with N(CH<sub>3</sub>)<sub>2</sub> substituted D5- $\pi$ -A. A similar trend in HLG is observed for the remaining systems which confirms the significance of the substituent effect in tuning  $\lambda_{\text{max}}$  (Table 3a and b). The HOMO and LUMO plots of the representative systems are shown in Fig. 6. The HOMO has a more delocalized distribution than the LUMO with more orbital contributions from the donor site while the LUMO is largely delocalized along the  $\pi$ -spacer and acceptor moiety.

### Photovoltaic performance

In Table 3a and b, electronic excitation energy, ground state oxidation potential  $E^{\text{dye}}$ , excited state oxidation potential  $E^{\text{dye}*}$ , free energy change of electron injection  $\Delta G_{\text{inject}}$ , free energy change of dye regeneration  $\Delta G_{\text{reg}}$ , and open-circuit voltage  $eV_{\text{OC}}$  of D- $\pi$ -A systems are described. The negative  $\Delta G_{\text{inject}}$  observed in the range -0.73 to -1.65 eV lies above the CB of TiO<sub>2</sub> (-4.0 eV) and indicates the possibility of a spontaneous electron injection process from CB to TiO<sub>2</sub>. Also a more electron-donating substituent enhances the electron injection process as  $\Delta G_{\text{inject}}$

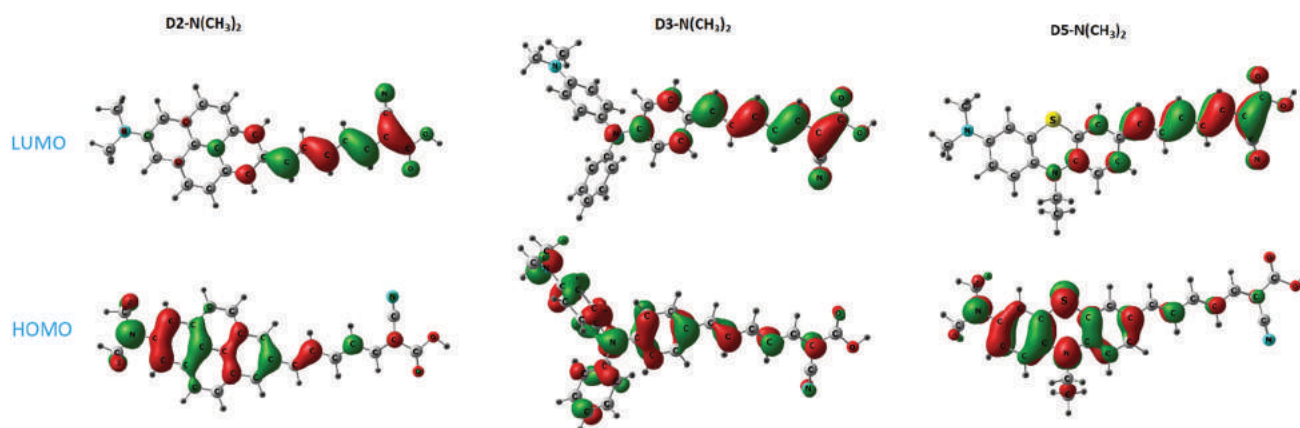


Fig. 6 Frontier molecular orbitals of representative N(CH<sub>3</sub>)<sub>2</sub> substituted D- $\pi$ -A systems at the B3LYP/cc-pVDZ level.

becomes more negative with such substituents. Alkyls, and PhCH<sub>3</sub> substituted D- $\pi$ -A systems are less efficient for electron injection than the OH, OCH<sub>3</sub>, OC<sub>2</sub>H<sub>5</sub>, NH<sub>2</sub> and N(CH<sub>3</sub>)<sub>2</sub> substituted systems. Among all, the most negative  $\Delta G_{\text{inject}} - 1.65$  eV is observed for phenothiazine system D5-N(CH<sub>3</sub>)<sub>2</sub>. The smaller electron injection efficiency ( $-0.79$  to  $-0.81$  eV) observed for alkyls and PhCH<sub>3</sub> substituted coumarin systems can be attributed to their lower electron-donating strength than others.

From the previous studies, it is understood that the PCE of DSSCs depends on the free energy change for dye regeneration.<sup>89,90</sup> The lower the  $\Delta G_{\text{reg}}$ , the faster the dye regeneration will be, leading to higher efficiency for the electron injection from the dye to the TiO<sub>2</sub> semiconductor. In the studied systems, the fastest dye regeneration force 0.08 eV has been attained by the N(CH<sub>3</sub>)<sub>2</sub> substituted phenothiazine system (D5-N(CH<sub>3</sub>)<sub>2</sub>), whereas the least dye regeneration (1.27–1.29 eV) has been possessed by alkyls, and PhCH<sub>3</sub> substituted coumarin systems. The unsubstituted systems always possess higher  $\Delta G_{\text{reg}}$  values (0.48–1.39 eV) than substituted ones (0.08–1.29 eV) and this suggests that the introduction of electron-donating substituents on the donor moiety gives better  $\Delta G_{\text{reg}}$  values and improves electron regeneration efficiency. Similarly, a positive effect of substituents on  $eV_{\text{OC}}$  is always observed confirming that by tuning the donating strength of the substituents, significant improvement in the performance of DSSCs can be achieved. In all the six sets, N(CH<sub>3</sub>)<sub>2</sub> substituted systems possess the best  $eV_{\text{OC}}$  and among them, the highest is observed for D1-N(CH<sub>3</sub>)<sub>2</sub> (1.38 eV) whereas the lowest  $eV_{\text{OC}}$  (0.72 eV) is observed for D4-PhCH<sub>3</sub>.

By considering the above-mentioned results, we analyzed the relation between electron donating strength  $\Delta V_{\text{MA}}$  and open-circuit voltage  $eV_{\text{OC}}$  (Fig. 7 and Fig. S1, ESI<sup>†</sup>). The excellent linear correlation observed in all six series of different D- $\pi$ -A systems shows that  $eV_{\text{OC}}$  increases with enhancement in the donating strength of the substituents. Overall the study suggests that by selecting the appropriate donor and substituent, precise tuning of the optical and photovoltaic properties of the D- $\pi$ -A systems can be achieved. Also these results point out that the theoretical examination of the donating strength of the substituents using MESP analysis is promising for dye designing and efficiency prediction of D- $\pi$ -A systems.

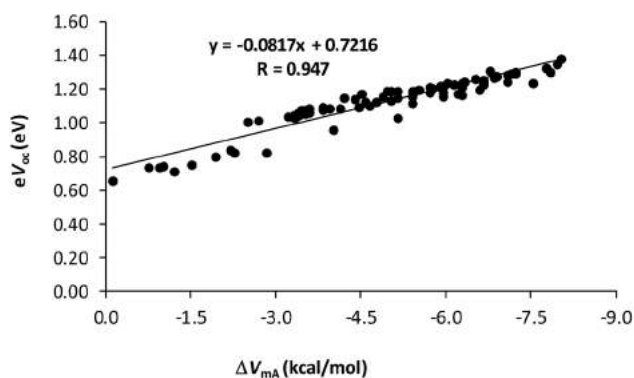


Fig. 7 Correlation between donating strength  $\Delta V_{\text{MA}}$  and open-circuit voltage  $eV_{\text{OC}}$  of D- $\pi$ -A systems.

## Conclusions

The electron-donating strength of the donors in the D- $\pi$ -A system affects the optical and photovoltaic performance of DSSCs, leading to better PCE in the solar cell. In the study using MESP analysis, we have characterized the donating strength ( $\Delta V_{\text{MA}}$ ) of six different sets of D- $\pi$ -A systems, wherein the  $\pi$  and A systems are butadiene and cyanoacrylic acid, respectively. The significance of eleven electron releasing groups at the donors is also examined for a total of seventy-two D- $\pi$ -A systems and achieved the fine-tuning of the electron donation from the donor to the acceptor. In all the six different sets of D- $\pi$ -A systems, the N(CH<sub>3</sub>)<sub>2</sub> substituted D- $\pi$ -A systems show the highest donating strength which can be attributed to the highest electron releasing nature of the N(CH<sub>3</sub>)<sub>2</sub> group. Also, the electron releasing groups at the donors tune the HOMO and LUMO energies of all the corresponding D- $\pi$ -A systems for better optical properties than unsubstituted systems. The optical and photovoltaic performance of the D- $\pi$ -A system is described at the CAM-B3LYP/cc-pVDZ/SMD//B3LYP/cc-pVDZ level. The enhanced performance of these properties achieved with enhanced donating strength conveys the role of tuning the donating strength for better PCE. Among all, the N(CH<sub>3</sub>)<sub>2</sub> substituted D1 system (benzene) possesses the highest  $eV_{\text{OC}}$  which can be attributed to its highest donating strength. These findings suggest that we can improve the photovoltaic performance of DSSCs by tuning the ground state property,  $\Delta V_{\text{MA}}$  at the acceptor site. All the findings imply that incorporation of more electron-releasing substituents on an electron-rich donor moiety improves/tunes the photovoltaic performance by facilitating efficient intramolecular charge transfer in the D- $\pi$ -A system. The correlation plot of  $\Delta V_{\text{MA}}$  with  $eV_{\text{OC}}$  will provide an efficient guideline for developing an effective dye designing strategy for desirable photovoltaic properties.

## Conflicts of interest

There are no conflicts to declare.

## Acknowledgements

The authors thank DST-SERB for funding through GAP1397 and also gratefully acknowledge the CSIR 4th PI for the HPC facility and NIIST IT lab for computational support. V. V. Divya thanks CSIR, India, for the senior research fellowship.

## References

- 1 J. Gong, K. Sumathy, Q. Qiao and Z. Zhou, *Renewable Sustainable Energy Rev.*, 2017, **68**, 234–246.
- 2 Y.-H. Chen, V. S. Nguyen, H.-H. Chou, Y. S. Tingare, T.-C. Wei and C.-Y. Yeh, *ACS Appl. Energy Mater.*, 2020, **3**, 5479–5486.
- 3 N. Mariotti, M. Bonomo, L. Fagiolari, N. Barbero, C. Gerbaldi, F. Bella and C. Barolo, *Green Chem.*, 2020, **22**, 7168–7218.

- 4 B. O'regan and M. Grätzel, *Nature*, 1991, **353**, 737.
- 5 M. K. Nazeeruddin, F. De Angelis, S. Fantacci, A. Selloni, G. Viscardi, P. Liska, S. Ito, B. Takeru and M. Grätzel, *J. Am. Chem. Soc.*, 2005, **127**, 16835–16847.
- 6 G. Marotta, M. A. Reddy, S. P. Singh, A. Islam, L. Han, F. De Angelis, M. Pastore and M. Chandrasekharam, *ACS Appl. Mater. Interfaces*, 2013, **5**, 9635–9647.
- 7 S. Yun, Y. Qin, A. R. Uhl, N. Vlachopoulos, M. Yin, D. Li, X. Han and A. Hagfeldt, *Energy Environ. Sci.*, 2018, **11**, 476–526.
- 8 L. L. Estrella, M. P. Balanay and D. H. Kim, *J. Phys. Chem. A*, 2018, **122**, 6328–6342.
- 9 M. Grätzel, *Nature*, 2001, **414**, 338–344.
- 10 S. Ito, S. M. Zakeeruddin, R. Humphry-Baker, P. Liska, R. Charvet, P. Comte, M. K. Nazeeruddin, P. Péchy, M. Takata and H. Miura, *Adv. Mater.*, 2006, **18**, 1202–1205.
- 11 S. Ito, H. Miura, S. Uchida, M. Takata, K. Sumioka, P. Liska, P. Comte, P. Péchy and M. Grätzel, *Chem. Commun.*, 2008, 5194–5196.
- 12 Q. Yu, Y. Wang, Z. Yi, N. Zu, J. Zhang, M. Zhang and P. Wang, *ACS Nano*, 2010, **4**, 6032–6038.
- 13 L. Han, A. Islam, H. Chen, C. Malapaka, B. Chiranjeevi, S. Zhang, X. Yang and M. Yanagida, *Energy Environ. Sci.*, 2012, **5**, 6057–6060.
- 14 L. E. Polander, A. Yella, J. Teuscher, R. Humphry-Baker, B. F. E. Curchod, N. Ashari Astani, P. Gao, J.-E. Moser, I. Tavernelli, U. Rothlisberger, M. Grätzel, M. K. Nazeeruddin and J. Frey, *Chem. Mater.*, 2013, **25**, 2642–2648.
- 15 S. Mathew, A. Yella, P. Gao, R. Humphry-Baker, B. F. Curchod, N. Ashari-Astani, I. Tavernelli, U. Rothlisberger, M. K. Nazeeruddin and M. Grätzel, *Nat. Chem.*, 2014, **6**, 242–247.
- 16 K. Kakiage, Y. Aoyama, T. Yano, T. Otsuka, T. Kyomen, M. Unno and M. Hanaya, *Chem. Commun.*, 2014, **50**, 6379–6381.
- 17 Y. S. Tingare, N. S. n. Vinh, H. H. Chou, Y. C. Liu, Y. S. Long, T. C. Wu, T. C. Wei and C. Y. Yeh, *Adv. Energy Mater.*, 2017, **7**, 1700032.
- 18 K. Sharma, V. Sharma and S. S. Sharma, *Nanoscale Res. Lett.*, 2018, **13**, 381.
- 19 X. Song, X. Yang, H. Wang, J. An, Z. Yu, X. Wang, A. Hagfeldt and L. Sun, *Sol. Energy*, 2019, **187**, 274–280.
- 20 P. Ferdowsi, Y. Saygili, F. Jazaeri, T. Edvinsson, J. Mokhtari, S. M. Zakeeruddin, Y. Liu, M. Grätzel and A. Hagfeldt, *ChemSusChem*, 2020, **13**, 212–220.
- 21 Y.-Q. Yan, Y.-Z. Zhu, P.-P. Dai, J. Han, M. Yan and J.-Y. Zheng, *New J. Chem.*, 2020, **44**, 12909–12915.
- 22 Y. Chiba, A. Islam, Y. Watanabe, R. Komiya, N. Koide and L. Han, *Jpn. J. Appl. Phys.*, 2006, **45**, L638.
- 23 F. Gao, Y. Wang, D. Shi, J. Zhang, M. Wang, X. Jing, R. Humphry-Baker, P. Wang, S. M. Zakeeruddin and M. Grätzel, *J. Am. Chem. Soc.*, 2008, **130**, 10720–10728.
- 24 S. Tan, J. Zhai, H. Fang, T. Jiu, J. Ge, Y. Li, L. Jiang and D. Zhu, *Chem. – Eur. J.*, 2005, **11**, 6272–6276.
- 25 A. Mishra, M. K. Fischer and P. Bäuerle, *Angew. Chem., Int. Ed.*, 2009, **48**, 2474–2499.
- 26 T. Mori, H. Saomoto, K. Machitani, K. Inoue, Y. Aoki, T. Koshitani, N. Koumura and T. N. Murakami, *RSC Adv.*, 2016, **6**, 13964–13970.
- 27 K. Hara, Y. Dan-oh, C. Kasada, Y. Ohga, A. Shinpo, S. Suga, K. Sayama and H. Arakawa, *Langmuir*, 2004, **20**, 4205–4210.
- 28 K. Hara, T. Sato, R. Katoh, A. Furube, T. Yoshihara, M. Murai, M. Kurashige, S. Ito, A. Shinpo and S. Suga, *Adv. Funct. Mater.*, 2005, **15**, 246–252.
- 29 R. Chen, X. Yang, H. Tian, X. Wang, A. Hagfeldt and L. Sun, *Chem. Mater.*, 2007, **19**, 4007–4015.
- 30 Z.-S. Wang, Y. Cui, Y. Dan-oh, C. Kasada, A. Shinpo and K. Hara, *J. Phys. Chem. C*, 2007, **111**, 7224–7230.
- 31 S. Hwang, J. H. Lee, C. Park, H. Lee, C. Kim, C. Park, M.-H. Lee, W. Lee, J. Park and K. Kim, *Chem. Commun.*, 2007, 4887–4889.
- 32 J. Preat, D. Jacquemin, C. Michaux and E. A. Perpète, *Chem. Phys.*, 2010, **376**, 56–68.
- 33 H. Tian, I. Bora, X. Jiang, E. Gabrielsson, K. M. Karlsson, A. Hagfeldt and L. Sun, *J. Mater. Chem.*, 2011, **21**, 12462–12472.
- 34 A. Dhar, N. Siva Kumar, M. Asif and R. L. Vekariya, *New J. Chem.*, 2018, **42**, 12024–12031.
- 35 Y. Ren, D. Sun, Y. Cao, H. N. Tsao, Y. Yuan, S. M. Zakeeruddin, P. Wang and M. Grätzel, *J. Am. Chem. Soc.*, 2018, **140**, 2405–2408.
- 36 T. Kitamura, M. Ikeda, K. Shigaki, T. Inoue, N. A. Anderson, X. Ai, T. Lian and S. Yanagida, *Chem. Mater.*, 2004, **16**, 1806–1812.
- 37 D. P. Hagberg, T. Marinado, K. M. Karlsson, K. Nonomura, P. Qin, G. Boschloo, T. Brinck, A. Hagfeldt and L. Sun, *J. Org. Chem.*, 2007, **72**, 9550–9556.
- 38 H. Tian, X. Yang, R. Chen, R. Zhang, A. Hagfeldt and L. Sun, *J. Phys. Chem. C*, 2008, **112**, 11023–11033.
- 39 J. Zhang, H.-B. Li, S.-L. Sun, Y. Geng, Y. Wu and Z.-M. Su, *J. Mater. Chem.*, 2012, **22**, 568–576.
- 40 J. Zhang, Y.-H. Kan, H.-B. Li, Y. Geng, Y. Wu and Z.-M. Su, *Dyes Pigm.*, 2012, **95**, 313–321.
- 41 Z. Yao, L. Yang, Y. Cai, C. Yan, M. Zhang, N. Cai, X. Dong and P. Wang, *J. Phys. Chem. C*, 2014, **118**, 2977–2986.
- 42 T. Horiuchi, H. Miura, K. Sumioka and S. Uchida, *J. Am. Chem. Soc.*, 2004, **126**, 12218–12219.
- 43 W. Xu, B. Peng, J. Chen, M. Liang and F. Cai, *J. Phys. Chem. C*, 2008, **112**, 874–880.
- 44 J. Preat, *J. Phys. Chem. C*, 2010, **114**, 16716–16725.
- 45 D. Patil, M. Jadhav, K. Avhad, T. H. Chowdhury, A. Islam, I. Bedja and N. Sekar, *New J. Chem.*, 2018, **42**, 11555–11564.
- 46 H.-L. Jia, Z.-J. Peng, Y.-C. Chen, C.-Y. Huang and M.-Y. Guan, *New J. Chem.*, 2018, **42**, 18702–18707.
- 47 L. Zhang, W. Shen, R. He, X. Liu, Z. Fu and M. Li, *J. Mol.*, 2014, **20**, 2489.
- 48 N. Inostroza, F. Mendizabal, R. Arratia-Pérez, C. Orellana and C. Linares-Flores, *J. Mol. Model.*, 2016, **22**, 25.
- 49 S. Gauthier, F. Robin-Le Guen, L. Wojcik, N. Le Poul, A. Planchat, Y. Pellegrin, P. G. Level, N. Szuwarski, M. Boujtita and D. Jacquemin, *Dyes Pigm.*, 2019, **171**, 107747.

- 50 V. V. Divya, F. B. Sayyed and C. H. Suresh, *ChemPhysChem*, 2019, **20**, 1752–1758.
- 51 S. R. Gadre, S. A. Kulkarni and I. H. Shrivastava, *J. Chem. Phys.*, 1992, **96**, 5253–5260.
- 52 S. R. Gadre and R. N. Shirsat, *Electrostatics of Atoms and Molecules*, Universities Press, 2000.
- 53 P. Politzer and D. G. Truhlar, *Chemical Applications of Atomic and Molecular Electrostatic potentials: Reactivity, Structure, Scattering, and Energetics of Organic, Inorganic, and Biological systems*, Springer Science & Business Media, 2013.
- 54 C. H. Suresh and N. Koga, *Inorg. Chem.*, 2002, **41**, 1573–1578.
- 55 C. H. Suresh, *Inorg. Chem.*, 2006, **45**, 4982–4986.
- 56 J. Mathew, T. Thomas and C. H. Suresh, *Inorg. Chem.*, 2007, **2007**(46), 10800–10809.
- 57 G. S. Remya and C. H. Suresh, *Phys. Chem. Chem. Phys.*, 2016, **18**, 20615–20626.
- 58 E. Scrocco and J. Tomasi, *New concepts II*, Springer, 1973, pp. 95–170.
- 59 J. S. Murray and P. Politzer, *Wiley Interdiscip. Rev.: Comput. Mol. Sci.*, 2011, **1**, 153–163.
- 60 F. B. Sayyed and C. H. Suresh, *New J. Chem.*, 2009, **33**, 2465–2471.
- 61 C. H. Suresh, P. Alexander, K. P. Vijayalakshmi, P. K. Sajith and S. R. Gadre, *Phys. Chem. Chem. Phys.*, 2008, **10**, 6492–6499.
- 62 F. B. Sayyed and C. H. Suresh, *Tetrahedron Lett.*, 2009, **50**, 7351–7354.
- 63 P. K. Sajith and C. H. Suresh, *Inorg. Chem.*, 2012, **51**, 967–977.
- 64 F. B. Sayyed and C. H. Suresh, *J. Phys. Chem. A*, 2011, **115**, 9300–9307.
- 65 V. V. Divya and C. H. Suresh, *New J. Chem.*, 2020, **44**, 7200–7209.
- 66 L. Liu, L. Miao, L. Li, F. Li, Y. Lu, Z. Shang and J. Chen, *J. Phys. Chem. Lett.*, 2018, **9**, 3573–3579.
- 67 M. R. Narayan, *Renewable Sustainable Energy Rev.*, 2012, **16**, 208–215.
- 68 L. M. Fraas and L. D. Partain, *Solar Cells and Their Applications*, John Wiley & Sons, 2010.
- 69 Y. Tachibana, K. Hara, K. Sayama and H. Arakawa, *Chem. Mater.*, 2002, **2002**(14), 2527–2535.
- 70 A. Mihi and H. Míguez, *J. Phys. Chem. B*, 2005, **109**, 15968–15976.
- 71 J. Preat, C. Michaux, D. Jacquemin and E. A. Perpète, *J. Phys. Chem. C*, 2009, **113**, 16821–16833.
- 72 R. Katoh, A. Furube, T. Yoshihara, K. Hara, G. Fujihashi, S. Takano, S. Murata, H. Arakawa and M. Tachiya, *J. Phys. Chem. B*, 2004, **108**, 4818–4822.
- 73 N. N. Ghosh, M. Habib, A. Pramanik, P. Sarkar and S. Pal, *New J. Chem.*, 2019, **43**, 6480–6491.
- 74 J. B. Asbury, Y.-Q. Wang, E. Hao, H. N. Ghosh and T. Lian, *Res. Chem. Intermed.*, 2001, **27**, 393–406.
- 75 T. Koopmans, *Physica*, 1933, **1**, 104–113.
- 76 W.-L. Ding, D.-M. Wang, Z.-Y. Geng, X.-L. Zhao and Y.-F. Yan, *J. Phys. Chem. C*, 2013, **117**, 17382–17398.
- 77 G. Boschloo and A. Hagfeldt, *Acc. Chem. Res.*, 2009, **42**, 1819–1826.
- 78 C.-R. Zhang, Z.-J. Liu, Y.-H. Chen, H.-S. Chen, Y.-Z. Wu, W. Feng and D.-B. Wang, *Curr. Appl. Phys.*, 2010, **10**, 77–83.
- 79 A. D. Becke, *J. Chem. Phys.*, 1993, **98**, 1372–1377.
- 80 T. H. Dunning Jr, *Chem. Phys.*, 1989, **90**, 1007–1023.
- 81 H. Gotfredsen, T. Neumann, F. E. Storm, A. V. Muñoz, M. Jevric, O. Hammerich, K. V. Mikkelsen, M. Freitag, G. Boschloo and M. B. Nielsen, *ChemPhotoChem*, 2018, **2**, 976–985.
- 82 M. Pastore, E. Mosconi, F. De Angelis and M. Grätzel, *J. Phys. Chem. C*, 2010, **114**, 7205–7212.
- 83 T. Yanai, D. P. Tew and N. C. Handy, *Chem. Phys. Lett.*, 2004, **393**, 51–57.
- 84 A. V. Marenich, C. J. Cramer and D. G. Truhlar, *J. Phys. Chem. B*, 2009, **113**, 6378–6396.
- 85 M. J. Frisch, G. W. Trucks, H. B. Schlegel, G. E. Scuseria, M. A. Robb, J. R. Cheeseman, G. Scalmani, V. Barone, G. A. Petersson, H. Nakatsuji, X. Li, M. Caricato, A. V. Marenich, J. Bloino, B. G. Janesko, R. Gomperts, B. Mennucci, H. P. Hratchian, J. V. Ortiz, A. F. Izmaylov, J. L. Sonnenberg, D. Williams-Young, F. Ding, F. Lipparini, F. Egidi, J. Goings, B. Peng, A. Petrone, T. Henderson, D. Ranasinghe, V. G. Zakrzewski, J. Gao, N. Rega, G. Zheng, W. Liang, M. Hada, M. Ehara, K. Toyota, R. Fukuda, J. Hasegawa, M. Ishida, T. Nakajima, Y. Honda, O. Kitao, H. Nakai, T. Vreven, K. Throssell, J. A. Montgomery Jr., J. E. Peralta, F. Ogliaro, M. J. Bearpark, J. J. Heyd, E. N. Brothers, K. N. Kudin, V. N. Staroverov, T. A. Keith, R. Kobayashi, J. Normand, K. Raghavachari, A. P. Rendell, J. C. Burant, S. S. Iyengar, J. Tomasi, M. Cossi, J. M. Millam, M. Klene, C. Adamo, R. Cammi, J. W. Ochterski, R. L. Martin, K. Morokuma, O. Farkas, J. B. Foresman and D. J. Fox, *Gaussian 16, Revision A.03*, Gaussian, Wallingford, CT, 2016.
- 86 R. Menzel, D. Ogermann, S. Kupfer, D. Wei, G. Helmar, K. Kleinermanns, L. González and R. Beckert, *Dyes Pigm.*, 2012, **94**, 512–524.
- 87 S. Kupfer, J. Guthmuller and L. Gonzalez, *J. Chem. Theory Comput.*, 2013, **9**, 543–554.
- 88 A. Kumar, S. R. Gadre, N. Mohan and C. H. Suresh, *J. Phys. Chem. A*, 2014, **118**, 526–532.
- 89 S. M. Feldt, G. Wang, G. Boschloo and A. Hagfeldt, *J. Phys. Chem. C*, 2011, **115**, 21500–21507.
- 90 W. Yang, N. Vlachopoulos, Y. Hao, A. Hagfeldt and G. Boschloo, *Phys. Chem. Chem. Phys.*, 2015, **17**, 15868–15875.





Cite this: DOI: 10.1039/d1nj00881a

# Design and DFT study of nitrogen-rich donor systems for improved photovoltaic performance in dye-sensitized solar cells†

 Velayudhan V. Divya<sup>ab</sup> and Cherumuttathu H. Suresh \*<sup>ab</sup>

Eighteen electron-rich nitrogen incorporated donors with a butadiene  $\pi$ -spacer and a cyanoacrylic acid acceptor (A) as photosensitizers (D1- $\pi$ -A to D18- $\pi$ -A) for dye-sensitized solar cell (DSSC) applications have been designed for improving the photovoltaic performance. The significance of the nitrogen centres for revamping the donating strength ( $\Delta V_{\text{MA}}$ ) of D- $\pi$ -A is scrutinized using molecular electrostatic potential (MESP) analysis at the B3LYP/cc-pVDZ level of density functional theory (DFT). During the transformation of a donor (D) to D- $\pi$ -A, a certain delocalization of electron density from D to  $\pi$ -A has occurred, and the change in the MESP minimum ( $\Delta V_{\text{MA}}$ ) observed at the cyano region of D- $\pi$ -A is related to the donating strength of D. Optical and photovoltaic properties are analyzed at the TD/CAM-B3LYP/cc-pVDZ/SMD//B3LYP/cc-pVDZ level. In D1- $\pi$ -A to D18- $\pi$ -A,  $\Delta V_{\text{MA}}$  is in the range  $-7.0$  to  $-19.0$  kcal mol<sup>-1</sup> and the increase in donating strength is found to be proportional to the number of planar nitrogens in the donors. D12- $\pi$ -A exhibited the most negative  $\Delta V_{\text{MA}}$  ( $-19.0$  kcal mol<sup>-1</sup>), indicating the highest electron-donating strength of D12, whereas the least negative  $\Delta V_{\text{MA}}$  ( $-7.0$  kcal mol<sup>-1</sup>) displayed by D7- $\pi$ -A is correlated to the weak donating character of D7. By increasing the electron-donating strength of D in D- $\pi$ -A, a red-shift in the absorption maximum ( $\Delta\lambda_{\text{max}}$ ) by 162 to 294 nm is observed. Further, the open-circuit voltage ( $eV_{\text{oc}}$ ) calculated for the D- $\pi$ -A systems showed a strong linear relationship with  $\Delta V_{\text{MA}}$ . The LUMO (lowest unoccupied molecular orbital) energy of all the D- $\pi$ -A systems ( $-1.79$  to  $-2.79$  eV) is observed above the conduction band (CB) energy of TiO<sub>2</sub> ( $-4.0$  eV), which ensured a desirable electron injection efficiency ( $\Delta G_{\text{inject}}$ ) for them. The analysis of the adsorption energy ( $E_{\text{ads}}$ ) of the D- $\pi$ -A systems on the TiO<sub>2</sub> semiconductor (D- $\pi$ -A/TiO<sub>2</sub>) showed that D12- $\pi$ -A has the highest adsorption stability. Improving the adsorption stability is better for improving  $eV_{\text{oc}}$  and the power conversion efficiency (PCE). The maximum absorption wavelength ( $\lambda_{\text{max}}$ ) of the D- $\pi$ -A/TiO<sub>2</sub> systems ranges from 513 to 703 nm and all of them display a red-shift with respect to the bare D- $\pi$ -A systems. The study suggests D12 as the most efficient photosensitizer for DSSC applications. Further, it deepens the understanding of the structure-performance relationship of D- $\pi$ -A systems as photosensitizers.

 Received 21st February 2021,  
 Accepted 22nd May 2021

DOI: 10.1039/d1nj00881a

[rsc.li/njc](http://rsc.li/njc)

## Introduction

The utilization of a renewable source of energy, preferably solar energy, for the ever-growing energy demand could diminish global climate change, which leads to sustainable livelihood on earth.<sup>1-4</sup> Since solar energy is the most abundant green energy alternative for the future energy crisis, more research efforts have to invest in the development of photovoltaic strategies

based on solar power.<sup>1,3-5</sup> Over the past three decades, the third generation photovoltaic technology employed in dye-sensitized solar cells (DSSCs) has acquired a notable position over conventional silicon-based solar cells due to the simple synthetic strategy, easier structure modification, large absorption coefficient, and low production cost.<sup>3,5-11</sup> The major components employed in a DSSC device include photosensitizers, electrolytes, and electrode materials; modifications in those components lead to the enhancement of the power conversion efficiency (PCE) of the solar cell.<sup>12</sup> Generally in DSSCs, Ru-based sensitizers have greater PCEs than organic dye sensitizers, which show a comparable PCE to silicon-based solar cells.<sup>3</sup> Whereas, the highly expensive nature and rare chance of occurrence of Ru-metal mean that its practical application in DSSCs is limited.<sup>3,13</sup>

<sup>a</sup> Chemical Sciences and Technology Division, CSIR-National Institute for Interdisciplinary Science and Technology, Thiruvananthapuram, Kerala 695 019, India. E-mail: sureshch@niist.res.in

<sup>b</sup> Academy of Scientific and Innovative Research (AcSIR), Ghaziabad 201002, India

† Electronic supplementary information (ESI) available. See DOI: 10.1039/d1nj00881a

After the invention of the DSSC device by O'Regan and Grätzel in 1991,<sup>6</sup> extensive research efforts have been invested in the synthesis and device modelling of metal-free organic sensitizers, which leads to the improvement of the PCE.<sup>13–21</sup> Usually, organic sensitizers comprise a D- $\pi$ -A framework where D,  $\pi$ , and A denote the donor,  $\pi$ -spacer and acceptor, respectively. So far large varieties of structural modifications in the D- $\pi$ -A structural framework have been performed, reveal that tuning the donating strength of the donor could significantly influence the absorption range and photovoltaic parameters.<sup>12,22–29</sup> In our previous study, we quantified the electron-donating strength of eight typically used donor systems, *viz* pyrene, perylene, chrysene, triphenylamine, carbazole, phenothiazine, julolidine, *N,N*-dialkylaniline, ullazine and coumarin, in the D- $\pi$ -A system and revealed that julolidine and *N,N*-dialkylaniline based  $\pi$ -A systems are the most efficient sensitizers for DSSCs.<sup>22</sup> For improved optical and photovoltaic properties of D- $\pi$ -A systems the particular analysis recommends the incorporation of electron-rich heteroatoms (preferably nitrogen) in donors. The literature shows that non-planar donors, especially triphenylamine, carbazole and indoline, reduce the electron transfer ability and overall conjugation in the donor group with the  $\pi$ -A system leading to lower light-harvesting efficiency of the dye sensitizer.<sup>30,31</sup> The mentioned reducing factors are rectified through the introduction of planarized nitrogen incorporated donors *viz.* ullazine and indolizine as photosensitizers.<sup>30–33</sup> Further, the rational design of photosensitizers with nitrogen annulation at the bay region of a polycyclic aromatic hydrocarbon (PAH) system provides a remarkable PCE in DSSCs.<sup>34</sup> For example, perylene based PAH systems as donors in DSSCs have disappointing PCEs,<sup>35–37</sup> whereas an N-annulated perylene (NP) core as a donor with phenyl functional groups results in an improved PCE of about 10.5%.<sup>38</sup> Later, Wang *et al.* modified the NP core with bulky substituents to obtain PCEs up to 10.4%.<sup>39</sup> This re-engineered chromophore was again modified with an N-annulated indenoperylene unit as the donor and reached a PCE of 12.5%.<sup>40</sup> The aforementioned studies reveal that structural modifications with N-annulation in PAH systems enhance the intramolecular charge transfer (ICT) due to the planar structure. Also, the multiple substitution sites involved in PAHs increase the possibility of molecular engineering. Recently Subramanian *et al.* described that a more N-doped polyaromatic hydrocarbon analogue of ullazine contributes a large dipole moment and more planarization to the dye-sensitizers, thus resulting in higher light-harvesting efficiency (LHE) than the donors with a single N-doping site.<sup>25</sup>

In this context, the most significant approach for an efficient photosensitizer is the engineering of electron-rich planar donors. Correspondingly, it is worthwhile to evaluate the role of nitrogen centres in donors for enhancing the donating strength. To tackle the failings of the electron transfer ability and overall conjugation in the donor group with the  $\pi$ -A system, we designed eighteen electron-rich nitrogen incorporated donors (D1–D18) as dye sensitizers for DSSC application (Fig. 1). For the  $\pi$ -A framework, butadiene and cyanoacrylic acid have been considered. In our previous study,<sup>41</sup> we proved

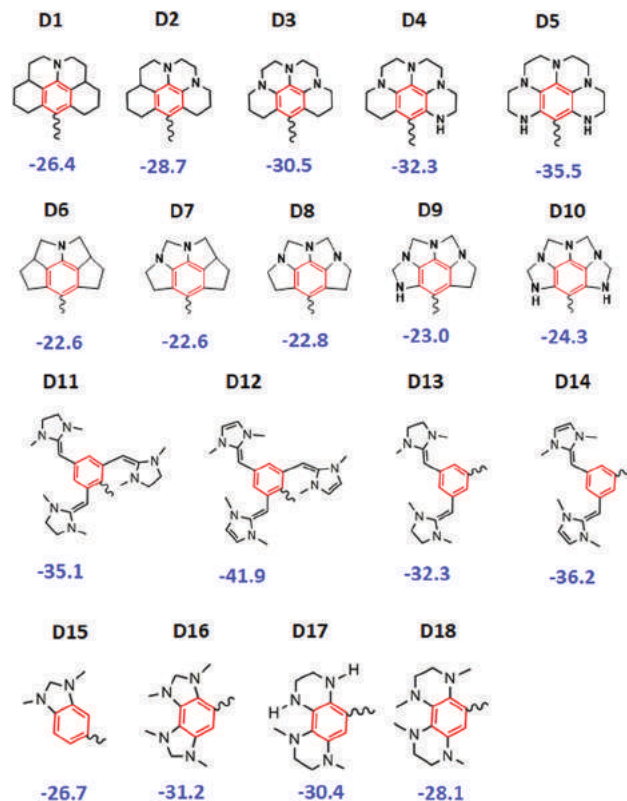


Fig. 1 Designed donor systems. The MESP minimum over the phenyl ring ( $V_{md}$ ) is given in kcal mol<sup>-1</sup>.

that butadiene exhibits better electronic effect transmitting power than thiophene, furan and benzylic spacers. Hence, for better electronic charge transfer from D to A, a butadiene  $\pi$ -spacer and cyanoacrylic acid as an acceptor have been considered.

In the analysis, the D1–D5 donors are designed from known donor julolidine (Fig. S1a, ESI<sup>†</sup>), where the possibility of N-annulation in the julolidine core has been attempted (D1 to D5) to enhance the electron-donating strength of the designed systems compared to julolidine (the calculated electron-donating strength,  $\Delta V_{MA}$ , of julolidine by MESP analysis is  $-9.2$  kcal mol<sup>-1</sup><sup>22</sup>). Julolidine is an N-heterocyclic aromatic compound which comprises alkyl bridges between amino nitrogen and ring *ortho* carbon atoms.<sup>42,43</sup> Because of the high efficiency in energy conversion and fluorescent properties, julolidine derivatives have been used in the construction of dye-sensitized solar cells and photoconductive materials, as fluorescent sensors for bio-imaging, *etc.*<sup>44</sup> The conjugation of the aromatic part of the molecule with its amino substituent is an indicator of the ability of the nitrogen atom to possess  $sp^2$ -hybridization, which enhances the donating strength of this class of compounds.<sup>45</sup> In D6–D10, five-membered rings at the aromatic ring system have been considered for N-annulation; those systems are derived from 1,2,4,5-tetrahydropyrrolo[3,2,1-hi]indole (Fig. S1b, ESI<sup>†</sup>).<sup>43</sup> Among the designed N-heterocyclic systems (D1–D10), some of the derivatives are known and they are the best candidates for intramolecular cyclization and for generating diboryne nanowires.<sup>46,47</sup> Donors D11–D14 are

designed from the electron-rich nature of the phenyl/ $\pi$ -system. According to various experimental and theoretical studies, the electron-rich nature of the phenyl/ $\pi$ -system could be fine-tuned by electron-donating substituents and hence the aromatic ring of 1,3,5-*N,N*-dimethyltriaminobenzene could be considered as the most electron-rich neutral six-membered ring.<sup>48</sup> Previously, Suresh and Sayyed described that the electron density at the phenyl ring could be significantly improved by the treatment of *N*-heterocyclic ring substitution and they proposed two highly electron rich systems *viz.* D11 and D12 as shown in Fig. 1.<sup>48</sup> Since those systems are considered as electron rich (involving six nitrogen lone pairs), we could test the suitability of those systems as photosensitizers for DSSC application. Finally, two, and four nitrogens have been integrated in D15–D18, where the likelihood of *N*-annulation has been attained through *N*-heterocyclic five and six membered rings.<sup>49,50</sup>

For evaluating the donating strength of the donors in *D*– $\pi$ –*A*, the intramolecular charge transfer (ICT) from *D* to *A* has to be assessed. Here it has been quantified in terms of the change in the molecular electrostatic potential (MESP) minimum,  $\Delta V_m$ , at the cyano group of *A*. Very recently we proved that the MESP is an excellent tool to quantify the electron-donating strength ( $\Delta V_m$ ) of *D*– $\pi$ –*A* systems.<sup>22,26</sup> It is a real physical property which is experimentally observable from X-ray diffraction studies. To understand the reactivity of molecular systems, theoretically derived MESP have been extensively used in the work of Tomasi,<sup>51</sup> Pullman,<sup>52,53</sup> Politzer<sup>54–57</sup> and Gadre,<sup>58–60</sup> and the wide range of applications in chemical and biological phenomena shows the acceptability of this area of research. Further, our group has contributed to several applications of the MESP parameter in organic and inorganic chemistry and described that the MESP is an excellent tool for the prediction of structure–property relationships.<sup>61–71</sup> In the present study the significance of *N*-annulation for improved optical and photovoltaic properties has been evaluated using density functional theory (DFT) and time-dependent DFT (TDDFT) calculations. Currently, quantum chemical calculations have emerged as an elementary tactic to identify potential sensitizers before long-running expensive synthesis.<sup>72–78</sup> Thus our computationally engineered dye sensitizers could open up new synthetic strategies for the development of photosensitizers for DSSC application.

## Computational details

Density functional theory (DFT) calculations at the B3LYP/cc-pVDZ level have been conducted for the optimization of the ground state geometries of the *D*– $\pi$ –*A* systems.<sup>79,80</sup> It is substantiated that the B3LYP level is adequate for the explanation of the electronic structure of dye molecules in DSSC applications.<sup>26,81,82</sup> The ground state geometries of all *D*– $\pi$ –*A* systems after binding to the (TiO<sub>2</sub>)<sub>9</sub> cluster are optimized at the same level of DFT with the LANL2DZ basis set for the Ti atom and cc-pVDZ for non-metal atoms.<sup>83</sup> Vibrational frequencies are calculated at the same level and it is confirmed that there are no imaginary frequencies. Studies show that the (TiO<sub>2</sub>)<sub>9</sub>

cluster size is sufficient to model the dye–TiO<sub>2</sub> interfaces for simulating the electronic structure, optical properties, and binding modes of TiO<sub>2</sub>.<sup>84</sup> Frontier molecular orbital energies of all *D*– $\pi$ –*A* and *D*– $\pi$ –*A* adsorbed on (TiO<sub>2</sub>)<sub>9</sub> cluster systems (*D*– $\pi$ –*A*/TiO<sub>2</sub>) are reported for the ground-state geometries. The optical properties of the *D*– $\pi$ –*A* systems before and after binding to the (TiO<sub>2</sub>)<sub>9</sub> cluster are simulated using time-dependent DFT (TD DFT) at the CAM-B3LYP level<sup>85</sup> on the ground state geometry with mixed basis sets. To account for the solvent effect (dichloromethane as the solvent), SCRF-SMD (self-consistent reaction field-density simulation model) incorporated in the Gaussian 16 suite of programs has been considered. The CAM-B3LYP exchange–correlation functional is widely used in theoretical calculations for the excited state properties and provides results that are close to experimental results.<sup>86–88</sup> In our previous study, the absorption properties of experimentally known dye sensitizers have been benchmarked including julolidine based dye-sensitizers and it is found that the TD-CAM B3LYP/cc-pVDZ/SMD//B3LYP/cc-pVDZ level is adequate to describe the electronic, optical and photovoltaic properties.<sup>22</sup> The higher excitation energy associated with the CAM-B3LYP exchange functional than the B3LYP functional can be attributed to the higher bond length alteration index (BLA) of *D*– $\pi$ –*A* systems.<sup>26</sup> Moreover, for the examination of the intramolecular charge transfer characteristics of *D*– $\pi$ –*A* systems, molecular electrostatic potential based topographical analysis has been performed on the ground state geometry at the B3LYP/cc-pVDZ level. All the calculations are performed with the Gaussian 16 program package.<sup>89</sup>

The molecular electrostatic potential (MESP),  $V(\mathbf{r})$ , is an important property of a molecule that its nuclei and electrons create at every point  $\mathbf{r}$  in the surrounding space, which is defined in eqn (1) as

$$V(\mathbf{r}) = \sum_A^N \frac{Z_A}{|\mathbf{r} - \mathbf{R}_A|} - \int \frac{\rho(\mathbf{r}')d\mathbf{r}'}{|\mathbf{r} - \mathbf{r}'|} \quad (1)$$

where  $N$  is the total number of nuclei,  $Z_A$  is the charge on nucleus  $A$  located at distance  $R_A$ ,  $\rho(\mathbf{r}')$  is the electron density of the molecule, and  $\mathbf{r}'$  is a dummy integration variable. In the equation, the sign of  $V(\mathbf{r})$  at any  $\mathbf{r}$  depends upon whether the positive contribution of the nuclei or the negative one of the electrons is dominant there.

## Results and discussion

### MESP analysis of the donors

The MESP minimum  $V_m$  gives a clear idea regarding the most electron-rich region in a molecular system. In all the donor systems (D1–D18), an aromatic phenyl ring (shown in a red colour, Fig. 1) has been observed and  $V_m$  observed at that phenyl ring,  $V_{mD}$ , has been considered as the donor strength of each system. The most negative  $V_m$  depicts the most electron-rich nature of the molecular system. From D1 to D5, a systematic increase in the *N*-centers (up to 5 nitrogens) is introduced and  $V_{mD}$  reached  $-35.5$  kcal mol<sup>-1</sup> from  $-26.4$  kcal mol<sup>-1</sup>. The more

negative  $V_{\text{mD}}$  in D5 ( $-35.5 \text{ kcal mol}^{-1}$ ) than those of D1–D4 characterizes the more electron-rich nature, which can be attributed to the occurrence of five nitrogen centers. In the D6–D10 donors, an increase in the negative character of  $V_{\text{mD}}$  (from  $-22.6$  to  $-24.3 \text{ kcal mol}^{-1}$ ) has been attained by a systematic increase of the nitrogen atoms (up to 5 nitrogens). Meanwhile, due to the presence of more pyramidalized nitrogens, the D6–D10 donors provide less negative  $V_{\text{mD}}$  than those of D1–D5.

In the D11–D12 donors, imidazolidine and imidazole ring systems have been introduced at the 1, 3, and 5 positions of the benzene ring. In D11, the electron-rich aminal functional groups increase the electron density over the phenyl ring, resulting in a comparable  $V_{\text{mD}}$  of  $-35.1 \text{ kcal mol}^{-1}$  to D5 ( $-35.5 \text{ kcal mol}^{-1}$ ). In D12 the conjugation in the CC bond enhances the electron density over the phenyl ring, leading to a more negative  $V_{\text{mD}}$  ( $-41.9 \text{ kcal mol}^{-1}$ ) than D11. Due to the reduced number of aminal functional groups at the phenyl ring, D13 shows a less negative  $V_{\text{mD}}$  ( $-32.3 \text{ kcal mol}^{-1}$ ) than those of D11 and D12. In D14, conjugation increases the electron density of the donor system, resulting in a more negative  $V_{\text{mD}}$  ( $-36.2 \text{ kcal mol}^{-1}$ ) than D13. It is noted that the imidazolidine and imidazole substituted donor systems *viz.* D12 and D14 exhibit more negative  $V_{\text{mD}}$  than D5, which can be considered as their better donor strength. Finally, for verifying the effectiveness of the introduced strategy, the D15–D18 donors are examined. In D16 the increased number of *N*-alkyl substitutions at the phenyl ring resulted in a more negative  $V_{\text{mD}}$  ( $-31.2 \text{ kcal mol}^{-1}$ ) than D15 ( $V_{\text{mD}} = -26.7 \text{ kcal mol}^{-1}$ ). Compared to D15, a more negative  $V_{\text{mD}}$  is observed for D17, which can be attributed to the presence of an additional two nitrogen centres. Finally, in D18 the additional two methyl groups at nitrogen atoms promote pyramidalization of the *N*-centres, resulting in a less negative  $V_{\text{mD}}$  ( $-28.1 \text{ kcal mol}^{-1}$ ) than D17.

### Donating strength of the D- $\pi$ -A systems

The influence of the electron-rich nitrogen lone pairs in the donors (D) for enhancing the electron-donating strength of the D- $\pi$ -A system ( $\Delta V_{\text{mA}}$ ) has been elucidated with MESP analysis. In D- $\pi$ -A systems, the  $\pi$ -A linkage with the donor involves intramolecular charge transfer (ICT) from D to A, and the transferred electron density accumulated at A depends on the donor strength of each system.<sup>22,26</sup> The electron density distribution *via* ICT at various regions of a representative D- $\pi$ -A system (D1- $\pi$ -A), *viz.* D, the  $\pi$ -spacer and A, has been shown in Fig. 2b as the MESP minima at the donor  $V_{\text{mD}'}$ , spacer  $V_{\text{mS}'}$  and acceptor  $V_{\text{mA}'}$ . Since the  $\pi$ -A part (butadiene) involved in the study is the same for all D- $\pi$ -A systems, the MESP minimum observed at the CN group of A has been considered as the reference  $V_{\text{mA}}$  to evaluate the changes observed at that minimum with the attachment of D (Fig. 2a). Also, it is proved that one could take other  $V_{\text{m}}$  regions at A as the reference  $V_{\text{m}}$  *viz.*  $V_{\text{m(OH)}}$  and  $V_{\text{m(CO)}}$  for monitoring the changes at the respective sites due to the parallel behavior exhibited by those parameters.<sup>26</sup> In the study,  $V_{\text{mA}'}$  (observed at the CN region) has been selected as the reference point due to the most negative  $V_{\text{m}}$  character.

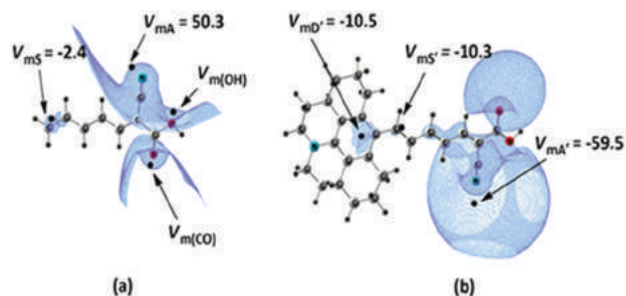


Fig. 2 (a) MESP isosurface at various sites of (a) the reference system, and (b) a representative D- $\pi$ -A system, where the MESP minimum is shown in  $\text{kcal mol}^{-1}$ .

Table 1  $V_{\text{m}}$  ( $\text{kcal mol}^{-1}$ ) of the D- $\pi$ -A systems calculated at the B3LYP/cc-pVDZ level

Systems	$V_{\text{mD}}$	$V_{\text{mD}'}$	$\Delta V_{\text{mD}}$	$V_{\text{mS}'}$	$V_{\text{mS}}$	$\Delta V_{\text{mS}}$	$V_{\text{mA}'}$	$V_{\text{mA}}$	$\Delta V_{\text{mA}}$
D1	-26.4	-10.5	15.9	-10.3	-2.4	-7.9	-59.5	-50.3	-9.2
D2	-28.7	-13.0	15.7	-11.7	-2.4	-9.3	-60.3	-50.3	-10.0
D3	-30.5	-14.1	16.4	-12.3	-2.4	-9.9	-60.8	-50.3	-10.5
D4	-32.3	-14.9	17.4	-13.2	-2.4	-10.9	-61.3	-50.3	-11.0
D5	-35.5	-17.6	17.9	-18.6	-2.4	-16.3	-63.8	-50.3	-13.5
D6	-22.6	-9.0	13.6	-9.3	-2.4	-7.0	-58.2	-50.3	-7.8
D7	-22.6	-9.7	12.9	-8.8	-2.4	-6.4	-57.4	-50.3	-7.0
D8	-22.8	-10.6	12.2	-8.3	-2.4	-6.0	-56.2	-50.3	-5.9
D9	-23.0	-10.5	12.5	-9.5	-2.4	-7.1	-57.9	-50.3	-7.5
D10	-24.3	-12.0	12.4	-10.4	-2.4	-8.0	-58.7	-50.3	-8.4
D11	-35.1	-22.8	12.3	-18.4	-2.4	-16.1	-64.0	-50.3	-13.7
D12	-41.9	-28.7	13.2	-18.4	-2.4	-16.1	-69.3	-50.3	-19.0
D13	-32.3	-20.7	11.6	-11.1	-2.4	-8.7	-58.2	-50.3	-7.9
D14	-36.2	-24.1	12.1	-14.6	-2.4	-12.2	-60.0	-50.3	-9.7
D15	-26.7	-11.6	15.1	-10.4	-2.4	-8.0	-58.5	-50.3	-8.2
D16	-31.2	-13.9	17.3	-13.1	-2.4	-10.7	-62.0	-50.3	-11.7
D17	-30.4	-16.2	14.2	-11.6	-2.4	-9.2	-58.9	-50.3	-8.5
D18	-28.1	-13.5	14.6	-9.9	-2.4	-7.5	-58.4	-50.3	-8.1

In Table 1,  $V_{\text{m}}$  values at D, the  $\pi$ -spacer and A of the D- $\pi$ -A systems are reported along with the change in  $V_{\text{m}}$  at those regions with the attachment of  $\pi$ -A to D. The change in  $V_{\text{m}}$  occurring at the D site ( $\Delta V_{\text{mD}}$ ) has been calculated by subtracting  $V_{\text{m}}$  observed at the donor ( $V_{\text{mD}}$ ) from the corresponding  $V_{\text{m}}$  observed at D of D- $\pi$ -A ( $V_{\text{mD}'}$ ). Likewise,  $\Delta V_{\text{mS}}$  and  $\Delta V_{\text{mA}}$  have been calculated by subtracting  $V_{\text{m}}$  observed at the respective sites of the reference system ( $V_{\text{mS}}$  and  $V_{\text{mA}}$ ) from the corresponding values of the D- $\pi$ -A systems ( $V_{\text{mS}'}$  and  $V_{\text{mA}'}$ ). In the table  $\Delta V_{\text{mD}}$  ranges from 12.2 to 17.9  $\text{kcal mol}^{-1}$ ; the positive  $\Delta V_{\text{mD}}$  value shows electron deficiency at D.

In all, the less negative  $V_{\text{m}}$  observed at the D site of D- $\pi$ -A ( $V_{\text{mD}'}$ ) than  $V_{\text{m}}$  of the donor ( $V_{\text{mD}}$ ) confirms the ICT from D to A. Further, the ICT from D to A enhances the electron density at the spacer; the gained electron density at the spacer has been denoted as negative  $\Delta V_{\text{mS}}$ , which ranges from  $-6.0$  to  $-16.3 \text{ kcal mol}^{-1}$ . As per  $\Delta V_{\text{mS}}$ , the highest electron-donating strength has been attained by the D5- $\pi$ -A system while the least is possessed by the D8- $\pi$ -A system.  $V_{\text{mA}'}$  ranges from  $-7.0$  to  $-13.5 \text{ kcal mol}^{-1}$ . The donors having greater electron-donating strength exhibit a more negative  $V_{\text{mA}'}$ . As a result, the change in the MESP appearing on the acceptor ( $\Delta V_{\text{mA}}$ ) with the



attachment of D to  $\pi$ -A has been regarded as the donating strength of the D- $\pi$ -A system.<sup>22</sup>

In the D1-D5 based  $\pi$ -A systems, the least negative  $\Delta V_{\text{mA}}$  ( $-9.2 \text{ kcal mol}^{-1}$ ) has been attained by the one nitrogen system D1- $\pi$ -A, which shows its poor electron-donating strength. Also, from D1- $\pi$ -A to D5- $\pi$ -A, a systematic enhancement in the donating strength has been observed for an increased number of nitrogen centres ( $n = 1-5$ ) and the most negative  $\Delta V_{\text{mA}}$  ( $-13.5 \text{ kcal mol}^{-1}$ ) has been shown by D5- $\pi$ -A (incorporating 5 nitrogen lone pairs). In D6 to D10- $\pi$ -A the more pyramidalized nitrogen centres in the donors impart less negative  $\Delta V_{\text{mA}}$  in the range  $-5.9$  to  $-8.4 \text{ kcal mol}^{-1}$  than the D1- $\pi$ -A-D5- $\pi$ -A systems. In D11- $\pi$ -A, the incorporation of six nitrogen lone pairs through imidazolidine rings at the phenyl ring enhances the electron density at the donor site, resulting in a  $\Delta V_{\text{mA}}$  of  $-13.7 \text{ kcal mol}^{-1}$ . Whereas, in D12- $\pi$ -A, the conjugation in the CC bond (imidazole ring) enhances the electron density at the donor more than in D11- $\pi$ -A, which leads to a more negative  $\Delta V_{\text{mA}}$  of  $-19.0 \text{ kcal mol}^{-1}$ . In the D13- $\pi$ -A and D14- $\pi$ -A systems, a relatively lower donating strength is observed in terms of  $\Delta V_{\text{mA}}$  ( $-7.9 \text{ kcal mol}^{-1}$  and  $-9.7 \text{ kcal mol}^{-1}$ ) than that of the D11 and D12- $\pi$ -A systems. This can be attributed to their reduced number of nitrogen centres (4 nitrogens). Since the nitrogens involved in the D1 to D4- $\pi$ -A systems are more planarized than those of D13 and D14- $\pi$ -A, the former systems show greater electron-donating strength. The integration of four nitrogens at the donor enhances the donating strength of the D16- $\pi$ -A system ( $-11.7 \text{ kcal mol}^{-1}$ ) over D15- $\pi$ -A ( $-8.2 \text{ kcal mol}^{-1}$ ). Further, the nearly planar nitrogens involved in D16- $\pi$ -A provide a similar donating strength  $-11.0 \text{ kcal mol}^{-1}$  to D4- $\pi$ -A ( $-11.7 \text{ kcal mol}^{-1}$ ). D17- $\pi$ -A with four nitrogen atoms incorporated through two fused six-membered rings at the phenyl ring attains a less negative  $\Delta V_{\text{mA}}$  ( $-8.5 \text{ kcal mol}^{-1}$ ) than D16- $\pi$ -A.

The additional two methyl groups in D18- $\pi$ -A at the nitrogen atoms are pyramidalized and lead to a less negative  $\Delta V_{\text{mA}}$  ( $8.1 \text{ kcal mol}^{-1}$ ) than D17. Finally, from the elucidated examples it is clear that donors having more planarized nitrogen centres enhance the donating strength of the D- $\pi$ -A systems. Among all, the D12, D11 and D5 based  $\pi$ -A systems are the best candidates for DSSC application.

### Absorption spectra

In Table 2, the optical properties of the donor and D- $\pi$ -A systems are given. Since we have used the same  $-\pi$ - and A units in all the designed D- $\pi$ -A systems, the influence of  $\pi$ -A on the absorption maximum ( $\lambda_{\text{max}}$ ) can be considered the same for all donors, and the shift in the absorption maximum ( $\Delta\lambda_{\text{max}}$ ) occurring during the transformation of D to D- $\pi$ -A can be recognized as due to the influence of the donating strength of the donor units.  $\Delta\lambda_{\text{max}}$  is calculated by subtracting  $\lambda_{\text{max}}$  of D from the analogous D- $\pi$ -A system. For the analysis the HOMO  $\rightarrow$  LUMO transition has been considered. The influence of the donor strength ( $V_{\text{mD}}$ ) on the  $\lambda_{\text{max}}$  of donors is observed in the range 280 to 329 nm. In Table 2, when a donor changes to D- $\pi$ -A, the absorption shifts to higher wavelengths in the range 454 to 619 nm. According to our previous study,  $\Delta\lambda_{\text{max}}$  in the range of 162 to 294 nm can be recognized as due to the influence of the donating strength ( $\Delta V_{\text{mA}}$ ) of the D- $\pi$ -A systems.<sup>22</sup> The significant correlation observed between  $\Delta V_{\text{mA}}$  and  $\Delta\lambda_{\text{max}}$  with a correlation coefficient of 0.940 confirms the significance of  $\Delta V_{\text{mA}}$  to  $\Delta\lambda_{\text{max}}$  (Fig. 3, deviations are neglected for the  $R$  calculation). It shows that  $\Delta\lambda_{\text{max}}$  increases with enhanced donating strength of the D- $\pi$ -A systems. In the table, the D1-D5 based  $\pi$ -A systems display a systematic increase in  $\Delta\lambda_{\text{max}}$  (from 203 to 257 nm) which can be recognized as due to the enhanced donating strength of those systems with an

**Table 2** Maximum absorption wavelength  $\lambda_{\text{max}}$  (nm), oscillator strength  $f$ , MO contribution, percentage of MO contribution (MO%), and shift in absorption maximum  $\Delta\lambda_{\text{max}}$  (nm) of the donor and D- $\pi$ -A systems at the TD-CAM-B3LYP/cc-pVDZ/SMD//B3LYP/cc-pVDZ level

Systems	Donor				D- $\pi$ -A system			
	$\lambda_{\text{max}}$ (nm)	$f$	MO contribution	$\lambda_{\text{max}}$ (nm)	$f$	MO contribution	MO (%)	$\Delta\lambda_{\text{max}}$ (nm)
D1	272	0.08	H $\rightarrow$ L	476	1.77	H $\rightarrow$ L	92	203
D2	286	0.11	H $\rightarrow$ L	513	1.53	H $\rightarrow$ L	92	227
D3	280	0.02	H $\rightarrow$ L	520	1.54	H $\rightarrow$ L	92	240
D4	285	0.03	H $\rightarrow$ L	542	1.31	H $\rightarrow$ L	89	257
D5	285	0.04	H $\rightarrow$ L	527	1.58	H $\rightarrow$ L	91	241
D6	285	0.04	H $\rightarrow$ L	471	1.74	H $\rightarrow$ L	94	187
D7	301	0.05	H $\rightarrow$ L	481	1.42	H $\rightarrow$ L	92	180
D8	304	0.03	H $\rightarrow$ L	475	1.46	H $\rightarrow$ L	91	171
D9	329	0.06	H $\rightarrow$ L	531	0.97	H $\rightarrow$ L	92	202
D10	341	0.07	H $\rightarrow$ L	522	0.04	H $\rightarrow$ L	87	181
D11	304	0.11	H $\rightarrow$ L	549	1.30	H $\rightarrow$ L	88	245
D12	325	0.60	H $\rightarrow$ L	619	0.27	H $\rightarrow$ L	79	294
				600	1.41	H-1 $\rightarrow$ L	49	275
D13	292	1.17	H $\rightarrow$ L	454	0.03	H $\rightarrow$ L	91	162
				423	1.19	H-1 $\rightarrow$ L	68	131
D14	324	1.14	H $\rightarrow$ L	583	0.03	H $\rightarrow$ L	93	259
				512	0.14	H-1 $\rightarrow$ L	93	188
D15	272	0.18	H $\rightarrow$ L	481	1.62	H $\rightarrow$ L	92	209
D16	282	0.06	H $\rightarrow$ L	509	0.99	H $\rightarrow$ L	93	227
D17	282	0.09	H $\rightarrow$ L	500	0.83	H $\rightarrow$ L	92	218
D18	288	0.07	H $\rightarrow$ L	487	0.97	H $\rightarrow$ L	90	199

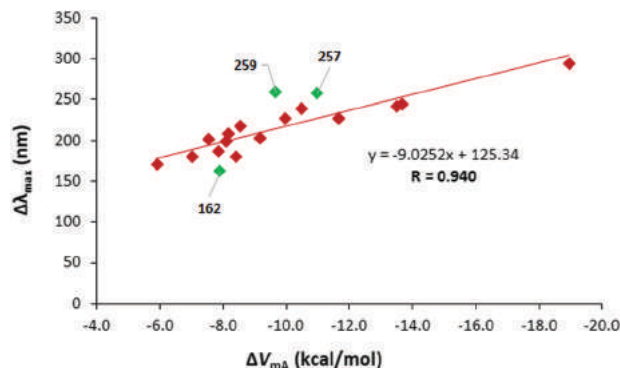


Fig. 3 Correlation between  $\Delta V_{MA}$  and  $\Delta\lambda_{max}$  of the D- $\pi$ -A systems (the  $R$  value has been calculated by excluding the deviations shown in a green colour).

increased number of nitrogen centres ( $n = 1-5$ ). Among those systems, the D4 based  $\pi$ -A system shows greater  $\Delta\lambda_{max}$  than D5- $\pi$ -A, which displays a slight deviation in the correlation (marked in a green colour, Fig. 3). The lower  $\Delta\lambda_{max}$  values exhibited by the D6- $\pi$ -A to D10- $\pi$ -A systems in the range of 171–202 nm are recognized as due to the lower donating strength of those systems. Compared to the D6- $\pi$ -A to D10- $\pi$ -A systems, the greater  $\Delta\lambda_{max}$  in D11- $\pi$ -A (245 nm) can be recognized as due to its larger donating strength. The presence of conjugation in CC bonds enhances the donating strength of D12- $\pi$ -A, resulting in the highest  $\Delta\lambda_{max}$  of 294 nm. The highest  $\Delta\lambda_{max}$  (294 nm) can be attributed to the utmost  $\Delta V_{MA}$  and  $\lambda_{max}$  of D12- $\pi$ -A (619 nm). In the D13- $\pi$ -A and D14- $\pi$ -A systems,  $\Delta\lambda_{max}$  values of 162 and 259 nm are observed with a  $\lambda_{max}$  of 454 and 583 nm, respectively. In those systems a slight deviation in the correlation has been observed, which may be due to the poor oscillator strength ( $f \rightarrow 0.03$ ). The higher  $\Delta\lambda_{max}$  of 227 nm in D16- $\pi$ -A than D15- $\pi$ -A (209 nm) can be spotted as due to the better electron-donating strength (because of the increased number of nitrogens (four)) of D16- $\pi$ -A. In D17- $\pi$ -A,  $\lambda_{max}$  and  $\Delta\lambda_{max}$  are 500 nm and 218 nm, respectively. Even though there is an equal number of nitrogens (four) in the donor site, the higher  $\Delta\lambda_{max}$  in D17- $\pi$ -A than D18- $\pi$ -A (199 nm) can be recognized as due to the influence of more planar NH centres.

Finally, for the dye sensitizers, the HOMO (highest occupied molecular orbital) and LUMO (lowest unoccupied molecular orbital) energies are crucial for determining the efficiency of the sensitizers (Table 5). For the effective regeneration of the oxidized dye, it is important to have a HOMO energy ( $e_h$ ) lower than the redox potential of the  $\Gamma^-/I_3^-$  electrolyte ( $-4.8$  eV). The  $e_h$  values of the D3–D5, D11–D14, and D16 based  $\pi$ -A systems are in the range of  $-4.68$  to  $-4.74$  eV, lying above the redox potential of the  $\Gamma^-/I_3^-$  electrolyte. It is therefore suggesting that the oxidized dye might not efficiently regenerate in those systems from the  $\Gamma^-/I_3^-$  electrolyte. Whereas, for the rest of the D- $\pi$ -A systems,  $e_h$  ( $-4.82$  to  $-5.29$  eV) lying below the redox potential of the electrolyte facilitates effective dye regeneration. For the D1- $\pi$ -A to D18- $\pi$ -A systems, the LUMO energies ( $e_l$ ) are in the range of  $-1.79$  to  $-2.79$  eV, lying above the conduction band (CB) energy of the  $TiO_2$  semiconductor ( $-4.0$  eV), which

ensures effective electron injection into the  $TiO_2$  conduction band. The HOMO–LUMO gap (HLG) energy of the designed D- $\pi$ -A systems ranges from 1.64 to 2.65 eV and it shows a decreasing trend with increasing electron donating strength. In DSSCs, HLG values give a clear idea regarding the PCE of the dye-sensitizer. As per various theoretical studies, a lower HLG ensures better optical and photovoltaic properties, thereby improving the PCE of DSSC devices.<sup>90–92</sup> Herein, we could recognize that the lower HLG energy obtained with D12- $\pi$ -A (2.17 eV) is accompanied by the highest absorption maximum (619 nm), good adsorption stability ( $-28.6$  kcal mol $^{-1}$ ), and highest  $eV_{oc}$  (2.21 eV). Consequently, among all, the D12- $\pi$ -A system having the lowest LUMO energy ( $-1.79$  eV) may provide a better PCE in DSSC devices.

According to the basic principle of DSSCs, when the dye molecule gets adsorbed on the  $TiO_2$  semiconductor, the interaction between the dye and semiconductor can shift their energy levels and prompt electron injection into the semiconductor, which is desirable for a better PCE.<sup>73</sup> To determine the energy levels of the adsorbed D- $\pi$ -A systems on  $TiO_2$ , we have designed a bidentate bridging mode for binding the D- $\pi$ -A systems on  $TiO_2$  (Fig. 4a). It has been reported that the bidentate bridging mode is the most stable adsorption mode for anchoring groups.<sup>93,94</sup> Further, the LUMO energy levels ( $-3.50$  to  $-3.79$  eV) of the adsorbed D- $\pi$ -A systems are deeper than the bare D- $\pi$ -A systems ( $-1.79$  to  $-2.79$  eV) and ensure that the LUMO is above the CB energy of  $TiO_2$ , which could promote efficient electron injection from the excited dye molecule into the CB of  $TiO_2$ . The absorption properties of the D1- $\pi$ -A to D18- $\pi$ -A systems adsorbed on  $TiO_2$  are reported in Table 3. We denote D- $\pi$ -A adsorbed on  $TiO_2$  as D- $\pi$ -A/ $TiO_2$ . The observed  $\lambda_{max}$  in the range 513 to 703 nm is favourable for an improved PCE, and shows a red shift with respect to the pure D- $\pi$ -A system. Among all, D12- $\pi$ -A/ $TiO_2$  shows the highest  $\lambda_{max}$  (703 nm), whereas D13- $\pi$ -A/ $TiO_2$  displays the lowest  $\lambda_{max}$  (513 nm). The HLG of the D- $\pi$ -A/ $TiO_2$  systems ranges from 0.61 to 1.89 eV, indicating that the adsorption of the dye with the semiconductor significantly reduces the HLG related to the bare D- $\pi$ -A systems. The electron density shifts in the D- $\pi$ -A/ $TiO_2$  systems between the HOMO and LUMO are given in the representative example (D12- $\pi$ -A/ $TiO_2$ ) shown in Fig. 4b. In all the D- $\pi$ -A/ $TiO_2$  systems, the HOMO is localized on the donor region whereas the LUMO is distributed on  $TiO_2$ . This kind of charge delocalization is anticipated for a better PCE of dye sensitizers.

Quantitatively, the adsorption stability of the D- $\pi$ -A systems on the  $(TiO_2)_9$  cluster has been evaluated using the adsorption energy ( $E_{ads}$ ), which is listed in Table 4. It is defined as  $E_{ads} = E_{dye/TiO_2} - (E_{dye} + E_{TiO_2})$ , where  $E_{dye/TiO_2}$ ,  $E_{dye}$ , and  $E_{TiO_2}$  denote the energies of dye/ $TiO_2$ , the isolated dye and the  $TiO_2$  cluster, respectively.<sup>95</sup> It is clear that a more negative adsorption energy could reveal higher adsorption stability between the dye molecule and  $TiO_2$ . In Table 4, we observed that all the adsorbed systems that have a more negative adsorption energy contain greater N-annulation. Among all, the most negative adsorption energy ( $-28.6$  kcal mol $^{-1}$ ) is attained with D12- $\pi$ -A/ $TiO_2$ , which

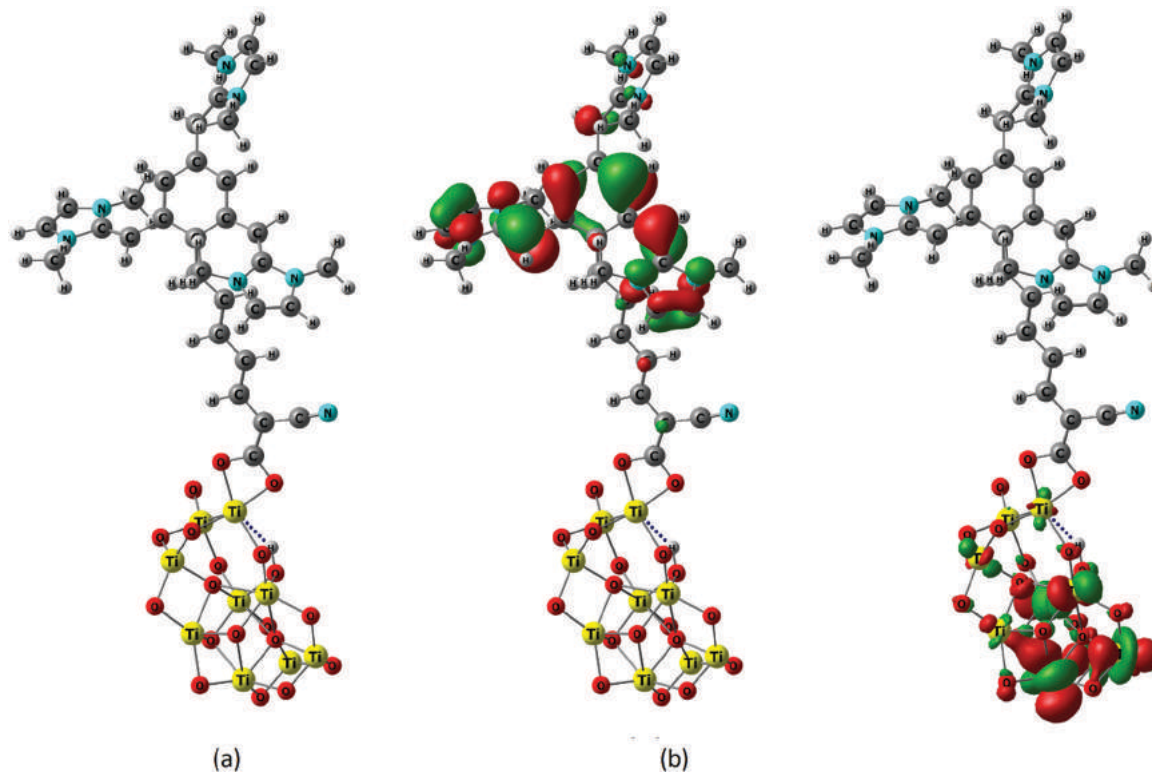


Fig. 4 (a) Optimized geometry of a representative D- $\pi$ -A system on the (TiO<sub>2</sub>)<sub>9</sub> cluster (D12- $\pi$ -A/TiO<sub>2</sub>). (b) Electron density shift in the frontier molecular orbitals.

**Table 3** HOMO (eV), LUMO (eV), and HOMO-LUMO energy gap, HLG (eV), for the D- $\pi$ -A/TiO<sub>2</sub> systems at the B3LYP/GenECP level. The maximum absorption wavelength  $\lambda_{\max}$  (nm), and oscillator strength ( $f$ ) adsorbed on TiO<sub>2</sub> are simulated at the TD CAM-B3LYP/GenECP/SMD//B3LYP/GenECP level

D- $\pi$ -A/TiO <sub>2</sub> systems	HOMO (eV)	LUMO (eV)	HLG (eV)	$\lambda_{\max}$ (nm)	$f$
D1	-5.43	-3.68	1.75	538	2.36
D2	-5.17	-3.66	1.52	583	2.03
D3	-5.10	-3.64	1.46	593	2.07
D4	-5.07	-3.62	1.45	611	1.73
D5	-5.09	-3.55	1.54	592	0.60
D6	-5.63	-3.74	1.89	526	2.24
D7	-5.53	-3.76	1.77	538	1.85
D8	-5.57	-3.79	1.77	531	1.87
D9	-5.37	-3.74	1.64	611	1.73
D10	-5.39	-3.71	1.69	574	0.05
D11	-4.85	-3.50	1.34	630	1.79
D12	-4.38	-3.25	1.13	703	0.29
D13	-4.99	-3.78	1.21	513	0.03
D14	-4.32	-3.71	0.61	697	0.02
D15	-5.44	-3.74	1.71	545	2.01
D16	-5.08	-3.60	1.48	610	1.91
D17	-5.25	-3.72	1.53	573	1.02
D18	-5.31	-3.72	1.59	558	1.22

indicates the most stable adsorption. Apart from N-annulation, the adsorption stability increases with enhanced electron-donating strength of D- $\pi$ -A. The excellent linear correlation between  $\Delta V_{\text{mA}}$  and  $E_{\text{ads}}$  with a correlation coefficient of 0.947 confirms that the donating strength of the donor systems of D- $\pi$ -A assessed in terms of  $\Delta V_{\text{mA}}$  is useful to assess the  $E_{\text{ads}}$  values of the dye on the semiconductor (Fig. 5a). Since stronger adsorption leads to deeper

**Table 4** The adsorption energies ( $E_{\text{ads}}$ ) of all the D- $\pi$ -A/(TiO<sub>2</sub>)<sub>9</sub> systems where the  $E_{\text{ads}}$  values are given in kcal mol<sup>-1</sup>

D- $\pi$ -A/(TiO <sub>2</sub> ) <sub>9</sub> systems	$E_{\text{ads}}$ (kcal mol <sup>-1</sup> )
D1- $\pi$ -A/(TiO <sub>2</sub> ) <sub>9</sub>	-23.6
D2- $\pi$ -A/(TiO <sub>2</sub> ) <sub>9</sub>	-23.8
D3- $\pi$ -A/(TiO <sub>2</sub> ) <sub>9</sub>	-23.9
D4- $\pi$ -A/(TiO <sub>2</sub> ) <sub>9</sub>	-24.3
D5- $\pi$ -A/(TiO <sub>2</sub> ) <sub>9</sub>	-25.0
D6- $\pi$ -A/(TiO <sub>2</sub> ) <sub>9</sub>	-23.3
D7- $\pi$ -A/(TiO <sub>2</sub> ) <sub>9</sub>	-23.0
D8- $\pi$ -A/(TiO <sub>2</sub> ) <sub>9</sub>	-22.8
D9- $\pi$ -A/(TiO <sub>2</sub> ) <sub>9</sub>	-23.4
D10- $\pi$ -A/(TiO <sub>2</sub> ) <sub>9</sub>	-23.8
D11- $\pi$ -A/(TiO <sub>2</sub> ) <sub>9</sub>	-25.4
D12- $\pi$ -A/(TiO <sub>2</sub> ) <sub>9</sub>	-28.6
D13- $\pi$ -A/(TiO <sub>2</sub> ) <sub>9</sub>	-22.2
D14- $\pi$ -A/(TiO <sub>2</sub> ) <sub>9</sub>	-23.3
D15- $\pi$ -A/(TiO <sub>2</sub> ) <sub>9</sub>	-22.6
D16- $\pi$ -A/(TiO <sub>2</sub> ) <sub>9</sub>	-24.5
D17- $\pi$ -A/(TiO <sub>2</sub> ) <sub>9</sub>	-23.2
D18- $\pi$ -A/(TiO <sub>2</sub> ) <sub>9</sub>	-23.3

LUMO energy levels, a more donating dye is expected to give higher adsorption stability and higher  $eV_{\text{oc}}$  (Table 4 and Fig. 5b). In the D12- $\pi$ -A/TiO<sub>2</sub> system, the highest adsorption stability and  $eV_{\text{oc}}$  (2.21 eV) have been observed, which predicts superior photovoltaic performance of the adsorbed dye.

### Photovoltaic performance

The photovoltaic parameters of the D- $\pi$ -A systems are listed in Table 5. The electron injection-free energy change ( $\Delta G_{\text{inject}}$ ) is

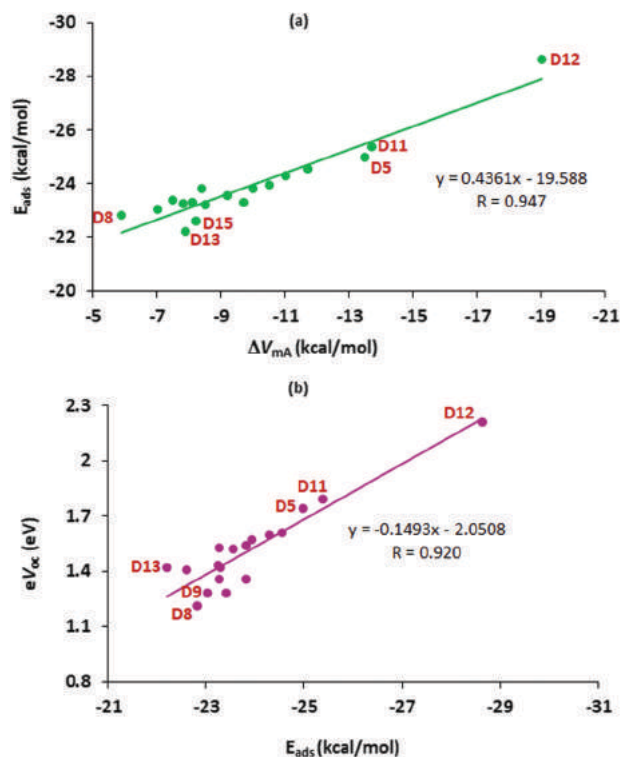


Fig. 5 (a) Correlation between  $\Delta V_{MA}$  and  $E_{ads}$  and (b)  $E_{ads}$  and  $eV_{OC}$ .

in the range  $-1.28$  to  $-2.10$  eV. It is defined as  $\Delta G_{inject} = E^{dye*} - |E_{CB}|$ ,<sup>96–98</sup> where  $E^{dye*}$  is the excited state oxidation potential and  $E_{CB}$  is the energy of the conduction band edge of the  $TiO_2$  semiconductor ( $-4.0$  eV).  $E^{dye*}$  can be calculated as  $(-e_h - \text{vertical excitation energy})$ .<sup>96,99</sup> The more negative  $\Delta G_{inject}$  will have more ability to inject electrons from the excited state of D- $\pi$ -A to the CB of  $TiO_2$ . Since  $\Delta G_{inject}$  is related to short-circuit current density  $J_{sc}$ , by improving the electron injection ability, an enhancement in the PCE can occur.<sup>6,22,26,98</sup> Among all,

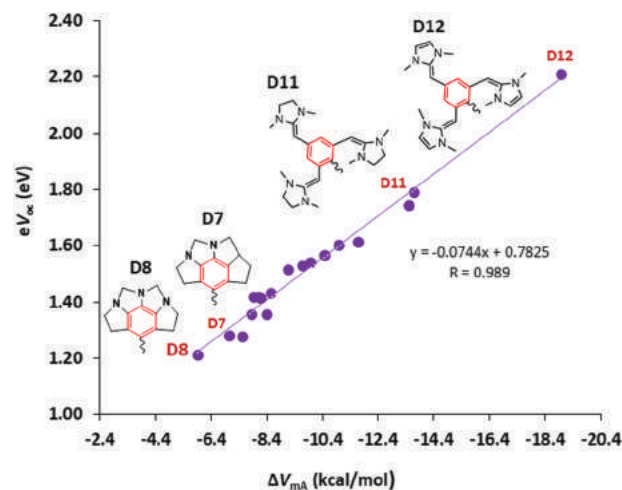


Fig. 6 Correlation between the donating strength ( $\Delta V_{MA}$ ) of the D- $\pi$ -A system and the open-circuit voltage ( $eV_{OC}$ ).

$\Delta G_{inject}$  is more negative in D14- $\pi$ -A ( $-2.10$  eV) while it is the least negative in D9- $\pi$ -A ( $-1.28$  eV). Further, it is noted that the donating strength improves the electron injection efficiency. The  $\Delta G_{reg}$  value measures the dye regeneration efficiency of the systems, which can be written as  $(E^{dye} - 4.8)$  eV or  $(-e_h) - 4.8$  eV.<sup>100,101</sup> The smallest  $\Delta G_{reg}$  ( $-0.84$  eV) observed in D12- $\pi$ -A shows the highest dye regeneration efficiency, while the highest value  $0.49$  observed in D6- $\pi$ -A indicates the lowest dye regeneration efficiency. Finally, the open-circuit voltage ( $eV_{OC} = e_1 - (-4.0)$ )<sup>102</sup> lies in the range  $1.21$  eV to  $2.21$  eV, which shows an excellent correlation with  $\Delta V_{MA}$  (Fig. 6), and suggests that  $eV_{OC}$  increases with enhanced strength of the D- $\pi$ -A systems. The correlation in Fig. 6 also suggests that the MESP approach offers an easy analysis tool for the quantification of the donating strength of D- $\pi$ -A systems in DSSC applications, and the correlation plot provides a guideline for designing dye sensitizers for desirable photovoltaic applications.

**Table 5** HOMO (eV), LUMO (eV), and HOMO–LUMO energy gap (eV) at the B3LYP/cc-pVDZ level. Ground and excited state oxidation potential ( $E^{dye}$ ,  $E^{dye*}$ ), excitation energy, free energy of electron injection  $\Delta G_{inject}$ , dye regeneration efficiency  $\Delta G_{reg}$ , and open-circuit voltage  $eV_{OC}$  at the TD-CAM-B3LYP/SMD/cc-pVDZ//B3LYP/cc-pVDZ level

Systems	Excitation energy (eV)	HOMO (eV)	LUMO (eV)	HLG (eV)	$E^{dye}$ (eV)	$E^{dye*}$ (eV)	$\Delta G_{inject}$ (eV)	$\Delta G_{reg}$ (eV)	$eV_{OC}$ (eV)
D1	2.61	-5.09	-2.48	2.61	5.09	2.48	-1.52	0.29	1.52
D2	2.42	-4.82	-2.46	2.36	4.82	2.40	-1.60	0.02	1.54
D3	2.38	-4.74	-2.43	2.31	4.74	2.36	-1.64	-0.06	1.57
D4	2.29	-4.69	-2.40	2.29	4.69	2.40	-1.60	-0.11	1.60
D5	2.35	-4.68	-2.26	2.42	4.68	2.33	-1.67	-0.12	1.74
D6	2.63	-5.29	-2.64	2.65	5.29	2.66	-1.34	0.49	1.36
D7	2.58	-5.22	-2.72	2.50	5.22	2.64	-1.36	0.42	1.28
D8	2.61	-5.27	-2.79	2.48	5.27	2.66	-1.34	0.47	1.21
D9	2.33	-5.05	-2.72	2.33	5.05	2.72	-1.28	0.25	1.28
D10	2.38	-5.04	-2.64	2.40	5.04	2.66	-1.34	0.24	1.36
D11	2.26	-4.50	-2.21	2.29	4.50	2.24	-1.76	-0.30	1.79
D12	2.00	-3.96	-1.79	2.17	3.96	1.96	-2.04	-0.84	2.21
D13	2.73	-4.77	-2.58	2.19	4.77	2.04	-1.96	-0.03	1.42
D14	2.21	-4.11	-2.47	1.64	4.11	1.90	-2.10	-0.69	1.53
D15	2.58	-5.11	-2.59	2.52	5.11	2.53	-1.47	0.31	1.41
D16	2.29	-4.72	-2.39	2.33	4.72	2.43	-1.57	-0.08	1.61
D17	2.48	-4.96	-2.57	2.39	4.96	2.48	-1.52	0.16	1.43
D18	2.55	-5.04	-2.58	2.46	5.04	2.49	-1.51	0.24	1.42



In the analysis, the highest donating strength observed in D12- $\pi$ -A correlates to the highest  $eV_{oc}$  (2.21 eV). The pyramidalized nitrogen centres observed in D8- $\pi$ -A retard the efficient electron injection to  $\pi$ -A, and it shows the lowest  $eV_{oc}$  (1.21 eV) due to inferior donating strength.

## Conclusions

Donor modifications, especially through the integration of electron-rich nitrogen atoms (N-annulation), significantly affect the structure–performance relationship of D- $\pi$ -A systems for dye-sensitized solar cell applications. For tuning the electron-donating ability of D- $\pi$ -A systems, eighteen electron-rich nitrogen incorporated donors are designed with butadiene and cyanoacrylic acid as a  $\pi$ -spacer and an acceptor, respectively. The implication of planarized nitrogens for improving the electron-donating strength ( $\Delta V_{mA}$ ) of D- $\pi$ -A systems is investigated using MESP topographical analysis, which states that the magnitude of  $\Delta V_{mA}$  increases with an increased number of planar nitrogens. The  $\lambda_{max}$  values of the D- $\pi$ -A systems are fine-tuned by the extent of  $\pi$ -conjugation and N-annulation in the donors. The significance of  $\Delta V_{mA}$  in shifting the absorption maximum ( $\Delta\lambda_{max}$ ) is confirmed by the linear correlation observed between  $\Delta V_{mA}$  and  $\Delta\lambda_{max}$ . Regarding the frontier molecular orbitals of the D- $\pi$ -A systems, the HOMO and LUMO energies are affected by the electron-rich nature of the donors in D- $\pi$ -A. The sufficiently more negative LUMO energy of the D- $\pi$ -A systems than the CB energy of TiO<sub>2</sub> provides high electron injection efficiency. The open-circuit voltage ( $eV_{oc}$ ), and free energy of electron injection ( $\Delta G_{inject}$ ) have been analysed for the D- $\pi$ -A systems and reveal that  $eV_{oc}$  is increased with enhanced  $\Delta V_{mA}$ . Also, the adsorption stability of the D- $\pi$ -A systems on TiO<sub>2</sub> has been evaluated and indicates that the adsorption stability ( $E_{ads}$ ) increased with enhanced electron-donating strength of the D- $\pi$ -A system. Since adsorption of the D- $\pi$ -A system on TiO<sub>2</sub> shifts the LUMO energy, the stability of the D- $\pi$ -A/TiO<sub>2</sub> system affects  $eV_{oc}$  and thus the efficiency of the solar cell. The strong linear correlation observed between  $E_{ads}$  and  $eV_{oc}$  proves this conclusion. Among all the cases studied, D12- $\pi$ -A/TiO<sub>2</sub> shows the highest adsorption stability; furthermore, D12- $\pi$ -A displays the highest  $\Delta\lambda_{max}$ , the best  $eV_{oc}$  and the highest magnitude for  $\Delta V_{mA}$ . Consequently, from the aforementioned fundamental parameters, it can be concluded that the D12 based photosensitizer is very effective for improving the PCE. Also, the N-annulation design strategy will pave the way for attaining high efficiency in the field of dye-sensitized solar cells.

## Conflicts of interest

There are no conflicts to declare.

## Acknowledgements

The authors thank DST-SERB for funding through GAP1397 and also gratefully acknowledge the CSIR 4th PI for HPC facility

and NIIST IT lab for computational support. V. V. Divya thanks CSIR, India, for the senior research fellowship.

## References

- 1 A. Baheti, C.-P. Lee, K. J. Thomas and K.-C. Ho, *Phys. Chem. Chem. Phys.*, 2011, **13**, 17210–17221.
- 2 Y.-H. Chen, V. S. Nguyen, H.-H. Chou, Y. S. Tingare, T.-C. Wei and C.-Y. Yeh, *ACS Appl. Energy Mater.*, 2020, **3**, 5479–5486.
- 3 J. Gong, K. Sumathy, Q. Qiao and Z. Zhou, *Renewable Sustainable Energy Rev.*, 2017, **68**, 234–246.
- 4 G. Boschloo, *Front. Chem.*, 2019, **7**, 77.
- 5 M. Grätzel, *Acc. Chem. Res.*, 2009, **42**, 1788–1798.
- 6 B. O'Regan and M. Grätzel, *Nature*, 1991, **353**, 737–740.
- 7 M. K. Nazeeruddin, F. De Angelis, S. Fantacci, A. Selloni, G. Viscardi, P. Liska, S. Ito, B. Takeru and M. Grätzel, *J. Am. Chem. Soc.*, 2005, **127**, 16835–16847.
- 8 G. Marotta, M. A. Reddy, S. P. Singh, A. Islam, L. Han, F. De Angelis, M. Pastore and M. Chandrasekharam, *ACS Appl. Mater. Interfaces*, 2013, **5**, 9635–9647.
- 9 S. Yun, Y. Qin, A. R. Uhl, N. Vlachopoulos, M. Yin, D. Li, X. Han and A. Hagfeldt, *Energy Environ. Sci.*, 2018, **11**, 476–526.
- 10 A. Fakharuddin, R. Jose, T. M. Brown, F. Fabregat-Santiago and J. Bisquert, *Energy Environ. Sci.*, 2014, **7**, 3952–3981.
- 11 A. Hinsch, W. Veurman, H. Brandt, K. F. Jensen and S. Mastroianni, *ChemPhysChem*, 2014, **15**, 1076–1087.
- 12 A. Hagfeldt, G. Boschloo, L. Sun, L. Kloo and H. Pettersson, *Chem. Rev.*, 2010, **110**, 6595–6663.
- 13 Y. Kurumisawa, T. Higashino, S. Nimura, Y. Tsuji, H. Iiyama and H. Imahori, *J. Am. Chem. Soc.*, 2019, **141**, 9910–9919.
- 14 H. Zhou, J.-M. Ji, S. H. Kang, M. S. Kim, H. S. Lee, C. H. Kim and H. K. Kim, *J. Mater. Chem. C*, 2019, **7**, 2843–2852.
- 15 K. Kakiage, Y. Aoyama, T. Yano, K. Oya, T. Kyomen and M. Hanaya, *Chem. Commun.*, 2015, **51**, 6315–6317.
- 16 K. Kakiage, Y. Aoyama, T. Yano, K. Oya, J.-I. Fujisawa and M. Hanaya, *Chem. Commun.*, 2015, **51**, 15894–15897.
- 17 S. Mathew, A. Yella, P. Gao, R. Humphry-Baker, B. F. Curchod, N. Ashari-Astani, I. Tavernelli, U. Rothlisberger, M. K. Nazeeruddin and M. Grätzel, *Nat. Chem.*, 2014, **6**, 242–247.
- 18 F.-S. Lin, P. Priyanka, M.-S. Fan, S. Vegiraju, J.-S. Ni, Y.-C. Wu, Y.-H. Li, G.-H. Lee, Y. Ezhumalai and R.-J. Jeng, *J. Mater. Chem. C*, 2020, **8**, 15322–15330.
- 19 Y. Ren, Y. Li, S. Chen, J. Liu, J. Zhang and P. Wang, *Energy Environ. Sci.*, 2016, **9**, 1390–1399.
- 20 K. Sharma, V. Sharma and S. Sharma, *Nanoscale Res. Lett.*, 2018, **13**, 381.
- 21 X. Song, X. Yang, H. Wang, J. An, Z. Yu, X. Wang, A. Hagfeldt and L. Sun, *Sol. Energy*, 2019, **187**, 274–280.
- 22 V. V. Divya and C. H. Suresh, *New J. Chem.*, 2020, **44**, 7200–7209.

- 23 M. Jadhav, J. V. Vaghasiya, D. Patil, S. S. Soni and N. Sekar, *New J. Chem.*, 2019, **43**, 8970–8981.
- 24 R. Tarsang, V. Promarak, T. Sudyoadsuk, S. Namuangruk and S. Jungsuttiwong, *J. Photochem. Photobiol., A*, 2014, **273**, 8–16.
- 25 M. Karuppusamy, V. S. K. Choutipalli, D. Vijay and V. Subramanian, *J. Chem. Sci.*, 2020, **132**, 20.
- 26 V. V. Divya and C. H. Suresh, *New J. Chem.*, 2021, **45**, 2496–2507.
- 27 Y. K. Eom, S. H. Kang, I. T. Choi, Y. Yoo, J. Kim and H. K. Kim, *J. Mater. Chem. A*, 2017, **5**, 2297–2308.
- 28 Y.-Q. Yan, Y.-Z. Zhu, P.-P. Dai, J. Han, M. Yan and J.-Y. Zheng, *Sol. Energy*, 2020, **207**, 428–435.
- 29 H. Zhang, Z.-E. Chen and H.-R. Tian, *Sol. Energy*, 2020, **198**, 239–246.
- 30 A. J. Huckaba, F. Giordano, L. E. McNamara, K. M. Dreux, N. I. Hammer, G. S. Tschumper, S. M. Zakeeruddin, M. Grätzel, M. K. Nazeeruddin and J. H. Delcamp, *Adv. Energy Mater.*, 2015, **5**, 1401629.
- 31 Y. Zhang, H. Cheema, L. McNamara, L. A. Hunt, N. I. Hammer and J. H. Delcamp, *Chem. – Eur. J.*, 2018, **24**, 5939–5949.
- 32 J. Feng, Y. Jiao, W. Ma, M. K. Nazeeruddin, M. Grätzel and S. Meng, *J. Phys. Chem. C*, 2013, **117**, 3772–3778.
- 33 J. H. Delcamp, A. Yella, T. W. Holcombe, M. K. Nazeeruddin and M. Grätzel, *Angew. Chem., Int. Ed.*, 2013, **125**, 394–398.
- 34 C. Yan, W. Ma, Y. Ren, M. Zhang and P. Wang, *ACS Appl. Mater. Interfaces*, 2015, **7**, 801–809.
- 35 U. B. Cappel, M. H. Karlsson, N. G. Pschirer, F. Eickemeyer, J. Schöneboom, P. Erk, G. Boschloo and A. Hagfeldt, *J. Phys. Chem. C*, 2009, **113**, 14595–14597.
- 36 C. Li, Z. Liu, J. Schöneboom, F. Eickemeyer, N. G. Pschirer, P. Erk, A. Herrmann and K. Müllen, *J. Mater. Chem. C*, 2009, **19**, 5405–5415.
- 37 Y. Jin, J. Hua, W. Wu, X. Ma and F. Meng, *Synth. Met.*, 2008, **158**, 64–71.
- 38 J. Luo, M. Xu, R. Li, K.-W. Huang, C. Jiang, Q. Qi, W. Zeng, J. Zhang, C. Chi, P. Wang and J. Wu, *J. Am. Chem. Soc.*, 2014, **136**, 265–272.
- 39 Z. Yao, H. Wu, Y. Ren, Y. Guo and P. Wang, *Energy Environ. Sci.*, 2015, **8**, 1438–1442.
- 40 Z. Yao, M. Zhang, H. Wu, L. Yang, R. Li and P. Wang, *J. Am. Chem. Soc.*, 2015, **137**, 3799–3802.
- 41 V. V. Divya, F. B. Sayyed and C. H. Suresh, *ChemPhysChem*, 2019, **20**, 1752–1758.
- 42 F. Effenberger, P. Fischer, W. W. Schöllner and W.-D. Stohrer, *Tetrahedron*, 1978, **34**, 2409–2417.
- 43 A. Zakrzewska, R. Gawinecki, E. Kolehmainen and B. Osmiałowski, *Int. J. Mol. Sci.*, 2005, **6**, 52–62.
- 44 J. O. S. Varejão, E. V. V. Varejão and S. A. Fernandes, *Eur. J. Org. Chem.*, 2019, 4273–4310.
- 45 J. E. Kuder, W. W. Limburg, J. M. Pochan and D. Wychick, *J. Chem. Soc. Perkin Trans. 2*, 1977, 1643–1651.
- 46 G. Shishkin, *Chem. Heterocycl. Compd.*, 1983, **19**, 549–553.
- 47 F. Fantuzzi, C. B. Coutinho, R. R. Oliveira and M. A. C. Nascimento, *Inorg. Chem.*, 2018, **57**, 3931–3940.
- 48 C. H. Suresh and F. B. Sayyed, *J. Phys. Chem. A*, 2013, **117**, 10455–10461.
- 49 S. Rohrbach, R. S. Shah, T. Tuttle and J. A. Murphy, *Angew. Chem.*, 2019, **131**, 11576–11580.
- 50 J. S. Miller, D. A. Dixon, J. C. Calabrese, C. Vazquez, P. J. Krusic, M. D. Ward, E. Wasserman and R. L. Harlow, *J. Am. Chem. Soc.*, 1990, **112**, 381–398.
- 51 E. Scrocco and J. Tomasi, in *Advances Quantum Chemistry*, ed. P.-O. Löwdin, Academic Press, 1978, vol. 11, pp. 115–193.
- 52 B. Pullman, *Int. J. Quantum Chem.*, 1990, **38**, 81–92.
- 53 A. Pullman and B. Pullman, *Q. Rev. Biophys.*, 1981, **14**, 289–380.
- 54 P. Politzer and J. S. Murray, *J. Mol. Struct.*, 1996, **376**, 419–424.
- 55 P. Politzer, J. S. Murray and T. Clark, *Phys. Chem. Chem. Phys.*, 2013, **15**, 11178–11189.
- 56 P. Politzer and J. S. Murray, *Cryst. Growth Des.*, 2015, **15**, 3767–3774.
- 57 P. Politzer and J. S. Murray, *ChemPhysChem*, 2020, **21**, 579–588.
- 58 C. H. Suresh and S. R. Gadre, *J. Org. Chem.*, 1999, **64**, 2505–2512.
- 59 S. R. Gadre and R. N. Shirsat, *Electrostatics of Atoms and Molecules*, Universities Press, 2000.
- 60 S. R. Gadre, S. A. Kulkarni and I. H. Shrivastava, *J. Chem. Phys.*, 1992, **96**, 5253–5260.
- 61 F. B. Sayyed and C. H. Suresh, *Tetrahedron Lett.*, 2009, **50**, 7351–7354.
- 62 F. B. Sayyed and C. H. Suresh, *New J. Chem.*, 2009, **33**, 2465–2471.
- 63 P. Sajith and C. H. Suresh, *Inorg. Chem.*, 2012, **51**, 967–977.
- 64 J. Mathew and C. H. Suresh, *Organometallics*, 2011, **30**, 1438–1444.
- 65 K. Sandhya and C. H. Suresh, *Dalton Trans.*, 2014, **43**, 12279–12287.
- 66 B. A. Anjali, F. B. Sayyed and C. H. Suresh, *J. Phys. Chem. C*, 2016, **120**, 1112–1119.
- 67 B. A. Anjali and C. H. Suresh, *ACS Omega*, 2017, **2**, 4196–4206.
- 68 P. V. Bijina and C. H. Suresh, *J. Chem. Sci.*, 2016, **128**, 1677–1686.
- 69 R. Rakhi and C. H. Suresh, *Phys. Chem. Chem. Phys.*, 2016, **18**, 24631–24641.
- 70 K. Remya and C. H. Suresh, *Phys. Chem. Chem. Phys.*, 2015, **17**, 27035–27044.
- 71 T. D. Della and C. H. Suresh, *Phys. Chem. Chem. Phys.*, 2016, **18**, 14588–14602.
- 72 F. Arkan and M. Izadyar, *Renewable Sustainable Energy Rev.*, 2018, **94**, 609–655.
- 73 W. Zhang, L. Wang, L. Mao, J. Jiang, H. Ren, P. Heng, H. Ågren and J. Zhang, *J. Phys. Chem. C*, 2020, **124**, 3980–3987.
- 74 A. D. Laurent, C. Adamo and D. Jacquemin, *Phys. Chem. Chem. Phys.*, 2014, **16**, 14334–14356.
- 75 M. Y. Mehboob, M. U. Khan, R. Hussain, K. Ayub, A. Sattar, M. K. Ahmad, Z. Irshad and M. Adnan, *Spectrochim. Acta, Part A*, 2021, **244**, 118873.

- 76 M. Y. Mehboob, M. U. Khan, R. Hussain, R. Fatima, Z. Irshad and M. Adnan, *J. Theory Comput. Chem.*, 2020, **19**, 2050034.
- 77 M. Y. Mehboob, R. Hussain, M. U. Khan, M. Adnan, A. Umar, M. U. Alvi, M. Ahmed, M. Khalid, J. Iqbal and M. N. Akhtar, *Comput. Theor. Chem.*, 2020, **1186**, 112908.
- 78 M. Y. Mehboob, R. Hussain, M. U. Khan, M. Adnan, M. A. Ehsan, A. Rehman and M. R. S. A. Janjua, *J. Phys. Org. Chem.*, 2021, e4204.
- 79 A. D. Becke, *J. Chem. Phys.*, 1993, **98**, 1372–1377.
- 80 T. H. Dunning Jr, *Chem. Phys.*, 1989, **90**, 1007–1023.
- 81 J. K. Roy, S. Kar and J. Leszczynski, *J. Phys. Chem. C*, 2019, **123**, 3309–3320.
- 82 S. Kupfer, J. Guthmuller and L. Gonzalez, *J. Chem. Theory Comput.*, 2013, **9**, 543–554.
- 83 P. J. Hay and W. R. Wadt, *J. Chem. Phys.*, 1985, **82**, 270–283.
- 84 R. Sánchez-de-Armas, M. A. San Miguel, J. Oviedo and J. F. Sanz, *Phys. Chem. Chem. Phys.*, 2012, **14**, 225–233.
- 85 T. Yanai, D. P. Tew and N. C. Handy, *Chem. Phys. Lett.*, 2004, **393**, 51–57.
- 86 G. Deogratias, N. Seriani, T. Pogrebnyaya and A. Pogrebnoi, *J. Mol. Graphics Modell.*, 2020, **94**, 107480.
- 87 J. Zhang, H.-C. Zhu, R.-L. Zhong, L. Wang and Z.-M. Su, *Org. Electron.*, 2018, **54**, 104–113.
- 88 H.-C. Zhu, C.-F. Li, Z.-H. Fu, S.-S. Wei, X.-F. Zhu and J. Zhang, *Appl. Surf. Sci.*, 2018, **455**, 1095–1105.
- 89 M. J. Frisch, G. W. Trucks, H. B. Schlegel, G. E. Scuseria, M. A. Robb, J. R. Cheeseman, G. Scalmani, V. Barone, G. A. Petersson, H. Nakatsuji, X. Li, M. Caricato, A. V. Marenich, J. Bloino, B. G. Janesko, R. Gomperts, B. Mennucci, H. P. Hratchian, J. V. Ortiz, A. F. Izmaylov, J. L. Sonnenberg, D. Williams-Young, F. Ding, F. Lipparini, F. Egidi, J. Goings, B. Peng, A. Petrone, T. Henderson, D. Ranasinghe, V. G. Zakrzewski, J. Gao, N. Rega, G. Zheng, W. Liang, M. Hada, M. Ehara, K. Toyota, R. Fukuda, J. Hasegawa, M. Ishida, T. Nakajima, Y. Honda, O. Kitao, H. Nakai, T. Vreven, K. Throssell, J. A. Montgomery Jr., J. E. Peralta, F. Ogliaro, M. J. Bearpark, J. J. Heyd, E. N. Brothers, K. N. Kudin, V. N. Staroverov, T. A. Keith, R. Kobayashi, J. Normand, K. Raghavachari, A. P. Rendell, J. C. Burant, S. S. Iyengar, J. Tomasi, M. Cossi, J. M. Millam, M. Klene, C. Adamo, R. Cammi, J. W. Ochterski, R. L. Martin, K. Morokuma, O. Farkas, J. B. Foresman and D. J. Fox, *Gaussian 16, Revision A.03*, Gaussian, Wallingford, CT, 2016.
- 90 M. Y. Mehboob, R. Hussain, Z. Irshad and M. Adnan, *J. Phys. Org. Chem.*, 2021, e4210.
- 91 R. Hussain, M. Y. Mehboob, M. U. Khan, M. Khalid, Z. Irshad, R. Fatima, A. Anwar, S. Nawab and M. Adnan, *J. Mater. Sci.*, 2021, **56**, 5113–5131.
- 92 M. Y. Mehboob, R. Hussain, Z. Irshad and M. Adnan, *Bull. Korean Chem. Soc.*, 2021, **42**, 597–610.
- 93 L. Zhang and J. M. Cole, *ACS Appl. Mater. Interfaces*, 2015, **7**, 3427–3455.
- 94 M. Pastore and F. De Angelis, *Phys. Chem. Chem. Phys.*, 2012, **14**, 920–928.
- 95 P. Li, Z. Wang, C. Song and H. Zhang, *J. Mater. Chem. A*, 2017, **5**, 11454–11465.
- 96 R. Katoh, A. Furube, T. Yoshihara, K. Hara, G. Fujihashi, S. Takano, S. Murata, H. Arakawa and M. Tachiya, *J. Phys. Chem. B*, 2004, **108**, 4818–4822.
- 97 J. Preat, C. Michaux, D. Jacquemin and E. A. Perpète, *J. Phys. Chem. C*, 2009, **113**, 16821–16833.
- 98 N. N. Ghosh, M. Habib, A. Pramanik, P. Sarkar and S. Pal, *New J. Chem.*, 2019, **43**, 6480–6491.
- 99 J. Zhang, H.-B. Li, S.-L. Sun, Y. Geng, Y. Wu and Z.-M. Su, *J. Mater. Chem.*, 2012, **22**, 568–576.
- 100 G. Boschloo and A. Hagfeldt, *Acc. Chem. Res.*, 2009, **42**, 1819–1826.
- 101 T. Koopmans, *Physica*, 1933, **1**, 104–113.
- 102 C.-R. Zhang, Z.-J. Liu, Y.-H. Chen, H.-S. Chen, Y.-Z. Wu, W. Feng and D.-B. Wang, *Curr. Appl. Phys.*, 2010, **10**, 77–83.

## ABSTRACT

---

Name of the Student: Divya Velayudhan V. V.

Registration No.: 10CC15A39004

Faculty of Study: Chemical Sciences

Year of Submission: 2021

AcSIR academic centre/CSIRLab: CSIR-NIIST

Name of the Supervisor: Dr. C. H. Suresh

**Title of the thesis:** Density Functional Theory Studies on D- $\pi$ -A Systems Used in Dye-Sensitized Solar Cells: Donor-Acceptor Effect, Spacer Effect, and Molecular Design Strategies

---

Dye-sensitized solar cells (DSSCs) have a fundamental role in photovoltaic technology as an alternative to highly expensive conventional silicon based solar cell. Theoretical studies are greatly acknowledged for the reliable prediction of efficiency of dye-sensitizers and understanding the fundamental processes involved in DSSC device. The thesis is organized into four chapters. Chapter 1 gives an overview of both DSSCs and computational chemistry methods. In chapter 2, using molecular electrostatic potential (MESP) analysis, the electronic effect transmission power ( $\gamma$ ) of various spacer (G in the notation) units in a Y-G-X type molecular model and electron donating strength ( $\Delta V_{mA}$ ) of typically used donors in D- $\pi$ -A type dye-sensitizers have been computed. Among the studied spacers units, alkenyl spacers with shorter spacer chain length showed the highest  $\gamma$ , which will be effective for the better power conversion efficiency (PCE) in DSSCs. Further,  $\Delta V_{mA}$  is found to be proportional to absorptional redshift and open-circuit voltage ( $eV_{OC}$ ) which shows the relevance of  $\Delta V_{mA}$  for the enhancement of optical and photovoltaic properties of dye-sensitizers. In chapter 3, the role of electron donating substituents on the donor region of D- $\pi$ -A systems has been analysed and found that  $\Delta V_{mA}$ , optical, and photovoltaic properties have been improved in substituted D- $\pi$ -A systems than bare D- $\pi$ -A. Finally in chapter 4, the significance of nitrogen centres for revamping the donating strength of D- $\pi$ -A is scrutinized. The results show that absorption maxima, adsorption stability of dye/TiO<sub>2</sub> interface, and photovoltaic properties enhanced with number of N-centres at donor region. In all chapters, the strong linear correlation observed for the ground state property  $\Delta V_{mA}$  and  $eV_{OC}$  provides guidelines for effective dye design with a desirable photovoltaic applications. For the prediction of PCE, the study developed a new theoretical strategy (MESP based).



# **SCI Publications**

# Substituent Effect Transmission Power of Alkyl, Alkenyl, Alkynyl, Phenyl, Thiophenyl, and Polyacene Spacers

Velayudhan V. Divya,<sup>[a, b]</sup> Fared Bhasha Sayyed,<sup>[a]</sup> and Cherumuttathu H. Suresh<sup>\*[a, b]</sup>

The transmission of substituent effect through a variety of spacers, that is to say, alkyl, alkenyl, alkynyl, phenyl, thiophenyl, and polyacene has been studied by modeling Y-G-X type molecular systems (Y: reaction center; G: spacer moiety; X: substituent) using B3LYP/6-31G(d,p) density functional theory calculations. The reaction center is always kept as a C=C double bond and the molecular electrostatic potential (MESP) minimum ( $V_{\min}$ ) observed for this bond showed subtle variation with respect to the changes in the spacer unit and the nature of substituent. Strong linear correlations are observed between Hammett substituent constants ( $\sigma_i$  and  $\sigma_p$ ) and  $V_{\min}$ , which

recommend the aptness of  $V_{\min}$  as an electronic descriptor to quantify the substituent effect. Since  $V_{\min}$  offers an alternative measure of substituent effect, the correlation between  $V_{\min}$  and  $\sigma_p$  has been used for assessing the transmission of substituent effect through a variety of spacer moieties. The highest transmission coefficient ( $\gamma$ ) is always observed for smaller spacer length. Among all the spacers, alkenyl showed the highest and alkyl showed the lowest transmission power. The study recommends the use of short chains of C=C double, C≡C triple or a combination of both as spacers for the effective transmission of substituent effect to the reaction center.

## 1. Introduction

Substituents in molecules are regarded as functional groups and tuning of various chemical properties can be achieved by controlling the substituent effects.<sup>[1]</sup> The theory of substituent effect has been considered as fundamental to the prediction of molecular reactivity.<sup>[1–2]</sup> The electronic effect of a substituent can be transmitted to the reaction center via a transmitting moiety. For example in a molecule Y-G-X, (Y: reaction center; G: spacer moiety; X: substituent), the effect of X at Y through G can be interpreted with the famous Hammett relationship  $\log(K_X/K_0) = \rho\sigma$ , where  $\rho$  is the reaction constant and  $\sigma$  is the substituent constant. Hammett equation and several of its modifications<sup>[2a,3]</sup> have been used in a quantitative way for the effective interpretation of substituent effects.<sup>[4]</sup> The applicability of  $\sigma$ -constants for a variety of molecules assisted the understanding of structure-activity and structure-property relationships in chemistry.<sup>[5]</sup>

Substituent effects are classified into inductive (through  $\sigma$  bond),  $\pi$  – resonance and through space (field) effects.<sup>[1a,2a,6]</sup> The separation of the substituent effect into inductive ( $\sigma_i$  or F) and resonance effect ( $\sigma_r$  or R) was done by Swain and Lupton.<sup>[7]</sup> They interpreted that the negative and positive values of substituent constant indicate electron donating and withdrawing nature of substituents, respectively. Using quantum chemical approaches, many efforts have been made to model the

substituent effect.<sup>[4–5,8]</sup> Substituent effects are responsible for small perturbations on the molecular electron density distribution, which can be measured by means of correlating them with the computed quantities of total energy, atomic charges, and electrostatic potentials resulting from ab initio quantum chemical or semiempirical methods.<sup>[9,9]</sup> Further, several experimental studies have utilized Y-G-X type systems to understand the substituent effect transmission ability of various spacer moieties using geometrical variables, ionization techniques, and NMR chemical shifts etc.<sup>[8f,10]</sup>

Among the several theoretical quantities used to interpret Hammett constants, topographical analysis of molecular electrostatic potential (MESP) provided a clean approach to substituent effects.<sup>[5a–c,8c–e]</sup> The prediction and rationalization of reactivity trends using MESP have been pioneered by Scrocco, Tomasi, and co-workers.<sup>[11]</sup> Politzer and Murry widely used the MESP plots calculated using standard electronic structure theory to interpret while the topographical analysis of MESP has been pioneered by Gadre et al.<sup>[12]</sup> From MESP topographical studies on conjugated organic molecular systems, Suresh et al. have shown that critical features of MESP are useful for the quantification of inductive,<sup>[13]</sup> resonance,<sup>[14]</sup> steric<sup>[15]</sup> and proximity effects<sup>[8b]</sup> of substituents. Also, MESP minimum ( $V_{\min}$ ) has been used as a powerful electronic descriptor to quantify substituent effect, trans influence and two electron donor character of ligands.<sup>[5a,c,16]</sup> Here we intend to study Y-G-X type systems using  $V_{\min}$  analysis. The substituent effect transmission power of X through the spacer will be assessed by the  $V_{\min}$  observed over Y, an olefinic moiety. Although the significance of such spacers in donor-acceptor systems is well known, quantification of substituent effect transmission power of a variety of spacer systems is yet to be systematically analyzed. Previous studies showed that modifications in spacer units such as their  $\pi$ -bond character, conjugation length, and planarity had a significant role in electron transmission power, absorption

[a] V. V. Divya, Dr. F. B. Sayyed, Dr. C. H. Suresh  
Chemical Sciences and Technology Division  
CSIR – National Institute for Interdisciplinary Science and Technology  
Thiruvananthapuram, Kerala, 695 019, India  
E-mail: sureshch@niist.res.in

[b] V. V. Divya, Dr. C. H. Suresh  
Academy of Scientific and Innovative Research (AcSIR)  
Ghaziabad-201002, India

Supporting information for this article is available on the WWW under <https://doi.org/10.1002/cphc.201900206>

wavelength, and other related photophysical properties.<sup>[17]</sup> Here spacers such as alkyl, alkenyl, alkynyl, phenyl, thiophenyl, and polyacenes have been selected to include the inductive, and resonance effect aspects. We envision that this study will provide useful information regarding the future dye designing and other related studies.

## 2. Results and Discussion

### 2.1. MESP Topography and Spacer Effects

MESP is one of the most appropriate electronic descriptors to understand the electron withdrawing and donating nature of substituents and ligands.<sup>[5a,b,12d, 16a, 18]</sup> It is recognized that electron rich region in a molecule experiences a significant change in MESP minimum ( $V_{min}$ ) due to substituent effects. Here we consider an olefinic bond (Figure 1) as a sensitive region to

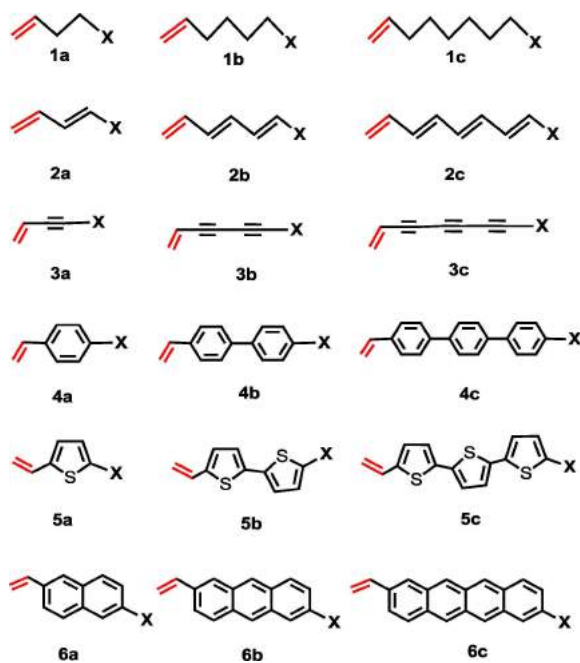


**Figure 1.** Various spacers considered to quantify the transmission power of spacers. The double bond marked in red is the region where MESP minimum is located for  $X=\text{NH}_2$ ,  $\text{OH}$ ,  $\text{CH}_3$ ,  $\text{H}$ ,  $\text{F}$ ,  $\text{Cl}$ ,  $\text{CF}_3$ ,  $\text{CHO}$ ,  $\text{CN}$  and  $\text{NO}_2$ .

understand the precise variation of  $V_{min}$  with respect to the substituent effect. A general notation  $\text{C}_2\text{H}_3\text{-G}_n\text{-X}$  has been used to denote the molecule, where  $\text{G}_n$  stands for the repeating 'n' spacer G units between  $\text{C}_2\text{H}_3$  and X. The effect of substituent on  $\text{C}_2\text{H}_3\text{-}$  has been measured in terms of  $V_{min}$  on its CC double bond. Electron donating and withdrawing substituents used in this study include  $\text{NH}_2$ ,  $\text{OH}$ ,  $\text{CH}_3$ ,  $\text{H}$ ,  $\text{F}$ ,  $\text{Cl}$ ,  $\text{CF}_3$ ,  $\text{CHO}$ ,  $\text{CN}$  and  $\text{NO}_2$ . The spacers selected for the study are alkyl, alkenyl, alkynyl, phenyl, thiophenyl, and polyacenes (Figure 1). For a reasonable understanding about the spacer length, systems up to  $n=3$  have been considered. In studies related to the substituent

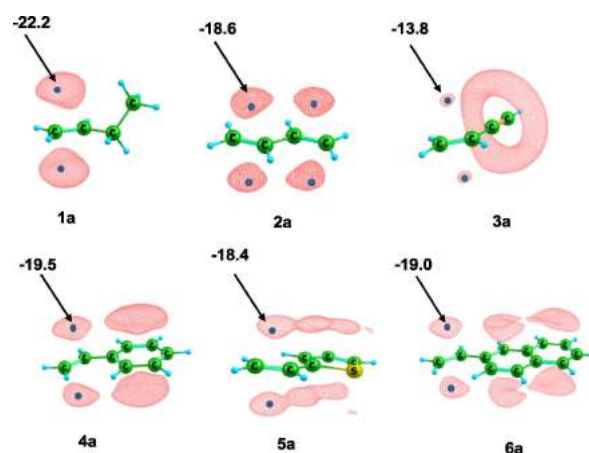


**Figure 2.** MESP isosurface at  $-13.0 \text{ kcal mol}^{-1}$  for **1a**, **2a**, **3a**, **4a**, **5a** and **6a**.  $V_{min}$  values in  $\text{kcal mol}^{-1}$  are also depicted.

effect, a system with  $X=\text{H}$  is described as the unsubstituted reference system. Hence the change in  $V_{min}$  due to substitution is designated as  $\Delta V_{min}$  which gives a direct estimation of the substituent effect.<sup>[8c]</sup>

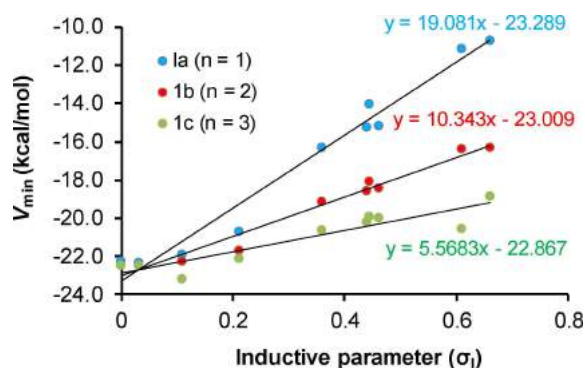
MESP isosurface for **1a**, **2a**, **3a**, **4a**, **5a** and **6a** ( $X=\text{H}$ ) is shown in Figure 2 along with the respective  $V_{min}$  values at the terminal double bond, viz.  $-22.2$ ,  $-18.6$ ,  $-13.8$ ,  $-19.5$ ,  $-18.4$ ,  $-19.0 \text{ kcal/mol}$ . The  $V_{min}$  at the terminal double bond for all the substituted systems (total 180 systems) is depicted in Table 1. The  $V_{min}$  ranges from  $-30.5$  to  $3.8 \text{ kcal/mol}$  which indicates the effect of both spacer moiety and the substituent on tuning the electron distribution on the double bond. In  $\text{C}_2\text{H}_3\text{-alkyl-X}$  systems (**1a–1c**), the inductive effect is the prime factor for electron transmission. A less negative  $V_{min}$  is observed for  $X=\text{NH}_2$  and  $X=\text{OH}$  than  $X=\text{H}$  suggesting the electron withdrawing inductive ( $-I$ ) character of the highly electronegative N and O atoms. For  $X=\text{CH}_3$  and  $n=1$ ,  $V_{min}$  is slightly more negative than  $X=\text{H}$  indicating the electron donating inductive ( $+I$ ) effect of the methyl group. An increase in alkyl chain length slightly enhances this electron donation. Further, the  $-I$  effect of substituents  $\text{Cl}$ ,  $\text{CF}_3$ ,  $\text{CN}$ ,  $\text{NO}_2$  etc. are clearly reflected on their respective  $V_{min}$ . The diminishing  $-I$  effect with an increase in alkyl chain length is pronounced in the case of  $\text{CN}$  and  $\text{NO}_2$ . For example,  $V_{min}$  of  $\text{NH}_2$  substituted systems shows a variation of  $\sim 1.3 \text{ kcal mol}^{-1}$  from  $n=1$  to  $n=3$ , while  $\text{CN}$  and  $\text{NO}_2$  exhibits a variation of  $9.4$  and  $8.1 \text{ kcal mol}^{-1}$ , respectively. The inductive control of electronic transmission in alkyl systems is confirmed by the strong linear correlation between  $V_{min}$  and inductive substituent constant ( $\sigma_I$ ) (Figure 3 and Table S1). The slope of the correlation plot  $19.081$  observed for spacer length  $n=1$  is the highest and it decreases to  $10.343$  for  $n=2$  and further decreases to  $5.5683$  for  $n=3$ . This data indicates the rapidly decreasing behavior of  $I$  with the increase in the number of CC single bonds.<sup>[13]</sup>

For the case of unsubstituted alkenyl systems (**2a–2c**),  $V_{min}$  values are observed at  $-18.6$ ,  $-18.4$ , and  $-18.3 \text{ kcal/mol}$  respectively. The small variation in  $V_{min}$  indicates the negligible impact of spacer length on electronic transmission whereas the

**Table 1.**  $V_{\min}$  (in kcal mol<sup>-1</sup>) obtained over the terminal double bond of various spacer systems.

X	NH <sub>2</sub>	OH	CH <sub>3</sub>	H	F	Cl	CF <sub>3</sub>	CHO	CN	NO <sub>2</sub>
1a	-21.9	-20.7	-22.3	-22.2	-16.3	-14.0	-15.2	-15.1	-11.1	-10.7
1b	-22.3	-21.6	-22.5	-22.5	-19.1	-18.1	-18.6	-18.4	-16.4	-16.3
1c	-23.2	-22.1	-22.5	-22.5	-20.6	-19.9	-20.2	-20.0	-20.5	-18.8
2a	-30.5	-25.4	-21.6	-18.6	-17.0	-13.3	-8.6	-7.3	-3.6	0.1
2b	-28.6	-24.3	-20.8	-18.4	-17.9	-14.8	-10.7	-9.0	-6.8	-3.5
2c	-24.3	-23.3	-20.4	-18.3	-18.1	-15.6	-12.2	-10.5	-8.9	-6.0
3a	-25.9	-20.6	-18.4	-13.8	-14.0	-11.9	-3.7	-3.0	1.4	3.8
3b	-20.1	-16.3	-14.3	-10.2	-11.0	-9.7	-2.7	-2.0	1.3	3.1
3c	-13.2	-13.1	-11.5	-8.0	-8.9	-7.9	-2.1	-1.5	1.1	2.5
4a	-25.8	-21.8	-21.0	-19.5	-17.5	-15.1	-12.5	-11.1	-8.5	-6.7
4b	-22.0	-20.2	-19.8	-19.1	-17.9	-16.7	-15.4	-14.8	-13.2	-12.4
4c	-20.0	-19.4	-19.3	-18.9	-18.1	-15.1	-16.8	-16.4	-15.5	-15.0
5a	-24.5	-20.8	-20.1	-18.4	-16.3	-14.4	-10.5	-8.7	-6.2	-3.5
5b	-20.8	-19.1	-18.2	-17.1	-15.9	-14.8	-12.5	-10.7	-9.6	-7.3
5c	-18.6	-17.4	-17.2	-16.6	-15.8	-15.1	-13.5	-12.3	-11.5	-9.8
6a	-23.5	-20.6	-20.2	-19.0	-17.4	-15.8	-13.9	-12.8	-11.0	-9.5
6b	-22.1	-20.1	-19.6	-18.8	-17.5	-16.1	-14.8	-13.8	-12.4	-11.2
6c	-20.5	-19.5	-19.2	-18.6	-17.4	-16.4	-15.4	-14.6	-13.5	-12.6

individual effect of a substituent on  $V_{\min}$  is very high in **2** series. For instance,  $\Delta V_{\min}$  of NH<sub>2</sub> and OH in **2** is significantly more negative than those in **1**. In **2**, NH<sub>2</sub> and OH donate electrons


**Figure 3.** Correlation between the  $V_{\min}$  of **1a–1c** with the inductive parameter ( $\sigma_I$ ).

mainly through resonance mechanism. NH<sub>2</sub> is the most electron donating with  $\Delta V_{\min}$  -11.9, -10.2 and -6.0 kcal mol<sup>-1</sup> for **2a**, **2b**, and **2c**, respectively (Table 2 while the most electron withdrawing NO<sub>2</sub> shows  $\Delta V_{\min}$  18.7, 14.9 and 12.4 kcal mol<sup>-1</sup>. Increasing the spacer length diminishes the power of electron transmission. Further, in the case of CH<sub>3</sub>,  $V_{\min}$  is more negative than the unsubstituted system which can be mainly attributed to the electron donating hyperconjugation and +I effect of CH<sub>3</sub>. Here the magnitude of electron donation for **2a–2c** in terms of  $\Delta V_{\min}$  is -3.0, -2.4, and -2.1 kcal/mol (Table 2). Substituents F, Cl, CF<sub>3</sub>, CHO, CN, and NO<sub>2</sub> show a considerable decrease in the magnitude of  $V_{\min}$  compared to the reference system, which authenticates their electron withdrawing inductive and resonance effects. The  $\Delta V_{\min}$  18.7, 15.0, 11.3, 10.0, 5.3, 1.6 kcal mol<sup>-1</sup> observed for the substituents NO<sub>2</sub>, CN, CHO, CF<sub>3</sub>, Cl and F, respectively suggest that their electron withdrawing power follows the order NO<sub>2</sub> > CN > CHO > CF<sub>3</sub> > Cl > F (Table 2). The strong linear correlations observed between  $V_{\min}$  of **2a**, **2b**, and **2c** systems with Hammett constant  $\sigma_p$  (Figure 4 and

**Table 2.**  $\Delta V_{\min}$  in kcal mol<sup>-1</sup> of various spacer systems.

X	$V_{\min}$ H	NH <sub>2</sub>	$\Delta V_{\min}$ OH	CH <sub>3</sub>	F	Cl	CF <sub>3</sub>	CHO	CN	NO <sub>2</sub>
1a	-22.2	0.3	1.5	-0.1	6.0	8.2	7.0	7.1	11.1	11.5
1b	-22.5	0.2	0.8	0.0	3.3	4.4	3.9	4.1	6.1	6.1
1c	-22.5	-0.7	0.4	0.0	1.9	2.6	2.3	2.5	1.9	3.6
2a	-18.6	-11.9	-6.8	-3.1	1.6	5.3	10	11.3	15.0	18.7
2b	-18.4	-10.2	-6.0	-2.4	0.5	3.6	7.7	9.3	11.6	14.9
2c	-18.3	-6.0	-5.0	-2.1	0.3	2.7	6.1	7.8	9.4	12.4
3a	-13.8	-12.1	-6.8	-4.6	-0.2	1.9	10.1	10.8	15.2	17.6
3b	-10.2	-9.9	-6.0	-4.1	-0.8	0.5	7.5	8.2	11.5	13.3
3c	-8.0	-5.2	-5.0	-3.5	-0.9	0.1	5.9	6.5	9.2	10.5
4a	-19.5	-6.3	-2.3	-1.4	2.0	4.5	7.1	8.4	11.0	12.8
4b	-19.1	-2.9	-1.1	-0.8	1.2	2.4	3.7	4.3	5.8	6.7
4c	-18.9	-1.1	-0.5	-0.4	0.8	3.8	2.1	2.4	3.4	3.9
5a	-18.4	-6.1	-2.4	-1.7	2.1	4	7.8	9.7	12.2	14.9
5b	-17.1	-3.7	-2.0	-1.1	1.1	2.3	4.6	6.4	7.5	9.7
5c	-16.6	-2.1	-0.8	-0.6	0.8	1.5	3.1	4.2	5.1	6.8
6a	-19.0	-4.5	-1.6	-1.2	1.6	3.3	5.1	6.2	8.0	9.5
6b	-18.8	-3.3	-1.3	-0.9	1.3	2.6	4.0	5.0	6.3	7.5
6c	-18.6	-1.9	-0.9	-0.6	1.1	2.1	3.2	4.0	5.1	6.0

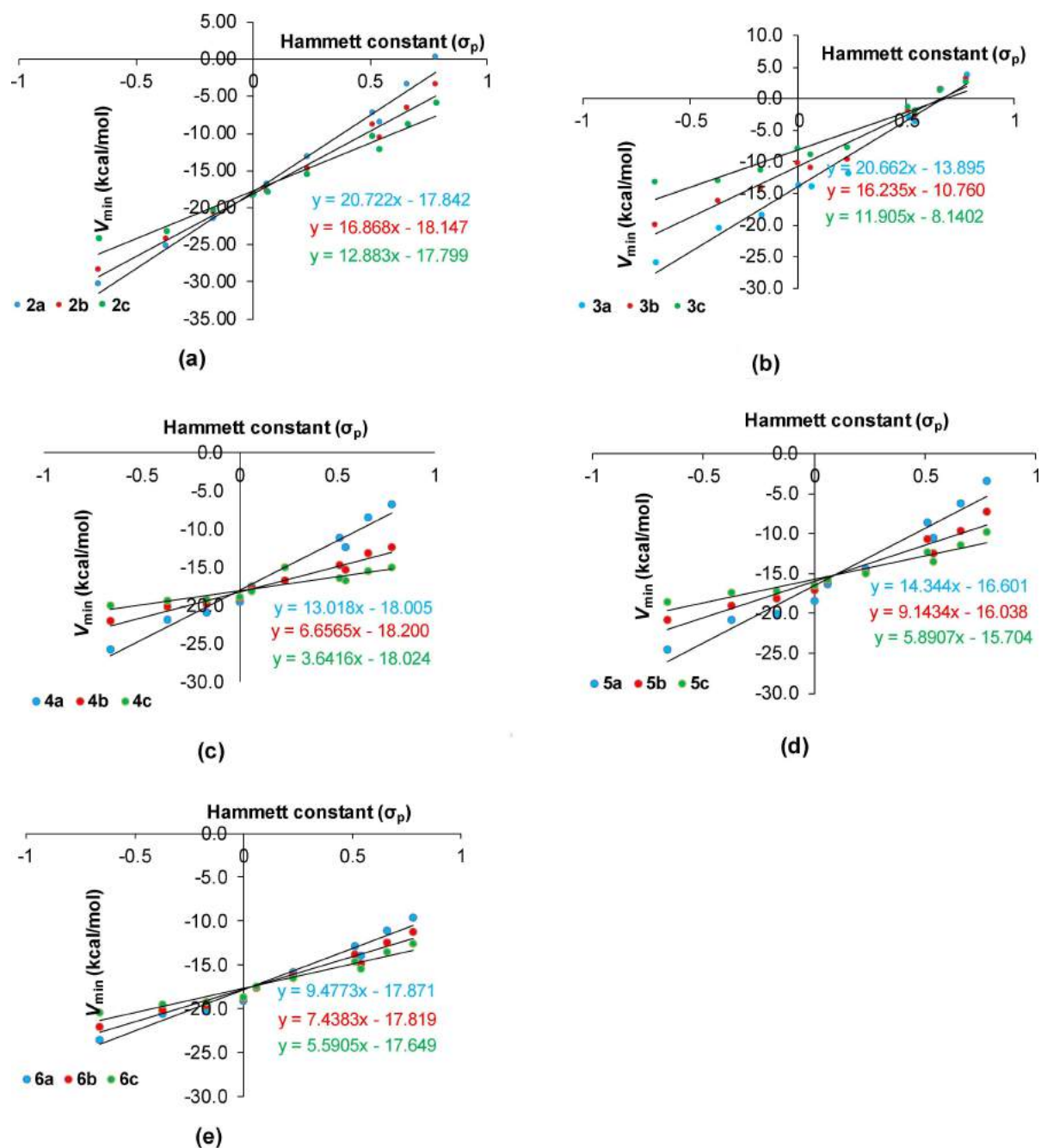


Figure 4. Correlation of  $V_{\min}$  with Hammett parameter ( $\sigma_p$ ) of a) alkenyl, b) alkylnyl, c) phenyl, d) thiophenyl, and e) polyacene systems.

Table S1) suggests that the MESP topographical quantity  $V_{\min}$  is highly suited as an electronic descriptor to quantify the electron donating and withdrawing nature of a substituent. The slope of the correlation plots decreases as  $n$  increase in the spacer length. Since  $\sigma_p = 0$  stands for the unsubstituted systems, the Y-intercept of the correlation plot corresponds to  $V_{\min}$  of the unsubstituted system. Indeed, the Y-intercept and  $V_{\min}$  of the unsubstituted system show very close agreement.

The unsubstituted alkylnyl systems, (**3a–3c**) shows  $V_{\min}$  values at  $-13.8$ ,  $-10.2$ , and  $-8.0$  kcal mol $^{-1}$ , respectively. The magnitude of these values are smaller than the unsubstituted

alkenyl systems indicating the more electronegative  $C_{sp}$  hybridized carbons in alkylnyl systems than  $C_{sp2}$  in alkenyl systems. Similar to **2**, resonance effect dominates in **3** except for  $X=CH_3$  and  $X=CF_3$ . The magnitude of electron withdrawing effect ( $\Delta V_{\min}$ ) obtained for substituents such as  $NO_2$ ,  $CN$ ,  $CHO$ ,  $CF_3$ ,  $Cl$ , and  $F$  is very similar to that found for  $C_2H_3$ -alkenyl- $X$  systems which indicates that substituent effect transmission power is similar for  $C=C$  double bonds and  $C\equiv C$  triple bonds.

The unsubstituted systems with phenyl ring spacers, **4a–4c** show  $V_{\min}$  values at  $-19.5$ ,  $-19.1$ , and  $-18.9$  kcal mol $^{-1}$ , respectively. The electron donating  $NH_2$ ,  $OH$ , and  $CH_3$  substitu-



ents enhance the negative character of  $V_{min}$  while the electron withdrawing F, Cl,  $CF_3$ , CHO, CN, and  $NO_2$  substituents diminish it. The similar  $V_{min}$  feature has been noticed for systems containing thiophenyl spacers, **5a–5c** and polyacene spacers, **6a–6c** (Table 1). In **4** series with  $n=2$  and 3, adjacent two phenyl units are twisted away from planarity which gives a diminishing effect on the electron donating/withdrawing ability of the substituent. The C–C single bond connection between two phenyl units in **4** proposes a significant inductive effect along with resonance. In polyacenes, resonance effect dominates over the inductive effect. In **4**, **5** and **6** series, increase in spacer length has a decreasing effect on the transmission power of the substituent effect.

## 2.2. $V_{min}$ -Based Quantification of Substituent Effect Transmission Power of Spacers

When a reacting center and substituent are separated by a variety of spacers, significant variations in the molecular properties can be observed.<sup>[19]</sup> The transmission of the substituent effect through olefinic systems showed the applicability of  $\rho$  in calculating the substituent effect transmission power. From the previous studies,<sup>[10b,d]</sup> it is understood that the transmission power of a spacer can be quantified by the transmission coefficient ( $\gamma$ ) defined as  $\gamma = \rho_s / \rho_o$ , where  $\rho_s$  is the reaction constant of a spacer for which the transmission power has to be quantified and  $\rho_o$  is the reaction constant of the reference group. Since  $V_{min}$  provides an alternative measure of substituent effects for  $\pi$ -conjugated systems, the correlation of  $V_{min}$  with  $\sigma_p$  can be used to evaluate the transmission ability of various spacers using the equation,  $V_{min} = \rho\sigma_p + \text{constant}$ . Therefore, linear regression analysis between  $V_{min}$  and  $\sigma_p$  values is carried out to find the  $\rho$  values (Table 3). In order to calculate the transmission coefficients ( $\gamma$ ), the phenyl group substituted **4a** is taken as the reference system for all the spacers. For **4a** systems,  $V_{min} = 13.018(\sigma_p) - 18.00$  and the slope of this equation ( $\rho_{4a}$ ) is used as  $\rho_o$  to determine  $\gamma$ . For example, the  $\gamma$  value for **2a** is calculated as  $\gamma = \rho_{2a} / \rho_{4a} = 20.722 / 13.018 = 1.592$  meaning that the transmission power of **2a** is 1.592 times higher than

**Table 3.** Slope, intercept, reaction constant ( $\rho_s$ ), correlation coefficient (R) and transmission coefficient ( $\gamma$ ) of various spacers.

X	Slope	Intercept	$\rho_s$	R	$\gamma$
<b>2a</b>	20.722	-17.84	20.722	0.994	1.592
<b>2b</b>	16.868	-18.15	16.868	0.993	1.296
<b>2c</b>	12.883	-17.80	12.883	0.981	0.989
<b>3a</b>	20.662	-13.90	20.662	0.988	1.587
<b>3b</b>	16.235	-10.76	16.235	0.985	1.247
<b>3c</b>	11.905	-8.14	11.905	0.962	0.914
<b>4a</b>	13.018	-18.00	13.018	0.987	1.000
<b>4b</b>	6.667	-18.20	6.667	0.984	0.512
<b>4c</b>	3.642	-18.02	3.642	0.895	0.280
<b>5a</b>	14.344	-16.60	14.344	0.979	1.102
<b>5b</b>	9.143	-16.03	9.143	0.973	0.702
<b>5c</b>	5.891	-15.70	5.891	0.961	0.452
<b>6a</b>	9.477	-17.87	9.477	0.984	0.728
<b>6b</b>	7.438	-17.81	7.438	0.983	0.571
<b>6c</b>	5.591	-17.65	5.591	0.974	0.429

phenyl ring. Among the  $\pi$ -bonded spacers, for  $n=1$ , the order of substituent effect transmission power of spacers is **2a**  $\approx$  **3a** > **5a** > **4a** > **6a**. On the basis of the average of all the  $\gamma$  values for a particular spacer from  $n=1-3$ , the order of transmission power of substituent effects is as follows: **2a–2c** > **3a–3c** > **5a–5c** > **4a–4c** > **6a–6c**. This order is in agreement with the experimental findings<sup>[10b]</sup> and suggesting the appropriateness of  $V_{min}$  method for the present study.

## 2.3. Combination of Two Different Spacers and Substituent Selectivity

To understand the transmission ability of a combination of two different spacers, we selected six types of spacers as shown in Figure 5. In **7a** and **7b** the substituent is connected to the double bonded carbon and an aromatic ring, respectively. In Table 4, the  $V_{min}$  values obtained for all the hetero spacers are reported. For substituent 'H' the  $V_{min}$  values of **7a** and **7b** are  $-18.76$  and  $-18.89$  kcal/mol showing a variation of  $0.13$  kcal mol<sup>-1</sup> between the two isomers. However, for other substituents, the difference in  $V_{min}$  is found to be less than  $\sim 1.0$  kcal mol<sup>-1</sup> suggesting that the electron donating or withdrawing nature is not highly affected whether 'X' is attached to the double bond or the phenyl ring. The  $V_{min}$  values for substituent 'H' of **8a** and **8b** are  $-16.32$  and  $-15.88$  kcal mol<sup>-1</sup> indicating that total electron withdrawing nature of ethynylbenzene is more when ethyne is attached directly to the olefinic

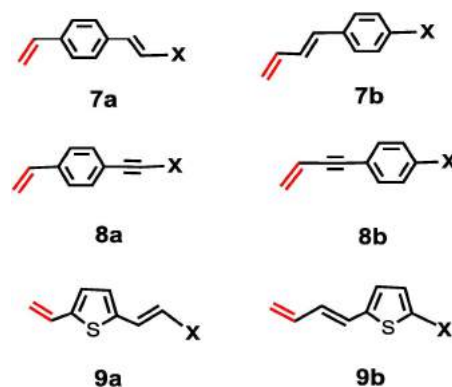


**Figure 5.** Spacers considered to quantifying the effect of the combination of two different spacers.

**Table 4.**  $V_{min}$  values (kcal/mol) obtained for hetero spacers.

X	7a	7b	8a	8b	9a	9b
<b>NH<sub>2</sub></b>	-24.85	-24.22	-22.78	-21.02	-24.16	-23.72
<b>OH</b>	-21.96	-21.08	-20.27	-17.95	-21.52	-20.83
<b>Me</b>	-20.21	-20.21	-18.83	-17.07	-19.39	-19.77
<b>H</b>	-18.76	-18.89	-16.32	-15.88	-17.51	-18.32
<b>F</b>	-17.70	-17.70	-16.50	-14.56	-16.75	-17.13
<b>Cl</b>	-15.81	-15.75	-15.44	-12.80	-14.56	-15.44
<b>CF<sub>3</sub></b>	-13.24	-13.49	-10.86	-10.67	-11.42	-12.30
<b>CHO</b>	-12.05	-12.17	-9.79	-9.60	-8.85	-10.35
<b>CN</b>	-10.17	-10.48	-10.48	-7.78	-7.97	-8.85
<b>NO<sub>2</sub></b>	-7.97	-8.79	-8.79	-6.28	-5.21	-6.34

moiety. Further, the electron withdrawing and donating substituents show maximum influence when they are attached to the phenyl ring. Additionally, for **9a** and **9b**,  $V_{\min}$  values for the unsubstituted systems are observed at  $-17.51$  and  $-18.32$  kcal/mol, respectively meaning that the variation is only  $0.81$  kcal/mol. In fact, for all the substituent except CHO and  $\text{NO}_2$ , the variation is less than  $\sim 1$  kcal/mol. This confirms that electronic effect is not highly affected whether 'X' is attached to a double bond or thiophenyl ring. In general, a spacer made up of two different moieties, substituent effect transmission power of 'X' can show a minor variation depending on the connectivity of X with the spacer unit.

### 3. Conclusions

The substituent effect transmission power of electron donating and withdrawing substituents on a terminal CC double bond has been assessed using MESP  $V_{\min}$  analysis. The  $V_{\min}$  observed on this bond showed significant change with respect to the electron donating/withdrawing nature of the substituent as well as the nature and length of the spacer unit. The  $V_{\min}$  correlates strongly with an inductive parameter for systems consisting of alkyl spacers. Similarly, for all the  $\pi$ -conjugated systems, strong linear correlations were observed between Hammett substituent constant and  $V_{\min}$ . The decreasing trend of slope values with an increase in the size of spacer length revealed the strongly diminishing nature of the substituent effect transmission. From the slope of the correlation plots, the transmission power of spacers are obtained which can be arranged in the order alkenyl > alkynyl > thiophenyl > phenyl > polyacene. For systems having alkyl spacers, transmission of substituent effect is the least as the inductive effect has a rapidly diminishing character with the increase in the size of the spacer unit. In summary, among all the spacer groups, alkenyl and alkynyl units are the most effective for the substituent effect transmission.

### 4. Computational Details

Geometry optimization has been carried out with B3LYP/6-31G(d, p) density functional theory method.<sup>[20]</sup> MESP computations are also done at the same level of theory. Previous studies showed that this method is adequate for calculating MESP features.<sup>[5b,h,21]</sup> MESP,  $V(\mathbf{r})$  at a point  $\mathbf{r}$  due to a molecular system with nuclear charges located at  $\mathbf{R}_A$  and electron density  $\rho(\mathbf{r})$  is expressed in Equation (1) where  $N$  is the total number of nuclei in the molecule and  $Z_A$  is the charge on nucleus  $A$ , located at the distance  $|\mathbf{R}_A|$ .

$$V(\mathbf{r}) = \sum_A^N \frac{Z_A}{|\mathbf{r} - \mathbf{R}_A|} - \int \frac{\rho(\mathbf{r}') d^3\mathbf{r}'}{|\mathbf{r} - \mathbf{r}'|} \quad (1)$$

In MESP topography, a negative-valued minimum ( $V_{\min}$ ) is often observed in electron-rich regions such as lone pair,  $\pi$ -bonds, and anionic sites of a molecular system. Gaussian 09

programme package has been used for all the calculations.<sup>[22]</sup> Vibrational frequency analysis is done with the same level of theory to confirm that the number of imaginary frequencies is zero for all the optimized geometries.

### Acknowledgements

Authors thank DST-SERB for funding through GAP137239 and also gratefully acknowledge the CSIR 4th PI for HPC facility and NIIST IT lab for computational support.

### Conflict of Interest

The authors declare no conflict of interest.

**Keywords:** density functional calculations · molecular electrostatic potential · spacers · substituent effect · transmission power.

- [1] a) T. M. Krygowski, B. T. Stepień, *Chem. Rev.* **2005**, *105*, 3482–3512; b) O. Exner, T. M. Krygowski, *Chem. Soc. Rev.* **1996**, *25*, 71–75.
- [2] a) C. Hansch, A. Leo, R. W. Taft, *Chem. Rev.* **1991**, *91*, 165–195; b) W. Adcock, N. A. Trout, *Chem. Rev.* **1999**, *99*, 1415–1435; c) O. Exner, S. Bohm, *Curr. Org. Chem.* **2006**, *10*, 763–778; d) L. P. Hammett, *J. Am. Chem. Soc.* **1937**, *59*, 96–103.
- [3] H. H. Jaffé, *Chem. Rev.* **1953**, *53*, 191–261.
- [4] T. M. Krygowski, M. A. Dobrowolski, K. Zborowski, M. K. Cyranski, *J. Phys. Chem.* **2006**, *19*, 889–895.
- [5] a) C. H. Suresh, S. R. Gadre, *J. Am. Chem. Soc.* **1998**, *120*, 7049–7055; b) C. H. Suresh, S. R. Gadre, *J. Phys. Chem. A* **2007**, *111*, 710–714; c) G. S. Remya, C. H. Suresh, *Phys. Chem. Chem. Phys.* **2016**, *18*, 20615–20626; d) T. M. Krygowski, K. Ejsmont, B. T. Stepień, M. K. Cyranski, J. Poater, M. Sola, *J. Org. Chem.* **2004**, *69*, 6634–6640; e) T. M. Krygowski, M. Palusiak, A. Płonka, J. E. Zachara-Horeglad, *J. Phys. Org. Chem.* **2007**, *20*, 297–306; f) T. M. Krygowski, J. E. Zachara-Horeglad, M. Palusiak, *J. Org. Chem.* **2010**, *75*, 4944–4949; g) T. M. Krygowski, W. P. Oziminski, *J. Mol. Model.* **2014**, *20*, 2352; h) S. E. Wheeler, K. N. Houk, *J. Am. Chem. Soc.* **2009**, *131*, 3126–3127; i) S. E. Wheeler, K. N. Houk, *J. Am. Chem. Soc.* **2009**, *131*, 3126–3127; j) S. E. Wheeler, *J. Am. Chem. Soc.* **2011**, *133*, 10262–10274; k) S. E. Wheeler, *Acc. Chem. Res.* **2013**, *46*, 1029–1038; l) B. Galabov, S. Ilieva, H. F. Schaefer, *J. Org. Chem.* **2006**, *71*, 6382–6387; m) B. Galabov, V. Nikolova, S. Ilieva, *Chem. Eur. J.* **2013**, *19*, 5149–5155.
- [6] a) R. W. Taft, *J. Am. Chem. Soc.* **1953**, *75*, 4231–4238; b) M. Charton, *Prog. Phys. Org. Chem.* **1981**, *119*–251.
- [7] C. G. Swain, E. C. Lupton, *J. Am. Chem. Soc.* **1968**, *90*, 4328–4337.
- [8] a) B. Galabov, S. Ilieva, G. Koleva, W. D. Allen, H. F. Schaefer III, P. von R. Schleyer, *Wiley Interdiscip. Rev.: Comput. Mol. Sci.* **2013**, *3*, 37–55; b) F. B. Sayyed, C. H. Suresh, *New J. Chem.* **2009**, *33*, 2465–2471; c) F. B. Sayyed, C. H. Suresh, S. R. Gadre, *J. Phys. Chem. A* **2010**, *114*, 12330–12333; d) F. B. Sayyed, C. H. Suresh, *J. Phys. Chem. A* **2011**, *115*, 9300–9307; e) F. B. Sayyed, C. H. Suresh, *J. Phys. Chem. A* **2011**, *115*, 5660–5664; f) F. B. Sayyed, C. H. Suresh, *Chem. Phys. Lett.* **2012**, *523*, 11–14.
- [9] a) S. Böhm, J. Kuthan, *Int. J. Quantum Chem.* **1984**, *26*, 21–33; b) K. H. Kim, Y. C. Martin, *J. Org. Chem.* **1991**, *56*, 2723–2729; c) J. S. Murray, T. Brinck, P. Politzer, *J. Mol. Struct.* **1992**, *255*, 271–281; d) H. Szatylowicz, T. Siodla, O. A. Stasyuk, T. M. Krygowski, *Phys. Chem. Chem. Phys.* **2016**, *18*, 11711–11721; e) T. Krygowski, N. Sadlej-Sosnowska, *Struct. Chem.* **2011**, *22*, 17–22.
- [10] a) C. A. van Walree, L. W. Jenneskens, *Tetrahedron* **1997**, *53*, 5825–5830; b) M. Charton, *J. Org. Chem.* **1961**, *26*, 735–738; c) S. A. Myers, R. A. Assink, D. A. Loyb, K. J. Sheac, *J. Chem. Soc. Perkin Trans. 2* **2000**, 545–549; d) K. Bowden, *Can. J. Chem.* **1963**, *41*, 2781–2793; e) K. Waisser, J. Kunes, L. Kubicova, M. Budesinsky, O. Exner, *Magn. Reson. Chem.* **1997**, *35*, 543–548; f) W. Adcock, *J. Phys. Org. Chem.* **2009**, *22*, 1065–1069; g) W. Adcock, A. Krstic, *Magn. Reson. Chem.* **2000**, *38*, 115–122; h) W.

- Adcock, N. Trout, *Magn. Reson. Chem.* **1998**, *36*, 181–195; i) A. R. Campanelli, A. Domenicano, G. Piacente, F. Ramondo, *J. Phys. Chem. A* **2010**, *114*, 5162–5170.
- [11] a) E. Scrocco, J. Tomasi, in *New concepts II*, Springer, **1973**, pp. 95–170; b) E. Scrocco, J. Tomasi, in *Advances in quantum chemistry*, Vol. 11, Elsevier, **1978**, pp. 115–193.
- [12] a) S. R. Gadre, I. H. Shrivastava, *J. Chem. Phys.* **1991**, *94*, 4384–4390; b) F. Luque, M. Orozco, P. Bhadane, S. Gadre, *J. Chem. Phys.* **1994**, *100*, 6718–6726; c) S. R. Gadre, P. K. Bhadane, *J. Chem. Phys.* **1997**, *107*, 5625–5626; d) S. R. Gadre, C. H. Suresh, *J. Org. Chem.* **1997**, *62*, 2625–2627.
- [13] C. H. Suresh, P. Alexander, K. P. Vijayalakshmi, P. K. Sajith, S. R. Gadre, *Phys. Chem. Chem. Phys.* **2008**, *10*, 6492–6499.
- [14] F. B. Sayyed, C. H. Suresh, *Tetrahedron Lett.* **2009**, *50*, 7351–7354.
- [15] C. H. Suresh, *Inorg. Chem.* **2006**, *45*, 4982–4986.
- [16] a) P. K. Sajith, C. H. Suresh, *Inorg. Chem.* **2012**, *51*, 967–977; b) P. K. Sajith, C. H. Suresh, *Dalton Trans.* **2010**, *39*, 815–822; c) J. Mathew, T. Thomas, C. H. Suresh, *Inorg. Chem.* **2007**, *46*, 10800–10809; d) J. Mathew, C. H. Suresh, *Inorg. Chem.* **2010**, *49*, 4665–4669.
- [17] a) C.-J. Tan, C.-S. Yang, Y.-C. Sheng, H. W. Amini, H.-H. G. Tsai, *J. Phys. Chem. C* **2016**, *120*, 21272–21284; b) C. Teng, X. Yang, C. Yang, H. Tian, S. Li, X. Wang, A. Hagfeldt, L. Sun, *J. Phys. Chem. C* **2010**, *114*, 11305–11313; c) Y. Hua, J. He, C. Zhang, C. Qin, L. Han, J. Zhao, T. Chen, W.-Y. Wong, W.-K. Wong, X. Zhu, *J. Mater. Chem. A* **2015**, *3*, 3103–3112; d) Y. Ding, Y. Jiang, W. Zhang, L. Zhang, X. Lu, Q. Wang, G. Zhou, J.-m. Liu, K. Kempa, J. Gao, *J. Phys. Chem. C* **2017**, *121*, 16731–16738.
- [18] a) F. Massoth, P. Politzer, M. Concha, J. Murray, J. Jakowski, J. Simons, *J. Phys. Chem. B* **2006**, *110*, 14283–14291; b) P. Politzer, L. Abrahmsen, P. Sjöberg, *J. Am. Chem. Soc.* **1984**, *106*, 855–860.
- [19] J. Frederick, J. Dippy, *Chem. Rev.* **1939**, *25*, 151–211.
- [20] a) A. D. Becke, *J. Chem. Phys.* **1993**, *98*, 5648–5652; b) C. Lee, W. Yang, R. G. Parr, *Phys. Rev. B* **1988**, *37*, 785.
- [21] F. B. Sayyed, C. H. Suresh, *New J. Chem.* **2009**, *33*, 2465–2471.
- [22] M. J. Frisch, G. W. Trucks, H. B. Schlegel, G. E. Scuseria, M. A. Robb, J. R. Cheeseman, G. Scalmani, V. Barone, B. Mennucci, G. A. Petersson, H. Nakatsuji, M. Caricato, X. Li, H. P. Hratchian, A. F. Izmaylov, J. Bloino, G. Zheng, J. L. Sonnenberg, M. Hada, M. Ehara, K. Toyota, R. Fukuda, J. Hasegawa, M. Ishida, T. Nakajima, Y. Honda, O. Kitao, H. Nakai, T. Vreven, J. J. A. Montgomery, J. E. Peralta, F. Ogliaro, M. Bearpark, J. J. Heyd, E. Brothers, K. N. Kudin, V. N. Staroverov, T. Keith, R. Kobayashi, J. Normand, K. Raghavachari, A. Rendell, J. C. Burant, S. S. Iyengar, J. Tomasi, M. Cossi, N. Rega, J. M. Millam, M. Klene, J. E. Knox, J. B. Cross, V. Bakken, C. Adamo, J. Jaramillo, R. Gomperts, R. E. Stratmann, O. Yazyev, A. J. Austin, R. Cammi, C. Pomelli, J. W. Ochterski, R. L. Martin, K. Morokuma, V. G. Zakrzewski, G. A. Voth, P. Salvador, J. J. Dannenberg, S. Dapprich, A. D. Daniels, O. Farkas, J. B. Foresman, J. V. Ortiz, J. Cioslowski, D. J. Fox, Gaussian 09, Revision D.01; Gaussian, Inc. Wallingford, CT, 2013.

---

Manuscript received: February 28, 2019  
Accepted manuscript online: April 11, 2019  
Version of record online: June 13, 2019





Cite this: *New J. Chem.*, 2020, **44**, 7200

# Density functional theory study on the donating strength of donor systems in dye-sensitized solar cells†

Velayudhan V. Divya<sup>ab</sup> and Cherumuttathu H. Suresh<sup>id</sup> \*<sup>ab</sup>

The electron-donating strengths of donor (D) moieties in thirteen donor- $\pi$ -acceptor systems (D1- $\pi$ -A to D13- $\pi$ -A wherein  $\pi$ - and A represent butadiene and cyanoacrylic acid units, respectively) have been studied using B3LYP/cc-pVDZ level density functional theory (DFT) calculations. The selected D moieties are encountered as a part of an organic sensitizer molecule in dye-sensitized solar cell (DSSC) applications. When the D moiety is joined with  $\pi$ -A, a certain amount of electron donation from D to A occurs leading to an increase in electron density at the A site of D- $\pi$ -A compared to the A site of  $\pi$ -A. This electron reorganization is quantified in terms of a change in molecular electrostatic potential (MESP) minimum ( $\Delta V_{\text{mA}}$ ) at the acceptor site, the CN group of the cyanoacrylic acid. The  $\Delta V_{\text{mA}}$  is always negative, in the range of  $-11.0$  to  $-2.6$  kcal mol<sup>-1</sup> which provides a quick assessment of the rank order of the electron-donating nature of the D moieties in the ground state of D- $\pi$ -A. The optical and photovoltaic properties of D and D- $\pi$ -A systems are also determined at the TD-CAM-B3LYP/cc-pVDZ//B3LYP/cc-pVDZ level. An absorption red shift ( $\Delta\lambda_{\text{max}}$ ) in the range of 81–242 nm is observed when D moieties change to D- $\pi$ -A systems. The ground state property  $\Delta V_{\text{mA}}$  showed a strong linear correlation with the excited state property  $\Delta\lambda_{\text{max}}$ . Furthermore,  $\Delta V_{\text{mA}}$  is found to be proportional to the open-circuit voltage ( $V_{\text{OC}}$ ). The resemblance of highest occupied molecular orbital (HOMO) and lowest unoccupied molecular orbital (LUMO) energies of the D- $\pi$ -A system with the respective energies of donor and  $\pi$ -A systems shows that the donor tunes the HOMO, while  $\pi$ -A tunes the LUMO. Among the thirteen D- $\pi$ -A systems, *N,N*-dialkylaniline, and julolidine are rated as the best donors for the photovoltaic applications. This study shows that the MESP based assessment of the donating strength of donor systems offers a powerful rational design strategy for the development of efficient dyes for DSSC applications.

Received 11th February 2020,  
Accepted 1st April 2020

DOI: 10.1039/d0nj00723d

rsc.li/njc

## Introduction

Dye-sensitized solar cells (DSSCs) have been regarded as a highly potential alternative to conventional silicon-based solar cells due to their high molar extinction coefficient, low production cost, simple synthetic strategy and easy structural modifications.<sup>1–5</sup> DSSCs also perform relatively better than other traditional solar cells under diffuse light conditions and at higher temperatures.<sup>4–6</sup> In DSSC applications, the sensitizers synthesized can be divided into two broad areas, *viz.* metal-based systems such as Ru(II) polypyridyl complexes, and Zn(II) porphyrins<sup>7</sup> and the metal-free donor- $\pi$ -acceptor (D- $\pi$ -A) type organic dyes.<sup>8</sup> The Ru-based

polypyridyl sensitizers attained the highest power conversion efficiency over 11% more than most of the metal-free sensitizers.<sup>9–14</sup>

This is due to the ability of metal sensitizers to absorb solar irradiation up to the near-infrared region, while other metal-free dye sensitizers are absorbed in the shorter wavelength region.<sup>8,13,15</sup> So, a highly efficient sensitizer should have an absorption maximum near to the Vis-NIR region associated with a long-lived charge excited state.<sup>16,17</sup> Due to the highly expensive and toxic synthetic procedures involved in metal sensitizers, the organic dyes exhibit remarkable importance in DSSC applications.<sup>8</sup> Recent studies proposed important structural modifications in organic dyes<sup>18,19</sup> to achieve a high power conversion efficiency (PCE) and over 12% has been achieved with a metal-free alkoxy-silyl carbazole dye as a sensitizer.<sup>20</sup> Yao *et al.* reported an improved PCE of 12.5% with a metal-free indenoperylene based D- $\pi$ -A dye,<sup>21</sup> the best-known metal-free organic dye. In 2017, a simple designing strategy over the phenothiazine moiety with ethynyl-pyrene enabled a PCE of 12%.<sup>22</sup> The other recent milestones in DSSCs include co-sensitization, which enables higher photovoltaic performance

<sup>a</sup> Chemical Sciences and Technology Division, CSIR-National Institute for Interdisciplinary Science and Technology (CSIR-NIIST), Thiruvananthapuram, Kerala 695 019, India. E-mail: sureshch@niist.res.in, sureshch@gmail.com

<sup>b</sup> Academy of Scientific and Innovative Research (AcSIR), CSIR-NIIST Campus, Trivandrum, India

† Electronic supplementary information (ESI) available: See DOI: 10.1039/d0nj00723d

over 14% with a collaborative sensitization by silyl and carboxy anchoring groups.<sup>23</sup> Many studies proposed the structural modification of the donor group of the D- $\pi$ -A dye to achieve higher efficiency as increasing the electron donating strength generally broadens and intensifies the region of absorption.<sup>24–26</sup>

In general, a dye sensitizer with a D- $\pi$ -A framework can be modified at donor,<sup>27,28</sup> spacer,<sup>29–32</sup> and anchoring groups<sup>33–35</sup> to improve the PCE. Typically, the acceptor portion (A) of the dye anchored onto the TiO<sub>2</sub> semiconductor favours the charge transfer of the excited electrons to the conduction band of the semiconductor.<sup>36</sup> The oxidized dye is then regenerated by the electron transfer from the electrolyte (I<sup>-</sup>/I<sub>3</sub><sup>-</sup> couple), while the electrolyte couple regains the electron from the platinum counter electrode.<sup>4,37</sup> Therefore, for an efficient dye sensitizer, an effective electron injection can occur from the dye to the TiO<sub>2</sub> semiconductor if its highest occupied molecular orbital (HOMO) is observed at a level slightly below the redox couple of the I<sup>-</sup>/I<sub>3</sub><sup>-</sup> electrolyte (-4.8 eV) and the lowest unoccupied molecular orbital (LUMO) is observed above the conduction band of TiO<sub>2</sub> (-4.0 eV).<sup>8,38,39</sup>

Apart from the simple D- $\pi$ -A framework, several other configurations like D-D- $\pi$ -A,<sup>40–42</sup> D-A- $\pi$ -A,<sup>43–46</sup> D- $\pi$ -A-A,<sup>47</sup> (D- $\pi$ -A)<sub>2</sub>,<sup>48</sup> and double D- $\pi$ -A bridges<sup>49</sup> were also introduced and revealed that the introduction of additional donors, acceptors, and the extension of  $\pi$  conjugation reduces the HOMO-LUMO energy gap and redshifts the absorption maximum. In other words, for the improved PCE, the donor should be stable, and electron-rich for the effective electron injection to the TiO<sub>2</sub> conduction band,<sup>28,50,51</sup> thereby broadening their absorption to the Vis-NIR region.<sup>50,51</sup> Therefore, for effective dye designing, it is very important to understand the electronic and photophysical properties of the dye systems.<sup>44</sup> Density functional theory (DFT) and Time-dependent density functional theory (TD-DFT) can afford a more efficient approach to understand and predict these structural and electronic features without any time delay compared to the traditional trial and error methods.<sup>52–63</sup> Previous studies have shown that the donor strength has a significant role in absorption maximum, the kinetics of electron injection and light-harvesting efficiency.<sup>64,65</sup> Recently, the relevance of the theoretical estimation of donor strength in organic electronics has been explained by Köse.<sup>66</sup>

Thirteen typically used donor building blocks (Fig. 1) in the DSSC applications are selected for this DFT/TDDFT study (D1–D13).<sup>24,31,67–72</sup> Among them, D1–D4 are aromatic hydrocarbon systems whereas the remaining donor moieties contain at least one lone pair bearing a nitrogen centre (D5–D13). The estimation of the donating strength is assessed by molecular electrostatic potential (MESP) topographical features of these donor molecules and their corresponding D- $\pi$ -A systems. The MESP distribution is useful to understand the charge distribution within a molecule,<sup>73–76</sup> and the regions with negative MESP values indicate electron-dense regions while positive-valued areas represent electron-deficient regions. The MESP based interpretation has been used for the study of substituent effects, intermolecular interactions, non-covalent interactions, hydrogen bonding, cation- $\pi$  interactions, aromaticity and a variety of chemical phenomena.<sup>77–80</sup> MESP analysis has been used in the

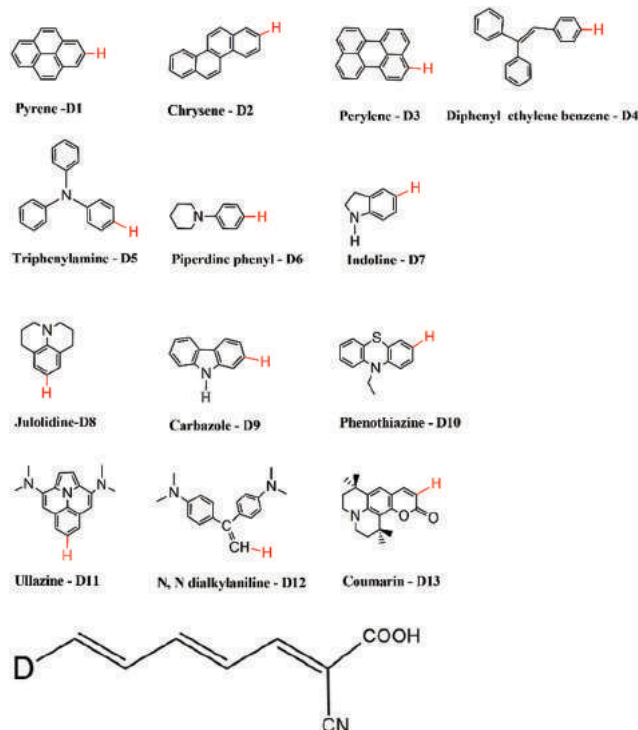


Fig. 1 ChemDraw representation of donors (D1–D13) and D- $\pi$ -A systems. The bond shown in red colour is replaced with the  $\pi$ -A part to design the D- $\pi$ -A system.

field of organometallic chemistry for the quantification of the electron-donating strength of phosphine and N-heterocyclic ligands.<sup>73</sup> The global minimum ( $V_{\min}$ ) of MESP near the two electron donor atom (P or N) indicates the net donating ability of the ligand for making a coordination bond with a metal centre. Furthermore, Suresh and co-workers proved that MESP minimum ( $V_{\min}$ ) analysis is very effective for the quantification of the inductive, resonance, steric and proximity effects of substituents.<sup>75,81–84</sup> Recently the substituent effect transmitting power ( $\gamma$ ) through various spacer units is also calculated *via* MESP analysis and showed that  $V_{\min}$  values are beneficial for the quantification of the transmission power of spacers.<sup>85</sup> The study recommends the usage of short alkenyl systems as spacers for effective electronic transmission. Moreover, the above reliable studies confirmed that MESP is a powerful descriptor, capable of predicting the electronic properties of the molecular systems effectively. The present study focuses on the MESP analysis of D- $\pi$ -A systems towards photovoltaic applications. The butadiene moiety (-HC=CH-CH=CH-) and the cyanoacrylic acid unit (-H<sub>2</sub>C=C(CN)-COOH) are used as the  $\pi$ -spacer and anchoring (A) group, respectively.

## Computational method

The ground state geometry optimization has been carried out using the B3LYP density functional theory (DFT) method<sup>86</sup> with the cc-pVDZ basis set.<sup>87</sup> This DFT method has been extensively used in the theoretical studies of organic dyes for dye-sensitized

solar cell applications.<sup>45,60</sup> Frequency calculations were also done at the same level of theory and confirmed that there were no imaginary frequencies. Vertical excitation energy calculations have been done for the first 7 states by using a long-range and solvation effect-corrected CAM-B3LYP/cc-pVDZ DFT method<sup>56</sup> in dichloromethane. The reliability of this method has been checked by doing the computation on experimentally known systems (Fig. S1, ESI†) using three more methods, *viz.* B3LYP,<sup>86</sup> PBE1PBE,<sup>88</sup> and  $\omega$ B97XD.<sup>89</sup> For all these methods, the solvation effects are incorporated through the self-consistent reaction field (SCRF) calculation implemented in the SMD (solvation model based on electron density) model.<sup>90</sup> The TD-DFT calculations showed that the result given by CAM-B3LYP is the most reliable to reproduce the experimental absorption maximum (Table S1, ESI†). DFT and TD-DFT calculations are done using the Gaussian 16 program package.<sup>91</sup> For quantifying the electron donating strength of donors in the D- $\pi$ -A system, molecular electrostatic potential (MESP) analysis has been performed at the B3LYP/cc-pVDZ level. MESP,  $V(r)$  at point  $r$  in the vicinity of a molecular system in the atomic unit can be calculated from the electron density  $\rho(r')$ , using eqn (1)

$$V(r) = \sum_A^N \frac{Z_A}{|r - R_A|} - \int \frac{\rho(r') dr'}{|r - r'|} \quad (1)$$

where  $N$  is the total number of nuclei present in the molecular system,  $Z_A$  is the charge on the nucleus  $A$  at a distance  $R_A$  and  $r'$  is a dummy integration variable.<sup>92,93</sup>

## Results and discussion

### MESP analysis of donor molecules

The MESP minima  $V_m$  are useful for locating the most electron-rich regions in the molecules. The  $V_m$  appears on the aromatic rings, hetero atoms and CC double bonds of donor molecules (D1–D13) which are shown in Fig. 2. Since all the systems contain at least one aromatic ring, the ring showing the most negative  $V_m$  ( $V_{mD}$ ) is taken for comparing the donor strength of each system. The  $V_{mD}$  values of all the systems are depicted in Fig. 2 along with other  $V_m$  values. In polycyclic aromatic hydrocarbon (PAH) systems (D1–D3),  $V_{mD}$  values lie in a small range of  $-14.4$  to  $-14.9$  kcal mol<sup>-1</sup> which can be attributed to the similar  $\pi$ -conjugation features which are not affected by a hetero atom or a substituent. In the D4 system, two phenyl rings show a nearly coplanar arrangement with the CC double bond and their  $V_{mD}$  ( $-16.1$  and  $-16.8$  kcal mol<sup>-1</sup>) values are more negative than a PAH while the third phenyl ring has a highly twisted arrangement with respect to the CC double bond and shows  $V_{mD} -13.7$  kcal mol<sup>-1</sup>. It appears that the presence of a conjugated CC bond in D4 enhances its electron density over the corresponding aromatic rings. In D5, three phenyl rings share the lone pair electron density from the nitrogen centre leading to a more negative character for  $V_{mD} -15.6$  kcal mol<sup>-1</sup> than a PAH. In D6, D7 and D8, an amino nitrogen centre is connected with an arene ring. In the piperidine-phenyl system D6, the nitrogen centre is more pyramidalized than the other

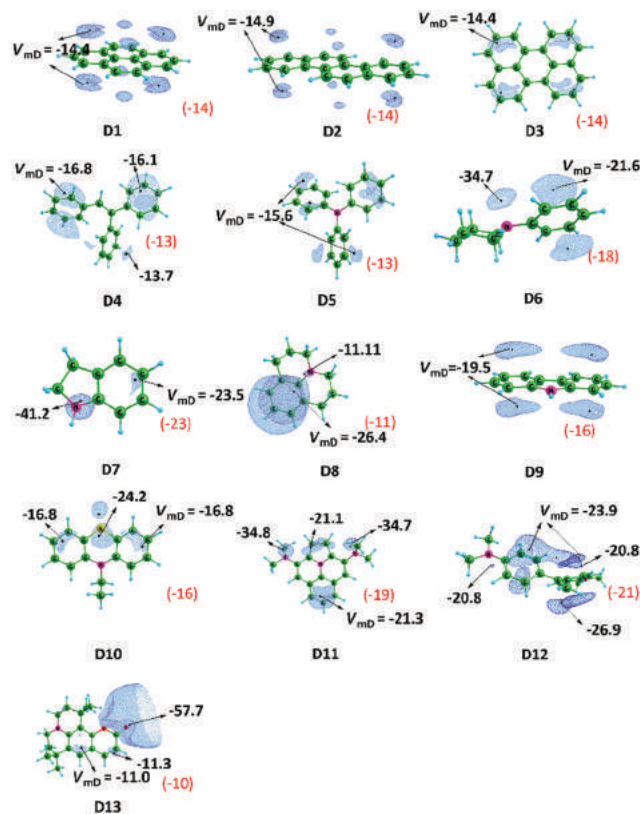


Fig. 2 MESP minima at the donor site, the  $V_{mD}$  of the donor systems. Isosurface values in kcal mol<sup>-1</sup> are given in brackets. Here carbon atoms are shown in green colour, while nitrogen, sulfur and oxygen atoms are shown in pink, yellow and red colours, respectively.

two and shows the least negative  $V_{mD}$  ( $-21.6$  kcal mol<sup>-1</sup>) among the three. In D7 and D8, fusing the  $N$ -alkyl unit/s with the aromatic ring improves the planarization of the  $N$ -centre, leading to more electron donation *via* +R effect to the arene ring. As a result, julolidine D8 shows the most electron-rich arene ring in terms of  $V_{mD} -26.4$  kcal mol<sup>-1</sup> followed by D7 ( $-23.5$  kcal mol<sup>-1</sup>). Compared to a PAH, carbazole arene rings show significantly more negative  $V_{mD}$  ( $-19.5$  kcal mol<sup>-1</sup>); here the sharing of the  $N$ -centre lone pair is with two aromatic rings which leads to less negative  $V_{mD}$  than D6–D8. Similarly, in D10, the sharing of the  $N$ -lone pair with two arene rings can be seen in addition to the effect of the hetero S atom. In this case,  $V_{mD}$  is less negative than carbazole. In D11, the combined effect of three  $N$ -centres can be attributed to the electron-rich nature of the arene ring ( $V_{mD} -21.3$  kcal mol<sup>-1</sup>) and among the  $N$ -centres, the  $N,N$ -dimethyl units are not fully effective for the influence of the +R contribution due to slight pyramidalization caused by steric congestions from the alkyl moiety of the adjacent five-membered ring. In D12, along with the +R contribution of  $N,N$ -dimethyl substituents, the conjugation effect of CC double bonds leads to relatively more electron-rich arene rings. The least negative  $V_{mD} -11.0$  kcal mol<sup>-1</sup> is observed in D13, the coumarin system. Here, the presence of a highly electron-withdrawing carbonyl group at the heterocyclic ring reduces the electron density on the aromatic ring.



### MESP analysis of D- $\pi$ -A systems

The donating strength of donor fragments in the D- $\pi$ -A system has been studied by MESP analysis. The MESP isosurface plot of a representative D- $\pi$ -A system (D12) is shown in Fig. 3a along with MESP minimum ( $V_m$ ) values at various positions. The positions selected for  $V_m$  analysis are (i) the donor site ( $V_{mD}$ ), (ii) the spacer site nearer to the donor ( $V_{mS}$ ) and (iii) the anchor site ( $V_{mA}$ ). The  $\pi$ -A portion is built by linking a butadiene moiety ( $\pi$ -spacer) with the cyanoacrylic acid moiety (A). Since the  $\pi$ -spacer and anchor units are the same for all donors, they have been considered as a reference system and the corresponding MESP minimum at their spacer ( $V_{mS}$ ) and anchoring sites ( $V_{mA}$ ) are evaluated for comparison with those of the D- $\pi$ -A system (Fig. 3b). The various MESP minimum values, *viz.*  $V_{mD}$ ,  $V_{mS}$ , and  $V_{mA}$  (Fig. S3, ESI<sup>†</sup>), are shown in Table 1 along with the most negative  $V_m$  of the donor molecule ( $V_{mD}$ ). In Table 1, the quantities  $\Delta V_{mD}$ ,  $\Delta V_{mS}$ , and  $\Delta V_{mA}$  represent the change that occurs in the minimum potential of the donor, spacer and anchoring sites with the introduction of the  $\pi$ -A system. Furthermore, in order to calculate  $\Delta V_{mD}$ , the most negative minima at the phenyl ring of each donor ( $V_{mD}$ ) have been subtracted from the corresponding minima ( $V_{mD}$ ) of the D- $\pi$ -A system. Similarly,  $\Delta V_{mS}$  and  $\Delta V_{mA}$  have been calculated by subtracting the  $V_m$  values at spacer and anchoring moieties of the reference system ( $V_{mS}$  and  $V_{mA}$ ) from the corresponding minima ( $V_{mS}$  and  $V_{mA}$ ) of the D- $\pi$ -A system.

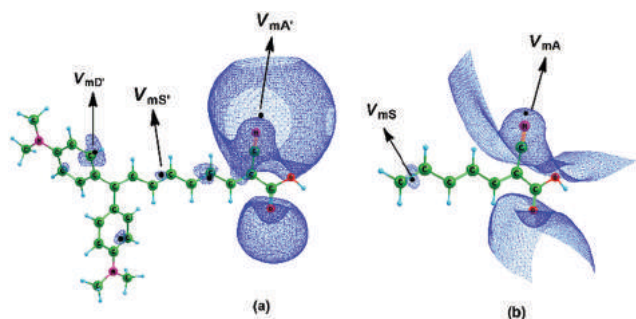


Fig. 3 MESP isosurface plot of (a) representative D- $\pi$ -A system and (b) reference system.

Table 1  $V_m$  (kcal mol<sup>-1</sup>) of the D- $\pi$ -A systems calculated at the B3LYP/cc-pVDZ level

Systems	$V_{mD}$	$V_{mD}'$	$\Delta V_{mD}$	$V_{mS}$	$V_{mS}'$	$\Delta V_{mS}$	$V_{mA}$	$V_{mA}'$	$\Delta V_{mA}$
D1	-14.4	-8.2	6.2	-2.4	-3.3	-0.9	-50.3	-53.0	-2.7
D2	-14.9	-9.8	5.1	-2.4	-3.3	-0.9	-50.3	-53.0	-2.6
D3	-14.4	-8.0	6.4	-2.4	-4.0	-1.6	-50.3	-54.2	-3.8
D4	-16.8	-7.8	9.0	-2.4	-4.3	-1.9	-50.3	-54.2	-3.8
D5	-15.6	-7.7	7.9	-2.4	-6.3	-3.9	-50.3	-56.0	-5.7
D6	-21.6	-9.3	12.3	-2.4	-8.0	-5.6	-50.3	-57.5	-7.2
D7	-23.5	-8.8	14.7	-2.4	-8.3	-5.9	-50.3	-57.5	-7.2
D8	-26.4	-10.0	16.4	-2.4	-10.8	-8.4	-50.3	-59.5	-9.2
D9	-19.5	-12.0	7.5	-2.4	-4.8	-2.4	-50.3	-54.8	-4.5
D10	-16.8	-9.4	7.4	-2.4	-5.3	-2.9	-50.3	-55.2	-4.9
D11	-21.3	-11.0	10.3	-2.4	-7.5	-5.1	-50.3	-55.4	-5.1
D12	-23.9	-14.1	9.8	-2.4	-12.9	-10.5	-50.3	-61.4	-11.0
D13	-11.0	-1.9	9.1	-2.4	-8.0	-5.6	-50.3	-56.5	-6.2

From Table 1, it is clear that when a donor part is being attached with a  $\pi$ -A system, the minimum potential of the donor site ( $V_{mD}$ ) becomes less negative indicating the electron transferring ability from the donor site to the  $\pi$ -A site. The term  $\Delta V_{mD}$  in Table 1 represents the change that occurred on the minimum potential at the donor site during the  $\pi$ -A linkage which varies from 5.1 to 16.4 kcal mol<sup>-1</sup> and indicates the intramolecular charge transfer involved in the D- $\pi$ -A system. Furthermore, at the spacer site of the D- $\pi$ -A system, electron density gain is observed represented by negative  $\Delta V_{mS}$  which lies in the range of -0.9 to -10.5 kcal mol<sup>-1</sup>. On the basis of  $\Delta V_{mS}$ , the highest donating strength can be attributed to the D12, while the least donating strength can be assigned for PAHs.

The  $V_{mA}$  values indicate that the minimum potential at the anchor moiety, for example at the cyano group, shows significant variations with respect to different donor units. The most electron-donating donor is expected to show the most negative  $V_{mA}$ . For the application of DSSCs, the cyanoacrylic portion has to be linked to the TiO<sub>2</sub> semiconductor for efficient electron transfer. By making the anchoring group electron-rich, efficient electron transfer from the dye to TiO<sub>2</sub> can occur. In other words, the efficiency of the DSSC system can be directly related to the electron-donating strength of the donor moieties. Due to this reason, the change in MESP minimum that appeared on the anchoring part ( $\Delta V_{mA}$ ) has been considered as the donating strength of the donor moiety. The PAHs (D1-D3) showed the least negative value of  $\Delta V_{mA}$  (-2.7 to -3.8 kcal mol<sup>-1</sup>), indicating their poor electron-donating strength. Furthermore, in the D4 system, a similar donating strength of -3.8 kcal mol<sup>-1</sup> is observed. In D5, the introduction of the N-centre imparts more negative  $\Delta V_{mA}$  values (-5.7 kcal mol<sup>-1</sup>) than PAHs which explains its better electron-donating strength compared to polyacenes. In D6 and D7, the more planarized nitrogen centres in the donor part impart a more negative  $\Delta V_{mA}$  value of -7.2 kcal mol<sup>-1</sup> and suggests its higher electron-donating strength than D5. In the D8 system, the fused N-centre with the aromatic ring further improves its planarization and leads to more negative  $\Delta V_{mA}$  -9.2 kcal mol<sup>-1</sup> than D5, D6, and D7. In carbazole (D9), the N-lone pair is shared between two aromatic rings through resonance, and as a result, the electron-donating strength in terms of  $\Delta V_{mA}$  (-4.5 kcal mol<sup>-1</sup>) appears weaker than those (D6-D8) having only one aromatic ring for sharing an N-lone pair. In D10, the presence of sulfur slightly enhances the negative value of  $\Delta V_{mA}$  to -5.0 kcal mol<sup>-1</sup>. Even though there are three nitrogen centres in ullazine, it shows a donating strength of -5.1 kcal mol<sup>-1</sup> which can be attributed to the influence of pyramidalized *N,N*-dimethyl groups in ullazine. In D12, a more negative  $\Delta V_{mA}$  value of -11.0 kcal mol<sup>-1</sup> can be recognized with the +R effect of mostly planarized *N,N*-dimethyl substituents. Finally, in D13 a more negative  $\Delta V_{mA}$  value (-6.2 kcal mol<sup>-1</sup>) than that of PAHs has been observed due to the interplay of the electron-rich nitrogen centre and the electron-withdrawing carbonyl group. These results strongly suggest that the incorporation of an electron-rich heteroatom in the donor region can have a positive influence on the electronic transmission to the acceptor moiety. On the basis of  $\Delta V_{mA}$ ,

**Table 2** Maximum absorption wavelength (nm), oscillator strength  $f$ , absorptional shift  $\Delta\lambda_{\max}$  and the percentage MO contribution of donor and D- $\pi$ -A systems at the TD-CAM-B3LYP/SMD/cc-pVDZ//B3LYP/cc-pVDZ level

Donor				D- $\pi$ -A			
Systems	$\lambda_{\max}$	$f$	MO contribution	$\lambda_{\max}$	$f$	MO contribution	$\Delta\lambda_{\max}$
D1	320	0.52	H $\rightarrow$ L (93.2%)	401	2.21	H-1 $\rightarrow$ L (94.2%)	81
D2	306	0.03	H-1 $\rightarrow$ L (33.6%)	376	0.03	H $\rightarrow$ L (74.6%)	56
			H $\rightarrow$ L (19.9%)	409	2.47	H $\rightarrow$ L (79.3%)	103
			H $\rightarrow$ L+1 (39.5%)				
D3	300	0.23	H $\rightarrow$ L (68.5%)				109
	408	0.59	H $\rightarrow$ L (98.7%)	518	1.73	H $\rightarrow$ L (90.4%)	110
D4	300	0.78	H $\rightarrow$ L (97.0%)	434	2.21	H $\rightarrow$ L (88.6%)	134
D5	284	0.03	H $\rightarrow$ L (90.8%)	453	2.02	H $\rightarrow$ L (86.7%)	169
D6	279	0.38	H $\rightarrow$ L+1 (98.8%)				174
	256	0.05	H $\rightarrow$ L (87.8%)	446	2.00	H $\rightarrow$ L (92.6%)	190
	236	0.37	H $\rightarrow$ L+1 (91.7%)				210
D7	261	0.09	H $\rightarrow$ L (90.5%)	448	1.86	H $\rightarrow$ L (93.7%)	187
	226	0.18	H $\rightarrow$ L+1 (90.0%)				222
D8	277	0.08	H $\rightarrow$ L (92.9%)	480	1.95	H $\rightarrow$ L (93.2%)	203
	243	0.29	H $\rightarrow$ L+1 (92.9%)				237
	286	0.06	H $\rightarrow$ L (87.6%)	419	2.21	H $\rightarrow$ L (93.2%)	133
D9	262	0.31	H-1 $\rightarrow$ L (84.2%)				157
	319	0.02	H $\rightarrow$ L (95.2%)	459	1.67	H $\rightarrow$ L (84.8%)	140
D10	275	0.18	H $\rightarrow$ L+2 (84.6%)				184
	324	0.38	H $\rightarrow$ L (90.8%)	448	0.02	H $\rightarrow$ L (89.2%)	124
D11				411	2.11	H-1 $\rightarrow$ L (73.6%)	87
	278	0.20	H $\rightarrow$ L (78.0%)	520	1.95	H $\rightarrow$ L (92.6%)	242
D12	334	0.64	H $\rightarrow$ L (95.3%)	503	1.99	H $\rightarrow$ L (89.3%)	169

the order of the donating strength of donor groups can be written as D2 < D1 < D3 = D4 < D9 < D10 < D11 < D5 < D13 < D6 = D7 < D8 < D12. The julolidine based donor system D8 and the *N,N*-dialkyl aniline incorporated D12 are the most efficient among the studied systems.

### Absorption spectra of donor and D- $\pi$ -A systems

The absorption maxima of all the systems (donor and D- $\pi$ -A) along with oscillator strength ( $f$ ) are summarized in Table 2. For the assessment of the absorptional shift,  $\Delta\lambda_{\max}$ , the absorption maximum of the D- $\pi$ -A system was subtracted from the donor system. For calculating  $\Delta\lambda_{\max}$ , HOMO  $\rightarrow$  LUMO orbital transition has been considered, except for D1. In D1,  $\lambda_{\max}$  is observed for the HOMO-1  $\rightarrow$  LUMO transition, while its HOMO  $\rightarrow$  LUMO transition is nearly forbidden due to very small  $f$  values. The data in Table 2 clearly suggest that the absorption maximum ( $\lambda_{\max}$ ) of D- $\pi$ -A shifts significantly to a higher wavelength region compared to donor D. Since in all systems we used the same spacer and anchoring moiety (the  $\pi$ -A unit), their influence on the absorptional shift ( $\Delta\lambda_{\max}$ ) can be considered to be the same. This implies that the large variation in  $\Delta\lambda_{\max}$  exhibited by the D- $\pi$ -A system is due to the variation in the donating strength of donor moieties. For instance, among all donor moieties, D1 with  $\Delta\lambda_{\max}$  81 nm is the least donating while D12 with  $\Delta\lambda_{\max}$  242 nm is the most donating (Table 2). Furthermore,  $\Delta V_{\text{MA}}$  with  $\Delta\lambda_{\max}$  with a correlation coefficient shows a linear correlation of 0.966 (Fig. 4) which shows the significance of the donating strength of  $\Delta V_{\text{MA}}$  on  $\Delta\lambda_{\max}$ . In the linear correlation plot, D1 and D11 based D- $\pi$ -A systems exhibit a slight deviation, which can be attributed as their less intense ( $f \rightarrow 0.02$ - $0.03$ ) and nearly forbidden HOMO  $\rightarrow$  LUMO charge transfer character of the

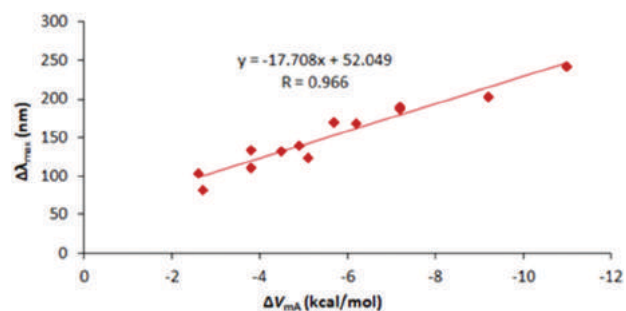


**Fig. 4** Correlation between the donating strength ( $\Delta V_{\text{MA}}$ ) of the D- $\pi$ -A system and the change in absorption maxima ( $\Delta\lambda_{\max}$ ).

orbital excitation. From these results the shift in absorption maxima ( $\Delta\lambda_{\max}$ ) follows the order D12 > D8 > D7 > D6 > D10 > D5 > D13 > D9 > D4 > D3 > D2 > D11 > D1, preferably due to the nature of donor groups. Therefore, to improve the wavelength of absorption to a preferred region (Vis to NIR), its donating ability has to be tuned with the introduction of better electron-donating donor groups (preferably more nitrogen centres).

The frontier molecular orbital energy levels given in Fig. 5 show the HOMO-LUMO band gap features of D, D- $\pi$ -A and  $\pi$ -A systems (butadiene moieties linked with cyano acrylic acid). The HOMO value ( $\epsilon_{\text{h}}$ ) of the D systems is in the range of -4.66 to -5.70 eV, whereas that of the D- $\pi$ -A system is in the range of -4.96 to -5.89 eV. These data indicate the close resemblance of the HOMO level of the D and D- $\pi$ -A systems. On the other hand, the LUMO energy level ( $\epsilon_{\text{l}}$ ) of D shows a large deviation from the  $\epsilon_{\text{l}}$  of the D- $\pi$ -A system indicating clear



Fig. 5 Frontier molecular energy level diagram of D- $\pi$ -A systems at the B3LYP/cc-pVDZ level.

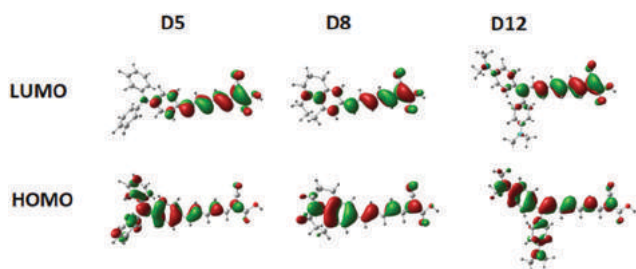


Fig. 6 Frontier molecular orbitals of representative D- $\pi$ -A systems at the B3LYP/cc-pVDZ level.

dissimilarity. In fact,  $\epsilon_1$  of D- $\pi$ -A in the range of  $-2.52$  to  $-3.10$  eV is very close to  $\epsilon_1$   $-2.97$  eV observed for  $\pi$ -A. Thus, the data shown in Fig. 5 indicate that the HOMO of D- $\pi$ -A is more like the HOMO of the donor and its LUMO is more like that of  $\pi$ -A. This feature is clearly evident in the frontier molecular orbital diagram given in the D- $\pi$ -A system for representative cases (Fig. 6). HOMOs are more localized towards the donor region with decreasing orbital contributions from the  $\pi$ -A system, while the LUMO is mostly localized in the  $\pi$ -A region. D1- $\pi$ -A is an exception wherein HOMO-1 to the LUMO is the allowed transition and its HOMO has a different  $\pi$  character, localized exclusively on the pyrene ring. The data shown in Fig. 5 clearly suggest that linking the donor system to the  $\pi$ -A unit is very effective for reducing the band gap. For all cases, the HOMO level is tuned towards the value of the  $\text{I}^-/\text{I}_3^-$  electrolyte couple while the LUMO level appears closer to the conduction band (CB) of  $\text{TiO}_2$ . The HOMO and LUMO distribution and their energy levels suggest a significant charge separation in the excited state leading to the strong electron coupling of the dye with the  $\text{TiO}_2$  semiconductor which promotes the electron transfer to the conduction band.<sup>94</sup>

In general, compared to D systems, the absorption maxima of D- $\pi$ -A systems show a significant red shift (Table 2) in the range of 81–242 nm. In D1- $\pi$ -A and D2- $\pi$ -A,  $\lambda_{\text{max}}$  is observed at

401 and 409 nm, respectively. The major electronic excitation of pyrene incorporated D1- $\pi$ -A is assigned to the transition of HOMO-1 to the LUMO. The forbidden HOMO to LUMO transition of D1- $\pi$ -A can be changed to allow one by appropriate substitution such as a substitution by the methyl group at the first or second position (Table S2 and Fig. S2, ESI<sup>†</sup>). The D3- $\pi$ -A system showed a broad absorption coverage in the visible region with  $\lambda_{\text{max}}$  518 nm corresponding to the HOMO-LUMO transition. Among all, D3- $\pi$ -A has the lowest HOMO-LUMO band gap of 2.26 eV (Fig. 5). The D4 in D4- $\pi$ -A is more electron-donating than a PAH moiety and it shows a smaller band gap of 2.71 eV compared to D1 to D2 incorporated systems. Furthermore, in nitrogen-containing D- $\pi$ -A systems (D5-D13), the band gap energy decreases to a greater extent by 2.31–2.75 eV for all except D9- $\pi$ -A (2.87 eV) than hydrocarbon systems. Among the nitrogen-containing systems, D12- $\pi$ -A showed the highest  $\lambda_{\text{max}}$  520 nm with a band gap of 2.39 eV while D11- $\pi$ -A showed the lowest band gap of 2.31 eV. The  $\lambda_{\text{max}}$  value of D11- $\pi$ -A observed at 411 nm is due to the transition of HOMO-1 to LUMO. Among them all, the HOMO energy level of D12- $\pi$ -A appeared nearest to the energy level of the redox electrolyte while its LUMO level is 1.44 eV higher than the CB of  $\text{TiO}_2$ . The LUMO energy levels of all systems offer a favourable electron injection from the excited state to the conduction band of  $\text{TiO}_2$  while HOMO energies lower than the oxidation potential of the  $\text{I}^-/\text{I}_3^-$  electrolyte ( $-4.8$  eV) indicate effective dye regeneration. These results support their effective utilization in the DSSC application. The D3- $\pi$ -A, D11- $\pi$ -A and D12- $\pi$ -A systems are among the lowest band gap systems, desirable for harvesting more light in the UV-visible region.

#### Analysis of photovoltaic parameters

According to Koopman's theorem,<sup>95</sup> the ground state oxidation potential ( $E_{\text{ox}}^{\text{dye}}$ ) of a dye can be approximated as the negative HOMO energy ( $-\epsilon_{\text{h}}$ ). Furthermore, the excited state dye regeneration

**Table 3** Calculated vertical excitation energy, absorption maxima, oscillator strength  $f$ , HOMO LUMO energy, HOMO–LUMO energy gap (HLG), ground and excited-state oxidation potentials ( $E_{\text{ox}}^{\text{dye}}$  and  $E_{\text{ox}}^{\text{dye}*}$ ), free energy change for electron injection ( $\Delta G_{\text{inject}}$ ), dye regeneration driving force ( $\Delta G_{\text{reg}}$ ), and the open circuit voltage ( $eV_{\text{OC}}$ ) of D- $\pi$ -A systems at the TD-CAM-B3LYP/SMD/cc-pVDZ//B3LYP/cc-pVDZ level

Systems	Excitation energy (eV)	$\lambda_{\text{absmax}}$ (nm)	$f$	HOMO (eV)	LUMO (eV)	HLG (eV)	$E_{\text{ox}}^{\text{dye}}$ (eV)	$E_{\text{ox}}^{\text{dye}*}$ (eV)	$\Delta G_{\text{inject}}$ (eV)	$\Delta G_{\text{reg}}$ (eV)	( $eV_{\text{OC}}$ ) (eV)
D1	3.09	401	2.22	-5.88	-2.99	2.89	5.88	2.79	-1.21	1.08	1.01
D2	3.03	409	2.47	-5.89	-3.00	2.89	5.89	2.86	-1.14	1.09	1.00
D3	2.39	518	1.73	-5.35	-3.10	2.26	5.35	2.96	-1.04	0.55	0.90
D4	2.86	434	2.21	-5.70	-2.98	2.71	5.70	2.84	-1.16	0.90	1.02
D5	2.73	453	2.02	-5.37	-2.79	2.58	5.37	2.64	-1.36	0.57	1.21
D6	2.78	446	2.00	-5.42	-2.68	2.74	5.42	2.64	-1.36	0.62	1.32
D7	2.59	448	1.95	-5.40	-2.65	2.75	5.40	2.81	-1.19	0.60	1.35
D8	2.77	480	1.86	-5.12	-2.52	2.60	5.12	2.35	-1.65	0.32	1.48
D9	2.96	419	2.21	-5.78	-2.91	2.87	5.78	2.82	-1.18	0.98	1.09
D10	2.70	459	1.67	-5.28	-2.84	2.44	5.28	2.58	-1.42	0.48	1.16
D11	3.01	411	2.11	-5.07	-2.76	2.31	5.07	2.06	-1.94	0.27	1.24
D12	2.39	520	1.95	-4.96	-2.56	2.39	4.96	2.57	-1.43	0.16	1.44
D13	2.46	503	1.99	-5.35	-2.87	2.49	5.35	2.89	-1.11	0.55	1.13

driving force ( $\Delta G_{\text{reg}}$ ) can be approximated as ( $E_{\text{ox}}^{\text{dye}} - 4.8$ ) eV or  $(-\varepsilon_{\text{h}} - 4.8)$  eV where  $-4.8$  eV stands for the redox potential of the  $\text{I}^-/\text{I}_3^-$  electrolyte couple.<sup>22,96</sup> The free energy change for electron injection ( $\Delta G_{\text{inject}}$ ) from the excited state of the dye to the semiconductor<sup>53,97,98</sup> is generally defined as,

$$\Delta G_{\text{inject}} = E_{\text{ox}}^{\text{dye}*} - 4.0 \quad (2)$$

where  $E_{\text{ox}}^{\text{dye}*}$  is the excited state oxidation potential and  $-4.0$  eV stands for the conduction band (CB) edge of the  $\text{TiO}_2$  semiconductor.<sup>22,99</sup> Assuming that the electron injection occurs from the unrelaxed excited state,  $E_{\text{ox}}^{\text{dye}*}$  can be explained as the difference between the ground state oxidation potential of the dye and the vertical transition energy  $\lambda_{\text{max}}$ ,<sup>96,97,100</sup>

$$E_{\text{ox}}^{\text{dye}*} = (-\varepsilon_{\text{h}}) - \lambda_{\text{max}} \quad (3)$$

Furthermore, the difference between the energy of the LUMO ( $\varepsilon_{\text{l}}$ ) of the dye and the energy of the conduction band edge of  $\text{TiO}_2$  is regarded as the open circuit voltage (eqn (4)).<sup>100</sup>

$$eV_{\text{OC}} = \varepsilon_{\text{l}} - (-4.0) \quad (4)$$

In Table 3, the  $\Delta G_{\text{inject}}$  values fall in the range of  $-1.04$  to  $-1.94$  eV, and the D11- $\pi$ -A system with the most negative value has the highest electron injection efficiency while D2 to D4 based D- $\pi$ -A systems show the lowest efficiency. The smallest  $\Delta G_{\text{reg}}$  value of 0.16 eV is observed for D12- $\pi$ -A and suggests its fastest dye regeneration efficiency. A good linear correlation between  $\Delta V_{\text{mA}}$  and  $eV_{\text{OC}}$  is observed for all the cases (Fig. 7)

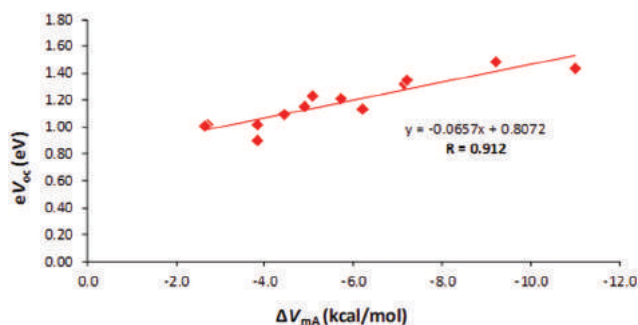


**Fig. 7** Correlation between  $\Delta V_{\text{mA}}$  ( $\text{kcal mol}^{-1}$ ) and  $eV_{\text{OC}}$  (eV).

suggesting that the electron accepting tendency of the acceptor part is well reflected at the LUMO levels. Among all the systems, julolidine based D8- $\pi$ -A possesses the highest  $\varepsilon_{\text{l}}$  value resulting in the highest  $eV_{\text{OC}}$  value of 1.48 eV. The second highest  $eV_{\text{OC}}$  value of 1.44 eV is observed for D12- $\pi$ -A. The  $\Delta V_{\text{mA}}$  values suggest that the electron donating ability of PAH moieties is the lowest among all the donors and the corresponding D1 to D3 based D- $\pi$ -A systems show the lowest range of  $eV_{\text{OC}}$  0.90–1.01 eV.

## Conclusions

Using MESP topographical analysis, the donating strength of thirteen known (D1–D13) typically used donor systems in the DSSC applications has been quantified. The red shift in the absorption maximum ( $\Delta\lambda_{\text{max}}$ ) observed for the D- $\pi$ -A systems is rationalized in terms of the amount of electron donation from the donor D moieties to the  $\pi$ -A system using the MESP parameter  $\Delta V_{\text{mA}}$ . The highest electron donating strength  $\Delta V_{\text{mA}}$  observed in D12- $\pi$ -A shows the highest  $\Delta\lambda_{\text{max}}$  and maximum absorption wavelength  $\lambda_{\text{max}}$  with a small band gap energy of 2.39 eV. In poor electron donating D1 and D2 based D- $\pi$ -A systems, the smallest  $\Delta\lambda_{\text{max}}$  and  $\lambda_{\text{max}}$  values are observed. A linear correlation obtained between  $\Delta V_{\text{mA}}$  and  $\Delta\lambda_{\text{max}}$  confirms that  $\Delta\lambda_{\text{max}}$  increases with an increase in  $\Delta V_{\text{mA}}$ . The frontier molecular energy levels showed that the HOMO of the D- $\pi$ -A system has a greater resemblance to the HOMO of the donor, whereas the LUMO has a greater resemblance to the LUMO of  $\pi$ -A. Thus, the donor tunes the HOMO, while  $\pi$ -A tunes the LUMO energy of the D- $\pi$ -A system for efficient dye regeneration and electron injection. Among all the systems, D12- $\pi$ -A showed the highest electron injection efficiency. Since  $eV_{\text{OC}}$  is directly proportional to the power conversion efficiency of the solar cell, D8- $\pi$ -A and D12- $\pi$ -A having the highest  $eV_{\text{OC}}$  can be regarded as the most efficient sensitizers for DSSCs while the lowest  $eV_{\text{OC}}$  values displayed by the PAH based (D1–D3) D- $\pi$ -A systems offer poor efficiency. The linear correlation between  $\Delta V_{\text{mA}}$  and  $eV_{\text{OC}}$  shows that  $eV_{\text{OC}}$  increases with an increase in the negative character of  $\Delta V_{\text{mA}}$  and also proves that better sensitizers can be developed by connecting a powerful electron donor to a  $\pi$ -A system. One way to do this is by incorporating multiple lone pair



bearing nitrogen centres in donors. Thus, the MESP approach offers an easy analysis tool for the quantification of the donating strength of D- $\pi$ -A systems in DSSC applications.

## Conflicts of interest

There are no conflicts to declare.

## Acknowledgements

Authors acknowledge the DST-SERB for funding through GAP1397 and also gratefully acknowledge the CSIR 4th PI for the HPC facility and the NIIST IT lab for computational support. V. V. Divya thanks the CSIR, India, for the senior research fellowship.

## Notes and references

- B. O'regan and M. Grätzel, *Nature*, 1991, **353**, 737.
- N. Anscombe, *Nat. Photonics*, 2011, **5**, 266–267.
- F. Odobel, L. Le Pleux, Y. Pellegrin and E. Blart, *Acc. Chem. Res.*, 2010, **43**, 1063–1071.
- A. Hagfeldt, G. Boschloo, L. Sun, L. Kloo and H. Pettersson, *Chem. Rev.*, 2010, **110**, 6595–6663.
- N. Sharifi, F. Tajabadi and N. Taghavinia, *ChemPhysChem*, 2014, **15**, 3902–3927.
- J. Gong, K. Sumathy, Q. Qiao and Z. Zhou, *Renewable Sustainable Energy Rev.*, 2017, **68**, 234–246.
- A. Yella, H.-W. Lee, H. N. Tsao, C. Yi, A. K. Chandiran, M. K. Nazeeruddin, E. W.-G. Diau, C.-Y. Yeh, S. M. Zakeeruddin and M. Grätzel, *Science*, 2011, **334**, 629–634.
- A. Mishra, M. K. Fischer and P. Bäuerle, *Angew. Chem., Int. Ed.*, 2009, **48**, 2474–2499.
- M. K. Nazeeruddin, A. Kay, I. Rodicio, R. Humphry-Baker, E. Mueller, P. Liska, N. Vlachopoulos and M. Graetzel, *J. Am. Chem. Soc.*, 1993, **115**, 6382–6390.
- M. K. Nazeeruddin, P. Péchy, T. Renouard, S. M. Zakeeruddin, R. Humphry-Baker, P. Comte, P. Liska, L. Cevey, E. Costa, V. Shklover, L. Spiccia, G. B. Deacon, C. A. Bignozzi and M. Grätzel, *J. Am. Chem. Soc.*, 2001, **123**, 1613–1624.
- M. K. Nazeeruddin, R. Splivallo, P. Liska, P. Comte and M. Grätzel, *Chem. Commun.*, 2003, 1456–1457.
- M. K. Nazeeruddin, F. De Angelis, S. Fantacci, A. Selloni, G. Viscardi, P. Liska, S. Ito, B. Takeru and M. Grätzel, *J. Am. Chem. Soc.*, 2005, **127**, 16835–16847.
- F. Gao, Y. Wang, J. Zhang, D. Shi, M. Wang, R. Humphry-Baker, P. Wang, S. M. Zakeeruddin and M. Grätzel, *Chem. Commun.*, 2008, 2635–2637.
- C.-Y. Chen, M. Wang, J.-Y. Li, N. Pootrakulchote, L. Alibabaei, C.-H. Ngoc-le, J.-D. Decoppet, J.-H. Tsai, C. Grätzel, C.-G. Wu, S. M. Zakeeruddin and M. Grätzel, *ACS Nano*, 2009, **3**, 3103–3109.
- Y. Cao, Y. Bai, Q. Yu, Y. Cheng, S. Liu, D. Shi, F. Gao and P. Wang, *J. Phys. Chem. C*, 2009, **113**, 6290–6297.
- M. Pastore, E. Mosconi and F. De Angelis, *J. Phys. Chem. C*, 2012, **116**, 5965–5973.
- M. Cheng, X. Yang, J. Li, F. Zhang and L. Sun, *ChemSusChem*, 2013, **6**, 70–77.
- S. Ito, H. Miura, S. Uchida, M. Takata, K. Sumioka, P. Liska, P. Comte, P. Péchy and M. Grätzel, *Chem. Commun.*, 2008, 5194–5196.
- W. Zeng, Y. Cao, Y. Bai, Y. Wang, Y. Shi, M. Zhang, F. Wang, C. Pan and P. Wang, *Chem. Mater.*, 2010, **22**, 1915–1925.
- K. Kakiage, Y. Aoyama, T. Yano, T. Otsuka, T. Kyomen, M. Unno and M. Hanaya, *Chem. Commun.*, 2014, **50**, 6379–6381.
- Z. Yao, M. Zhang, H. Wu, L. Yang, R. Li and P. Wang, *J. Am. Chem. Soc.*, 2015, **137**, 3799–3802.
- B. Nagarajan, S. Kushwaha, R. Elumalai, S. Mandal, K. Ramanujam and D. Raghavachari, *J. Mater. Chem. A*, 2017, **5**, 10289–10300.
- K. Kakiage, Y. Aoyama, T. Yano, K. Oya, J.-I. Fujisawa and M. Hanaya, *Chem. Commun.*, 2015, **51**, 15894–15897.
- T. Kitamura, M. Ikeda, K. Shigaki, T. Inoue, N. A. Anderson, X. Ai, T. Lian and S. Yanagida, *Chem. Mater.*, 2004, **16**, 1806–1812.
- Z.-S. Wang, Y. Cui, Y. Dan-oh, C. Kasada, A. Shinpo and K. Hara, *J. Phys. Chem. C*, 2007, **111**, 7224–7230.
- Z.-S. Wang, N. Koumura, Y. Cui, M. Takahashi, H. Sekiguchi, A. Mori, T. Kubo, A. Furube and K. Hara, *Chem. Mater.*, 2008, **20**, 3993–4003.
- A. Venkateswararao, K. R. J. Thomas, C.-P. Lee, C.-T. Li and K.-C. Ho, *ACS Appl. Mater. Interfaces*, 2014, **6**, 2528–2539.
- A. J. Huckaba, F. Giordano, L. E. McNamara, K. M. Dreux, N. I. Hammer, G. S. Tschumper, S. M. Zakeeruddin, M. Grätzel, M. K. Nazeeruddin and J. H. Delcamp, *Adv. Energy Mater.*, 2015, **5**, 1401629.
- K. Hara, M. Kurashige, Y. Dan-oh, C. Kasada, A. Shinpo, S. Suga, K. Sayama and H. Arakawa, *New J. Chem.*, 2003, **27**, 783–785.
- C. Teng, X. Yang, C. Yang, H. Tian, S. Li, X. Wang, A. Hagfeldt and L. Sun, *J. Phys. Chem. C*, 2010, **114**, 11305–11313.
- A. Baheti, C.-P. Lee, K. J. Thomas and K.-C. Ho, *Phys. Chem. Chem. Phys.*, 2011, **13**, 17210–17221.
- K. Srinivas, C. R. Kumar, M. A. Reddy, K. Bhanuprakash, V. J. Rao and L. Giribabu, *Synth. Met.*, 2011, **161**, 96–105.
- Y. Ooyama, S. Inoue, T. Nagano, K. Kushimoto, J. Ohshita, I. Imae, K. Komaguchi and Y. Harima, *Angew. Chem., Int. Ed.*, 2011, **50**, 7429–7433.
- B. Hosseinzadeh, A. S. Beni, M. Azari, M. Zarandi and M. Karami, *New J. Chem.*, 2016, **40**, 8371–8381.
- D. Patil, M. Jadhav, K. Avhad, T. H. Chowdhury, A. Islam, I. Bedja and N. Sekar, *New J. Chem.*, 2018, **42**, 11555–11564.
- J. Feng, Y. Jiao, W. Ma, M. K. Nazeeruddin, M. Grätzel and S. Meng, *J. Phys. Chem. C*, 2013, **117**, 3772–3778.
- S. Ardo and G. J. Meyer, *Chem. Soc. Rev.*, 2009, **38**, 115–164.
- R. Argazzi, C. A. Bignozzi, T. A. Heimer, F. N. Castellano and G. J. Meyer, *J. Am. Chem. Soc.*, 1995, **117**, 11815–11816.
- N. Hirata, J. J. Lagref, E. J. Palomares, J. R. Durrant, M. K. Nazeeruddin, M. Grätzel and D. Di Censo, *Chem. – Eur. J.*, 2004, **10**, 595–602.
- Z. Ning, Q. Zhang, W. Wu, H. Pei, B. Liu and H. Tian, *J. Org. Chem.*, 2008, **73**, 3791–3797.



- 41 L. Li, Y. Hao, X. Yang, J. Zhao, H. Tian, C. Teng, A. Hagfeldt and L. Sun, *ChemSusChem*, 2011, **4**, 609–612.
- 42 J. Tang, J. Hua, W. Wu, J. Li, Z. Jin, Y. Long and H. Tian, *Energy Environ. Sci.*, 2010, **3**, 1736–1745.
- 43 W. Li, Y. Wu, Q. Zhang, H. Tian and W. Zhu, *ACS Appl. Mater. Interfaces*, 2012, **4**, 1822–1830.
- 44 R. Tarsang, V. Promarak, T. Sudyoasuk, S. Namuangruk, N. Kungwan and S. Jungstittiwong, *ChemPhysChem*, 2014, **15**, 3809–3818.
- 45 H.-Q. Xia, C.-P. Kong, J. Wang, F.-Q. Bai and H.-X. Zhang, *RSC Adv.*, 2014, **4**, 50338–50350.
- 46 A. Dessi, A. Sinicropi, S. Mohammadpourasl, R. Basosi, M. Taddei, F. Fabrizi de Biani, M. Calamante, L. Zani, A. Mordini, P. Bracq, D. Franchi and G. Reginato, *ACS Omega*, 2019, **4**, 7614–7627.
- 47 L.-Y. Lin, C.-H. Tsai, F. Lin, T.-W. Huang, S.-H. Chou, C.-C. Wu and K.-T. Wong, *Tetrahedron*, 2012, **68**, 7509–7516.
- 48 K. D. Seo, B. S. You, I. T. Choi, M. J. Ju, M. You, H. S. Kang and H. K. Kim, *J. Mater. Chem. A*, 2013, **1**, 9947–9953.
- 49 Y. Hong, J.-Y. Liao, J. Fu, D.-B. Kuang, H. Meier, C.-Y. Su and D. Cao, *Dyes Pigm.*, 2012, **94**, 481–489.
- 50 A. Dualeh, R. Humphry-Baker, J. H. Delcamp, M. K. Nazeeruddin and M. Grätzel, *Adv. Energy Mater.*, 2013, **3**, 496–504.
- 51 J. H. Delcamp, A. Yella, T. W. Holcombe, M. K. Nazeeruddin and M. Grätzel, *Angew. Chem., Int. Ed.*, 2013, **125**, 394–398.
- 52 K. Srinivas, K. Yesudas, K. Bhanuprakash, V. J. Rao and L. Giribabu, *J. Phys. Chem. C*, 2009, **113**, 20117–20126.
- 53 J. Preat, C. Michaux, D. Jacquemin and E. A. Perpète, *J. Phys. Chem. C*, 2009, **113**, 16821–16833.
- 54 J. Preat, *J. Phys. Chem. C*, 2010, **114**, 16716–16725.
- 55 J. Preat, D. Jacquemin and E. A. Perpète, *Environ. Sci. Technol.*, 2010, **44**, 5666–5671.
- 56 M. Pastore, E. Mosconi, F. De Angelis and M. Grätzel, *J. Phys. Chem. C*, 2010, **114**, 7205–7212.
- 57 D. Casanova, F. P. Rotzinger and M. Grätzel, *J. Chem. Theory Comput.*, 2010, **6**, 1219–1227.
- 58 S. Meng, E. Kaxiras, M. K. Nazeeruddin and M. Grätzel, *J. Phys. Chem. C*, 2011, **115**, 9276–9282.
- 59 R. Sánchez-de-Armas, M. Á. San Miguel, J. Oviedo and J. F. Sanz, *Phys. Chem. Chem. Phys.*, 2012, **14**, 225–233.
- 60 J. Zhang, H.-B. Li, S.-L. Sun, Y. Geng, Y. Wu and Z.-M. Su, *J. Mater. Chem.*, 2012, **22**, 568–576.
- 61 W. Fan, D. Tan and W. Q. Deng, *ChemPhysChem*, 2012, **13**, 2051–2060.
- 62 J. Zhang, Y.-H. Kan, H.-B. Li, Y. Geng, Y. Wu and Z.-M. Su, *Dyes Pigm.*, 2012, **95**, 313–321.
- 63 J. Zhang, H.-B. Li, J.-Z. Zhang, Y. Wu, Y. Geng, Q. Fu and Z.-M. Su, *J. Mater. Chem. A*, 2013, **1**, 14000–14007.
- 64 W.-L. Ding, D.-M. Wang, Z.-Y. Geng, X.-L. Zhao and Y.-F. Yan, *J. Phys. Chem. C*, 2013, **117**, 17382–17398.
- 65 R. Tarsang, V. Promarak, T. Sudyoasuk, S. Namuangruk and S. Jungstittiwong, *J. Photochem. Photobiol., A*, 2014, **273**, 8–16.
- 66 M. E. Köse, *J. Phys. Chem. A*, 2019, **123**, 5566–5573.
- 67 K. Hara, T. Sato, R. Katoh, A. Furube, Y. Ohga, A. Shinpo, S. Suga, K. Sayama, H. Sugihara and H. Arakawa, *J. Phys. Chem. B*, 2003, **107**, 597–606.
- 68 J. Li and A. C. Grimsdale, *Chem. Soc. Rev.*, 2010, **39**, 2399–2410.
- 69 G. Wu, F. Kong, J. Li, W. Chen, X. Fang, C. Zhang, Q. Chen, X. Zhang and S. Dai, *Dyes Pigm.*, 2013, **99**, 653–660.
- 70 Z.-S. Huang, H. Meier and D. Cao, *J. Mater. Chem.*, 2016, **4**, 2404–2426.
- 71 Y. Zhang, H. Cheema, L. McNamara, L. A. Hunt, N. I. Hammer and J. H. Delcamp, *Chem. – Eur. J.*, 2018, **24**, 5939–5949.
- 72 Z. Yang, C. Shao and D. Cao, *RSC Adv.*, 2015, **5**, 22892–22898.
- 73 C. H. Suresh and N. Koga, *Inorg. Chem.*, 2002, **41**, 1573–1578.
- 74 O. Kühl, *Coord. Chem. Rev.*, 2005, **249**, 693–704.
- 75 C. H. Suresh, *Inorg. Chem.*, 2006, **45**, 4982–4986.
- 76 J. Mathew, T. Thomas and C. H. Suresh, *Inorg. Chem.*, 2007, **46**, 10800–10809.
- 77 S. Mecozzi, A. P. West and D. A. Dougherty, *J. Am. Chem. Soc.*, 1996, **118**, 2307–2308.
- 78 S. E. Wheeler and K. N. Houk, *J. Chem. Theory Comput.*, 2009, **5**, 2301–2312.
- 79 S. E. Wheeler and K. Houk, *J. Am. Chem. Soc.*, 2009, **131**, 3126–3127.
- 80 F. B. Sayyed and C. H. Suresh, *J. Phys. Chem. A*, 2011, **115**, 9300–9307.
- 81 C. H. Suresh, P. Alexander, K. P. Vijayalakshmi, P. K. Sajith and S. R. Gadre, *Phys. Chem. Chem. Phys.*, 2008, **10**, 6492–6499.
- 82 F. B. Sayyed and C. H. Suresh, *Tetrahedron Lett.*, 2009, **50**, 7351–7354.
- 83 F. B. Sayyed and C. H. Suresh, *New J. Chem.*, 2009, **33**, 2465–2471.
- 84 F. B. Sayyed and C. H. Suresh, *J. Phys. Chem. A*, 2011, **115**, 5660–5664.
- 85 V. V. Divya, F. B. Sayyed and C. H. Suresh, *ChemPhysChem*, 2019, **20**, 1752–1758.
- 86 A. D. Becke, *J. Chem. Phys.*, 1993, **98**, 1372–1377.
- 87 T. H. Dunning Jr, *J. Chem. Phys.*, 1989, **90**, 1007–1023.
- 88 C. Adamo and V. Barone, *J. Chem. Phys.*, 1999, **110**, 6158–6170.
- 89 J.-D. Chai and M. Head-Gordon, *Phys. Chem. Chem. Phys.*, 2008, **10**, 6615–6620.
- 90 A. V. Marenich, C. J. Cramer and D. G. Truhlar, *J. Phys. Chem. B*, 2009, **113**, 6378–6396.
- 91 M. J. Frisch, G. W. Trucks, H. B. Schlegel, G. E. Scuseria, M. A. Robb, J. R. Cheeseman, G. Scalmani, V. Barone, G. A. Petersson, H. Nakatsuji, X. Li, M. Caricato, A. V. Marenich, J. Bloino, B. G. Janesko, R. Gomperts, B. Mennucci, H. P. Hratchian, J. V. Ortiz, A. F. Izmaylov, J. L. Sonnenberg, D. Williams-Young, F. Ding, F. Lipparini, F. Egidi, J. Goings, B. Peng, A. Petrone, T. Henderson, D. Ranasinghe, V. G. Zakrzewski, J. Gao, N. Rega, G. Zheng, W. Liang, M. Hada, M. Ehara, K. Toyota, R. Fukuda, J. Hasegawa, M. Ishida, T. Nakajima, Y. Honda, O. Kitao, H. Nakai, T. Vreven, K. Throssell, J. A. Montgomery, J. E. Peralta, F. Ogliaro, M. J. Bearpark, J. J. Heyd, E. N. Brothers, K. N. Kudin, V. N. Staroverov, T. A. Keith, R. Kobayashi, J. Normand, K. Raghavachari, A. P. Rendell, J. C. Burant, S. S. Iyengar, J. Tomasi, M. Cossi, J. M. Millam, M. Klene, C. Adamo, R. Cammi, J. W. Ochterski, R. L. Martin, K. Morokuma,

- O. Farkas, J. B. Foresman and D. J. Fox, *Gaussian 16, Revision A.03*, Gaussian, Inc., Wallingford CT, 2016.
- 92 S. R. Gadre and R. N. Shirsat, *Electrostatics of atoms and molecules*, Universities Press, 2000.
- 93 P. Politzer and D. G. Truhlar, *Chemical applications of atomic and molecular electrostatic potentials: reactivity, structure, scattering, and energetics of organic, inorganic, and biological systems*, Springer Science & Business Media, 2013.
- 94 J. Yang, X. Wang, W.-L. Yim and Q. Wang, *J. Phys. Chem. C*, 2015, **119**, 26355–26361.
- 95 T. Koopmans, *Physica*, 1933, **1**, 104–113.
- 96 J.-H. Luo, Q.-S. Li, L.-N. Yang, Z.-Z. Sun and Z.-S. Li, *RSC Adv.*, 2014, **4**, 20200–20207.
- 97 R. Katoh, A. Furube, T. Yoshihara, K. Hara, G. Fujihashi, S. Takano, S. Murata, H. Arakawa and M. Tachiya, *J. Phys. Chem. B*, 2004, **108**, 4818–4822.
- 98 N. N. Ghosh, M. Habib, A. Pramanik, P. Sarkar and S. Pal, *New J. Chem.*, 2019, **43**, 6480–6491.
- 99 J. B. Asbury, Y.-Q. Wang, E. Hao, H. N. Ghosh and T. Lian, *Res. Chem. Intermed.*, 2001, **27**, 393–406.
- 100 W. Sang-aroon, S. Saekow and V. Amornkitbamrung, *J. Photochem. Photobiol., A*, 2012, **236**, 35–40.



Cite this: *New J. Chem.*, 2021, 45, 2496

# Tuning the donating strength of dye sensitizers using molecular electrostatic potential analysis†

Velayudhan V. Divya<sup>ab</sup> and Cherumuttathu H. Suresh<sup>id</sup>\*<sup>ab</sup>

Donor- $\pi$ -acceptor (D- $\pi$ -A) systems typically used in dye-sensitized solar cells (DSSC) have been studied for assessing the donating strength of six donors (D1-D6) under the influence of substituents such as CH<sub>3</sub>, C<sub>5</sub>H<sub>11</sub>, isopropyl, *t*-butyl, OH, OCH<sub>3</sub>, OC<sub>2</sub>H<sub>5</sub>, NH<sub>2</sub>, N(CH<sub>3</sub>)<sub>2</sub>, PhCH<sub>3</sub>, and PhNH<sub>2</sub> along with  $\pi$ -spacer butadiene and acceptor moiety cyanoacrylic acid. The substituent effect enhances electron donation from D to A through the  $\pi$ -spacer. The enhancement in electron density at A has been quantified in terms of the difference in the molecular electrostatic potential (MESP) minimum at the cyano nitrogen ( $\Delta V_{\text{mA}}$ ) between  $\pi$ -A and D- $\pi$ -A. For unsubstituted D- $\pi$ -A systems,  $\Delta V_{\text{mA}}$  is in the range -0.1 to -5.7 kcal mol<sup>-1</sup>, whereas the substitution enhances the negative character of  $\Delta V_{\text{mA}}$  in the range -0.8 to -8.0 kcal mol<sup>-1</sup>. In alkyls and Ph-CH<sub>3</sub> substituted D- $\pi$ -A systems,  $\Delta V_{\text{mA}}$  lies in the range -0.8 to -6.7 kcal mol<sup>-1</sup>, whereas the N(CH<sub>3</sub>)<sub>2</sub> substituted systems exhibit more negative  $\Delta V_{\text{mA}}$  (more enhanced donating strength) in the range -5.1 to -8.0 kcal mol<sup>-1</sup>. The more negative value of  $\Delta V_{\text{mA}}$  implies the greater electron-donating ability of the D- $\pi$ -A system. Optical and photovoltaic parameters ( $\Delta G_{\text{reg}}$ ,  $\Delta G_{\text{inject}}$ ,  $eV_{\text{OC}}$ ) are analyzed at the TD-CAM-B3LYP/SMD/cc-pVDZ//B3LYP/cc-pVDZ level of DFT. An excellent linear correlation is observed in all six sets between  $\Delta V_{\text{mA}}$  and the absorption maximum ( $\lambda_{\text{max}}$ ) showing that  $\lambda_{\text{max}}$  increases with enhanced donating strength. The higher absorption maximum obtained by N(CH<sub>3</sub>)<sub>2</sub> substituted D- $\pi$ -A systems lies in the range 430 nm to 490 nm, explaining the outstanding donating ability of N(CH<sub>3</sub>)<sub>2</sub> compared to other substituents. The reduced highest occupied molecular orbital (HOMO) – lowest unoccupied molecular orbital (LUMO) gap (from 3.14 to 2.17 eV) with enhanced donating strength confirms the influence of substituent effects in broadening the absorption maximum. Furthermore, in photovoltaic parameters, a strong influence of the substituent effect is observed. The N(CH<sub>3</sub>)<sub>2</sub> substituted D1- $\pi$ -A (D1-N(CH<sub>3</sub>)<sub>2</sub>) exhibits the highest  $eV_{\text{OC}}$  (1.38 eV). The strong linear correlation observed for the ground state property  $\Delta V_{\text{mA}}$  and open-circuit voltage  $eV_{\text{OC}}$  provides guidelines for developing an effective strategy for designing dye sensitizers for desirable photovoltaic applications.

Received 29th September 2020,  
Accepted 21st November 2020

DOI: 10.1039/d0nj04797j

rsc.li/njc

## Introduction

Over the past 30 years, dye-sensitized solar cells (DSSCs) and their structural modification have become an emerging research area in the field of photovoltaics.<sup>1-3</sup> DSSCs are considered as the most inventive candidate for the next generation of clean renewable sources due to their easier structure modification, simple synthetic strategy, large absorption coefficient, and low production cost.<sup>1,4-7</sup> Nonetheless, the performance of DSSC is still in a bottleneck due to their lower power conversion efficiency (PCE) than the conventional silicon-based solar cells due to the inherent voltage loss during the dye regeneration

and poor long term stability.<sup>8</sup> In order to improve the PCE over conventional silicon-based solar cells, extensive research efforts like modification on electrolytes, semiconductors, and sensitizers have been executed and result in the development of new and efficient dye sensitizers.<sup>3,5,9-21</sup> Among the DSSCs, the Ru based sensitizers achieved the best PCE of 11%, which attains a comparable PCE to a silicon-based solar cell.<sup>5,22,23</sup> But due to the scarce resources and highly expensive nature of Ru metal, its practical application is limited, and more research efforts have resulted in the development of Ru-free organic sensitizers.<sup>6,11,24</sup> However, the major challenge of organic solar cells is the enhancement of PCE, durability, and stability to compete with silicon-based solar cells. One of the key strategies for the synthesis of Ru free sensitizers is the designing of the D- $\pi$ -A architecture, which enables efficient electron transfer from a donor (D) to the acceptor (A) through a spacer ( $\pi$ ).<sup>25,26</sup>

From the literature, it is understood that for the design of highly efficient photosensitizers, different kinds of building

<sup>a</sup> Chemical Sciences and Technology Division, CSIR-National Institute for Interdisciplinary Science and Technology, Thiruvananthapuram, Kerala 695019, India. E-mail: sureshch@niist.res.in, sureshch@gmail.com

<sup>b</sup> Academy of Scientific and Innovative Research (AcSIR), Ghaziabad 201002, India

† Electronic supplementary information (ESI) available. See DOI: 10.1039/d0nj04797j

blocks such as donors,<sup>27–35</sup> spacers,<sup>36–41</sup> and anchoring units<sup>42–46</sup> are required in the D– $\pi$ –A architecture to tune the electronic structure of the synthesized product. The fine-tuning of the HOMO–LUMO (highest occupied molecular orbital – lowest unoccupied molecular orbital) energy levels of a photosensitizer is often achieved by adjusting the substituent effect on the donor by the incorporation of electron-donating/withdrawing groups. In most of the cases, the electron-donating groups on the donor moiety act as substituents and they have a profound impact on the electronic structure and efficiency of the desired dye sensitizer.<sup>6,47–49</sup> *A priori* knowledge on the donating strength of the donor can become helpful for the prediction of the PCE of the designed/synthesized system. A quantitative/mathematical comparison of donating strength of the typically used donors is lacking in the literature.

Here we have selected six different donor systems (D1–D6), substituted with electron-donating groups such as CH<sub>3</sub>, C<sub>5</sub>H<sub>11</sub>, isopropyl, *t*-butyl, OH, OCH<sub>3</sub>, O–C<sub>2</sub>H<sub>5</sub>, NH<sub>2</sub>, N(CH<sub>3</sub>)<sub>2</sub>, N(C<sub>2</sub>H<sub>5</sub>)<sub>2</sub>, Ph–CH<sub>3</sub>, and Ph–NH<sub>2</sub> to evaluate the donating strength on a  $\pi$ –A system made up of a butadiene  $\pi$ -spacer and cyanoacrylic acid (Fig. 1). According to our previous study, the butadiene spacer is rated as having the highest substituent effect transmitting power compared to triple bonded, aromatic, and hetero-aromatic conjugated systems.<sup>50</sup> Hence this moiety is employed in the study as a  $\pi$ -spacer for effective intramolecular charge transfer (ICT) and cyanoacrylic acid is used as an acceptor (A). The molecular electrostatic potential (MESP) topographical analysis is used as a tool to measure the electronic effect of the substituted D on the acceptor A. MESP is a well-established tool for deriving many structure–property relationships for chemical and biological systems.<sup>51–57</sup> According to Scrocco, Tomasi, and coworkers, the MESP describes the charge distribution around a molecule and the regions with more negative MESP indicate the more electron-dense region of that system.<sup>58,59</sup> Suresh and coworkers widely used MESP for the quantification

of the substituent effect,<sup>60</sup> inductive effect,<sup>61</sup> resonance effect,<sup>62</sup> trans influence,<sup>63</sup> cation  $\pi$ -interaction,<sup>64</sup> *etc.* In a recent study, we have shown that MESP analysis is very useful for assessing the donating strength of D in the D– $\pi$ –A system.<sup>65</sup> MESP becomes a new theoretical tool for predicting the feasibility of organic electrode materials for lithium-ion batteries,<sup>66</sup> explained by Shang, Chen, and co-workers. The wide range of applications in various fields supports the validity of MESP based studies for analyzing the photovoltaic properties of dye-sensitized solar cells. The present study focuses on the substituent effect in tuning various ground state electronic and photovoltaic properties of D– $\pi$ –A systems for solar cell applications.

## Theoretical background and computational methodology

The three key parameters involved in the calculations of power conversion efficiency ( $\eta$ ) of a solar cell include open-circuit voltage ( $V_{OC}$ ), short-circuit current density ( $J_{SC}$ ), and the fill factor (FF). Thus, as compared to incident solar power on the cell ( $P_{inc}$ ), the  $\eta$  can be calculated as<sup>67</sup>

$$\eta = FF \frac{V_{OC} J_{SC}}{P_{inc}} \quad (1)$$

In the above equation,  $J_{SC}$  is related to the interaction between a sensitizer and semiconductor. In DSSCs,  $J_{SC}$  is calculated as<sup>39,40,68–70</sup>

$$J_{SC} = \int_{\lambda} LHE(\lambda) \phi_{inject} \eta_{collect} d\lambda \quad (2)$$

From the above equation, it is clear that  $J_{SC}$  is related to the light-harvesting efficiency (LHE) and electron injection efficiency  $\phi_{inject}$ .

*i.e.*, LHE =  $1 - 10^{-f}$ , where  $f$  represents the oscillator strength of the adsorbed dye molecule.<sup>71</sup>

Furthermore, the electron injection efficiency  $\phi_{inject}$  is related to electron injection-free energy change ( $\Delta G_{inject}$ ), and the enhancement in the  $J_{SC}$  can be carried out by the improvement of  $\Delta G_{inject}$ . Since electron injection takes place from the excited state of the dye to the conduction band of TiO<sub>2</sub>,  $\Delta G_{inject}$  can be calculated as follows.<sup>71–73</sup>

$$\Delta G_{inject} = E^{dye*} - |E_{CB}| \quad (3)$$

where  $E^{dye*}$  is the excited state oxidation potential and  $E_{CB}$  is the energy of the conduction band edge of the TiO<sub>2</sub> semiconductor. The negative  $\Delta G_{inject}$  values indicate that free energy change is spontaneous. It is well known that the conduction band (CB) of semiconductors is sensitive to conditions (*e.g.* pH of the solution) and it is very difficult to determine experimentally. Hence in this study, we used a widely accepted value of  $-4.00$  eV (an experimental value where the semiconductor is in contact with aqueous redox electrolytes of fixed pH 7.0) for doing the calculations.<sup>74</sup> For calculating  $E^{dye*}$ , it is assumed that electron injection occurs from the unrelaxed excited state and  $E^{dye*}$  can be written as<sup>39,72</sup>

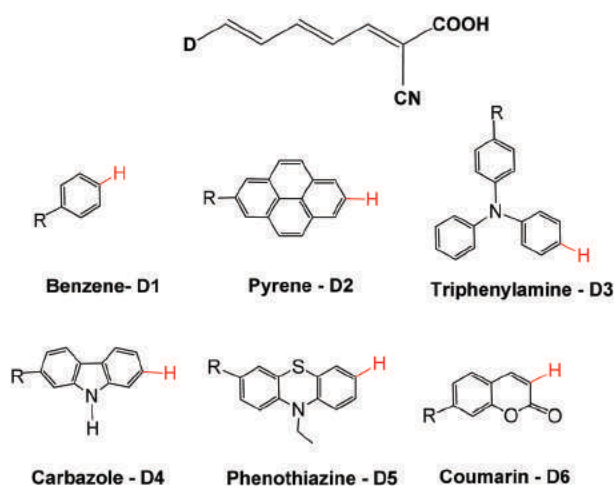


Fig. 1 Chemdraw diagram of the D– $\pi$ –A system (top) and the donors D1–D6. The R substituents are CH<sub>3</sub>, C<sub>5</sub>H<sub>11</sub>, isopropyl, *t*-butyl, OH, OCH<sub>3</sub>, O–C<sub>2</sub>H<sub>5</sub>, NH<sub>2</sub>, N(CH<sub>3</sub>)<sub>2</sub>, Ph–CH<sub>3</sub>, and Ph–NH<sub>2</sub>. The bond shown in red colour indicates the connecting position of D with  $\pi$ –A.



$$E^{\text{dye}*} = E^{\text{dye}} - \lambda_{\text{max}} \quad (4)$$

where  $E^{\text{dye}}$  is the ground state oxidation potential of the dye and  $\lambda_{\text{max}}$  is the vertical transition energy. According to Koopman's theorem, the ground state oxidation potential can be calculated as negative HOMO energy,<sup>75</sup> and this approximation has been giving good agreement with experimental results.<sup>76</sup>

The excited state dye regeneration can be predicted from the ground state oxidation potential as follows.<sup>77</sup>

$$\Delta G_{\text{reg}} = E^{\text{dye}} - 4.8 \text{ eV} \quad (5)$$

Thus from eqn (2)–(4), it is clear that  $J_{\text{SC}}$  will increase with the enhancement of light-harvesting efficiency and  $\Delta G_{\text{inject}}$ .

Theoretically, the open-circuit voltage can be approximated as the difference between the energy of the LUMO of the dye and the energy of the conduction band edge of  $\text{TiO}_2$ .<sup>78</sup>

$$eV_{\text{OC}} = E_{\text{LUMO}} - E_{\text{CB}} \quad (6)$$

Thus, the overall efficiency  $\eta$  of a solar cell can be enhanced by the improvement in  $J_{\text{SC}}$ ,  $eV_{\text{OC}}$  and FF values. (Since FF can be calculated from current–voltage characteristics, it is beyond the scope of this study).

For the ground state geometry optimization of the D- $\pi$ -A systems, the widely utilized B3LYP density functional theory (DFT) method<sup>79</sup> with the cc-pVDZ basis set<sup>65,80,81</sup> has been considered. Vibrational frequency calculation was also carried out at the same level of theory and basis set, and confirms that there are no imaginary frequencies. Absorption maxima and vertical excitation energies for the first seven states are calculated using time-dependent DFT at the CAM-B3LYP/SMD/cc-pVDZ//B3LYP/cc-pVDZ level.<sup>82,83</sup> Here SMD stands for the incorporation of the solvation effect of dichloromethane in the self-consistent reaction field (SCRF) approach<sup>84</sup> as implemented in the Gaussian16 suite of programmes.<sup>85</sup> The dependency of bond localization of single and double bonds in the ground state on the excited state properties has been analyzed using bond length alteration index (BLA).<sup>86,87</sup> The BLA index for the unsubstituted D1 to D6- $\pi$ -A systems are calculated with B3LYP and CAM-B3LYP geometries (Table S1 and Fig. S2, ESI†). For all a positive BLA index has been observed and larger BLA index has been observed with CAM-B3LYP. This indicates that carbon-carbon single and double bonds are more localized with CAM-B3LYP than B3LYP. Also, the BLA index for the S1 state of a representative set of TPA systems has been calculated with CAM-B3LYP (Table S2, ESI†). The reduced BLA index for S1 than the S0 state indicates the delocalized nature of the system and also supports the ICT transfer involved in D- $\pi$ -A systems. Previously, González *et al.* noted that B3LYP fails to predict the excitation energies due to its intrinsic problems in describing charge transfer (CT) states whereas the long-range correction on them using CAM delivers good agreement with the experimental UV/vis absorption.<sup>87</sup> They also observed that excited state properties are highly dependent on the localization of single and double bonds in the ground state structure which can be quantified in terms of the BLA index. Our previous study also showed that the calculated absorption maximum of known D- $\pi$ -A systems at the

CAM-B3LYP/SMD/cc-pVDZ//B3LYP/cc-pVDZ level of theory agrees well with the experimental absorption maximum.<sup>65</sup> The MESP,  $V(\mathbf{r})$  as defined in eqn (1) has been evaluated using the electron density  $\rho(\mathbf{r}')$  computed at the B3LYP/cc-pVDZ level.

$$V(\mathbf{r}) = \sum_A^N \frac{Z_A}{|\mathbf{r} - \mathbf{R}_A|} - \int \frac{\rho(\mathbf{r}') d\mathbf{r}'}{|\mathbf{r} - \mathbf{r}'|}$$

The  $N$  in eqn (1) is the total number of nuclei present in the molecular system,  $Z_A$  is the charge on the nucleus  $A$  at a distance  $R_A$  and  $\mathbf{r}'$  is a dummy integration variable.<sup>52,53</sup> All calculations have been carried out using the Gaussian 16 program package.<sup>85</sup>

### MESP analysis

The MESP plot of two representative donors (D1 and D4) and their corresponding D- $\pi$ -A systems (unsubstituted) are shown in Fig. 2 along with the respective MESP minimum ( $V_m$ ) at various sites.

In donor systems,  $V_{\text{mD}'}$  represents  $V_m$  of the donor. For example,  $V_{\text{mD}'}$  of benzene (D1) and carbazole (D4) are  $-16.6$  and  $-19.5 \text{ kcal mol}^{-1}$  (Fig. 2). In D- $\pi$ -A systems,  $V_{\text{mD}}$  and  $V_{\text{mS}}$  represent the MESP minimum at the donor and spacer (nearer to D), respectively while  $V_{\text{m(OH)}}$ ,  $V_{\text{m(CO)}}$ , and  $V_{\text{mA}}$  represent the MESP minimum at the lone pair regions of OH, CO and CN of the acceptor moiety, respectively. Previous studies by Suresh and Gadre *et al.* have shown that lone pair regions in molecules can be characterized using MESP topographical analysis.<sup>88</sup> The

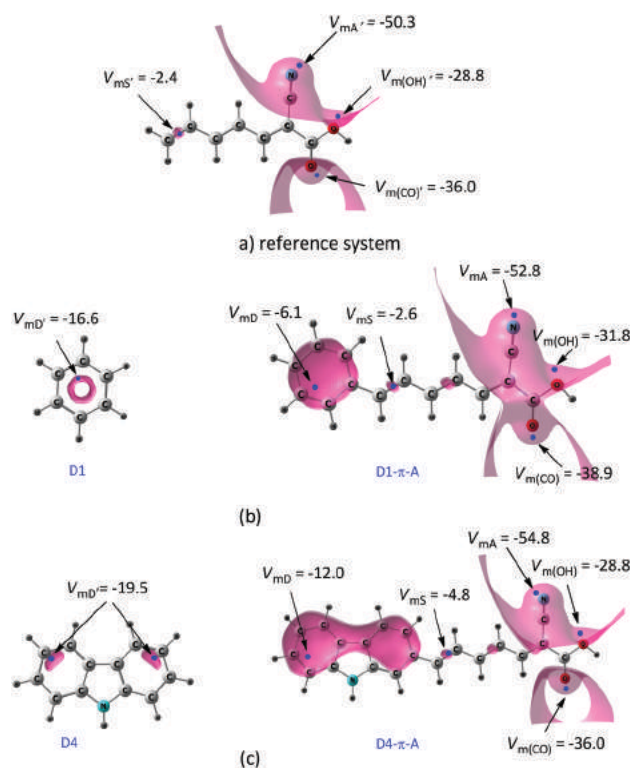


Fig. 2 MESP isosurfaces at various sites of the (a) reference system, (b) D1 and D1- $\pi$ -A system, and (c) D4 and D4- $\pi$ -A system.  $V_m$  values are in  $\text{kcal mol}^{-1}$ .

Table 1  $V_m$  (kcal mol<sup>-1</sup>) at various sites of D- $\pi$ -A systems calculated at B3LYP/cc-pVDZ levels

D moiety	D- $\pi$ -A system	$V_{mD'}$	$V_{mD}$	$V_{mS}$	$V_{m(OH)}$	$V_{m(CO)}$	$V_{mA}$	$\Delta V_{mD}$	$\Delta V_{mS}$	$\Delta V_{m(OH)}$	$\Delta V_{m(CO)}$	$\Delta V_{mA}$	
(a) Benzene	D1	-16.6	-6.1	-2.6	-31.8	-38.9	-52.8	10.5	-0.2	-2.9	-2.9	-2.5	
	D1-CH <sub>3</sub>	-18.1	-6.5	-3.8	-32.7	-39.9	-53.8	11.5	-1.4	-3.9	-3.9	-3.5	
	D1-C <sub>5</sub> H <sub>11</sub>	-18.7	-7.2	-4.3	-33.1	-40.1	-54.2	11.5	-1.9	-4.3	-4.1	-3.8	
	D1-isopropyl	-17.9	-6.7	-3.8	-32.9	-39.9	-53.8	11.2	-1.4	-4.1	-3.9	-3.5	
	D1- <i>t</i> -but	-18.1	-6.9	-4.0	-32.9	-40.0	-53.9	11.2	-1.6	-4.1	-4.0	-3.6	
	D1-OH	-17.9	-5.0	-4.3	-33.8	-40.9	-54.5	12.9	-1.9	-5.0	-4.8	-4.2	
	D1-OCH <sub>3</sub>	-18.8	-6.0	-5.0	-34.3	-41.4	-54.8	12.8	-2.6	-5.5	-5.4	-4.5	
	D1-OC <sub>2</sub> H <sub>5</sub>	-19.3	-6.5	-5.3	-34.5	-41.6	-55.3	12.7	-2.9	-5.6	-5.6	-5.0	
	D1-NH <sub>2</sub>	-23.1	-8.6	-7.6	-36.4	-43.7	-57.1	14.5	-5.2	-7.6	-7.7	-6.8	
	D1-N(CH <sub>3</sub> ) <sub>2</sub>	-24.0	-9.1	-9.0	-37.7	-45.1	-58.4	14.9	-6.7	-8.8	-9.0	-8.0	
	D1-PhCH <sub>3</sub>	-16.7	-7.0	-3.7	-32.8	-39.8	-53.5	9.7	-1.3	-4.0	-3.8	-3.2	
	D1-PhNH <sub>2</sub>	-19.7	-9.5	-5.9	-34.5	-41.7	-55.0	10.2	-3.5	-5.6	-5.6	-4.7	
	Pyrene	D2	-14.4	-8.2	-3.3	-32.0	-39.3	-53.0	6.2	-0.9	-3.2	-3.3	-2.7
		D2-CH <sub>3</sub>	-15.4	-8.7	-4.0	-32.6	-39.8	-53.7	6.7	-1.6	-3.8	-3.8	-3.3
		D2-C <sub>5</sub> H <sub>11</sub>	-15.8	-9.2	-4.2	-32.8	-40.0	-53.9	6.7	-1.8	-4.0	-4.0	-3.6
		D2-isopropyl	-15.3	-8.8	-4.0	-32.4	-39.7	-53.7	6.5	-1.6	-3.6	-3.7	-3.4
		D2- <i>t</i> -but	-15.5	-8.9	-4.1	-32.4	-39.8	-53.8	6.6	-1.7	-3.6	-3.8	-3.5
		D2-OH	-15.2	-8.2	-4.0	-32.8	-39.9	-53.7	7.0	-1.6	-4.0	-3.9	-3.4
		D2-OCH <sub>3</sub>	-15.9	-8.8	-4.5	-32.9	-40.2	-54.2	7.1	-2.1	-4.1	-4.1	-3.8
		D2-OC <sub>2</sub> H <sub>5</sub>	-16.3	-9.2	-4.6	-33.3	-40.5	-54.3	7.1	-2.3	-4.5	-4.5	-4.0
D2-NH <sub>2</sub>		-18.1	-11.0	-5.8	-34.1	-41.2	-54.7	7.2	-3.4	-5.3	-5.2	-4.4	
D2-N(CH <sub>3</sub> ) <sub>2</sub>		-18.9	-11.5	-6.7	-34.7	-42.1	-55.8	7.3	-4.3	-5.9	-6.1	-5.5	
D2-PhCH <sub>3</sub>		-14.7	-8.6	-3.8	-32.6	-39.7	-53.7	6.1	-1.4	-3.8	-3.7	-3.3	
D2-PhNH <sub>2</sub>		-16.7	-10.7	-5.0	-33.4	-40.6	-54.5	6.0	-2.6	-4.6	-4.6	-4.1	
TPA	D3	-15.6	-7.7	-6.3	-35.6	-42.5	-56.0	7.9	-3.9	-6.8	-6.5	-5.7	
	D3-CH <sub>3</sub>	-16.5	-8.3	-6.9	-36.0	-43.2	-56.7	8.2	-4.5	-7.2	-7.2	-6.3	
	D3-C <sub>5</sub> H <sub>11</sub>	-16.8	-8.7	-7.2	-36.0	-43.3	-57.0	8.2	-4.8	-7.2	-7.3	-6.7	
	D3-isopropyl	-16.4	-8.3	-6.8	-35.8	-43.1	-56.6	8.1	-4.5	-7.0	-7.1	-6.3	
	D3- <i>t</i> -but	-16.4	-8.3	-6.9	-36.1	-43.1	-56.4	8.2	-4.5	-7.3	-7.1	-6.0	
	D3-OH	-17.5	-8.2	-7.5	-36.3	-43.5	-57.2	9.3	-5.1	-7.5	-7.5	-6.8	
	D3-OCH <sub>3</sub>	-17.9	-8.7	-7.7	-36.6	-43.7	-57.2	9.2	-5.3	-7.8	-7.7	-6.9	
	D3-OC <sub>2</sub> H <sub>5</sub>	-18.1	-8.9	-7.8	-36.7	-43.9	-57.4	9.2	-5.5	-7.9	-7.9	-7.1	
	D3-NH <sub>2</sub>	-19.4	-10.2	-8.7	-37.3	-44.5	-58.1	9.2	-6.3	-8.5	-8.5	-7.8	
	D3-N(CH <sub>3</sub> ) <sub>2</sub>	-20.0	-11.0	-9.2	-37.7	-44.8	-58.3	9.0	-6.8	-8.9	-8.8	-8.0	
	D3-PhCH <sub>3</sub>	-15.3	-7.8	-6.4	-35.6	-42.7	-56.3	7.5	-4.0	-6.8	-6.7	-6.0	
	D3-PhNH <sub>2</sub>	-17.4	-9.7	-7.5	-36.3	-43.5	-57.2	7.7	-5.1	-7.5	-7.5	-6.8	
(b) Carbazole	D4	-19.5	-12.0	-4.8	-33.6	-40.6	-54.8	7.5	-2.4	-4.8	-4.6	-4.5	
	D4-CH <sub>3</sub>	-20.6	-12.3	-5.6	-34.2	-41.3	-55.3	8.3	-3.2	-5.4	-5.3	-5.0	
	D4-C <sub>5</sub> H <sub>11</sub>	-21.0	-12.7	-5.9	-34.3	-41.4	-55.5	8.3	-3.5	-5.5	-5.3	-5.1	
	D4-isopropyl	-20.3	-12.2	-5.5	-34.0	-41.0	-55.1	8.1	-3.1	-5.2	-5.0	-4.8	
	D4- <i>t</i> -but	-20.4	-12.4	-5.5	-34.1	-41.1	-54.9	8.0	-3.1	-5.3	-5.1	-4.6	
	D4-OH	-21.0	-11.4	-6.0	-34.8	-41.5	-55.7	9.6	-3.6	-6.0	-5.5	-5.4	
	D4-OCH <sub>3</sub>	-21.6	-12.0	-6.5	-35.1	-42.0	-56.0	9.5	-4.1	-6.3	-6.0	-5.7	
	D4-OC <sub>2</sub> H <sub>5</sub>	-21.8	-12.4	-6.7	-35.1	-42.1	-55.8	9.4	-4.3	-6.3	-6.1	-5.5	
	D4-NH <sub>2</sub>	-23.6	-14.5	-7.9	-36.0	-43.2	-57.0	9.1	-5.5	-7.2	-7.2	-6.7	
	D4-N(CH <sub>3</sub> ) <sub>2</sub>	-24.6	-14.7	-8.8	-36.8	-43.7	-57.5	9.9	-6.5	-8.0	-7.7	-7.2	
	D4-PhCH <sub>3</sub>	-19.5	-12.2	-5.2	-33.9	-41.0	-55.0	7.2	-2.8	-5.1	-5.0	-4.6	
	D4-PhNH <sub>2</sub>	-21.8	-14.6	-6.5	-34.9	-42.0	-55.7	7.2	-4.1	-6.1	-6.0	-5.4	
	Phenothiazine	D5	-16.8	-9.4	-5.3	-34.6	-41.7	-55.2	7.4	-2.9	-5.8	-5.6	-4.9
		D5-CH <sub>3</sub>	-17.6	-9.0	-5.8	-34.7	-42.2	-55.7	8.6	-3.5	-5.9	-6.1	-5.4
		D5-C <sub>5</sub> H <sub>11</sub>	-17.9	-9.5	-6.1	-35.2	-42.5	-55.8	8.4	-3.8	-6.4	-6.5	-5.5
		D5-isopropyl	-17.5	-9.0	-5.9	-35.0	-42.3	-55.3	8.5	-3.5	-6.2	-6.3	-5.0
		D5- <i>t</i> -but	-17.6	-9.0	-6.0	-35.1	-42.4	-55.7	8.6	-3.6	-6.3	-6.3	-5.4
		D5-OH	-18.1	-7.2	-6.3	-35.4	-42.9	-56.1	10.9	-4.0	-6.6	-6.8	-5.8
		D5-OCH <sub>3</sub>	-18.4	-9.4	-6.7	-35.5	-42.7	-56.2	9.0	-4.3	-6.7	-6.7	-5.9
		D5-OC <sub>2</sub> H <sub>5</sub>	-18.6	-9.8	-6.7	-35.7	-43.1	-56.5	8.8	-4.3	-6.9	-7.1	-6.1
D5-NH <sub>2</sub>		-19.5	-11.4	-7.3	-36.1	-43.4	-56.9	8.2	-5.0	-7.3	-7.4	-6.5	
D5-N(CH <sub>3</sub> ) <sub>2</sub>		-20.6	-12.4	-8.2	-36.6	-44.1	-57.5	8.3	-5.8	-7.8	-8.1	-7.2	
D5-PhCH <sub>3</sub>		-16.7	-9.0	-5.5	-34.8	-42.0	-55.5	7.7	-3.1	-6.0	-6.0	-5.1	
D5-PhNH <sub>2</sub>		-18.2	-11.2	-6.6	-35.4	-42.9	-56.2	7.0	-4.2	-6.6	-6.8	-5.9	
Coumarin	D6	-5.7	-0.1	0.0	-30.1	-37.8	-50.5	5.6	2.4	-1.3	-1.8	-0.2	
	D6-CH <sub>3</sub>	-6.5	-0.4	-1.2	-31.0	-38.7	-51.3	6.1	1.2	-2.2	-2.7	-0.9	
	D6-C <sub>5</sub> H <sub>11</sub>	-7.2	-1.1	-1.6	-31.2	-39.0	-51.8	6.1	0.8	-2.4	-3.0	-1.5	
	D6-isopropyl	-6.7	-0.6	-1.2	-30.7	-38.7	-51.1	6.0	1.2	-1.9	-2.7	-0.8	
	D6- <i>t</i> -but	-6.9	-0.9	-1.4	-31.2	-38.9	-51.3	6.0	0.9	-2.4	-2.9	-1.0	
	D6-OH	-6.1	-	-1.9	-31.8	-39.5	-52.3	6.1	0.5	-3.0	-3.5	-1.9	
D6-OCH <sub>3</sub>	-7.0	-0.1	-2.6	-32.1	-40.0	-52.6	7.0	-0.2	-3.3	-4.0	-2.3		

Table 1 (continued)

D moiety	D- $\pi$ -A system	$V_{mD'}$	$V_{mD}$	$V_{mS}$	$V_{m(OH)}$	$V_{m(CO)}$	$V_{mA}$	$\Delta V_{mD}$	$\Delta V_{mS}$	$\Delta V_{m(OH)}$	$\Delta V_{m(CO)}$	$\Delta V_{mA}$
	D6-OC <sub>2</sub> H <sub>5</sub>	-7.5	-0.4	-2.9	-32.3	-40.2	-52.5	7.0	-0.6	-3.5	-4.2	-2.2
	D6-NH <sub>2</sub>	-10.4	-2.1	-5.0	-33.9	-41.8	-54.3	8.3	-2.6	-5.1	-5.8	-4.0
	D6-N(CH <sub>3</sub> ) <sub>2</sub>	-11.3	-2.6	-6.3	-35.0	-43.0	-55.5	8.7	-4.0	-6.2	-7.0	-5.1
	D6-PhCH <sub>3</sub>	-7.2	-1.6	-1.6	-31.2	-38.8	-51.5	5.6	0.8	-2.4	-2.8	-1.2
	D6-PhNH <sub>2</sub>	-10.2	-4.2	-3.6	-32.8	-40.6	-53.2	6.0	-1.2	-4.0	-4.6	-2.8

MESP minimum observed at the CN unit of  $\pi$ -A is considered as a reference value,  $V_{mA'}$  (Fig. 2a) ( $-50.3 \text{ kcal mol}^{-1}$ ) to monitor the changes observed at this minimum due to the incorporation of D to  $\pi$ -A. One could also consider the MESP minimum  $V_{m(OH)}$  or  $V_{m(CO)}$  of  $\pi$ -A as a reference point similar to  $V_{mA'}$  because in general the trends observed for these quantities show a parallel behavior. Here  $V_{mA'}$  is selected as the reference point on the basis of its most negative character compared to all other minima.

In Table 1a and b,  $V_m$  of D- $\pi$ -A systems at various sites *viz.* donor ( $V_{mD}$ ), spacer ( $V_{mS}$ ) and acceptor ( $V_{m(OH)}$ ,  $V_{m(CO)}$  and  $V_{mA}$ ) are reported along with  $V_{mD'}$ . The unsubstituted D- $\pi$ -A systems are denoted as D1, D2, D3, D4, D5, and D6, and the substituents attached at D1-D6 are represented as D1-CH<sub>3</sub>, D1-C<sub>5</sub>H<sub>11</sub>, D2-CH<sub>3</sub>, D2-C<sub>5</sub>H<sub>11</sub>, *etc.* The quantities  $\Delta V_{mD}$ ,  $\Delta V_{mS}$ ,  $\Delta V_{m(OH)}$ ,  $\Delta V_{m(CO)}$ , and  $\Delta V_{mA}$  represent the change in  $V_m$  at the respective

sites with the attachment of  $\pi$ -A to D.  $\Delta V_{mD}$  has been calculated by subtracting the  $V_m$  observed at the donor ( $V_{mD'}$ ) from the respective  $V_m$  observed at the D site of D- $\pi$ -A ( $V_{mD}$ ). Likewise  $\Delta V_{mS}$ ,  $\Delta V_{m(OH)}$ ,  $\Delta V_{m(CO)}$ , and  $\Delta V_{mA}$  are estimated by subtracting the respective  $V_m$  at  $\pi$ -A *viz.*  $V_{mS}$ ,  $V_{m(OH)}$ ,  $V_{m(CO)}$  and  $V_{mA'}$  (Fig. 2) from the corresponding values at D- $\pi$ -A ( $V_{mS}$ ,  $V_{m(OH)}$ ,  $V_{m(CO)}$  and  $V_{mA}$ ) (Table 1a and b).

The data in Table 1a and b show that the  $V_{mD}$  of the D- $\pi$ -A system is always less negative than the  $V_{mD'}$  of the donor D. For various donor systems,  $\Delta V_{mD}$  lies in the range 5.6 to 14.9  $\text{kcal mol}^{-1}$  which clearly suggests that the D site of the D- $\pi$ -A system becomes electron deficient compared to a normal D. The electron deficiency at D can be attributed to ICT of electrons from D to the  $\pi$ -A region which implies that  $V_m$  at the acceptor sites of D- $\pi$ -A becomes more negative compared to  $\pi$ -A and as a result always negative values are observed for

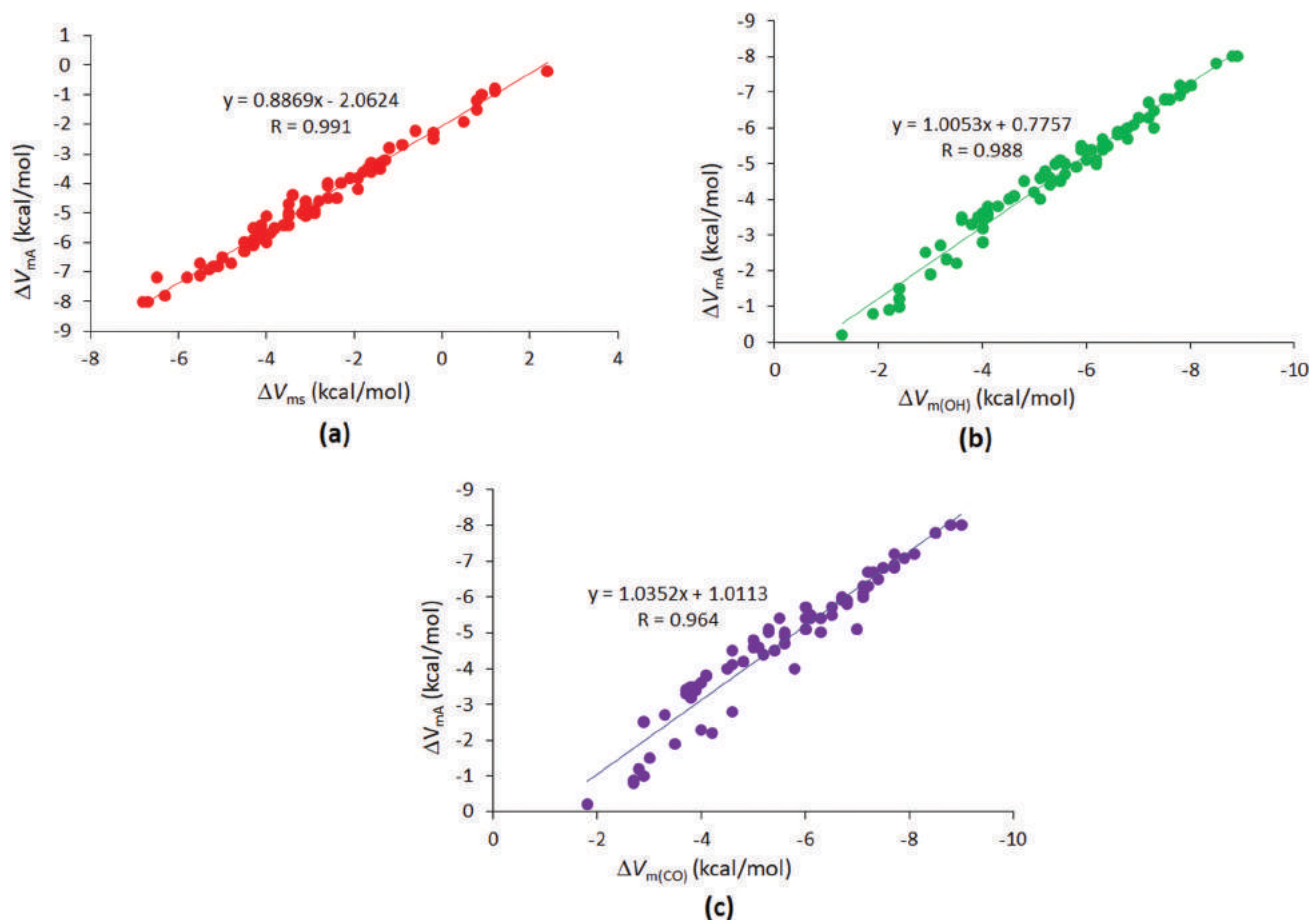


Fig. 3 Correlation between MESP parameters  $\Delta V_{mS}$ ,  $\Delta V_{m(OH)}$ ,  $\Delta V_{m(CO)}$ , and  $\Delta V_{mA}$ .

**Table 2** HOMO, LUMO and HOMO–LUMO energy gap (HLG) (in eV) observed for the ground state at the B3LYP/cc-pVDZ level and absorption maximum  $\lambda_{\max}$  (nm), and oscillator strength ( $f$ ) at the CAM-B3LYP/SMD/cc-pVDZ//B3LYP/cc-pVDZ level

D- $\pi$ -A system	HOMO	LUMO	HLG	$\lambda_{\max}$	$f$	D- $\pi$ -A system	HOMO	LUMO	HLG	$\lambda_{\max}$	$f$
Benzene						Pyrene					
D1	-6.13	-2.99	3.14	388	1.74	D2	-5.88	-2.99	2.89	401	2.22
D1-CH <sub>3</sub>	-6.01	-2.92	3.08	396	1.82	D2-CH <sub>3</sub>	-5.84	-2.95	2.89	404	2.27
D1-C <sub>5</sub> H <sub>11</sub>	-5.97	-2.90	3.07	398	1.86	D2-C <sub>5</sub> H <sub>11</sub>	-5.81	-2.94	2.87	404	2.32
D1-isopropyl	-6.01	-2.92	3.08	396	1.86	D2-isopropyl	-5.83	-2.95	2.88	404	2.30
D1- <i>t</i> -but	-6.00	-2.92	3.08	397	1.89	D2- <i>t</i> -but	-5.82	-2.95	2.87	404	2.33
D1-OH	-5.84	-2.85	2.99	408	1.78	D2-OH	-5.85	-2.94	2.91	409	2.19
D1-OCH <sub>3</sub>	-5.79	-2.83	2.97	412	1.81	D2-OCH <sub>3</sub>	-5.79	-2.92	2.87	410	2.20
D1-OC <sub>2</sub> H <sub>5</sub>	-5.77	-2.81	2.96	413	1.84	D2-OC <sub>2</sub> H <sub>5</sub>	-5.77	-2.91	2.86	410	2.23
D1-NH <sub>2</sub>	-5.53	-2.69	2.84	434	1.85	D2-NH <sub>2</sub>	-5.62	-2.86	2.76	419	2.20
D1-N(CH <sub>3</sub> ) <sub>2</sub>	-5.34	-2.62	2.72	457	1.94	D2-N(CH <sub>3</sub> ) <sub>2</sub>	-5.39	-2.81	2.58	430	2.21
D1-PhCH <sub>3</sub>	-5.89	-2.96	2.93	410	2.15	D2-PhCH <sub>3</sub>	-5.86	-2.97	2.89	406	2.49
D1-PhNH <sub>2</sub>	-5.52	-2.86	2.66	428	2.17	D2-PhNH <sub>2</sub>	-5.53	-2.91	2.62	411	2.53
TPA						Carbazole					
D3	-5.37	-2.79	2.58	453	2.02	D4	-5.78	-2.91	2.87	419	2.21
D3-CH <sub>3</sub>	-5.31	-2.76	2.55	457	2.03	D4-CH <sub>3</sub>	-5.69	-2.87	2.83	424	2.27
D3-C <sub>5</sub> H <sub>11</sub>	-5.29	-2.75	2.55	458	2.06	D4-C <sub>5</sub> H <sub>11</sub>	-5.67	-2.85	2.82	425	2.31
D3-isopropyl	-5.31	-2.76	2.55	457	2.03	D4-isopropyl	-5.71	-2.88	2.83	424	2.30
D3- <i>t</i> -but	-5.31	-2.76	2.55	457	2.02	D4- <i>t</i> -but	-5.70	-2.87	2.83	424	2.31
D3-OH	-5.26	-2.73	2.53	460	2.02	D4-OH	-5.58	-2.84	2.74	432	2.22
D3-OCH <sub>3</sub>	-5.24	-2.72	2.52	461	2.03	D4-OCH <sub>3</sub>	-5.54	-2.82	2.72	433	2.27
D3-OC <sub>2</sub> H <sub>5</sub>	-5.23	-2.71	2.51	461	2.03	D4-OC <sub>2</sub> H <sub>5</sub>	-5.52	-2.81	2.71	434	2.29
D3-NH <sub>2</sub>	-5.13	-2.67	2.46	468	2.00	D4-NH <sub>2</sub>	-5.33	-2.75	2.58	447	2.23
D3-N(CH <sub>3</sub> ) <sub>2</sub>	-5.03	-2.65	2.38	472	2.00	D4-N(CH <sub>3</sub> ) <sub>2</sub>	-5.14	-2.71	2.44	461	2.26
D3-PhCH <sub>3</sub>	-5.31	-2.78	2.52	457	2.12	D4-PhCH <sub>3</sub>	-5.66	-2.90	2.76	427	2.53
D3-PhNH <sub>2</sub>	-5.17	-2.73	2.44	460	2.12	D4-PhNH <sub>2</sub>	-5.37	-2.83	2.53	433	2.57
Phenothiazine						Coumarin					
D5	-5.28	-2.84	2.44	459	1.67	D6	-6.19	-3.34	2.85	424	1.71
D5-CH <sub>3</sub>	-5.22	-2.81	2.41	464	1.69	D6-CH <sub>3</sub>	-6.09	-3.26	2.82	431	1.78
D5-C <sub>5</sub> H <sub>11</sub>	-5.20	-2.80	2.40	464	1.72	D6-C <sub>5</sub> H <sub>11</sub>	-6.07	-3.25	2.82	431	1.84
D5-isopropyl	-5.21	-2.81	2.40	465	1.68	D6-isopropyl	-6.09	-3.27	2.82	431	1.83
D5- <i>t</i> -but	-5.22	-2.81	2.40	464	1.71	D6- <i>t</i> -but	-6.07	-3.25	2.82	432	1.84
D5-OH	-5.15	-2.79	2.36	469	1.66	D6-OH	-5.98	-3.20	2.78	439	1.77
D5-OCH <sub>3</sub>	-5.14	-2.78	2.36	469	1.70	D6-OCH <sub>3</sub>	-5.94	-3.18	2.76	442	1.82
D5-OC <sub>2</sub> H <sub>5</sub>	-5.12	-2.77	2.35	470	1.71	D6-OC <sub>2</sub> H <sub>5</sub>	-5.92	-3.16	2.76	443	1.85
D5-NH <sub>2</sub>	-4.99	-2.74	2.25	482	1.62	D6-NH <sub>2</sub>	-5.71	-3.04	2.67	463	1.86
D5-N(CH <sub>3</sub> ) <sub>2</sub>	-4.88	-2.70	2.17	490	1.62	D6-N(CH <sub>3</sub> ) <sub>2</sub>	-5.56	-2.97	2.59	481	1.96
D5-PhCH <sub>3</sub>	-5.22	-2.81	2.41	464	1.69	D6-PhCH <sub>3</sub>	-6.00	-3.28	2.72	444	2.10
D5-PhNH <sub>2</sub>	-5.07	-2.78	2.29	469	1.78	D6-PhNH <sub>2</sub>	-5.68	-3.17	2.51	461	2.18

$\Delta V_{m(OH)}$ ,  $\Delta V_{m(CO)}$ , and  $\Delta V_{mA}$ . For example, when  $\pi$ -A changes to D1- $\pi$ -A,  $V_m$  at the cyano region turns out to be more negative ( $V_{mA} = -52.8 \text{ kcal mol}^{-1}$ ) than the respective  $V_m$  on the reference system ( $\pi$ -A),  $V_{mA}$  ( $-50.3 \text{ kcal mol}^{-1}$ ). A similar trend in  $V_{mA}$  is observed for all the remaining systems. Also compared to  $\pi$ -A, the  $\pi$ -spacer region of D- $\pi$ -A shows more negative character for  $V_{mS}$  in all cases except some of the coumarin-based systems. Among the donors, the  $V_{mD}$  value is the least negative for coumarin systems, which can be attributed to the presence of an electron withdrawing carbonyl group in it. The quantities  $\Delta V_{mS}$ ,  $\Delta V_{m(OH)}$ ,  $\Delta V_{m(CO)}$  and  $\Delta V_{mA}$  show a parallel trend as shown in the correlation plots given in Fig. 3a–c. This suggests that any of these quantities can be used as a parameter to measure the donating strength of donor moieties to a common acceptor. Here  $\Delta V_{mA}$  (for the CN group) is selected for this purpose. It may be noted that variation in  $\Delta V_{mD}$  is not similar to  $\Delta V_{mA}$  (Fig. S3, ESI<sup>†</sup>) because it accounts for the property of various donors whereas  $\Delta V_{mA}$  accounts for the accepting ability of a CN unit from various donors.

In Table 1a and b, the lower  $\Delta V_{mA}$  in the range  $-0.2$  to  $-5.1 \text{ kcal mol}^{-1}$  have been attained by coumarin-based D- $\pi$ -A

systems which can be attributed to the presence of an electron-withdrawing CO group in the donor site. In benzene and pyrene based systems, the strong conjugation feature in donors increases the negative character of the  $\Delta V_{mA}$  values ( $-2.5$  to  $-8.0 \text{ kcal mol}^{-1}$ ) leading to better-donating strength than coumarin systems.

In carbazole and phenothiazine systems, the charge transfer to the acceptor is enhanced ( $\Delta V_{mA} -4.5$  to  $-7.2 \text{ kcal mol}^{-1}$ ) due to donation from hetero atoms *viz.* nitrogen and sulphur. Among all, the TPA based systems have the highest electron-donating strength ( $-5.7$  to  $-8.0 \text{ kcal mol}^{-1}$ ).

Substituents at the donor region can be utilized for tuning the electron-donating strength of the donor. For instance, alkyl substituents *viz.* CH<sub>3</sub>, C<sub>5</sub>H<sub>11</sub>, isopropyl, and *t*-butyl at the donor unit enhance the electron-donating strength of all the corresponding substituted D- $\pi$ -A systems by a +I inductive effect. The substituents bearing lone pairs such as OH, OCH<sub>3</sub>, NH<sub>2</sub>, and N(CH<sub>3</sub>)<sub>2</sub> improve the electron density of the donor unit, resulting in better electron-donating power than alkyl substituents ( $\Delta V_{mA}$  in the range  $-3.4$  to  $-8.0 \text{ kcal mol}^{-1}$ ) +R resonance effect. Among all, N(CH<sub>3</sub>)<sub>2</sub> substituted benzene and TPA based D- $\pi$ -A systems show



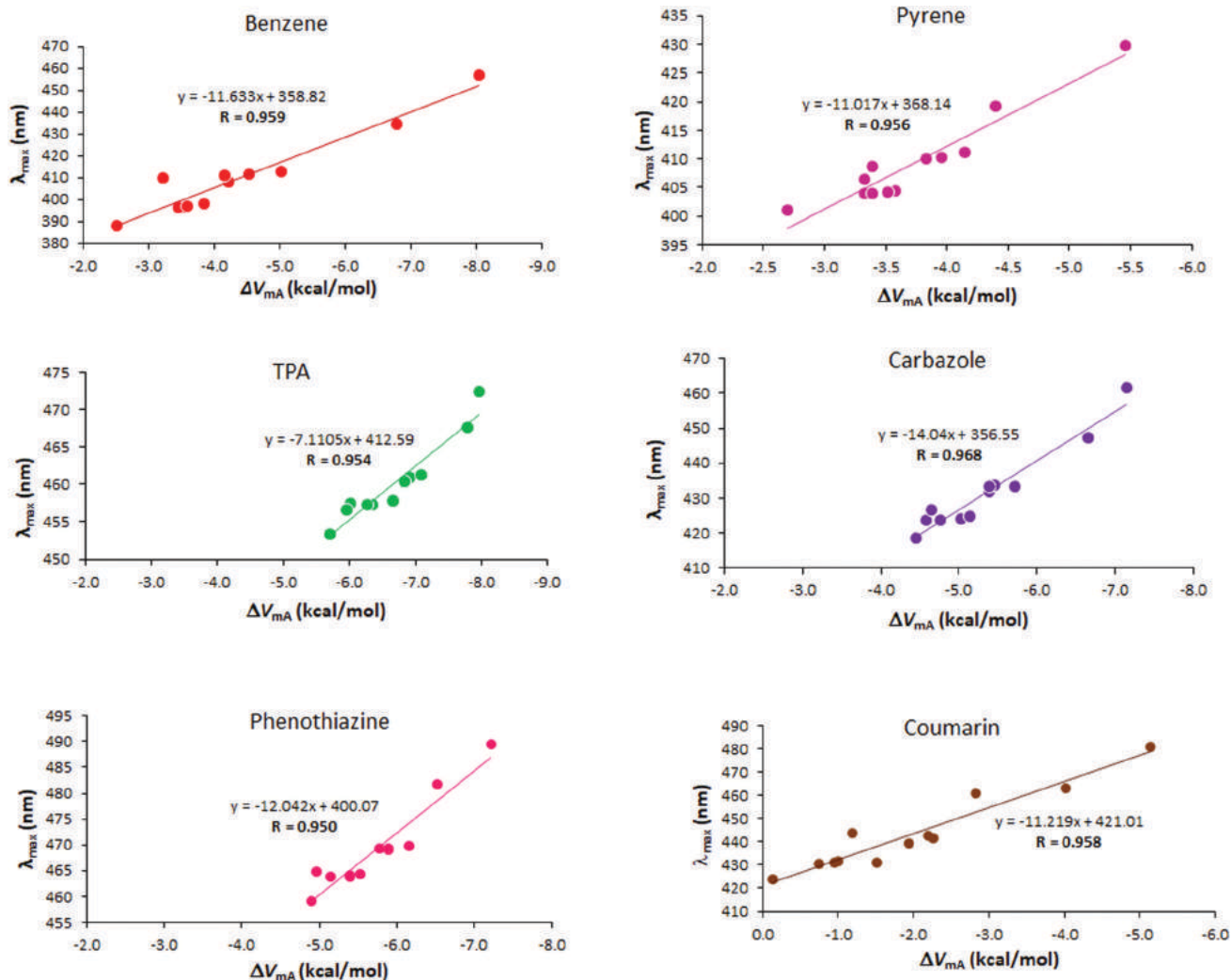


Fig. 4 Correlation between absorption maximum ( $\lambda_{\max}$ ) and donating strength ( $\Delta V_{mA}$ ) of various D- $\pi$ -A systems with different substituents.

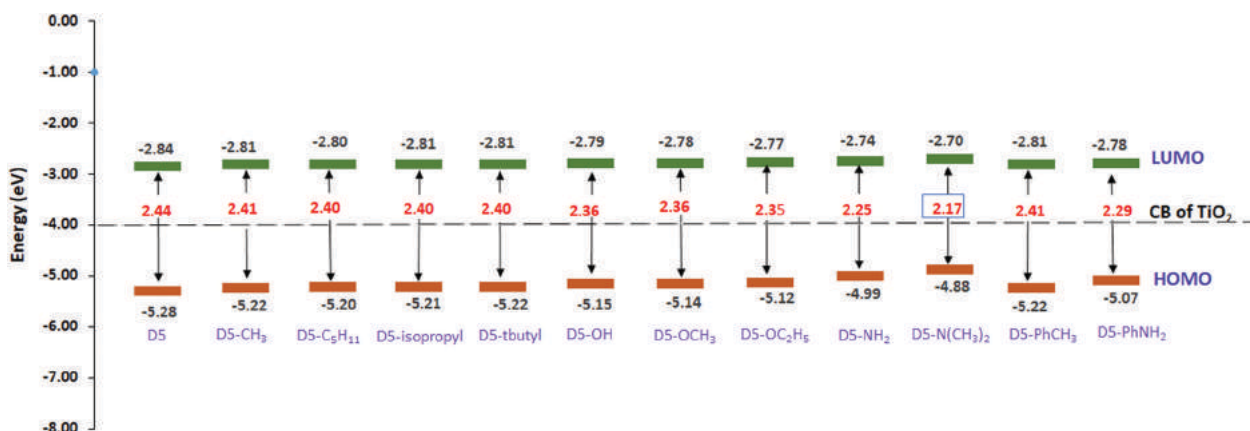


Fig. 5 Frontier molecular energy levels of phenothiazine based  $\pi$ -A with various substituents at the B3LYP/cc-pVDZ level.

the highest donation from donor to acceptor. The donating strength of various substituents attached on the D- $\pi$ -A system follows the order PhCH<sub>3</sub>  $\sim$  alkyls  $<$  -OH, -OR, PhNH<sub>2</sub>  $<$  NH<sub>2</sub>  $<$  N(CH<sub>3</sub>)<sub>2</sub>.

**Table 3** HOMO, LUMO and HOMO–LUMO energy gap (HLG) (in eV) observed for the ground state at the B3LYP/cc-pVDZ level. Excitation energy, ground and excited state oxidation potential ( $E^{\text{dye}}$ ,  $E^{\text{dye*}}$ ), free energy of electron injection  $\Delta G_{\text{inject}}$ , dye regeneration efficiency  $\Delta G_{\text{reg}}$ , and open-circuit voltage  $eV_{\text{OC}}$  at the TD-CAM-B3LYP/SMD/cc-pVDZ//B3LYP/cc-pVDZ level

D- $\pi$ -A	Excitation energy (eV)	HOMO (eV)	LUMO (eV)	HLG (eV)	$E^{\text{dye}}$ (eV)	$E^{\text{dye*}}$ (eV)	$\Delta G_{\text{inject}}$ (eV)	$\Delta G_{\text{reg}}$ (eV)	$eV_{\text{OC}}$ (eV)
(a)									
Benzene									
D1	3.20	-6.13	-2.99	3.14	6.13	2.93	-1.07	1.33	1.01
D1-CH <sub>3</sub>	3.13	-6.01	-2.92	3.08	6.01	2.88	-1.12	1.21	1.08
D1-C <sub>5</sub> H <sub>11</sub>	3.11	-5.97	-2.90	3.07	5.97	2.86	-1.14	1.17	1.10
D1-isopropyl	3.13	-6.01	-2.92	3.08	6.01	2.88	-1.12	1.21	1.08
D1- <i>t</i> -but	3.13	-6.00	-2.92	3.08	6.00	2.87	-1.13	1.20	1.08
D1-OH	3.04	-5.84	-2.85	2.99	5.84	2.80	-1.20	1.04	1.15
D1-OCH <sub>3</sub>	3.01	-5.79	-2.83	2.97	5.79	2.78	-1.22	0.99	1.17
D1-OC <sub>2</sub> H <sub>5</sub>	3.00	-5.77	-2.81	2.96	5.77	2.77	-1.23	0.97	1.19
D1-NH <sub>2</sub>	2.85	-5.53	-2.69	2.84	5.53	2.68	-1.32	0.73	1.31
D1-N(CH <sub>3</sub> ) <sub>2</sub>	2.71	-5.34	-2.62	2.72	5.34	2.63	-1.37	0.54	1.38
D1-PhCH <sub>3</sub>	3.02	-5.89	-2.96	2.93	5.89	2.87	-1.13	1.09	1.04
D1-PhNH <sub>2</sub>	2.90	-5.52	-2.86	2.66	5.52	2.62	-1.38	0.73	1.14
Pyrene									
D2	3.09	-5.88	-2.99	2.89	5.88	2.79	-1.21	1.08	1.01
D2-CH <sub>3</sub>	3.07	-5.84	-2.95	2.89	5.84	2.77	-1.23	1.04	1.05
D2-C <sub>5</sub> H <sub>11</sub>	3.07	-5.81	-2.94	2.87	5.81	2.74	-1.26	1.01	1.06
D2-isopropyl	3.07	-5.83	-2.95	2.88	5.83	2.76	-1.24	1.03	1.05
D2- <i>t</i> -but	3.07	-5.82	-2.95	2.87	5.82	2.75	-1.25	1.02	1.05
D2-OH	3.03	-5.85	-2.94	2.91	5.85	2.82	-1.18	1.05	1.06
D2-OCH <sub>3</sub>	3.02	-5.79	-2.92	2.87	5.79	2.77	-1.23	0.99	1.08
D2-OC <sub>2</sub> H <sub>5</sub>	3.02	-5.77	-2.91	2.86	5.77	2.75	-1.25	0.97	1.09
D2-NH <sub>2</sub>	2.96	-5.62	-2.86	2.76	5.62	2.66	-1.34	0.82	1.14
D2-N(CH <sub>3</sub> ) <sub>2</sub>	2.88	-5.39	-2.81	2.58	5.39	2.51	-1.49	0.59	1.19
D2-PhCH <sub>3</sub>	3.05	-5.86	-2.97	2.89	5.86	2.81	-1.19	1.06	1.03
D2-PhNH <sub>2</sub>	3.02	-5.53	-2.91	2.62	5.53	2.51	-1.49	0.73	1.09
TPA									
D3	2.73	-5.37	-2.79	2.58	5.37	2.64	-1.36	0.57	1.21
D3-CH <sub>3</sub>	2.71	-5.31	-2.76	2.55	5.31	2.60	-1.40	0.51	1.24
D3-C <sub>5</sub> H <sub>11</sub>	2.71	-5.29	-2.75	2.55	5.29	2.58	-1.42	0.49	1.25
D3-isopropyl	2.71	-5.31	-2.76	2.55	5.31	2.60	-1.40	0.51	1.24
D3- <i>t</i> -but	2.71	-5.31	-2.76	2.55	5.31	2.60	-1.40	0.51	1.24
D3-OH	2.69	-5.26	-2.73	2.53	5.26	2.57	-1.43	0.46	1.27
D3-OCH <sub>3</sub>	2.69	-5.24	-2.72	2.52	5.24	2.55	-1.45	0.44	1.28
D3-OC <sub>2</sub> H <sub>5</sub>	2.69	-5.23	-2.71	2.51	5.23	2.54	-1.46	0.43	1.29
D3-NH <sub>2</sub>	2.65	-5.13	-2.67	2.46	5.13	2.48	-1.52	0.33	1.33
D3-N(CH <sub>3</sub> ) <sub>2</sub>	2.62	-5.03	-2.65	2.38	5.03	2.41	-1.59	0.23	1.35
D3-PhCH <sub>3</sub>	2.72	-5.31	-2.78	2.52	5.31	2.60	-1.41	0.51	1.22
D3-PhNH <sub>2</sub>	2.69	-5.17	-2.73	2.44	5.17	2.48	-1.52	0.37	1.27
(b)									
Carbazole									
D4	2.96	-5.78	-2.91	2.87	5.78	2.82	-1.18	0.98	1.09
D4-CH <sub>3</sub>	2.92	-5.69	-2.87	2.83	5.69	2.77	-1.23	0.89	1.13
D4-C <sub>5</sub> H <sub>11</sub>	2.92	-5.67	-2.85	2.82	5.67	2.75	-1.25	0.87	1.15
D4-isopropyl	2.93	-5.71	-2.88	2.83	5.71	2.78	-1.22	0.91	1.12
D4- <i>t</i> -but	2.93	-5.70	-2.87	2.83	5.70	2.77	-1.23	0.90	1.13
D4-OH	2.87	-5.58	-2.84	2.74	5.58	2.71	-1.29	0.78	1.16
D4-OCH <sub>3</sub>	2.86	-5.54	-2.82	2.72	5.54	2.68	-1.32	0.74	1.18
D4-OC <sub>2</sub> H <sub>5</sub>	2.86	-5.52	-2.81	2.71	5.52	2.66	-1.34	0.72	1.19
D4-NH <sub>2</sub>	2.77	-5.33	-2.75	2.58	5.33	2.56	-1.44	0.53	1.25
D4-N(CH <sub>3</sub> ) <sub>2</sub>	2.69	-5.14	-2.71	2.44	5.14	2.45	-1.55	0.34	1.29
D4-PhCH <sub>3</sub>	2.91	-5.66	-2.90	2.76	5.66	2.75	-1.25	0.86	1.10
D4-PhNH <sub>2</sub>	2.86	-5.37	-2.83	2.53	5.37	2.51	-1.49	0.57	1.17
Phenothiazine									
D5	2.70	-5.28	-2.84	2.44	5.28	2.58	-1.42	0.48	1.16
D5-CH <sub>3</sub>	2.67	-5.22	-2.81	2.41	5.22	2.55	-1.45	0.42	1.19
D5-C <sub>5</sub> H <sub>11</sub>	2.67	-5.20	-2.80	2.40	5.20	2.53	-1.47	0.40	1.20
D5-isopropyl	2.67	-5.21	-2.81	2.40	5.21	2.54	-1.46	0.41	1.19
D5- <i>t</i> -but	2.67	-5.22	-2.81	2.40	5.22	2.55	-1.45	0.42	1.19
D5-OH	2.64	-5.15	-2.79	2.36	5.15	2.51	-1.49	0.35	1.21
D5-OCH <sub>3</sub>	2.64	-5.14	-2.78	2.36	5.14	2.50	-1.50	0.34	1.22
D5-OC <sub>2</sub> H <sub>5</sub>	2.64	-5.12	-2.77	2.35	5.12	2.48	-1.52	0.32	1.23
D5-NH <sub>2</sub>	2.57	-4.99	-2.74	2.25	4.99	2.42	-1.58	0.19	1.26
D5-N(CH <sub>3</sub> ) <sub>2</sub>	2.53	-4.88	-2.70	2.17	4.88	2.35	-1.65	0.08	1.30
D5-PhCH <sub>3</sub>	2.67	-5.22	-2.81	2.41	5.22	2.55	-1.45	0.42	1.19
D5-PhNH <sub>2</sub>	2.64	-5.07	-2.78	2.29	5.07	2.43	-1.57	0.27	1.22

Table 3 (continued)

D- $\pi$ -A	Excitation energy (eV)	HOMO (eV)	LUMO (eV)	HLG (eV)	$E^{\text{dye}}$ (eV)	$E^{\text{dye}*}$ (eV)	$\Delta G_{\text{inject}}$ (eV)	$\Delta G_{\text{reg}}$ (eV)	$eV_{\text{OC}}$ (eV)
Coumarin									
D6	2.93	-6.19	-3.34	2.85	6.19	3.27	-0.73	1.39	0.66
D6-CH <sub>3</sub>	2.88	-6.09	-3.26	2.82	6.09	3.21	-0.79	1.29	0.74
D6-C <sub>5</sub> H <sub>11</sub>	2.87	-6.07	-3.25	2.82	6.07	3.19	-0.81	1.27	0.75
D6-isopropyl	2.88	-6.09	-3.27	2.82	6.09	3.21	-0.79	1.29	0.73
D6- <i>t</i> -but	2.87	-6.07	-3.25	2.82	6.07	3.20	-0.80	1.27	0.75
D6-OH	2.82	-5.98	-3.20	2.78	5.98	3.15	-0.85	1.18	0.80
D6-OCH <sub>3</sub>	2.81	-5.94	-3.18	2.76	5.94	3.13	-0.87	1.14	0.82
D6-OC <sub>2</sub> H <sub>5</sub>	2.80	-5.92	-3.16	2.76	5.92	3.11	-0.89	1.12	0.84
D6-NH <sub>2</sub>	2.68	-5.71	-3.04	2.67	5.71	3.04	-0.96	0.91	0.96
D6-N(CH <sub>3</sub> ) <sub>2</sub>	2.58	-5.56	-2.97	2.59	5.56	2.98	-1.02	0.76	1.03
D6-PhCH <sub>3</sub>	2.80	-6.00	-3.28	2.72	6.00	3.21	-0.79	1.20	0.72
D6-PhNH <sub>2</sub>	2.69	-5.68	-3.17	2.51	5.68	2.99	-1.01	0.88	0.83

### Absorption spectra

In Table 2, the HOMO and LUMO energies, HOMO-LUMO energy gap (HLG), absorption maximum ( $\lambda_{\text{max}}$ ), and oscillator strength ( $f$ ) of six different D- $\pi$ -A systems with various substituents are reported. In all kinds of D- $\pi$ -A systems, a systematic increase in  $\lambda_{\text{max}}$  with respect to various substituents has been observed (388 to 490 nm), which can be correlated with the electron donating strength of the donors in the D- $\pi$ -A system. This is evident in the excellent linear correlations between  $\Delta V_{\text{MA}}$  and  $\lambda_{\text{max}}$  obtained for all six kinds of D- $\pi$ -A systems (Fig. 4). Also with an improved electron-donating strength of a D- $\pi$ -A system, lowering of HLG is noted in every system, which lies in the range 3.14 to 2.17 eV. Among all, the highest  $\lambda_{\text{max}}$  490 nm has been shown by (NH<sub>3</sub>)<sub>2</sub> substituted phenothiazine system D5-N(CH<sub>3</sub>)<sub>2</sub>. For the six D- $\pi$ -A systems and the selected eleven substituents, 102 nm width is available for tuning  $\lambda_{\text{max}}$  to a preferred region. For individual donors, the substituent effect alone can account for a tuning width of 69 nm for benzene, 29 nm for pyrene, 19 nm for TPA, 42 nm for carbazole, 31 nm for phenothiazine and 57 nm for coumarin, respectively.

The  $\Delta V_{\text{MA}}$  versus  $\lambda_{\text{max}}$  correlations given in Fig. 4 suggest that the substituent effects tune the HOMO-LUMO energy gap (HLG). The HLG plot of a representative system D5- $\pi$ -A

(phenothiazine-based) is given in Fig. 5 which shows that the introduction of substituents on the core D unit lowers the HLG from 2.41 to 2.17 eV. Poor electron-donating ability is observed in alkyls and PhCH<sub>3</sub> substituted systems display higher HLG (2.40 to 2.41 eV), while the lowest HLG has been attained with N(CH<sub>3</sub>)<sub>2</sub> substituted D5- $\pi$ -A. A similar trend in HLG is observed for the remaining systems which confirms the significance of the substituent effect in tuning  $\lambda_{\text{max}}$  (Table 3a and b). The HOMO and LUMO plots of the representative systems are shown in Fig. 6. The HOMO has a more delocalized distribution than the LUMO with more orbital contributions from the donor site while the LUMO is largely delocalized along the  $\pi$ -spacer and acceptor moiety.

### Photovoltaic performance

In Table 3a and b, electronic excitation energy, ground state oxidation potential  $E^{\text{dye}}$ , excited state oxidation potential  $E^{\text{dye}*}$ , free energy change of electron injection  $\Delta G_{\text{inject}}$ , free energy change of dye regeneration  $\Delta G_{\text{reg}}$ , and open-circuit voltage  $eV_{\text{OC}}$  of D- $\pi$ -A systems are described. The negative  $\Delta G_{\text{inject}}$  observed in the range -0.73 to -1.65 eV lies above the CB of TiO<sub>2</sub> (-4.0 eV) and indicates the possibility of a spontaneous electron injection process from CB to TiO<sub>2</sub>. Also a more electron-donating substituent enhances the electron injection process as  $\Delta G_{\text{inject}}$

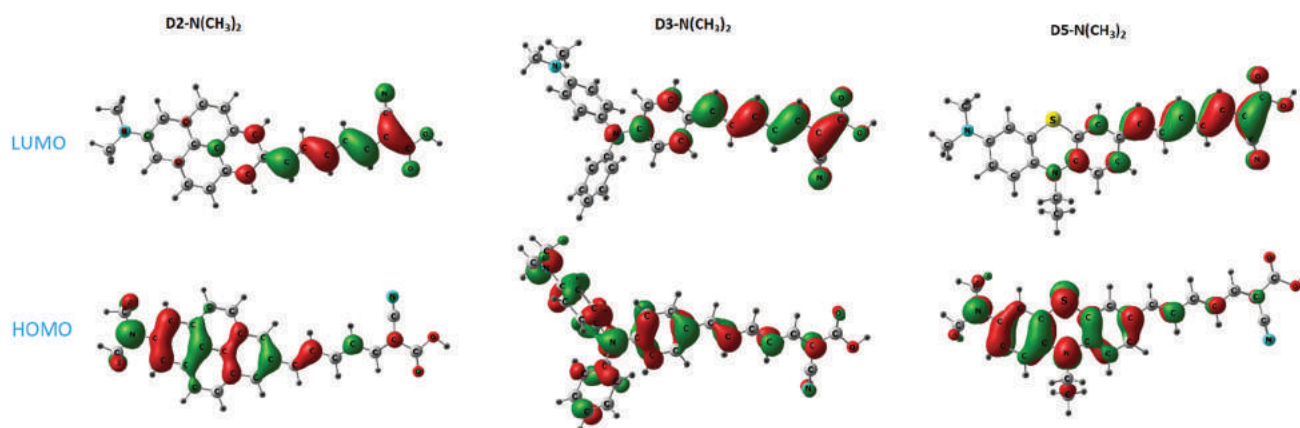


Fig. 6 Frontier molecular orbitals of representative N(CH<sub>3</sub>)<sub>2</sub> substituted D- $\pi$ -A systems at the B3LYP/cc-pVDZ level.

becomes more negative with such substituents. Alkyls, and PhCH<sub>3</sub> substituted D- $\pi$ -A systems are less efficient for electron injection than the OH, OCH<sub>3</sub>, OC<sub>2</sub>H<sub>5</sub>, NH<sub>2</sub> and N(CH<sub>3</sub>)<sub>2</sub> substituted systems. Among all, the most negative  $\Delta G_{\text{inject}} - 1.65$  eV is observed for phenothiazine system D5-N(CH<sub>3</sub>)<sub>2</sub>. The smaller electron injection efficiency ( $-0.79$  to  $-0.81$  eV) observed for alkyls and PhCH<sub>3</sub> substituted coumarin systems can be attributed to their lower electron-donating strength than others.

From the previous studies, it is understood that the PCE of DSSCs depends on the free energy change for dye regeneration.<sup>89,90</sup> The lower the  $\Delta G_{\text{reg}}$ , the faster the dye regeneration will be, leading to higher efficiency for the electron injection from the dye to the TiO<sub>2</sub> semiconductor. In the studied systems, the fastest dye regeneration force 0.08 eV has been attained by the N(CH<sub>3</sub>)<sub>2</sub> substituted phenothiazine system (D5-N(CH<sub>3</sub>)<sub>2</sub>), whereas the least dye regeneration (1.27–1.29 eV) has been possessed by alkyls, and PhCH<sub>3</sub> substituted coumarin systems. The unsubstituted systems always possess higher  $\Delta G_{\text{reg}}$  values (0.48–1.39 eV) than substituted ones (0.08–1.29 eV) and this suggests that the introduction of electron-donating substituents on the donor moiety gives better  $\Delta G_{\text{reg}}$  values and improves electron regeneration efficiency. Similarly, a positive effect of substituents on  $eV_{\text{OC}}$  is always observed confirming that by tuning the donating strength of the substituents, significant improvement in the performance of DSSCs can be achieved. In all the six sets, N(CH<sub>3</sub>)<sub>2</sub> substituted systems possess the best  $eV_{\text{OC}}$  and among them, the highest is observed for D1-N(CH<sub>3</sub>)<sub>2</sub> (1.38 eV) whereas the lowest  $eV_{\text{OC}}$  (0.72 eV) is observed for D4-PhCH<sub>3</sub>.

By considering the above-mentioned results, we analyzed the relation between electron donating strength  $\Delta V_{\text{MA}}$  and open-circuit voltage  $eV_{\text{OC}}$  (Fig. 7 and Fig. S1, ESI<sup>†</sup>). The excellent linear correlation observed in all six series of different D- $\pi$ -A systems shows that  $eV_{\text{OC}}$  increases with enhancement in the donating strength of the substituents. Overall the study suggests that by selecting the appropriate donor and substituent, precise tuning of the optical and photovoltaic properties of the D- $\pi$ -A systems can be achieved. Also these results point out that the theoretical examination of the donating strength of the substituents using MESP analysis is promising for dye designing and efficiency prediction of D- $\pi$ -A systems.

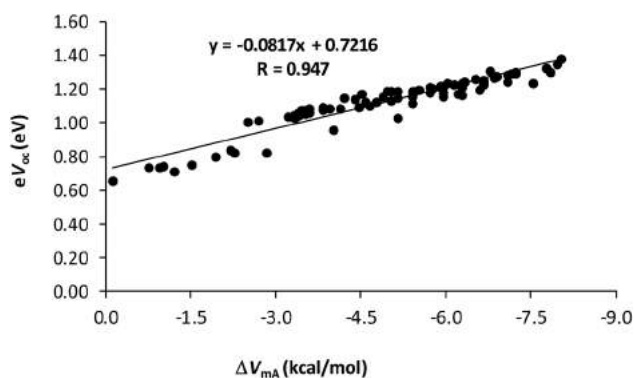


Fig. 7 Correlation between donating strength  $\Delta V_{\text{MA}}$  and open-circuit voltage  $eV_{\text{OC}}$  of D- $\pi$ -A systems.

## Conclusions

The electron-donating strength of the donors in the D- $\pi$ -A system affects the optical and photovoltaic performance of DSSCs, leading to better PCE in the solar cell. In the study using MESP analysis, we have characterized the donating strength ( $\Delta V_{\text{MA}}$ ) of six different sets of D- $\pi$ -A systems, wherein the  $\pi$  and A systems are butadiene and cyanoacrylic acid, respectively. The significance of eleven electron releasing groups at the donors is also examined for a total of seventy-two D- $\pi$ -A systems and achieved the fine-tuning of the electron donation from the donor to the acceptor. In all the six different sets of D- $\pi$ -A systems, the N(CH<sub>3</sub>)<sub>2</sub> substituted D- $\pi$ -A systems show the highest donating strength which can be attributed to the highest electron releasing nature of the N(CH<sub>3</sub>)<sub>2</sub> group. Also, the electron releasing groups at the donors tune the HOMO and LUMO energies of all the corresponding D- $\pi$ -A systems for better optical properties than unsubstituted systems. The optical and photovoltaic performance of the D- $\pi$ -A system is described at the CAM-B3LYP/cc-pVDZ/SMD//B3LYP/cc-pVDZ level. The enhanced performance of these properties achieved with enhanced donating strength conveys the role of tuning the donating strength for better PCE. Among all, the N(CH<sub>3</sub>)<sub>2</sub> substituted D1 system (benzene) possesses the highest  $eV_{\text{OC}}$  which can be attributed to its highest donating strength. These findings suggest that we can improve the photovoltaic performance of DSSCs by tuning the ground state property,  $\Delta V_{\text{MA}}$  at the acceptor site. All the findings imply that incorporation of more electron-releasing substituents on an electron-rich donor moiety improves/tunes the photovoltaic performance by facilitating efficient intramolecular charge transfer in the D- $\pi$ -A system. The correlation plot of  $\Delta V_{\text{MA}}$  with  $eV_{\text{OC}}$  will provide an efficient guideline for developing an effective dye designing strategy for desirable photovoltaic properties.

## Conflicts of interest

There are no conflicts to declare.

## Acknowledgements

The authors thank DST-SERB for funding through GAP1397 and also gratefully acknowledge the CSIR 4th PI for the HPC facility and NIIST IT lab for computational support. V. V. Divya thanks CSIR, India, for the senior research fellowship.

## References

- 1 J. Gong, K. Sumathy, Q. Qiao and Z. Zhou, *Renewable Sustainable Energy Rev.*, 2017, **68**, 234–246.
- 2 Y.-H. Chen, V. S. Nguyen, H.-H. Chou, Y. S. Tingare, T.-C. Wei and C.-Y. Yeh, *ACS Appl. Energy Mater.*, 2020, **3**, 5479–5486.
- 3 N. Mariotti, M. Bonomo, L. Fagiolari, N. Barbero, C. Gerbaldi, F. Bella and C. Barolo, *Green Chem.*, 2020, **22**, 7168–7218.



- 4 B. O'regan and M. Grätzel, *Nature*, 1991, **353**, 737.
- 5 M. K. Nazeeruddin, F. De Angelis, S. Fantacci, A. Selloni, G. Viscardi, P. Liska, S. Ito, B. Takeru and M. Grätzel, *J. Am. Chem. Soc.*, 2005, **127**, 16835–16847.
- 6 G. Marotta, M. A. Reddy, S. P. Singh, A. Islam, L. Han, F. De Angelis, M. Pastore and M. Chandrasekharam, *ACS Appl. Mater. Interfaces*, 2013, **5**, 9635–9647.
- 7 S. Yun, Y. Qin, A. R. Uhl, N. Vlachopoulos, M. Yin, D. Li, X. Han and A. Hagfeldt, *Energy Environ. Sci.*, 2018, **11**, 476–526.
- 8 L. L. Estrella, M. P. Balanay and D. H. Kim, *J. Phys. Chem. A*, 2018, **122**, 6328–6342.
- 9 M. Grätzel, *Nature*, 2001, **414**, 338–344.
- 10 S. Ito, S. M. Zakeeruddin, R. Humphry-Baker, P. Liska, R. Charvet, P. Comte, M. K. Nazeeruddin, P. Péchy, M. Takata and H. Miura, *Adv. Mater.*, 2006, **18**, 1202–1205.
- 11 S. Ito, H. Miura, S. Uchida, M. Takata, K. Sumioka, P. Liska, P. Comte, P. Péchy and M. Grätzel, *Chem. Commun.*, 2008, 5194–5196.
- 12 Q. Yu, Y. Wang, Z. Yi, N. Zu, J. Zhang, M. Zhang and P. Wang, *ACS Nano*, 2010, **4**, 6032–6038.
- 13 L. Han, A. Islam, H. Chen, C. Malapaka, B. Chiranjeevi, S. Zhang, X. Yang and M. Yanagida, *Energy Environ. Sci.*, 2012, **5**, 6057–6060.
- 14 L. E. Polander, A. Yella, J. Teuscher, R. Humphry-Baker, B. F. E. Curchod, N. Ashari Astani, P. Gao, J.-E. Moser, I. Tavernelli, U. Rothlisberger, M. Grätzel, M. K. Nazeeruddin and J. Frey, *Chem. Mater.*, 2013, **25**, 2642–2648.
- 15 S. Mathew, A. Yella, P. Gao, R. Humphry-Baker, B. F. Curchod, N. Ashari-Astani, I. Tavernelli, U. Rothlisberger, M. K. Nazeeruddin and M. Grätzel, *Nat. Chem.*, 2014, **6**, 242–247.
- 16 K. Kakiage, Y. Aoyama, T. Yano, T. Otsuka, T. Kyomen, M. Unno and M. Hanaya, *Chem. Commun.*, 2014, **50**, 6379–6381.
- 17 Y. S. Tingare, N. S. n. Vinh, H. H. Chou, Y. C. Liu, Y. S. Long, T. C. Wu, T. C. Wei and C. Y. Yeh, *Adv. Energy Mater.*, 2017, **7**, 1700032.
- 18 K. Sharma, V. Sharma and S. S. Sharma, *Nanoscale Res. Lett.*, 2018, **13**, 381.
- 19 X. Song, X. Yang, H. Wang, J. An, Z. Yu, X. Wang, A. Hagfeldt and L. Sun, *Sol. Energy*, 2019, **187**, 274–280.
- 20 P. Ferdowsi, Y. Saygili, F. Jazaeri, T. Edvinsson, J. Mokhtari, S. M. Zakeeruddin, Y. Liu, M. Grätzel and A. Hagfeldt, *ChemSusChem*, 2020, **13**, 212–220.
- 21 Y.-Q. Yan, Y.-Z. Zhu, P.-P. Dai, J. Han, M. Yan and J.-Y. Zheng, *New J. Chem.*, 2020, **44**, 12909–12915.
- 22 Y. Chiba, A. Islam, Y. Watanabe, R. Komiya, N. Koide and L. Han, *Jpn. J. Appl. Phys.*, 2006, **45**, L638.
- 23 F. Gao, Y. Wang, D. Shi, J. Zhang, M. Wang, X. Jing, R. Humphry-Baker, P. Wang, S. M. Zakeeruddin and M. Grätzel, *J. Am. Chem. Soc.*, 2008, **130**, 10720–10728.
- 24 S. Tan, J. Zhai, H. Fang, T. Jiu, J. Ge, Y. Li, L. Jiang and D. Zhu, *Chem. – Eur. J.*, 2005, **11**, 6272–6276.
- 25 A. Mishra, M. K. Fischer and P. Bäuerle, *Angew. Chem., Int. Ed.*, 2009, **48**, 2474–2499.
- 26 T. Mori, H. Saomoto, K. Machitani, K. Inoue, Y. Aoki, T. Koshitani, N. Koumura and T. N. Murakami, *RSC Adv.*, 2016, **6**, 13964–13970.
- 27 K. Hara, Y. Dan-oh, C. Kasada, Y. Ohga, A. Shinpo, S. Suga, K. Sayama and H. Arakawa, *Langmuir*, 2004, **20**, 4205–4210.
- 28 K. Hara, T. Sato, R. Katoh, A. Furube, T. Yoshihara, M. Murai, M. Kurashige, S. Ito, A. Shinpo and S. Suga, *Adv. Funct. Mater.*, 2005, **15**, 246–252.
- 29 R. Chen, X. Yang, H. Tian, X. Wang, A. Hagfeldt and L. Sun, *Chem. Mater.*, 2007, **19**, 4007–4015.
- 30 Z.-S. Wang, Y. Cui, Y. Dan-oh, C. Kasada, A. Shinpo and K. Hara, *J. Phys. Chem. C*, 2007, **111**, 7224–7230.
- 31 S. Hwang, J. H. Lee, C. Park, H. Lee, C. Kim, C. Park, M.-H. Lee, W. Lee, J. Park and K. Kim, *Chem. Commun.*, 2007, 4887–4889.
- 32 J. Preat, D. Jacquemin, C. Michaux and E. A. Perpète, *Chem. Phys.*, 2010, **376**, 56–68.
- 33 H. Tian, I. Bora, X. Jiang, E. Gabrielsson, K. M. Karlsson, A. Hagfeldt and L. Sun, *J. Mater. Chem.*, 2011, **21**, 12462–12472.
- 34 A. Dhar, N. Siva Kumar, M. Asif and R. L. Vekariya, *New J. Chem.*, 2018, **42**, 12024–12031.
- 35 Y. Ren, D. Sun, Y. Cao, H. N. Tsao, Y. Yuan, S. M. Zakeeruddin, P. Wang and M. Grätzel, *J. Am. Chem. Soc.*, 2018, **140**, 2405–2408.
- 36 T. Kitamura, M. Ikeda, K. Shigaki, T. Inoue, N. A. Anderson, X. Ai, T. Lian and S. Yanagida, *Chem. Mater.*, 2004, **16**, 1806–1812.
- 37 D. P. Hagberg, T. Marinado, K. M. Karlsson, K. Nonomura, P. Qin, G. Boschloo, T. Brinck, A. Hagfeldt and L. Sun, *J. Org. Chem.*, 2007, **72**, 9550–9556.
- 38 H. Tian, X. Yang, R. Chen, R. Zhang, A. Hagfeldt and L. Sun, *J. Phys. Chem. C*, 2008, **112**, 11023–11033.
- 39 J. Zhang, H.-B. Li, S.-L. Sun, Y. Geng, Y. Wu and Z.-M. Su, *J. Mater. Chem.*, 2012, **22**, 568–576.
- 40 J. Zhang, Y.-H. Kan, H.-B. Li, Y. Geng, Y. Wu and Z.-M. Su, *Dyes Pigm.*, 2012, **95**, 313–321.
- 41 Z. Yao, L. Yang, Y. Cai, C. Yan, M. Zhang, N. Cai, X. Dong and P. Wang, *J. Phys. Chem. C*, 2014, **118**, 2977–2986.
- 42 T. Horiuchi, H. Miura, K. Sumioka and S. Uchida, *J. Am. Chem. Soc.*, 2004, **126**, 12218–12219.
- 43 W. Xu, B. Peng, J. Chen, M. Liang and F. Cai, *J. Phys. Chem. C*, 2008, **112**, 874–880.
- 44 J. Preat, *J. Phys. Chem. C*, 2010, **114**, 16716–16725.
- 45 D. Patil, M. Jadhav, K. Avhad, T. H. Chowdhury, A. Islam, I. Bedja and N. Sekar, *New J. Chem.*, 2018, **42**, 11555–11564.
- 46 H.-L. Jia, Z.-J. Peng, Y.-C. Chen, C.-Y. Huang and M.-Y. Guan, *New J. Chem.*, 2018, **42**, 18702–18707.
- 47 L. Zhang, W. Shen, R. He, X. Liu, Z. Fu and M. Li, *J. Mol.*, 2014, **20**, 2489.
- 48 N. Inostroza, F. Mendizabal, R. Arratia-Pérez, C. Orellana and C. Linares-Flores, *J. Mol. Model.*, 2016, **22**, 25.
- 49 S. Gauthier, F. Robin-Le Guen, L. Wojcik, N. Le Poul, A. Planchat, Y. Pellegrin, P. G. Level, N. Szuwarski, M. Boujtita and D. Jacquemin, *Dyes Pigm.*, 2019, **171**, 107747.

- 50 V. V. Divya, F. B. Sayyed and C. H. Suresh, *ChemPhysChem*, 2019, **20**, 1752–1758.
- 51 S. R. Gadre, S. A. Kulkarni and I. H. Shrivastava, *J. Chem. Phys.*, 1992, **96**, 5253–5260.
- 52 S. R. Gadre and R. N. Shirsat, *Electrostatics of Atoms and Molecules*, Universities Press, 2000.
- 53 P. Politzer and D. G. Truhlar, *Chemical Applications of Atomic and Molecular Electrostatic potentials: Reactivity, Structure, Scattering, and Energetics of Organic, Inorganic, and Biological systems*, Springer Science & Business Media, 2013.
- 54 C. H. Suresh and N. Koga, *Inorg. Chem.*, 2002, **41**, 1573–1578.
- 55 C. H. Suresh, *Inorg. Chem.*, 2006, **45**, 4982–4986.
- 56 J. Mathew, T. Thomas and C. H. Suresh, *Inorg. Chem.*, 2007, **2007**(46), 10800–10809.
- 57 G. S. Remya and C. H. Suresh, *Phys. Chem. Chem. Phys.*, 2016, **18**, 20615–20626.
- 58 E. Scrocco and J. Tomasi, *New concepts II*, Springer, 1973, pp. 95–170.
- 59 J. S. Murray and P. Politzer, *Wiley Interdiscip. Rev.: Comput. Mol. Sci.*, 2011, **1**, 153–163.
- 60 F. B. Sayyed and C. H. Suresh, *New J. Chem.*, 2009, **33**, 2465–2471.
- 61 C. H. Suresh, P. Alexander, K. P. Vijayalakshmi, P. K. Sajith and S. R. Gadre, *Phys. Chem. Chem. Phys.*, 2008, **10**, 6492–6499.
- 62 F. B. Sayyed and C. H. Suresh, *Tetrahedron Lett.*, 2009, **50**, 7351–7354.
- 63 P. K. Sajith and C. H. Suresh, *Inorg. Chem.*, 2012, **51**, 967–977.
- 64 F. B. Sayyed and C. H. Suresh, *J. Phys. Chem. A*, 2011, **115**, 9300–9307.
- 65 V. V. Divya and C. H. Suresh, *New J. Chem.*, 2020, **44**, 7200–7209.
- 66 L. Liu, L. Miao, L. Li, F. Li, Y. Lu, Z. Shang and J. Chen, *J. Phys. Chem. Lett.*, 2018, **9**, 3573–3579.
- 67 M. R. Narayan, *Renewable Sustainable Energy Rev.*, 2012, **16**, 208–215.
- 68 L. M. Fraas and L. D. Partain, *Solar Cells and Their Applications*, John Wiley & Sons, 2010.
- 69 Y. Tachibana, K. Hara, K. Sayama and H. Arakawa, *Chem. Mater.*, 2002, **2002**(14), 2527–2535.
- 70 A. Mihi and H. Míguez, *J. Phys. Chem. B*, 2005, **109**, 15968–15976.
- 71 J. Preat, C. Michaux, D. Jacquemin and E. A. Perpète, *J. Phys. Chem. C*, 2009, **113**, 16821–16833.
- 72 R. Katoh, A. Furube, T. Yoshihara, K. Hara, G. Fujihashi, S. Takano, S. Murata, H. Arakawa and M. Tachiya, *J. Phys. Chem. B*, 2004, **108**, 4818–4822.
- 73 N. N. Ghosh, M. Habib, A. Pramanik, P. Sarkar and S. Pal, *New J. Chem.*, 2019, **43**, 6480–6491.
- 74 J. B. Asbury, Y.-Q. Wang, E. Hao, H. N. Ghosh and T. Lian, *Res. Chem. Intermed.*, 2001, **27**, 393–406.
- 75 T. Koopmans, *Physica*, 1933, **1**, 104–113.
- 76 W.-L. Ding, D.-M. Wang, Z.-Y. Geng, X.-L. Zhao and Y.-F. Yan, *J. Phys. Chem. C*, 2013, **117**, 17382–17398.
- 77 G. Boschloo and A. Hagfeldt, *Acc. Chem. Res.*, 2009, **42**, 1819–1826.
- 78 C.-R. Zhang, Z.-J. Liu, Y.-H. Chen, H.-S. Chen, Y.-Z. Wu, W. Feng and D.-B. Wang, *Curr. Appl. Phys.*, 2010, **10**, 77–83.
- 79 A. D. Becke, *J. Chem. Phys.*, 1993, **98**, 1372–1377.
- 80 T. H. Dunning Jr, *Chem. Phys.*, 1989, **90**, 1007–1023.
- 81 H. Gotfredsen, T. Neumann, F. E. Storm, A. V. Muñoz, M. Jevric, O. Hammerich, K. V. Mikkelsen, M. Freitag, G. Boschloo and M. B. Nielsen, *ChemPhotoChem*, 2018, **2**, 976–985.
- 82 M. Pastore, E. Mosconi, F. De Angelis and M. Grätzel, *J. Phys. Chem. C*, 2010, **114**, 7205–7212.
- 83 T. Yanai, D. P. Tew and N. C. Handy, *Chem. Phys. Lett.*, 2004, **393**, 51–57.
- 84 A. V. Marenich, C. J. Cramer and D. G. Truhlar, *J. Phys. Chem. B*, 2009, **113**, 6378–6396.
- 85 M. J. Frisch, G. W. Trucks, H. B. Schlegel, G. E. Scuseria, M. A. Robb, J. R. Cheeseman, G. Scalmani, V. Barone, G. A. Petersson, H. Nakatsuji, X. Li, M. Caricato, A. V. Marenich, J. Bloino, B. G. Janesko, R. Gomperts, B. Mennucci, H. P. Hratchian, J. V. Ortiz, A. F. Izmaylov, J. L. Sonnenberg, D. Williams-Young, F. Ding, F. Lipparini, F. Egidi, J. Goings, B. Peng, A. Petrone, T. Henderson, D. Ranasinghe, V. G. Zakrzewski, J. Gao, N. Rega, G. Zheng, W. Liang, M. Hada, M. Ehara, K. Toyota, R. Fukuda, J. Hasegawa, M. Ishida, T. Nakajima, Y. Honda, O. Kitao, H. Nakai, T. Vreven, K. Throssell, J. A. Montgomery Jr., J. E. Peralta, F. Ogliaro, M. J. Bearpark, J. J. Heyd, E. N. Brothers, K. N. Kudin, V. N. Staroverov, T. A. Keith, R. Kobayashi, J. Normand, K. Raghavachari, A. P. Rendell, J. C. Burant, S. S. Iyengar, J. Tomasi, M. Cossi, J. M. Millam, M. Klene, C. Adamo, R. Cammi, J. W. Ochterski, R. L. Martin, K. Morokuma, O. Farkas, J. B. Foresman and D. J. Fox, *Gaussian 16, Revision A.03*, Gaussian, Wallingford, CT, 2016.
- 86 R. Menzel, D. Ogermann, S. Kupfer, D. Wei, G. Helmar, K. Kleinermanns, L. González and R. Beckert, *Dyes Pigm.*, 2012, **94**, 512–524.
- 87 S. Kupfer, J. Guthmuller and L. Gonzalez, *J. Chem. Theory Comput.*, 2013, **9**, 543–554.
- 88 A. Kumar, S. R. Gadre, N. Mohan and C. H. Suresh, *J. Phys. Chem. A*, 2014, **118**, 526–532.
- 89 S. M. Feldt, G. Wang, G. Boschloo and A. Hagfeldt, *J. Phys. Chem. C*, 2011, **115**, 21500–21507.
- 90 W. Yang, N. Vlachopoulos, Y. Hao, A. Hagfeldt and G. Boschloo, *Phys. Chem. Chem. Phys.*, 2015, **17**, 15868–15875.



Cite this: DOI: 10.1039/d1nj00881a

# Design and DFT study of nitrogen-rich donor systems for improved photovoltaic performance in dye-sensitized solar cells†

 Velayudhan V. Divya<sup>ab</sup> and Cherumuttathu H. Suresh \*<sup>ab</sup>

Eighteen electron-rich nitrogen incorporated donors with a butadiene  $\pi$ -spacer and a cyanoacrylic acid acceptor (A) as photosensitizers (D1- $\pi$ -A to D18- $\pi$ -A) for dye-sensitized solar cell (DSSC) applications have been designed for improving the photovoltaic performance. The significance of the nitrogen centres for revamping the donating strength ( $\Delta V_{\text{mA}}$ ) of D- $\pi$ -A is scrutinized using molecular electrostatic potential (MESP) analysis at the B3LYP/cc-pVDZ level of density functional theory (DFT). During the transformation of a donor (D) to D- $\pi$ -A, a certain delocalization of electron density from D to  $\pi$ -A has occurred, and the change in the MESP minimum ( $\Delta V_{\text{mA}}$ ) observed at the cyano region of D- $\pi$ -A is related to the donating strength of D. Optical and photovoltaic properties are analyzed at the TD/CAM-B3LYP/cc-pVDZ/SMD//B3LYP/cc-pVDZ level. In D1- $\pi$ -A to D18- $\pi$ -A,  $\Delta V_{\text{mA}}$  is in the range  $-7.0$  to  $-19.0$  kcal mol<sup>-1</sup> and the increase in donating strength is found to be proportional to the number of planar nitrogens in the donors. D12- $\pi$ -A exhibited the most negative  $\Delta V_{\text{mA}}$  ( $-19.0$  kcal mol<sup>-1</sup>), indicating the highest electron-donating strength of D12, whereas the least negative  $\Delta V_{\text{mA}}$  ( $-7.0$  kcal mol<sup>-1</sup>) displayed by D7- $\pi$ -A is correlated to the weak donating character of D7. By increasing the electron-donating strength of D in D- $\pi$ -A, a red-shift in the absorption maximum ( $\Delta\lambda_{\text{max}}$ ) by 162 to 294 nm is observed. Further, the open-circuit voltage ( $eV_{\text{oc}}$ ) calculated for the D- $\pi$ -A systems showed a strong linear relationship with  $\Delta V_{\text{mA}}$ . The LUMO (lowest unoccupied molecular orbital) energy of all the D- $\pi$ -A systems ( $-1.79$  to  $-2.79$  eV) is observed above the conduction band (CB) energy of TiO<sub>2</sub> ( $-4.0$  eV), which ensured a desirable electron injection efficiency ( $\Delta G_{\text{inject}}$ ) for them. The analysis of the adsorption energy ( $E_{\text{ads}}$ ) of the D- $\pi$ -A systems on the TiO<sub>2</sub> semiconductor (D- $\pi$ -A/TiO<sub>2</sub>) showed that D12- $\pi$ -A has the highest adsorption stability. Improving the adsorption stability is better for improving  $eV_{\text{oc}}$  and the power conversion efficiency (PCE). The maximum absorption wavelength ( $\lambda_{\text{max}}$ ) of the D- $\pi$ -A/TiO<sub>2</sub> systems ranges from 513 to 703 nm and all of them display a red-shift with respect to the bare D- $\pi$ -A systems. The study suggests D12 as the most efficient photosensitizer for DSSC applications. Further, it deepens the understanding of the structure-performance relationship of D- $\pi$ -A systems as photosensitizers.

 Received 21st February 2021,  
 Accepted 22nd May 2021

DOI: 10.1039/d1nj00881a

[rsc.li/njc](http://rsc.li/njc)

## Introduction

The utilization of a renewable source of energy, preferably solar energy, for the ever-growing energy demand could diminish global climate change, which leads to sustainable livelihood on earth.<sup>1-4</sup> Since solar energy is the most abundant green energy alternative for the future energy crisis, more research efforts have to invest in the development of photovoltaic strategies

based on solar power.<sup>1,3-5</sup> Over the past three decades, the third generation photovoltaic technology employed in dye-sensitized solar cells (DSSCs) has acquired a notable position over conventional silicon-based solar cells due to the simple synthetic strategy, easier structure modification, large absorption coefficient, and low production cost.<sup>3,5-11</sup> The major components employed in a DSSC device include photosensitizers, electrolytes, and electrode materials; modifications in those components lead to the enhancement of the power conversion efficiency (PCE) of the solar cell.<sup>12</sup> Generally in DSSCs, Ru-based sensitizers have greater PCEs than organic dye sensitizers, which show a comparable PCE to silicon-based solar cells.<sup>3</sup> Whereas, the highly expensive nature and rare chance of occurrence of Ru-metal mean that its practical application in DSSCs is limited.<sup>3,13</sup>

<sup>a</sup> Chemical Sciences and Technology Division, CSIR-National Institute for Interdisciplinary Science and Technology, Thiruvananthapuram, Kerala 695 019, India. E-mail: sureshch@niist.res.in

<sup>b</sup> Academy of Scientific and Innovative Research (AcSIR), Ghaziabad 201002, India

† Electronic supplementary information (ESI) available. See DOI: 10.1039/d1nj00881a

After the invention of the DSSC device by O'Regan and Grätzel in 1991,<sup>6</sup> extensive research efforts have been invested in the synthesis and device modelling of metal-free organic sensitizers, which leads to the improvement of the PCE.<sup>13–21</sup> Usually, organic sensitizers comprise a D- $\pi$ -A framework where D,  $\pi$ , and A denote the donor,  $\pi$ -spacer and acceptor, respectively. So far large varieties of structural modifications in the D- $\pi$ -A structural framework have been performed, reveal that tuning the donating strength of the donor could significantly influence the absorption range and photovoltaic parameters.<sup>12,22–29</sup> In our previous study, we quantified the electron-donating strength of eight typically used donor systems, *viz* pyrene, perylene, chrysene, triphenylamine, carbazole, phenothiazine, julolidine, *N,N*-dialkylaniline, ullazine and coumarin, in the D- $\pi$ -A system and revealed that julolidine and *N,N*-dialkylaniline based  $\pi$ -A systems are the most efficient sensitizers for DSSCs.<sup>22</sup> For improved optical and photovoltaic properties of D- $\pi$ -A systems the particular analysis recommends the incorporation of electron-rich heteroatoms (preferably nitrogen) in donors. The literature shows that non-planar donors, especially triphenylamine, carbazole and indoline, reduce the electron transfer ability and overall conjugation in the donor group with the  $\pi$ -A system leading to lower light-harvesting efficiency of the dye sensitizer.<sup>30,31</sup> The mentioned reducing factors are rectified through the introduction of planarized nitrogen incorporated donors *viz.* ullazine and indolizine as photosensitizers.<sup>30–33</sup> Further, the rational design of photosensitizers with nitrogen annulation at the bay region of a polycyclic aromatic hydrocarbon (PAH) system provides a remarkable PCE in DSSCs.<sup>34</sup> For example, perylene based PAH systems as donors in DSSCs have disappointing PCEs,<sup>35–37</sup> whereas an N-annulated perylene (NP) core as a donor with phenyl functional groups results in an improved PCE of about 10.5%.<sup>38</sup> Later, Wang *et al.* modified the NP core with bulky substituents to obtain PCEs up to 10.4%.<sup>39</sup> This re-engineered chromophore was again modified with an N-annulated indenoperylene unit as the donor and reached a PCE of 12.5%.<sup>40</sup> The aforementioned studies reveal that structural modifications with N-annulation in PAH systems enhance the intramolecular charge transfer (ICT) due to the planar structure. Also, the multiple substitution sites involved in PAHs increase the possibility of molecular engineering. Recently Subramanian *et al.* described that a more N-doped polyaromatic hydrocarbon analogue of ullazine contributes a large dipole moment and more planarization to the dye-sensitizers, thus resulting in higher light-harvesting efficiency (LHE) than the donors with a single N-doping site.<sup>25</sup>

In this context, the most significant approach for an efficient photosensitizer is the engineering of electron-rich planar donors. Correspondingly, it is worthwhile to evaluate the role of nitrogen centres in donors for enhancing the donating strength. To tackle the failings of the electron transfer ability and overall conjugation in the donor group with the  $\pi$ -A system, we designed eighteen electron-rich nitrogen incorporated donors (D1–D18) as dye sensitizers for DSSC application (Fig. 1). For the  $\pi$ -A framework, butadiene and cyanoacrylic acid have been considered. In our previous study,<sup>41</sup> we proved

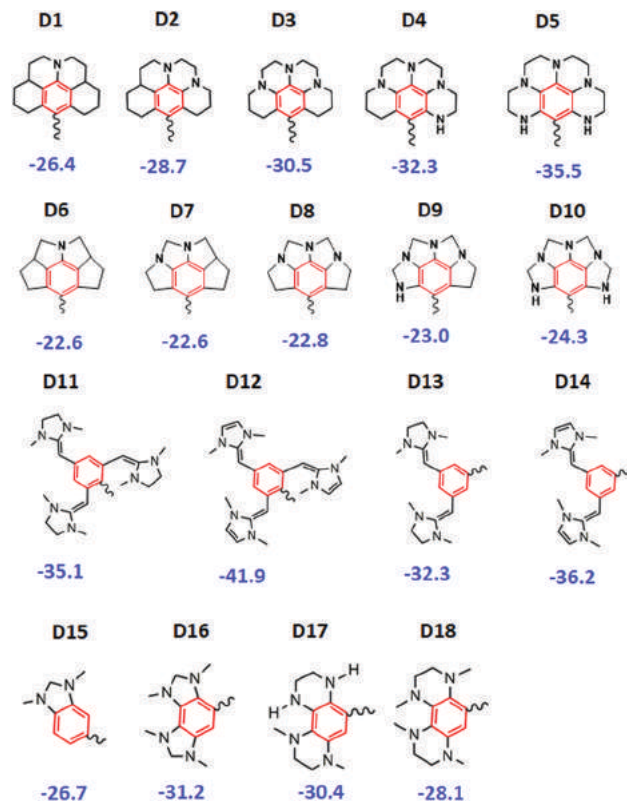


Fig. 1 Designed donor systems. The MESP minimum over the phenyl ring ( $V_{md}$ ) is given in kcal mol<sup>-1</sup>.

that butadiene exhibits better electronic effect transmitting power than thiophene, furan and benzylic spacers. Hence, for better electronic charge transfer from D to A, a butadiene  $\pi$ -spacer and cyanoacrylic acid as an acceptor have been considered.

In the analysis, the D1–D5 donors are designed from known donor julolidine (Fig. S1a, ESI<sup>†</sup>), where the possibility of N-annulation in the julolidine core has been attempted (D1 to D5) to enhance the electron-donating strength of the designed systems compared to julolidine (the calculated electron-donating strength,  $\Delta V_{mA}$ , of julolidine by MESP analysis is  $-9.2$  kcal mol<sup>-1</sup><sup>22</sup>). Julolidine is an N-heterocyclic aromatic compound which comprises alkyl bridges between amino nitrogen and ring *ortho* carbon atoms.<sup>42,43</sup> Because of the high efficiency in energy conversion and fluorescent properties, julolidine derivatives have been used in the construction of dye-sensitized solar cells and photoconductive materials, as fluorescent sensors for bio-imaging, *etc.*<sup>44</sup> The conjugation of the aromatic part of the molecule with its amino substituent is an indicator of the ability of the nitrogen atom to possess  $sp^2$ -hybridization, which enhances the donating strength of this class of compounds.<sup>45</sup> In D6–D10, five-membered rings at the aromatic ring system have been considered for N-annulation; those systems are derived from 1,2,4,5-tetrahydropyrrolo[3,2,1-hi]indole (Fig. S1b, ESI<sup>†</sup>).<sup>43</sup> Among the designed N-heterocyclic systems (D1–D10), some of the derivatives are known and they are the best candidates for intramolecular cyclization and for generating diboryne nanowires.<sup>46,47</sup> Donors D11–D14 are



designed from the electron-rich nature of the phenyl/ $\pi$ -system. According to various experimental and theoretical studies, the electron-rich nature of the phenyl/ $\pi$ -system could be fine-tuned by electron-donating substituents and hence the aromatic ring of 1,3,5-*N,N*-dimethyltriaminobenzene could be considered as the most electron-rich neutral six-membered ring.<sup>48</sup> Previously, Suresh and Sayyed described that the electron density at the phenyl ring could be significantly improved by the treatment of *N*-heterocyclic ring substitution and they proposed two highly electron rich systems *viz.* D11 and D12 as shown in Fig. 1.<sup>48</sup> Since those systems are considered as electron rich (involving six nitrogen lone pairs), we could test the suitability of those systems as photosensitizers for DSSC application. Finally, two, and four nitrogens have been integrated in D15–D18, where the likelihood of *N*-annulation has been attained through *N*-heterocyclic five and six membered rings.<sup>49,50</sup>

For evaluating the donating strength of the donors in *D*– $\pi$ –*A*, the intramolecular charge transfer (ICT) from *D* to *A* has to be assessed. Here it has been quantified in terms of the change in the molecular electrostatic potential (MESP) minimum,  $\Delta V_m$ , at the cyano group of *A*. Very recently we proved that the MESP is an excellent tool to quantify the electron-donating strength ( $\Delta V_m$ ) of *D*– $\pi$ –*A* systems.<sup>22,26</sup> It is a real physical property which is experimentally observable from X-ray diffraction studies. To understand the reactivity of molecular systems, theoretically derived MESP have been extensively used in the work of Tomasi,<sup>51</sup> Pullman,<sup>52,53</sup> Politzer<sup>54–57</sup> and Gadre,<sup>58–60</sup> and the wide range of applications in chemical and biological phenomena shows the acceptability of this area of research. Further, our group has contributed to several applications of the MESP parameter in organic and inorganic chemistry and described that the MESP is an excellent tool for the prediction of structure–property relationships.<sup>61–71</sup> In the present study the significance of *N*-annulation for improved optical and photovoltaic properties has been evaluated using density functional theory (DFT) and time-dependent DFT (TDDFT) calculations. Currently, quantum chemical calculations have emerged as an elementary tactic to identify potential sensitizers before long-running expensive synthesis.<sup>72–78</sup> Thus our computationally engineered dye sensitizers could open up new synthetic strategies for the development of photosensitizers for DSSC application.

## Computational details

Density functional theory (DFT) calculations at the B3LYP/cc-pVDZ level have been conducted for the optimization of the ground state geometries of the *D*– $\pi$ –*A* systems.<sup>79,80</sup> It is substantiated that the B3LYP level is adequate for the explanation of the electronic structure of dye molecules in DSSC applications.<sup>26,81,82</sup> The ground state geometries of all *D*– $\pi$ –*A* systems after binding to the (TiO<sub>2</sub>)<sub>9</sub> cluster are optimized at the same level of DFT with the LANL2DZ basis set for the Ti atom and cc-pVDZ for non-metal atoms.<sup>83</sup> Vibrational frequencies are calculated at the same level and it is confirmed that there are no imaginary frequencies. Studies show that the (TiO<sub>2</sub>)<sub>9</sub>

cluster size is sufficient to model the dye–TiO<sub>2</sub> interfaces for simulating the electronic structure, optical properties, and binding modes of TiO<sub>2</sub>.<sup>84</sup> Frontier molecular orbital energies of all *D*– $\pi$ –*A* and *D*– $\pi$ –*A* adsorbed on (TiO<sub>2</sub>)<sub>9</sub> cluster systems (*D*– $\pi$ –*A*/TiO<sub>2</sub>) are reported for the ground-state geometries. The optical properties of the *D*– $\pi$ –*A* systems before and after binding to the (TiO<sub>2</sub>)<sub>9</sub> cluster are simulated using time-dependent DFT (TD DFT) at the CAM-B3LYP level<sup>85</sup> on the ground state geometry with mixed basis sets. To account for the solvent effect (dichloromethane as the solvent), SCRF-SMD (self-consistent reaction field-density simulation model) incorporated in the Gaussian 16 suite of programs has been considered. The CAM-B3LYP exchange–correlation functional is widely used in theoretical calculations for the excited state properties and provides results that are close to experimental results.<sup>86–88</sup> In our previous study, the absorption properties of experimentally known dye sensitizers have been benchmarked including julolidine based dye-sensitizers and it is found that the TD-CAM B3LYP/cc-pVDZ/SMD//B3LYP/cc-pVDZ level is adequate to describe the electronic, optical and photovoltaic properties.<sup>22</sup> The higher excitation energy associated with the CAM-B3LYP exchange functional than the B3LYP functional can be attributed to the higher bond length alteration index (BLA) of *D*– $\pi$ –*A* systems.<sup>26</sup> Moreover, for the examination of the intramolecular charge transfer characteristics of *D*– $\pi$ –*A* systems, molecular electrostatic potential based topographical analysis has been performed on the ground state geometry at the B3LYP/cc-pVDZ level. All the calculations are performed with the Gaussian 16 program package.<sup>89</sup>

The molecular electrostatic potential (MESP),  $V(\mathbf{r})$ , is an important property of a molecule that its nuclei and electrons create at every point  $\mathbf{r}$  in the surrounding space, which is defined in eqn (1) as

$$V(\mathbf{r}) = \sum_A^N \frac{Z_A}{|\mathbf{r} - \mathbf{R}_A|} - \int \frac{\rho(\mathbf{r}')d\mathbf{r}'}{|\mathbf{r} - \mathbf{r}'|} \quad (1)$$

where  $N$  is the total number of nuclei,  $Z_A$  is the charge on nucleus  $A$  located at distance  $R_A$ ,  $\rho(\mathbf{r}')$  is the electron density of the molecule, and  $\mathbf{r}'$  is a dummy integration variable. In the equation, the sign of  $V(\mathbf{r})$  at any  $\mathbf{r}$  depends upon whether the positive contribution of the nuclei or the negative one of the electrons is dominant there.

## Results and discussion

### MESP analysis of the donors

The MESP minimum  $V_m$  gives a clear idea regarding the most electron-rich region in a molecular system. In all the donor systems (D1–D18), an aromatic phenyl ring (shown in a red colour, Fig. 1) has been observed and  $V_m$  observed at that phenyl ring,  $V_{mD}$ , has been considered as the donor strength of each system. The most negative  $V_m$  depicts the most electron-rich nature of the molecular system. From D1 to D5, a systematic increase in the *N*-centers (up to 5 nitrogens) is introduced and  $V_{mD}$  reached  $-35.5$  kcal mol<sup>-1</sup> from  $-26.4$  kcal mol<sup>-1</sup>. The more

negative  $V_{\text{mD}}$  in D5 ( $-35.5 \text{ kcal mol}^{-1}$ ) than those of D1–D4 characterizes the more electron-rich nature, which can be attributed to the occurrence of five nitrogen centers. In the D6–D10 donors, an increase in the negative character of  $V_{\text{mD}}$  (from  $-22.6$  to  $-24.3 \text{ kcal mol}^{-1}$ ) has been attained by a systematic increase of the nitrogen atoms (up to 5 nitrogens). Meanwhile, due to the presence of more pyramidalized nitrogens, the D6–D10 donors provide less negative  $V_{\text{mD}}$  than those of D1–D5.

In the D11–D12 donors, imidazolidine and imidazole ring systems have been introduced at the 1, 3, and 5 positions of the benzene ring. In D11, the electron-rich aminal functional groups increase the electron density over the phenyl ring, resulting in a comparable  $V_{\text{mD}}$  of  $-35.1 \text{ kcal mol}^{-1}$  to D5 ( $-35.5 \text{ kcal mol}^{-1}$ ). In D12 the conjugation in the CC bond enhances the electron density over the phenyl ring, leading to a more negative  $V_{\text{mD}}$  ( $-41.9 \text{ kcal mol}^{-1}$ ) than D11. Due to the reduced number of aminal functional groups at the phenyl ring, D13 shows a less negative  $V_{\text{mD}}$  ( $-32.3 \text{ kcal mol}^{-1}$ ) than those of D11 and D12. In D14, conjugation increases the electron density of the donor system, resulting in a more negative  $V_{\text{mD}}$  ( $-36.2 \text{ kcal mol}^{-1}$ ) than D13. It is noted that the imidazolidine and imidazole substituted donor systems *viz.* D12 and D14 exhibit more negative  $V_{\text{mD}}$  than D5, which can be considered as their better donor strength. Finally, for verifying the effectiveness of the introduced strategy, the D15–D18 donors are examined. In D16 the increased number of *N*-alkyl substitutions at the phenyl ring resulted in a more negative  $V_{\text{mD}}$  ( $-31.2 \text{ kcal mol}^{-1}$ ) than D15 ( $V_{\text{mD}} = -26.7 \text{ kcal mol}^{-1}$ ). Compared to D15, a more negative  $V_{\text{mD}}$  is observed for D17, which can be attributed to the presence of an additional two nitrogen centres. Finally, in D18 the additional two methyl groups at nitrogen atoms promote pyramidalization of the *N*-centres, resulting in a less negative  $V_{\text{mD}}$  ( $-28.1 \text{ kcal mol}^{-1}$ ) than D17.

### Donating strength of the D- $\pi$ -A systems

The influence of the electron-rich nitrogen lone pairs in the donors (D) for enhancing the electron-donating strength of the D- $\pi$ -A system ( $\Delta V_{\text{mA}}$ ) has been elucidated with MESP analysis. In D- $\pi$ -A systems, the  $\pi$ -A linkage with the donor involves intramolecular charge transfer (ICT) from D to A, and the transferred electron density accumulated at A depends on the donor strength of each system.<sup>22,26</sup> The electron density distribution *via* ICT at various regions of a representative D- $\pi$ -A system (D1- $\pi$ -A), *viz.* D, the  $\pi$ -spacer and A, has been shown in Fig. 2b as the MESP minima at the donor  $V_{\text{mD}'}$ , spacer  $V_{\text{mS}'}$  and acceptor  $V_{\text{mA}'}$ . Since the  $\pi$ -A part (butadiene) involved in the study is the same for all D- $\pi$ -A systems, the MESP minimum observed at the CN group of A has been considered as the reference  $V_{\text{mA}}$  to evaluate the changes observed at that minimum with the attachment of D (Fig. 2a). Also, it is proved that one could take other  $V_{\text{m}}$  regions at A as the reference  $V_{\text{m}}$  *viz.*  $V_{\text{m(OH)}}$  and  $V_{\text{m(CO)}}$  for monitoring the changes at the respective sites due to the parallel behavior exhibited by those parameters.<sup>26</sup> In the study,  $V_{\text{mA}'}$  (observed at the CN region) has been selected as the reference point due to the most negative  $V_{\text{m}}$  character.

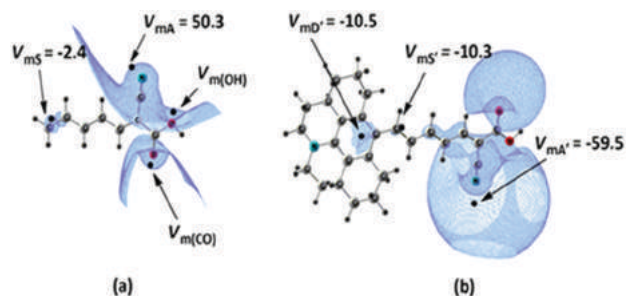


Fig. 2 (a) MESP isosurface at various sites of (a) the reference system, and (b) a representative D- $\pi$ -A system, where the MESP minimum is shown in  $\text{kcal mol}^{-1}$ .

Table 1  $V_{\text{m}}$  ( $\text{kcal mol}^{-1}$ ) of the D- $\pi$ -A systems calculated at the B3LYP/cc-pVDZ level

Systems	$V_{\text{mD}}$	$V_{\text{mD}'}$	$\Delta V_{\text{mD}}$	$V_{\text{mS}'}$	$V_{\text{mS}}$	$\Delta V_{\text{mS}}$	$V_{\text{mA}'}$	$V_{\text{mA}}$	$\Delta V_{\text{mA}}$
D1	-26.4	-10.5	15.9	-10.3	-2.4	-7.9	-59.5	-50.3	-9.2
D2	-28.7	-13.0	15.7	-11.7	-2.4	-9.3	-60.3	-50.3	-10.0
D3	-30.5	-14.1	16.4	-12.3	-2.4	-9.9	-60.8	-50.3	-10.5
D4	-32.3	-14.9	17.4	-13.2	-2.4	-10.9	-61.3	-50.3	-11.0
D5	-35.5	-17.6	17.9	-18.6	-2.4	-16.3	-63.8	-50.3	-13.5
D6	-22.6	-9.0	13.6	-9.3	-2.4	-7.0	-58.2	-50.3	-7.8
D7	-22.6	-9.7	12.9	-8.8	-2.4	-6.4	-57.4	-50.3	-7.0
D8	-22.8	-10.6	12.2	-8.3	-2.4	-6.0	-56.2	-50.3	-5.9
D9	-23.0	-10.5	12.5	-9.5	-2.4	-7.1	-57.9	-50.3	-7.5
D10	-24.3	-12.0	12.4	-10.4	-2.4	-8.0	-58.7	-50.3	-8.4
D11	-35.1	-22.8	12.3	-18.4	-2.4	-16.1	-64.0	-50.3	-13.7
D12	-41.9	-28.7	13.2	-18.4	-2.4	-16.1	-69.3	-50.3	-19.0
D13	-32.3	-20.7	11.6	-11.1	-2.4	-8.7	-58.2	-50.3	-7.9
D14	-36.2	-24.1	12.1	-14.6	-2.4	-12.2	-60.0	-50.3	-9.7
D15	-26.7	-11.6	15.1	-10.4	-2.4	-8.0	-58.5	-50.3	-8.2
D16	-31.2	-13.9	17.3	-13.1	-2.4	-10.7	-62.0	-50.3	-11.7
D17	-30.4	-16.2	14.2	-11.6	-2.4	-9.2	-58.9	-50.3	-8.5
D18	-28.1	-13.5	14.6	-9.9	-2.4	-7.5	-58.4	-50.3	-8.1

In Table 1,  $V_{\text{m}}$  values at D, the  $\pi$ -spacer and A of the D- $\pi$ -A systems are reported along with the change in  $V_{\text{m}}$  at those regions with the attachment of  $\pi$ -A to D. The change in  $V_{\text{m}}$  occurring at the D site ( $\Delta V_{\text{mD}}$ ) has been calculated by subtracting  $V_{\text{m}}$  observed at the donor ( $V_{\text{mD}}$ ) from the corresponding  $V_{\text{m}}$  observed at D of D- $\pi$ -A ( $V_{\text{mD}'}$ ). Likewise,  $\Delta V_{\text{mS}}$  and  $\Delta V_{\text{mA}}$  have been calculated by subtracting  $V_{\text{m}}$  observed at the respective sites of the reference system ( $V_{\text{mS}}$  and  $V_{\text{mA}}$ ) from the corresponding values of the D- $\pi$ -A systems ( $V_{\text{mS}'}$  and  $V_{\text{mA}'}$ ). In the table  $\Delta V_{\text{mD}}$  ranges from 12.2 to 17.9  $\text{kcal mol}^{-1}$ ; the positive  $\Delta V_{\text{mD}}$  value shows electron deficiency at D.

In all, the less negative  $V_{\text{m}}$  observed at the D site of D- $\pi$ -A ( $V_{\text{mD}'}$ ) than  $V_{\text{m}}$  of the donor ( $V_{\text{mD}}$ ) confirms the ICT from D to A. Further, the ICT from D to A enhances the electron density at the spacer; the gained electron density at the spacer has been denoted as negative  $\Delta V_{\text{mS}}$ , which ranges from  $-6.0$  to  $-16.3 \text{ kcal mol}^{-1}$ . As per  $\Delta V_{\text{mS}}$ , the highest electron-donating strength has been attained by the D5- $\pi$ -A system while the least is possessed by the D8- $\pi$ -A system.  $V_{\text{mA}'}$  ranges from  $-7.0$  to  $-13.5 \text{ kcal mol}^{-1}$ . The donors having greater electron-donating strength exhibit a more negative  $V_{\text{mA}'}$ . As a result, the change in the MESP appearing on the acceptor ( $\Delta V_{\text{mA}}$ ) with the

attachment of D to  $\pi$ -A has been regarded as the donating strength of the D- $\pi$ -A system.<sup>22</sup>

In the D1-D5 based  $\pi$ -A systems, the least negative  $\Delta V_{\text{mA}}$  ( $-9.2 \text{ kcal mol}^{-1}$ ) has been attained by the one nitrogen system D1- $\pi$ -A, which shows its poor electron-donating strength. Also, from D1- $\pi$ -A to D5- $\pi$ -A, a systematic enhancement in the donating strength has been observed for an increased number of nitrogen centres ( $n = 1-5$ ) and the most negative  $\Delta V_{\text{mA}}$  ( $-13.5 \text{ kcal mol}^{-1}$ ) has been shown by D5- $\pi$ -A (incorporating 5 nitrogen lone pairs). In D6 to D10- $\pi$ -A the more pyramidalized nitrogen centres in the donors impart less negative  $\Delta V_{\text{mA}}$  in the range  $-5.9$  to  $-8.4 \text{ kcal mol}^{-1}$  than the D1- $\pi$ -A-D5- $\pi$ -A systems. In D11- $\pi$ -A, the incorporation of six nitrogen lone pairs through imidazolidine rings at the phenyl ring enhances the electron density at the donor site, resulting in a  $\Delta V_{\text{mA}}$  of  $-13.7 \text{ kcal mol}^{-1}$ . Whereas, in D12- $\pi$ -A, the conjugation in the CC bond (imidazole ring) enhances the electron density at the donor more than in D11- $\pi$ -A, which leads to a more negative  $\Delta V_{\text{mA}}$  of  $-19.0 \text{ kcal mol}^{-1}$ . In the D13- $\pi$ -A and D14- $\pi$ -A systems, a relatively lower donating strength is observed in terms of  $\Delta V_{\text{mA}}$  ( $-7.9 \text{ kcal mol}^{-1}$  and  $-9.7 \text{ kcal mol}^{-1}$ ) than that of the D11 and D12- $\pi$ -A systems. This can be attributed to their reduced number of nitrogen centres (4 nitrogens). Since the nitrogens involved in the D1 to D4- $\pi$ -A systems are more planarized than those of D13 and D14- $\pi$ -A, the former systems show greater electron-donating strength. The integration of four nitrogens at the donor enhances the donating strength of the D16- $\pi$ -A system ( $-11.7 \text{ kcal mol}^{-1}$ ) over D15- $\pi$ -A ( $-8.2 \text{ kcal mol}^{-1}$ ). Further, the nearly planar nitrogens involved in D16- $\pi$ -A provide a similar donating strength  $-11.0 \text{ kcal mol}^{-1}$  to D4- $\pi$ -A ( $-11.7 \text{ kcal mol}^{-1}$ ). D17- $\pi$ -A with four nitrogen atoms incorporated through two fused six-membered rings at the phenyl ring attains a less negative  $\Delta V_{\text{mA}}$  ( $-8.5 \text{ kcal mol}^{-1}$ ) than D16- $\pi$ -A.

The additional two methyl groups in D18- $\pi$ -A at the nitrogen atoms are pyramidalized and lead to a less negative  $\Delta V_{\text{mA}}$  ( $8.1 \text{ kcal mol}^{-1}$ ) than D17. Finally, from the elucidated examples it is clear that donors having more planarized nitrogen centres enhance the donating strength of the D- $\pi$ -A systems. Among all, the D12, D11 and D5 based  $\pi$ -A systems are the best candidates for DSSC application.

### Absorption spectra

In Table 2, the optical properties of the donor and D- $\pi$ -A systems are given. Since we have used the same  $-\pi$ - and A units in all the designed D- $\pi$ -A systems, the influence of  $\pi$ -A on the absorption maximum ( $\lambda_{\text{max}}$ ) can be considered the same for all donors, and the shift in the absorption maximum ( $\Delta\lambda_{\text{max}}$ ) occurring during the transformation of D to D- $\pi$ -A can be recognized as due to the influence of the donating strength of the donor units.  $\Delta\lambda_{\text{max}}$  is calculated by subtracting  $\lambda_{\text{max}}$  of D from the analogous D- $\pi$ -A system. For the analysis the HOMO  $\rightarrow$  LUMO transition has been considered. The influence of the donor strength ( $V_{\text{mD}}$ ) on the  $\lambda_{\text{max}}$  of donors is observed in the range 280 to 329 nm. In Table 2, when a donor changes to D- $\pi$ -A, the absorption shifts to higher wavelengths in the range 454 to 619 nm. According to our previous study,  $\Delta\lambda_{\text{max}}$  in the range of 162 to 294 nm can be recognized as due to the influence of the donating strength ( $\Delta V_{\text{mA}}$ ) of the D- $\pi$ -A systems.<sup>22</sup> The significant correlation observed between  $\Delta V_{\text{mA}}$  and  $\Delta\lambda_{\text{max}}$  with a correlation coefficient of 0.940 confirms the significance of  $\Delta V_{\text{mA}}$  to  $\Delta\lambda_{\text{max}}$  (Fig. 3, deviations are neglected for the  $R$  calculation). It shows that  $\Delta\lambda_{\text{max}}$  increases with enhanced donating strength of the D- $\pi$ -A systems. In the table, the D1-D5 based  $\pi$ -A systems display a systematic increase in  $\Delta\lambda_{\text{max}}$  (from 203 to 257 nm) which can be recognized as due to the enhanced donating strength of those systems with an

**Table 2** Maximum absorption wavelength  $\lambda_{\text{max}}$  (nm), oscillator strength  $f$ , MO contribution, percentage of MO contribution (MO%), and shift in absorption maximum  $\Delta\lambda_{\text{max}}$  (nm) of the donor and D- $\pi$ -A systems at the TD-CAM-B3LYP/cc-pVDZ/SMD//B3LYP/cc-pVDZ level

Systems	Donor			D- $\pi$ -A system				
	$\lambda_{\text{max}}$ (nm)	$f$	MO contribution	$\lambda_{\text{max}}$ (nm)	$f$	MO contribution	MO (%)	$\Delta\lambda_{\text{max}}$ (nm)
D1	272	0.08	H $\rightarrow$ L	476	1.77	H $\rightarrow$ L	92	203
D2	286	0.11	H $\rightarrow$ L	513	1.53	H $\rightarrow$ L	92	227
D3	280	0.02	H $\rightarrow$ L	520	1.54	H $\rightarrow$ L	92	240
D4	285	0.03	H $\rightarrow$ L	542	1.31	H $\rightarrow$ L	89	257
D5	285	0.04	H $\rightarrow$ L	527	1.58	H $\rightarrow$ L	91	241
D6	285	0.04	H $\rightarrow$ L	471	1.74	H $\rightarrow$ L	94	187
D7	301	0.05	H $\rightarrow$ L	481	1.42	H $\rightarrow$ L	92	180
D8	304	0.03	H $\rightarrow$ L	475	1.46	H $\rightarrow$ L	91	171
D9	329	0.06	H $\rightarrow$ L	531	0.97	H $\rightarrow$ L	92	202
D10	341	0.07	H $\rightarrow$ L	522	0.04	H $\rightarrow$ L	87	181
D11	304	0.11	H $\rightarrow$ L	549	1.30	H $\rightarrow$ L	88	245
D12	325	0.60	H $\rightarrow$ L	619	0.27	H $\rightarrow$ L	79	294
				600	1.41	H-1 $\rightarrow$ L	49	275
D13	292	1.17	H $\rightarrow$ L	454	0.03	H $\rightarrow$ L	91	162
				423	1.19	H-1 $\rightarrow$ L	68	131
D14	324	1.14	H $\rightarrow$ L	583	0.03	H $\rightarrow$ L	93	259
				512	0.14	H-1 $\rightarrow$ L	93	188
D15	272	0.18	H $\rightarrow$ L	481	1.62	H $\rightarrow$ L	92	209
D16	282	0.06	H $\rightarrow$ L	509	0.99	H $\rightarrow$ L	93	227
D17	282	0.09	H $\rightarrow$ L	500	0.83	H $\rightarrow$ L	92	218
D18	288	0.07	H $\rightarrow$ L	487	0.97	H $\rightarrow$ L	90	199

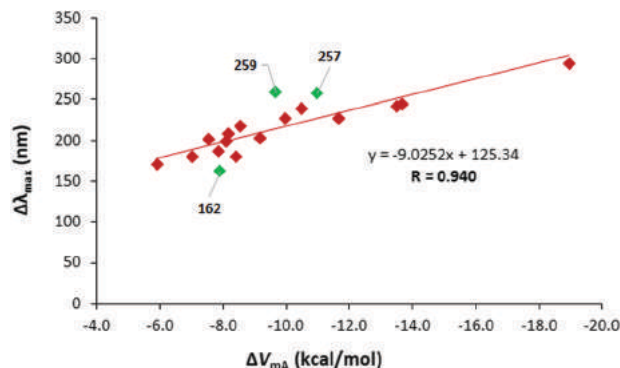


Fig. 3 Correlation between  $\Delta V_{MA}$  and  $\Delta\lambda_{max}$  of the D- $\pi$ -A systems (the  $R$  value has been calculated by excluding the deviations shown in a green colour).

increased number of nitrogen centres ( $n = 1-5$ ). Among those systems, the D4 based  $\pi$ -A system shows greater  $\Delta\lambda_{max}$  than D5- $\pi$ -A, which displays a slight deviation in the correlation (marked in a green colour, Fig. 3). The lower  $\Delta\lambda_{max}$  values exhibited by the D6- $\pi$ -A to D10- $\pi$ -A systems in the range of 171–202 nm are recognized as due to the lower donating strength of those systems. Compared to the D6- $\pi$ -A to D10- $\pi$ -A systems, the greater  $\Delta\lambda_{max}$  in D11- $\pi$ -A (245 nm) can be recognized as due to its larger donating strength. The presence of conjugation in CC bonds enhances the donating strength of D12- $\pi$ -A, resulting in the highest  $\Delta\lambda_{max}$  of 294 nm. The highest  $\Delta\lambda_{max}$  (294 nm) can be attributed to the utmost  $\Delta V_{MA}$  and  $\lambda_{max}$  of D12- $\pi$ -A (619 nm). In the D13- $\pi$ -A and D14- $\pi$ -A systems,  $\Delta\lambda_{max}$  values of 162 and 259 nm are observed with a  $\lambda_{max}$  of 454 and 583 nm, respectively. In those systems a slight deviation in the correlation has been observed, which may be due to the poor oscillator strength ( $f \rightarrow 0.03$ ). The higher  $\Delta\lambda_{max}$  of 227 nm in D16- $\pi$ -A than D15- $\pi$ -A (209 nm) can be spotted as due to the better electron-donating strength (because of the increased number of nitrogens (four)) of D16- $\pi$ -A. In D17- $\pi$ -A,  $\lambda_{max}$  and  $\Delta\lambda_{max}$  are 500 nm and 218 nm, respectively. Even though there is an equal number of nitrogens (four) in the donor site, the higher  $\Delta\lambda_{max}$  in D17- $\pi$ -A than D18- $\pi$ -A (199 nm) can be recognized as due to the influence of more planar NH centres.

Finally, for the dye sensitizers, the HOMO (highest occupied molecular orbital) and LUMO (lowest unoccupied molecular orbital) energies are crucial for determining the efficiency of the sensitizers (Table 5). For the effective regeneration of the oxidized dye, it is important to have a HOMO energy ( $e_h$ ) lower than the redox potential of the  $\Gamma^-/I_3^-$  electrolyte ( $-4.8$  eV). The  $e_h$  values of the D3–D5, D11–D14, and D16 based  $\pi$ -A systems are in the range of  $-4.68$  to  $-4.74$  eV, lying above the redox potential of the  $\Gamma^-/I_3^-$  electrolyte. It is therefore suggesting that the oxidized dye might not efficiently regenerate in those systems from the  $\Gamma^-/I_3^-$  electrolyte. Whereas, for the rest of the D- $\pi$ -A systems,  $e_h$  ( $-4.82$  to  $-5.29$  eV) lying below the redox potential of the electrolyte facilitates effective dye regeneration. For the D1- $\pi$ -A to D18- $\pi$ -A systems, the LUMO energies ( $e_l$ ) are in the range of  $-1.79$  to  $-2.79$  eV, lying above the conduction band (CB) energy of the  $TiO_2$  semiconductor ( $-4.0$  eV), which

ensures effective electron injection into the  $TiO_2$  conduction band. The HOMO–LUMO gap (HLG) energy of the designed D- $\pi$ -A systems ranges from 1.64 to 2.65 eV and it shows a decreasing trend with increasing electron donating strength. In DSSCs, HLG values give a clear idea regarding the PCE of the dye-sensitizer. As per various theoretical studies, a lower HLG ensures better optical and photovoltaic properties, thereby improving the PCE of DSSC devices.<sup>90–92</sup> Herein, we could recognize that the lower HLG energy obtained with D12- $\pi$ -A (2.17 eV) is accompanied by the highest absorption maximum (619 nm), good adsorption stability ( $-28.6$  kcal mol<sup>-1</sup>), and highest  $eV_{oc}$  (2.21 eV). Consequently, among all, the D12- $\pi$ -A system having the lowest LUMO energy ( $-1.79$  eV) may provide a better PCE in DSSC devices.

According to the basic principle of DSSCs, when the dye molecule gets adsorbed on the  $TiO_2$  semiconductor, the interaction between the dye and semiconductor can shift their energy levels and prompt electron injection into the semiconductor, which is desirable for a better PCE.<sup>73</sup> To determine the energy levels of the adsorbed D- $\pi$ -A systems on  $TiO_2$ , we have designed a bidentate bridging mode for binding the D- $\pi$ -A systems on  $TiO_2$  (Fig. 4a). It has been reported that the bidentate bridging mode is the most stable adsorption mode for anchoring groups.<sup>93,94</sup> Further, the LUMO energy levels ( $-3.50$  to  $-3.79$  eV) of the adsorbed D- $\pi$ -A systems are deeper than the bare D- $\pi$ -A systems ( $-1.79$  to  $-2.79$  eV) and ensure that the LUMO is above the CB energy of  $TiO_2$ , which could promote efficient electron injection from the excited dye molecule into the CB of  $TiO_2$ . The absorption properties of the D1- $\pi$ -A to D18- $\pi$ -A systems adsorbed on  $TiO_2$  are reported in Table 3. We denote D- $\pi$ -A adsorbed on  $TiO_2$  as D- $\pi$ -A/ $TiO_2$ . The observed  $\lambda_{max}$  in the range 513 to 703 nm is favourable for an improved PCE, and shows a red shift with respect to the pure D- $\pi$ -A system. Among all, D12- $\pi$ -A/ $TiO_2$  shows the highest  $\lambda_{max}$  (703 nm), whereas D13- $\pi$ -A/ $TiO_2$  displays the lowest  $\lambda_{max}$  (513 nm). The HLG of the D- $\pi$ -A/ $TiO_2$  systems ranges from 0.61 to 1.89 eV, indicating that the adsorption of the dye with the semiconductor significantly reduces the HLG related to the bare D- $\pi$ -A systems. The electron density shifts in the D- $\pi$ -A/ $TiO_2$  systems between the HOMO and LUMO are given in the representative example (D12- $\pi$ -A/ $TiO_2$ ) shown in Fig. 4b. In all the D- $\pi$ -A/ $TiO_2$  systems, the HOMO is localized on the donor region whereas the LUMO is distributed on  $TiO_2$ . This kind of charge delocalization is anticipated for a better PCE of dye sensitizers.

Quantitatively, the adsorption stability of the D- $\pi$ -A systems on the  $(TiO_2)_9$  cluster has been evaluated using the adsorption energy ( $E_{ads}$ ), which is listed in Table 4. It is defined as  $E_{ads} = E_{dye/TiO_2} - (E_{dye} + E_{TiO_2})$ , where  $E_{dye/TiO_2}$ ,  $E_{dye}$ , and  $E_{TiO_2}$  denote the energies of dye/ $TiO_2$ , the isolated dye and the  $TiO_2$  cluster, respectively.<sup>95</sup> It is clear that a more negative adsorption energy could reveal higher adsorption stability between the dye molecule and  $TiO_2$ . In Table 4, we observed that all the adsorbed systems that have a more negative adsorption energy contain greater N-annulation. Among all, the most negative adsorption energy ( $-28.6$  kcal mol<sup>-1</sup>) is attained with D12- $\pi$ -A/ $TiO_2$ , which



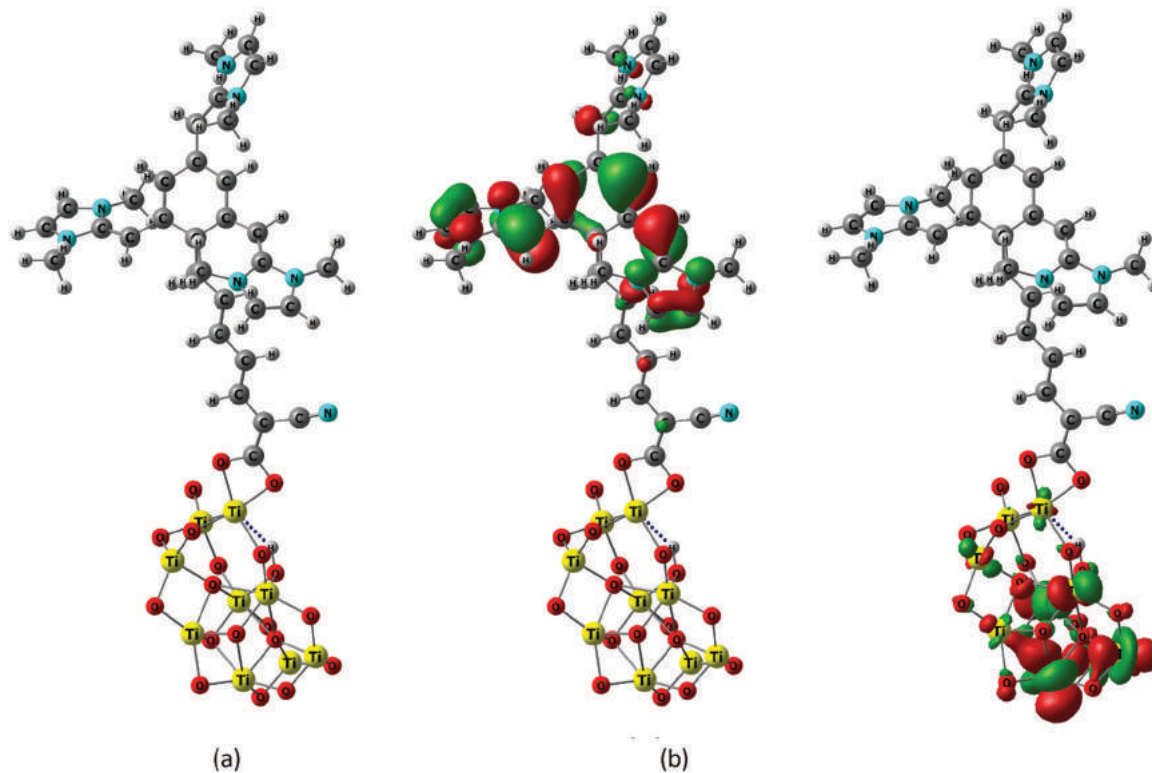


Fig. 4 (a) Optimized geometry of a representative D- $\pi$ -A system on the (TiO<sub>2</sub>)<sub>9</sub> cluster (D12- $\pi$ -A/TiO<sub>2</sub>). (b) Electron density shift in the frontier molecular orbitals.

**Table 3** HOMO (eV), LUMO (eV), and HOMO-LUMO energy gap, HLG (eV), for the D- $\pi$ -A/TiO<sub>2</sub> systems at the B3LYP/GenECP level. The maximum absorption wavelength  $\lambda_{\text{max}}$  (nm), and oscillator strength ( $f$ ) adsorbed on TiO<sub>2</sub> are simulated at the TD CAM-B3LYP/GenECP/SMD//B3LYP/GenECP level

D- $\pi$ -A/TiO <sub>2</sub> systems	HOMO (eV)	LUMO (eV)	HLG (eV)	$\lambda_{\text{max}}$ (nm)	$f$
D1	-5.43	-3.68	1.75	538	2.36
D2	-5.17	-3.66	1.52	583	2.03
D3	-5.10	-3.64	1.46	593	2.07
D4	-5.07	-3.62	1.45	611	1.73
D5	-5.09	-3.55	1.54	592	0.60
D6	-5.63	-3.74	1.89	526	2.24
D7	-5.53	-3.76	1.77	538	1.85
D8	-5.57	-3.79	1.77	531	1.87
D9	-5.37	-3.74	1.64	611	1.73
D10	-5.39	-3.71	1.69	574	0.05
D11	-4.85	-3.50	1.34	630	1.79
D12	-4.38	-3.25	1.13	703	0.29
D13	-4.99	-3.78	1.21	513	0.03
D14	-4.32	-3.71	0.61	697	0.02
D15	-5.44	-3.74	1.71	545	2.01
D16	-5.08	-3.60	1.48	610	1.91
D17	-5.25	-3.72	1.53	573	1.02
D18	-5.31	-3.72	1.59	558	1.22

indicates the most stable adsorption. Apart from N-annulation, the adsorption stability increases with enhanced electron-donating strength of D- $\pi$ -A. The excellent linear correlation between  $\Delta V_{\text{mA}}$  and  $E_{\text{ads}}$  with a correlation coefficient of 0.947 confirms that the donating strength of the donor systems of D- $\pi$ -A assessed in terms of  $\Delta V_{\text{mA}}$  is useful to assess the  $E_{\text{ads}}$  values of the dye on the semiconductor (Fig. 5a). Since stronger adsorption leads to deeper

**Table 4** The adsorption energies ( $E_{\text{ads}}$ ) of all the D- $\pi$ -A/(TiO<sub>2</sub>)<sub>9</sub> systems where the  $E_{\text{ads}}$  values are given in kcal mol<sup>-1</sup>

D- $\pi$ -A/(TiO <sub>2</sub> ) <sub>9</sub> systems	$E_{\text{ads}}$ (kcal mol <sup>-1</sup> )
D1- $\pi$ -A/(TiO <sub>2</sub> ) <sub>9</sub>	-23.6
D2- $\pi$ -A/(TiO <sub>2</sub> ) <sub>9</sub>	-23.8
D3- $\pi$ -A/(TiO <sub>2</sub> ) <sub>9</sub>	-23.9
D4- $\pi$ -A/(TiO <sub>2</sub> ) <sub>9</sub>	-24.3
D5- $\pi$ -A/(TiO <sub>2</sub> ) <sub>9</sub>	-25.0
D6- $\pi$ -A/(TiO <sub>2</sub> ) <sub>9</sub>	-23.3
D7- $\pi$ -A/(TiO <sub>2</sub> ) <sub>9</sub>	-23.0
D8- $\pi$ -A/(TiO <sub>2</sub> ) <sub>9</sub>	-22.8
D9- $\pi$ -A/(TiO <sub>2</sub> ) <sub>9</sub>	-23.4
D10- $\pi$ -A/(TiO <sub>2</sub> ) <sub>9</sub>	-23.8
D11- $\pi$ -A/(TiO <sub>2</sub> ) <sub>9</sub>	-25.4
D12- $\pi$ -A/(TiO <sub>2</sub> ) <sub>9</sub>	-28.6
D13- $\pi$ -A/(TiO <sub>2</sub> ) <sub>9</sub>	-22.2
D14- $\pi$ -A/(TiO <sub>2</sub> ) <sub>9</sub>	-23.3
D15- $\pi$ -A/(TiO <sub>2</sub> ) <sub>9</sub>	-22.6
D16- $\pi$ -A/(TiO <sub>2</sub> ) <sub>9</sub>	-24.5
D17- $\pi$ -A/(TiO <sub>2</sub> ) <sub>9</sub>	-23.2
D18- $\pi$ -A/(TiO <sub>2</sub> ) <sub>9</sub>	-23.3

LUMO energy levels, a more donating dye is expected to give higher adsorption stability and higher  $eV_{\text{oc}}$  (Table 4 and Fig. 5b). In the D12- $\pi$ -A/TiO<sub>2</sub> system, the highest adsorption stability and  $eV_{\text{oc}}$  (2.21 eV) have been observed, which predicts superior photovoltaic performance of the adsorbed dye.

### Photovoltaic performance

The photovoltaic parameters of the D- $\pi$ -A systems are listed in Table 5. The electron injection-free energy change ( $\Delta G_{\text{inject}}$ ) is

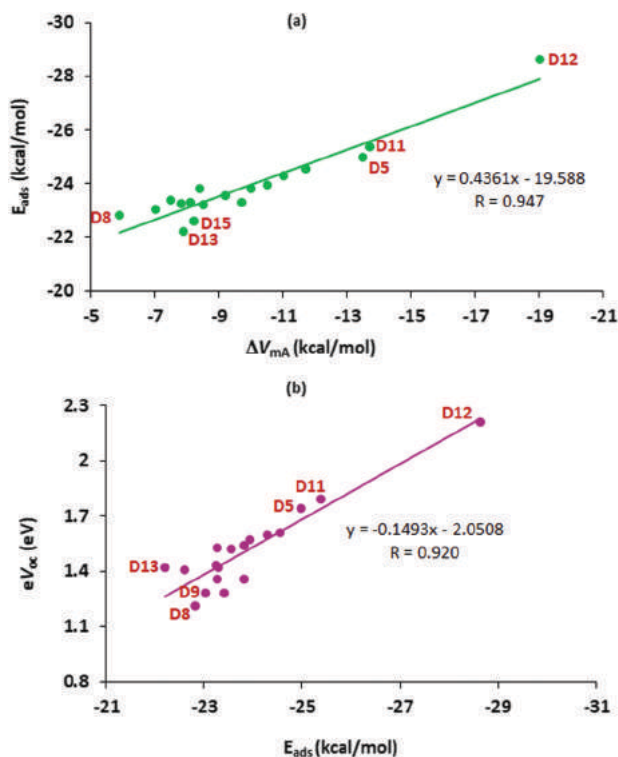


Fig. 5 (a) Correlation between  $\Delta V_{MA}$  and  $E_{ads}$  and (b)  $E_{ads}$  and  $eV_{OC}$ .

in the range  $-1.28$  to  $-2.10$  eV. It is defined as  $\Delta G_{inject} = E^{dye*} - |E_{CB}|$ ,<sup>96–98</sup> where  $E^{dye*}$  is the excited state oxidation potential and  $E_{CB}$  is the energy of the conduction band edge of the  $TiO_2$  semiconductor ( $-4.0$  eV).  $E^{dye*}$  can be calculated as  $(-e_h - \text{vertical excitation energy})$ .<sup>96,99</sup> The more negative  $\Delta G_{inject}$  will have more ability to inject electrons from the excited state of D- $\pi$ -A to the CB of  $TiO_2$ . Since  $\Delta G_{inject}$  is related to short-circuit current density  $J_{sc}$ , by improving the electron injection ability, an enhancement in the PCE can occur.<sup>6,22,26,98</sup> Among all,

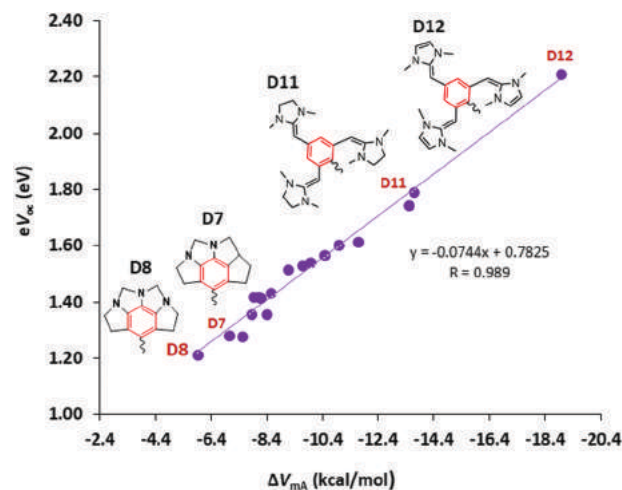


Fig. 6 Correlation between the donating strength ( $\Delta V_{MA}$ ) of the D- $\pi$ -A system and the open-circuit voltage ( $eV_{OC}$ ).

$\Delta G_{inject}$  is more negative in D14- $\pi$ -A ( $-2.10$  eV) while it is the least negative in D9- $\pi$ -A ( $-1.28$  eV). Further, it is noted that the donating strength improves the electron injection efficiency. The  $\Delta G_{reg}$  value measures the dye regeneration efficiency of the systems, which can be written as  $(E^{dye} - 4.8)$  eV or  $(-e_h) - 4.8$  eV.<sup>100,101</sup> The smallest  $\Delta G_{reg}$  ( $-0.84$  eV) observed in D12- $\pi$ -A shows the highest dye regeneration efficiency, while the highest value  $0.49$  observed in D6- $\pi$ -A indicates the lowest dye regeneration efficiency. Finally, the open-circuit voltage ( $eV_{OC} = e_1 - (-4.0)$ )<sup>102</sup> lies in the range  $1.21$  eV to  $2.21$  eV, which shows an excellent correlation with  $\Delta V_{MA}$  (Fig. 6), and suggests that  $eV_{OC}$  increases with enhanced strength of the D- $\pi$ -A systems. The correlation in Fig. 6 also suggests that the MESP approach offers an easy analysis tool for the quantification of the donating strength of D- $\pi$ -A systems in DSSC applications, and the correlation plot provides a guideline for designing dye sensitizers for desirable photovoltaic applications.

Table 5 HOMO (eV), LUMO (eV), and HOMO–LUMO energy gap (eV) at the B3LYP/cc-pVDZ level. Ground and excited state oxidation potential ( $E^{dye}$ ,  $E^{dye*}$ ), excitation energy, free energy of electron injection  $\Delta G_{inject}$ , dye regeneration efficiency  $\Delta G_{reg}$ , and open-circuit voltage  $eV_{OC}$  at the TD-CAM-B3LYP/SMD/cc-pVDZ//B3LYP/cc-pVDZ level

Systems	Excitation energy (eV)	HOMO (eV)	LUMO (eV)	HLG (eV)	$E^{dye}$ (eV)	$E^{dye*}$ (eV)	$\Delta G_{inject}$ (eV)	$\Delta G_{reg}$ (eV)	$eV_{OC}$ (eV)
D1	2.61	-5.09	-2.48	2.61	5.09	2.48	-1.52	0.29	1.52
D2	2.42	-4.82	-2.46	2.36	4.82	2.40	-1.60	0.02	1.54
D3	2.38	-4.74	-2.43	2.31	4.74	2.36	-1.64	-0.06	1.57
D4	2.29	-4.69	-2.40	2.29	4.69	2.40	-1.60	-0.11	1.60
D5	2.35	-4.68	-2.26	2.42	4.68	2.33	-1.67	-0.12	1.74
D6	2.63	-5.29	-2.64	2.65	5.29	2.66	-1.34	0.49	1.36
D7	2.58	-5.22	-2.72	2.50	5.22	2.64	-1.36	0.42	1.28
D8	2.61	-5.27	-2.79	2.48	5.27	2.66	-1.34	0.47	1.21
D9	2.33	-5.05	-2.72	2.33	5.05	2.72	-1.28	0.25	1.28
D10	2.38	-5.04	-2.64	2.40	5.04	2.66	-1.34	0.24	1.36
D11	2.26	-4.50	-2.21	2.29	4.50	2.24	-1.76	-0.30	1.79
D12	2.00	-3.96	-1.79	2.17	3.96	1.96	-2.04	-0.84	2.21
D13	2.73	-4.77	-2.58	2.19	4.77	2.04	-1.96	-0.03	1.42
D14	2.21	-4.11	-2.47	1.64	4.11	1.90	-2.10	-0.69	1.53
D15	2.58	-5.11	-2.59	2.52	5.11	2.53	-1.47	0.31	1.41
D16	2.29	-4.72	-2.39	2.33	4.72	2.43	-1.57	-0.08	1.61
D17	2.48	-4.96	-2.57	2.39	4.96	2.48	-1.52	0.16	1.43
D18	2.55	-5.04	-2.58	2.46	5.04	2.49	-1.51	0.24	1.42

In the analysis, the highest donating strength observed in D12- $\pi$ -A correlates to the highest  $eV_{oc}$  (2.21 eV). The pyramidalized nitrogen centres observed in D8- $\pi$ -A retard the efficient electron injection to  $\pi$ -A, and it shows the lowest  $eV_{oc}$  (1.21 eV) due to inferior donating strength.

## Conclusions

Donor modifications, especially through the integration of electron-rich nitrogen atoms (N-annulation), significantly affect the structure–performance relationship of D- $\pi$ -A systems for dye-sensitized solar cell applications. For tuning the electron-donating ability of D- $\pi$ -A systems, eighteen electron-rich nitrogen incorporated donors are designed with butadiene and cyanoacrylic acid as a  $\pi$ -spacer and an acceptor, respectively. The implication of planarized nitrogens for improving the electron-donating strength ( $\Delta V_{mA}$ ) of D- $\pi$ -A systems is investigated using MESP topographical analysis, which states that the magnitude of  $\Delta V_{mA}$  increases with an increased number of planar nitrogens. The  $\lambda_{max}$  values of the D- $\pi$ -A systems are fine-tuned by the extent of  $\pi$ -conjugation and N-annulation in the donors. The significance of  $\Delta V_{mA}$  in shifting the absorption maximum ( $\Delta\lambda_{max}$ ) is confirmed by the linear correlation observed between  $\Delta V_{mA}$  and  $\Delta\lambda_{max}$ . Regarding the frontier molecular orbitals of the D- $\pi$ -A systems, the HOMO and LUMO energies are affected by the electron-rich nature of the donors in D- $\pi$ -A. The sufficiently more negative LUMO energy of the D- $\pi$ -A systems than the CB energy of TiO<sub>2</sub> provides high electron injection efficiency. The open-circuit voltage ( $eV_{oc}$ ), and free energy of electron injection ( $\Delta G_{inject}$ ) have been analysed for the D- $\pi$ -A systems and reveal that  $eV_{oc}$  is increased with enhanced  $\Delta V_{mA}$ . Also, the adsorption stability of the D- $\pi$ -A systems on TiO<sub>2</sub> has been evaluated and indicates that the adsorption stability ( $E_{ads}$ ) increased with enhanced electron-donating strength of the D- $\pi$ -A system. Since adsorption of the D- $\pi$ -A system on TiO<sub>2</sub> shifts the LUMO energy, the stability of the D- $\pi$ -A/TiO<sub>2</sub> system affects  $eV_{oc}$  and thus the efficiency of the solar cell. The strong linear correlation observed between  $E_{ads}$  and  $eV_{oc}$  proves this conclusion. Among all the cases studied, D12- $\pi$ -A/TiO<sub>2</sub> shows the highest adsorption stability; furthermore, D12- $\pi$ -A displays the highest  $\Delta\lambda_{max}$ , the best  $eV_{oc}$  and the highest magnitude for  $\Delta V_{mA}$ . Consequently, from the aforementioned fundamental parameters, it can be concluded that the D12 based photosensitizer is very effective for improving the PCE. Also, the N-annulation design strategy will pave the way for attaining high efficiency in the field of dye-sensitized solar cells.

## Conflicts of interest

There are no conflicts to declare.

## Acknowledgements

The authors thank DST-SERB for funding through GAP1397 and also gratefully acknowledge the CSIR 4th PI for HPC facility

and NIIST IT lab for computational support. V. V. Divya thanks CSIR, India, for the senior research fellowship.

## References

- 1 A. Baheti, C.-P. Lee, K. J. Thomas and K.-C. Ho, *Phys. Chem. Chem. Phys.*, 2011, **13**, 17210–17221.
- 2 Y.-H. Chen, V. S. Nguyen, H.-H. Chou, Y. S. Tingare, T.-C. Wei and C.-Y. Yeh, *ACS Appl. Energy Mater.*, 2020, **3**, 5479–5486.
- 3 J. Gong, K. Sumathy, Q. Qiao and Z. Zhou, *Renewable Sustainable Energy Rev.*, 2017, **68**, 234–246.
- 4 G. Boschloo, *Front. Chem.*, 2019, **7**, 77.
- 5 M. Grätzel, *Acc. Chem. Res.*, 2009, **42**, 1788–1798.
- 6 B. O'Regan and M. Grätzel, *Nature*, 1991, **353**, 737–740.
- 7 M. K. Nazeeruddin, F. De Angelis, S. Fantacci, A. Selloni, G. Viscardi, P. Liska, S. Ito, B. Takeru and M. Grätzel, *J. Am. Chem. Soc.*, 2005, **127**, 16835–16847.
- 8 G. Marotta, M. A. Reddy, S. P. Singh, A. Islam, L. Han, F. De Angelis, M. Pastore and M. Chandrasekharam, *ACS Appl. Mater. Interfaces*, 2013, **5**, 9635–9647.
- 9 S. Yun, Y. Qin, A. R. Uhl, N. Vlachopoulos, M. Yin, D. Li, X. Han and A. Hagfeldt, *Energy Environ. Sci.*, 2018, **11**, 476–526.
- 10 A. Fakharuddin, R. Jose, T. M. Brown, F. Fabregat-Santiago and J. Bisquert, *Energy Environ. Sci.*, 2014, **7**, 3952–3981.
- 11 A. Hinsch, W. Veurman, H. Brandt, K. F. Jensen and S. Mastroianni, *ChemPhysChem*, 2014, **15**, 1076–1087.
- 12 A. Hagfeldt, G. Boschloo, L. Sun, L. Kloo and H. Pettersson, *Chem. Rev.*, 2010, **110**, 6595–6663.
- 13 Y. Kurumisawa, T. Higashino, S. Nimura, Y. Tsuji, H. Iiyama and H. Imahori, *J. Am. Chem. Soc.*, 2019, **141**, 9910–9919.
- 14 H. Zhou, J.-M. Ji, S. H. Kang, M. S. Kim, H. S. Lee, C. H. Kim and H. K. Kim, *J. Mater. Chem. C*, 2019, **7**, 2843–2852.
- 15 K. Kakiage, Y. Aoyama, T. Yano, K. Oya, T. Kyomen and M. Hanaya, *Chem. Commun.*, 2015, **51**, 6315–6317.
- 16 K. Kakiage, Y. Aoyama, T. Yano, K. Oya, J.-I. Fujisawa and M. Hanaya, *Chem. Commun.*, 2015, **51**, 15894–15897.
- 17 S. Mathew, A. Yella, P. Gao, R. Humphry-Baker, B. F. Curchod, N. Ashari-Astani, I. Tavernelli, U. Rothlisberger, M. K. Nazeeruddin and M. Grätzel, *Nat. Chem.*, 2014, **6**, 242–247.
- 18 F.-S. Lin, P. Priyanka, M.-S. Fan, S. Vegiraju, J.-S. Ni, Y.-C. Wu, Y.-H. Li, G.-H. Lee, Y. Ezhumalai and R.-J. Jeng, *J. Mater. Chem. C*, 2020, **8**, 15322–15330.
- 19 Y. Ren, Y. Li, S. Chen, J. Liu, J. Zhang and P. Wang, *Energy Environ. Sci.*, 2016, **9**, 1390–1399.
- 20 K. Sharma, V. Sharma and S. Sharma, *Nanoscale Res. Lett.*, 2018, **13**, 381.
- 21 X. Song, X. Yang, H. Wang, J. An, Z. Yu, X. Wang, A. Hagfeldt and L. Sun, *Sol. Energy*, 2019, **187**, 274–280.
- 22 V. V. Divya and C. H. Suresh, *New J. Chem.*, 2020, **44**, 7200–7209.

- 23 M. Jadhav, J. V. Vaghasiya, D. Patil, S. S. Soni and N. Sekar, *New J. Chem.*, 2019, **43**, 8970–8981.
- 24 R. Tarsang, V. Promarak, T. Sudyoadsuk, S. Namuangruk and S. Jungsuttiwong, *J. Photochem. Photobiol., A*, 2014, **273**, 8–16.
- 25 M. Karuppusamy, V. S. K. Choutipalli, D. Vijay and V. Subramanian, *J. Chem. Sci.*, 2020, **132**, 20.
- 26 V. V. Divya and C. H. Suresh, *New J. Chem.*, 2021, **45**, 2496–2507.
- 27 Y. K. Eom, S. H. Kang, I. T. Choi, Y. Yoo, J. Kim and H. K. Kim, *J. Mater. Chem. A*, 2017, **5**, 2297–2308.
- 28 Y.-Q. Yan, Y.-Z. Zhu, P.-P. Dai, J. Han, M. Yan and J.-Y. Zheng, *Sol. Energy*, 2020, **207**, 428–435.
- 29 H. Zhang, Z.-E. Chen and H.-R. Tian, *Sol. Energy*, 2020, **198**, 239–246.
- 30 A. J. Huckaba, F. Giordano, L. E. McNamara, K. M. Dreux, N. I. Hammer, G. S. Tschumper, S. M. Zakeeruddin, M. Grätzel, M. K. Nazeeruddin and J. H. Delcamp, *Adv. Energy Mater.*, 2015, **5**, 1401629.
- 31 Y. Zhang, H. Cheema, L. McNamara, L. A. Hunt, N. I. Hammer and J. H. Delcamp, *Chem. – Eur. J.*, 2018, **24**, 5939–5949.
- 32 J. Feng, Y. Jiao, W. Ma, M. K. Nazeeruddin, M. Grätzel and S. Meng, *J. Phys. Chem. C*, 2013, **117**, 3772–3778.
- 33 J. H. Delcamp, A. Yella, T. W. Holcombe, M. K. Nazeeruddin and M. Grätzel, *Angew. Chem., Int. Ed.*, 2013, **125**, 394–398.
- 34 C. Yan, W. Ma, Y. Ren, M. Zhang and P. Wang, *ACS Appl. Mater. Interfaces*, 2015, **7**, 801–809.
- 35 U. B. Cappel, M. H. Karlsson, N. G. Pschirer, F. Eickemeyer, J. Schöneboom, P. Erk, G. Boschloo and A. Hagfeldt, *J. Phys. Chem. C*, 2009, **113**, 14595–14597.
- 36 C. Li, Z. Liu, J. Schöneboom, F. Eickemeyer, N. G. Pschirer, P. Erk, A. Herrmann and K. Müllen, *J. Mater. Chem. C*, 2009, **19**, 5405–5415.
- 37 Y. Jin, J. Hua, W. Wu, X. Ma and F. Meng, *Synth. Met.*, 2008, **158**, 64–71.
- 38 J. Luo, M. Xu, R. Li, K.-W. Huang, C. Jiang, Q. Qi, W. Zeng, J. Zhang, C. Chi, P. Wang and J. Wu, *J. Am. Chem. Soc.*, 2014, **136**, 265–272.
- 39 Z. Yao, H. Wu, Y. Ren, Y. Guo and P. Wang, *Energy Environ. Sci.*, 2015, **8**, 1438–1442.
- 40 Z. Yao, M. Zhang, H. Wu, L. Yang, R. Li and P. Wang, *J. Am. Chem. Soc.*, 2015, **137**, 3799–3802.
- 41 V. V. Divya, F. B. Sayyed and C. H. Suresh, *ChemPhysChem*, 2019, **20**, 1752–1758.
- 42 F. Effenberger, P. Fischer, W. W. Schöllner and W.-D. Stohrer, *Tetrahedron*, 1978, **34**, 2409–2417.
- 43 A. Zakrzewska, R. Gawinecki, E. Kolehmainen and B. Osmiałowski, *Int. J. Mol. Sci.*, 2005, **6**, 52–62.
- 44 J. O. S. Varejão, E. V. V. Varejão and S. A. Fernandes, *Eur. J. Org. Chem.*, 2019, 4273–4310.
- 45 J. E. Kuder, W. W. Limburg, J. M. Pochan and D. Wychick, *J. Chem. Soc. Perkin Trans. 2*, 1977, 1643–1651.
- 46 G. Shishkin, *Chem. Heterocycl. Compd.*, 1983, **19**, 549–553.
- 47 F. Fantuzzi, C. B. Coutinho, R. R. Oliveira and M. A. C. Nascimento, *Inorg. Chem.*, 2018, **57**, 3931–3940.
- 48 C. H. Suresh and F. B. Sayyed, *J. Phys. Chem. A*, 2013, **117**, 10455–10461.
- 49 S. Rohrbach, R. S. Shah, T. Tuttle and J. A. Murphy, *Angew. Chem.*, 2019, **131**, 11576–11580.
- 50 J. S. Miller, D. A. Dixon, J. C. Calabrese, C. Vazquez, P. J. Krusic, M. D. Ward, E. Wasserman and R. L. Harlow, *J. Am. Chem. Soc.*, 1990, **112**, 381–398.
- 51 E. Scrocco and J. Tomasi, in *Advances Quantum Chemistry*, ed. P.-O. Löwdin, Academic Press, 1978, vol. 11, pp. 115–193.
- 52 B. Pullman, *Int. J. Quantum Chem.*, 1990, **38**, 81–92.
- 53 A. Pullman and B. Pullman, *Q. Rev. Biophys.*, 1981, **14**, 289–380.
- 54 P. Politzer and J. S. Murray, *J. Mol. Struct.*, 1996, **376**, 419–424.
- 55 P. Politzer, J. S. Murray and T. Clark, *Phys. Chem. Chem. Phys.*, 2013, **15**, 11178–11189.
- 56 P. Politzer and J. S. Murray, *Cryst. Growth Des.*, 2015, **15**, 3767–3774.
- 57 P. Politzer and J. S. Murray, *ChemPhysChem*, 2020, **21**, 579–588.
- 58 C. H. Suresh and S. R. Gadre, *J. Org. Chem.*, 1999, **64**, 2505–2512.
- 59 S. R. Gadre and R. N. Shirsat, *Electrostatics of Atoms and Molecules*, Universities Press, 2000.
- 60 S. R. Gadre, S. A. Kulkarni and I. H. Shrivastava, *J. Chem. Phys.*, 1992, **96**, 5253–5260.
- 61 F. B. Sayyed and C. H. Suresh, *Tetrahedron Lett.*, 2009, **50**, 7351–7354.
- 62 F. B. Sayyed and C. H. Suresh, *New J. Chem.*, 2009, **33**, 2465–2471.
- 63 P. Sajith and C. H. Suresh, *Inorg. Chem.*, 2012, **51**, 967–977.
- 64 J. Mathew and C. H. Suresh, *Organometallics*, 2011, **30**, 1438–1444.
- 65 K. Sandhya and C. H. Suresh, *Dalton Trans.*, 2014, **43**, 12279–12287.
- 66 B. A. Anjali, F. B. Sayyed and C. H. Suresh, *J. Phys. Chem. C*, 2016, **120**, 1112–1119.
- 67 B. A. Anjali and C. H. Suresh, *ACS Omega*, 2017, **2**, 4196–4206.
- 68 P. V. Bijina and C. H. Suresh, *J. Chem. Sci.*, 2016, **128**, 1677–1686.
- 69 R. Rakhi and C. H. Suresh, *Phys. Chem. Chem. Phys.*, 2016, **18**, 24631–24641.
- 70 K. Remya and C. H. Suresh, *Phys. Chem. Chem. Phys.*, 2015, **17**, 27035–27044.
- 71 T. D. Della and C. H. Suresh, *Phys. Chem. Chem. Phys.*, 2016, **18**, 14588–14602.
- 72 F. Arkan and M. Izadyar, *Renewable Sustainable Energy Rev.*, 2018, **94**, 609–655.
- 73 W. Zhang, L. Wang, L. Mao, J. Jiang, H. Ren, P. Heng, H. Ågren and J. Zhang, *J. Phys. Chem. C*, 2020, **124**, 3980–3987.
- 74 A. D. Laurent, C. Adamo and D. Jacquemin, *Phys. Chem. Chem. Phys.*, 2014, **16**, 14334–14356.
- 75 M. Y. Mehboob, M. U. Khan, R. Hussain, K. Ayub, A. Sattar, M. K. Ahmad, Z. Irshad and M. Adnan, *Spectrochim. Acta, Part A*, 2021, **244**, 118873.



- 76 M. Y. Mehboob, M. U. Khan, R. Hussain, R. Fatima, Z. Irshad and M. Adnan, *J. Theory Comput. Chem.*, 2020, **19**, 2050034.
- 77 M. Y. Mehboob, R. Hussain, M. U. Khan, M. Adnan, A. Umar, M. U. Alvi, M. Ahmed, M. Khalid, J. Iqbal and M. N. Akhtar, *Comput. Theor. Chem.*, 2020, **1186**, 112908.
- 78 M. Y. Mehboob, R. Hussain, M. U. Khan, M. Adnan, M. A. Ehsan, A. Rehman and M. R. S. A. Janjua, *J. Phys. Org. Chem.*, 2021, e4204.
- 79 A. D. Becke, *J. Chem. Phys.*, 1993, **98**, 1372–1377.
- 80 T. H. Dunning Jr, *Chem. Phys.*, 1989, **90**, 1007–1023.
- 81 J. K. Roy, S. Kar and J. Leszczynski, *J. Phys. Chem. C*, 2019, **123**, 3309–3320.
- 82 S. Kupfer, J. Guthmuller and L. Gonzalez, *J. Chem. Theory Comput.*, 2013, **9**, 543–554.
- 83 P. J. Hay and W. R. Wadt, *J. Chem. Phys.*, 1985, **82**, 270–283.
- 84 R. Sánchez-de-Armas, M. A. San Miguel, J. Oviedo and J. F. Sanz, *Phys. Chem. Chem. Phys.*, 2012, **14**, 225–233.
- 85 T. Yanai, D. P. Tew and N. C. Handy, *Chem. Phys. Lett.*, 2004, **393**, 51–57.
- 86 G. Deogratias, N. Seriani, T. Pogrebnyaya and A. Pogrebnoi, *J. Mol. Graphics Modell.*, 2020, **94**, 107480.
- 87 J. Zhang, H.-C. Zhu, R.-L. Zhong, L. Wang and Z.-M. Su, *Org. Electron.*, 2018, **54**, 104–113.
- 88 H.-C. Zhu, C.-F. Li, Z.-H. Fu, S.-S. Wei, X.-F. Zhu and J. Zhang, *Appl. Surf. Sci.*, 2018, **455**, 1095–1105.
- 89 M. J. Frisch, G. W. Trucks, H. B. Schlegel, G. E. Scuseria, M. A. Robb, J. R. Cheeseman, G. Scalmani, V. Barone, G. A. Petersson, H. Nakatsuji, X. Li, M. Caricato, A. V. Marenich, J. Bloino, B. G. Janesko, R. Gomperts, B. Mennucci, H. P. Hratchian, J. V. Ortiz, A. F. Izmaylov, J. L. Sonnenberg, D. Williams-Young, F. Ding, F. Lipparini, F. Egidi, J. Goings, B. Peng, A. Petrone, T. Henderson, D. Ranasinghe, V. G. Zakrzewski, J. Gao, N. Rega, G. Zheng, W. Liang, M. Hada, M. Ehara, K. Toyota, R. Fukuda, J. Hasegawa, M. Ishida, T. Nakajima, Y. Honda, O. Kitao, H. Nakai, T. Vreven, K. Throssell, J. A. Montgomery Jr., J. E. Peralta, F. Ogliaro, M. J. Bearpark, J. J. Heyd, E. N. Brothers, K. N. Kudin, V. N. Staroverov, T. A. Keith, R. Kobayashi, J. Normand, K. Raghavachari, A. P. Rendell, J. C. Burant, S. S. Iyengar, J. Tomasi, M. Cossi, J. M. Millam, M. Klene, C. Adamo, R. Cammi, J. W. Ochterski, R. L. Martin, K. Morokuma, O. Farkas, J. B. Foresman and D. J. Fox, *Gaussian 16, Revision A.03*, Gaussian, Wallingford, CT, 2016.
- 90 M. Y. Mehboob, R. Hussain, Z. Irshad and M. Adnan, *J. Phys. Org. Chem.*, 2021, e4210.
- 91 R. Hussain, M. Y. Mehboob, M. U. Khan, M. Khalid, Z. Irshad, R. Fatima, A. Anwar, S. Nawab and M. Adnan, *J. Mater. Sci.*, 2021, **56**, 5113–5131.
- 92 M. Y. Mehboob, R. Hussain, Z. Irshad and M. Adnan, *Bull. Korean Chem. Soc.*, 2021, **42**, 597–610.
- 93 L. Zhang and J. M. Cole, *ACS Appl. Mater. Interfaces*, 2015, **7**, 3427–3455.
- 94 M. Pastore and F. De Angelis, *Phys. Chem. Chem. Phys.*, 2012, **14**, 920–928.
- 95 P. Li, Z. Wang, C. Song and H. Zhang, *J. Mater. Chem. A*, 2017, **5**, 11454–11465.
- 96 R. Katoh, A. Furube, T. Yoshihara, K. Hara, G. Fujihashi, S. Takano, S. Murata, H. Arakawa and M. Tachiya, *J. Phys. Chem. B*, 2004, **108**, 4818–4822.
- 97 J. Preat, C. Michaux, D. Jacquemin and E. A. Perpète, *J. Phys. Chem. C*, 2009, **113**, 16821–16833.
- 98 N. N. Ghosh, M. Habib, A. Pramanik, P. Sarkar and S. Pal, *New J. Chem.*, 2019, **43**, 6480–6491.
- 99 J. Zhang, H.-B. Li, S.-L. Sun, Y. Geng, Y. Wu and Z.-M. Su, *J. Mater. Chem.*, 2012, **22**, 568–576.
- 100 G. Boschloo and A. Hagfeldt, *Acc. Chem. Res.*, 2009, **42**, 1819–1826.
- 101 T. Koopmans, *Physica*, 1933, **1**, 104–113.
- 102 C.-R. Zhang, Z.-J. Liu, Y.-H. Chen, H.-S. Chen, Y.-Z. Wu, W. Feng and D.-B. Wang, *Curr. Appl. Phys.*, 2010, **10**, 77–83.

## ABSTRACT

---

Name of the Student: Divya Velayudhan V. V.

Registration No.: 10CC15A39004

Faculty of Study: Chemical Sciences

Year of Submission: 2021

AcSIR academic centre/CSIRLab: CSIR-NIIST

Name of the Supervisor: Dr. C. H. Suresh

**Title of the thesis:** Density Functional Theory Studies on D- $\pi$ -A Systems Used in Dye-Sensitized Solar Cells: Donor-Acceptor Effect, Spacer Effect, and Molecular Design Strategies

---

Dye-sensitized solar cells (DSSCs) have a fundamental role in photovoltaic technology as an alternative to highly expensive conventional silicon based solar cell. Theoretical studies are greatly acknowledged for the reliable prediction of efficiency of dye-sensitizers and understanding the fundamental processes involved in DSSC device. The thesis is organized into four chapters. Chapter 1 gives an overview of both DSSCs and computational chemistry methods. In chapter 2, using molecular electrostatic potential (MESP) analysis, the electronic effect transmission power ( $\gamma$ ) of various spacer (G in the notation) units in a Y-G-X type molecular model and electron donating strength ( $\Delta V_{mA}$ ) of typically used donors in D- $\pi$ -A type dye-sensitizers have been computed. Among the studied spacers units, alkenyl spacers with shorter spacer chain length showed the highest  $\gamma$ , which will be effective for the better power conversion efficiency (PCE) in DSSCs. Further,  $\Delta V_{mA}$  is found to be proportional to absorptional redshift and open-circuit voltage ( $eV_{OC}$ ) which shows the relevance of  $\Delta V_{mA}$  for the enhancement of optical and photovoltaic properties of dye-sensitizers. In chapter 3, the role of electron donating substituents on the donor region of D- $\pi$ -A systems has been analysed and found that  $\Delta V_{mA}$ , optical, and photovoltaic properties have been improved in substituted D- $\pi$ -A systems than bare D- $\pi$ -A. Finally in chapter 4, the significance of nitrogen centres for revamping the donating strength of D- $\pi$ -A is scrutinized. The results show that absorption maxima, adsorption stability of dye/TiO<sub>2</sub> interface, and photovoltaic properties enhanced with number of N-centres at donor region. In all chapters, the strong linear correlation observed for the ground state property  $\Delta V_{mA}$  and  $eV_{OC}$  provides guidelines for effective dye design with a desirable photovoltaic applications. For the prediction of PCE, the study developed a new theoretical strategy (MESP based).

## List of Publications

### I. Publications related to thesis

1. Substituent Effect Transmission Power of Alkyl, Alkenyl, Alkynyl, Phenyl, Thiophenyl, and Polyacene Spacers, **Velayudhan V. Divya**, Fareed Bhasha Sayyed, and Cherumuttathu H. Suresh,\* *ChemPhysChem* **2019**, 20, 1752– 1758
2. Density functional theory study on the donating strength of donor systems in dye-sensitized solar cells, **Velayudhan V. Divya** and Cherumuttathu H. Suresh,\* *New J. Chem.*, **2020**, 44, 7200
3. Tuning the donating strength of dye sensitizers using molecular electrostatic potential analysis, **Velayudhan V. Divya** and Cherumuttathu H. Suresh,\* *New J. Chem.*, **2021**, 45, 2496
4. Design and DFT study of nitrogen-rich donor systems for improved photovoltaic performance in dye-sensitized solar cells, **Velayudhan V. Divya** and Cherumuttathu H. Suresh,\* *New J. Chem.*, **2021**, 45, 11585-11595

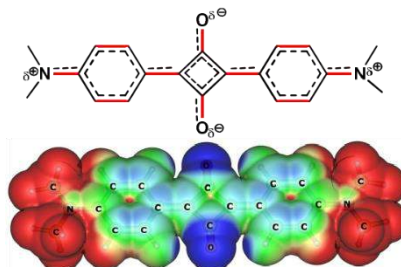
### II. Publications out of thesis

1. Electronic Structure of Bis (4-dimethylaminophenyl) squaraine, **Velayudhan V. Divya** and Cherumuttathu H. Suresh, \* *ChemistrySelect*, **2019**, 4, 3387 –3394
2. Solution Processable Deep-Red Phosphorescent Pt (II) Complex: Direct Conversion from Its Pt(IV) Species via a Base-Promoted Reduction, Ilene Allison, Hyunsoo Lim, Atul Shukla, Viqar Ahmad, Monirul Hasan, Kedar Deshmukh, Robert Wawrzinek, Sarah K. M. McGregor, Jack K. Clegg, **Velayudhan V. Divya**, Chinju Govind, Cherumuttathu H. Suresh, Venugopal Karunakaran, Narayanan Unni K. N., Ayyappanpillai Ajayaghosh, Ebinazar B. Namdas\* and Shih-Chun Lo,\* *ACS Appl. Electron. Mater.*, **2019**, 1, 1304–1313
3. Regulating Back Electron Transfer through Donor and  $\pi$ -Spacer Alterations in Benzothieno[3,2-b]indole-based Dye-sensitized Solar Cells, P. R Nitha, V. Jayadev, Sourava C. Pradhan, **Velayudhan V. Divya**, Cherumuttathu H. Suresh, Jubi John,\* Suraj Soman,\* Ayyappanpillai Ajayaghosh\* *Chem Asian J.*, **2020**, 15, 3 503–3512

### III. Published contributions to academic conferences

1. Presented a poster entitled “Electronic Structure of Bis(4-dimethylaminophenyl) Squaraine” at the Theoretical Chemistry Symposium (TCS), BITS Pilani, Pilani, Rajasthan, 13-16 February, 2019.

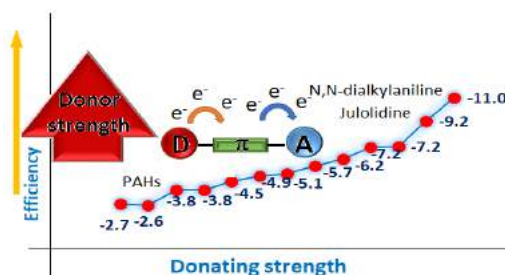
**Abstract:** Squaraine is a well-known organic functional material in the field of photovoltaics due to its energy harvesting characteristics. The aim of the present study is to understand in detail the electronic structure of squaraine dye as well as its



noncovalent interaction with solvent molecules. The structural and electronic features of bis (4dimethylaminophenyl) squaraine (1) has been studied using density functional BLYP/631G(d,p) level of theory. The quinoid character of 1 is correlated to partial double bond character of C-NMe<sub>2</sub> (1.386 Å) and C-O (1.243 Å) bonds which leads to accumulation of positive charge on NMe<sub>2</sub> groups and negative charge on carbonyl oxygen. Further, the diagonal C1C3 (2.089 Å) and C2C4 (2.126 Å) distances of the squaric ring indicated a 1,3 type C-C orbital interaction. Molecular electrostatic potential (MESP) topographical analysis confirmed the charge separated quadrupolar nature of 1. The MESP minimum, V<sub>min</sub> located at the carbonyl oxygen, -63.9 kcal/mol, confirmed its highly electron rich character arising from the quinoid structure. The electronic structure of 1 revealed from MESP confirmed its quadrupolar nature and suggested the location of positive charge on NMe<sub>2</sub> groups. The typically used chemical structure drawing of 1 showing +2 charge on the squaraine ring is inaccurate and misleading. The solvatochromic behaviour of 1 can be attributed to its quadrupolar electronic structure wherein the electron rich carbonyl groups provide room for noncovalent interactions with multiple solvent molecules.

2. Presented a Poster entitled “Density functional theory study on the donating strength of donor systems in dye-sensitized solar cells” - 14th International Conference on Ecomaterials (ICEM-14), CSIR-National Institute for Interdisciplinary Science and Technology (NIIST), Industrial Estate (P.O.), Thiruvananthapuram, Kerala, 5 – 7 February, 2020.

**Abstract:** Developing a highly efficient D- $\pi$ -A system for dye-sensitized solar cell (DSSC) application *via* improved donor strength became an emerging area of interest for the last two decades.<sup>1</sup> Since the electron-donating strength of the donor fragment determines the electronic and optical properties of the system, it is highly essential to know the donating strength of such units beforehand. Herein, a TD-CAM B3LYP/cc-pVDZ//B3LYP/cc-pVDZ density functional theory study has been carried out on 13 typically used donor systems for the analysis of optical, and photovoltaic properties. The electron-donating strength of the donor system has been quantified in terms of the molecular electrostatic potential at anchoring moiety. Further, a remarkable linear correlation obtained between donating strength ( $\Delta V_{mA}$ ) and absorption shift ( $\Delta\lambda_{max}$ ), open-circuit voltage ( $V_{oc}$ ) shows the significance of  $\Delta V_{mA}$  on  $\Delta\lambda_{max}$  and  $V_{oc}$ . Among the investigated D- $\pi$ -A systems, N,N-dialkyl aniline, and julolidine were found to be the best donors for the photovoltaic application. In general, by tuning the donating strength we can able to enhance  $V_{oc}$ , thereby enhances the efficiency of the D- $\pi$ -A system.



# **SCI Publications**

# Substituent Effect Transmission Power of Alkyl, Alkenyl, Alkynyl, Phenyl, Thiophenyl, and Polyacene Spacers

Velayudhan V. Divya,<sup>[a, b]</sup> Fared Bhasha Sayyed,<sup>[a]</sup> and Cherumuttathu H. Suresh<sup>\*[a, b]</sup>

The transmission of substituent effect through a variety of spacers, that is to say, alkyl, alkenyl, alkynyl, phenyl, thiophenyl, and polyacene has been studied by modeling Y-G-X type molecular systems (Y: reaction center; G: spacer moiety; X: substituent) using B3LYP/6-31G(d,p) density functional theory calculations. The reaction center is always kept as a C=C double bond and the molecular electrostatic potential (MESP) minimum ( $V_{\min}$ ) observed for this bond showed subtle variation with respect to the changes in the spacer unit and the nature of substituent. Strong linear correlations are observed between Hammett substituent constants ( $\sigma_I$  and  $\sigma_P$ ) and  $V_{\min}$ , which

recommend the aptness of  $V_{\min}$  as an electronic descriptor to quantify the substituent effect. Since  $V_{\min}$  offers an alternative measure of substituent effect, the correlation between  $V_{\min}$  and  $\sigma_P$  has been used for assessing the transmission of substituent effect through a variety of spacer moieties. The highest transmission coefficient ( $\gamma$ ) is always observed for smaller spacer length. Among all the spacers, alkenyl showed the highest and alkyl showed the lowest transmission power. The study recommends the use of short chains of C=C double, C≡C triple or a combination of both as spacers for the effective transmission of substituent effect to the reaction center.

## 1. Introduction

Substituents in molecules are regarded as functional groups and tuning of various chemical properties can be achieved by controlling the substituent effects.<sup>[1]</sup> The theory of substituent effect has been considered as fundamental to the prediction of molecular reactivity.<sup>[1–2]</sup> The electronic effect of a substituent can be transmitted to the reaction center via a transmitting moiety. For example in a molecule Y-G-X, (Y: reaction center; G: spacer moiety; X: substituent), the effect of X at Y through G can be interpreted with the famous Hammett relationship  $\log(K_X/K_0) = \rho\sigma$ , where  $\rho$  is the reaction constant and  $\sigma$  is the substituent constant. Hammett equation and several of its modifications<sup>[2a,3]</sup> have been used in a quantitative way for the effective interpretation of substituent effects.<sup>[4]</sup> The applicability of  $\sigma$ -constants for a variety of molecules assisted the understanding of structure-activity and structure-property relationships in chemistry.<sup>[5]</sup>

Substituent effects are classified into inductive (through  $\sigma$  bond),  $\pi$  – resonance and through space (field) effects.<sup>[1a,2a,6]</sup> The separation of the substituent effect into inductive ( $\sigma_I$  or F) and resonance effect ( $\sigma_R$  or R) was done by Swain and Lupton.<sup>[7]</sup> They interpreted that the negative and positive values of substituent constant indicate electron donating and withdrawing nature of substituents, respectively. Using quantum chemical approaches, many efforts have been made to model the

substituent effect.<sup>[4–5,8]</sup> Substituent effects are responsible for small perturbations on the molecular electron density distribution, which can be measured by means of correlating them with the computed quantities of total energy, atomic charges, and electrostatic potentials resulting from ab initio quantum chemical or semiempirical methods.<sup>[5a,9]</sup> Further, several experimental studies have utilized Y-G-X type systems to understand the substituent effect transmission ability of various spacer moieties using geometrical variables, ionization techniques, and NMR chemical shifts etc.<sup>[8f,10]</sup>

Among the several theoretical quantities used to interpret Hammett constants, topographical analysis of molecular electrostatic potential (MESP) provided a clean approach to substituent effects.<sup>[5a–c,8c–e]</sup> The prediction and rationalization of reactivity trends using MESP have been pioneered by Scrocco, Tomasi, and co-workers.<sup>[11]</sup> Politzer and Murry widely used the MESP plots calculated using standard electronic structure theory to interpret while the topographical analysis of MESP has been pioneered by Gadre et al.<sup>[12]</sup> From MESP topographical studies on conjugated organic molecular systems, Suresh et al. have shown that critical features of MESP are useful for the quantification of inductive,<sup>[13]</sup> resonance,<sup>[14]</sup> steric<sup>[15]</sup> and proximity effects<sup>[8b]</sup> of substituents. Also, MESP minimum ( $V_{\min}$ ) has been used as a powerful electronic descriptor to quantify substituent effect, trans influence and two electron donor character of ligands.<sup>[5a,c,16]</sup> Here we intend to study Y-G-X type systems using  $V_{\min}$  analysis. The substituent effect transmission power of X through the spacer will be assessed by the  $V_{\min}$  observed over Y, an olefinic moiety. Although the significance of such spacers in donor-acceptor systems is well known, quantification of substituent effect transmission power of a variety of spacer systems is yet to be systematically analyzed. Previous studies showed that modifications in spacer units such as their  $\pi$ -bond character, conjugation length, and planarity had a significant role in electron transmission power, absorption

[a] V. V. Divya, Dr. F. B. Sayyed, Dr. C. H. Suresh  
Chemical Sciences and Technology Division  
CSIR – National Institute for Interdisciplinary Science and Technology  
Thiruvananthapuram, Kerala, 695 019, India  
E-mail: sureshch@niist.res.in

[b] V. V. Divya, Dr. C. H. Suresh  
Academy of Scientific and Innovative Research (AcSIR)  
Ghaziabad-201002, India

Supporting information for this article is available on the WWW under <https://doi.org/10.1002/cphc.201900206>

wavelength, and other related photophysical properties.<sup>[17]</sup> Here spacers such as alkyl, alkenyl, alkynyl, phenyl, thiophenyl, and polyacenes have been selected to include the inductive, and resonance effect aspects. We envision that this study will provide useful information regarding the future dye designing and other related studies.

## 2. Results and Discussion

### 2.1. MESP Topography and Spacer Effects

MESP is one of the most appropriate electronic descriptors to understand the electron withdrawing and donating nature of substituents and ligands.<sup>[5a,b,12d, 16a, 18]</sup> It is recognized that electron rich region in a molecule experiences a significant change in MESP minimum ( $V_{min}$ ) due to substituent effects. Here we consider an olefinic bond (Figure 1) as a sensitive region to

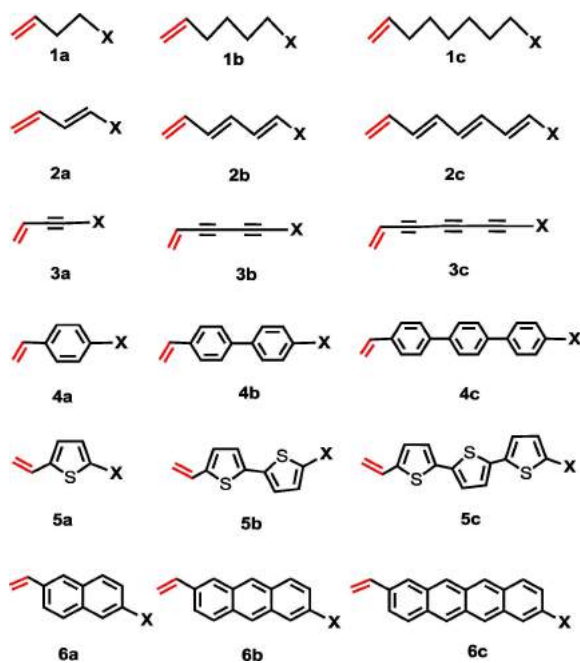


**Figure 1.** Various spacers considered to quantify the transmission power of spacers. The double bond marked in red is the region where MESP minimum is located for  $X=\text{NH}_2$ ,  $\text{OH}$ ,  $\text{CH}_3$ ,  $\text{H}$ ,  $\text{F}$ ,  $\text{Cl}$ ,  $\text{CF}_3$ ,  $\text{CHO}$ ,  $\text{CN}$  and  $\text{NO}_2$ .

understand the precise variation of  $V_{min}$  with respect to the substituent effect. A general notation  $\text{C}_2\text{H}_3\text{-G}_n\text{-X}$  has been used to denote the molecule, where  $\text{G}_n$  stands for the repeating 'n' spacer G units between  $\text{C}_2\text{H}_3$  and X. The effect of substituent on  $\text{C}_2\text{H}_3\text{-}$  has been measured in terms of  $V_{min}$  on its CC double bond. Electron donating and withdrawing substituents used in this study include  $\text{NH}_2$ ,  $\text{OH}$ ,  $\text{CH}_3$ ,  $\text{H}$ ,  $\text{F}$ ,  $\text{Cl}$ ,  $\text{CF}_3$ ,  $\text{CHO}$ ,  $\text{CN}$  and  $\text{NO}_2$ . The spacers selected for the study are alkyl, alkenyl, alkynyl, phenyl, thiophenyl, and polyacenes (Figure 1). For a reasonable understanding about the spacer length, systems up to  $n=3$  have been considered. In studies related to the substituent

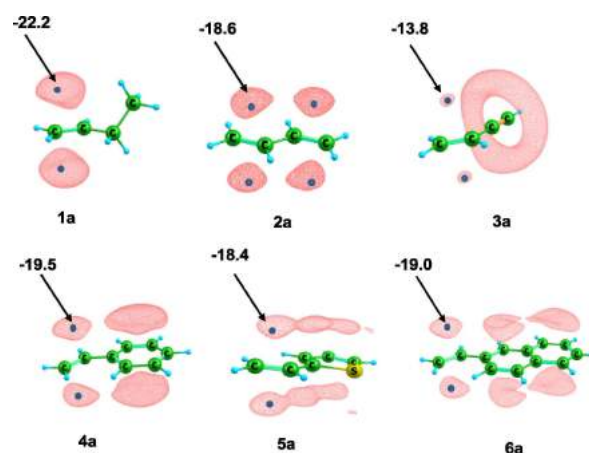


**Figure 2.** MESP isosurface at  $-13.0 \text{ kcal mol}^{-1}$  for **1a**, **2a**, **3a**, **4a**, **5a** and **6a**.  $V_{min}$  values in  $\text{kcal mol}^{-1}$  are also depicted.

effect, a system with  $X=\text{H}$  is described as the unsubstituted reference system. Hence the change in  $V_{min}$  due to substitution is designated as  $\Delta V_{min}$  which gives a direct estimation of the substituent effect.<sup>[8c]</sup>

MESP isosurface for **1a**, **2a**, **3a**, **4a**, **5a** and **6a** ( $X=\text{H}$ ) is shown in Figure 2 along with the respective  $V_{min}$  values at the terminal double bond, viz.  $-22.2$ ,  $-18.6$ ,  $-13.8$ ,  $-19.5$ ,  $-18.4$ ,  $-19.0 \text{ kcal/mol}$ . The  $V_{min}$  at the terminal double bond for all the substituted systems (total 180 systems) is depicted in Table 1. The  $V_{min}$  ranges from  $-30.5$  to  $3.8 \text{ kcal/mol}$  which indicates the effect of both spacer moiety and the substituent on tuning the electron distribution on the double bond. In  $\text{C}_2\text{H}_3\text{-alkyl-X}$  systems (**1a–1c**), the inductive effect is the prime factor for electron transmission. A less negative  $V_{min}$  is observed for  $X=\text{NH}_2$  and  $X=\text{OH}$  than  $X=\text{H}$  suggesting the electron withdrawing inductive ( $-I$ ) character of the highly electronegative N and O atoms. For  $X=\text{CH}_3$  and  $n=1$ ,  $V_{min}$  is slightly more negative than  $X=\text{H}$  indicating the electron donating inductive ( $+I$ ) effect of the methyl group. An increase in alkyl chain length slightly enhances this electron donation. Further, the  $-I$  effect of substituents  $\text{Cl}$ ,  $\text{CF}_3$ ,  $\text{CN}$ ,  $\text{NO}_2$  etc. are clearly reflected on their respective  $V_{min}$ . The diminishing  $-I$  effect with an increase in alkyl chain length is pronounced in the case of  $\text{CN}$  and  $\text{NO}_2$ . For example,  $V_{min}$  of  $\text{NH}_2$  substituted systems shows a variation of  $\sim 1.3 \text{ kcal mol}^{-1}$  from  $n=1$  to  $n=3$ , while  $\text{CN}$  and  $\text{NO}_2$  exhibits a variation of  $9.4$  and  $8.1 \text{ kcal mol}^{-1}$ , respectively. The inductive control of electronic transmission in alkyl systems is confirmed by the strong linear correlation between  $V_{min}$  and inductive substituent constant ( $\sigma_I$ ) (Figure 3 and Table S1). The slope of the correlation plot  $19.081$  observed for spacer length  $n=1$  is the highest and it decreases to  $10.343$  for  $n=2$  and further decreases to  $5.5683$  for  $n=3$ . This data indicates the rapidly decreasing behavior of  $I$  with the increase in the number of CC single bonds.<sup>[13]</sup>

For the case of unsubstituted alkenyl systems (**2a–2c**),  $V_{min}$  values are observed at  $-18.6$ ,  $-18.4$ , and  $-18.3 \text{ kcal/mol}$  respectively. The small variation in  $V_{min}$  indicates the negligible impact of spacer length on electronic transmission whereas the



**Table 1.**  $V_{\min}$  (in kcal mol<sup>-1</sup>) obtained over the terminal double bond of various spacer systems.

X	NH <sub>2</sub>	OH	CH <sub>3</sub>	H	F	Cl	CF <sub>3</sub>	CHO	CN	NO <sub>2</sub>
1a	-21.9	-20.7	-22.3	-22.2	-16.3	-14.0	-15.2	-15.1	-11.1	-10.7
1b	-22.3	-21.6	-22.5	-22.5	-19.1	-18.1	-18.6	-18.4	-16.4	-16.3
1c	-23.2	-22.1	-22.5	-22.5	-20.6	-19.9	-20.2	-20.0	-20.5	-18.8
2a	-30.5	-25.4	-21.6	-18.6	-17.0	-13.3	-8.6	-7.3	-3.6	0.1
2b	-28.6	-24.3	-20.8	-18.4	-17.9	-14.8	-10.7	-9.0	-6.8	-3.5
2c	-24.3	-23.3	-20.4	-18.3	-18.1	-15.6	-12.2	-10.5	-8.9	-6.0
3a	-25.9	-20.6	-18.4	-13.8	-14.0	-11.9	-3.7	-3.0	1.4	3.8
3b	-20.1	-16.3	-14.3	-10.2	-11.0	-9.7	-2.7	-2.0	1.3	3.1
3c	-13.2	-13.1	-11.5	-8.0	-8.9	-7.9	-2.1	-1.5	1.1	2.5
4a	-25.8	-21.8	-21.0	-19.5	-17.5	-15.1	-12.5	-11.1	-8.5	-6.7
4b	-22.0	-20.2	-19.8	-19.1	-17.9	-16.7	-15.4	-14.8	-13.2	-12.4
4c	-20.0	-19.4	-19.3	-18.9	-18.1	-15.1	-16.8	-16.4	-15.5	-15.0
5a	-24.5	-20.8	-20.1	-18.4	-16.3	-14.4	-10.5	-8.7	-6.2	-3.5
5b	-20.8	-19.1	-18.2	-17.1	-15.9	-14.8	-12.5	-10.7	-9.6	-7.3
5c	-18.6	-17.4	-17.2	-16.6	-15.8	-15.1	-13.5	-12.3	-11.5	-9.8
6a	-23.5	-20.6	-20.2	-19.0	-17.4	-15.8	-13.9	-12.8	-11.0	-9.5
6b	-22.1	-20.1	-19.6	-18.8	-17.5	-16.1	-14.8	-13.8	-12.4	-11.2
6c	-20.5	-19.5	-19.2	-18.6	-17.4	-16.4	-15.4	-14.6	-13.5	-12.6

individual effect of a substituent on  $V_{\min}$  is very high in **2** series. For instance,  $\Delta V_{\min}$  of NH<sub>2</sub> and OH in **2** is significantly more negative than those in **1**. In **2**, NH<sub>2</sub> and OH donate electrons

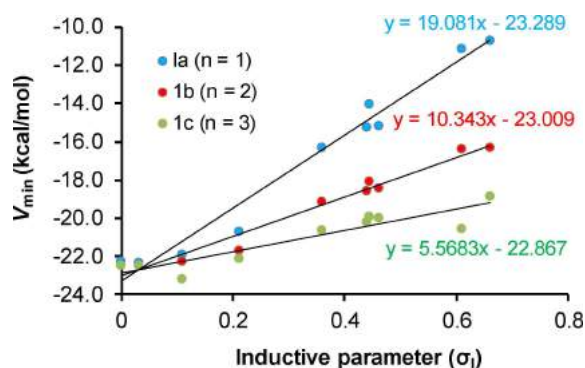


**Figure 3.** Correlation between the  $V_{\min}$  of **1a–1c** with the inductive parameter ( $\sigma_I$ ).

mainly through resonance mechanism. NH<sub>2</sub> is the most electron donating with  $\Delta V_{\min}$  -11.9, -10.2 and -6.0 kcal mol<sup>-1</sup> for **2a**, **2b**, and **2c**, respectively (Table 2 while the most electron withdrawing NO<sub>2</sub> shows  $\Delta V_{\min}$  18.7, 14.9 and 12.4 kcal mol<sup>-1</sup>. Increasing the spacer length diminishes the power of electron transmission. Further, in the case of CH<sub>3</sub>,  $V_{\min}$  is more negative than the unsubstituted system which can be mainly attributed to the electron donating hyperconjugation and +I effect of CH<sub>3</sub>. Here the magnitude of electron donation for **2a–2c** in terms of  $\Delta V_{\min}$  is -3.0, -2.4, and -2.1 kcal/mol (Table 2). Substituents F, Cl, CF<sub>3</sub>, CHO, CN, and NO<sub>2</sub> show a considerable decrease in the magnitude of  $V_{\min}$  compared to the reference system, which authenticates their electron withdrawing inductive and resonance effects. The  $\Delta V_{\min}$  18.7, 15.0, 11.3, 10.0, 5.3, 1.6 kcal mol<sup>-1</sup> observed for the substituents NO<sub>2</sub>, CN, CHO, CF<sub>3</sub>, Cl and F, respectively suggest that their electron withdrawing power follows the order NO<sub>2</sub> > CN > CHO > CF<sub>3</sub> > Cl > F (Table 2). The strong linear correlations observed between  $V_{\min}$  of **2a**, **2b**, and **2c** systems with Hammett constant  $\sigma_p$  (Figure 4 and

**Table 2.**  $\Delta V_{\min}$  in kcal mol<sup>-1</sup> of various spacer systems.

X	$V_{\min}$ H	NH <sub>2</sub>	$\Delta V_{\min}$ OH	CH <sub>3</sub>	F	Cl	CF <sub>3</sub>	CHO	CN	NO <sub>2</sub>
1a	-22.2	0.3	1.5	-0.1	6.0	8.2	7.0	7.1	11.1	11.5
1b	-22.5	0.2	0.8	0.0	3.3	4.4	3.9	4.1	6.1	6.1
1c	-22.5	-0.7	0.4	0.0	1.9	2.6	2.3	2.5	1.9	3.6
2a	-18.6	-11.9	-6.8	-3.1	1.6	5.3	10	11.3	15.0	18.7
2b	-18.4	-10.2	-6.0	-2.4	0.5	3.6	7.7	9.3	11.6	14.9
2c	-18.3	-6.0	-5.0	-2.1	0.3	2.7	6.1	7.8	9.4	12.4
3a	-13.8	-12.1	-6.8	-4.6	-0.2	1.9	10.1	10.8	15.2	17.6
3b	-10.2	-9.9	-6.0	-4.1	-0.8	0.5	7.5	8.2	11.5	13.3
3c	-8.0	-5.2	-5.0	-3.5	-0.9	0.1	5.9	6.5	9.2	10.5
4a	-19.5	-6.3	-2.3	-1.4	2.0	4.5	7.1	8.4	11.0	12.8
4b	-19.1	-2.9	-1.1	-0.8	1.2	2.4	3.7	4.3	5.8	6.7
4c	-18.9	-1.1	-0.5	-0.4	0.8	3.8	2.1	2.4	3.4	3.9
5a	-18.4	-6.1	-2.4	-1.7	2.1	4	7.8	9.7	12.2	14.9
5b	-17.1	-3.7	-2.0	-1.1	1.1	2.3	4.6	6.4	7.5	9.7
5c	-16.6	-2.1	-0.8	-0.6	0.8	1.5	3.1	4.2	5.1	6.8
6a	-19.0	-4.5	-1.6	-1.2	1.6	3.3	5.1	6.2	8.0	9.5
6b	-18.8	-3.3	-1.3	-0.9	1.3	2.6	4.0	5.0	6.3	7.5
6c	-18.6	-1.9	-0.9	-0.6	1.1	2.1	3.2	4.0	5.1	6.0

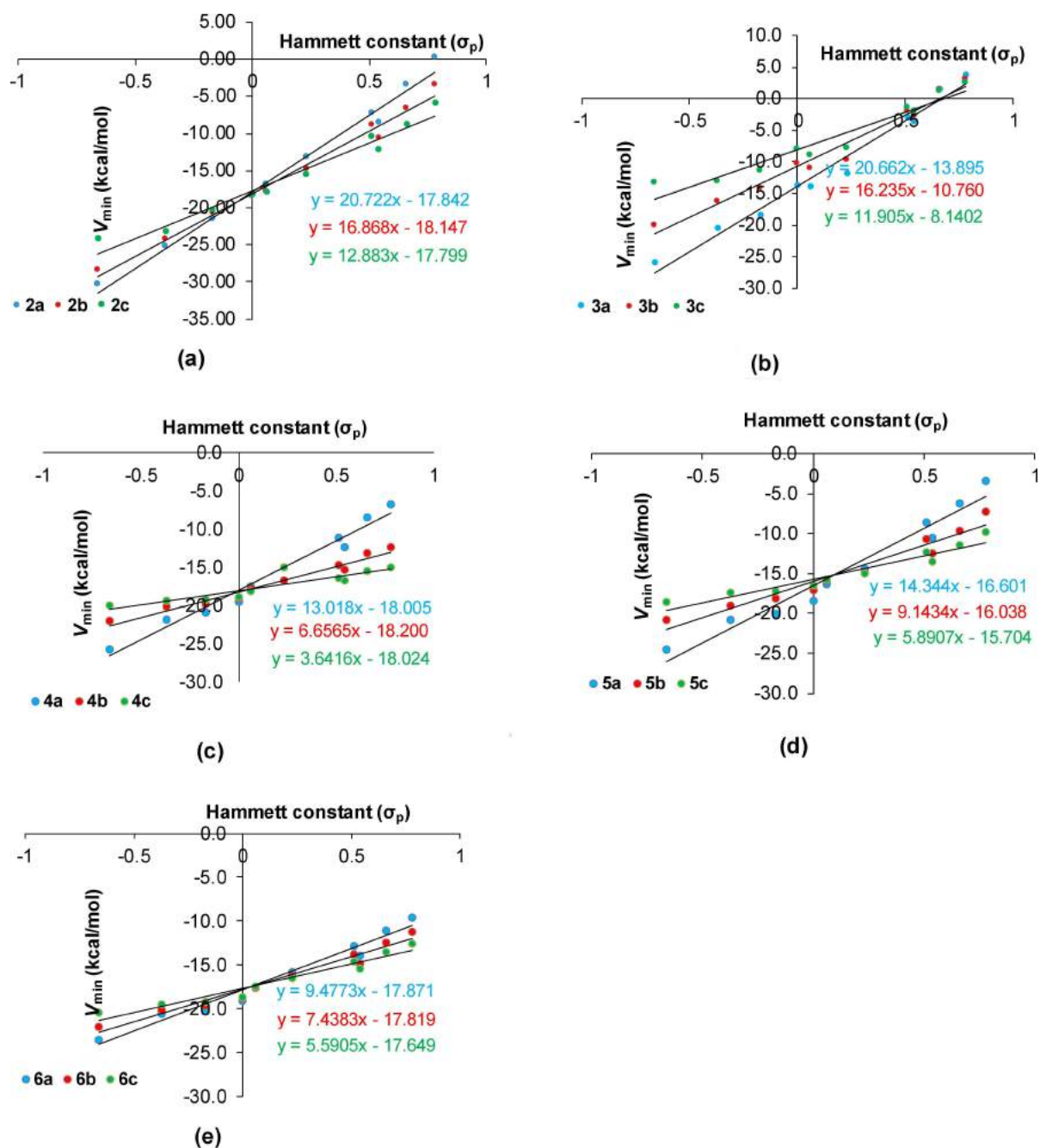


Figure 4. Correlation of  $V_{\min}$  with Hammett parameter ( $\sigma_p$ ) of a) alkenyl, b) alkylnyl, c) phenyl, d) thiophenyl, and e) polyacene systems.

Table S1) suggests that the MESP topographical quantity  $V_{\min}$  is highly suited as an electronic descriptor to quantify the electron donating and withdrawing nature of a substituent. The slope of the correlation plots decreases as  $n$  increase in the spacer length. Since  $\sigma_p = 0$  stands for the unsubstituted systems, the Y-intercept of the correlation plot corresponds to  $V_{\min}$  of the unsubstituted system. Indeed, the Y-intercept and  $V_{\min}$  of the unsubstituted system show very close agreement.

The unsubstituted alkylnyl systems, (**3a–3c**) shows  $V_{\min}$  values at  $-13.8$ ,  $-10.2$ , and  $-8.0$  kcal mol $^{-1}$ , respectively. The magnitude of these values are smaller than the unsubstituted

alkenyl systems indicating the more electronegative  $C_{sp}$  hybridized carbons in alkylnyl systems than  $C_{sp2}$  in alkenyl systems. Similar to **2**, resonance effect dominates in **3** except for  $X=CH_3$  and  $X=CF_3$ . The magnitude of electron withdrawing effect ( $\Delta V_{\min}$ ) obtained for substituents such as  $NO_2$ ,  $CN$ ,  $CHO$ ,  $CF_3$ ,  $Cl$ , and  $F$  is very similar to that found for  $C_2H_3$ -alkenyl- $X$  systems which indicates that substituent effect transmission power is similar for  $C=C$  double bonds and  $C\equiv C$  triple bonds.

The unsubstituted systems with phenyl ring spacers, **4a–4c** show  $V_{\min}$  values at  $-19.5$ ,  $-19.1$ , and  $-18.9$  kcal mol $^{-1}$ , respectively. The electron donating  $NH_2$ ,  $OH$ , and  $CH_3$  substitu-

ents enhance the negative character of  $V_{min}$  while the electron withdrawing F, Cl,  $CF_3$ , CHO, CN, and  $NO_2$  substituents diminish it. The similar  $V_{min}$  feature has been noticed for systems containing thiophenyl spacers, **5a–5c** and polyacene spacers, **6a–6c** (Table 1). In **4** series with  $n=2$  and 3, adjacent two phenyl units are twisted away from planarity which gives a diminishing effect on the electron donating/withdrawing ability of the substituent. The C–C single bond connection between two phenyl units in **4** proposes a significant inductive effect along with resonance. In polyacenes, resonance effect dominates over the inductive effect. In **4**, **5** and **6** series, increase in spacer length has a decreasing effect on the transmission power of the substituent effect.

## 2.2. $V_{min}$ -Based Quantification of Substituent Effect Transmission Power of Spacers

When a reacting center and substituent are separated by a variety of spacers, significant variations in the molecular properties can be observed.<sup>[19]</sup> The transmission of the substituent effect through olefinic systems showed the applicability of  $\rho$  in calculating the substituent effect transmission power. From the previous studies,<sup>[10b,d]</sup> it is understood that the transmission power of a spacer can be quantified by the transmission coefficient ( $\gamma$ ) defined as  $\gamma = \rho_s / \rho_o$ , where  $\rho_s$  is the reaction constant of a spacer for which the transmission power has to be quantified and  $\rho_o$  is the reaction constant of the reference group. Since  $V_{min}$  provides an alternative measure of substituent effects for  $\pi$ -conjugated systems, the correlation of  $V_{min}$  with  $\sigma_p$  can be used to evaluate the transmission ability of various spacers using the equation,  $V_{min} = \rho\sigma_p + \text{constant}$ . Therefore, linear regression analysis between  $V_{min}$  and  $\sigma_p$  values is carried out to find the  $\rho$  values (Table 3). In order to calculate the transmission coefficients ( $\gamma$ ), the phenyl group substituted **4a** is taken as the reference system for all the spacers. For **4a** systems,  $V_{min} = 13.018(\sigma_p) - 18.00$  and the slope of this equation ( $\rho_{4a}$ ) is used as  $\rho_o$  to determine  $\gamma$ . For example, the  $\gamma$  value for **2a** is calculated as  $\gamma = \rho_{2a} / \rho_{4a} = 20.722 / 13.018 = 1.592$  meaning that the transmission power of **2a** is 1.592 times higher than

**Table 3.** Slope, intercept, reaction constant ( $\rho_s$ ), correlation coefficient (R) and transmission coefficient ( $\gamma$ ) of various spacers.

X	Slope	Intercept	$\rho_s$	R	$\gamma$
<b>2a</b>	20.722	−17.84	20.722	0.994	1.592
<b>2b</b>	16.868	−18.15	16.868	0.993	1.296
<b>2c</b>	12.883	−17.80	12.883	0.981	0.989
<b>3a</b>	20.662	−13.90	20.662	0.988	1.587
<b>3b</b>	16.235	−10.76	16.235	0.985	1.247
<b>3c</b>	11.905	−8.14	11.905	0.962	0.914
<b>4a</b>	13.018	−18.00	13.018	0.987	1.000
<b>4b</b>	6.667	−18.20	6.667	0.984	0.512
<b>4c</b>	3.642	−18.02	3.642	0.895	0.280
<b>5a</b>	14.344	−16.60	14.344	0.979	1.102
<b>5b</b>	9.143	−16.03	9.143	0.973	0.702
<b>5c</b>	5.891	−15.70	5.891	0.961	0.452
<b>6a</b>	9.477	−17.87	9.477	0.984	0.728
<b>6b</b>	7.438	−17.81	7.438	0.983	0.571
<b>6c</b>	5.591	−17.65	5.591	0.974	0.429

phenyl ring. Among the  $\pi$ -bonded spacers, for  $n=1$ , the order of substituent effect transmission power of spacers is **2a**  $\approx$  **3a** > **5a** > **4a** > **6a**. On the basis of the average of all the  $\gamma$  values for a particular spacer from  $n=1–3$ , the order of transmission power of substituent effects is as follows: **2a–2c** > **3a–3c** > **5a–5c** > **4a–4c** > **6a–6c**. This order is in agreement with the experimental findings<sup>[10b]</sup> and suggesting the appropriateness of  $V_{min}$  method for the present study.

## 2.3. Combination of Two Different Spacers and Substituent Selectivity

To understand the transmission ability of a combination of two different spacers, we selected six types of spacers as shown in Figure 5. In **7a** and **7b** the substituent is connected to the double bonded carbon and an aromatic ring, respectively. In Table 4, the  $V_{min}$  values obtained for all the hetero spacers are reported. For substituent 'H' the  $V_{min}$  values of **7a** and **7b** are  $-18.76$  and  $-18.89$  kcal/mol showing a variation of  $0.13$  kcal mol<sup>−1</sup> between the two isomers. However, for other substituents, the difference in  $V_{min}$  is found to be less than  $\sim 1.0$  kcal mol<sup>−1</sup> suggesting that the electron donating or withdrawing nature is not highly affected whether 'X' is attached to the double bond or the phenyl ring. The  $V_{min}$  values for substituent 'H' of **8a** and **8b** are  $-16.32$  and  $-15.88$  kcal mol<sup>−1</sup> indicating that total electron withdrawing nature of ethynylbenzene is more when ethyne is attached directly to the olefinic

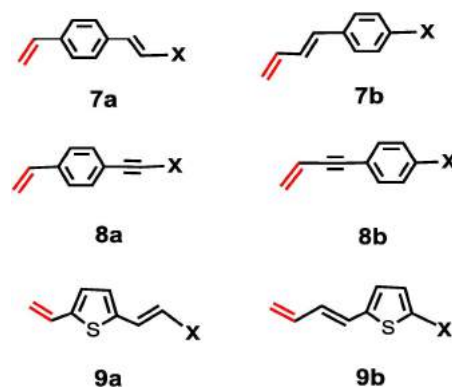


**Figure 5.** Spacers considered to quantifying the effect of the combination of two different spacers.

**Table 4.**  $V_{min}$  values (kcal/mol) obtained for hetero spacers.

X	7a	7b	8a	8b	9a	9b
<b>NH<sub>2</sub></b>	−24.85	−24.22	−22.78	−21.02	−24.16	−23.72
<b>OH</b>	−21.96	−21.08	−20.27	−17.95	−21.52	−20.83
<b>Me</b>	−20.21	−20.21	−18.83	−17.07	−19.39	−19.77
<b>H</b>	−18.76	−18.89	−16.32	−15.88	−17.51	−18.32
<b>F</b>	−17.70	−17.70	−16.50	−14.56	−16.75	−17.13
<b>Cl</b>	−15.81	−15.75	−15.44	−12.80	−14.56	−15.44
<b>CF<sub>3</sub></b>	−13.24	−13.49	−10.86	−10.67	−11.42	−12.30
<b>CHO</b>	−12.05	−12.17	−9.79	−9.60	−8.85	−10.35
<b>CN</b>	−10.17	−10.48	−10.48	−7.78	−7.97	−8.85
<b>NO<sub>2</sub></b>	−7.97	−8.79	−8.79	−6.28	−5.21	−6.34

moiety. Further, the electron withdrawing and donating substituents show maximum influence when they are attached to the phenyl ring. Additionally, for **9a** and **9b**,  $V_{\min}$  values for the unsubstituted systems are observed at  $-17.51$  and  $-18.32$  kcal/mol, respectively meaning that the variation is only  $0.81$  kcal/mol. In fact, for all the substituent except CHO and  $\text{NO}_2$ , the variation is less than  $\sim 1$  kcal/mol. This confirms that electronic effect is not highly affected whether 'X' is attached to a double bond or thiophenyl ring. In general, a spacer made up of two different moieties, substituent effect transmission power of 'X' can show a minor variation depending on the connectivity of X with the spacer unit.

### 3. Conclusions

The substituent effect transmission power of electron donating and withdrawing substituents on a terminal CC double bond has been assessed using MESP  $V_{\min}$  analysis. The  $V_{\min}$  observed on this bond showed significant change with respect to the electron donating/withdrawing nature of the substituent as well as the nature and length of the spacer unit. The  $V_{\min}$  correlates strongly with an inductive parameter for systems consisting of alkyl spacers. Similarly, for all the  $\pi$ -conjugated systems, strong linear correlations were observed between Hammett substituent constant and  $V_{\min}$ . The decreasing trend of slope values with an increase in the size of spacer length revealed the strongly diminishing nature of the substituent effect transmission. From the slope of the correlation plots, the transmission power of spacers are obtained which can be arranged in the order alkenyl > alkynyl > thiophenyl > phenyl > polyacene. For systems having alkyl spacers, transmission of substituent effect is the least as the inductive effect has a rapidly diminishing character with the increase in the size of the spacer unit. In summary, among all the spacer groups, alkenyl and alkynyl units are the most effective for the substituent effect transmission.

### 4. Computational Details

Geometry optimization has been carried out with B3LYP/6-31G(d, p) density functional theory method.<sup>[20]</sup> MESP computations are also done at the same level of theory. Previous studies showed that this method is adequate for calculating MESP features.<sup>[5b,h,21]</sup> MESP,  $V(\mathbf{r})$  at a point  $\mathbf{r}$  due to a molecular system with nuclear charges located at  $\mathbf{R}_A$  and electron density  $\rho(\mathbf{r})$  is expressed in Equation (1) where  $N$  is the total number of nuclei in the molecule and  $Z_A$  is the charge on nucleus  $A$ , located at the distance  $|\mathbf{R}_A|$ .

$$V(\mathbf{r}) = \sum_A^N \frac{Z_A}{|\mathbf{r} - \mathbf{R}_A|} - \int \frac{\rho(\mathbf{r}') d^3r'}{|\mathbf{r} - \mathbf{r}'|} \quad (1)$$

In MESP topography, a negative-valued minimum ( $V_{\min}$ ) is often observed in electron-rich regions such as lone pair,  $\pi$ -bonds, and anionic sites of a molecular system. Gaussian 09

programme package has been used for all the calculations.<sup>[22]</sup> Vibrational frequency analysis is done with the same level of theory to confirm that the number of imaginary frequencies is zero for all the optimized geometries.

### Acknowledgements

Authors thank DST-SERB for funding through GAP137239 and also gratefully acknowledge the CSIR 4th PI for HPC facility and NIIST IT lab for computational support.

### Conflict of Interest

The authors declare no conflict of interest.

**Keywords:** density functional calculations · molecular electrostatic potential · spacers · substituent effect · transmission power.

- [1] a) T. M. Krygowski, B. T. Stepień, *Chem. Rev.* **2005**, *105*, 3482–3512; b) O. Exner, T. M. Krygowski, *Chem. Soc. Rev.* **1996**, *25*, 71–75.
- [2] a) C. Hansch, A. Leo, R. W. Taft, *Chem. Rev.* **1991**, *91*, 165–195; b) W. Adcock, N. A. Trout, *Chem. Rev.* **1999**, *99*, 1415–1435; c) O. Exner, S. Bohm, *Curr. Org. Chem.* **2006**, *10*, 763–778; d) L. P. Hammett, *J. Am. Chem. Soc.* **1937**, *59*, 96–103.
- [3] H. H. Jaffé, *Chem. Rev.* **1953**, *53*, 191–261.
- [4] T. M. Krygowski, M. A. Dobrowolski, K. Zborowski, M. K. Cyranski, *J. Phys. Chem.* **2006**, *19*, 889–895.
- [5] a) C. H. Suresh, S. R. Gadre, *J. Am. Chem. Soc.* **1998**, *120*, 7049–7055; b) C. H. Suresh, S. R. Gadre, *J. Phys. Chem. A* **2007**, *111*, 710–714; c) G. S. Remya, C. H. Suresh, *Phys. Chem. Chem. Phys.* **2016**, *18*, 20615–20626; d) T. M. Krygowski, K. Ejsmont, B. T. Stepień, M. K. Cyranski, J. Poater, M. Sola, *J. Org. Chem.* **2004**, *69*, 6634–6640; e) T. M. Krygowski, M. Palusiak, A. Płonka, J. E. Zachara-Horeglad, *J. Phys. Org. Chem.* **2007**, *20*, 297–306; f) T. M. Krygowski, J. E. Zachara-Horeglad, M. Palusiak, *J. Org. Chem.* **2010**, *75*, 4944–4949; g) T. M. Krygowski, W. P. Oziminski, *J. Mol. Model.* **2014**, *20*, 2352; h) S. E. Wheeler, K. N. Houk, *J. Am. Chem. Soc.* **2009**, *131*, 3126–3127; i) S. E. Wheeler, K. N. Houk, *J. Am. Chem. Soc.* **2009**, *131*, 3126–3127; j) S. E. Wheeler, *J. Am. Chem. Soc.* **2011**, *133*, 10262–10274; k) S. E. Wheeler, *Acc. Chem. Res.* **2013**, *46*, 1029–1038; l) B. Galabov, S. Ilieva, H. F. Schaefer, *J. Org. Chem.* **2006**, *71*, 6382–6387; m) B. Galabov, V. Nikolova, S. Ilieva, *Chem. Eur. J.* **2013**, *19*, 5149–5155.
- [6] a) R. W. Taft, *J. Am. Chem. Soc.* **1953**, *75*, 4231–4238; b) M. Charton, *Prog. Phys. Org. Chem.* **1981**, *119*–251.
- [7] C. G. Swain, E. C. Lupton, *J. Am. Chem. Soc.* **1968**, *90*, 4328–4337.
- [8] a) B. Galabov, S. Ilieva, G. Koleva, W. D. Allen, H. F. Schaefer III, P. von R. Schleyer, *Wiley Interdiscip. Rev.: Comput. Mol. Sci.* **2013**, *3*, 37–55; b) F. B. Sayyed, C. H. Suresh, *New J. Chem.* **2009**, *33*, 2465–2471; c) F. B. Sayyed, C. H. Suresh, S. R. Gadre, *J. Phys. Chem. A* **2010**, *114*, 12330–12333; d) F. B. Sayyed, C. H. Suresh, *J. Phys. Chem. A* **2011**, *115*, 9300–9307; e) F. B. Sayyed, C. H. Suresh, *J. Phys. Chem. A* **2011**, *115*, 5660–5664; f) F. B. Sayyed, C. H. Suresh, *Chem. Phys. Lett.* **2012**, *523*, 11–14.
- [9] a) S. Böhm, J. Kuthan, *Int. J. Quantum Chem.* **1984**, *26*, 21–33; b) K. H. Kim, Y. C. Martin, *J. Org. Chem.* **1991**, *56*, 2723–2729; c) J. S. Murray, T. Brinck, P. Politzer, *J. Mol. Struct.* **1992**, *255*, 271–281; d) H. Szatylowicz, T. Siodla, O. A. Stasyuk, T. M. Krygowski, *Phys. Chem. Chem. Phys.* **2016**, *18*, 11711–11721; e) T. Krygowski, N. Sadlej-Sosnowska, *Struct. Chem.* **2011**, *22*, 17–22.
- [10] a) C. A. van Walree, L. W. Jenneskens, *Tetrahedron* **1997**, *53*, 5825–5830; b) M. Charton, *J. Org. Chem.* **1961**, *26*, 735–738; c) S. A. Myers, R. A. Assink, D. A. Loyb, K. J. Sheac, *J. Chem. Soc. Perkin Trans. 2* **2000**, 545–549; d) K. Bowden, *Can. J. Chem.* **1963**, *41*, 2781–2793; e) K. Waisser, J. Kunes, L. Kubicova, M. Budesinsky, O. Exner, *Magn. Reson. Chem.* **1997**, *35*, 543–548; f) W. Adcock, *J. Phys. Org. Chem.* **2009**, *22*, 1065–1069; g) W. Adcock, A. Krstic, *Magn. Reson. Chem.* **2000**, *38*, 115–122; h) W.

- Adcock, N. Trout, *Magn. Reson. Chem.* **1998**, *36*, 181–195; i) A. R. Campanelli, A. Domenicano, G. Piacente, F. Ramondo, *J. Phys. Chem. A* **2010**, *114*, 5162–5170.
- [11] a) E. Scrocco, J. Tomasi, in *New concepts II*, Springer, **1973**, pp. 95–170; b) E. Scrocco, J. Tomasi, in *Advances in quantum chemistry*, Vol. 11, Elsevier, **1978**, pp. 115–193.
- [12] a) S. R. Gadre, I. H. Shrivastava, *J. Chem. Phys.* **1991**, *94*, 4384–4390; b) F. Luque, M. Orozco, P. Bhadane, S. Gadre, *J. Chem. Phys.* **1994**, *100*, 6718–6726; c) S. R. Gadre, P. K. Bhadane, *J. Chem. Phys.* **1997**, *107*, 5625–5626; d) S. R. Gadre, C. H. Suresh, *J. Org. Chem.* **1997**, *62*, 2625–2627.
- [13] C. H. Suresh, P. Alexander, K. P. Vijayalakshmi, P. K. Sajith, S. R. Gadre, *Phys. Chem. Chem. Phys.* **2008**, *10*, 6492–6499.
- [14] F. B. Sayyed, C. H. Suresh, *Tetrahedron Lett.* **2009**, *50*, 7351–7354.
- [15] C. H. Suresh, *Inorg. Chem.* **2006**, *45*, 4982–4986.
- [16] a) P. K. Sajith, C. H. Suresh, *Inorg. Chem.* **2012**, *51*, 967–977; b) P. K. Sajith, C. H. Suresh, *Dalton Trans.* **2010**, *39*, 815–822; c) J. Mathew, T. Thomas, C. H. Suresh, *Inorg. Chem.* **2007**, *46*, 10800–10809; d) J. Mathew, C. H. Suresh, *Inorg. Chem.* **2010**, *49*, 4665–4669.
- [17] a) C.-J. Tan, C.-S. Yang, Y.-C. Sheng, H. W. Amini, H.-H. G. Tsai, *J. Phys. Chem. C* **2016**, *120*, 21272–21284; b) C. Teng, X. Yang, C. Yang, H. Tian, S. Li, X. Wang, A. Hagfeldt, L. Sun, *J. Phys. Chem. C* **2010**, *114*, 11305–11313; c) Y. Hua, J. He, C. Zhang, C. Qin, L. Han, J. Zhao, T. Chen, W.-Y. Wong, W.-K. Wong, X. Zhu, *J. Mater. Chem. A* **2015**, *3*, 3103–3112; d) Y. Ding, Y. Jiang, W. Zhang, L. Zhang, X. Lu, Q. Wang, G. Zhou, J.-m. Liu, K. Kempa, J. Gao, *J. Phys. Chem. C* **2017**, *121*, 16731–16738.
- [18] a) F. Massoth, P. Politzer, M. Concha, J. Murray, J. Jakowski, J. Simons, *J. Phys. Chem. B* **2006**, *110*, 14283–14291; b) P. Politzer, L. Abrahamsen, P. Sjöberg, *J. Am. Chem. Soc.* **1984**, *106*, 855–860.
- [19] J. Frederick, J. Dippy, *Chem. Rev.* **1939**, *25*, 151–211.
- [20] a) A. D. Becke, *J. Chem. Phys.* **1993**, *98*, 5648–5652; b) C. Lee, W. Yang, R. G. Parr, *Phys. Rev. B* **1988**, *37*, 785.
- [21] F. B. Sayyed, C. H. Suresh, *New J. Chem.* **2009**, *33*, 2465–2471.
- [22] M. J. Frisch, G. W. Trucks, H. B. Schlegel, G. E. Scuseria, M. A. Robb, J. R. Cheeseman, G. Scalmani, V. Barone, B. Mennucci, G. A. Petersson, H. Nakatsuji, M. Caricato, X. Li, H. P. Hratchian, A. F. Izmaylov, J. Bloino, G. Zheng, J. L. Sonnenberg, M. Hada, M. Ehara, K. Toyota, R. Fukuda, J. Hasegawa, M. Ishida, T. Nakajima, Y. Honda, O. Kitao, H. Nakai, T. Vreven, J. J. A. Montgomery, J. E. Peralta, F. Ogliaro, M. Bearpark, J. J. Heyd, E. Brothers, K. N. Kudin, V. N. Staroverov, T. Keith, R. Kobayashi, J. Normand, K. Raghavachari, A. Rendell, J. C. Burant, S. S. Iyengar, J. Tomasi, M. Cossi, N. Rega, J. M. Millam, M. Klene, J. E. Knox, J. B. Cross, V. Bakken, C. Adamo, J. Jaramillo, R. Gomperts, R. E. Stratmann, O. Yazyev, A. J. Austin, R. Cammi, C. Pomelli, J. W. Ochterski, R. L. Martin, K. Morokuma, V. G. Zakrzewski, G. A. Voth, P. Salvador, J. J. Dannenberg, S. Dapprich, A. D. Daniels, O. Farkas, J. B. Foresman, J. V. Ortiz, J. Cioslowski, D. J. Fox, Gaussian 09, Revision D.01; Gaussian, Inc. Wallingford, CT, 2013.

---

Manuscript received: February 28, 2019  
Accepted manuscript online: April 11, 2019  
Version of record online: June 13, 2019





Cite this: *New J. Chem.*, 2020, **44**, 7200

# Density functional theory study on the donating strength of donor systems in dye-sensitized solar cells†

Velayudhan V. Divya<sup>ab</sup> and Cherumuttathu H. Suresh<sup>id</sup> \*<sup>ab</sup>

The electron-donating strengths of donor (D) moieties in thirteen donor- $\pi$ -acceptor systems (D1- $\pi$ -A to D13- $\pi$ -A wherein  $\pi$ - and A represent butadiene and cyanoacrylic acid units, respectively) have been studied using B3LYP/cc-pVDZ level density functional theory (DFT) calculations. The selected D moieties are encountered as a part of an organic sensitizer molecule in dye-sensitized solar cell (DSSC) applications. When the D moiety is joined with  $\pi$ -A, a certain amount of electron donation from D to A occurs leading to an increase in electron density at the A site of D- $\pi$ -A compared to the A site of  $\pi$ -A. This electron reorganization is quantified in terms of a change in molecular electrostatic potential (MESP) minimum ( $\Delta V_{\text{mA}}$ ) at the acceptor site, the CN group of the cyanoacrylic acid. The  $\Delta V_{\text{mA}}$  is always negative, in the range of  $-11.0$  to  $-2.6$  kcal mol<sup>-1</sup> which provides a quick assessment of the rank order of the electron-donating nature of the D moieties in the ground state of D- $\pi$ -A. The optical and photovoltaic properties of D and D- $\pi$ -A systems are also determined at the TD-CAM-B3LYP/cc-pVDZ//B3LYP/cc-pVDZ level. An absorption red shift ( $\Delta\lambda_{\text{max}}$ ) in the range of 81–242 nm is observed when D moieties change to D- $\pi$ -A systems. The ground state property  $\Delta V_{\text{mA}}$  showed a strong linear correlation with the excited state property  $\Delta\lambda_{\text{max}}$ . Furthermore,  $\Delta V_{\text{mA}}$  is found to be proportional to the open-circuit voltage ( $V_{\text{OC}}$ ). The resemblance of highest occupied molecular orbital (HOMO) and lowest unoccupied molecular orbital (LUMO) energies of the D- $\pi$ -A system with the respective energies of donor and  $\pi$ -A systems shows that the donor tunes the HOMO, while  $\pi$ -A tunes the LUMO. Among the thirteen D- $\pi$ -A systems, *N,N*-dialkylaniline, and julolidine are rated as the best donors for the photovoltaic applications. This study shows that the MESP based assessment of the donating strength of donor systems offers a powerful rational design strategy for the development of efficient dyes for DSSC applications.

Received 11th February 2020,  
Accepted 1st April 2020

DOI: 10.1039/d0nj00723d

rsc.li/njc

## Introduction

Dye-sensitized solar cells (DSSCs) have been regarded as a highly potential alternative to conventional silicon-based solar cells due to their high molar extinction coefficient, low production cost, simple synthetic strategy and easy structural modifications.<sup>1–5</sup> DSSCs also perform relatively better than other traditional solar cells under diffuse light conditions and at higher temperatures.<sup>4–6</sup> In DSSC applications, the sensitizers synthesized can be divided into two broad areas, *viz.* metal-based systems such as Ru(II) polypyridyl complexes, and Zn(II) porphyrins<sup>7</sup> and the metal-free donor- $\pi$ -acceptor (D- $\pi$ -A) type organic dyes.<sup>8</sup> The Ru-based

polypyridyl sensitizers attained the highest power conversion efficiency over 11% more than most of the metal-free sensitizers.<sup>9–14</sup>

This is due to the ability of metal sensitizers to absorb solar irradiation up to the near-infrared region, while other metal-free dye sensitizers are absorbed in the shorter wavelength region.<sup>8,13,15</sup> So, a highly efficient sensitizer should have an absorption maximum near to the Vis-NIR region associated with a long-lived charge excited state.<sup>16,17</sup> Due to the highly expensive and toxic synthetic procedures involved in metal sensitizers, the organic dyes exhibit remarkable importance in DSSC applications.<sup>8</sup> Recent studies proposed important structural modifications in organic dyes<sup>18,19</sup> to achieve a high power conversion efficiency (PCE) and over 12% has been achieved with a metal-free alkoxy-silyl carbazole dye as a sensitizer.<sup>20</sup> Yao *et al.* reported an improved PCE of 12.5% with a metal-free indenoperylene based D- $\pi$ -A dye,<sup>21</sup> the best-known metal-free organic dye. In 2017, a simple designing strategy over the phenothiazine moiety with ethynyl-pyrene enabled a PCE of 12%.<sup>22</sup> The other recent milestones in DSSCs include co-sensitization, which enables higher photovoltaic performance

<sup>a</sup> Chemical Sciences and Technology Division, CSIR-National Institute for Interdisciplinary Science and Technology (CSIR-NIIST), Thiruvananthapuram, Kerala 695 019, India. E-mail: sureshch@niist.res.in, sureshch@gmail.com

<sup>b</sup> Academy of Scientific and Innovative Research (AcSIR), CSIR-NIIST Campus, Trivandrum, India

† Electronic supplementary information (ESI) available: See DOI: 10.1039/d0nj00723d

over 14% with a collaborative sensitization by silyl and carboxy anchoring groups.<sup>23</sup> Many studies proposed the structural modification of the donor group of the D- $\pi$ -A dye to achieve higher efficiency as increasing the electron donating strength generally broadens and intensifies the region of absorption.<sup>24-26</sup>

In general, a dye sensitizer with a D- $\pi$ -A framework can be modified at donor,<sup>27,28</sup> spacer,<sup>29-32</sup> and anchoring groups<sup>33-35</sup> to improve the PCE. Typically, the acceptor portion (A) of the dye anchored onto the TiO<sub>2</sub> semiconductor favours the charge transfer of the excited electrons to the conduction band of the semiconductor.<sup>36</sup> The oxidized dye is then regenerated by the electron transfer from the electrolyte (I<sup>-</sup>/I<sub>3</sub><sup>-</sup> couple), while the electrolyte couple regains the electron from the platinum counter electrode.<sup>4,37</sup> Therefore, for an efficient dye sensitizer, an effective electron injection can occur from the dye to the TiO<sub>2</sub> semiconductor if its highest occupied molecular orbital (HOMO) is observed at a level slightly below the redox couple of the I<sup>-</sup>/I<sub>3</sub><sup>-</sup> electrolyte (-4.8 eV) and the lowest unoccupied molecular orbital (LUMO) is observed above the conduction band of TiO<sub>2</sub> (-4.0 eV).<sup>8,38,39</sup>

Apart from the simple D- $\pi$ -A framework, several other configurations like D-D- $\pi$ -A,<sup>40-42</sup> D-A- $\pi$ -A,<sup>43-46</sup> D- $\pi$ -A-A,<sup>47</sup> (D- $\pi$ -A)<sub>2</sub>,<sup>48</sup> and double D- $\pi$ -A bridges<sup>49</sup> were also introduced and revealed that the introduction of additional donors, acceptors, and the extension of  $\pi$  conjugation reduces the HOMO-LUMO energy gap and redshifts the absorption maximum. In other words, for the improved PCE, the donor should be stable, and electron-rich for the effective electron injection to the TiO<sub>2</sub> conduction band,<sup>28,50,51</sup> thereby broadening their absorption to the Vis-NIR region.<sup>50,51</sup> Therefore, for effective dye designing, it is very important to understand the electronic and photophysical properties of the dye systems.<sup>44</sup> Density functional theory (DFT) and Time-dependent density functional theory (TD-DFT) can afford a more efficient approach to understand and predict these structural and electronic features without any time delay compared to the traditional trial and error methods.<sup>52-63</sup> Previous studies have shown that the donor strength has a significant role in absorption maximum, the kinetics of electron injection and light-harvesting efficiency.<sup>64,65</sup> Recently, the relevance of the theoretical estimation of donor strength in organic electronics has been explained by Köse.<sup>66</sup>

Thirteen typically used donor building blocks (Fig. 1) in the DSSC applications are selected for this DFT/TDDFT study (D1-D13).<sup>24,31,67-72</sup> Among them, D1-D4 are aromatic hydrocarbon systems whereas the remaining donor moieties contain at least one lone pair bearing a nitrogen centre (D5-D13). The estimation of the donating strength is assessed by molecular electrostatic potential (MESP) topographical features of these donor molecules and their corresponding D- $\pi$ -A systems. The MESP distribution is useful to understand the charge distribution within a molecule,<sup>73-76</sup> and the regions with negative MESP values indicate electron-dense regions while positive-valued areas represent electron-deficient regions. The MESP based interpretation has been used for the study of substituent effects, intermolecular interactions, non-covalent interactions, hydrogen bonding, cation- $\pi$  interactions, aromaticity and a variety of chemical phenomena.<sup>77-80</sup> MESP analysis has been used in the

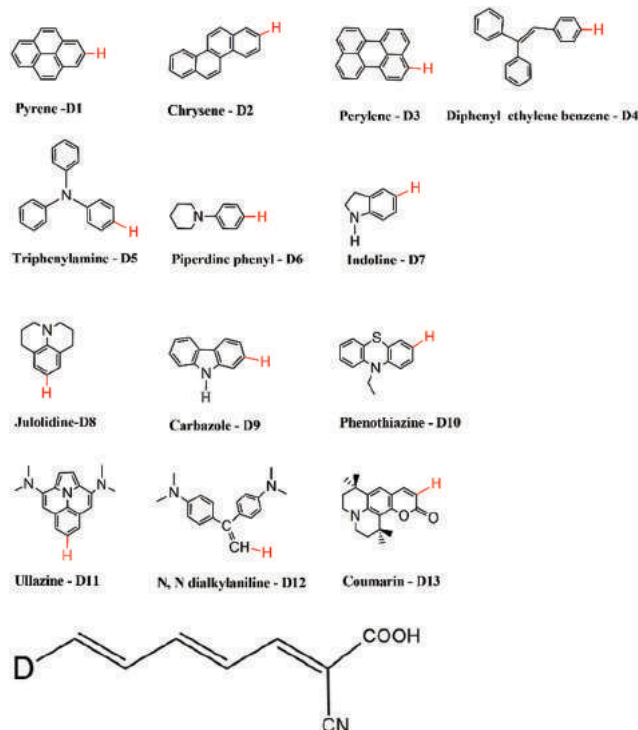


Fig. 1 ChemDraw representation of donors (D1–D13) and D- $\pi$ -A systems. The bond shown in red colour is replaced with the  $\pi$ -A part to design the D- $\pi$ -A system.

field of organometallic chemistry for the quantification of the electron-donating strength of phosphine and N-heterocyclic ligands.<sup>73</sup> The global minimum ( $V_{\min}$ ) of MESP near the two electron donor atom (P or N) indicates the net donating ability of the ligand for making a coordination bond with a metal centre. Furthermore, Suresh and co-workers proved that MESP minimum ( $V_{\min}$ ) analysis is very effective for the quantification of the inductive, resonance, steric and proximity effects of substituents.<sup>75,81-84</sup> Recently the substituent effect transmitting power ( $\gamma$ ) through various spacer units is also calculated *via* MESP analysis and showed that  $V_{\min}$  values are beneficial for the quantification of the transmission power of spacers.<sup>85</sup> The study recommends the usage of short alkenyl systems as spacers for effective electronic transmission. Moreover, the above reliable studies confirmed that MESP is a powerful descriptor, capable of predicting the electronic properties of the molecular systems effectively. The present study focuses on the MESP analysis of D- $\pi$ -A systems towards photovoltaic applications. The butadiene moiety (-HC=CH-CH=CH-) and the cyanoacrylic acid unit (-H<sub>2</sub>C=C(CN)-COOH) are used as the  $\pi$ -spacer and anchoring (A) group, respectively.

## Computational method

The ground state geometry optimization has been carried out using the B3LYP density functional theory (DFT) method<sup>86</sup> with the cc-pVDZ basis set.<sup>87</sup> This DFT method has been extensively used in the theoretical studies of organic dyes for dye-sensitized

solar cell applications.<sup>45,60</sup> Frequency calculations were also done at the same level of theory and confirmed that there were no imaginary frequencies. Vertical excitation energy calculations have been done for the first 7 states by using a long-range and solvation effect-corrected CAM-B3LYP/cc-pVDZ DFT method<sup>56</sup> in dichloromethane. The reliability of this method has been checked by doing the computation on experimentally known systems (Fig. S1, ESI†) using three more methods, *viz.* B3LYP,<sup>86</sup> PBE1PBE,<sup>88</sup> and  $\omega$ B97XD.<sup>89</sup> For all these methods, the solvation effects are incorporated through the self-consistent reaction field (SCRF) calculation implemented in the SMD (solvation model based on electron density) model.<sup>90</sup> The TD-DFT calculations showed that the result given by CAM-B3LYP is the most reliable to reproduce the experimental absorption maximum (Table S1, ESI†). DFT and TD-DFT calculations are done using the Gaussian 16 program package.<sup>91</sup> For quantifying the electron donating strength of donors in the D- $\pi$ -A system, molecular electrostatic potential (MESP) analysis has been performed at the B3LYP/cc-pVDZ level. MESP,  $V(r)$  at point  $r$  in the vicinity of a molecular system in the atomic unit can be calculated from the electron density  $\rho(r')$ , using eqn (1)

$$V(r) = \sum_A^N \frac{Z_A}{|r - R_A|} - \int \frac{\rho(r') dr'}{|r - r'|} \quad (1)$$

where  $N$  is the total number of nuclei present in the molecular system,  $Z_A$  is the charge on the nucleus  $A$  at a distance  $R_A$  and  $r'$  is a dummy integration variable.<sup>92,93</sup>

## Results and discussion

### MESP analysis of donor molecules

The MESP minima  $V_m$  are useful for locating the most electron-rich regions in the molecules. The  $V_m$  appears on the aromatic rings, hetero atoms and CC double bonds of donor molecules (D1–D13) which are shown in Fig. 2. Since all the systems contain at least one aromatic ring, the ring showing the most negative  $V_m$  ( $V_{mD}$ ) is taken for comparing the donor strength of each system. The  $V_{mD}$  values of all the systems are depicted in Fig. 2 along with other  $V_m$  values. In polycyclic aromatic hydrocarbon (PAH) systems (D1–D3),  $V_{mD}$  values lie in a small range of  $-14.4$  to  $-14.9$  kcal mol<sup>-1</sup> which can be attributed to the similar  $\pi$ -conjugation features which are not affected by a hetero atom or a substituent. In the D4 system, two phenyl rings show a nearly coplanar arrangement with the CC double bond and their  $V_{mD}$  ( $-16.1$  and  $-16.8$  kcal mol<sup>-1</sup>) values are more negative than a PAH while the third phenyl ring has a highly twisted arrangement with respect to the CC double bond and shows  $V_{mD} -13.7$  kcal mol<sup>-1</sup>. It appears that the presence of a conjugated CC bond in D4 enhances its electron density over the corresponding aromatic rings. In D5, three phenyl rings share the lone pair electron density from the nitrogen centre leading to a more negative character for  $V_{mD} -15.6$  kcal mol<sup>-1</sup> than a PAH. In D6, D7 and D8, an amino nitrogen centre is connected with an arene ring. In the piperidine-phenyl system D6, the nitrogen centre is more pyramidalized than the other

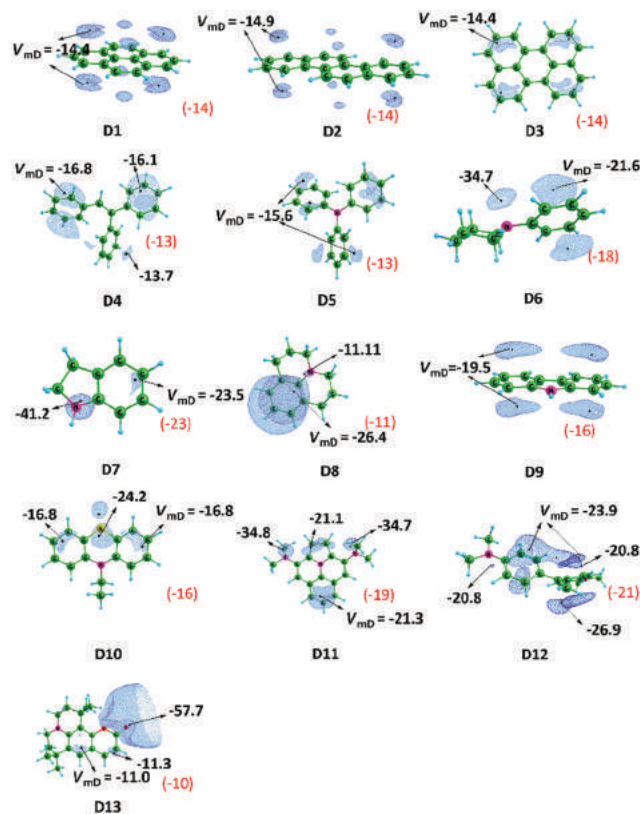


Fig. 2 MESP minima at the donor site, the  $V_{mD}$  of the donor systems. Isosurface values in kcal mol<sup>-1</sup> are given in brackets. Here carbon atoms are shown in green colour, while nitrogen, sulfur and oxygen atoms are shown in pink, yellow and red colours, respectively.

two and shows the least negative  $V_{mD}$  ( $-21.6$  kcal mol<sup>-1</sup>) among the three. In D7 and D8, fusing the  $N$ -alkyl unit/s with the aromatic ring improves the planarization of the  $N$ -centre, leading to more electron donation *via* +R effect to the arene ring. As a result, julolidine D8 shows the most electron-rich arene ring in terms of  $V_{mD} -26.4$  kcal mol<sup>-1</sup> followed by D7 ( $-23.5$  kcal mol<sup>-1</sup>). Compared to a PAH, carbazole arene rings show significantly more negative  $V_{mD}$  ( $-19.5$  kcal mol<sup>-1</sup>); here the sharing of the  $N$ -centre lone pair is with two aromatic rings which leads to less negative  $V_{mD}$  than D6–D8. Similarly, in D10, the sharing of the  $N$ -lone pair with two arene rings can be seen in addition to the effect of the hetero S atom. In this case,  $V_{mD}$  is less negative than carbazole. In D11, the combined effect of three  $N$ -centres can be attributed to the electron-rich nature of the arene ring ( $V_{mD} -21.3$  kcal mol<sup>-1</sup>) and among the  $N$ -centres, the  $N,N$ -dimethyl units are not fully effective for the influence of the +R contribution due to slight pyramidalization caused by steric congestions from the alkyl moiety of the adjacent five-membered ring. In D12, along with the +R contribution of  $N,N$ -dimethyl substituents, the conjugation effect of CC double bonds leads to relatively more electron-rich arene rings. The least negative  $V_{mD} -11.0$  kcal mol<sup>-1</sup> is observed in D13, the coumarin system. Here, the presence of a highly electron-withdrawing carbonyl group at the heterocyclic ring reduces the electron density on the aromatic ring.



### MESP analysis of D- $\pi$ -A systems

The donating strength of donor fragments in the D- $\pi$ -A system has been studied by MESP analysis. The MESP isosurface plot of a representative D- $\pi$ -A system (D12) is shown in Fig. 3a along with MESP minimum ( $V_m$ ) values at various positions. The positions selected for  $V_m$  analysis are (i) the donor site ( $V_{mD}$ ), (ii) the spacer site nearer to the donor ( $V_{mS}$ ) and (iii) the anchor site ( $V_{mA}$ ). The  $\pi$ -A portion is built by linking a butadiene moiety ( $\pi$ -spacer) with the cyanoacrylic acid moiety (A). Since the  $\pi$ -spacer and anchor units are the same for all donors, they have been considered as a reference system and the corresponding MESP minimum at their spacer ( $V_{mS}$ ) and anchoring sites ( $V_{mA}$ ) are evaluated for comparison with those of the D- $\pi$ -A system (Fig. 3b). The various MESP minimum values, *viz.*  $V_{mD}$ ,  $V_{mS}$ , and  $V_{mA}$  (Fig. S3, ESI<sup>†</sup>), are shown in Table 1 along with the most negative  $V_m$  of the donor molecule ( $V_{mD}$ ). In Table 1, the quantities  $\Delta V_{mD}$ ,  $\Delta V_{mS}$ , and  $\Delta V_{mA}$  represent the change that occurs in the minimum potential of the donor, spacer and anchoring sites with the introduction of the  $\pi$ -A system. Furthermore, in order to calculate  $\Delta V_{mD}$ , the most negative minima at the phenyl ring of each donor ( $V_{mD}$ ) have been subtracted from the corresponding minima ( $V_{mD}$ ) of the D- $\pi$ -A system. Similarly,  $\Delta V_{mS}$  and  $\Delta V_{mA}$  have been calculated by subtracting the  $V_m$  values at spacer and anchoring moieties of the reference system ( $V_{mS}$  and  $V_{mA}$ ) from the corresponding minima ( $V_{mS}$  and  $V_{mA}$ ) of the D- $\pi$ -A system.

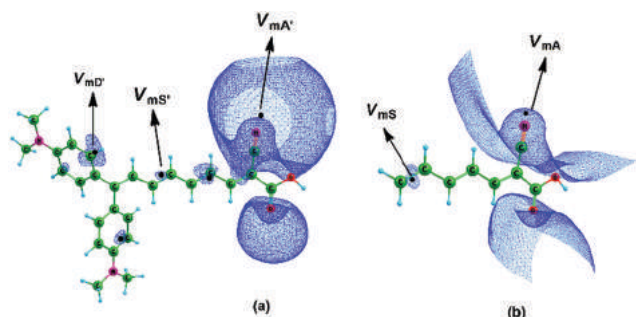


Fig. 3 MESP isosurface plot of (a) representative D- $\pi$ -A system and (b) reference system.

Table 1  $V_m$  (kcal mol<sup>-1</sup>) of the D- $\pi$ -A systems calculated at the B3LYP/cc-pVDZ level

Systems	$V_{mD}$	$V_{mD}'$	$\Delta V_{mD}$	$V_{mS}$	$V_{mS}'$	$\Delta V_{mS}$	$V_{mA}$	$V_{mA}'$	$\Delta V_{mA}$
D1	-14.4	-8.2	6.2	-2.4	-3.3	-0.9	-50.3	-53.0	-2.7
D2	-14.9	-9.8	5.1	-2.4	-3.3	-0.9	-50.3	-53.0	-2.6
D3	-14.4	-8.0	6.4	-2.4	-4.0	-1.6	-50.3	-54.2	-3.8
D4	-16.8	-7.8	9.0	-2.4	-4.3	-1.9	-50.3	-54.2	-3.8
D5	-15.6	-7.7	7.9	-2.4	-6.3	-3.9	-50.3	-56.0	-5.7
D6	-21.6	-9.3	12.3	-2.4	-8.0	-5.6	-50.3	-57.5	-7.2
D7	-23.5	-8.8	14.7	-2.4	-8.3	-5.9	-50.3	-57.5	-7.2
D8	-26.4	-10.0	16.4	-2.4	-10.8	-8.4	-50.3	-59.5	-9.2
D9	-19.5	-12.0	7.5	-2.4	-4.8	-2.4	-50.3	-54.8	-4.5
D10	-16.8	-9.4	7.4	-2.4	-5.3	-2.9	-50.3	-55.2	-4.9
D11	-21.3	-11.0	10.3	-2.4	-7.5	-5.1	-50.3	-55.4	-5.1
D12	-23.9	-14.1	9.8	-2.4	-12.9	-10.5	-50.3	-61.4	-11.0
D13	-11.0	-1.9	9.1	-2.4	-8.0	-5.6	-50.3	-56.5	-6.2

From Table 1, it is clear that when a donor part is being attached with a  $\pi$ -A system, the minimum potential of the donor site ( $V_{mD}$ ) becomes less negative indicating the electron transferring ability from the donor site to the  $\pi$ -A site. The term  $\Delta V_{mD}$  in Table 1 represents the change that occurred on the minimum potential at the donor site during the  $\pi$ -A linkage which varies from 5.1 to 16.4 kcal mol<sup>-1</sup> and indicates the intramolecular charge transfer involved in the D- $\pi$ -A system. Furthermore, at the spacer site of the D- $\pi$ -A system, electron density gain is observed represented by negative  $\Delta V_{mS}$  which lies in the range of -0.9 to -10.5 kcal mol<sup>-1</sup>. On the basis of  $\Delta V_{mS}$ , the highest donating strength can be attributed to the D12, while the least donating strength can be assigned for PAHs.

The  $V_{mA}$  values indicate that the minimum potential at the anchor moiety, for example at the cyano group, shows significant variations with respect to different donor units. The most electron-donating donor is expected to show the most negative  $V_{mA}$ . For the application of DSSCs, the cyanoacrylic portion has to be linked to the TiO<sub>2</sub> semiconductor for efficient electron transfer. By making the anchoring group electron-rich, efficient electron transfer from the dye to TiO<sub>2</sub> can occur. In other words, the efficiency of the DSSC system can be directly related to the electron-donating strength of the donor moieties. Due to this reason, the change in MESP minimum that appeared on the anchoring part ( $\Delta V_{mA}$ ) has been considered as the donating strength of the donor moiety. The PAHs (D1-D3) showed the least negative value of  $\Delta V_{mA}$  (-2.7 to -3.8 kcal mol<sup>-1</sup>), indicating their poor electron-donating strength. Furthermore, in the D4 system, a similar donating strength of -3.8 kcal mol<sup>-1</sup> is observed. In D5, the introduction of the N-centre imparts more negative  $\Delta V_{mA}$  values (-5.7 kcal mol<sup>-1</sup>) than PAHs which explains its better electron-donating strength compared to polyacenes. In D6 and D7, the more planarized nitrogen centres in the donor part impart a more negative  $\Delta V_{mA}$  value of -7.2 kcal mol<sup>-1</sup> and suggests its higher electron-donating strength than D5. In the D8 system, the fused N-centre with the aromatic ring further improves its planarization and leads to more negative  $\Delta V_{mA}$  -9.2 kcal mol<sup>-1</sup> than D5, D6, and D7. In carbazole (D9), the N-lone pair is shared between two aromatic rings through resonance, and as a result, the electron-donating strength in terms of  $\Delta V_{mA}$  (-4.5 kcal mol<sup>-1</sup>) appears weaker than those (D6-D8) having only one aromatic ring for sharing an N-lone pair. In D10, the presence of sulfur slightly enhances the negative value of  $\Delta V_{mA}$  to -5.0 kcal mol<sup>-1</sup>. Even though there are three nitrogen centres in ullazine, it shows a donating strength of -5.1 kcal mol<sup>-1</sup> which can be attributed to the influence of pyramidalized *N,N*-dimethyl groups in ullazine. In D12, a more negative  $\Delta V_{mA}$  value of -11.0 kcal mol<sup>-1</sup> can be recognized with the +R effect of mostly planarized *N,N*-dimethyl substituents. Finally, in D13 a more negative  $\Delta V_{mA}$  value (-6.2 kcal mol<sup>-1</sup>) than that of PAHs has been observed due to the interplay of the electron-rich nitrogen centre and the electron-withdrawing carbonyl group. These results strongly suggest that the incorporation of an electron-rich heteroatom in the donor region can have a positive influence on the electronic transmission to the acceptor moiety. On the basis of  $\Delta V_{mA}$ ,

**Table 2** Maximum absorption wavelength (nm), oscillator strength  $f$ , absorptional shift  $\Delta\lambda_{\max}$  and the percentage MO contribution of donor and D- $\pi$ -A systems at the TD-CAM-B3LYP/SMD/cc-pVDZ//B3LYP/cc-pVDZ level

Donor				D- $\pi$ -A			
Systems	$\lambda_{\max}$	$f$	MO contribution	$\lambda_{\max}$	$f$	MO contribution	$\Delta\lambda_{\max}$
D1	320	0.52	H $\rightarrow$ L (93.2%)	401	2.21	H-1 $\rightarrow$ L (94.2%)	81
D2	306	0.03	H-1 $\rightarrow$ L (33.6%)	376	0.03	H $\rightarrow$ L (74.6%)	56
			H $\rightarrow$ L (19.9%)	409	2.47	H $\rightarrow$ L (79.3%)	103
			H $\rightarrow$ L+1 (39.5%)				
D3	300	0.23	H $\rightarrow$ L (68.5%)				109
	408	0.59	H $\rightarrow$ L (98.7%)	518	1.73	H $\rightarrow$ L (90.4%)	110
D4	300	0.78	H $\rightarrow$ L (97.0%)	434	2.21	H $\rightarrow$ L (88.6%)	134
D5	284	0.03	H $\rightarrow$ L (90.8%)	453	2.02	H $\rightarrow$ L (86.7%)	169
D6	279	0.38	H $\rightarrow$ L+1 (98.8%)				174
	256	0.05	H $\rightarrow$ L (87.8%)	446	2.00	H $\rightarrow$ L (92.6%)	190
	236	0.37	H $\rightarrow$ L+1 (91.7%)				210
D7	261	0.09	H $\rightarrow$ L (90.5%)	448	1.86	H $\rightarrow$ L (93.7%)	187
	226	0.18	H $\rightarrow$ L+1 (90.0%)				222
D8	277	0.08	H $\rightarrow$ L (92.9%)	480	1.95	H $\rightarrow$ L (93.2%)	203
	243	0.29	H $\rightarrow$ L+1 (92.9%)				237
	286	0.06	H $\rightarrow$ L (87.6%)	419	2.21	H $\rightarrow$ L (93.2%)	133
D9	262	0.31	H-1 $\rightarrow$ L (84.2%)				157
	319	0.02	H $\rightarrow$ L (95.2%)	459	1.67	H $\rightarrow$ L (84.8%)	140
D10	275	0.18	H $\rightarrow$ L+2 (84.6%)				184
	324	0.38	H $\rightarrow$ L (90.8%)	448	0.02	H $\rightarrow$ L (89.2%)	124
D11				411	2.11	H-1 $\rightarrow$ L (73.6%)	87
	278	0.20	H $\rightarrow$ L (78.0%)	520	1.95	H $\rightarrow$ L (92.6%)	242
D12	334	0.64	H $\rightarrow$ L (95.3%)	503	1.99	H $\rightarrow$ L (89.3%)	169

the order of the donating strength of donor groups can be written as D2 < D1 < D3 = D4 < D9 < D10 < D11 < D5 < D13 < D6 = D7 < D8 < D12. The julolidine based donor system D8 and the *N,N*-dialkyl aniline incorporated D12 are the most efficient among the studied systems.

### Absorption spectra of donor and D- $\pi$ -A systems

The absorption maxima of all the systems (donor and D- $\pi$ -A) along with oscillator strength ( $f$ ) are summarized in Table 2. For the assessment of the absorptional shift,  $\Delta\lambda_{\max}$ , the absorption maximum of the D- $\pi$ -A system was subtracted from the donor system. For calculating  $\Delta\lambda_{\max}$ , HOMO  $\rightarrow$  LUMO orbital transition has been considered, except for D1. In D1,  $\lambda_{\max}$  is observed for the HOMO-1  $\rightarrow$  LUMO transition, while its HOMO  $\rightarrow$  LUMO transition is nearly forbidden due to very small  $f$  values. The data in Table 2 clearly suggest that the absorption maximum ( $\lambda_{\max}$ ) of D- $\pi$ -A shifts significantly to a higher wavelength region compared to donor D. Since in all systems we used the same spacer and anchoring moiety (the  $\pi$ -A unit), their influence on the absorptional shift ( $\Delta\lambda_{\max}$ ) can be considered to be the same. This implies that the large variation in  $\Delta\lambda_{\max}$  exhibited by the D- $\pi$ -A system is due to the variation in the donating strength of donor moieties. For instance, among all donor moieties, D1 with  $\Delta\lambda_{\max}$  81 nm is the least donating while D12 with  $\Delta\lambda_{\max}$  242 nm is the most donating (Table 2). Furthermore,  $\Delta V_{\text{MA}}$  with  $\Delta\lambda_{\max}$  with a correlation coefficient shows a linear correlation of 0.966 (Fig. 4) which shows the significance of the donating strength of  $\Delta V_{\text{MA}}$  on  $\Delta\lambda_{\max}$ . In the linear correlation plot, D1 and D11 based D- $\pi$ -A systems exhibit a slight deviation, which can be attributed as their less intense ( $f \rightarrow 0.02$ - $0.03$ ) and nearly forbidden HOMO  $\rightarrow$  LUMO charge transfer character of the

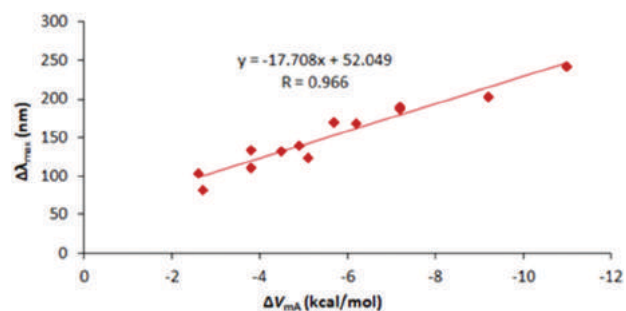


**Fig. 4** Correlation between the donating strength ( $\Delta V_{\text{MA}}$ ) of the D- $\pi$ -A system and the change in absorption maxima ( $\Delta\lambda_{\max}$ ).

orbital excitation. From these results the shift in absorption maxima ( $\Delta\lambda_{\max}$ ) follows the order D12 > D8 > D7 > D6 > D10 > D5 > D13 > D9 > D4 > D3 > D2 > D11 > D1, preferably due to the nature of donor groups. Therefore, to improve the wavelength of absorption to a preferred region (Vis to NIR), its donating ability has to be tuned with the introduction of better electron-donating donor groups (preferably more nitrogen centres).

The frontier molecular orbital energy levels given in Fig. 5 show the HOMO-LUMO band gap features of D, D- $\pi$ -A and  $\pi$ -A systems (butadiene moieties linked with cyano acrylic acid). The HOMO value ( $\epsilon_h$ ) of the D systems is in the range of -4.66 to -5.70 eV, whereas that of the D- $\pi$ -A system is in the range of -4.96 to -5.89 eV. These data indicate the close resemblance of the HOMO level of the D and D- $\pi$ -A systems. On the other hand, the LUMO energy level ( $\epsilon_l$ ) of D shows a large deviation from the  $\epsilon_l$  of the D- $\pi$ -A system indicating clear



Fig. 5 Frontier molecular energy level diagram of D- $\pi$ -A systems at the B3LYP/cc-pVDZ level.

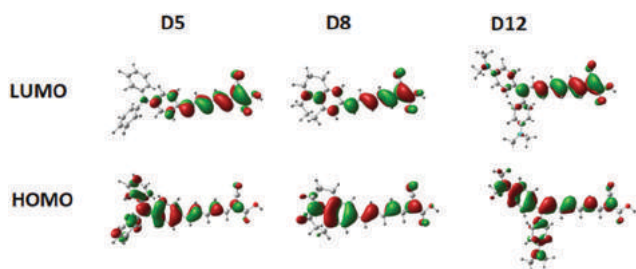


Fig. 6 Frontier molecular orbitals of representative D- $\pi$ -A systems at the B3LYP/cc-pVDZ level.

dissimilarity. In fact,  $\epsilon_1$  of D- $\pi$ -A in the range of  $-2.52$  to  $-3.10$  eV is very close to  $\epsilon_1$   $-2.97$  eV observed for  $\pi$ -A. Thus, the data shown in Fig. 5 indicate that the HOMO of D- $\pi$ -A is more like the HOMO of the donor and its LUMO is more like that of  $\pi$ -A. This feature is clearly evident in the frontier molecular orbital diagram given in the D- $\pi$ -A system for representative cases (Fig. 6). HOMOs are more localized towards the donor region with decreasing orbital contributions from the  $\pi$ -A system, while the LUMO is mostly localized in the  $\pi$ -A region. D1- $\pi$ -A is an exception wherein HOMO-1 to the LUMO is the allowed transition and its HOMO has a different  $\pi$  character, localized exclusively on the pyrene ring. The data shown in Fig. 5 clearly suggest that linking the donor system to the  $\pi$ -A unit is very effective for reducing the band gap. For all cases, the HOMO level is tuned towards the value of the  $\Gamma/I_3^-$  electrolyte couple while the LUMO level appears closer to the conduction band (CB) of TiO<sub>2</sub>. The HOMO and LUMO distribution and their energy levels suggest a significant charge separation in the excited state leading to the strong electron coupling of the dye with the TiO<sub>2</sub> semiconductor which promotes the electron transfer to the conduction band.<sup>94</sup>

In general, compared to D systems, the absorption maxima of D- $\pi$ -A systems show a significant red shift (Table 2) in the range of 81–242 nm. In D1- $\pi$ -A and D2- $\pi$ -A,  $\lambda_{\max}$  is observed at

401 and 409 nm, respectively. The major electronic excitation of pyrene incorporated D1- $\pi$ -A is assigned to the transition of HOMO-1 to the LUMO. The forbidden HOMO to LUMO transition of D1- $\pi$ -A can be changed to allow one by appropriate substitution such as a substitution by the methyl group at the first or second position (Table S2 and Fig. S2, ESI<sup>†</sup>). The D3- $\pi$ -A system showed a broad absorption coverage in the visible region with  $\lambda_{\max}$  518 nm corresponding to the HOMO-LUMO transition. Among all, D3- $\pi$ -A has the lowest HOMO-LUMO band gap of 2.26 eV (Fig. 5). The D4 in D4- $\pi$ -A is more electron-donating than a PAH moiety and it shows a smaller band gap of 2.71 eV compared to D1 to D2 incorporated systems. Furthermore, in nitrogen-containing D- $\pi$ -A systems (D5-D13), the band gap energy decreases to a greater extent by 2.31–2.75 eV for all except D9- $\pi$ -A (2.87 eV) than hydrocarbon systems. Among the nitrogen-containing systems, D12- $\pi$ -A showed the highest  $\lambda_{\max}$  520 nm with a band gap of 2.39 eV while D11- $\pi$ -A showed the lowest band gap of 2.31 eV. The  $\lambda_{\max}$  value of D11- $\pi$ -A observed at 411 nm is due to the transition of HOMO-1 to LUMO. Among them all, the HOMO energy level of D12- $\pi$ -A appeared nearest to the energy level of the redox electrolyte while its LUMO level is 1.44 eV higher than the CB of TiO<sub>2</sub>. The LUMO energy levels of all systems offer a favourable electron injection from the excited state to the conduction band of TiO<sub>2</sub> while HOMO energies lower than the oxidation potential of the  $\Gamma/I_3^-$  electrolyte ( $-4.8$  eV) indicate effective dye regeneration. These results support their effective utilization in the DSSC application. The D3- $\pi$ -A, D11- $\pi$ -A and D12- $\pi$ -A systems are among the lowest band gap systems, desirable for harvesting more light in the UV-visible region.

#### Analysis of photovoltaic parameters

According to Koopman's theorem,<sup>95</sup> the ground state oxidation potential ( $E_{\text{ox}}^{\text{dye}}$ ) of a dye can be approximated as the negative HOMO energy ( $-\epsilon_h$ ). Furthermore, the excited state dye regeneration

**Table 3** Calculated vertical excitation energy, absorption maxima, oscillator strength  $f$ , HOMO LUMO energy, HOMO–LUMO energy gap (HLG), ground and excited-state oxidation potentials ( $E_{\text{ox}}^{\text{dye}}$  and  $E_{\text{ox}}^{\text{dye*}}$ ), free energy change for electron injection ( $\Delta G_{\text{inject}}$ ), dye regeneration driving force ( $\Delta G_{\text{reg}}$ ), and the open circuit voltage ( $eV_{\text{OC}}$ ) of D– $\pi$ –A systems at the TD-CAM-B3LYP/SMD/cc-pVDZ//B3LYP/cc-pVDZ level

Systems	Excitation energy (eV)	$\lambda_{\text{absmax}}$ (nm)	$f$	HOMO (eV)	LUMO (eV)	HLG (eV)	$E_{\text{ox}}^{\text{dye}}$ (eV)	$E_{\text{ox}}^{\text{dye*}}$ (eV)	$\Delta G_{\text{inject}}$ (eV)	$\Delta G_{\text{reg}}$ (eV)	( $eV_{\text{OC}}$ ) (eV)
D1	3.09	401	2.22	-5.88	-2.99	2.89	5.88	2.79	-1.21	1.08	1.01
D2	3.03	409	2.47	-5.89	-3.00	2.89	5.89	2.86	-1.14	1.09	1.00
D3	2.39	518	1.73	-5.35	-3.10	2.26	5.35	2.96	-1.04	0.55	0.90
D4	2.86	434	2.21	-5.70	-2.98	2.71	5.70	2.84	-1.16	0.90	1.02
D5	2.73	453	2.02	-5.37	-2.79	2.58	5.37	2.64	-1.36	0.57	1.21
D6	2.78	446	2.00	-5.42	-2.68	2.74	5.42	2.64	-1.36	0.62	1.32
D7	2.59	448	1.95	-5.40	-2.65	2.75	5.40	2.81	-1.19	0.60	1.35
D8	2.77	480	1.86	-5.12	-2.52	2.60	5.12	2.35	-1.65	0.32	1.48
D9	2.96	419	2.21	-5.78	-2.91	2.87	5.78	2.82	-1.18	0.98	1.09
D10	2.70	459	1.67	-5.28	-2.84	2.44	5.28	2.58	-1.42	0.48	1.16
D11	3.01	411	2.11	-5.07	-2.76	2.31	5.07	2.06	-1.94	0.27	1.24
D12	2.39	520	1.95	-4.96	-2.56	2.39	4.96	2.57	-1.43	0.16	1.44
D13	2.46	503	1.99	-5.35	-2.87	2.49	5.35	2.89	-1.11	0.55	1.13

driving force ( $\Delta G_{\text{reg}}$ ) can be approximated as ( $E_{\text{ox}}^{\text{dye}} - 4.8$ ) eV or  $(-\varepsilon_{\text{h}} - 4.8)$  eV where  $-4.8$  eV stands for the redox potential of the  $\text{I}^-/\text{I}_3^-$  electrolyte couple.<sup>22,96</sup> The free energy change for electron injection ( $\Delta G_{\text{inject}}$ ) from the excited state of the dye to the semiconductor<sup>53,97,98</sup> is generally defined as,

$$\Delta G_{\text{inject}} = E_{\text{ox}}^{\text{dye*}} - 4.0 \quad (2)$$

where  $E_{\text{ox}}^{\text{dye*}}$  is the excited state oxidation potential and  $-4.0$  eV stands for the conduction band (CB) edge of the  $\text{TiO}_2$  semiconductor.<sup>22,99</sup> Assuming that the electron injection occurs from the unrelaxed excited state,  $E_{\text{ox}}^{\text{dye*}}$  can be explained as the difference between the ground state oxidation potential of the dye and the vertical transition energy  $\lambda_{\text{max}}$ ,<sup>96,97,100</sup>

$$E_{\text{ox}}^{\text{dye*}} = (-\varepsilon_{\text{h}}) - \lambda_{\text{max}} \quad (3)$$

Furthermore, the difference between the energy of the LUMO ( $\varepsilon_{\text{l}}$ ) of the dye and the energy of the conduction band edge of  $\text{TiO}_2$  is regarded as the open circuit voltage (eqn (4)).<sup>100</sup>

$$eV_{\text{OC}} = \varepsilon_{\text{l}} - (-4.0) \quad (4)$$

In Table 3, the  $\Delta G_{\text{inject}}$  values fall in the range of  $-1.04$  to  $-1.94$  eV, and the D11– $\pi$ –A system with the most negative value has the highest electron injection efficiency while D2 to D4 based D– $\pi$ –A systems show the lowest efficiency. The smallest  $\Delta G_{\text{reg}}$  value of 0.16 eV is observed for D12– $\pi$ –A and suggests its fastest dye regeneration efficiency. A good linear correlation between  $\Delta V_{\text{mA}}$  and  $eV_{\text{OC}}$  is observed for all the cases (Fig. 7)

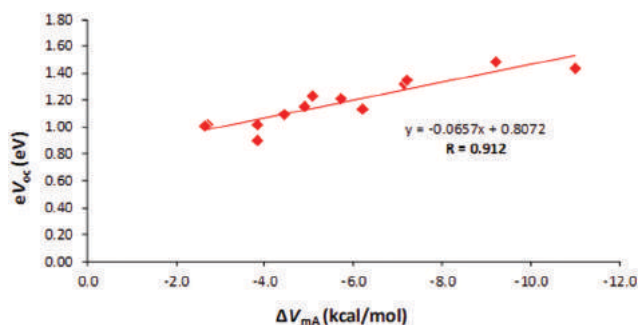


**Fig. 7** Correlation between  $\Delta V_{\text{mA}}$  ( $\text{kcal mol}^{-1}$ ) and  $eV_{\text{OC}}$  (eV).

suggesting that the electron accepting tendency of the acceptor part is well reflected at the LUMO levels. Among all the systems, julolidine based D8– $\pi$ –A possesses the highest  $\varepsilon_{\text{l}}$  value resulting in the highest  $eV_{\text{OC}}$  value of 1.48 eV. The second highest  $eV_{\text{OC}}$  value of 1.44 eV is observed for D12– $\pi$ –A. The  $\Delta V_{\text{mA}}$  values suggest that the electron donating ability of PAH moieties is the lowest among all the donors and the corresponding D1 to D3 based D– $\pi$ –A systems show the lowest range of  $eV_{\text{OC}}$  0.90–1.01 eV.

## Conclusions

Using MESP topographical analysis, the donating strength of thirteen known (D1–D13) typically used donor systems in the DSSC applications has been quantified. The red shift in the absorption maximum ( $\Delta\lambda_{\text{max}}$ ) observed for the D– $\pi$ –A systems is rationalized in terms of the amount of electron donation from the donor D moieties to the  $\pi$ –A system using the MESP parameter  $\Delta V_{\text{mA}}$ . The highest electron donating strength  $\Delta V_{\text{mA}}$  observed in D12– $\pi$ –A shows the highest  $\Delta\lambda_{\text{max}}$  and maximum absorption wavelength  $\lambda_{\text{max}}$  with a small band gap energy of 2.39 eV. In poor electron donating D1 and D2 based D– $\pi$ –A systems, the smallest  $\Delta\lambda_{\text{max}}$  and  $\lambda_{\text{max}}$  values are observed. A linear correlation obtained between  $\Delta V_{\text{mA}}$  and  $\Delta\lambda_{\text{max}}$  confirms that  $\Delta\lambda_{\text{max}}$  increases with an increase in  $\Delta V_{\text{mA}}$ . The frontier molecular energy levels showed that the HOMO of the D– $\pi$ –A system has a greater resemblance to the HOMO of the donor, whereas the LUMO has a greater resemblance to the LUMO of  $\pi$ –A. Thus, the donor tunes the HOMO, while  $\pi$ –A tunes the LUMO energy of the D– $\pi$ –A system for efficient dye regeneration and electron injection. Among all the systems, D12– $\pi$ –A showed the highest electron injection efficiency. Since  $eV_{\text{OC}}$  is directly proportional to the power conversion efficiency of the solar cell, D8– $\pi$ –A and D12– $\pi$ –A having the highest  $eV_{\text{OC}}$  can be regarded as the most efficient sensitizers for DSSCs while the lowest  $eV_{\text{OC}}$  values displayed by the PAH based (D1–D3) D– $\pi$ –A systems offer poor efficiency. The linear correlation between  $\Delta V_{\text{mA}}$  and  $eV_{\text{OC}}$  shows that  $eV_{\text{OC}}$  increases with an increase in the negative character of  $\Delta V_{\text{mA}}$  and also proves that better sensitizers can be developed by connecting a powerful electron donor to a  $\pi$ –A system. One way to do this is by incorporating multiple lone pair



bearing nitrogen centres in donors. Thus, the MESP approach offers an easy analysis tool for the quantification of the donating strength of D- $\pi$ -A systems in DSSC applications.

## Conflicts of interest

There are no conflicts to declare.

## Acknowledgements

Authors acknowledge the DST-SERB for funding through GAP1397 and also gratefully acknowledge the CSIR 4th PI for the HPC facility and the NIIST IT lab for computational support. V. V. Divya thanks the CSIR, India, for the senior research fellowship.

## Notes and references

- B. O'regan and M. Grätzel, *Nature*, 1991, **353**, 737.
- N. Anscombe, *Nat. Photonics*, 2011, **5**, 266–267.
- F. Odobel, L. Le Pleux, Y. Pellegrin and E. Blart, *Acc. Chem. Res.*, 2010, **43**, 1063–1071.
- A. Hagfeldt, G. Boschloo, L. Sun, L. Kloo and H. Pettersson, *Chem. Rev.*, 2010, **110**, 6595–6663.
- N. Sharifi, F. Tajabadi and N. Taghavinia, *ChemPhysChem*, 2014, **15**, 3902–3927.
- J. Gong, K. Sumathy, Q. Qiao and Z. Zhou, *Renewable Sustainable Energy Rev.*, 2017, **68**, 234–246.
- A. Yella, H.-W. Lee, H. N. Tsao, C. Yi, A. K. Chandiran, M. K. Nazeeruddin, E. W.-G. Diau, C.-Y. Yeh, S. M. Zakeeruddin and M. Grätzel, *Science*, 2011, **334**, 629–634.
- A. Mishra, M. K. Fischer and P. Bäuerle, *Angew. Chem., Int. Ed.*, 2009, **48**, 2474–2499.
- M. K. Nazeeruddin, A. Kay, I. Rodicio, R. Humphry-Baker, E. Mueller, P. Liska, N. Vlachopoulos and M. Graetzel, *J. Am. Chem. Soc.*, 1993, **115**, 6382–6390.
- M. K. Nazeeruddin, P. Péchy, T. Renouard, S. M. Zakeeruddin, R. Humphry-Baker, P. Comte, P. Liska, L. Cevey, E. Costa, V. Shklover, L. Spiccia, G. B. Deacon, C. A. Bignozzi and M. Grätzel, *J. Am. Chem. Soc.*, 2001, **123**, 1613–1624.
- M. K. Nazeeruddin, R. Splivallo, P. Liska, P. Comte and M. Grätzel, *Chem. Commun.*, 2003, 1456–1457.
- M. K. Nazeeruddin, F. De Angelis, S. Fantacci, A. Selloni, G. Viscardi, P. Liska, S. Ito, B. Takeru and M. Grätzel, *J. Am. Chem. Soc.*, 2005, **127**, 16835–16847.
- F. Gao, Y. Wang, J. Zhang, D. Shi, M. Wang, R. Humphry-Baker, P. Wang, S. M. Zakeeruddin and M. Grätzel, *Chem. Commun.*, 2008, 2635–2637.
- C.-Y. Chen, M. Wang, J.-Y. Li, N. Pootrakulchote, L. Alibabaei, C.-H. Ngoc-le, J.-D. Decoppet, J.-H. Tsai, C. Grätzel, C.-G. Wu, S. M. Zakeeruddin and M. Grätzel, *ACS Nano*, 2009, **3**, 3103–3109.
- Y. Cao, Y. Bai, Q. Yu, Y. Cheng, S. Liu, D. Shi, F. Gao and P. Wang, *J. Phys. Chem. C*, 2009, **113**, 6290–6297.
- M. Pastore, E. Mosconi and F. De Angelis, *J. Phys. Chem. C*, 2012, **116**, 5965–5973.
- M. Cheng, X. Yang, J. Li, F. Zhang and L. Sun, *ChemSusChem*, 2013, **6**, 70–77.
- S. Ito, H. Miura, S. Uchida, M. Takata, K. Sumioka, P. Liska, P. Comte, P. Péchy and M. Grätzel, *Chem. Commun.*, 2008, 5194–5196.
- W. Zeng, Y. Cao, Y. Bai, Y. Wang, Y. Shi, M. Zhang, F. Wang, C. Pan and P. Wang, *Chem. Mater.*, 2010, **22**, 1915–1925.
- K. Kakiage, Y. Aoyama, T. Yano, T. Otsuka, T. Kyomen, M. Unno and M. Hanaya, *Chem. Commun.*, 2014, **50**, 6379–6381.
- Z. Yao, M. Zhang, H. Wu, L. Yang, R. Li and P. Wang, *J. Am. Chem. Soc.*, 2015, **137**, 3799–3802.
- B. Nagarajan, S. Kushwaha, R. Elumalai, S. Mandal, K. Ramanujam and D. Raghavachari, *J. Mater. Chem. A*, 2017, **5**, 10289–10300.
- K. Kakiage, Y. Aoyama, T. Yano, K. Oya, J.-I. Fujisawa and M. Hanaya, *Chem. Commun.*, 2015, **51**, 15894–15897.
- T. Kitamura, M. Ikeda, K. Shigaki, T. Inoue, N. A. Anderson, X. Ai, T. Lian and S. Yanagida, *Chem. Mater.*, 2004, **16**, 1806–1812.
- Z.-S. Wang, Y. Cui, Y. Dan-oh, C. Kasada, A. Shinpo and K. Hara, *J. Phys. Chem. C*, 2007, **111**, 7224–7230.
- Z.-S. Wang, N. Koumura, Y. Cui, M. Takahashi, H. Sekiguchi, A. Mori, T. Kubo, A. Furube and K. Hara, *Chem. Mater.*, 2008, **20**, 3993–4003.
- A. Venkateswararao, K. R. J. Thomas, C.-P. Lee, C.-T. Li and K.-C. Ho, *ACS Appl. Mater. Interfaces*, 2014, **6**, 2528–2539.
- A. J. Huckaba, F. Giordano, L. E. McNamara, K. M. Dreux, N. I. Hammer, G. S. Tschumper, S. M. Zakeeruddin, M. Grätzel, M. K. Nazeeruddin and J. H. Delcamp, *Adv. Energy Mater.*, 2015, **5**, 1401629.
- K. Hara, M. Kurashige, Y. Dan-oh, C. Kasada, A. Shinpo, S. Suga, K. Sayama and H. Arakawa, *New J. Chem.*, 2003, **27**, 783–785.
- C. Teng, X. Yang, C. Yang, H. Tian, S. Li, X. Wang, A. Hagfeldt and L. Sun, *J. Phys. Chem. C*, 2010, **114**, 11305–11313.
- A. Baheti, C.-P. Lee, K. J. Thomas and K.-C. Ho, *Phys. Chem. Chem. Phys.*, 2011, **13**, 17210–17221.
- K. Srinivas, C. R. Kumar, M. A. Reddy, K. Bhanuprakash, V. J. Rao and L. Giribabu, *Synth. Met.*, 2011, **161**, 96–105.
- Y. Ooyama, S. Inoue, T. Nagano, K. Kushimoto, J. Ohshita, I. Imae, K. Komaguchi and Y. Harima, *Angew. Chem., Int. Ed.*, 2011, **50**, 7429–7433.
- B. Hosseinzadeh, A. S. Beni, M. Azari, M. Zarandi and M. Karami, *New J. Chem.*, 2016, **40**, 8371–8381.
- D. Patil, M. Jadhav, K. Avhad, T. H. Chowdhury, A. Islam, I. Bedja and N. Sekar, *New J. Chem.*, 2018, **42**, 11555–11564.
- J. Feng, Y. Jiao, W. Ma, M. K. Nazeeruddin, M. Grätzel and S. Meng, *J. Phys. Chem. C*, 2013, **117**, 3772–3778.
- S. Ardo and G. J. Meyer, *Chem. Soc. Rev.*, 2009, **38**, 115–164.
- R. Argazzi, C. A. Bignozzi, T. A. Heimer, F. N. Castellano and G. J. Meyer, *J. Am. Chem. Soc.*, 1995, **117**, 11815–11816.
- N. Hirata, J. J. Lagref, E. J. Palomares, J. R. Durrant, M. K. Nazeeruddin, M. Gratzel and D. Di Censo, *Chem. – Eur. J.*, 2004, **10**, 595–602.
- Z. Ning, Q. Zhang, W. Wu, H. Pei, B. Liu and H. Tian, *J. Org. Chem.*, 2008, **73**, 3791–3797.

- 41 L. Li, Y. Hao, X. Yang, J. Zhao, H. Tian, C. Teng, A. Hagfeldt and L. Sun, *ChemSusChem*, 2011, **4**, 609–612.
- 42 J. Tang, J. Hua, W. Wu, J. Li, Z. Jin, Y. Long and H. Tian, *Energy Environ. Sci.*, 2010, **3**, 1736–1745.
- 43 W. Li, Y. Wu, Q. Zhang, H. Tian and W. Zhu, *ACS Appl. Mater. Interfaces*, 2012, **4**, 1822–1830.
- 44 R. Tarsang, V. Promarak, T. Sudyoasuk, S. Namuangruk, N. Kungwan and S. Jungstittiwong, *ChemPhysChem*, 2014, **15**, 3809–3818.
- 45 H.-Q. Xia, C.-P. Kong, J. Wang, F.-Q. Bai and H.-X. Zhang, *RSC Adv.*, 2014, **4**, 50338–50350.
- 46 A. Dessi, A. Sinicropi, S. Mohammadpourasl, R. Basosi, M. Taddei, F. Fabrizi de Biani, M. Calamante, L. Zani, A. Mordini, P. Bracq, D. Franchi and G. Reginato, *ACS Omega*, 2019, **4**, 7614–7627.
- 47 L.-Y. Lin, C.-H. Tsai, F. Lin, T.-W. Huang, S.-H. Chou, C.-C. Wu and K.-T. Wong, *Tetrahedron*, 2012, **68**, 7509–7516.
- 48 K. D. Seo, B. S. You, I. T. Choi, M. J. Ju, M. You, H. S. Kang and H. K. Kim, *J. Mater. Chem. A*, 2013, **1**, 9947–9953.
- 49 Y. Hong, J.-Y. Liao, J. Fu, D.-B. Kuang, H. Meier, C.-Y. Su and D. Cao, *Dyes Pigm.*, 2012, **94**, 481–489.
- 50 A. Dualeh, R. Humphry-Baker, J. H. Delcamp, M. K. Nazeeruddin and M. Grätzel, *Adv. Energy Mater.*, 2013, **3**, 496–504.
- 51 J. H. Delcamp, A. Yella, T. W. Holcombe, M. K. Nazeeruddin and M. Grätzel, *Angew. Chem., Int. Ed.*, 2013, **125**, 394–398.
- 52 K. Srinivas, K. Yesudas, K. Bhanuprakash, V. J. Rao and L. Giribabu, *J. Phys. Chem. C*, 2009, **113**, 20117–20126.
- 53 J. Preat, C. Michaux, D. Jacquemin and E. A. Perpète, *J. Phys. Chem. C*, 2009, **113**, 16821–16833.
- 54 J. Preat, *J. Phys. Chem. C*, 2010, **114**, 16716–16725.
- 55 J. Preat, D. Jacquemin and E. A. Perpète, *Environ. Sci. Technol.*, 2010, **44**, 5666–5671.
- 56 M. Pastore, E. Mosconi, F. De Angelis and M. Grätzel, *J. Phys. Chem. C*, 2010, **114**, 7205–7212.
- 57 D. Casanova, F. P. Rotzinger and M. Grätzel, *J. Chem. Theory Comput.*, 2010, **6**, 1219–1227.
- 58 S. Meng, E. Kaxiras, M. K. Nazeeruddin and M. Grätzel, *J. Phys. Chem. C*, 2011, **115**, 9276–9282.
- 59 R. Sánchez-de-Armas, M. Á. San Miguel, J. Oviedo and J. F. Sanz, *Phys. Chem. Chem. Phys.*, 2012, **14**, 225–233.
- 60 J. Zhang, H.-B. Li, S.-L. Sun, Y. Geng, Y. Wu and Z.-M. Su, *J. Mater. Chem.*, 2012, **22**, 568–576.
- 61 W. Fan, D. Tan and W. Q. Deng, *ChemPhysChem*, 2012, **13**, 2051–2060.
- 62 J. Zhang, Y.-H. Kan, H.-B. Li, Y. Geng, Y. Wu and Z.-M. Su, *Dyes Pigm.*, 2012, **95**, 313–321.
- 63 J. Zhang, H.-B. Li, J.-Z. Zhang, Y. Wu, Y. Geng, Q. Fu and Z.-M. Su, *J. Mater. Chem. A*, 2013, **1**, 14000–14007.
- 64 W.-L. Ding, D.-M. Wang, Z.-Y. Geng, X.-L. Zhao and Y.-F. Yan, *J. Phys. Chem. C*, 2013, **117**, 17382–17398.
- 65 R. Tarsang, V. Promarak, T. Sudyoasuk, S. Namuangruk and S. Jungstittiwong, *J. Photochem. Photobiol., A*, 2014, **273**, 8–16.
- 66 M. E. Köse, *J. Phys. Chem. A*, 2019, **123**, 5566–5573.
- 67 K. Hara, T. Sato, R. Katoh, A. Furube, Y. Ohga, A. Shinpo, S. Suga, K. Sayama, H. Sugihara and H. Arakawa, *J. Phys. Chem. B*, 2003, **107**, 597–606.
- 68 J. Li and A. C. Grimsdale, *Chem. Soc. Rev.*, 2010, **39**, 2399–2410.
- 69 G. Wu, F. Kong, J. Li, W. Chen, X. Fang, C. Zhang, Q. Chen, X. Zhang and S. Dai, *Dyes Pigm.*, 2013, **99**, 653–660.
- 70 Z.-S. Huang, H. Meier and D. Cao, *J. Mater. Chem.*, 2016, **4**, 2404–2426.
- 71 Y. Zhang, H. Cheema, L. McNamara, L. A. Hunt, N. I. Hammer and J. H. Delcamp, *Chem. – Eur. J.*, 2018, **24**, 5939–5949.
- 72 Z. Yang, C. Shao and D. Cao, *RSC Adv.*, 2015, **5**, 22892–22898.
- 73 C. H. Suresh and N. Koga, *Inorg. Chem.*, 2002, **41**, 1573–1578.
- 74 O. Kühl, *Coord. Chem. Rev.*, 2005, **249**, 693–704.
- 75 C. H. Suresh, *Inorg. Chem.*, 2006, **45**, 4982–4986.
- 76 J. Mathew, T. Thomas and C. H. Suresh, *Inorg. Chem.*, 2007, **46**, 10800–10809.
- 77 S. Mecozzi, A. P. West and D. A. Dougherty, *J. Am. Chem. Soc.*, 1996, **118**, 2307–2308.
- 78 S. E. Wheeler and K. N. Houk, *J. Chem. Theory Comput.*, 2009, **5**, 2301–2312.
- 79 S. E. Wheeler and K. Houk, *J. Am. Chem. Soc.*, 2009, **131**, 3126–3127.
- 80 F. B. Sayyed and C. H. Suresh, *J. Phys. Chem. A*, 2011, **115**, 9300–9307.
- 81 C. H. Suresh, P. Alexander, K. P. Vijayalakshmi, P. K. Sajith and S. R. Gadre, *Phys. Chem. Chem. Phys.*, 2008, **10**, 6492–6499.
- 82 F. B. Sayyed and C. H. Suresh, *Tetrahedron Lett.*, 2009, **50**, 7351–7354.
- 83 F. B. Sayyed and C. H. Suresh, *New J. Chem.*, 2009, **33**, 2465–2471.
- 84 F. B. Sayyed and C. H. Suresh, *J. Phys. Chem. A*, 2011, **115**, 5660–5664.
- 85 V. V. Divya, F. B. Sayyed and C. H. Suresh, *ChemPhysChem*, 2019, **20**, 1752–1758.
- 86 A. D. Becke, *J. Chem. Phys.*, 1993, **98**, 1372–1377.
- 87 T. H. Dunning Jr, *J. Chem. Phys.*, 1989, **90**, 1007–1023.
- 88 C. Adamo and V. Barone, *J. Chem. Phys.*, 1999, **110**, 6158–6170.
- 89 J.-D. Chai and M. Head-Gordon, *Phys. Chem. Chem. Phys.*, 2008, **10**, 6615–6620.
- 90 A. V. Marenich, C. J. Cramer and D. G. Truhlar, *J. Phys. Chem. B*, 2009, **113**, 6378–6396.
- 91 M. J. Frisch, G. W. Trucks, H. B. Schlegel, G. E. Scuseria, M. A. Robb, J. R. Cheeseman, G. Scalmani, V. Barone, G. A. Petersson, H. Nakatsuji, X. Li, M. Caricato, A. V. Marenich, J. Bloino, B. G. Janesko, R. Gomperts, B. Mennucci, H. P. Hratchian, J. V. Ortiz, A. F. Izmaylov, J. L. Sonnenberg, D. Williams-Young, F. Ding, F. Lipparini, F. Egidi, J. Goings, B. Peng, A. Petrone, T. Henderson, D. Ranasinghe, V. G. Zakrzewski, J. Gao, N. Rega, G. Zheng, W. Liang, M. Hada, M. Ehara, K. Toyota, R. Fukuda, J. Hasegawa, M. Ishida, T. Nakajima, Y. Honda, O. Kitao, H. Nakai, T. Vreven, K. Throssell, J. A. Montgomery, J. E. Peralta, F. Ogliaro, M. J. Bearpark, J. J. Heyd, E. N. Brothers, K. N. Kudin, V. N. Staroverov, T. A. Keith, R. Kobayashi, J. Normand, K. Raghavachari, A. P. Rendell, J. C. Burant, S. S. Iyengar, J. Tomasi, M. Cossi, J. M. Millam, M. Klene, C. Adamo, R. Cammi, J. W. Ochterski, R. L. Martin, K. Morokuma,

- O. Farkas, J. B. Foresman and D. J. Fox, *Gaussian 16, Revision A.03*, Gaussian, Inc., Wallingford CT, 2016.
- 92 S. R. Gadre and R. N. Shirsat, *Electrostatics of atoms and molecules*, Universities Press, 2000.
- 93 P. Politzer and D. G. Truhlar, *Chemical applications of atomic and molecular electrostatic potentials: reactivity, structure, scattering, and energetics of organic, inorganic, and biological systems*, Springer Science & Business Media, 2013.
- 94 J. Yang, X. Wang, W.-L. Yim and Q. Wang, *J. Phys. Chem. C*, 2015, **119**, 26355–26361.
- 95 T. Koopmans, *Physica*, 1933, **1**, 104–113.
- 96 J.-H. Luo, Q.-S. Li, L.-N. Yang, Z.-Z. Sun and Z.-S. Li, *RSC Adv.*, 2014, **4**, 20200–20207.
- 97 R. Katoh, A. Furube, T. Yoshihara, K. Hara, G. Fujihashi, S. Takano, S. Murata, H. Arakawa and M. Tachiya, *J. Phys. Chem. B*, 2004, **108**, 4818–4822.
- 98 N. N. Ghosh, M. Habib, A. Pramanik, P. Sarkar and S. Pal, *New J. Chem.*, 2019, **43**, 6480–6491.
- 99 J. B. Asbury, Y.-Q. Wang, E. Hao, H. N. Ghosh and T. Lian, *Res. Chem. Intermed.*, 2001, **27**, 393–406.
- 100 W. Sang-aroon, S. Saekow and V. Amornkitbamrung, *J. Photochem. Photobiol., A*, 2012, **236**, 35–40.



Cite this: *New J. Chem.*, 2021, 45, 2496

# Tuning the donating strength of dye sensitizers using molecular electrostatic potential analysis†

Velayudhan V. Divya<sup>ab</sup> and Cherumuttathu H. Suresh<sup>id</sup>\*<sup>ab</sup>

Donor- $\pi$ -acceptor (D- $\pi$ -A) systems typically used in dye-sensitized solar cells (DSSC) have been studied for assessing the donating strength of six donors (D1-D6) under the influence of substituents such as CH<sub>3</sub>, C<sub>5</sub>H<sub>11</sub>, isopropyl, *t*-butyl, OH, OCH<sub>3</sub>, OC<sub>2</sub>H<sub>5</sub>, NH<sub>2</sub>, N(CH<sub>3</sub>)<sub>2</sub>, PhCH<sub>3</sub>, and PhNH<sub>2</sub> along with  $\pi$ -spacer butadiene and acceptor moiety cyanoacrylic acid. The substituent effect enhances electron donation from D to A through the  $\pi$ -spacer. The enhancement in electron density at A has been quantified in terms of the difference in the molecular electrostatic potential (MESP) minimum at the cyano nitrogen ( $\Delta V_{\text{mA}}$ ) between  $\pi$ -A and D- $\pi$ -A. For unsubstituted D- $\pi$ -A systems,  $\Delta V_{\text{mA}}$  is in the range -0.1 to -5.7 kcal mol<sup>-1</sup>, whereas the substitution enhances the negative character of  $\Delta V_{\text{mA}}$  in the range -0.8 to -8.0 kcal mol<sup>-1</sup>. In alkyls and Ph-CH<sub>3</sub> substituted D- $\pi$ -A systems,  $\Delta V_{\text{mA}}$  lies in the range -0.8 to -6.7 kcal mol<sup>-1</sup>, whereas the N(CH<sub>3</sub>)<sub>2</sub> substituted systems exhibit more negative  $\Delta V_{\text{mA}}$  (more enhanced donating strength) in the range -5.1 to -8.0 kcal mol<sup>-1</sup>. The more negative value of  $\Delta V_{\text{mA}}$  implies the greater electron-donating ability of the D- $\pi$ -A system. Optical and photovoltaic parameters ( $\Delta G_{\text{reg}}$ ,  $\Delta G_{\text{inject}}$ ,  $eV_{\text{OC}}$ ) are analyzed at the TD-CAM-B3LYP/SMD/cc-pVDZ//B3LYP/cc-pVDZ level of DFT. An excellent linear correlation is observed in all six sets between  $\Delta V_{\text{mA}}$  and the absorption maximum ( $\lambda_{\text{max}}$ ) showing that  $\lambda_{\text{max}}$  increases with enhanced donating strength. The higher absorption maximum obtained by N(CH<sub>3</sub>)<sub>2</sub> substituted D- $\pi$ -A systems lies in the range 430 nm to 490 nm, explaining the outstanding donating ability of N(CH<sub>3</sub>)<sub>2</sub> compared to other substituents. The reduced highest occupied molecular orbital (HOMO) – lowest unoccupied molecular orbital (LUMO) gap (from 3.14 to 2.17 eV) with enhanced donating strength confirms the influence of substituent effects in broadening the absorption maximum. Furthermore, in photovoltaic parameters, a strong influence of the substituent effect is observed. The N(CH<sub>3</sub>)<sub>2</sub> substituted D1- $\pi$ -A (D1-N(CH<sub>3</sub>)<sub>2</sub>) exhibits the highest  $eV_{\text{OC}}$  (1.38 eV). The strong linear correlation observed for the ground state property  $\Delta V_{\text{mA}}$  and open-circuit voltage  $eV_{\text{OC}}$  provides guidelines for developing an effective strategy for designing dye sensitizers for desirable photovoltaic applications.

Received 29th September 2020,  
Accepted 21st November 2020

DOI: 10.1039/d0nj04797j

rsc.li/njc

## Introduction

Over the past 30 years, dye-sensitized solar cells (DSSCs) and their structural modification have become an emerging research area in the field of photovoltaics.<sup>1–3</sup> DSSCs are considered as the most inventive candidate for the next generation of clean renewable sources due to their easier structure modification, simple synthetic strategy, large absorption coefficient, and low production cost.<sup>1,4–7</sup> Nonetheless, the performance of DSSC is still in a bottleneck due to their lower power conversion efficiency (PCE) than the conventional silicon-based solar cells due to the inherent voltage loss during the dye regeneration

and poor long term stability.<sup>8</sup> In order to improve the PCE over conventional silicon-based solar cells, extensive research efforts like modification on electrolytes, semiconductors, and sensitizers have been executed and result in the development of new and efficient dye sensitizers.<sup>3,5,9–21</sup> Among the DSSCs, the Ru based sensitizers achieved the best PCE of 11%, which attains a comparable PCE to a silicon-based solar cell.<sup>5,22,23</sup> But due to the scarce resources and highly expensive nature of Ru metal, its practical application is limited, and more research efforts have resulted in the development of Ru-free organic sensitizers.<sup>6,11,24</sup> However, the major challenge of organic solar cells is the enhancement of PCE, durability, and stability to compete with silicon-based solar cells. One of the key strategies for the synthesis of Ru free sensitizers is the designing of the D- $\pi$ -A architecture, which enables efficient electron transfer from a donor (D) to the acceptor (A) through a spacer ( $\pi$ ).<sup>25,26</sup>

From the literature, it is understood that for the design of highly efficient photosensitizers, different kinds of building

<sup>a</sup> Chemical Sciences and Technology Division, CSIR-National Institute for Interdisciplinary Science and Technology, Thiruvananthapuram, Kerala 695019, India. E-mail: sureshch@niist.res.in, sureshch@gmail.com

<sup>b</sup> Academy of Scientific and Innovative Research (AcSIR), Ghaziabad 201002, India

† Electronic supplementary information (ESI) available. See DOI: 10.1039/d0nj04797j



blocks such as donors,<sup>27–35</sup> spacers,<sup>36–41</sup> and anchoring units<sup>42–46</sup> are required in the D- $\pi$ -A architecture to tune the electronic structure of the synthesized product. The fine-tuning of the HOMO-LUMO (highest occupied molecular orbital – lowest unoccupied molecular orbital) energy levels of a photosensitizer is often achieved by adjusting the substituent effect on the donor by the incorporation of electron-donating/withdrawing groups. In most of the cases, the electron-donating groups on the donor moiety act as substituents and they have a profound impact on the electronic structure and efficiency of the desired dye sensitizer.<sup>6,47–49</sup> *A priori* knowledge on the donating strength of the donor can become helpful for the prediction of the PCE of the designed/synthesized system. A quantitative/mathematical comparison of donating strength of the typically used donors is lacking in the literature.

Here we have selected six different donor systems (D1–D6), substituted with electron-donating groups such as CH<sub>3</sub>, C<sub>5</sub>H<sub>11</sub>, isopropyl, *t*-butyl, OH, OCH<sub>3</sub>, O-C<sub>2</sub>H<sub>5</sub>, NH<sub>2</sub>, N(CH<sub>3</sub>)<sub>2</sub>, N(C<sub>2</sub>H<sub>5</sub>)<sub>2</sub>, Ph-CH<sub>3</sub>, and Ph-NH<sub>2</sub> to evaluate the donating strength on a  $\pi$ -A system made up of a butadiene  $\pi$ -spacer and cyanoacrylic acid (Fig. 1). According to our previous study, the butadiene spacer is rated as having the highest substituent effect transmitting power compared to triple bonded, aromatic, and hetero-aromatic conjugated systems.<sup>50</sup> Hence this moiety is employed in the study as a  $\pi$ -spacer for effective intramolecular charge transfer (ICT) and cyanoacrylic acid is used as an acceptor (A). The molecular electrostatic potential (MESP) topographical analysis is used as a tool to measure the electronic effect of the substituted D on the acceptor A. MESP is a well-established tool for deriving many structure–property relationships for chemical and biological systems.<sup>51–57</sup> According to Scrocco, Tomasi, and coworkers, the MESP describes the charge distribution around a molecule and the regions with more negative MESP indicate the more electron-dense region of that system.<sup>58,59</sup> Suresh and coworkers widely used MESP for the quantification

of the substituent effect,<sup>60</sup> inductive effect,<sup>61</sup> resonance effect,<sup>62</sup> trans influence,<sup>63</sup> cation  $\pi$ -interaction,<sup>64</sup> *etc.* In a recent study, we have shown that MESP analysis is very useful for assessing the donating strength of D in the D- $\pi$ -A system.<sup>65</sup> MESP becomes a new theoretical tool for predicting the feasibility of organic electrode materials for lithium-ion batteries,<sup>66</sup> explained by Shang, Chen, and co-workers. The wide range of applications in various fields supports the validity of MESP based studies for analyzing the photovoltaic properties of dye-sensitized solar cells. The present study focuses on the substituent effect in tuning various ground state electronic and photovoltaic properties of D- $\pi$ -A systems for solar cell applications.

## Theoretical background and computational methodology

The three key parameters involved in the calculations of power conversion efficiency ( $\eta$ ) of a solar cell include open-circuit voltage ( $V_{OC}$ ), short-circuit current density ( $J_{SC}$ ), and the fill factor (FF). Thus, as compared to incident solar power on the cell ( $P_{inc}$ ), the  $\eta$  can be calculated as<sup>67</sup>

$$\eta = FF \frac{V_{OC} J_{SC}}{P_{inc}} \quad (1)$$

In the above equation,  $J_{SC}$  is related to the interaction between a sensitizer and semiconductor. In DSSCs,  $J_{SC}$  is calculated as<sup>39,40,68–70</sup>

$$J_{SC} = \int_{\lambda} LHE(\lambda) \phi_{inject} \eta_{collect} d\lambda \quad (2)$$

From the above equation, it is clear that  $J_{SC}$  is related to the light-harvesting efficiency (LHE) and electron injection efficiency  $\phi_{inject}$ .

*i.e.*, LHE =  $1 - 10^{-f}$ , where  $f$  represents the oscillator strength of the adsorbed dye molecule.<sup>71</sup>

Furthermore, the electron injection efficiency  $\phi_{inject}$  is related to electron injection-free energy change ( $\Delta G_{inject}$ ), and the enhancement in the  $J_{SC}$  can be carried out by the improvement of  $\Delta G_{inject}$ . Since electron injection takes place from the excited state of the dye to the conduction band of TiO<sub>2</sub>,  $\Delta G_{inject}$  can be calculated as follows.<sup>71–73</sup>

$$\Delta G_{inject} = E^{dye*} - |E_{CB}| \quad (3)$$

where  $E^{dye*}$  is the excited state oxidation potential and  $E_{CB}$  is the energy of the conduction band edge of the TiO<sub>2</sub> semiconductor. The negative  $\Delta G_{inject}$  values indicate that free energy change is spontaneous. It is well known that the conduction band (CB) of semiconductors is sensitive to conditions (*e.g.* pH of the solution) and it is very difficult to determine experimentally. Hence in this study, we used a widely accepted value of  $-4.00$  eV (an experimental value where the semiconductor is in contact with aqueous redox electrolytes of fixed pH 7.0) for doing the calculations.<sup>74</sup> For calculating  $E^{dye*}$ , it is assumed that electron injection occurs from the unrelaxed excited state and  $E^{dye*}$  can be written as<sup>39,72</sup>

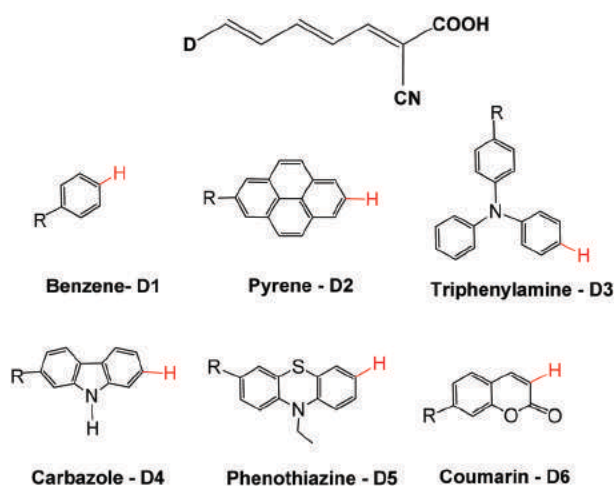


Fig. 1 Chemdraw diagram of the D- $\pi$ -A system (top) and the donors D1–D6. The R substituents are CH<sub>3</sub>, C<sub>5</sub>H<sub>11</sub>, isopropyl, *t*-butyl, OH, OCH<sub>3</sub>, O-C<sub>2</sub>H<sub>5</sub>, NH<sub>2</sub>, N(CH<sub>3</sub>)<sub>2</sub>, Ph-CH<sub>3</sub>, and Ph-NH<sub>2</sub>. The bond shown in red colour indicates the connecting position of D with  $\pi$ -A.

$$E^{\text{dye}*} = E^{\text{dye}} - \lambda_{\text{max}} \quad (4)$$

where  $E^{\text{dye}}$  is the ground state oxidation potential of the dye and  $\lambda_{\text{max}}$  is the vertical transition energy. According to Koopman's theorem, the ground state oxidation potential can be calculated as negative HOMO energy,<sup>75</sup> and this approximation has been giving good agreement with experimental results.<sup>76</sup>

The excited state dye regeneration can be predicted from the ground state oxidation potential as follows.<sup>77</sup>

$$\Delta G_{\text{reg}} = E^{\text{dye}} - 4.8 \text{ eV} \quad (5)$$

Thus from eqn (2)–(4), it is clear that  $J_{\text{SC}}$  will increase with the enhancement of light-harvesting efficiency and  $\Delta G_{\text{inject}}$ .

Theoretically, the open-circuit voltage can be approximated as the difference between the energy of the LUMO of the dye and the energy of the conduction band edge of  $\text{TiO}_2$ .<sup>78</sup>

$$eV_{\text{OC}} = E_{\text{LUMO}} - E_{\text{CB}} \quad (6)$$

Thus, the overall efficiency  $\eta$  of a solar cell can be enhanced by the improvement in  $J_{\text{SC}}$ ,  $eV_{\text{OC}}$  and FF values. (Since FF can be calculated from current–voltage characteristics, it is beyond the scope of this study).

For the ground state geometry optimization of the D- $\pi$ -A systems, the widely utilized B3LYP density functional theory (DFT) method<sup>79</sup> with the cc-pVDZ basis set<sup>65,80,81</sup> has been considered. Vibrational frequency calculation was also carried out at the same level of theory and basis set, and confirms that there are no imaginary frequencies. Absorption maxima and vertical excitation energies for the first seven states are calculated using time-dependent DFT at the CAM-B3LYP/SMD/cc-pVDZ//B3LYP/cc-pVDZ level.<sup>82,83</sup> Here SMD stands for the incorporation of the solvation effect of dichloromethane in the self-consistent reaction field (SCRf) approach<sup>84</sup> as implemented in the Gaussian16 suite of programmes.<sup>85</sup> The dependency of bond localization of single and double bonds in the ground state on the excited state properties has been analyzed using bond length alteration index (BLA).<sup>86,87</sup> The BLA index for the unsubstituted D1 to D6- $\pi$ -A systems are calculated with B3LYP and CAM-B3LYP geometries (Table S1 and Fig. S2, ESI†). For all a positive BLA index has been observed and larger BLA index has been observed with CAM-B3LYP. This indicates that carbon-carbon single and double bonds are more localized with CAM-B3LYP than B3LYP. Also, the BLA index for the S1 state of a representative set of TPA systems has been calculated with CAM-B3LYP (Table S2, ESI†). The reduced BLA index for S1 than the S0 state indicates the delocalized nature of the system and also supports the ICT transfer involved in D- $\pi$ -A systems. Previously, González *et al.* noted that B3LYP fails to predict the excitation energies due to its intrinsic problems in describing charge transfer (CT) states whereas the long-range correction on them using CAM delivers good agreement with the experimental UV/vis absorption.<sup>87</sup> They also observed that excited state properties are highly dependent on the localization of single and double bonds in the ground state structure which can be quantified in terms of the BLA index. Our previous study also showed that the calculated absorption maximum of known D- $\pi$ -A systems at the

CAM-B3LYP/SMD/cc-pVDZ//B3LYP/cc-pVDZ level of theory agrees well with the experimental absorption maximum.<sup>65</sup> The MESP,  $V(\mathbf{r})$  as defined in eqn (1) has been evaluated using the electron density  $\rho(\mathbf{r}')$  computed at the B3LYP/cc-pVDZ level.

$$V(\mathbf{r}) = \sum_A^N \frac{Z_A}{|\mathbf{r} - \mathbf{R}_A|} - \int \frac{\rho(\mathbf{r}') d\mathbf{r}'}{|\mathbf{r} - \mathbf{r}'|}$$

The  $N$  in eqn (1) is the total number of nuclei present in the molecular system,  $Z_A$  is the charge on the nucleus  $A$  at a distance  $R_A$  and  $\mathbf{r}'$  is a dummy integration variable.<sup>52,53</sup> All calculations have been carried out using the Gaussian 16 program package.<sup>85</sup>

### MESP analysis

The MESP plot of two representative donors (D1 and D4) and their corresponding D- $\pi$ -A systems (unsubstituted) are shown in Fig. 2 along with the respective MESP minimum ( $V_m$ ) at various sites.

In donor systems,  $V_{\text{mD}'}$  represents  $V_m$  of the donor. For example,  $V_{\text{mD}'}$  of benzene (D1) and carbazole (D4) are  $-16.6$  and  $-19.5$  kcal mol<sup>-1</sup> (Fig. 2). In D- $\pi$ -A systems,  $V_{\text{mD}}$  and  $V_{\text{mS}}$  represent the MESP minimum at the donor and spacer (nearer to D), respectively while  $V_{\text{m(OH)}}$ ,  $V_{\text{m(CO)}}$ , and  $V_{\text{mA}}$  represent the MESP minimum at the lone pair regions of OH, CO and CN of the acceptor moiety, respectively. Previous studies by Suresh and Gadre *et al.* have shown that lone pair regions in molecules can be characterized using MESP topographical analysis.<sup>88</sup> The

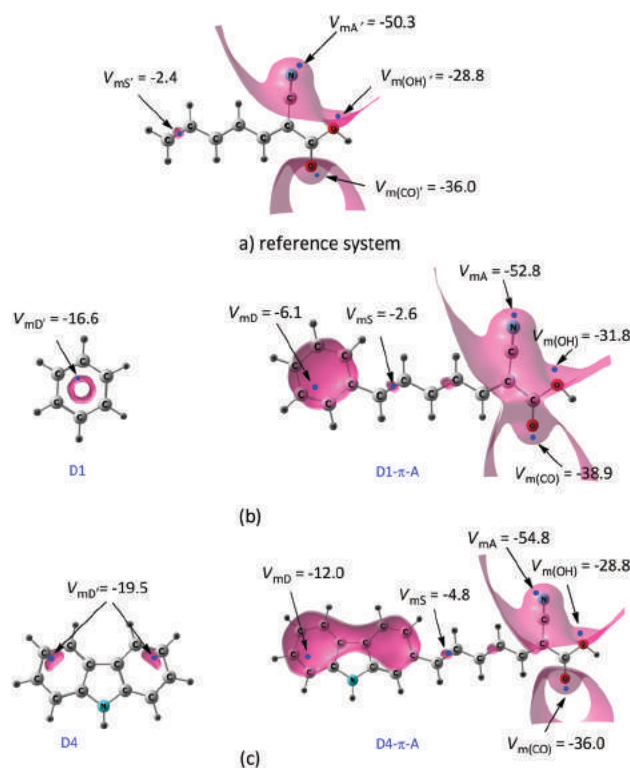


Fig. 2 MESP isosurfaces at various sites of the (a) reference system, (b) D1 and D1- $\pi$ -A system, and (c) D4 and D4- $\pi$ -A system.  $V_m$  values are in kcal mol<sup>-1</sup>.

Table 1  $V_m$  (kcal mol<sup>-1</sup>) at various sites of D- $\pi$ -A systems calculated at B3LYP/cc-pVDZ levels

D moiety	D- $\pi$ -A system	$V_{mD'}$	$V_{mD}$	$V_{mS}$	$V_{m(OH)}$	$V_{m(CO)}$	$V_{mA}$	$\Delta V_{mD}$	$\Delta V_{mS}$	$\Delta V_{m(OH)}$	$\Delta V_{m(CO)}$	$\Delta V_{mA}$	
(a) Benzene	D1	-16.6	-6.1	-2.6	-31.8	-38.9	-52.8	10.5	-0.2	-2.9	-2.9	-2.5	
	D1-CH <sub>3</sub>	-18.1	-6.5	-3.8	-32.7	-39.9	-53.8	11.5	-1.4	-3.9	-3.9	-3.5	
	D1-C <sub>5</sub> H <sub>11</sub>	-18.7	-7.2	-4.3	-33.1	-40.1	-54.2	11.5	-1.9	-4.3	-4.1	-3.8	
	D1-isopropyl	-17.9	-6.7	-3.8	-32.9	-39.9	-53.8	11.2	-1.4	-4.1	-3.9	-3.5	
	D1- <i>t</i> -but	-18.1	-6.9	-4.0	-32.9	-40.0	-53.9	11.2	-1.6	-4.1	-4.0	-3.6	
	D1-OH	-17.9	-5.0	-4.3	-33.8	-40.9	-54.5	12.9	-1.9	-5.0	-4.8	-4.2	
	D1-OCH <sub>3</sub>	-18.8	-6.0	-5.0	-34.3	-41.4	-54.8	12.8	-2.6	-5.5	-5.4	-4.5	
	D1-OC <sub>2</sub> H <sub>5</sub>	-19.3	-6.5	-5.3	-34.5	-41.6	-55.3	12.7	-2.9	-5.6	-5.6	-5.0	
	D1-NH <sub>2</sub>	-23.1	-8.6	-7.6	-36.4	-43.7	-57.1	14.5	-5.2	-7.6	-7.7	-6.8	
	D1-N(CH <sub>3</sub> ) <sub>2</sub>	-24.0	-9.1	-9.0	-37.7	-45.1	-58.4	14.9	-6.7	-8.8	-9.0	-8.0	
	D1-PhCH <sub>3</sub>	-16.7	-7.0	-3.7	-32.8	-39.8	-53.5	9.7	-1.3	-4.0	-3.8	-3.2	
	D1-PhNH <sub>2</sub>	-19.7	-9.5	-5.9	-34.5	-41.7	-55.0	10.2	-3.5	-5.6	-5.6	-4.7	
	Pyrene	D2	-14.4	-8.2	-3.3	-32.0	-39.3	-53.0	6.2	-0.9	-3.2	-3.3	-2.7
		D2-CH <sub>3</sub>	-15.4	-8.7	-4.0	-32.6	-39.8	-53.7	6.7	-1.6	-3.8	-3.8	-3.3
		D2-C <sub>5</sub> H <sub>11</sub>	-15.8	-9.2	-4.2	-32.8	-40.0	-53.9	6.7	-1.8	-4.0	-4.0	-3.6
		D2-isopropyl	-15.3	-8.8	-4.0	-32.4	-39.7	-53.7	6.5	-1.6	-3.6	-3.7	-3.4
		D2- <i>t</i> -but	-15.5	-8.9	-4.1	-32.4	-39.8	-53.8	6.6	-1.7	-3.6	-3.8	-3.5
		D2-OH	-15.2	-8.2	-4.0	-32.8	-39.9	-53.7	7.0	-1.6	-4.0	-3.9	-3.4
		D2-OCH <sub>3</sub>	-15.9	-8.8	-4.5	-32.9	-40.2	-54.2	7.1	-2.1	-4.1	-4.1	-3.8
		D2-OC <sub>2</sub> H <sub>5</sub>	-16.3	-9.2	-4.6	-33.3	-40.5	-54.3	7.1	-2.3	-4.5	-4.5	-4.0
D2-NH <sub>2</sub>		-18.1	-11.0	-5.8	-34.1	-41.2	-54.7	7.2	-3.4	-5.3	-5.2	-4.4	
D2-N(CH <sub>3</sub> ) <sub>2</sub>		-18.9	-11.5	-6.7	-34.7	-42.1	-55.8	7.3	-4.3	-5.9	-6.1	-5.5	
D2-PhCH <sub>3</sub>		-14.7	-8.6	-3.8	-32.6	-39.7	-53.7	6.1	-1.4	-3.8	-3.7	-3.3	
D2-PhNH <sub>2</sub>		-16.7	-10.7	-5.0	-33.4	-40.6	-54.5	6.0	-2.6	-4.6	-4.6	-4.1	
TPA	D3	-15.6	-7.7	-6.3	-35.6	-42.5	-56.0	7.9	-3.9	-6.8	-6.5	-5.7	
	D3-CH <sub>3</sub>	-16.5	-8.3	-6.9	-36.0	-43.2	-56.7	8.2	-4.5	-7.2	-7.2	-6.3	
	D3-C <sub>5</sub> H <sub>11</sub>	-16.8	-8.7	-7.2	-36.0	-43.3	-57.0	8.2	-4.8	-7.2	-7.3	-6.7	
	D3-isopropyl	-16.4	-8.3	-6.8	-35.8	-43.1	-56.6	8.1	-4.5	-7.0	-7.1	-6.3	
	D3- <i>t</i> -but	-16.4	-8.3	-6.9	-36.1	-43.1	-56.4	8.2	-4.5	-7.3	-7.1	-6.0	
	D3-OH	-17.5	-8.2	-7.5	-36.3	-43.5	-57.2	9.3	-5.1	-7.5	-7.5	-6.8	
	D3-OCH <sub>3</sub>	-17.9	-8.7	-7.7	-36.6	-43.7	-57.2	9.2	-5.3	-7.8	-7.7	-6.9	
	D3-OC <sub>2</sub> H <sub>5</sub>	-18.1	-8.9	-7.8	-36.7	-43.9	-57.4	9.2	-5.5	-7.9	-7.9	-7.1	
	D3-NH <sub>2</sub>	-19.4	-10.2	-8.7	-37.3	-44.5	-58.1	9.2	-6.3	-8.5	-8.5	-7.8	
	D3-N(CH <sub>3</sub> ) <sub>2</sub>	-20.0	-11.0	-9.2	-37.7	-44.8	-58.3	9.0	-6.8	-8.9	-8.8	-8.0	
	D3-PhCH <sub>3</sub>	-15.3	-7.8	-6.4	-35.6	-42.7	-56.3	7.5	-4.0	-6.8	-6.7	-6.0	
	D3-PhNH <sub>2</sub>	-17.4	-9.7	-7.5	-36.3	-43.5	-57.2	7.7	-5.1	-7.5	-7.5	-6.8	
(b) Carbazole	D4	-19.5	-12.0	-4.8	-33.6	-40.6	-54.8	7.5	-2.4	-4.8	-4.6	-4.5	
	D4-CH <sub>3</sub>	-20.6	-12.3	-5.6	-34.2	-41.3	-55.3	8.3	-3.2	-5.4	-5.3	-5.0	
	D4-C <sub>5</sub> H <sub>11</sub>	-21.0	-12.7	-5.9	-34.3	-41.4	-55.5	8.3	-3.5	-5.5	-5.3	-5.1	
	D4-isopropyl	-20.3	-12.2	-5.5	-34.0	-41.0	-55.1	8.1	-3.1	-5.2	-5.0	-4.8	
	D4- <i>t</i> -but	-20.4	-12.4	-5.5	-34.1	-41.1	-54.9	8.0	-3.1	-5.3	-5.1	-4.6	
	D4-OH	-21.0	-11.4	-6.0	-34.8	-41.5	-55.7	9.6	-3.6	-6.0	-5.5	-5.4	
	D4-OCH <sub>3</sub>	-21.6	-12.0	-6.5	-35.1	-42.0	-56.0	9.5	-4.1	-6.3	-6.0	-5.7	
	D4-OC <sub>2</sub> H <sub>5</sub>	-21.8	-12.4	-6.7	-35.1	-42.1	-55.8	9.4	-4.3	-6.3	-6.1	-5.5	
	D4-NH <sub>2</sub>	-23.6	-14.5	-7.9	-36.0	-43.2	-57.0	9.1	-5.5	-7.2	-7.2	-6.7	
	D4-N(CH <sub>3</sub> ) <sub>2</sub>	-24.6	-14.7	-8.8	-36.8	-43.7	-57.5	9.9	-6.5	-8.0	-7.7	-7.2	
	D4-PhCH <sub>3</sub>	-19.5	-12.2	-5.2	-33.9	-41.0	-55.0	7.2	-2.8	-5.1	-5.0	-4.6	
	D4-PhNH <sub>2</sub>	-21.8	-14.6	-6.5	-34.9	-42.0	-55.7	7.2	-4.1	-6.1	-6.0	-5.4	
	Phenothiazine	D5	-16.8	-9.4	-5.3	-34.6	-41.7	-55.2	7.4	-2.9	-5.8	-5.6	-4.9
		D5-CH <sub>3</sub>	-17.6	-9.0	-5.8	-34.7	-42.2	-55.7	8.6	-3.5	-5.9	-6.1	-5.4
		D5-C <sub>5</sub> H <sub>11</sub>	-17.9	-9.5	-6.1	-35.2	-42.5	-55.8	8.4	-3.8	-6.4	-6.5	-5.5
		D5-isopropyl	-17.5	-9.0	-5.9	-35.0	-42.3	-55.3	8.5	-3.5	-6.2	-6.3	-5.0
		D5- <i>t</i> -but	-17.6	-9.0	-6.0	-35.1	-42.4	-55.7	8.6	-3.6	-6.3	-6.3	-5.4
		D5-OH	-18.1	-7.2	-6.3	-35.4	-42.9	-56.1	10.9	-4.0	-6.6	-6.8	-5.8
		D5-OCH <sub>3</sub>	-18.4	-9.4	-6.7	-35.5	-42.7	-56.2	9.0	-4.3	-6.7	-6.7	-5.9
		D5-OC <sub>2</sub> H <sub>5</sub>	-18.6	-9.8	-6.7	-35.7	-43.1	-56.5	8.8	-4.3	-6.9	-7.1	-6.1
D5-NH <sub>2</sub>		-19.5	-11.4	-7.3	-36.1	-43.4	-56.9	8.2	-5.0	-7.3	-7.4	-6.5	
D5-N(CH <sub>3</sub> ) <sub>2</sub>		-20.6	-12.4	-8.2	-36.6	-44.1	-57.5	8.3	-5.8	-7.8	-8.1	-7.2	
D5-PhCH <sub>3</sub>		-16.7	-9.0	-5.5	-34.8	-42.0	-55.5	7.7	-3.1	-6.0	-6.0	-5.1	
D5-PhNH <sub>2</sub>		-18.2	-11.2	-6.6	-35.4	-42.9	-56.2	7.0	-4.2	-6.6	-6.8	-5.9	
Coumarin	D6	-5.7	-0.1	0.0	-30.1	-37.8	-50.5	5.6	2.4	-1.3	-1.8	-0.2	
	D6-CH <sub>3</sub>	-6.5	-0.4	-1.2	-31.0	-38.7	-51.3	6.1	1.2	-2.2	-2.7	-0.9	
	D6-C <sub>5</sub> H <sub>11</sub>	-7.2	-1.1	-1.6	-31.2	-39.0	-51.8	6.1	0.8	-2.4	-3.0	-1.5	
	D6-isopropyl	-6.7	-0.6	-1.2	-30.7	-38.7	-51.1	6.0	1.2	-1.9	-2.7	-0.8	
	D6- <i>t</i> -but	-6.9	-0.9	-1.4	-31.2	-38.9	-51.3	6.0	0.9	-2.4	-2.9	-1.0	
	D6-OH	-6.1	-	-1.9	-31.8	-39.5	-52.3	6.1	0.5	-3.0	-3.5	-1.9	
D6-OCH <sub>3</sub>	-7.0	-0.1	-2.6	-32.1	-40.0	-52.6	7.0	-0.2	-3.3	-4.0	-2.3		

Table 1 (continued)

D moiety	D- $\pi$ -A system	$V_{mD'}$	$V_{mD}$	$V_{mS}$	$V_{m(OH)}$	$V_{m(CO)}$	$V_{mA}$	$\Delta V_{mD}$	$\Delta V_{mS}$	$\Delta V_{m(OH)}$	$\Delta V_{m(CO)}$	$\Delta V_{mA}$
	D6-OC <sub>2</sub> H <sub>5</sub>	-7.5	-0.4	-2.9	-32.3	-40.2	-52.5	7.0	-0.6	-3.5	-4.2	-2.2
	D6-NH <sub>2</sub>	-10.4	-2.1	-5.0	-33.9	-41.8	-54.3	8.3	-2.6	-5.1	-5.8	-4.0
	D6-N(CH <sub>3</sub> ) <sub>2</sub>	-11.3	-2.6	-6.3	-35.0	-43.0	-55.5	8.7	-4.0	-6.2	-7.0	-5.1
	D6-PhCH <sub>3</sub>	-7.2	-1.6	-1.6	-31.2	-38.8	-51.5	5.6	0.8	-2.4	-2.8	-1.2
	D6-PhNH <sub>2</sub>	-10.2	-4.2	-3.6	-32.8	-40.6	-53.2	6.0	-1.2	-4.0	-4.6	-2.8

MESP minimum observed at the CN unit of  $\pi$ -A is considered as a reference value,  $V_{mA'}$  (Fig. 2a) ( $-50.3 \text{ kcal mol}^{-1}$ ) to monitor the changes observed at this minimum due to the incorporation of D to  $\pi$ -A. One could also consider the MESP minimum  $V_{m(OH)}$  or  $V_{m(CO)}$  of  $\pi$ -A as a reference point similar to  $V_{mA'}$  because in general the trends observed for these quantities show a parallel behavior. Here  $V_{mA'}$  is selected as the reference point on the basis of its most negative character compared to all other minima.

In Table 1a and b,  $V_m$  of D- $\pi$ -A systems at various sites *viz.* donor ( $V_{mD}$ ), spacer ( $V_{mS}$ ) and acceptor ( $V_{m(OH)}$ ,  $V_{m(CO)}$  and  $V_{mA}$ ) are reported along with  $V_{mD'}$ . The unsubstituted D- $\pi$ -A systems are denoted as D1, D2, D3, D4, D5, and D6, and the substituents attached at D1-D6 are represented as D1-CH<sub>3</sub>, D1-C<sub>5</sub>H<sub>11</sub>, D2-CH<sub>3</sub>, D2-C<sub>5</sub>H<sub>11</sub>, *etc.* The quantities  $\Delta V_{mD}$ ,  $\Delta V_{mS}$ ,  $\Delta V_{m(OH)}$ ,  $\Delta V_{m(CO)}$ , and  $\Delta V_{mA}$  represent the change in  $V_m$  at the respective

sites with the attachment of  $\pi$ -A to D.  $\Delta V_{mD}$  has been calculated by subtracting the  $V_m$  observed at the donor ( $V_{mD'}$ ) from the respective  $V_m$  observed at the D site of D- $\pi$ -A ( $V_{mD}$ ). Likewise  $\Delta V_{mS}$ ,  $\Delta V_{m(OH)}$ ,  $\Delta V_{m(CO)}$ , and  $\Delta V_{mA}$  are estimated by subtracting the respective  $V_m$  at  $\pi$ -A *viz.*  $V_{mS}$ ,  $V_{m(OH)}$ ,  $V_{m(CO)}$  and  $V_{mA}$  (Fig. 2) from the corresponding values at D- $\pi$ -A ( $V_{mS}$ ,  $V_{m(OH)}$ ,  $V_{m(CO)}$  and  $V_{mA}$ ) (Table 1a and b).

The data in Table 1a and b show that the  $V_{mD}$  of the D- $\pi$ -A system is always less negative than the  $V_{mD'}$  of the donor D. For various donor systems,  $\Delta V_{mD}$  lies in the range 5.6 to 14.9  $\text{kcal mol}^{-1}$  which clearly suggests that the D site of the D- $\pi$ -A system becomes electron deficient compared to a normal D. The electron deficiency at D can be attributed to ICT of electrons from D to the  $\pi$ -A region which implies that  $V_m$  at the acceptor sites of D- $\pi$ -A becomes more negative compared to  $\pi$ -A and as a result always negative values are observed for

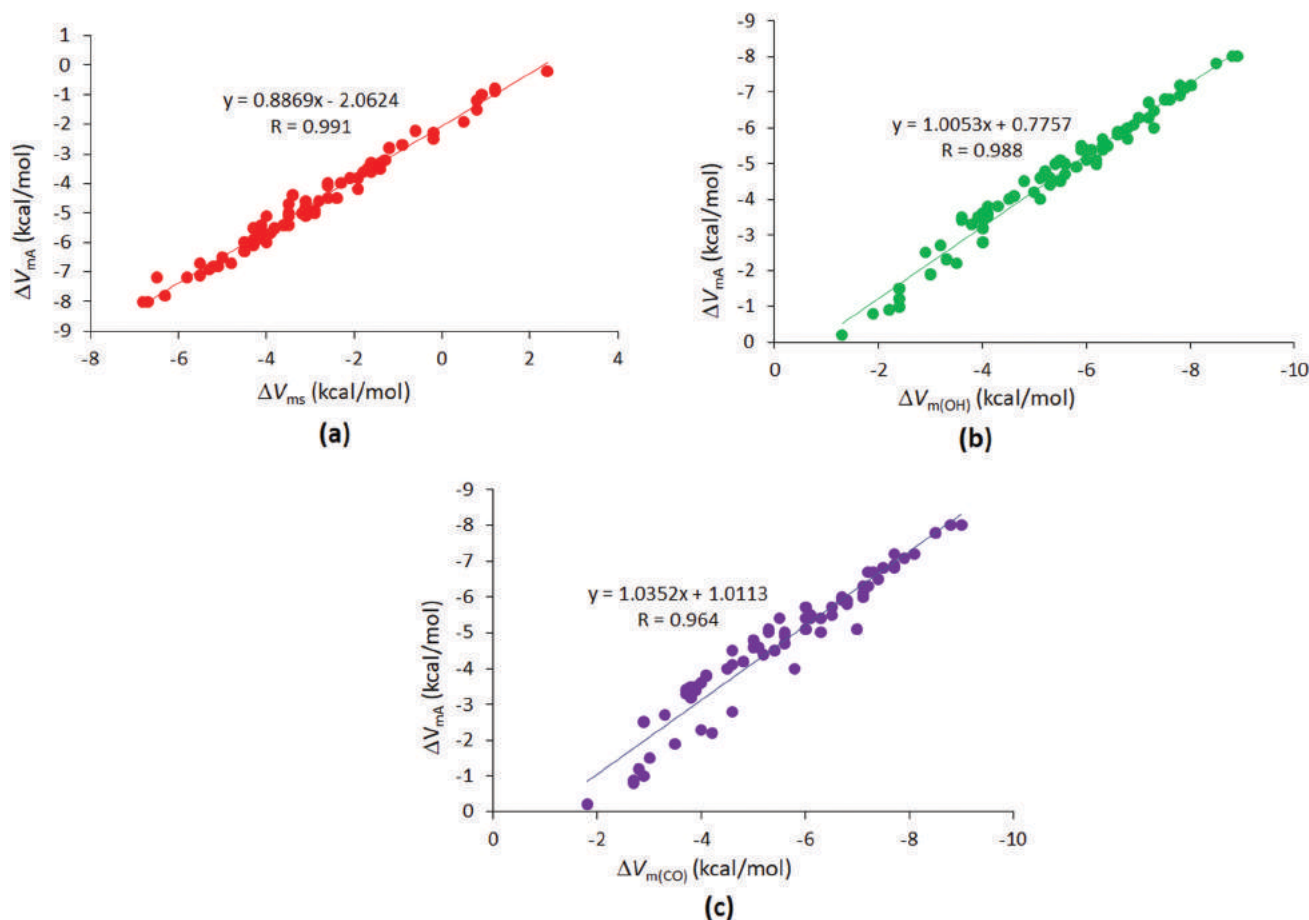


Fig. 3 Correlation between MESP parameters  $\Delta V_{mS}$ ,  $\Delta V_{m(OH)}$ ,  $\Delta V_{m(CO)}$ , and  $\Delta V_{mA}$ .



**Table 2** HOMO, LUMO and HOMO–LUMO energy gap (HLG) (in eV) observed for the ground state at the B3LYP/cc-pVDZ level and absorption maximum  $\lambda_{\max}$  (nm), and oscillator strength ( $f$ ) at the CAM-B3LYP/SMD/cc-pVDZ//B3LYP/cc-pVDZ level

D- $\pi$ -A system	HOMO	LUMO	HLG	$\lambda_{\max}$	$f$	D- $\pi$ -A system	HOMO	LUMO	HLG	$\lambda_{\max}$	$f$
Benzene						Pyrene					
D1	-6.13	-2.99	3.14	388	1.74	D2	-5.88	-2.99	2.89	401	2.22
D1-CH <sub>3</sub>	-6.01	-2.92	3.08	396	1.82	D2-CH <sub>3</sub>	-5.84	-2.95	2.89	404	2.27
D1-C <sub>5</sub> H <sub>11</sub>	-5.97	-2.90	3.07	398	1.86	D2-C <sub>5</sub> H <sub>11</sub>	-5.81	-2.94	2.87	404	2.32
D1-isopropyl	-6.01	-2.92	3.08	396	1.86	D2-isopropyl	-5.83	-2.95	2.88	404	2.30
D1- <i>t</i> -but	-6.00	-2.92	3.08	397	1.89	D2- <i>t</i> -but	-5.82	-2.95	2.87	404	2.33
D1-OH	-5.84	-2.85	2.99	408	1.78	D2-OH	-5.85	-2.94	2.91	409	2.19
D1-OCH <sub>3</sub>	-5.79	-2.83	2.97	412	1.81	D2-OCH <sub>3</sub>	-5.79	-2.92	2.87	410	2.20
D1-OC <sub>2</sub> H <sub>5</sub>	-5.77	-2.81	2.96	413	1.84	D2-OC <sub>2</sub> H <sub>5</sub>	-5.77	-2.91	2.86	410	2.23
D1-NH <sub>2</sub>	-5.53	-2.69	2.84	434	1.85	D2-NH <sub>2</sub>	-5.62	-2.86	2.76	419	2.20
D1-N(CH <sub>3</sub> ) <sub>2</sub>	-5.34	-2.62	2.72	457	1.94	D2-N(CH <sub>3</sub> ) <sub>2</sub>	-5.39	-2.81	2.58	430	2.21
D1-PhCH <sub>3</sub>	-5.89	-2.96	2.93	410	2.15	D2-PhCH <sub>3</sub>	-5.86	-2.97	2.89	406	2.49
D1-PhNH <sub>2</sub>	-5.52	-2.86	2.66	428	2.17	D2-PhNH <sub>2</sub>	-5.53	-2.91	2.62	411	2.53
TPA						Carbazole					
D3	-5.37	-2.79	2.58	453	2.02	D4	-5.78	-2.91	2.87	419	2.21
D3-CH <sub>3</sub>	-5.31	-2.76	2.55	457	2.03	D4-CH <sub>3</sub>	-5.69	-2.87	2.83	424	2.27
D3-C <sub>5</sub> H <sub>11</sub>	-5.29	-2.75	2.55	458	2.06	D4-C <sub>5</sub> H <sub>11</sub>	-5.67	-2.85	2.82	425	2.31
D3-isopropyl	-5.31	-2.76	2.55	457	2.03	D4-isopropyl	-5.71	-2.88	2.83	424	2.30
D3- <i>t</i> -but	-5.31	-2.76	2.55	457	2.02	D4- <i>t</i> -but	-5.70	-2.87	2.83	424	2.31
D3-OH	-5.26	-2.73	2.53	460	2.02	D4-OH	-5.58	-2.84	2.74	432	2.22
D3-OCH <sub>3</sub>	-5.24	-2.72	2.52	461	2.03	D4-OCH <sub>3</sub>	-5.54	-2.82	2.72	433	2.27
D3-OC <sub>2</sub> H <sub>5</sub>	-5.23	-2.71	2.51	461	2.03	D4-OC <sub>2</sub> H <sub>5</sub>	-5.52	-2.81	2.71	434	2.29
D3-NH <sub>2</sub>	-5.13	-2.67	2.46	468	2.00	D4-NH <sub>2</sub>	-5.33	-2.75	2.58	447	2.23
D3-N(CH <sub>3</sub> ) <sub>2</sub>	-5.03	-2.65	2.38	472	2.00	D4-N(CH <sub>3</sub> ) <sub>2</sub>	-5.14	-2.71	2.44	461	2.26
D3-PhCH <sub>3</sub>	-5.31	-2.78	2.52	457	2.12	D4-PhCH <sub>3</sub>	-5.66	-2.90	2.76	427	2.53
D3-PhNH <sub>2</sub>	-5.17	-2.73	2.44	460	2.12	D4-PhNH <sub>2</sub>	-5.37	-2.83	2.53	433	2.57
Phenothiazine						Coumarin					
D5	-5.28	-2.84	2.44	459	1.67	D6	-6.19	-3.34	2.85	424	1.71
D5-CH <sub>3</sub>	-5.22	-2.81	2.41	464	1.69	D6-CH <sub>3</sub>	-6.09	-3.26	2.82	431	1.78
D5-C <sub>5</sub> H <sub>11</sub>	-5.20	-2.80	2.40	464	1.72	D6-C <sub>5</sub> H <sub>11</sub>	-6.07	-3.25	2.82	431	1.84
D5-isopropyl	-5.21	-2.81	2.40	465	1.68	D6-isopropyl	-6.09	-3.27	2.82	431	1.83
D5- <i>t</i> -but	-5.22	-2.81	2.40	464	1.71	D6- <i>t</i> -but	-6.07	-3.25	2.82	432	1.84
D5-OH	-5.15	-2.79	2.36	469	1.66	D6-OH	-5.98	-3.20	2.78	439	1.77
D5-OCH <sub>3</sub>	-5.14	-2.78	2.36	469	1.70	D6-OCH <sub>3</sub>	-5.94	-3.18	2.76	442	1.82
D5-OC <sub>2</sub> H <sub>5</sub>	-5.12	-2.77	2.35	470	1.71	D6-OC <sub>2</sub> H <sub>5</sub>	-5.92	-3.16	2.76	443	1.85
D5-NH <sub>2</sub>	-4.99	-2.74	2.25	482	1.62	D6-NH <sub>2</sub>	-5.71	-3.04	2.67	463	1.86
D5-N(CH <sub>3</sub> ) <sub>2</sub>	-4.88	-2.70	2.17	490	1.62	D6-N(CH <sub>3</sub> ) <sub>2</sub>	-5.56	-2.97	2.59	481	1.96
D5-PhCH <sub>3</sub>	-5.22	-2.81	2.41	464	1.69	D6-PhCH <sub>3</sub>	-6.00	-3.28	2.72	444	2.10
D5-PhNH <sub>2</sub>	-5.07	-2.78	2.29	469	1.78	D6-PhNH <sub>2</sub>	-5.68	-3.17	2.51	461	2.18

$\Delta V_{m(OH)}$ ,  $\Delta V_{m(CO)}$ , and  $\Delta V_{mA}$ . For example, when  $\pi$ -A changes to D1- $\pi$ -A,  $V_m$  at the cyano region turns out to be more negative ( $V_{mA} = -52.8$  kcal mol<sup>-1</sup>) than the respective  $V_m$  on the reference system ( $\pi$ -A),  $V_{mA}$  ( $-50.3$  kcal mol<sup>-1</sup>). A similar trend in  $V_{mA}$  is observed for all the remaining systems. Also compared to  $\pi$ -A, the  $\pi$ -spacer region of D- $\pi$ -A shows more negative character for  $V_{mS}$  in all cases except some of the coumarin-based systems. Among the donors, the  $V_{mD}$  value is the least negative for coumarin systems, which can be attributed to the presence of an electron withdrawing carbonyl group in it. The quantities  $\Delta V_{mS}$ ,  $\Delta V_{m(OH)}$ ,  $\Delta V_{m(CO)}$  and  $\Delta V_{mA}$  show a parallel trend as shown in the correlation plots given in Fig. 3a–c. This suggests that any of these quantities can be used as a parameter to measure the donating strength of donor moieties to a common acceptor. Here  $\Delta V_{mA}$  (for the CN group) is selected for this purpose. It may be noted that variation in  $\Delta V_{mD}$  is not similar to  $\Delta V_{mA}$  (Fig. S3, ESI<sup>†</sup>) because it accounts for the property of various donors whereas  $\Delta V_{mA}$  accounts for the accepting ability of a CN unit from various donors.

In Table 1a and b, the lower  $\Delta V_{mA}$  in the range  $-0.2$  to  $-5.1$  kcal mol<sup>-1</sup> have been attained by coumarin-based D- $\pi$ -A

systems which can be attributed to the presence of an electron-withdrawing CO group in the donor site. In benzene and pyrene based systems, the strong conjugation feature in donors increases the negative character of the  $\Delta V_{mA}$  values ( $-2.5$  to  $-8.0$  kcal mol<sup>-1</sup>) leading to better-donating strength than coumarin systems.

In carbazole and phenothiazine systems, the charge transfer to the acceptor is enhanced ( $\Delta V_{mA} -4.5$  to  $-7.2$  kcal mol<sup>-1</sup>) due to donation from hetero atoms *viz.* nitrogen and sulphur. Among all, the TPA based systems have the highest electron-donating strength ( $-5.7$  to  $-8.0$  kcal mol<sup>-1</sup>).

Substituents at the donor region can be utilized for tuning the electron-donating strength of the donor. For instance, alkyl substituents *viz.* CH<sub>3</sub>, C<sub>5</sub>H<sub>11</sub>, isopropyl, and *t*-butyl at the donor unit enhance the electron-donating strength of all the corresponding substituted D- $\pi$ -A systems by a +I inductive effect. The substituents bearing lone pairs such as OH, OCH<sub>3</sub>, NH<sub>2</sub>, and N(CH<sub>3</sub>)<sub>2</sub> improve the electron density of the donor unit, resulting in better electron-donating power than alkyl substituents ( $\Delta V_{mA}$  in the range  $-3.4$  to  $-8.0$  kcal mol<sup>-1</sup>) +R resonance effect. Among all, N(CH<sub>3</sub>)<sub>2</sub> substituted benzene and TPA based D- $\pi$ -A systems show

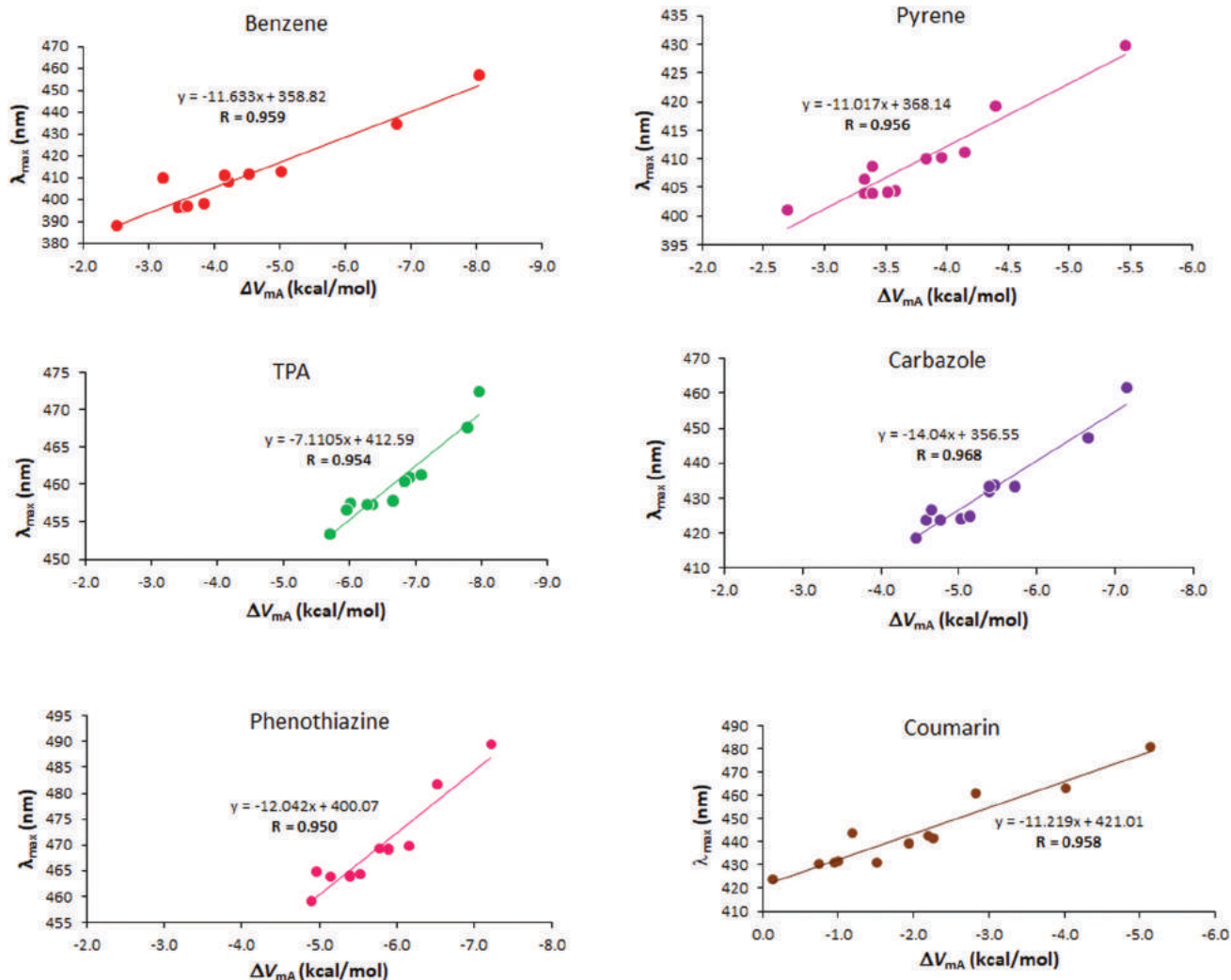


Fig. 4 Correlation between absorption maximum ( $\lambda_{\max}$ ) and donating strength ( $\Delta V_{mA}$ ) of various D- $\pi$ -A systems with different substituents.

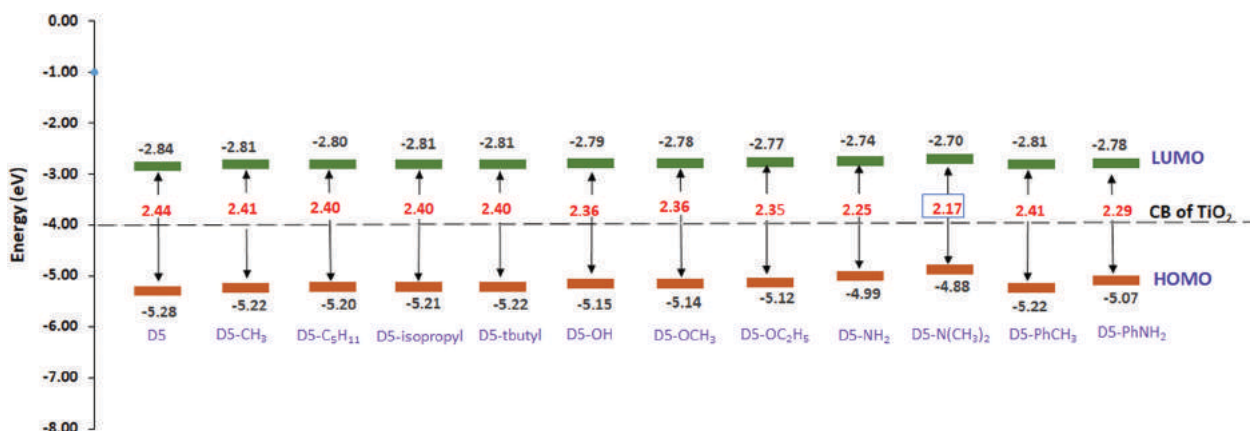


Fig. 5 Frontier molecular energy levels of phenothiazine based  $\pi$ -A with various substituents at the B3LYP/cc-pVDZ level.

the highest donation from donor to acceptor. The donating strength of various substituents attached on the D- $\pi$ -A system follows the order PhCH<sub>3</sub>  $\sim$  alkyls  $<$  -OH, -OR, PhNH<sub>2</sub>  $<$  NH<sub>2</sub>  $<$  N(CH<sub>3</sub>)<sub>2</sub>.

**Table 3** HOMO, LUMO and HOMO–LUMO energy gap (HLG) (in eV) observed for the ground state at the B3LYP/cc-pVDZ level. Excitation energy, ground and excited state oxidation potential ( $E^{\text{dye}}$ ,  $E^{\text{dye*}}$ ), free energy of electron injection  $\Delta G_{\text{inject}}$ , dye regeneration efficiency  $\Delta G_{\text{reg}}$ , and open-circuit voltage  $eV_{\text{OC}}$  at the TD-CAM-B3LYP/SMD/cc-pVDZ//B3LYP/cc-pVDZ level

D- $\pi$ -A	Excitation energy (eV)	HOMO (eV)	LUMO (eV)	HLG (eV)	$E^{\text{dye}}$ (eV)	$E^{\text{dye*}}$ (eV)	$\Delta G_{\text{inject}}$ (eV)	$\Delta G_{\text{reg}}$ (eV)	$eV_{\text{OC}}$ (eV)
(a)									
Benzene									
D1	3.20	-6.13	-2.99	3.14	6.13	2.93	-1.07	1.33	1.01
D1-CH <sub>3</sub>	3.13	-6.01	-2.92	3.08	6.01	2.88	-1.12	1.21	1.08
D1-C <sub>5</sub> H <sub>11</sub>	3.11	-5.97	-2.90	3.07	5.97	2.86	-1.14	1.17	1.10
D1-isopropyl	3.13	-6.01	-2.92	3.08	6.01	2.88	-1.12	1.21	1.08
D1- <i>t</i> -but	3.13	-6.00	-2.92	3.08	6.00	2.87	-1.13	1.20	1.08
D1-OH	3.04	-5.84	-2.85	2.99	5.84	2.80	-1.20	1.04	1.15
D1-OCH <sub>3</sub>	3.01	-5.79	-2.83	2.97	5.79	2.78	-1.22	0.99	1.17
D1-OC <sub>2</sub> H <sub>5</sub>	3.00	-5.77	-2.81	2.96	5.77	2.77	-1.23	0.97	1.19
D1-NH <sub>2</sub>	2.85	-5.53	-2.69	2.84	5.53	2.68	-1.32	0.73	1.31
D1-N(CH <sub>3</sub> ) <sub>2</sub>	2.71	-5.34	-2.62	2.72	5.34	2.63	-1.37	0.54	1.38
D1-PhCH <sub>3</sub>	3.02	-5.89	-2.96	2.93	5.89	2.87	-1.13	1.09	1.04
D1-PhNH <sub>2</sub>	2.90	-5.52	-2.86	2.66	5.52	2.62	-1.38	0.73	1.14
Pyrene									
D2	3.09	-5.88	-2.99	2.89	5.88	2.79	-1.21	1.08	1.01
D2-CH <sub>3</sub>	3.07	-5.84	-2.95	2.89	5.84	2.77	-1.23	1.04	1.05
D2-C <sub>5</sub> H <sub>11</sub>	3.07	-5.81	-2.94	2.87	5.81	2.74	-1.26	1.01	1.06
D2-isopropyl	3.07	-5.83	-2.95	2.88	5.83	2.76	-1.24	1.03	1.05
D2- <i>t</i> -but	3.07	-5.82	-2.95	2.87	5.82	2.75	-1.25	1.02	1.05
D2-OH	3.03	-5.85	-2.94	2.91	5.85	2.82	-1.18	1.05	1.06
D2-OCH <sub>3</sub>	3.02	-5.79	-2.92	2.87	5.79	2.77	-1.23	0.99	1.08
D2-OC <sub>2</sub> H <sub>5</sub>	3.02	-5.77	-2.91	2.86	5.77	2.75	-1.25	0.97	1.09
D2-NH <sub>2</sub>	2.96	-5.62	-2.86	2.76	5.62	2.66	-1.34	0.82	1.14
D2-N(CH <sub>3</sub> ) <sub>2</sub>	2.88	-5.39	-2.81	2.58	5.39	2.51	-1.49	0.59	1.19
D2-PhCH <sub>3</sub>	3.05	-5.86	-2.97	2.89	5.86	2.81	-1.19	1.06	1.03
D2-PhNH <sub>2</sub>	3.02	-5.53	-2.91	2.62	5.53	2.51	-1.49	0.73	1.09
TPA									
D3	2.73	-5.37	-2.79	2.58	5.37	2.64	-1.36	0.57	1.21
D3-CH <sub>3</sub>	2.71	-5.31	-2.76	2.55	5.31	2.60	-1.40	0.51	1.24
D3-C <sub>5</sub> H <sub>11</sub>	2.71	-5.29	-2.75	2.55	5.29	2.58	-1.42	0.49	1.25
D3-isopropyl	2.71	-5.31	-2.76	2.55	5.31	2.60	-1.40	0.51	1.24
D3- <i>t</i> -but	2.71	-5.31	-2.76	2.55	5.31	2.60	-1.40	0.51	1.24
D3-OH	2.69	-5.26	-2.73	2.53	5.26	2.57	-1.43	0.46	1.27
D3-OCH <sub>3</sub>	2.69	-5.24	-2.72	2.52	5.24	2.55	-1.45	0.44	1.28
D3-OC <sub>2</sub> H <sub>5</sub>	2.69	-5.23	-2.71	2.51	5.23	2.54	-1.46	0.43	1.29
D3-NH <sub>2</sub>	2.65	-5.13	-2.67	2.46	5.13	2.48	-1.52	0.33	1.33
D3-N(CH <sub>3</sub> ) <sub>2</sub>	2.62	-5.03	-2.65	2.38	5.03	2.41	-1.59	0.23	1.35
D3-PhCH <sub>3</sub>	2.72	-5.31	-2.78	2.52	5.31	2.60	-1.41	0.51	1.22
D3-PhNH <sub>2</sub>	2.69	-5.17	-2.73	2.44	5.17	2.48	-1.52	0.37	1.27
(b)									
Carbazole									
D4	2.96	-5.78	-2.91	2.87	5.78	2.82	-1.18	0.98	1.09
D4-CH <sub>3</sub>	2.92	-5.69	-2.87	2.83	5.69	2.77	-1.23	0.89	1.13
D4-C <sub>5</sub> H <sub>11</sub>	2.92	-5.67	-2.85	2.82	5.67	2.75	-1.25	0.87	1.15
D4-isopropyl	2.93	-5.71	-2.88	2.83	5.71	2.78	-1.22	0.91	1.12
D4- <i>t</i> -but	2.93	-5.70	-2.87	2.83	5.70	2.77	-1.23	0.90	1.13
D4-OH	2.87	-5.58	-2.84	2.74	5.58	2.71	-1.29	0.78	1.16
D4-OCH <sub>3</sub>	2.86	-5.54	-2.82	2.72	5.54	2.68	-1.32	0.74	1.18
D4-OC <sub>2</sub> H <sub>5</sub>	2.86	-5.52	-2.81	2.71	5.52	2.66	-1.34	0.72	1.19
D4-NH <sub>2</sub>	2.77	-5.33	-2.75	2.58	5.33	2.56	-1.44	0.53	1.25
D4-N(CH <sub>3</sub> ) <sub>2</sub>	2.69	-5.14	-2.71	2.44	5.14	2.45	-1.55	0.34	1.29
D4-PhCH <sub>3</sub>	2.91	-5.66	-2.90	2.76	5.66	2.75	-1.25	0.86	1.10
D4-PhNH <sub>2</sub>	2.86	-5.37	-2.83	2.53	5.37	2.51	-1.49	0.57	1.17
Phenothiazine									
D5	2.70	-5.28	-2.84	2.44	5.28	2.58	-1.42	0.48	1.16
D5-CH <sub>3</sub>	2.67	-5.22	-2.81	2.41	5.22	2.55	-1.45	0.42	1.19
D5-C <sub>5</sub> H <sub>11</sub>	2.67	-5.20	-2.80	2.40	5.20	2.53	-1.47	0.40	1.20
D5-isopropyl	2.67	-5.21	-2.81	2.40	5.21	2.54	-1.46	0.41	1.19
D5- <i>t</i> -but	2.67	-5.22	-2.81	2.40	5.22	2.55	-1.45	0.42	1.19
D5-OH	2.64	-5.15	-2.79	2.36	5.15	2.51	-1.49	0.35	1.21
D5-OCH <sub>3</sub>	2.64	-5.14	-2.78	2.36	5.14	2.50	-1.50	0.34	1.22
D5-OC <sub>2</sub> H <sub>5</sub>	2.64	-5.12	-2.77	2.35	5.12	2.48	-1.52	0.32	1.23
D5-NH <sub>2</sub>	2.57	-4.99	-2.74	2.25	4.99	2.42	-1.58	0.19	1.26
D5-N(CH <sub>3</sub> ) <sub>2</sub>	2.53	-4.88	-2.70	2.17	4.88	2.35	-1.65	0.08	1.30
D5-PhCH <sub>3</sub>	2.67	-5.22	-2.81	2.41	5.22	2.55	-1.45	0.42	1.19
D5-PhNH <sub>2</sub>	2.64	-5.07	-2.78	2.29	5.07	2.43	-1.57	0.27	1.22

Table 3 (continued)

D- $\pi$ -A	Excitation energy (eV)	HOMO (eV)	LUMO (eV)	HLG (eV)	$E^{\text{dye}}$ (eV)	$E^{\text{dye}*}$ (eV)	$\Delta G_{\text{inject}}$ (eV)	$\Delta G_{\text{reg}}$ (eV)	$eV_{\text{OC}}$ (eV)
Coumarin									
D6	2.93	-6.19	-3.34	2.85	6.19	3.27	-0.73	1.39	0.66
D6-CH <sub>3</sub>	2.88	-6.09	-3.26	2.82	6.09	3.21	-0.79	1.29	0.74
D6-C <sub>5</sub> H <sub>11</sub>	2.87	-6.07	-3.25	2.82	6.07	3.19	-0.81	1.27	0.75
D6-isopropyl	2.88	-6.09	-3.27	2.82	6.09	3.21	-0.79	1.29	0.73
D6- <i>t</i> -but	2.87	-6.07	-3.25	2.82	6.07	3.20	-0.80	1.27	0.75
D6-OH	2.82	-5.98	-3.20	2.78	5.98	3.15	-0.85	1.18	0.80
D6-OCH <sub>3</sub>	2.81	-5.94	-3.18	2.76	5.94	3.13	-0.87	1.14	0.82
D6-OC <sub>2</sub> H <sub>5</sub>	2.80	-5.92	-3.16	2.76	5.92	3.11	-0.89	1.12	0.84
D6-NH <sub>2</sub>	2.68	-5.71	-3.04	2.67	5.71	3.04	-0.96	0.91	0.96
D6-N(CH <sub>3</sub> ) <sub>2</sub>	2.58	-5.56	-2.97	2.59	5.56	2.98	-1.02	0.76	1.03
D6-PhCH <sub>3</sub>	2.80	-6.00	-3.28	2.72	6.00	3.21	-0.79	1.20	0.72
D6-PhNH <sub>2</sub>	2.69	-5.68	-3.17	2.51	5.68	2.99	-1.01	0.88	0.83

### Absorption spectra

In Table 2, the HOMO and LUMO energies, HOMO-LUMO energy gap (HLG), absorption maximum ( $\lambda_{\text{max}}$ ), and oscillator strength ( $f$ ) of six different D- $\pi$ -A systems with various substituents are reported. In all kinds of D- $\pi$ -A systems, a systematic increase in  $\lambda_{\text{max}}$  with respect to various substituents has been observed (388 to 490 nm), which can be correlated with the electron donating strength of the donors in the D- $\pi$ -A system. This is evident in the excellent linear correlations between  $\Delta V_{\text{MA}}$  and  $\lambda_{\text{max}}$  obtained for all six kinds of D- $\pi$ -A systems (Fig. 4). Also with an improved electron-donating strength of a D- $\pi$ -A system, lowering of HLG is noted in every system, which lies in the range 3.14 to 2.17 eV. Among all, the highest  $\lambda_{\text{max}}$  490 nm has been shown by (NH<sub>3</sub>)<sub>2</sub> substituted phenothiazine system D5-N(CH<sub>3</sub>)<sub>2</sub>. For the six D- $\pi$ -A systems and the selected eleven substituents, 102 nm width is available for tuning  $\lambda_{\text{max}}$  to a preferred region. For individual donors, the substituent effect alone can account for a tuning width of 69 nm for benzene, 29 nm for pyrene, 19 nm for TPA, 42 nm for carbazole, 31 nm for phenothiazine and 57 nm for coumarin, respectively.

The  $\Delta V_{\text{MA}}$  versus  $\lambda_{\text{max}}$  correlations given in Fig. 4 suggest that the substituent effects tune the HOMO-LUMO energy gap (HLG). The HLG plot of a representative system D5- $\pi$ -A

(phenothiazine-based) is given in Fig. 5 which shows that the introduction of substituents on the core D unit lowers the HLG from 2.41 to 2.17 eV. Poor electron-donating ability is observed in alkyls and PhCH<sub>3</sub> substituted systems display higher HLG (2.40 to 2.41 eV), while the lowest HLG has been attained with N(CH<sub>3</sub>)<sub>2</sub> substituted D5- $\pi$ -A. A similar trend in HLG is observed for the remaining systems which confirms the significance of the substituent effect in tuning  $\lambda_{\text{max}}$  (Table 3a and b). The HOMO and LUMO plots of the representative systems are shown in Fig. 6. The HOMO has a more delocalized distribution than the LUMO with more orbital contributions from the donor site while the LUMO is largely delocalized along the  $\pi$ -spacer and acceptor moiety.

### Photovoltaic performance

In Table 3a and b, electronic excitation energy, ground state oxidation potential  $E^{\text{dye}}$ , excited state oxidation potential  $E^{\text{dye}*}$ , free energy change of electron injection  $\Delta G_{\text{inject}}$ , free energy change of dye regeneration  $\Delta G_{\text{reg}}$ , and open-circuit voltage  $eV_{\text{OC}}$  of D- $\pi$ -A systems are described. The negative  $\Delta G_{\text{inject}}$  observed in the range -0.73 to -1.65 eV lies above the CB of TiO<sub>2</sub> (-4.0 eV) and indicates the possibility of a spontaneous electron injection process from CB to TiO<sub>2</sub>. Also a more electron-donating substituent enhances the electron injection process as  $\Delta G_{\text{inject}}$

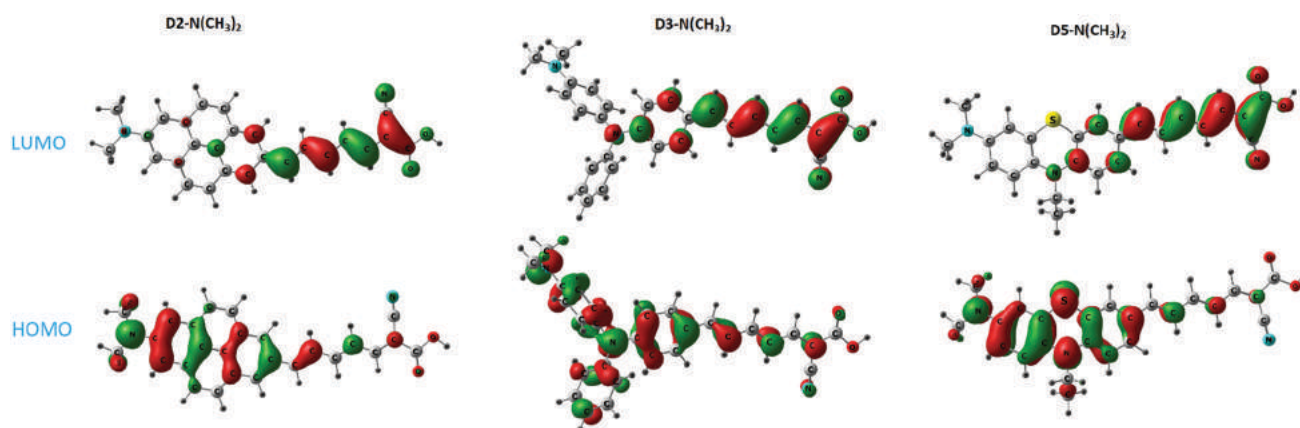


Fig. 6 Frontier molecular orbitals of representative N(CH<sub>3</sub>)<sub>2</sub> substituted D- $\pi$ -A systems at the B3LYP/cc-pVDZ level.



becomes more negative with such substituents. Alkyls, and PhCH<sub>3</sub> substituted D- $\pi$ -A systems are less efficient for electron injection than the OH, OCH<sub>3</sub>, OC<sub>2</sub>H<sub>5</sub>, NH<sub>2</sub> and N(CH<sub>3</sub>)<sub>2</sub> substituted systems. Among all, the most negative  $\Delta G_{\text{inject}} - 1.65$  eV is observed for phenothiazine system D5-N(CH<sub>3</sub>)<sub>2</sub>. The smaller electron injection efficiency ( $-0.79$  to  $-0.81$  eV) observed for alkyls and PhCH<sub>3</sub> substituted coumarin systems can be attributed to their lower electron-donating strength than others.

From the previous studies, it is understood that the PCE of DSSCs depends on the free energy change for dye regeneration.<sup>89,90</sup> The lower the  $\Delta G_{\text{reg}}$ , the faster the dye regeneration will be, leading to higher efficiency for the electron injection from the dye to the TiO<sub>2</sub> semiconductor. In the studied systems, the fastest dye regeneration force 0.08 eV has been attained by the N(CH<sub>3</sub>)<sub>2</sub> substituted phenothiazine system (D5-N(CH<sub>3</sub>)<sub>2</sub>), whereas the least dye regeneration (1.27–1.29 eV) has been possessed by alkyls, and PhCH<sub>3</sub> substituted coumarin systems. The unsubstituted systems always possess higher  $\Delta G_{\text{reg}}$  values (0.48–1.39 eV) than substituted ones (0.08–1.29 eV) and this suggests that the introduction of electron-donating substituents on the donor moiety gives better  $\Delta G_{\text{reg}}$  values and improves electron regeneration efficiency. Similarly, a positive effect of substituents on  $eV_{\text{OC}}$  is always observed confirming that by tuning the donating strength of the substituents, significant improvement in the performance of DSSCs can be achieved. In all the six sets, N(CH<sub>3</sub>)<sub>2</sub> substituted systems possess the best  $eV_{\text{OC}}$  and among them, the highest is observed for D1-N(CH<sub>3</sub>)<sub>2</sub> (1.38 eV) whereas the lowest  $eV_{\text{OC}}$  (0.72 eV) is observed for D4-PhCH<sub>3</sub>.

By considering the above-mentioned results, we analyzed the relation between electron donating strength  $\Delta V_{\text{MA}}$  and open-circuit voltage  $eV_{\text{OC}}$  (Fig. 7 and Fig. S1, ESI<sup>†</sup>). The excellent linear correlation observed in all six series of different D- $\pi$ -A systems shows that  $eV_{\text{OC}}$  increases with enhancement in the donating strength of the substituents. Overall the study suggests that by selecting the appropriate donor and substituent, precise tuning of the optical and photovoltaic properties of the D- $\pi$ -A systems can be achieved. Also these results point out that the theoretical examination of the donating strength of the substituents using MESP analysis is promising for dye designing and efficiency prediction of D- $\pi$ -A systems.

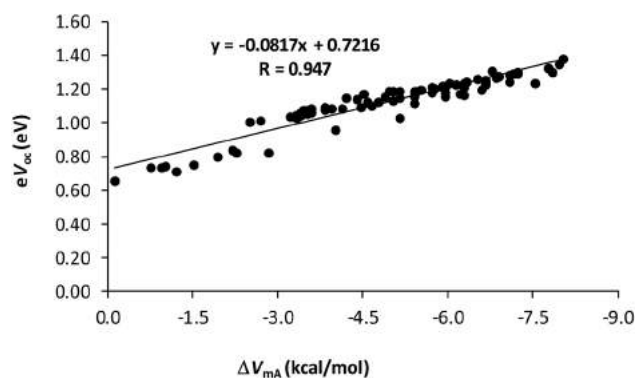


Fig. 7 Correlation between donating strength  $\Delta V_{\text{MA}}$  and open-circuit voltage  $eV_{\text{OC}}$  of D- $\pi$ -A systems.

## Conclusions

The electron-donating strength of the donors in the D- $\pi$ -A system affects the optical and photovoltaic performance of DSSCs, leading to better PCE in the solar cell. In the study using MESP analysis, we have characterized the donating strength ( $\Delta V_{\text{MA}}$ ) of six different sets of D- $\pi$ -A systems, wherein the  $\pi$  and A systems are butadiene and cyanoacrylic acid, respectively. The significance of eleven electron releasing groups at the donors is also examined for a total of seventy-two D- $\pi$ -A systems and achieved the fine-tuning of the electron donation from the donor to the acceptor. In all the six different sets of D- $\pi$ -A systems, the N(CH<sub>3</sub>)<sub>2</sub> substituted D- $\pi$ -A systems show the highest donating strength which can be attributed to the highest electron releasing nature of the N(CH<sub>3</sub>)<sub>2</sub> group. Also, the electron releasing groups at the donors tune the HOMO and LUMO energies of all the corresponding D- $\pi$ -A systems for better optical properties than unsubstituted systems. The optical and photovoltaic performance of the D- $\pi$ -A system is described at the CAM-B3LYP/cc-pVDZ/SMD//B3LYP/cc-pVDZ level. The enhanced performance of these properties achieved with enhanced donating strength conveys the role of tuning the donating strength for better PCE. Among all, the N(CH<sub>3</sub>)<sub>2</sub> substituted D1 system (benzene) possesses the highest  $eV_{\text{OC}}$  which can be attributed to its highest donating strength. These findings suggest that we can improve the photovoltaic performance of DSSCs by tuning the ground state property,  $\Delta V_{\text{MA}}$  at the acceptor site. All the findings imply that incorporation of more electron-releasing substituents on an electron-rich donor moiety improves/tunes the photovoltaic performance by facilitating efficient intramolecular charge transfer in the D- $\pi$ -A system. The correlation plot of  $\Delta V_{\text{MA}}$  with  $eV_{\text{OC}}$  will provide an efficient guideline for developing an effective dye designing strategy for desirable photovoltaic properties.

## Conflicts of interest

There are no conflicts to declare.

## Acknowledgements

The authors thank DST-SERB for funding through GAP1397 and also gratefully acknowledge the CSIR 4th PI for the HPC facility and NIIST IT lab for computational support. V. V. Divya thanks CSIR, India, for the senior research fellowship.

## References

- 1 J. Gong, K. Sumathy, Q. Qiao and Z. Zhou, *Renewable Sustainable Energy Rev.*, 2017, **68**, 234–246.
- 2 Y.-H. Chen, V. S. Nguyen, H.-H. Chou, Y. S. Tingare, T.-C. Wei and C.-Y. Yeh, *ACS Appl. Energy Mater.*, 2020, **3**, 5479–5486.
- 3 N. Mariotti, M. Bonomo, L. Fagiolari, N. Barbero, C. Gerbaldi, F. Bella and C. Barolo, *Green Chem.*, 2020, **22**, 7168–7218.

- 4 B. O'regan and M. Grätzel, *Nature*, 1991, **353**, 737.
- 5 M. K. Nazeeruddin, F. De Angelis, S. Fantacci, A. Selloni, G. Viscardi, P. Liska, S. Ito, B. Takeru and M. Grätzel, *J. Am. Chem. Soc.*, 2005, **127**, 16835–16847.
- 6 G. Marotta, M. A. Reddy, S. P. Singh, A. Islam, L. Han, F. De Angelis, M. Pastore and M. Chandrasekharam, *ACS Appl. Mater. Interfaces*, 2013, **5**, 9635–9647.
- 7 S. Yun, Y. Qin, A. R. Uhl, N. Vlachopoulos, M. Yin, D. Li, X. Han and A. Hagfeldt, *Energy Environ. Sci.*, 2018, **11**, 476–526.
- 8 L. L. Estrella, M. P. Balanay and D. H. Kim, *J. Phys. Chem. A*, 2018, **122**, 6328–6342.
- 9 M. Grätzel, *Nature*, 2001, **414**, 338–344.
- 10 S. Ito, S. M. Zakeeruddin, R. Humphry-Baker, P. Liska, R. Charvet, P. Comte, M. K. Nazeeruddin, P. Péchy, M. Takata and H. Miura, *Adv. Mater.*, 2006, **18**, 1202–1205.
- 11 S. Ito, H. Miura, S. Uchida, M. Takata, K. Sumioka, P. Liska, P. Comte, P. Péchy and M. Grätzel, *Chem. Commun.*, 2008, 5194–5196.
- 12 Q. Yu, Y. Wang, Z. Yi, N. Zu, J. Zhang, M. Zhang and P. Wang, *ACS Nano*, 2010, **4**, 6032–6038.
- 13 L. Han, A. Islam, H. Chen, C. Malapaka, B. Chiranjeevi, S. Zhang, X. Yang and M. Yanagida, *Energy Environ. Sci.*, 2012, **5**, 6057–6060.
- 14 L. E. Polander, A. Yella, J. Teuscher, R. Humphry-Baker, B. F. E. Curchod, N. Ashari Astani, P. Gao, J.-E. Moser, I. Tavernelli, U. Rothlisberger, M. Grätzel, M. K. Nazeeruddin and J. Frey, *Chem. Mater.*, 2013, **25**, 2642–2648.
- 15 S. Mathew, A. Yella, P. Gao, R. Humphry-Baker, B. F. Curchod, N. Ashari-Astani, I. Tavernelli, U. Rothlisberger, M. K. Nazeeruddin and M. Grätzel, *Nat. Chem.*, 2014, **6**, 242–247.
- 16 K. Kakiage, Y. Aoyama, T. Yano, T. Otsuka, T. Kyomen, M. Unno and M. Hanaya, *Chem. Commun.*, 2014, **50**, 6379–6381.
- 17 Y. S. Tingare, N. S. n. Vinh, H. H. Chou, Y. C. Liu, Y. S. Long, T. C. Wu, T. C. Wei and C. Y. Yeh, *Adv. Energy Mater.*, 2017, **7**, 1700032.
- 18 K. Sharma, V. Sharma and S. S. Sharma, *Nanoscale Res. Lett.*, 2018, **13**, 381.
- 19 X. Song, X. Yang, H. Wang, J. An, Z. Yu, X. Wang, A. Hagfeldt and L. Sun, *Sol. Energy*, 2019, **187**, 274–280.
- 20 P. Ferdowsi, Y. Saygili, F. Jazaeri, T. Edvinsson, J. Mokhtari, S. M. Zakeeruddin, Y. Liu, M. Grätzel and A. Hagfeldt, *ChemSusChem*, 2020, **13**, 212–220.
- 21 Y.-Q. Yan, Y.-Z. Zhu, P.-P. Dai, J. Han, M. Yan and J.-Y. Zheng, *New J. Chem.*, 2020, **44**, 12909–12915.
- 22 Y. Chiba, A. Islam, Y. Watanabe, R. Komiya, N. Koide and L. Han, *Jpn. J. Appl. Phys.*, 2006, **45**, L638.
- 23 F. Gao, Y. Wang, D. Shi, J. Zhang, M. Wang, X. Jing, R. Humphry-Baker, P. Wang, S. M. Zakeeruddin and M. Grätzel, *J. Am. Chem. Soc.*, 2008, **130**, 10720–10728.
- 24 S. Tan, J. Zhai, H. Fang, T. Jiu, J. Ge, Y. Li, L. Jiang and D. Zhu, *Chem. – Eur. J.*, 2005, **11**, 6272–6276.
- 25 A. Mishra, M. K. Fischer and P. Bäuerle, *Angew. Chem., Int. Ed.*, 2009, **48**, 2474–2499.
- 26 T. Mori, H. Saomoto, K. Machitani, K. Inoue, Y. Aoki, T. Koshitani, N. Koumura and T. N. Murakami, *RSC Adv.*, 2016, **6**, 13964–13970.
- 27 K. Hara, Y. Dan-oh, C. Kasada, Y. Ohga, A. Shinpo, S. Suga, K. Sayama and H. Arakawa, *Langmuir*, 2004, **20**, 4205–4210.
- 28 K. Hara, T. Sato, R. Katoh, A. Furube, T. Yoshihara, M. Murai, M. Kurashige, S. Ito, A. Shinpo and S. Suga, *Adv. Funct. Mater.*, 2005, **15**, 246–252.
- 29 R. Chen, X. Yang, H. Tian, X. Wang, A. Hagfeldt and L. Sun, *Chem. Mater.*, 2007, **19**, 4007–4015.
- 30 Z.-S. Wang, Y. Cui, Y. Dan-oh, C. Kasada, A. Shinpo and K. Hara, *J. Phys. Chem. C*, 2007, **111**, 7224–7230.
- 31 S. Hwang, J. H. Lee, C. Park, H. Lee, C. Kim, C. Park, M.-H. Lee, W. Lee, J. Park and K. Kim, *Chem. Commun.*, 2007, 4887–4889.
- 32 J. Preat, D. Jacquemin, C. Michaux and E. A. Perpète, *Chem. Phys.*, 2010, **376**, 56–68.
- 33 H. Tian, I. Bora, X. Jiang, E. Gabrielsson, K. M. Karlsson, A. Hagfeldt and L. Sun, *J. Mater. Chem.*, 2011, **21**, 12462–12472.
- 34 A. Dhar, N. Siva Kumar, M. Asif and R. L. Vekariya, *New J. Chem.*, 2018, **42**, 12024–12031.
- 35 Y. Ren, D. Sun, Y. Cao, H. N. Tsao, Y. Yuan, S. M. Zakeeruddin, P. Wang and M. Grätzel, *J. Am. Chem. Soc.*, 2018, **140**, 2405–2408.
- 36 T. Kitamura, M. Ikeda, K. Shigaki, T. Inoue, N. A. Anderson, X. Ai, T. Lian and S. Yanagida, *Chem. Mater.*, 2004, **16**, 1806–1812.
- 37 D. P. Hagberg, T. Marinado, K. M. Karlsson, K. Nonomura, P. Qin, G. Boschloo, T. Brinck, A. Hagfeldt and L. Sun, *J. Org. Chem.*, 2007, **72**, 9550–9556.
- 38 H. Tian, X. Yang, R. Chen, R. Zhang, A. Hagfeldt and L. Sun, *J. Phys. Chem. C*, 2008, **112**, 11023–11033.
- 39 J. Zhang, H.-B. Li, S.-L. Sun, Y. Geng, Y. Wu and Z.-M. Su, *J. Mater. Chem.*, 2012, **22**, 568–576.
- 40 J. Zhang, Y.-H. Kan, H.-B. Li, Y. Geng, Y. Wu and Z.-M. Su, *Dyes Pigm.*, 2012, **95**, 313–321.
- 41 Z. Yao, L. Yang, Y. Cai, C. Yan, M. Zhang, N. Cai, X. Dong and P. Wang, *J. Phys. Chem. C*, 2014, **118**, 2977–2986.
- 42 T. Horiuchi, H. Miura, K. Sumioka and S. Uchida, *J. Am. Chem. Soc.*, 2004, **126**, 12218–12219.
- 43 W. Xu, B. Peng, J. Chen, M. Liang and F. Cai, *J. Phys. Chem. C*, 2008, **112**, 874–880.
- 44 J. Preat, *J. Phys. Chem. C*, 2010, **114**, 16716–16725.
- 45 D. Patil, M. Jadhav, K. Avhad, T. H. Chowdhury, A. Islam, I. Bedja and N. Sekar, *New J. Chem.*, 2018, **42**, 11555–11564.
- 46 H.-L. Jia, Z.-J. Peng, Y.-C. Chen, C.-Y. Huang and M.-Y. Guan, *New J. Chem.*, 2018, **42**, 18702–18707.
- 47 L. Zhang, W. Shen, R. He, X. Liu, Z. Fu and M. Li, *J. Mol.*, 2014, **20**, 2489.
- 48 N. Inostroza, F. Mendizabal, R. Arratia-Pérez, C. Orellana and C. Linares-Flores, *J. Mol. Model.*, 2016, **22**, 25.
- 49 S. Gauthier, F. Robin-Le Guen, L. Wojcik, N. Le Poul, A. Planchat, Y. Pellegrin, P. G. Level, N. Szuwarski, M. Boujtita and D. Jacquemin, *Dyes Pigm.*, 2019, **171**, 107747.

- 50 V. V. Divya, F. B. Sayyed and C. H. Suresh, *ChemPhysChem*, 2019, **20**, 1752–1758.
- 51 S. R. Gadre, S. A. Kulkarni and I. H. Shrivastava, *J. Chem. Phys.*, 1992, **96**, 5253–5260.
- 52 S. R. Gadre and R. N. Shirsat, *Electrostatics of Atoms and Molecules*, Universities Press, 2000.
- 53 P. Politzer and D. G. Truhlar, *Chemical Applications of Atomic and Molecular Electrostatic potentials: Reactivity, Structure, Scattering, and Energetics of Organic, Inorganic, and Biological systems*, Springer Science & Business Media, 2013.
- 54 C. H. Suresh and N. Koga, *Inorg. Chem.*, 2002, **41**, 1573–1578.
- 55 C. H. Suresh, *Inorg. Chem.*, 2006, **45**, 4982–4986.
- 56 J. Mathew, T. Thomas and C. H. Suresh, *Inorg. Chem.*, 2007, **2007**(46), 10800–10809.
- 57 G. S. Remya and C. H. Suresh, *Phys. Chem. Chem. Phys.*, 2016, **18**, 20615–20626.
- 58 E. Scrocco and J. Tomasi, *New concepts II*, Springer, 1973, pp. 95–170.
- 59 J. S. Murray and P. Politzer, *Wiley Interdiscip. Rev.: Comput. Mol. Sci.*, 2011, **1**, 153–163.
- 60 F. B. Sayyed and C. H. Suresh, *New J. Chem.*, 2009, **33**, 2465–2471.
- 61 C. H. Suresh, P. Alexander, K. P. Vijayalakshmi, P. K. Sajith and S. R. Gadre, *Phys. Chem. Chem. Phys.*, 2008, **10**, 6492–6499.
- 62 F. B. Sayyed and C. H. Suresh, *Tetrahedron Lett.*, 2009, **50**, 7351–7354.
- 63 P. K. Sajith and C. H. Suresh, *Inorg. Chem.*, 2012, **51**, 967–977.
- 64 F. B. Sayyed and C. H. Suresh, *J. Phys. Chem. A*, 2011, **115**, 9300–9307.
- 65 V. V. Divya and C. H. Suresh, *New J. Chem.*, 2020, **44**, 7200–7209.
- 66 L. Liu, L. Miao, L. Li, F. Li, Y. Lu, Z. Shang and J. Chen, *J. Phys. Chem. Lett.*, 2018, **9**, 3573–3579.
- 67 M. R. Narayan, *Renewable Sustainable Energy Rev.*, 2012, **16**, 208–215.
- 68 L. M. Fraas and L. D. Partain, *Solar Cells and Their Applications*, John Wiley & Sons, 2010.
- 69 Y. Tachibana, K. Hara, K. Sayama and H. Arakawa, *Chem. Mater.*, 2002, **2002**(14), 2527–2535.
- 70 A. Mihi and H. Míguez, *J. Phys. Chem. B*, 2005, **109**, 15968–15976.
- 71 J. Preat, C. Michaux, D. Jacquemin and E. A. Perpète, *J. Phys. Chem. C*, 2009, **113**, 16821–16833.
- 72 R. Katoh, A. Furube, T. Yoshihara, K. Hara, G. Fujihashi, S. Takano, S. Murata, H. Arakawa and M. Tachiya, *J. Phys. Chem. B*, 2004, **108**, 4818–4822.
- 73 N. N. Ghosh, M. Habib, A. Pramanik, P. Sarkar and S. Pal, *New J. Chem.*, 2019, **43**, 6480–6491.
- 74 J. B. Asbury, Y.-Q. Wang, E. Hao, H. N. Ghosh and T. Lian, *Res. Chem. Intermed.*, 2001, **27**, 393–406.
- 75 T. Koopmans, *Physica*, 1933, **1**, 104–113.
- 76 W.-L. Ding, D.-M. Wang, Z.-Y. Geng, X.-L. Zhao and Y.-F. Yan, *J. Phys. Chem. C*, 2013, **117**, 17382–17398.
- 77 G. Boschloo and A. Hagfeldt, *Acc. Chem. Res.*, 2009, **42**, 1819–1826.
- 78 C.-R. Zhang, Z.-J. Liu, Y.-H. Chen, H.-S. Chen, Y.-Z. Wu, W. Feng and D.-B. Wang, *Curr. Appl. Phys.*, 2010, **10**, 77–83.
- 79 A. D. Becke, *J. Chem. Phys.*, 1993, **98**, 1372–1377.
- 80 T. H. Dunning Jr, *Chem. Phys.*, 1989, **90**, 1007–1023.
- 81 H. Gotfredsen, T. Neumann, F. E. Storm, A. V. Muñoz, M. Jevric, O. Hammerich, K. V. Mikkelsen, M. Freitag, G. Boschloo and M. B. Nielsen, *ChemPhotoChem*, 2018, **2**, 976–985.
- 82 M. Pastore, E. Mosconi, F. De Angelis and M. Grätzel, *J. Phys. Chem. C*, 2010, **114**, 7205–7212.
- 83 T. Yanai, D. P. Tew and N. C. Handy, *Chem. Phys. Lett.*, 2004, **393**, 51–57.
- 84 A. V. Marenich, C. J. Cramer and D. G. Truhlar, *J. Phys. Chem. B*, 2009, **113**, 6378–6396.
- 85 M. J. Frisch, G. W. Trucks, H. B. Schlegel, G. E. Scuseria, M. A. Robb, J. R. Cheeseman, G. Scalmani, V. Barone, G. A. Petersson, H. Nakatsuji, X. Li, M. Caricato, A. V. Marenich, J. Bloino, B. G. Janesko, R. Gomperts, B. Mennucci, H. P. Hratchian, J. V. Ortiz, A. F. Izmaylov, J. L. Sonnenberg, D. Williams-Young, F. Ding, F. Lipparini, F. Egidi, J. Goings, B. Peng, A. Petrone, T. Henderson, D. Ranasinghe, V. G. Zakrzewski, J. Gao, N. Rega, G. Zheng, W. Liang, M. Hada, M. Ehara, K. Toyota, R. Fukuda, J. Hasegawa, M. Ishida, T. Nakajima, Y. Honda, O. Kitao, H. Nakai, T. Vreven, K. Throssell, J. A. Montgomery Jr., J. E. Peralta, F. Ogliaro, M. J. Bearpark, J. J. Heyd, E. N. Brothers, K. N. Kudin, V. N. Staroverov, T. A. Keith, R. Kobayashi, J. Normand, K. Raghavachari, A. P. Rendell, J. C. Burant, S. S. Iyengar, J. Tomasi, M. Cossi, J. M. Millam, M. Klene, C. Adamo, R. Cammi, J. W. Ochterski, R. L. Martin, K. Morokuma, O. Farkas, J. B. Foresman and D. J. Fox, *Gaussian 16, Revision A.03*, Gaussian, Wallingford, CT, 2016.
- 86 R. Menzel, D. Ogermann, S. Kupfer, D. Wei, G. Helmar, K. Kleinermanns, L. González and R. Beckert, *Dyes Pigm.*, 2012, **94**, 512–524.
- 87 S. Kupfer, J. Guthmuller and L. Gonzalez, *J. Chem. Theory Comput.*, 2013, **9**, 543–554.
- 88 A. Kumar, S. R. Gadre, N. Mohan and C. H. Suresh, *J. Phys. Chem. A*, 2014, **118**, 526–532.
- 89 S. M. Feldt, G. Wang, G. Boschloo and A. Hagfeldt, *J. Phys. Chem. C*, 2011, **115**, 21500–21507.
- 90 W. Yang, N. Vlachopoulos, Y. Hao, A. Hagfeldt and G. Boschloo, *Phys. Chem. Chem. Phys.*, 2015, **17**, 15868–15875.



Cite this: DOI: 10.1039/d1nj00881a

# Design and DFT study of nitrogen-rich donor systems for improved photovoltaic performance in dye-sensitized solar cells†

 Velayudhan V. Divya<sup>ab</sup> and Cherumuttathu H. Suresh \*<sup>ab</sup>

Eighteen electron-rich nitrogen incorporated donors with a butadiene  $\pi$ -spacer and a cyanoacrylic acid acceptor (A) as photosensitizers (D1- $\pi$ -A to D18- $\pi$ -A) for dye-sensitized solar cell (DSSC) applications have been designed for improving the photovoltaic performance. The significance of the nitrogen centres for revamping the donating strength ( $\Delta V_{\text{MA}}$ ) of D- $\pi$ -A is scrutinized using molecular electrostatic potential (MESP) analysis at the B3LYP/cc-pVDZ level of density functional theory (DFT). During the transformation of a donor (D) to D- $\pi$ -A, a certain delocalization of electron density from D to  $\pi$ -A has occurred, and the change in the MESP minimum ( $\Delta V_{\text{MA}}$ ) observed at the cyano region of D- $\pi$ -A is related to the donating strength of D. Optical and photovoltaic properties are analyzed at the TD/CAM-B3LYP/cc-pVDZ/SMD//B3LYP/cc-pVDZ level. In D1- $\pi$ -A to D18- $\pi$ -A,  $\Delta V_{\text{MA}}$  is in the range  $-7.0$  to  $-19.0$  kcal mol<sup>-1</sup> and the increase in donating strength is found to be proportional to the number of planar nitrogens in the donors. D12- $\pi$ -A exhibited the most negative  $\Delta V_{\text{MA}}$  ( $-19.0$  kcal mol<sup>-1</sup>), indicating the highest electron-donating strength of D12, whereas the least negative  $\Delta V_{\text{MA}}$  ( $-7.0$  kcal mol<sup>-1</sup>) displayed by D7- $\pi$ -A is correlated to the weak donating character of D7. By increasing the electron-donating strength of D in D- $\pi$ -A, a red-shift in the absorption maximum ( $\Delta\lambda_{\text{max}}$ ) by 162 to 294 nm is observed. Further, the open-circuit voltage ( $eV_{\text{oc}}$ ) calculated for the D- $\pi$ -A systems showed a strong linear relationship with  $\Delta V_{\text{MA}}$ . The LUMO (lowest unoccupied molecular orbital) energy of all the D- $\pi$ -A systems ( $-1.79$  to  $-2.79$  eV) is observed above the conduction band (CB) energy of TiO<sub>2</sub> ( $-4.0$  eV), which ensured a desirable electron injection efficiency ( $\Delta G_{\text{inject}}$ ) for them. The analysis of the adsorption energy ( $E_{\text{ads}}$ ) of the D- $\pi$ -A systems on the TiO<sub>2</sub> semiconductor (D- $\pi$ -A/TiO<sub>2</sub>) showed that D12- $\pi$ -A has the highest adsorption stability. Improving the adsorption stability is better for improving  $eV_{\text{oc}}$  and the power conversion efficiency (PCE). The maximum absorption wavelength ( $\lambda_{\text{max}}$ ) of the D- $\pi$ -A/TiO<sub>2</sub> systems ranges from 513 to 703 nm and all of them display a red-shift with respect to the bare D- $\pi$ -A systems. The study suggests D12 as the most efficient photosensitizer for DSSC applications. Further, it deepens the understanding of the structure-performance relationship of D- $\pi$ -A systems as photosensitizers.

 Received 21st February 2021,  
 Accepted 22nd May 2021

DOI: 10.1039/d1nj00881a

[rsc.li/njc](http://rsc.li/njc)

## Introduction

The utilization of a renewable source of energy, preferably solar energy, for the ever-growing energy demand could diminish global climate change, which leads to sustainable livelihood on earth.<sup>1-4</sup> Since solar energy is the most abundant green energy alternative for the future energy crisis, more research efforts have to invest in the development of photovoltaic strategies

based on solar power.<sup>1,3-5</sup> Over the past three decades, the third generation photovoltaic technology employed in dye-sensitized solar cells (DSSCs) has acquired a notable position over conventional silicon-based solar cells due to the simple synthetic strategy, easier structure modification, large absorption coefficient, and low production cost.<sup>3,5-11</sup> The major components employed in a DSSC device include photosensitizers, electrolytes, and electrode materials; modifications in those components lead to the enhancement of the power conversion efficiency (PCE) of the solar cell.<sup>12</sup> Generally in DSSCs, Ru-based sensitizers have greater PCEs than organic dye sensitizers, which show a comparable PCE to silicon-based solar cells.<sup>3</sup> Whereas, the highly expensive nature and rare chance of occurrence of Ru-metal mean that its practical application in DSSCs is limited.<sup>3,13</sup>

<sup>a</sup> Chemical Sciences and Technology Division, CSIR-National Institute for Interdisciplinary Science and Technology, Thiruvananthapuram, Kerala 695 019, India. E-mail: sureshch@niist.res.in

<sup>b</sup> Academy of Scientific and Innovative Research (AcSIR), Ghaziabad 201002, India

† Electronic supplementary information (ESI) available. See DOI: 10.1039/d1nj00881a



After the invention of the DSSC device by O'Regan and Grätzel in 1991,<sup>6</sup> extensive research efforts have been invested in the synthesis and device modelling of metal-free organic sensitizers, which leads to the improvement of the PCE.<sup>13–21</sup> Usually, organic sensitizers comprise a D- $\pi$ -A framework where D,  $\pi$ , and A denote the donor,  $\pi$ -spacer and acceptor, respectively. So far large varieties of structural modifications in the D- $\pi$ -A structural framework have been performed, reveal that tuning the donating strength of the donor could significantly influence the absorption range and photovoltaic parameters.<sup>12,22–29</sup> In our previous study, we quantified the electron-donating strength of eight typically used donor systems, *viz* pyrene, perylene, chrysene, triphenylamine, carbazole, phenothiazine, julolidine, *N,N*-dialkylaniline, ullazine and coumarin, in the D- $\pi$ -A system and revealed that julolidine and *N,N*-dialkylaniline based  $\pi$ -A systems are the most efficient sensitizers for DSSCs.<sup>22</sup> For improved optical and photovoltaic properties of D- $\pi$ -A systems the particular analysis recommends the incorporation of electron-rich heteroatoms (preferably nitrogen) in donors. The literature shows that non-planar donors, especially triphenylamine, carbazole and indoline, reduce the electron transfer ability and overall conjugation in the donor group with the  $\pi$ -A system leading to lower light-harvesting efficiency of the dye sensitizer.<sup>30,31</sup> The mentioned reducing factors are rectified through the introduction of planarized nitrogen incorporated donors *viz.* ullazine and indolizine as photosensitizers.<sup>30–33</sup> Further, the rational design of photosensitizers with nitrogen annulation at the bay region of a polycyclic aromatic hydrocarbon (PAH) system provides a remarkable PCE in DSSCs.<sup>34</sup> For example, perylene based PAH systems as donors in DSSCs have disappointing PCEs,<sup>35–37</sup> whereas an N-annulated perylene (NP) core as a donor with phenyl functional groups results in an improved PCE of about 10.5%.<sup>38</sup> Later, Wang *et al.* modified the NP core with bulky substituents to obtain PCEs up to 10.4%.<sup>39</sup> This re-engineered chromophore was again modified with an N-annulated indenoperylene unit as the donor and reached a PCE of 12.5%.<sup>40</sup> The aforementioned studies reveal that structural modifications with N-annulation in PAH systems enhance the intramolecular charge transfer (ICT) due to the planar structure. Also, the multiple substitution sites involved in PAHs increase the possibility of molecular engineering. Recently Subramanian *et al.* described that a more N-doped polyaromatic hydrocarbon analogue of ullazine contributes a large dipole moment and more planarization to the dye-sensitizers, thus resulting in higher light-harvesting efficiency (LHE) than the donors with a single N-doping site.<sup>25</sup>

In this context, the most significant approach for an efficient photosensitizer is the engineering of electron-rich planar donors. Correspondingly, it is worthwhile to evaluate the role of nitrogen centres in donors for enhancing the donating strength. To tackle the failings of the electron transfer ability and overall conjugation in the donor group with the  $\pi$ -A system, we designed eighteen electron-rich nitrogen incorporated donors (D1–D18) as dye sensitizers for DSSC application (Fig. 1). For the  $\pi$ -A framework, butadiene and cyanoacrylic acid have been considered. In our previous study,<sup>41</sup> we proved

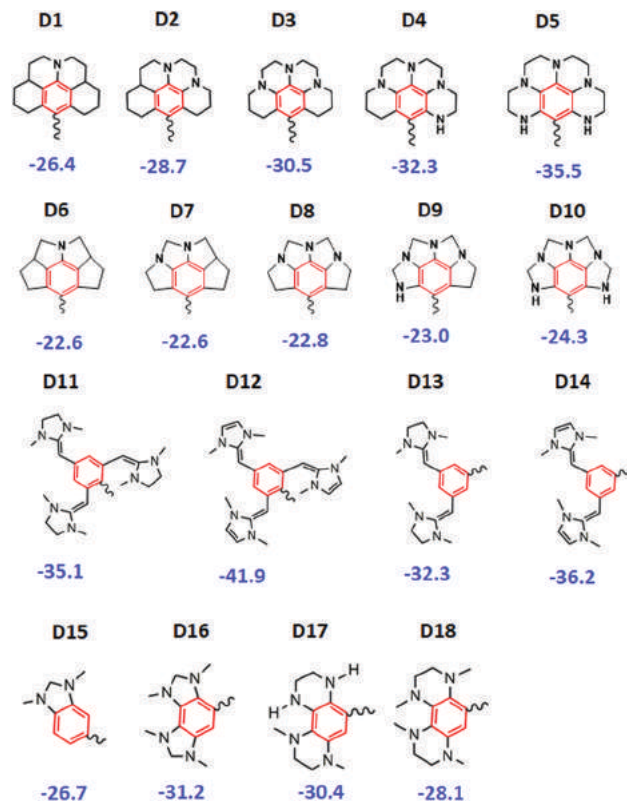


Fig. 1 Designed donor systems. The MESP minimum over the phenyl ring ( $V_{md}$ ) is given in kcal mol<sup>-1</sup>.

that butadiene exhibits better electronic effect transmitting power than thiophene, furan and benzylic spacers. Hence, for better electronic charge transfer from D to A, a butadiene  $\pi$ -spacer and cyanoacrylic acid as an acceptor have been considered.

In the analysis, the D1–D5 donors are designed from known donor julolidine (Fig. S1a, ESI<sup>†</sup>), where the possibility of N-annulation in the julolidine core has been attempted (D1 to D5) to enhance the electron-donating strength of the designed systems compared to julolidine (the calculated electron-donating strength,  $\Delta V_{MA}$ , of julolidine by MESP analysis is  $-9.2$  kcal mol<sup>-1</sup><sup>22</sup>). Julolidine is an N-heterocyclic aromatic compound which comprises alkyl bridges between amino nitrogen and ring *ortho* carbon atoms.<sup>42,43</sup> Because of the high efficiency in energy conversion and fluorescent properties, julolidine derivatives have been used in the construction of dye-sensitized solar cells and photoconductive materials, as fluorescent sensors for bio-imaging, *etc.*<sup>44</sup> The conjugation of the aromatic part of the molecule with its amino substituent is an indicator of the ability of the nitrogen atom to possess  $sp^2$ -hybridization, which enhances the donating strength of this class of compounds.<sup>45</sup> In D6–D10, five-membered rings at the aromatic ring system have been considered for N-annulation; those systems are derived from 1,2,4,5-tetrahydropyrrolo[3,2,1-hi]indole (Fig. S1b, ESI<sup>†</sup>).<sup>43</sup> Among the designed N-heterocyclic systems (D1–D10), some of the derivatives are known and they are the best candidates for intramolecular cyclization and for generating diboryne nanowires.<sup>46,47</sup> Donors D11–D14 are

designed from the electron-rich nature of the phenyl/ $\pi$ -system. According to various experimental and theoretical studies, the electron-rich nature of the phenyl/ $\pi$ -system could be fine-tuned by electron-donating substituents and hence the aromatic ring of 1,3,5-*N,N*-dimethyltriaminobenzene could be considered as the most electron-rich neutral six-membered ring.<sup>48</sup> Previously, Suresh and Sayyed described that the electron density at the phenyl ring could be significantly improved by the treatment of *N*-heterocyclic ring substitution and they proposed two highly electron rich systems *viz.* D11 and D12 as shown in Fig. 1.<sup>48</sup> Since those systems are considered as electron rich (involving six nitrogen lone pairs), we could test the suitability of those systems as photosensitizers for DSSC application. Finally, two, and four nitrogens have been integrated in D15–D18, where the likelihood of *N*-annulation has been attained through *N*-heterocyclic five and six membered rings.<sup>49,50</sup>

For evaluating the donating strength of the donors in *D*– $\pi$ –*A*, the intramolecular charge transfer (ICT) from *D* to *A* has to be assessed. Here it has been quantified in terms of the change in the molecular electrostatic potential (MESP) minimum,  $\Delta V_m$ , at the cyano group of *A*. Very recently we proved that the MESP is an excellent tool to quantify the electron-donating strength ( $\Delta V_m$ ) of *D*– $\pi$ –*A* systems.<sup>22,26</sup> It is a real physical property which is experimentally observable from X-ray diffraction studies. To understand the reactivity of molecular systems, theoretically derived MESP have been extensively used in the work of Tomasi,<sup>51</sup> Pullman,<sup>52,53</sup> Politzer<sup>54–57</sup> and Gadre,<sup>58–60</sup> and the wide range of applications in chemical and biological phenomena shows the acceptability of this area of research. Further, our group has contributed to several applications of the MESP parameter in organic and inorganic chemistry and described that the MESP is an excellent tool for the prediction of structure–property relationships.<sup>61–71</sup> In the present study the significance of *N*-annulation for improved optical and photovoltaic properties has been evaluated using density functional theory (DFT) and time-dependent DFT (TDDFT) calculations. Currently, quantum chemical calculations have emerged as an elementary tactic to identify potential sensitizers before long-running expensive synthesis.<sup>72–78</sup> Thus our computationally engineered dye sensitizers could open up new synthetic strategies for the development of photosensitizers for DSSC application.

## Computational details

Density functional theory (DFT) calculations at the B3LYP/cc-pVDZ level have been conducted for the optimization of the ground state geometries of the *D*– $\pi$ –*A* systems.<sup>79,80</sup> It is substantiated that the B3LYP level is adequate for the explanation of the electronic structure of dye molecules in DSSC applications.<sup>26,81,82</sup> The ground state geometries of all *D*– $\pi$ –*A* systems after binding to the (TiO<sub>2</sub>)<sub>9</sub> cluster are optimized at the same level of DFT with the LANL2DZ basis set for the Ti atom and cc-pVDZ for non-metal atoms.<sup>83</sup> Vibrational frequencies are calculated at the same level and it is confirmed that there are no imaginary frequencies. Studies show that the (TiO<sub>2</sub>)<sub>9</sub>

cluster size is sufficient to model the dye–TiO<sub>2</sub> interfaces for simulating the electronic structure, optical properties, and binding modes of TiO<sub>2</sub>.<sup>84</sup> Frontier molecular orbital energies of all *D*– $\pi$ –*A* and *D*– $\pi$ –*A* adsorbed on (TiO<sub>2</sub>)<sub>9</sub> cluster systems (*D*– $\pi$ –*A*/TiO<sub>2</sub>) are reported for the ground-state geometries. The optical properties of the *D*– $\pi$ –*A* systems before and after binding to the (TiO<sub>2</sub>)<sub>9</sub> cluster are simulated using time-dependent DFT (TD DFT) at the CAM-B3LYP level<sup>85</sup> on the ground state geometry with mixed basis sets. To account for the solvent effect (dichloromethane as the solvent), SCRF-SMD (self-consistent reaction field-density simulation model) incorporated in the Gaussian 16 suite of programs has been considered. The CAM-B3LYP exchange–correlation functional is widely used in theoretical calculations for the excited state properties and provides results that are close to experimental results.<sup>86–88</sup> In our previous study, the absorption properties of experimentally known dye sensitizers have been benchmarked including julolidine based dye-sensitizers and it is found that the TD-CAM B3LYP/cc-pVDZ/SMD//B3LYP/cc-pVDZ level is adequate to describe the electronic, optical and photovoltaic properties.<sup>22</sup> The higher excitation energy associated with the CAM-B3LYP exchange functional than the B3LYP functional can be attributed to the higher bond length alteration index (BLA) of *D*– $\pi$ –*A* systems.<sup>26</sup> Moreover, for the examination of the intramolecular charge transfer characteristics of *D*– $\pi$ –*A* systems, molecular electrostatic potential based topographical analysis has been performed on the ground state geometry at the B3LYP/cc-pVDZ level. All the calculations are performed with the Gaussian 16 program package.<sup>89</sup>

The molecular electrostatic potential (MESP),  $V(\mathbf{r})$ , is an important property of a molecule that its nuclei and electrons create at every point  $\mathbf{r}$  in the surrounding space, which is defined in eqn (1) as

$$V(\mathbf{r}) = \sum_A^N \frac{Z_A}{|\mathbf{r} - \mathbf{R}_A|} - \int \frac{\rho(\mathbf{r}')d\mathbf{r}'}{|\mathbf{r} - \mathbf{r}'|} \quad (1)$$

where  $N$  is the total number of nuclei,  $Z_A$  is the charge on nucleus  $A$  located at distance  $R_A$ ,  $\rho(\mathbf{r}')$  is the electron density of the molecule, and  $\mathbf{r}'$  is a dummy integration variable. In the equation, the sign of  $V(\mathbf{r})$  at any  $\mathbf{r}$  depends upon whether the positive contribution of the nuclei or the negative one of the electrons is dominant there.

## Results and discussion

### MESP analysis of the donors

The MESP minimum  $V_m$  gives a clear idea regarding the most electron-rich region in a molecular system. In all the donor systems (D1–D18), an aromatic phenyl ring (shown in a red colour, Fig. 1) has been observed and  $V_m$  observed at that phenyl ring,  $V_{mD}$ , has been considered as the donor strength of each system. The most negative  $V_m$  depicts the most electron-rich nature of the molecular system. From D1 to D5, a systematic increase in the *N*-centers (up to 5 nitrogens) is introduced and  $V_{mD}$  reached  $-35.5$  kcal mol<sup>-1</sup> from  $-26.4$  kcal mol<sup>-1</sup>. The more

negative  $V_{\text{mD}}$  in D5 ( $-35.5 \text{ kcal mol}^{-1}$ ) than those of D1–D4 characterizes the more electron-rich nature, which can be attributed to the occurrence of five nitrogen centers. In the D6–D10 donors, an increase in the negative character of  $V_{\text{mD}}$  (from  $-22.6$  to  $-24.3 \text{ kcal mol}^{-1}$ ) has been attained by a systematic increase of the nitrogen atoms (up to 5 nitrogens). Meanwhile, due to the presence of more pyramidalized nitrogens, the D6–D10 donors provide less negative  $V_{\text{mD}}$  than those of D1–D5.

In the D11–D12 donors, imidazolidine and imidazole ring systems have been introduced at the 1, 3, and 5 positions of the benzene ring. In D11, the electron-rich aminal functional groups increase the electron density over the phenyl ring, resulting in a comparable  $V_{\text{mD}}$  of  $-35.1 \text{ kcal mol}^{-1}$  to D5 ( $-35.5 \text{ kcal mol}^{-1}$ ). In D12 the conjugation in the CC bond enhances the electron density over the phenyl ring, leading to a more negative  $V_{\text{mD}}$  ( $-41.9 \text{ kcal mol}^{-1}$ ) than D11. Due to the reduced number of aminal functional groups at the phenyl ring, D13 shows a less negative  $V_{\text{mD}}$  ( $-32.3 \text{ kcal mol}^{-1}$ ) than those of D11 and D12. In D14, conjugation increases the electron density of the donor system, resulting in a more negative  $V_{\text{mD}}$  ( $-36.2 \text{ kcal mol}^{-1}$ ) than D13. It is noted that the imidazolidine and imidazole substituted donor systems *viz.* D12 and D14 exhibit more negative  $V_{\text{mD}}$  than D5, which can be considered as their better donor strength. Finally, for verifying the effectiveness of the introduced strategy, the D15–D18 donors are examined. In D16 the increased number of *N*-alkyl substitutions at the phenyl ring resulted in a more negative  $V_{\text{mD}}$  ( $-31.2 \text{ kcal mol}^{-1}$ ) than D15 ( $V_{\text{mD}} = -26.7 \text{ kcal mol}^{-1}$ ). Compared to D15, a more negative  $V_{\text{mD}}$  is observed for D17, which can be attributed to the presence of an additional two nitrogen centres. Finally, in D18 the additional two methyl groups at nitrogen atoms promote pyramidalization of the N-centres, resulting in a less negative  $V_{\text{mD}}$  ( $-28.1 \text{ kcal mol}^{-1}$ ) than D17.

### Donating strength of the D- $\pi$ -A systems

The influence of the electron-rich nitrogen lone pairs in the donors (D) for enhancing the electron-donating strength of the D- $\pi$ -A system ( $\Delta V_{\text{mA}}$ ) has been elucidated with MESP analysis. In D- $\pi$ -A systems, the  $\pi$ -A linkage with the donor involves intramolecular charge transfer (ICT) from D to A, and the transferred electron density accumulated at A depends on the donor strength of each system.<sup>22,26</sup> The electron density distribution *via* ICT at various regions of a representative D- $\pi$ -A system (D1- $\pi$ -A), *viz.* D, the  $\pi$ -spacer and A, has been shown in Fig. 2b as the MESP minima at the donor  $V_{\text{mD}'}$ , spacer  $V_{\text{mS}'}$  and acceptor  $V_{\text{mA}'}$ . Since the  $\pi$ -A part (butadiene) involved in the study is the same for all D- $\pi$ -A systems, the MESP minimum observed at the CN group of A has been considered as the reference  $V_{\text{mA}}$  to evaluate the changes observed at that minimum with the attachment of D (Fig. 2a). Also, it is proved that one could take other  $V_{\text{m}}$  regions at A as the reference  $V_{\text{m}}$  *viz.*  $V_{\text{m(OH)}}$  and  $V_{\text{m(CO)}}$  for monitoring the changes at the respective sites due to the parallel behavior exhibited by those parameters.<sup>26</sup> In the study,  $V_{\text{mA}'}$  (observed at the CN region) has been selected as the reference point due to the most negative  $V_{\text{m}}$  character.

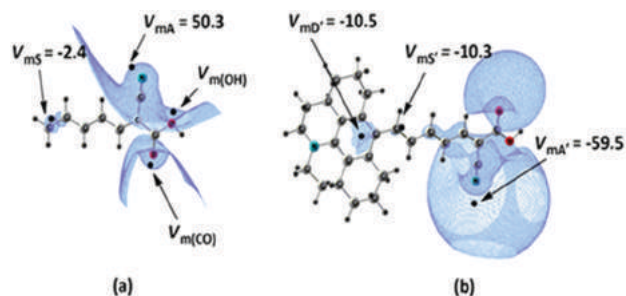


Fig. 2 (a) MESP isosurface at various sites of (a) the reference system, and (b) a representative D- $\pi$ -A system, where the MESP minimum is shown in  $\text{kcal mol}^{-1}$ .

Table 1  $V_{\text{m}}$  ( $\text{kcal mol}^{-1}$ ) of the D- $\pi$ -A systems calculated at the B3LYP/cc-pVDZ level

Systems	$V_{\text{mD}}$	$V_{\text{mD}'}$	$\Delta V_{\text{mD}}$	$V_{\text{mS}'}$	$V_{\text{mS}}$	$\Delta V_{\text{mS}}$	$V_{\text{mA}'}$	$V_{\text{mA}}$	$\Delta V_{\text{mA}}$
D1	-26.4	-10.5	15.9	-10.3	-2.4	-7.9	-59.5	-50.3	-9.2
D2	-28.7	-13.0	15.7	-11.7	-2.4	-9.3	-60.3	-50.3	-10.0
D3	-30.5	-14.1	16.4	-12.3	-2.4	-9.9	-60.8	-50.3	-10.5
D4	-32.3	-14.9	17.4	-13.2	-2.4	-10.9	-61.3	-50.3	-11.0
D5	-35.5	-17.6	17.9	-18.6	-2.4	-16.3	-63.8	-50.3	-13.5
D6	-22.6	-9.0	13.6	-9.3	-2.4	-7.0	-58.2	-50.3	-7.8
D7	-22.6	-9.7	12.9	-8.8	-2.4	-6.4	-57.4	-50.3	-7.0
D8	-22.8	-10.6	12.2	-8.3	-2.4	-6.0	-56.2	-50.3	-5.9
D9	-23.0	-10.5	12.5	-9.5	-2.4	-7.1	-57.9	-50.3	-7.5
D10	-24.3	-12.0	12.4	-10.4	-2.4	-8.0	-58.7	-50.3	-8.4
D11	-35.1	-22.8	12.3	-18.4	-2.4	-16.1	-64.0	-50.3	-13.7
D12	-41.9	-28.7	13.2	-18.4	-2.4	-16.1	-69.3	-50.3	-19.0
D13	-32.3	-20.7	11.6	-11.1	-2.4	-8.7	-58.2	-50.3	-7.9
D14	-36.2	-24.1	12.1	-14.6	-2.4	-12.2	-60.0	-50.3	-9.7
D15	-26.7	-11.6	15.1	-10.4	-2.4	-8.0	-58.5	-50.3	-8.2
D16	-31.2	-13.9	17.3	-13.1	-2.4	-10.7	-62.0	-50.3	-11.7
D17	-30.4	-16.2	14.2	-11.6	-2.4	-9.2	-58.9	-50.3	-8.5
D18	-28.1	-13.5	14.6	-9.9	-2.4	-7.5	-58.4	-50.3	-8.1

In Table 1,  $V_{\text{m}}$  values at D, the  $\pi$ -spacer and A of the D- $\pi$ -A systems are reported along with the change in  $V_{\text{m}}$  at those regions with the attachment of  $\pi$ -A to D. The change in  $V_{\text{m}}$  occurring at the D site ( $\Delta V_{\text{mD}}$ ) has been calculated by subtracting  $V_{\text{m}}$  observed at the donor ( $V_{\text{mD}}$ ) from the corresponding  $V_{\text{m}}$  observed at D of D- $\pi$ -A ( $V_{\text{mD}'}$ ). Likewise,  $\Delta V_{\text{mS}}$  and  $\Delta V_{\text{mA}}$  have been calculated by subtracting  $V_{\text{m}}$  observed at the respective sites of the reference system ( $V_{\text{mS}}$  and  $V_{\text{mA}}$ ) from the corresponding values of the D- $\pi$ -A systems ( $V_{\text{mS}'}$  and  $V_{\text{mA}'}$ ). In the table  $\Delta V_{\text{mD}}$  ranges from 12.2 to 17.9  $\text{kcal mol}^{-1}$ ; the positive  $\Delta V_{\text{mD}}$  value shows electron deficiency at D.

In all, the less negative  $V_{\text{m}}$  observed at the D site of D- $\pi$ -A ( $V_{\text{mD}'}$ ) than  $V_{\text{m}}$  of the donor ( $V_{\text{mD}}$ ) confirms the ICT from D to A. Further, the ICT from D to A enhances the electron density at the spacer; the gained electron density at the spacer has been denoted as negative  $\Delta V_{\text{mS}}$ , which ranges from  $-6.0$  to  $-16.3 \text{ kcal mol}^{-1}$ . As per  $\Delta V_{\text{mS}}$ , the highest electron-donating strength has been attained by the D5- $\pi$ -A system while the least is possessed by the D8- $\pi$ -A system.  $V_{\text{mA}'}$  ranges from  $-7.0$  to  $-13.5 \text{ kcal mol}^{-1}$ . The donors having greater electron-donating strength exhibit a more negative  $V_{\text{mA}'}$ . As a result, the change in the MESP appearing on the acceptor ( $\Delta V_{\text{mA}}$ ) with the

attachment of D to  $\pi$ -A has been regarded as the donating strength of the D- $\pi$ -A system.<sup>22</sup>

In the D1-D5 based  $\pi$ -A systems, the least negative  $\Delta V_{\text{mA}}$  ( $-9.2 \text{ kcal mol}^{-1}$ ) has been attained by the one nitrogen system D1- $\pi$ -A, which shows its poor electron-donating strength. Also, from D1- $\pi$ -A to D5- $\pi$ -A, a systematic enhancement in the donating strength has been observed for an increased number of nitrogen centres ( $n = 1-5$ ) and the most negative  $\Delta V_{\text{mA}}$  ( $-13.5 \text{ kcal mol}^{-1}$ ) has been shown by D5- $\pi$ -A (incorporating 5 nitrogen lone pairs). In D6 to D10- $\pi$ -A the more pyramidalized nitrogen centres in the donors impart less negative  $\Delta V_{\text{mA}}$  in the range  $-5.9$  to  $-8.4 \text{ kcal mol}^{-1}$  than the D1- $\pi$ -A-D5- $\pi$ -A systems. In D11- $\pi$ -A, the incorporation of six nitrogen lone pairs through imidazolidine rings at the phenyl ring enhances the electron density at the donor site, resulting in a  $\Delta V_{\text{mA}}$  of  $-13.7 \text{ kcal mol}^{-1}$ . Whereas, in D12- $\pi$ -A, the conjugation in the CC bond (imidazole ring) enhances the electron density at the donor more than in D11- $\pi$ -A, which leads to a more negative  $\Delta V_{\text{mA}}$  of  $-19.0 \text{ kcal mol}^{-1}$ . In the D13- $\pi$ -A and D14- $\pi$ -A systems, a relatively lower donating strength is observed in terms of  $\Delta V_{\text{mA}}$  ( $-7.9 \text{ kcal mol}^{-1}$  and  $-9.7 \text{ kcal mol}^{-1}$ ) than that of the D11 and D12- $\pi$ -A systems. This can be attributed to their reduced number of nitrogen centres (4 nitrogens). Since the nitrogens involved in the D1 to D4- $\pi$ -A systems are more planarized than those of D13 and D14- $\pi$ -A, the former systems show greater electron-donating strength. The integration of four nitrogens at the donor enhances the donating strength of the D16- $\pi$ -A system ( $-11.7 \text{ kcal mol}^{-1}$ ) over D15- $\pi$ -A ( $-8.2 \text{ kcal mol}^{-1}$ ). Further, the nearly planar nitrogens involved in D16- $\pi$ -A provide a similar donating strength  $-11.0 \text{ kcal mol}^{-1}$  to D4- $\pi$ -A ( $-11.7 \text{ kcal mol}^{-1}$ ). D17- $\pi$ -A with four nitrogen atoms incorporated through two fused six-membered rings at the phenyl ring attains a less negative  $\Delta V_{\text{mA}}$  ( $-8.5 \text{ kcal mol}^{-1}$ ) than D16- $\pi$ -A.

The additional two methyl groups in D18- $\pi$ -A at the nitrogen atoms are pyramidalized and lead to a less negative  $\Delta V_{\text{mA}}$  ( $8.1 \text{ kcal mol}^{-1}$ ) than D17. Finally, from the elucidated examples it is clear that donors having more planarized nitrogen centres enhance the donating strength of the D- $\pi$ -A systems. Among all, the D12, D11 and D5 based  $\pi$ -A systems are the best candidates for DSSC application.

### Absorption spectra

In Table 2, the optical properties of the donor and D- $\pi$ -A systems are given. Since we have used the same  $-\pi$ - and A units in all the designed D- $\pi$ -A systems, the influence of  $\pi$ -A on the absorption maximum ( $\lambda_{\text{max}}$ ) can be considered the same for all donors, and the shift in the absorption maximum ( $\Delta\lambda_{\text{max}}$ ) occurring during the transformation of D to D- $\pi$ -A can be recognized as due to the influence of the donating strength of the donor units.  $\Delta\lambda_{\text{max}}$  is calculated by subtracting  $\lambda_{\text{max}}$  of D from the analogous D- $\pi$ -A system. For the analysis the HOMO  $\rightarrow$  LUMO transition has been considered. The influence of the donor strength ( $V_{\text{mD}}$ ) on the  $\lambda_{\text{max}}$  of donors is observed in the range 280 to 329 nm. In Table 2, when a donor changes to D- $\pi$ -A, the absorption shifts to higher wavelengths in the range 454 to 619 nm. According to our previous study,  $\Delta\lambda_{\text{max}}$  in the range of 162 to 294 nm can be recognized as due to the influence of the donating strength ( $\Delta V_{\text{mA}}$ ) of the D- $\pi$ -A systems.<sup>22</sup> The significant correlation observed between  $\Delta V_{\text{mA}}$  and  $\Delta\lambda_{\text{max}}$  with a correlation coefficient of 0.940 confirms the significance of  $\Delta V_{\text{mA}}$  to  $\Delta\lambda_{\text{max}}$  (Fig. 3, deviations are neglected for the  $R$  calculation). It shows that  $\Delta\lambda_{\text{max}}$  increases with enhanced donating strength of the D- $\pi$ -A systems. In the table, the D1-D5 based  $\pi$ -A systems display a systematic increase in  $\Delta\lambda_{\text{max}}$  (from 203 to 257 nm) which can be recognized as due to the enhanced donating strength of those systems with an

**Table 2** Maximum absorption wavelength  $\lambda_{\text{max}}$  (nm), oscillator strength  $f$ , MO contribution, percentage of MO contribution (MO%), and shift in absorption maximum  $\Delta\lambda_{\text{max}}$  (nm) of the donor and D- $\pi$ -A systems at the TD-CAM-B3LYP/cc-pVDZ/SMD//B3LYP/cc-pVDZ level

Systems	Donor				D- $\pi$ -A system			
	$\lambda_{\text{max}}$ (nm)	$f$	MO contribution	$\lambda_{\text{max}}$ (nm)	$f$	MO contribution	MO (%)	$\Delta\lambda_{\text{max}}$ (nm)
D1	272	0.08	H $\rightarrow$ L	476	1.77	H $\rightarrow$ L	92	203
D2	286	0.11	H $\rightarrow$ L	513	1.53	H $\rightarrow$ L	92	227
D3	280	0.02	H $\rightarrow$ L	520	1.54	H $\rightarrow$ L	92	240
D4	285	0.03	H $\rightarrow$ L	542	1.31	H $\rightarrow$ L	89	257
D5	285	0.04	H $\rightarrow$ L	527	1.58	H $\rightarrow$ L	91	241
D6	285	0.04	H $\rightarrow$ L	471	1.74	H $\rightarrow$ L	94	187
D7	301	0.05	H $\rightarrow$ L	481	1.42	H $\rightarrow$ L	92	180
D8	304	0.03	H $\rightarrow$ L	475	1.46	H $\rightarrow$ L	91	171
D9	329	0.06	H $\rightarrow$ L	531	0.97	H $\rightarrow$ L	92	202
D10	341	0.07	H $\rightarrow$ L	522	0.04	H $\rightarrow$ L	87	181
D11	304	0.11	H $\rightarrow$ L	549	1.30	H $\rightarrow$ L	88	245
D12	325	0.60	H $\rightarrow$ L	619	0.27	H $\rightarrow$ L	79	294
				600	1.41	H-1 $\rightarrow$ L	49	275
D13	292	1.17	H $\rightarrow$ L	454	0.03	H $\rightarrow$ L	91	162
				423	1.19	H-1 $\rightarrow$ L	68	131
D14	324	1.14	H $\rightarrow$ L	583	0.03	H $\rightarrow$ L	93	259
				512	0.14	H-1 $\rightarrow$ L	93	188
D15	272	0.18	H $\rightarrow$ L	481	1.62	H $\rightarrow$ L	92	209
D16	282	0.06	H $\rightarrow$ L	509	0.99	H $\rightarrow$ L	93	227
D17	282	0.09	H $\rightarrow$ L	500	0.83	H $\rightarrow$ L	92	218
D18	288	0.07	H $\rightarrow$ L	487	0.97	H $\rightarrow$ L	90	199



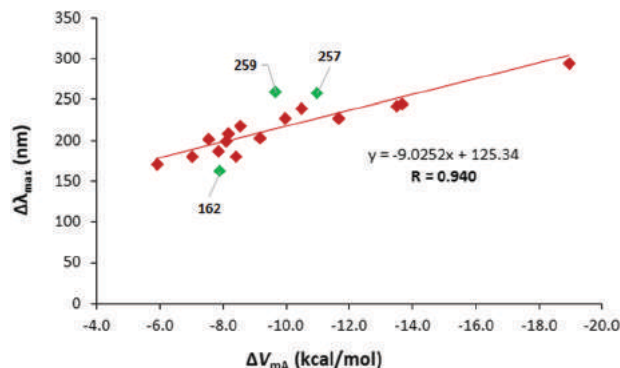


Fig. 3 Correlation between  $\Delta V_{MA}$  and  $\Delta\lambda_{max}$  of the D- $\pi$ -A systems (the  $R$  value has been calculated by excluding the deviations shown in a green colour).

increased number of nitrogen centres ( $n = 1-5$ ). Among those systems, the D4 based  $\pi$ -A system shows greater  $\Delta\lambda_{max}$  than D5- $\pi$ -A, which displays a slight deviation in the correlation (marked in a green colour, Fig. 3). The lower  $\Delta\lambda_{max}$  values exhibited by the D6- $\pi$ -A to D10- $\pi$ -A systems in the range of 171–202 nm are recognized as due to the lower donating strength of those systems. Compared to the D6- $\pi$ -A to D10- $\pi$ -A systems, the greater  $\Delta\lambda_{max}$  in D11- $\pi$ -A (245 nm) can be recognized as due to its larger donating strength. The presence of conjugation in CC bonds enhances the donating strength of D12- $\pi$ -A, resulting in the highest  $\Delta\lambda_{max}$  of 294 nm. The highest  $\Delta\lambda_{max}$  (294 nm) can be attributed to the utmost  $\Delta V_{MA}$  and  $\lambda_{max}$  of D12- $\pi$ -A (619 nm). In the D13- $\pi$ -A and D14- $\pi$ -A systems,  $\Delta\lambda_{max}$  values of 162 and 259 nm are observed with a  $\lambda_{max}$  of 454 and 583 nm, respectively. In those systems a slight deviation in the correlation has been observed, which may be due to the poor oscillator strength ( $f \rightarrow 0.03$ ). The higher  $\Delta\lambda_{max}$  of 227 nm in D16- $\pi$ -A than D15- $\pi$ -A (209 nm) can be spotted as due to the better electron-donating strength (because of the increased number of nitrogens (four)) of D16- $\pi$ -A. In D17- $\pi$ -A,  $\lambda_{max}$  and  $\Delta\lambda_{max}$  are 500 nm and 218 nm, respectively. Even though there is an equal number of nitrogens (four) in the donor site, the higher  $\Delta\lambda_{max}$  in D17- $\pi$ -A than D18- $\pi$ -A (199 nm) can be recognized as due to the influence of more planar NH centres.

Finally, for the dye sensitizers, the HOMO (highest occupied molecular orbital) and LUMO (lowest unoccupied molecular orbital) energies are crucial for determining the efficiency of the sensitizers (Table 5). For the effective regeneration of the oxidized dye, it is important to have a HOMO energy ( $e_h$ ) lower than the redox potential of the  $\Gamma^-/I_3^-$  electrolyte ( $-4.8$  eV). The  $e_h$  values of the D3–D5, D11–D14, and D16 based  $\pi$ -A systems are in the range of  $-4.68$  to  $-4.74$  eV, lying above the redox potential of the  $\Gamma^-/I_3^-$  electrolyte. It is therefore suggesting that the oxidized dye might not efficiently regenerate in those systems from the  $\Gamma^-/I_3^-$  electrolyte. Whereas, for the rest of the D- $\pi$ -A systems,  $e_h$  ( $-4.82$  to  $-5.29$  eV) lying below the redox potential of the electrolyte facilitates effective dye regeneration. For the D1- $\pi$ -A to D18- $\pi$ -A systems, the LUMO energies ( $e_l$ ) are in the range of  $-1.79$  to  $-2.79$  eV, lying above the conduction band (CB) energy of the  $TiO_2$  semiconductor ( $-4.0$  eV), which

ensures effective electron injection into the  $TiO_2$  conduction band. The HOMO–LUMO gap (HLG) energy of the designed D- $\pi$ -A systems ranges from 1.64 to 2.65 eV and it shows a decreasing trend with increasing electron donating strength. In DSSCs, HLG values give a clear idea regarding the PCE of the dye-sensitizer. As per various theoretical studies, a lower HLG ensures better optical and photovoltaic properties, thereby improving the PCE of DSSC devices.<sup>90–92</sup> Herein, we could recognize that the lower HLG energy obtained with D12- $\pi$ -A (2.17 eV) is accompanied by the highest absorption maximum (619 nm), good adsorption stability ( $-28.6$  kcal mol<sup>-1</sup>), and highest  $eV_{oc}$  (2.21 eV). Consequently, among all, the D12- $\pi$ -A system having the lowest LUMO energy ( $-1.79$  eV) may provide a better PCE in DSSC devices.

According to the basic principle of DSSCs, when the dye molecule gets adsorbed on the  $TiO_2$  semiconductor, the interaction between the dye and semiconductor can shift their energy levels and prompt electron injection into the semiconductor, which is desirable for a better PCE.<sup>73</sup> To determine the energy levels of the adsorbed D- $\pi$ -A systems on  $TiO_2$ , we have designed a bidentate bridging mode for binding the D- $\pi$ -A systems on  $TiO_2$  (Fig. 4a). It has been reported that the bidentate bridging mode is the most stable adsorption mode for anchoring groups.<sup>93,94</sup> Further, the LUMO energy levels ( $-3.50$  to  $-3.79$  eV) of the adsorbed D- $\pi$ -A systems are deeper than the bare D- $\pi$ -A systems ( $-1.79$  to  $-2.79$  eV) and ensure that the LUMO is above the CB energy of  $TiO_2$ , which could promote efficient electron injection from the excited dye molecule into the CB of  $TiO_2$ . The absorption properties of the D1- $\pi$ -A to D18- $\pi$ -A systems adsorbed on  $TiO_2$  are reported in Table 3. We denote D- $\pi$ -A adsorbed on  $TiO_2$  as D- $\pi$ -A/ $TiO_2$ . The observed  $\lambda_{max}$  in the range 513 to 703 nm is favourable for an improved PCE, and shows a red shift with respect to the pure D- $\pi$ -A system. Among all, D12- $\pi$ -A/ $TiO_2$  shows the highest  $\lambda_{max}$  (703 nm), whereas D13- $\pi$ -A/ $TiO_2$  displays the lowest  $\lambda_{max}$  (513 nm). The HLG of the D- $\pi$ -A/ $TiO_2$  systems ranges from 0.61 to 1.89 eV, indicating that the adsorption of the dye with the semiconductor significantly reduces the HLG related to the bare D- $\pi$ -A systems. The electron density shifts in the D- $\pi$ -A/ $TiO_2$  systems between the HOMO and LUMO are given in the representative example (D12- $\pi$ -A/ $TiO_2$ ) shown in Fig. 4b. In all the D- $\pi$ -A/ $TiO_2$  systems, the HOMO is localized on the donor region whereas the LUMO is distributed on  $TiO_2$ . This kind of charge delocalization is anticipated for a better PCE of dye sensitizers.

Quantitatively, the adsorption stability of the D- $\pi$ -A systems on the  $(TiO_2)_9$  cluster has been evaluated using the adsorption energy ( $E_{ads}$ ), which is listed in Table 4. It is defined as  $E_{ads} = E_{dye/TiO_2} - (E_{dye} + E_{TiO_2})$ , where  $E_{dye/TiO_2}$ ,  $E_{dye}$ , and  $E_{TiO_2}$  denote the energies of dye/ $TiO_2$ , the isolated dye and the  $TiO_2$  cluster, respectively.<sup>95</sup> It is clear that a more negative adsorption energy could reveal higher adsorption stability between the dye molecule and  $TiO_2$ . In Table 4, we observed that all the adsorbed systems that have a more negative adsorption energy contain greater N-annulation. Among all, the most negative adsorption energy ( $-28.6$  kcal mol<sup>-1</sup>) is attained with D12- $\pi$ -A/ $TiO_2$ , which

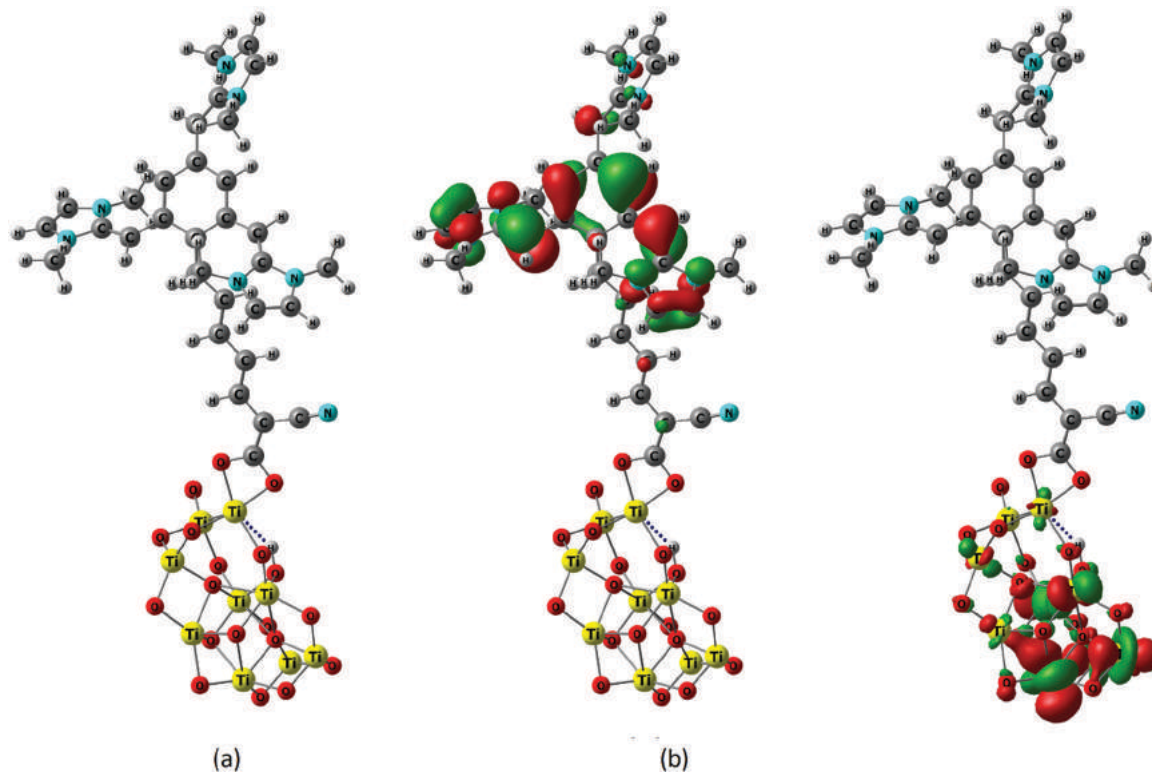


Fig. 4 (a) Optimized geometry of a representative D- $\pi$ -A system on the (TiO<sub>2</sub>)<sub>9</sub> cluster (D12- $\pi$ -A/TiO<sub>2</sub>). (b) Electron density shift in the frontier molecular orbitals.

**Table 3** HOMO (eV), LUMO (eV), and HOMO-LUMO energy gap, HLG (eV), for the D- $\pi$ -A/TiO<sub>2</sub> systems at the B3LYP/GenECP level. The maximum absorption wavelength  $\lambda_{\text{max}}$  (nm), and oscillator strength ( $f$ ) adsorbed on TiO<sub>2</sub> are simulated at the TD CAM-B3LYP/GenECP/SMD//B3LYP/GenECP level

D- $\pi$ -A/TiO <sub>2</sub> systems	HOMO (eV)	LUMO (eV)	HLG (eV)	$\lambda_{\text{max}}$ (nm)	$f$
D1	-5.43	-3.68	1.75	538	2.36
D2	-5.17	-3.66	1.52	583	2.03
D3	-5.10	-3.64	1.46	593	2.07
D4	-5.07	-3.62	1.45	611	1.73
D5	-5.09	-3.55	1.54	592	0.60
D6	-5.63	-3.74	1.89	526	2.24
D7	-5.53	-3.76	1.77	538	1.85
D8	-5.57	-3.79	1.77	531	1.87
D9	-5.37	-3.74	1.64	611	1.73
D10	-5.39	-3.71	1.69	574	0.05
D11	-4.85	-3.50	1.34	630	1.79
D12	-4.38	-3.25	1.13	703	0.29
D13	-4.99	-3.78	1.21	513	0.03
D14	-4.32	-3.71	0.61	697	0.02
D15	-5.44	-3.74	1.71	545	2.01
D16	-5.08	-3.60	1.48	610	1.91
D17	-5.25	-3.72	1.53	573	1.02
D18	-5.31	-3.72	1.59	558	1.22

indicates the most stable adsorption. Apart from N-annulation, the adsorption stability increases with enhanced electron-donating strength of D- $\pi$ -A. The excellent linear correlation between  $\Delta V_{\text{mA}}$  and  $E_{\text{ads}}$  with a correlation coefficient of 0.947 confirms that the donating strength of the donor systems of D- $\pi$ -A assessed in terms of  $\Delta V_{\text{mA}}$  is useful to assess the  $E_{\text{ads}}$  values of the dye on the semiconductor (Fig. 5a). Since stronger adsorption leads to deeper

**Table 4** The adsorption energies ( $E_{\text{ads}}$ ) of all the D- $\pi$ -A/(TiO<sub>2</sub>)<sub>9</sub> systems where the  $E_{\text{ads}}$  values are given in kcal mol<sup>-1</sup>

D- $\pi$ -A/(TiO <sub>2</sub> ) <sub>9</sub> systems	$E_{\text{ads}}$ (kcal mol <sup>-1</sup> )
D1- $\pi$ -A/(TiO <sub>2</sub> ) <sub>9</sub>	-23.6
D2- $\pi$ -A/(TiO <sub>2</sub> ) <sub>9</sub>	-23.8
D3- $\pi$ -A/(TiO <sub>2</sub> ) <sub>9</sub>	-23.9
D4- $\pi$ -A/(TiO <sub>2</sub> ) <sub>9</sub>	-24.3
D5- $\pi$ -A/(TiO <sub>2</sub> ) <sub>9</sub>	-25.0
D6- $\pi$ -A/(TiO <sub>2</sub> ) <sub>9</sub>	-23.3
D7- $\pi$ -A/(TiO <sub>2</sub> ) <sub>9</sub>	-23.0
D8- $\pi$ -A/(TiO <sub>2</sub> ) <sub>9</sub>	-22.8
D9- $\pi$ -A/(TiO <sub>2</sub> ) <sub>9</sub>	-23.4
D10- $\pi$ -A/(TiO <sub>2</sub> ) <sub>9</sub>	-23.8
D11- $\pi$ -A/(TiO <sub>2</sub> ) <sub>9</sub>	-25.4
D12- $\pi$ -A/(TiO <sub>2</sub> ) <sub>9</sub>	-28.6
D13- $\pi$ -A/(TiO <sub>2</sub> ) <sub>9</sub>	-22.2
D14- $\pi$ -A/(TiO <sub>2</sub> ) <sub>9</sub>	-23.3
D15- $\pi$ -A/(TiO <sub>2</sub> ) <sub>9</sub>	-22.6
D16- $\pi$ -A/(TiO <sub>2</sub> ) <sub>9</sub>	-24.5
D17- $\pi$ -A/(TiO <sub>2</sub> ) <sub>9</sub>	-23.2
D18- $\pi$ -A/(TiO <sub>2</sub> ) <sub>9</sub>	-23.3

LUMO energy levels, a more donating dye is expected to give higher adsorption stability and higher  $eV_{\text{oc}}$  (Table 4 and Fig. 5b). In the D12- $\pi$ -A/TiO<sub>2</sub> system, the highest adsorption stability and  $eV_{\text{oc}}$  (2.21 eV) have been observed, which predicts superior photovoltaic performance of the adsorbed dye.

### Photovoltaic performance

The photovoltaic parameters of the D- $\pi$ -A systems are listed in Table 5. The electron injection-free energy change ( $\Delta G_{\text{inject}}$ ) is

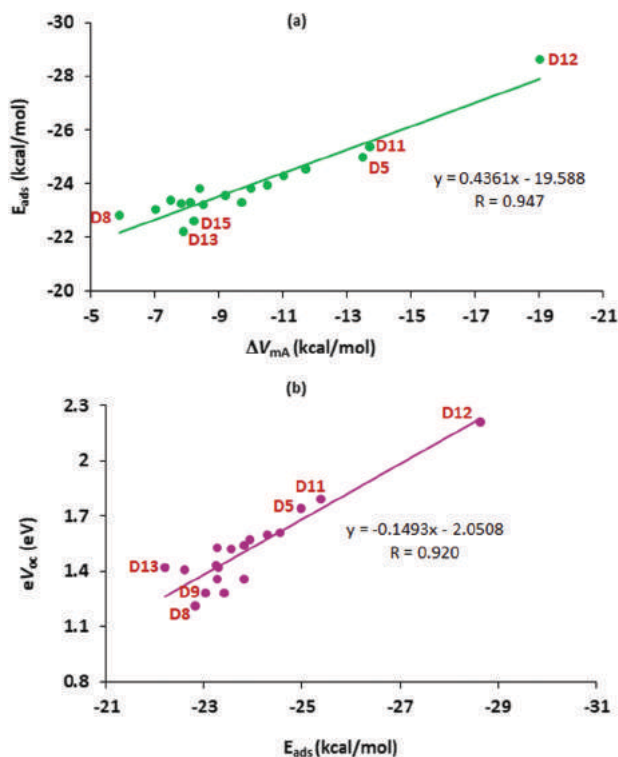


Fig. 5 (a) Correlation between  $\Delta V_{MA}$  and  $E_{ads}$  and (b)  $E_{ads}$  and  $eV_{OC}$ .

in the range  $-1.28$  to  $-2.10$  eV. It is defined as  $\Delta G_{inject} = E^{dye*} - |E_{CB}|$ ,<sup>96–98</sup> where  $E^{dye*}$  is the excited state oxidation potential and  $E_{CB}$  is the energy of the conduction band edge of the  $TiO_2$  semiconductor ( $-4.0$  eV).  $E^{dye*}$  can be calculated as  $(-e_h - \text{vertical excitation energy})$ .<sup>96,99</sup> The more negative  $\Delta G_{inject}$  will have more ability to inject electrons from the excited state of D- $\pi$ -A to the CB of  $TiO_2$ . Since  $\Delta G_{inject}$  is related to short-circuit current density  $J_{sc}$ , by improving the electron injection ability, an enhancement in the PCE can occur.<sup>6,22,26,98</sup> Among all,

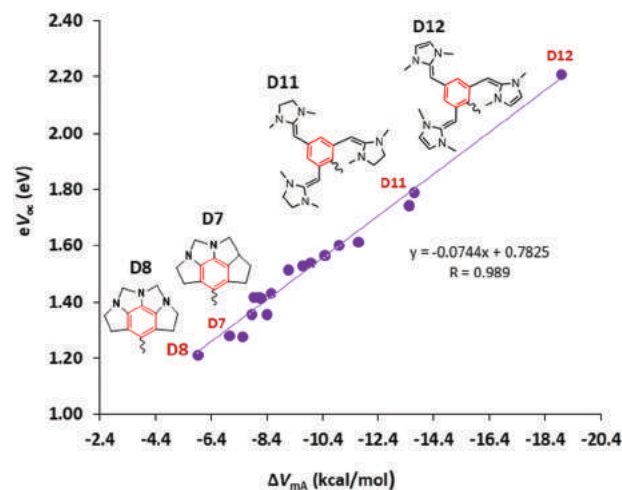


Fig. 6 Correlation between the donating strength ( $\Delta V_{MA}$ ) of the D- $\pi$ -A system and the open-circuit voltage ( $eV_{OC}$ ).

$\Delta G_{inject}$  is more negative in D14- $\pi$ -A ( $-2.10$  eV) while it is the least negative in D9- $\pi$ -A ( $-1.28$  eV). Further, it is noted that the donating strength improves the electron injection efficiency. The  $\Delta G_{reg}$  value measures the dye regeneration efficiency of the systems, which can be written as  $(E^{dye} - 4.8)$  eV or  $(-e_h) - 4.8$  eV.<sup>100,101</sup> The smallest  $\Delta G_{reg}$  ( $-0.84$  eV) observed in D12- $\pi$ -A shows the highest dye regeneration efficiency, while the highest value  $0.49$  observed in D6- $\pi$ -A indicates the lowest dye regeneration efficiency. Finally, the open-circuit voltage ( $eV_{OC} = e_1 - (-4.0)$ )<sup>102</sup> lies in the range  $1.21$  eV to  $2.21$  eV, which shows an excellent correlation with  $\Delta V_{MA}$  (Fig. 6), and suggests that  $eV_{OC}$  increases with enhanced strength of the D- $\pi$ -A systems. The correlation in Fig. 6 also suggests that the MESP approach offers an easy analysis tool for the quantification of the donating strength of D- $\pi$ -A systems in DSSC applications, and the correlation plot provides a guideline for designing dye sensitizers for desirable photovoltaic applications.

**Table 5** HOMO (eV), LUMO (eV), and HOMO–LUMO energy gap (eV) at the B3LYP/cc-pVDZ level. Ground and excited state oxidation potential ( $E^{dye}$ ,  $E^{dye*}$ ), excitation energy, free energy of electron injection  $\Delta G_{inject}$ , dye regeneration efficiency  $\Delta G_{reg}$ , and open-circuit voltage  $eV_{OC}$  at the TD-CAM-B3LYP/SMD/cc-pVDZ//B3LYP/cc-pVDZ level

Systems	Excitation energy (eV)	HOMO (eV)	LUMO (eV)	HLG (eV)	$E^{dye}$ (eV)	$E^{dye*}$ (eV)	$\Delta G_{inject}$ (eV)	$\Delta G_{reg}$ (eV)	$eV_{OC}$ (eV)
D1	2.61	-5.09	-2.48	2.61	5.09	2.48	-1.52	0.29	1.52
D2	2.42	-4.82	-2.46	2.36	4.82	2.40	-1.60	0.02	1.54
D3	2.38	-4.74	-2.43	2.31	4.74	2.36	-1.64	-0.06	1.57
D4	2.29	-4.69	-2.40	2.29	4.69	2.40	-1.60	-0.11	1.60
D5	2.35	-4.68	-2.26	2.42	4.68	2.33	-1.67	-0.12	1.74
D6	2.63	-5.29	-2.64	2.65	5.29	2.66	-1.34	0.49	1.36
D7	2.58	-5.22	-2.72	2.50	5.22	2.64	-1.36	0.42	1.28
D8	2.61	-5.27	-2.79	2.48	5.27	2.66	-1.34	0.47	1.21
D9	2.33	-5.05	-2.72	2.33	5.05	2.72	-1.28	0.25	1.28
D10	2.38	-5.04	-2.64	2.40	5.04	2.66	-1.34	0.24	1.36
D11	2.26	-4.50	-2.21	2.29	4.50	2.24	-1.76	-0.30	1.79
D12	2.00	-3.96	-1.79	2.17	3.96	1.96	-2.04	-0.84	2.21
D13	2.73	-4.77	-2.58	2.19	4.77	2.04	-1.96	-0.03	1.42
D14	2.21	-4.11	-2.47	1.64	4.11	1.90	-2.10	-0.69	1.53
D15	2.58	-5.11	-2.59	2.52	5.11	2.53	-1.47	0.31	1.41
D16	2.29	-4.72	-2.39	2.33	4.72	2.43	-1.57	-0.08	1.61
D17	2.48	-4.96	-2.57	2.39	4.96	2.48	-1.52	0.16	1.43
D18	2.55	-5.04	-2.58	2.46	5.04	2.49	-1.51	0.24	1.42

In the analysis, the highest donating strength observed in D12- $\pi$ -A correlates to the highest  $eV_{oc}$  (2.21 eV). The pyramidalized nitrogen centres observed in D8- $\pi$ -A retard the efficient electron injection to  $\pi$ -A, and it shows the lowest  $eV_{oc}$  (1.21 eV) due to inferior donating strength.

## Conclusions

Donor modifications, especially through the integration of electron-rich nitrogen atoms (N-annulation), significantly affect the structure–performance relationship of D- $\pi$ -A systems for dye-sensitized solar cell applications. For tuning the electron-donating ability of D- $\pi$ -A systems, eighteen electron-rich nitrogen incorporated donors are designed with butadiene and cyanoacrylic acid as a  $\pi$ -spacer and an acceptor, respectively. The implication of planarized nitrogens for improving the electron-donating strength ( $\Delta V_{mA}$ ) of D- $\pi$ -A systems is investigated using MESP topographical analysis, which states that the magnitude of  $\Delta V_{mA}$  increases with an increased number of planar nitrogens. The  $\lambda_{max}$  values of the D- $\pi$ -A systems are fine-tuned by the extent of  $\pi$ -conjugation and N-annulation in the donors. The significance of  $\Delta V_{mA}$  in shifting the absorption maximum ( $\Delta\lambda_{max}$ ) is confirmed by the linear correlation observed between  $\Delta V_{mA}$  and  $\Delta\lambda_{max}$ . Regarding the frontier molecular orbitals of the D- $\pi$ -A systems, the HOMO and LUMO energies are affected by the electron-rich nature of the donors in D- $\pi$ -A. The sufficiently more negative LUMO energy of the D- $\pi$ -A systems than the CB energy of TiO<sub>2</sub> provides high electron injection efficiency. The open-circuit voltage ( $eV_{oc}$ ), and free energy of electron injection ( $\Delta G_{inject}$ ) have been analysed for the D- $\pi$ -A systems and reveal that  $eV_{oc}$  is increased with enhanced  $\Delta V_{mA}$ . Also, the adsorption stability of the D- $\pi$ -A systems on TiO<sub>2</sub> has been evaluated and indicates that the adsorption stability ( $E_{ads}$ ) increased with enhanced electron-donating strength of the D- $\pi$ -A system. Since adsorption of the D- $\pi$ -A system on TiO<sub>2</sub> shifts the LUMO energy, the stability of the D- $\pi$ -A/TiO<sub>2</sub> system affects  $eV_{oc}$  and thus the efficiency of the solar cell. The strong linear correlation observed between  $E_{ads}$  and  $eV_{oc}$  proves this conclusion. Among all the cases studied, D12- $\pi$ -A/TiO<sub>2</sub> shows the highest adsorption stability; furthermore, D12- $\pi$ -A displays the highest  $\Delta\lambda_{max}$ , the best  $eV_{oc}$  and the highest magnitude for  $\Delta V_{mA}$ . Consequently, from the aforementioned fundamental parameters, it can be concluded that the D12 based photosensitizer is very effective for improving the PCE. Also, the N-annulation design strategy will pave the way for attaining high efficiency in the field of dye-sensitized solar cells.

## Conflicts of interest

There are no conflicts to declare.

## Acknowledgements

The authors thank DST-SERB for funding through GAP1397 and also gratefully acknowledge the CSIR 4th PI for HPC facility

and NIIST IT lab for computational support. V. V. Divya thanks CSIR, India, for the senior research fellowship.

## References

- 1 A. Baheti, C.-P. Lee, K. J. Thomas and K.-C. Ho, *Phys. Chem. Chem. Phys.*, 2011, **13**, 17210–17221.
- 2 Y.-H. Chen, V. S. Nguyen, H.-H. Chou, Y. S. Tingare, T.-C. Wei and C.-Y. Yeh, *ACS Appl. Energy Mater.*, 2020, **3**, 5479–5486.
- 3 J. Gong, K. Sumathy, Q. Qiao and Z. Zhou, *Renewable Sustainable Energy Rev.*, 2017, **68**, 234–246.
- 4 G. Boschloo, *Front. Chem.*, 2019, **7**, 77.
- 5 M. Grätzel, *Acc. Chem. Res.*, 2009, **42**, 1788–1798.
- 6 B. O'Regan and M. Grätzel, *Nature*, 1991, **353**, 737–740.
- 7 M. K. Nazeeruddin, F. De Angelis, S. Fantacci, A. Selloni, G. Viscardi, P. Liska, S. Ito, B. Takeru and M. Grätzel, *J. Am. Chem. Soc.*, 2005, **127**, 16835–16847.
- 8 G. Marotta, M. A. Reddy, S. P. Singh, A. Islam, L. Han, F. De Angelis, M. Pastore and M. Chandrasekharam, *ACS Appl. Mater. Interfaces*, 2013, **5**, 9635–9647.
- 9 S. Yun, Y. Qin, A. R. Uhl, N. Vlachopoulos, M. Yin, D. Li, X. Han and A. Hagfeldt, *Energy Environ. Sci.*, 2018, **11**, 476–526.
- 10 A. Fakharuddin, R. Jose, T. M. Brown, F. Fabregat-Santiago and J. Bisquert, *Energy Environ. Sci.*, 2014, **7**, 3952–3981.
- 11 A. Hinsch, W. Veurman, H. Brandt, K. F. Jensen and S. Mastroianni, *ChemPhysChem*, 2014, **15**, 1076–1087.
- 12 A. Hagfeldt, G. Boschloo, L. Sun, L. Kloo and H. Pettersson, *Chem. Rev.*, 2010, **110**, 6595–6663.
- 13 Y. Kurumisawa, T. Higashino, S. Nimura, Y. Tsuji, H. Iiyama and H. Imahori, *J. Am. Chem. Soc.*, 2019, **141**, 9910–9919.
- 14 H. Zhou, J.-M. Ji, S. H. Kang, M. S. Kim, H. S. Lee, C. H. Kim and H. K. Kim, *J. Mater. Chem. C*, 2019, **7**, 2843–2852.
- 15 K. Kakiage, Y. Aoyama, T. Yano, K. Oya, T. Kyomen and M. Hanaya, *Chem. Commun.*, 2015, **51**, 6315–6317.
- 16 K. Kakiage, Y. Aoyama, T. Yano, K. Oya, J.-I. Fujisawa and M. Hanaya, *Chem. Commun.*, 2015, **51**, 15894–15897.
- 17 S. Mathew, A. Yella, P. Gao, R. Humphry-Baker, B. F. Curchod, N. Ashari-Astani, I. Tavernelli, U. Rothlisberger, M. K. Nazeeruddin and M. Grätzel, *Nat. Chem.*, 2014, **6**, 242–247.
- 18 F.-S. Lin, P. Priyanka, M.-S. Fan, S. Vegiraju, J.-S. Ni, Y.-C. Wu, Y.-H. Li, G.-H. Lee, Y. Ezhumalai and R.-J. Jeng, *J. Mater. Chem. C*, 2020, **8**, 15322–15330.
- 19 Y. Ren, Y. Li, S. Chen, J. Liu, J. Zhang and P. Wang, *Energy Environ. Sci.*, 2016, **9**, 1390–1399.
- 20 K. Sharma, V. Sharma and S. Sharma, *Nanoscale Res. Lett.*, 2018, **13**, 381.
- 21 X. Song, X. Yang, H. Wang, J. An, Z. Yu, X. Wang, A. Hagfeldt and L. Sun, *Sol. Energy*, 2019, **187**, 274–280.
- 22 V. V. Divya and C. H. Suresh, *New J. Chem.*, 2020, **44**, 7200–7209.



- 23 M. Jadhav, J. V. Vaghasiya, D. Patil, S. S. Soni and N. Sekar, *New J. Chem.*, 2019, **43**, 8970–8981.
- 24 R. Tarsang, V. Promarak, T. Sudyoadsuk, S. Namuangruk and S. Jungsuttiwong, *J. Photochem. Photobiol., A*, 2014, **273**, 8–16.
- 25 M. Karuppusamy, V. S. K. Choutipalli, D. Vijay and V. Subramanian, *J. Chem. Sci.*, 2020, **132**, 20.
- 26 V. V. Divya and C. H. Suresh, *New J. Chem.*, 2021, **45**, 2496–2507.
- 27 Y. K. Eom, S. H. Kang, I. T. Choi, Y. Yoo, J. Kim and H. K. Kim, *J. Mater. Chem. A*, 2017, **5**, 2297–2308.
- 28 Y.-Q. Yan, Y.-Z. Zhu, P.-P. Dai, J. Han, M. Yan and J.-Y. Zheng, *Sol. Energy*, 2020, **207**, 428–435.
- 29 H. Zhang, Z.-E. Chen and H.-R. Tian, *Sol. Energy*, 2020, **198**, 239–246.
- 30 A. J. Huckaba, F. Giordano, L. E. McNamara, K. M. Dreux, N. I. Hammer, G. S. Tschumper, S. M. Zakeeruddin, M. Grätzel, M. K. Nazeeruddin and J. H. Delcamp, *Adv. Energy Mater.*, 2015, **5**, 1401629.
- 31 Y. Zhang, H. Cheema, L. McNamara, L. A. Hunt, N. I. Hammer and J. H. Delcamp, *Chem. – Eur. J.*, 2018, **24**, 5939–5949.
- 32 J. Feng, Y. Jiao, W. Ma, M. K. Nazeeruddin, M. Grätzel and S. Meng, *J. Phys. Chem. C*, 2013, **117**, 3772–3778.
- 33 J. H. Delcamp, A. Yella, T. W. Holcombe, M. K. Nazeeruddin and M. Grätzel, *Angew. Chem., Int. Ed.*, 2013, **125**, 394–398.
- 34 C. Yan, W. Ma, Y. Ren, M. Zhang and P. Wang, *ACS Appl. Mater. Interfaces*, 2015, **7**, 801–809.
- 35 U. B. Cappel, M. H. Karlsson, N. G. Pschirer, F. Eickemeyer, J. Schöneboom, P. Erk, G. Boschloo and A. Hagfeldt, *J. Phys. Chem. C*, 2009, **113**, 14595–14597.
- 36 C. Li, Z. Liu, J. Schöneboom, F. Eickemeyer, N. G. Pschirer, P. Erk, A. Herrmann and K. Müllen, *J. Mater. Chem. C*, 2009, **19**, 5405–5415.
- 37 Y. Jin, J. Hua, W. Wu, X. Ma and F. Meng, *Synth. Met.*, 2008, **158**, 64–71.
- 38 J. Luo, M. Xu, R. Li, K.-W. Huang, C. Jiang, Q. Qi, W. Zeng, J. Zhang, C. Chi, P. Wang and J. Wu, *J. Am. Chem. Soc.*, 2014, **136**, 265–272.
- 39 Z. Yao, H. Wu, Y. Ren, Y. Guo and P. Wang, *Energy Environ. Sci.*, 2015, **8**, 1438–1442.
- 40 Z. Yao, M. Zhang, H. Wu, L. Yang, R. Li and P. Wang, *J. Am. Chem. Soc.*, 2015, **137**, 3799–3802.
- 41 V. V. Divya, F. B. Sayyed and C. H. Suresh, *ChemPhysChem*, 2019, **20**, 1752–1758.
- 42 F. Effenberger, P. Fischer, W. W. Schöllner and W.-D. Stohrer, *Tetrahedron*, 1978, **34**, 2409–2417.
- 43 A. Zakrzewska, R. Gawinecki, E. Kolehmainen and B. Osmiałowski, *Int. J. Mol. Sci.*, 2005, **6**, 52–62.
- 44 J. O. S. Varejão, E. V. V. Varejão and S. A. Fernandes, *Eur. J. Org. Chem.*, 2019, 4273–4310.
- 45 J. E. Kuder, W. W. Limburg, J. M. Pochan and D. Wychick, *J. Chem. Soc. Perkin Trans. 2*, 1977, 1643–1651.
- 46 G. Shishkin, *Chem. Heterocycl. Compd.*, 1983, **19**, 549–553.
- 47 F. Fantuzzi, C. B. Coutinho, R. R. Oliveira and M. A. C. Nascimento, *Inorg. Chem.*, 2018, **57**, 3931–3940.
- 48 C. H. Suresh and F. B. Sayyed, *J. Phys. Chem. A*, 2013, **117**, 10455–10461.
- 49 S. Rohrbach, R. S. Shah, T. Tuttle and J. A. Murphy, *Angew. Chem.*, 2019, **131**, 11576–11580.
- 50 J. S. Miller, D. A. Dixon, J. C. Calabrese, C. Vazquez, P. J. Krusic, M. D. Ward, E. Wasserman and R. L. Harlow, *J. Am. Chem. Soc.*, 1990, **112**, 381–398.
- 51 E. Scrocco and J. Tomasi, in *Advances Quantum Chemistry*, ed. P.-O. Löwdin, Academic Press, 1978, vol. 11, pp. 115–193.
- 52 B. Pullman, *Int. J. Quantum Chem.*, 1990, **38**, 81–92.
- 53 A. Pullman and B. Pullman, *Q. Rev. Biophys.*, 1981, **14**, 289–380.
- 54 P. Politzer and J. S. Murray, *J. Mol. Struct.*, 1996, **376**, 419–424.
- 55 P. Politzer, J. S. Murray and T. Clark, *Phys. Chem. Chem. Phys.*, 2013, **15**, 11178–11189.
- 56 P. Politzer and J. S. Murray, *Cryst. Growth Des.*, 2015, **15**, 3767–3774.
- 57 P. Politzer and J. S. Murray, *ChemPhysChem*, 2020, **21**, 579–588.
- 58 C. H. Suresh and S. R. Gadre, *J. Org. Chem.*, 1999, **64**, 2505–2512.
- 59 S. R. Gadre and R. N. Shirsat, *Electrostatics of Atoms and Molecules*, Universities Press, 2000.
- 60 S. R. Gadre, S. A. Kulkarni and I. H. Shrivastava, *J. Chem. Phys.*, 1992, **96**, 5253–5260.
- 61 F. B. Sayyed and C. H. Suresh, *Tetrahedron Lett.*, 2009, **50**, 7351–7354.
- 62 F. B. Sayyed and C. H. Suresh, *New J. Chem.*, 2009, **33**, 2465–2471.
- 63 P. Sajith and C. H. Suresh, *Inorg. Chem.*, 2012, **51**, 967–977.
- 64 J. Mathew and C. H. Suresh, *Organometallics*, 2011, **30**, 1438–1444.
- 65 K. Sandhya and C. H. Suresh, *Dalton Trans.*, 2014, **43**, 12279–12287.
- 66 B. A. Anjali, F. B. Sayyed and C. H. Suresh, *J. Phys. Chem. C*, 2016, **120**, 1112–1119.
- 67 B. A. Anjali and C. H. Suresh, *ACS Omega*, 2017, **2**, 4196–4206.
- 68 P. V. Bijina and C. H. Suresh, *J. Chem. Sci.*, 2016, **128**, 1677–1686.
- 69 R. Rakhi and C. H. Suresh, *Phys. Chem. Chem. Phys.*, 2016, **18**, 24631–24641.
- 70 K. Remya and C. H. Suresh, *Phys. Chem. Chem. Phys.*, 2015, **17**, 27035–27044.
- 71 T. D. Della and C. H. Suresh, *Phys. Chem. Chem. Phys.*, 2016, **18**, 14588–14602.
- 72 F. Arkan and M. Izadyar, *Renewable Sustainable Energy Rev.*, 2018, **94**, 609–655.
- 73 W. Zhang, L. Wang, L. Mao, J. Jiang, H. Ren, P. Heng, H. Ågren and J. Zhang, *J. Phys. Chem. C*, 2020, **124**, 3980–3987.
- 74 A. D. Laurent, C. Adamo and D. Jacquemin, *Phys. Chem. Chem. Phys.*, 2014, **16**, 14334–14356.
- 75 M. Y. Mehboob, M. U. Khan, R. Hussain, K. Ayub, A. Sattar, M. K. Ahmad, Z. Irshad and M. Adnan, *Spectrochim. Acta, Part A*, 2021, **244**, 118873.

- 76 M. Y. Mehboob, M. U. Khan, R. Hussain, R. Fatima, Z. Irshad and M. Adnan, *J. Theory Comput. Chem.*, 2020, **19**, 2050034.
- 77 M. Y. Mehboob, R. Hussain, M. U. Khan, M. Adnan, A. Umar, M. U. Alvi, M. Ahmed, M. Khalid, J. Iqbal and M. N. Akhtar, *Comput. Theor. Chem.*, 2020, **1186**, 112908.
- 78 M. Y. Mehboob, R. Hussain, M. U. Khan, M. Adnan, M. A. Ehsan, A. Rehman and M. R. S. A. Janjua, *J. Phys. Org. Chem.*, 2021, e4204.
- 79 A. D. Becke, *J. Chem. Phys.*, 1993, **98**, 1372–1377.
- 80 T. H. Dunning Jr, *Chem. Phys.*, 1989, **90**, 1007–1023.
- 81 J. K. Roy, S. Kar and J. Leszczynski, *J. Phys. Chem. C*, 2019, **123**, 3309–3320.
- 82 S. Kupfer, J. Guthmuller and L. Gonzalez, *J. Chem. Theory Comput.*, 2013, **9**, 543–554.
- 83 P. J. Hay and W. R. Wadt, *J. Chem. Phys.*, 1985, **82**, 270–283.
- 84 R. Sánchez-de-Armas, M. A. San Miguel, J. Oviedo and J. F. Sanz, *Phys. Chem. Chem. Phys.*, 2012, **14**, 225–233.
- 85 T. Yanai, D. P. Tew and N. C. Handy, *Chem. Phys. Lett.*, 2004, **393**, 51–57.
- 86 G. Deogratias, N. Seriani, T. Pogrebnyaya and A. Pogrebnoi, *J. Mol. Graphics Modell.*, 2020, **94**, 107480.
- 87 J. Zhang, H.-C. Zhu, R.-L. Zhong, L. Wang and Z.-M. Su, *Org. Electron.*, 2018, **54**, 104–113.
- 88 H.-C. Zhu, C.-F. Li, Z.-H. Fu, S.-S. Wei, X.-F. Zhu and J. Zhang, *Appl. Surf. Sci.*, 2018, **455**, 1095–1105.
- 89 M. J. Frisch, G. W. Trucks, H. B. Schlegel, G. E. Scuseria, M. A. Robb, J. R. Cheeseman, G. Scalmani, V. Barone, G. A. Petersson, H. Nakatsuji, X. Li, M. Caricato, A. V. Marenich, J. Bloino, B. G. Janesko, R. Gomperts, B. Mennucci, H. P. Hratchian, J. V. Ortiz, A. F. Izmaylov, J. L. Sonnenberg, D. Williams-Young, F. Ding, F. Lipparini, F. Egidi, J. Goings, B. Peng, A. Petrone, T. Henderson, D. Ranasinghe, V. G. Zakrzewski, J. Gao, N. Rega, G. Zheng, W. Liang, M. Hada, M. Ehara, K. Toyota, R. Fukuda, J. Hasegawa, M. Ishida, T. Nakajima, Y. Honda, O. Kitao, H. Nakai, T. Vreven, K. Throssell, J. A. Montgomery Jr., J. E. Peralta, F. Ogliaro, M. J. Bearpark, J. J. Heyd, E. N. Brothers, K. N. Kudin, V. N. Staroverov, T. A. Keith, R. Kobayashi, J. Normand, K. Raghavachari, A. P. Rendell, J. C. Burant, S. S. Iyengar, J. Tomasi, M. Cossi, J. M. Millam, M. Klene, C. Adamo, R. Cammi, J. W. Ochterski, R. L. Martin, K. Morokuma, O. Farkas, J. B. Foresman and D. J. Fox, *Gaussian 16, Revision A.03*, Gaussian, Wallingford, CT, 2016.
- 90 M. Y. Mehboob, R. Hussain, Z. Irshad and M. Adnan, *J. Phys. Org. Chem.*, 2021, e4210.
- 91 R. Hussain, M. Y. Mehboob, M. U. Khan, M. Khalid, Z. Irshad, R. Fatima, A. Anwar, S. Nawab and M. Adnan, *J. Mater. Sci.*, 2021, **56**, 5113–5131.
- 92 M. Y. Mehboob, R. Hussain, Z. Irshad and M. Adnan, *Bull. Korean Chem. Soc.*, 2021, **42**, 597–610.
- 93 L. Zhang and J. M. Cole, *ACS Appl. Mater. Interfaces*, 2015, **7**, 3427–3455.
- 94 M. Pastore and F. De Angelis, *Phys. Chem. Chem. Phys.*, 2012, **14**, 920–928.
- 95 P. Li, Z. Wang, C. Song and H. Zhang, *J. Mater. Chem. A*, 2017, **5**, 11454–11465.
- 96 R. Katoh, A. Furube, T. Yoshihara, K. Hara, G. Fujihashi, S. Takano, S. Murata, H. Arakawa and M. Tachiya, *J. Phys. Chem. B*, 2004, **108**, 4818–4822.
- 97 J. Preat, C. Michaux, D. Jacquemin and E. A. Perpète, *J. Phys. Chem. C*, 2009, **113**, 16821–16833.
- 98 N. N. Ghosh, M. Habib, A. Pramanik, P. Sarkar and S. Pal, *New J. Chem.*, 2019, **43**, 6480–6491.
- 99 J. Zhang, H.-B. Li, S.-L. Sun, Y. Geng, Y. Wu and Z.-M. Su, *J. Mater. Chem.*, 2012, **22**, 568–576.
- 100 G. Boschloo and A. Hagfeldt, *Acc. Chem. Res.*, 2009, **42**, 1819–1826.
- 101 T. Koopmans, *Physica*, 1933, **1**, 104–113.
- 102 C.-R. Zhang, Z.-J. Liu, Y.-H. Chen, H.-S. Chen, Y.-Z. Wu, W. Feng and D.-B. Wang, *Curr. Appl. Phys.*, 2010, **10**, 77–83.